



TalentDetector

**TalentDetector2024\_Winter  
INTERNATIONAL STUDENTS SCIENTIFIC  
CONFERENCE**

**Scientific editor:  
Mirosław Bonek**

Department of Engineering Materials and Biomaterials,  
Faculty of Mechanical Engineering,  
Silesian University of Technology  
26<sup>th</sup> January 2024  
Gliwice, Poland



**Katedra Materiałów**  
Inżynierskich i Biomedycznych

**Katedra Materiałów Inżynierskich i Biomedycznych****Wydział Mechaniczny Technologiczny****Politechnika Śląska**

ul. Konarskiego 18a, 44-100 Gliwice tel. +48 (32) 2371322

**Redakcja techniczna i skład komputerowy:**

dr hab. inż. Mirosław Bonek, prof. PŚ

**Recenzenci:**

M. Bonek, Z. Brytan, A. Czupryński, A. Drygała, A. Kania, A. Kloc-Ptaszna, M. Kremzer, M. Król, B. Krupińska, L. Kuchariková, S. Lesz, G. Matula, C. Meran, J. Nowak, O. Polishchuk, M. Polok-Rubinić, M. Roszak, M. Spilka, M. Sroka, M. Staszuk, M. Szindler, A. Śliwa, T. Tański, E. Tillová, A. Włodarczyk-Fligier

Materiały są opublikowane na podstawie oryginałów dostarczonych przez Autorów, zaopiniowanych przez Zespół Recenzentów.

**Wydano za zgodą:**

Kierownika Katedry Materiałów Inżynierskich i Biomedycznych

Wydziału Mechanicznego Technologicznego

Politechniki Śląskiej

**Wydawca:**

Katedra Materiałów Inżynierskich i Biomedycznych

Wydział Mechaniczny Technologiczny

Politechnika Śląska

Gliwice 2024

Wszystkie opublikowane materiały stanowią utwór podlegający ochronie na mocy prawa autorskiego. Utwór ten w całości ani we fragmentach nie może być powielany ani rozpowszechniany za pomocą urządzeń elektronicznych, mechanicznych, kopiujących, nagrywających i innych. Ponadto utwór ten nie może być umieszczany ani rozpowszechniany w postaci cyfrowej zarówno w Internecie, jak i w sieciach lokalnych, bez pisemnej zgody posiadacza praw autorskich.

**Seria wydawnicza:**

Prace Katedry Materiałów Inżynierskich i Biomedycznych

Wydział Mechaniczny technologiczny

Politechnika Śląska

Publikacja: styczeń 2024

ISBN 978-83-65138-39-2



**INTERNATIONAL STUDENTS SCIENTIFIC CONFERENCE**  
**TALENTDETECTOR2024\_WINTER**  
**SILESIA UNIVERSITY OF TECHNOLOGY, GLIWICE, POLAND**  
**26<sup>TH</sup> JANUARY 2024**

The International Student Scientific Conference TalentDetector2024\_Winter aims to integrate the student and scientific community dealing with topics related to material technologies. It is a place that gives the opportunity to exchange experiences, knowledge, skills and present current scientific achievements, developing and expanding students' interests in the field of materials engineering, surface engineering, biomaterials and biomedical engineering, nanotechnology, pro-ecological technologies and computer materials science. The conference allows for the presentation of projects conducted with the industry as part of the activities of Student Scientific Circles, doctorates, projects implemented in the form of PBL - Project Based Learning as part of the Excellence Initiative - Research University at the Silesian University of Technology, PBL in the framework of EURECA PRO/European University in Responsible Consumption and Production, international bilateral cooperation and projects implemented as part of the Visegrad Scholarship Program 2023/2024.



**CONFERENCE ORGANIZER**

Materials Science Circle of the Association of Alumni of the Silesian University of Technology,  
Gliwice, Poland

**CONFERENCE CO-ORGANIZER**

Department of Engineering Materials and Biomaterials, Faculty of Mechanical Engineering,  
Silesian University of Technology, Gliwice, Poland

**INTERNATIONAL SCIENTIFIC COMMITTEE**

prof. Mirosław Bonek, Silesian University of Technology, Gliwice, Poland - *President of the International Scientific Committee*

prof. Marcin Adamiak, Silesian University of Technology, Gliwice, Poland  
prof. Sedat Alkoy, Gebze Technical University, Gebze, Turkey  
prof. Rafał Babilas, Silesian University of Technology, Gliwice, Poland  
prof. Ahmet Durgutlu, Gazi University, Ankara, Turkey  
prof. Otar Gelashvili, Georgian Technical University, Tbilisi, Georgia  
prof. Boris Gitolendia, Georgian Technical University, Tbilisi, Georgia  
prof. Adam Grajcar, Silesian University of Technology, Gliwice, Poland  
prof. Alexander Horn, Laserinstitut Hochschule Mittweida, Mittweida, Germany  
prof. Volkan Kılıçlı, Gazi University, Ankara, Turkey  
doc. Lenka Kuchariková, University of Zilina, Zilina, Slovakia  
prof. Martin Kusy, Slovak Technical University in Bratislava, Trnava, Slovakia  
prof. Grzegorz Matula, Silesian University of Technology, Gliwice, Poland  
prof. Janusz Mazurkiewicz, Silesian University of Technology, Gliwice, Poland  
prof. Serhii Matiukh, Khmelnytskyi National University, Khmelnytskyi, Ukraine  
prof. Cemal Meran, Pamukkale University, Denizli, Turkey  
prof. Oleh Polishchuk, Khmelnytskyi National University, Khmelnytskyi, Ukraine  
prof. Mykola Skyba, Khmelnytskyi National University, Khmelnytskyi, Ukraine  
prof. Tomasz Tański, Silesian University of Technology, Gliwice, Poland  
doc. Miroslava Tavodova, Technical University in Zvolen, Zvolen, Slovakia  
prof. Eva Tillova, University of Zilina, Zilina, Slovakia

**ORGANIZING COMMITTEE***Chairman*

prof. Mirosław Bonek

prof. Zbigniew Brytan	dr. Mariusz Król
prof. Sabina Lesz	dr. Agnieszka J. Nowak
prof. Daniel Pakuła	dr. Magdalena Polok-Rubiniec
prof. Marek Roszak	dr. Weronika Smok
prof. Marek Sroka	dr. Marcin Staszuk
prof. Agata Śliwa	dr. Magdalena Szindler
prof. Tomasz Tański	dr. Marek Szindler
dr. K. Cesarz-Andraczke	dr. Anna Włodarczyk-Fligier
dr. Aleksandra Drygała	dr. Anna Woźniak
dr. Rafał Honysz	Ksenia Czardyban MSc
dr. Aneta Kania	Amadeusz Dziwis MSc
dr. Anna Kloc-Ptaszna	Wojciech Mikotejko MSc
dr. Marek Kremzer	Marta Zaborowska MSc



26th January 2024  
Gliwice, Poland

DEPARTMENT OF ENGINEERING MATERIALS AND BIOMATERIALS  
FACULTY OF MECHANICAL ENGINEERING  
SILESIA UNIVERSITY OF TECHNOLOGY

## INTERNATIONAL STUDENTS SCIENTIFIC CONFERENCE

### Contents

The Influence of Metal Oxide Thin Films Deposited by ALD Method on the Properties of Dye Sensitized Solar Cells A.E. Adzo, W. Sitek, M. Szindler .....	1
Elevator Potential Recovery P. Ayoub .....	7
Charging and Maintenance System for Drone Fleet P. Bartosz, D. Bereta, J. Sarno, D. Myszor .....	12
VR and 3D Tiles as a catalyst for the creation of immersive flight simulators P. Bartosz, J. Sarno, D. Myszor .....	16
Modification of the machine for double pressing of fuel briquettes K. Beridze; G. Taturashvili .....	20
Wybrane własności stopu $Ni_{36,3}Co_{25}W_{23,7}B_{15}$ wytworzonego metodą melt-spinning M. Bigaj, W. Pilarczyk, I. Kredowska, K. Młynarek-Żak .....	28
The characteristics of the ABS polymer material used for 3D printing filaments I. Blumski, L. Gabiga, R. Gabryś, J. Pająk, M. Polok-Rubiniec, A. Włodarczyk-Fligier, A. Kania .....	34
Creating of layers on the surface of the materials A. Bodnar, K. Jędrzejczyk, M. Szafron, M. Bonek.....	38
Computer simulation of the welding process of various materials manufactured using SLM methods W. Borek, K. Elanany, M. Kremzer, S. Ebied.....	44
Wirtualna symulacja próby lejułości odlewniczych materiałów inżynierskich S. Borowski, R. Dąbrowski, M. Dudzik, R. Honysz .....	48

Co-sensitization of titanium dioxide layers for photovoltaic applications with dyes J. Budzynowski, K. Tyczyński, S. Bielec, J. Sobolewski, A. Drygała, J. Wyrwał, S. Lesz, E. Tillová, P. Palček.....	55
The application of surface layers in the construction of photovoltaic cells P. Bułka, G. Latacz, D. Pakuła, M. Staszuk.....	62
Scanning, modelling, and printing in 3D technology D. Celeban, G. Pośpiech, P. Kruczyński, M. Szczypiór, A. Kania, A. Włodarczyk-Fligier, M. Polok-Rubiniec.....	68
Consolidation of 18Ni300 maraging steel powder in the Gleeble 3800 simulator J. Chudy, M. Kremzer, W. Borek, B. Tomiczek .....	75
The influence of wood waste on the mechanical properties of cast epoxy resin N. Ciemała, S. Masoń, W. Kała, K. Konopka, K. Świerczok, Ł. Wantuch, M. Szymiczek, M. Chomiak .....	81
Improvement of the functional properties of the top layer of tool steel after laser processing P. Cisowski, S. Szeja, J. Badora, A. Kłapsia, J. Muszyńska, E. Krajewska, M. Bonek, U. Ozdemir.....	93
Effect of spindle rotations and feed speed on energy consumption of milling on a CNC machining centre T. Čuchor, P. Koleda, R. Kminiak, M. Ťavodová .....	101
Exploring the potential of duplex stainless steels in additive manufacturing: composition, corrosion, and challenges M.J. Dagnaw, Z. Brytan .....	111
Modern technologies for welding polymers - thermoplastics - review of research and techniques K. Dziedzic, A. Kleszcz, M. Bentkowski, M. Bonek .....	119
Improvement of work organization in a selected manufacturing company M. Dziubanowska, M. Spilka .....	125
Analysis of stress distribution in the bottle opener A.R. Dziwis, P. Bzdon, A. Dziwis, W. Mikołajko, A. Śliwa .....	131
Tribological properties of the surface layer of tool steels after laser remelting A. Dzwonek, K. Malon, M. Paluch, M. Święcicka, M. Volkmer, O. Więcek, M. Bonek, E. Tillova.....	138

Działanie wiązki laserowej na różne typy stali w oparciu o techniki wytwarzania A. Dzwonek, K. Malon, M. Świącicka, O. Więcek, J. Kuta, J. Osiewała, O. Sobek, N. Tomanek, J. Badora, A. Kłapsia, E. Krajewska, J. Muszyńska, M. Bonek.....	146
Materials and technologies used in 3D printing in production of organ prototypes and implants R. Gabryś, J. Pająk, K. Krochmal, I. Blumski, L. Gabiga M. Polok-Rubiniec, A. Włodarczyk-Fligier, A. Kania .....	152
Analysis of the influence of technological parameters of laser cutting of steel on surface quality D. Gajczowska, J. Kuta, J. Osiewała, O. Sobek, N. Tomanek, A. Zyzik, M. Bonek, O. Polishchuk, B. Gitolendia .....	158
Planning and organization of biopolymers material process for biomedical applications M. Gawlas, M. Rzepiela, M. Żydowicz, L. Ochocka, M. Nitszke, S. Bober, K. Cesarz-Andraczke, M. Adamiec-Organiecki .....	165
Research methods on coatings obtained by vapor phase deposition J. Glajcar, P. Rucki, D. Pakuła, M. Staszuk .....	170
Investigation of current-voltage relationships of photovoltaic cells D. Godula, P. Wawrów, M. Bednarski, J. Michłowicz, P. Nowak, S. Markocki, M. Musztyfaga-Staszuk, M. Staszuk, W. Filipowski.....	178
Static analysis of stainless steel AISI 316L applied in pendulum swings J. Górny, A. Olszewska, W. Wanczura, A. Śliwa .....	187
Implementation of 3D printing in the trade fairs J. Gryc, A. Kania .....	195
Comparison of surface topography and electrical properties of crystalline silicon solar cells (part II) J. Gwozdek, W. Szreter, P. Wilczek, A. Drygała, M. Musztyfaga-Staszuk, J. Budzynowski, M. Staszuk .....	201
Korózia horčíka a jeho zliatin Ľ. Halimovič, M. Uhrčík.....	207
Life cycle assessment (LCA) methodology W. Hankowska, A. Kania.....	213
Structure and selected properties of oxide ALD coatings for biomedical applications M. Herman, M. Rapacz, Ł. Reimann, D. Pakuła, M. Staszuk.....	217

Zváranie a zvariteľnosť hliníka a jeho zliatin E. Illichmanová, M. Uhrčík .....	223
Wiązka laserowa jako zaawansowane narzędzie w inżynierii powierzchni B. Jóźwiak, N. Juszczak, M. Bonek .....	231
Implementation guide for the 5S method in a micro-enterprise M. Kaiser, A. Kania .....	237
Influence of Wall Perimeters and Printing Temperature on Tensile Properties of 3D Printed PLA Test Specimens P. Karski, N. Nokielski, J. Krzykawska-Szczepańska, R. Dziembała, M. Dratwiński, J. Banaszek, M. Rudnicka, J. Ptaszny, F. Pawełczyk, M. Kłusek, D.J. Michczyńska, M. Jędrzejowski .....	241
Innovative strategies for integrating fibre optic sensors into composite structures for optimized health monitoring of engineering structures M. Knutelski, Z. Brytan .....	249
Numerical analysis of the effect of environment and operating conditions on the performance of electric cables K. Kojm, Ł. Lomania, C. Zach, J. Polis, W. Mikołajko, A. Śliwa, A. Dziwis, M. Sroka .....	257
Wpływ metody wytwarzania na wybrane własności węglików spiekanych I. Kredowska, W. Pilarczyk, J. Śliwka, W. Pakieła, M. Bigaj, K. Gajewski .....	264
The comparison of materials used for 3D printing technology and their environmental impact P. Kruczyński, G. Pośpiech, D. Celeban, M. Szczypiór, A. Kania, M. Polok-Rubiniak, A. Włodarczyk-Fligier .....	273
Numerical analysis of the effect of operating conditions on steering components in a passenger car Ł. Lomania, C. Zach, K. Kojm, D. Towarnicki, R. Trojnar, M. Musialik, W. Mikołajko, A. Śliwa, M. Sroka, A. Dziwis .....	277
Measuring the angle of repose of granulates made from automotive waste V. Mancel, T. Kuvik, J. Krilek, M. Ľavodová.....	284
A Review on Wear and Friction in Bio-Implants A.S. Mekonnin, M.G. Jiru, M. Bonek, K. Waclawski.....	290
Easily Maneuverable and Portable Cable Reel Design C. Meran, S. Aydoğan, İ. Demirci, U. Emanet, K. Doğan, F. Oztekin .....	297

---

Investigation of the Effect of Mechanical Loosing on Vibration Amplitude and Energy Consumption in Cable Production Line Caterpillar Machine C. Meran, O. Eren, A. Alp, M. Irmak, V. Toprak, B. Calhan .....	305
Investigation of the Effect of Unbalance on Vibration Amplitude and Energy Consumption in a Copper Wire Twisting Machine C. Meran, K. Ilhan, M. Dinç, H. Saribay Y.B. Duman, O. Eren.....	313
Investigation of the Effect of Axial Misalignment on Vibration Amplitude and Energy Consumption in Plastic Granule Production Machine Main Motor C. Meran, I. Koksal, A.O. Baş, B. Bozdağ, B.N. Kerimoğlu, F. Oztekin. ....	321
Aplikácia DLC povlakov na valivé ložiská M. Murín, M. Vicen .....	329
Brain-Computer-Interface-based screen numeric keyboard D. Myszor, M. Lasak, S. Sadza .....	337
Efficient Data Loader for Training a Pyramid Stereo Matching Network on Synthetic CARLA-Generated Dataset D. Myszor, M. Paszkuta, T. Kukuczka, E. Szmyt, D. Sobieraj, P. Michalski, K. Pawełczyk, M. Polończyk.....	342
Designing and developing a station for testing the quality of EEG gels D. Myszor, J. Sarno, P. Bartosz, M. Wieczorek, M. Wola, K. Cichecka, M. Łoś, M. Polak, N. Krzywda.....	348
Numerical research of gear-lever of the planetary drive mechanisms of basic needles of warp knitting machines with the use of the software environment PRANS-PK V. Neimak, O. Polishchuk, T. Romanets, S. Smutko, M. Bonek.....	352
Development of a material for 3D printing that ensures self-cooling S. Nowak, S. Bijański, Ł. Hajduk, P. Zawisza, J. Wojnarowski, M. Mikulski, M.M. Szindler, M. Szindler, K. Wrzeźniowska, J. Popis.....	357
Computer programs supporting the design and modeling of injection molding technology J. Nowak, A.J. Nowak.....	363
Impact of laser surface modification in chosen fields M. Paluch, D. Gajczowska, P. Cisowski, M. Bonek, E. Tillova, U. Ozdemir, O. Polishchuk, B. Gitolendia .....	371

---

Point Cloud Acquisition Using Multiple Azure Kinect DK Sensors Based on ArUco Cube Spatial Calibration M. Paszkuta, E. Szmyt, T. Kukuczka, D. Myszor .....	379
Application of the NORAXON myoMotion system in the scope of 5S methodology applications W. Piętakiewicz, A. Sykała, P. Trybuszkiewicz, R. Trepia, K. Szczyrba, M. Roszak, R. Michnik, M. Molenda, A. Miller-Banaś .....	386
Personalized sensory accessories for children with disabilities manufactured with 3D printing technology A. Piątek, W. Wyleżoł, M. Słowiak, Sz. Modliński, A.J. Nowak, W. Walke, M. Król.....	396
Finite elements analysis of hip joint endoprosthesis J. Polis, J. Bicz, Z. Buchaj, R. Szymik, Z. Zielińska, M. Szojda, A. Śliwa, M. Sroka, A. Dziwis, W. Mikołajko .....	405
The influence of environmental conditions on the solar panel work P. Radek, M. Sładek, P. Kołodziejczyk, J. Tłołka, S. Nowak, G. Nowak, M.M. Szindler, J. Popis, M. Szindler .....	413
Recycled filament- a review M. Rejek, S. Jędrzejewski, Ł. Kołodziej, D. Markusik, D. Tatar, A. Woszczak, B. Chadzima, M. Król, A.J. Nowak .....	418
Investigation of the mechanical properties of components manufactured from recycled high-density polyethylene M. Rejek, S. Jędrzejewski, Ł. Kołodziej, D. Markusik, D. Tatar, A. Woszczak, B. Chadzima, M. Król, A.J. Nowak .....	428
Wpływ teksturowania laserowego na własności tribologiczne Poli-eter-eter ketonu K. Roskosz, O. Białas.....	436
Laser jako innowacyjne narzędzie do cięcia stali w wielkogabarytowych konstrukcjach T. Setnik, J. Płocica, M. Bonek.....	441
The use of smart coatings as corrosion protection in the automotive industry G. Sikorski, R. Łosoń, J. Zawadzki, M. Bonek.....	447
Comparison of surface topography and electrical properties of crystalline silicon solar cells (part I) B. Śmieszek, W. Pelka, O. Płaczek, M. Musztyfaga-Staszuk, A. Drygała, J. Popis, M. Staszuk .....	455



---

Quality management of the laser cutting process in the manufacture of stainless steel parts Iu. Sokolan, K. Sokolan, P. Maidan, O. Polishchuk, M. Bonek.....	463
Ewolucja mikrostruktury złącza spawanego ze stali X10CrWMoVNB9-2 po wyżarzaniu przez 10000h K. Sówka, M. Sroka.....	473
Wpływ obróbki cieplno-plastycznej na konduktywność miedzi chromowej M. Szafran, M.M. Krupiński, W. Borek, M. Krupiński.....	479
Technologie laserowe w przemyśle S. Szeja, A. Zyzik, M. Volkmer, M. Bonek .....	486
Morphology of Polymer Clay Nanocomposite Fibres Y.M. Tsekpo, W. Smok, P. Jarka, T. Tanski .....	491
The system for collecting data on failures in the maintenance department D. Wala, M. Spilka .....	496
Development of a hand prosthesis model using Reverse Engineering Ł. Wantuch, M.M. Szindler.....	502
The corrosion resistance of electro-deposited zinc coatings applied to the structural steel J. Wieczorek, J. Nosiadek, M. Milewski, K. Pepel, T. Markefka, J. Krawczyk, M. Bodio, W. Pakieła, A. Zarychta, A. Drygała, B. Grzegorzczuk, J. Kubisztal, K. Gołombek, S. Lesz.....	510
Optimization of the CuTi4 alloy melting and casting process K. Wiśniewski, Z. Rdzawski, W. Głuchowski, M. Łagoda, M. Musztyfaga-Staszuk.....	518
Biomaterials, Bioceramic Materials, and Metals for Bone Scaffold Formation and Scaffold Fabrication Methodologies S. Worku, M. Bonek.....	526
Torch Holder Design and Thermal Analysis of Hybrid Welding Machine C. Yildiz, S. Korucu .....	534
Structural and mechanical properties of an innovative composite coating for intense abrasive wear J. Żuławska, M. Wnętrzak, M. Dziergas, B. Siedlaczek, A. Czupryński, W. Kwaśny.....	540
Biopolymers as coating materials for zinc alloys and their biological evaluation M. Żydowicz, L. Ochocka, S. Bober, M. Gawlas, M. Rzepiela, K. Cesarz-Andraczke, M. Nitszke, M. Adamiec-Organisciok, M. Skonieczna .....	550





26th January 2024  
Gliwice, Poland

DEPARTMENT OF ENGINEERING MATERIALS AND BIOMATERIALS  
FACULTY OF MECHANICAL ENGINEERING  
SILESIA UNIVERSITY OF TECHNOLOGY

## INTERNATIONAL STUDENTS SCIENTIFIC CONFERENCE

### **The Influence of Metal Oxide Thin Films Deposited by ALD Method on the Properties of Dye Sensitized Solar Cells**

Addae Elizabeth Adzo<sup>a</sup>, Wojciech Sitek<sup>b</sup>, Marek Szindler<sup>c</sup>

<sup>a</sup> Silesian University of Technology, Faculty of Mechanical Engineering, Department of Engineering Materials and Biomaterials  
email: eaddae@polsl.pl

<sup>b</sup> Silesian University of Technology, Faculty of Mechanical Engineering, Department of Engineering Materials and Biomaterials  
email: Wojciech.Sitek@polsl.pl

<sup>c</sup> Silesian University of Technology, Faculty of Mechanical Engineering, Department of Engineering Materials and Biomaterials  
email: Marek.Szindler@polsl.pl

**Abstract:** Materials may be precisely synthesized at the atomic level using atomic layer deposition (ALD). This approach is particularly attractive for a wide range of applications since it can tailor the material composition, film thickness with great conformality, allow low-temperature processing, and provide in-situ real-time monitoring. We concentrate on the use of ALD layers in a variety of solar cells in this review. We concentrate on the use of ALD layers in a dye sensitized solar cells in this review. The presence of an ALD thin film in the structure of the dye-sensitized solar cell between the FTO layer and the printed TiO<sub>2</sub> layer has a positive effect on its final efficiency.

**Keywords:** Dye Sensitized Solar Cell, Atomic Layer Deposition, metal oxides

## 1. INTRODUCTION

Dye-sensitized solar cells (DSSCs) are an efficient photovoltaic technology for powering electronic applications such as wireless sensors with indoor light. Their low cost and abundant materials, as well as their capability to be manufactured as thin and light-weight flexible solar modules highlight their potential for economic indoor photovoltaics. However, their fabrication methods must be scaled to industrial manufacturing with high photovoltaic efficiency and performance stability under typical indoor conditions. This paper reviews the influence of metal oxide thin films deposited by ALD method on the properties of dye sensitized solar cells. We discuss how each functional component of a DSSC has been improved with these new materials and fabrication techniques. In addition, we propose a scalable cell fabrication process that integrates these developments to a new monolithic cell design based on several features including inkjet and screen printing of the dye, a solid state hole conductor, TCO contact,

compact TiO<sub>2</sub>, mesoporous TiO<sub>2</sub>, carbon nanotubes counter electrode, epoxy encapsulation layers and silver conductors. Finally, we discuss the need to design new stability testing protocols to assess the probable deployment of DSSCs in portable electronics and internet-of-things devices. [1]

The development of dye-sensitized solar cells (DSSCs) has made them a technically and financially viable substitute for p-n junction photovoltaic systems. It was found in the late 1960s that electrochemical cells containing lit organic dyes might produce energy. Chlorophyll was isolated from spinach at the University of California, Berkeley (photosynthesis). In 1972, the first zinc oxide (ZnO) electrode that was chlorophyll-sensitized was created. For the first time, photons were turned into electricity by injecting excited dye molecules' electrons into a semiconductor with a large band gap. Numerous studies have been conducted on ZnO single crystals, however due to the dye molecules' limited ability to absorb incident light in a monolayer, the dye-sensitized solar cells' efficiency was extremely low, with just 1% of the light being absorbed. In order to increase dye absorption across the electrode and, therefore, light harvesting efficiency (LHE), the porosity of the electrode composed of fine oxide powder was optimized [2,9].

ALD thin films find application in various kinds of solar cells as transparent conductive oxide, buffer layer, absorber layer, window layer, electron/hole contact, or surface passivation layer. A portion of these ALD layers are being used in large-scale production, most notably for silicon solar cells, which are presently leading the photovoltaic market. The growing interest in ALD and its potential uses beyond traditional semiconductor sectors are accelerated by the current shrinking of electronic devices and the advancement of analytical instruments. Because dye-sensitized solar cells (DSSCs) have several interfaces based on mesoporous structure, which necessitates engineering them for an effective electron transport system, we used ALD to increase the performance of DSSCs in our investigations. We will synthesize ALD TiO<sub>2</sub> on FTO and examine the ALD TiO<sub>2</sub> phase transition at various annealing temperatures. Because of the stable anatase TiO<sub>2</sub> phase, the conformal and thin ALD TiO<sub>2</sub> sheet is highly photocatalytic and highly stabilized [3, 10].

## **2. CONSTRUCTION OF A DYE-SENSITIZED SOLAR CELL AND A PROPOSAL FOR ITS MODIFICATION**

A dye-based solar cell consists of several basic elements. This solar cell containing a counter electrode, liquid electrolyte and photoanode is characterized by the fact that the photoanode is a glass plate connected to a layer of transparent conductive oxide TCO and an n-type semiconductor in the form of nanocrystalline titanium oxide with an adsorbed dye, for to which a layer of liquid electrolyte is attached, connected to a counter electrode consisting of a layer of platinum deposited by screen printing and a layer of transparent conductive oxide TCO and a glass plate [5,6].

The base of the glass substrate is covered with a transparent and electrically conductive layer which help a substrate for the deposition of the semiconductor and catalyst, acting also as current collectors. There are two main characteristics of a substrate being used in a DSSC: Firstly, more than 80% of transparency is required by the substrate to permit the passage of optimum sunlight to the effective area of the cell. Secondly, for the efficient charge transfer and reduced energy loss in DSSCs, it should have a high electrical conductivity. The fluorine-doped tin oxide (FTO, SnO<sub>2</sub>: F) and indium-doped tin oxide (ITO, In<sub>2</sub>O<sub>3</sub>: Sn) are usually applied as a

conductive substrate in DSSCs. Research is also being carried out on the use of zinc oxide doped with AZO aluminum. The prepared substrate is used to produce a working electrode and a counter electrode [8].

The working electrodes (WE) are prepared by depositing a thin layer of oxide semiconducting materials such as  $\text{TiO}_2$ ,  $\text{Nb}_2\text{O}_5$ ,  $\text{ZnO}$ ,  $\text{SnO}_2$  (n-type), and  $\text{NiO}$  (p-type) on a transparent conducting glass plate made of FTO or ITO. These oxides have a wide energy band gap of 3–3.2 eV. The application of an anatase allotropic form of  $\text{TiO}_2$  is more commendable in DSSCs as compared to a rutile form due to its higher energy band gap of 3.2 eV whereas the rutile form has a band gap of about 3 eV, although alternative wide band gap oxides such as  $\text{ZnO}$  and  $\text{Nb}_2\text{O}_5$  have also given promising results. Due to being non-toxic and less expensive and its easy availability,  $\text{TiO}_2$  is mostly used as a semiconducting layer. However, these semiconducting layers absorb only a small fraction of light in the UV region; hence, these working electrodes are then immersed in a mixture of a photosensitive molecular sensitizer and a solvent. After soaking the film within the dye solution, the dye gets covalently bonded to the  $\text{TiO}_2$  surface [7].

The dye is the component of DSSC responsible for the maximum absorption of the incident light. Any material being dye should have the following photophysical and electrochemical properties:

1. Firstly, the dye should be luminescent.
2. Secondly, the absorption spectra of the dye should cover ultraviolet-visible (UV-vis) and near-infrared region (NIR) regions.
3. The highest occupied molecular orbital (HOMO) should be located far from the surface of the conduction band of  $\text{TiO}_2$  and the lowest unoccupied molecular orbital (LUMO) should be placed as close to the surface of the  $\text{TiO}_2$ , and subsequently should be higher with respect to the  $\text{TiO}_2$  conduction band potential.
4. HOMO should lie lower than that of redox electrolytes.
5. The periphery of the dye should be hydrophobic to enhance the long-term stability of cells, as it results in minimized direct contact between electrolyte and anode; otherwise, water-induced distortion of the dye from the  $\text{TiO}_2$  surface can appear which may reduce the stability of cells.
6. To avoid the aggregation of the dye over the  $\text{TiO}_2$  surface, co-absorbents like chenodeoxycholic acid (CDCA) and anchoring groups like alkoxy-silyl, phosphoric acid, and carboxylic acid group were inserted between the dye and  $\text{TiO}_2$ . This results in the prevention of dye aggregation and thus limits the recombination reaction between redox electrolyte and electrons in the  $\text{TiO}_2$  nanolayer as well as results in the formation of stable linkage.

A glass plate with a TCO layer is also used to produce the CE counter electrode, which is another essential element of the DSSC. CE in DSSCs are mostly prepared by using platinum (Pt) or carbon (C). Both working and counter electrodes are sealed together, and subsequently, an electrolyte is filled with a help of a syringe. Counter electrode catalyzes the reduction of  $\text{I}^-/\text{I}_3^-$  liquid electrolyte and collects holes from the hole transport materials (HTMs). Pt is used mostly as a counter electrode as it demonstrates higher efficiencies, but the replacement of Pt was much needed due to its higher cost and less abundance. Thus, several alternatives have developed to replace Pt in DSSCs, such as carbon, carbonylsulfide (CoS), Au/GNP, alloy CEs

like FeSe and  $\text{CoNi}_{0.25}$ , although the different types of the CEs are also discussed by Jihuai Wu et al. [11].

The working electrode and counter electrode are connected with active elements facing each other, and the space between them is filled with electrolyte, which is another important element of the dssc structure. An electrolyte (such as  $\text{I}^-/\text{I}_3^-$ ,  $\text{Br}^-/\text{Br}_2$ ,  $\text{SCN}^-/\text{SCN}_2$ , and  $\text{Co(II)/Co(III)}$ ) has five main components, i.e., redox couple, solvent, additives, ionic liquids, and cations. The following properties should be present in an electrolyte [1]:

1. Redox couple should be able to regenerate the oxidized dye efficiently.
2. Should have long-term chemical, thermal, and electrochemical stability.
3. Should be non-corrosive with DSSC components.
4. Should be able to permit fast diffusion of charge carriers, enhance conductivity, and create effective contact between the working and counter electrodes.
5. Absorption spectra of an electrolyte should not overlap with the absorption spectra of a dye.

The classic procedure for producing a dye-sensitized solar cell is shown in Figure 1.

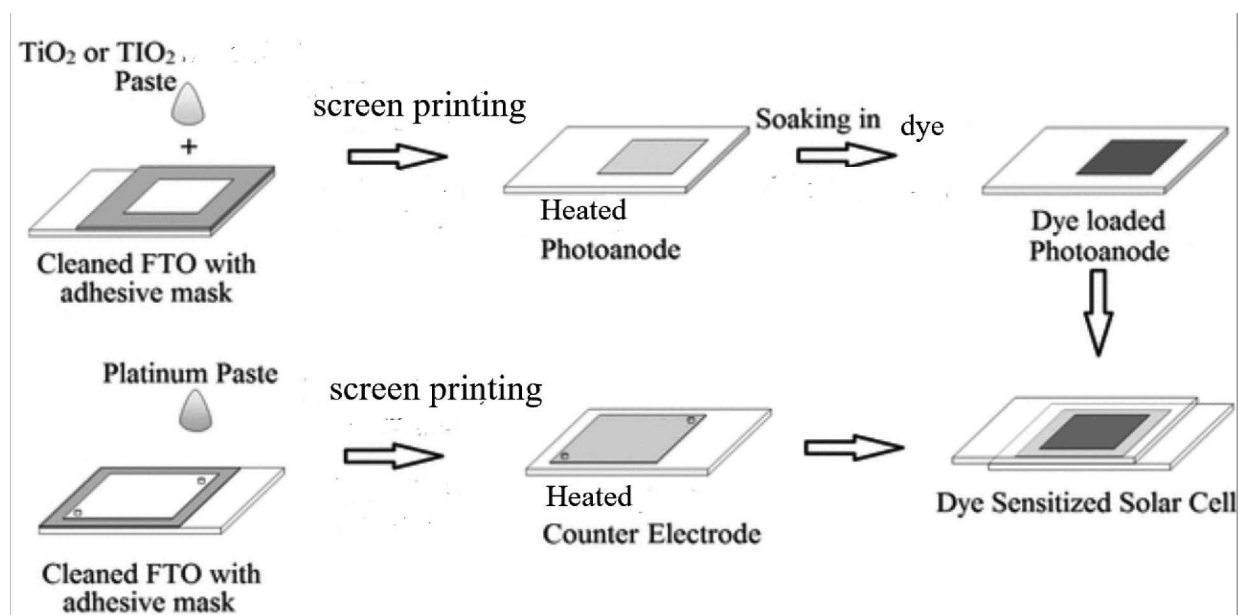


Fig. 1. Schematic illustration of stepwise procedure of DSSC fabrication

The authors propose a modification of this procedure by depositing a thin  $\text{TiO}_2$  film deposited using the ALD method on a substrate with an FTO layer. In this way, a passivating layer, the so-called blocking layer, will be introduced into the dssc structure (Fig.2). It will be located between the FTO layer and the titanium oxide layer deposited by screen printing. There are already reports that this procedure can increase the efficiency of the finished solar cell by more than 1% [4]. We will deposit ALD  $\text{TiO}_2$  on FTO and examine the ALD  $\text{TiO}_2$  phase transition at various deposition temperature and annealing temperatures. Because of the stable anatase  $\text{TiO}_2$  phase, the conformal and thin ALD  $\text{TiO}_2$  sheet is highly photocatalytic and highly stabilized.

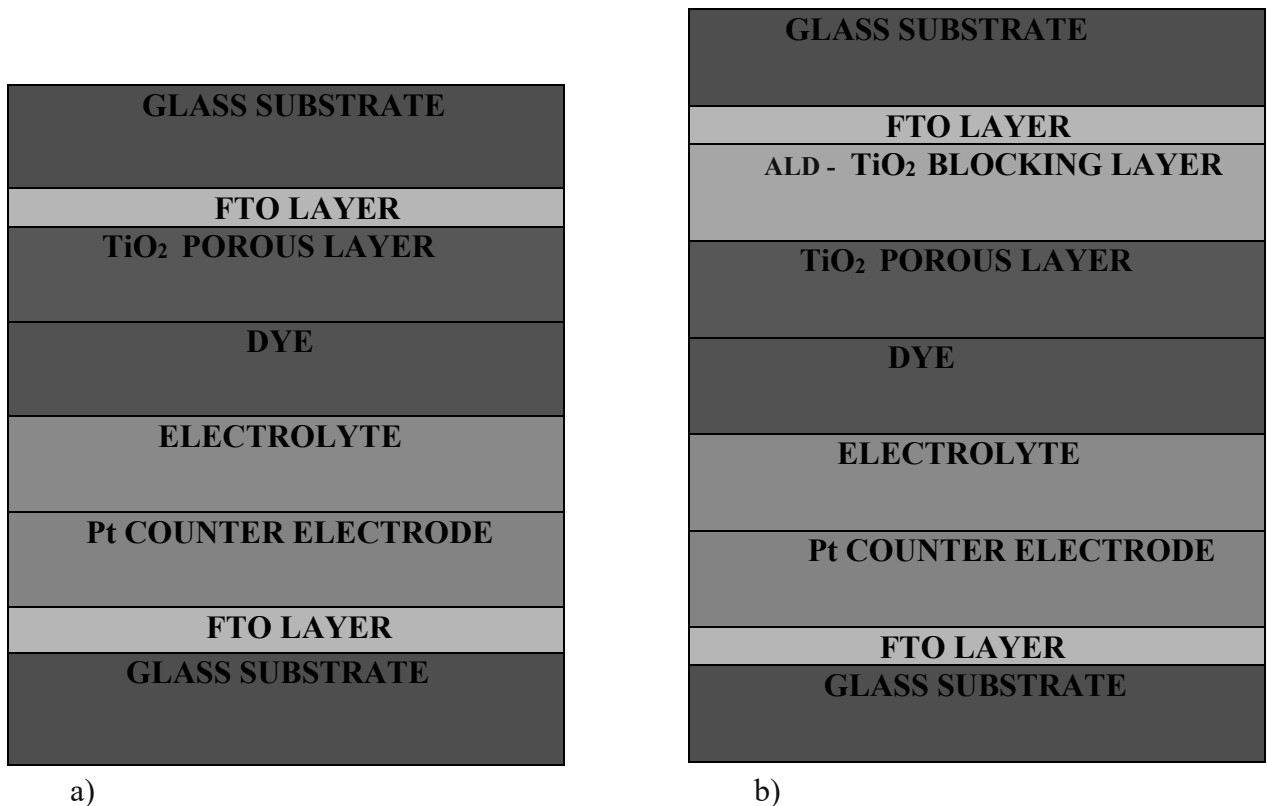


Fig. 2. Comparison of the construction of a classic DSSC with a DSSC containing a blocking layer prepared by the ALD method

After the fabrication of the dye sensitized solar cells the following experimental analysis will be done

- Literature Study: Background study, empirical study, data interpretation
- Microscopic observation and Atomic Force Microscopy: Morphological analysis
- Transmission electron microscopy (TEM), X-Ray Diffraction Analysis and Auger Electron Spectroscopy (AES): To study the structure of the metal oxide layer
- Scanning Electron Microscopy (SEM): Analyses of microstructure
- Reflectometry, UV/VIS spectroscopy and a four-blade probe: Testing of optical and electrical properties
- Solar simulation: Testing of the electrical properties of ready-made dye sensitized solar cells containing thin ALD thin films in their structure.

The research methodology planned in this way should enable comprehensive characterization of the deposited layers and manufactured solar cells. Moreover, it should enable the examination and writing of the influence of deposition parameters and additional heat treatment on the efficiency of ready-made solar cells.

### 3. CONCLUSION

The main goal of the article was to present the structure and principle of operation of a dye-sensitized solar cell and then propose a modification of this structure. The aim of this research include the usage of latest metal oxides thin films (Titanium Oxide, Aluminum Oxide and Zinc

Oxide) as blocking and passivating thin films in the fabrication of Dye Sensitized Solar Cells (DSSCs) using Atomic Layer Deposition (ALD). Furthermore, to improve the stability and lifetime of Dye Sensitized Solar Cells, the dye needs to be passivated. This process involves coating the dye molecules with a protective layer that prevents the dye molecules from reacting with other molecules, such as oxygen and water. This thin film also helps to prevent the dye from degrading over time. Additionally, the layer helps to reduce the energy losses due to recombination of generated electrons and holes.

## BIBLIOGRAPHY

1. A. Yella, H.-W. Lee, H. N. Tsao, C. Yi, A. K. Chandiran, M. K. Nazeeruddin, E. W.-G. Diau, C.-Y. Yeh, S. M. Zakeeruddin and M. Grätzel; Porphyrin-sensitized solar cells with cobalt (II/III)-based redox electrolyte exceed 12 percent efficiency. *Science*, 2011, 334, 629–634. doi: 10.1126/science.1209688.
2. S. G. Hashmi, M. Özkan, J. Halme, S. M. Zakeeruddin, J. Paltakari, M. Grätzel and P. D. Lund; Dye-sensitized solar cells with inkjet-printed dyes. *Energy Environ. Sci.*, 2016, 9, 2453–2462. doi: 10.1039/C6EE00826G
3. Kamppinen, A., Aitola, K., Poskela, A., Miettunen, K., & Lund, P. D. (2020). *Stability of cobalt complex based dye solar cells with PEDOT and Pt catalysts and different electrolyte concentrations*. *Electrochimica Acta*, 335, Article 135652. doi:/10.1016/j.electacta.2020.135652
4. S. G. Hashmi, G. G. Sonai, H. Iftikhar, P. D. Lund and A. F.; Nogueira, *Printed single-walled carbon-nanotubes-based counter electrodes for dye-sensitized solar cells with copper-based redox mediators*. *Semicond. Sci. Technol.*, 2019, 34, 105001 doi: 10.1088/1361-6641/ab39f0
5. Y. Cao, Y. Liu, S. M. Zakeeruddin, A. Hagfeldt and M. Grätzel, ; *Direct Contact of Selective Charge Extraction Layers Enables High-Efficiency Molecular Photovoltaics*. *Joule*, 2018, 2, 1108–1117 doi:/10.1016/j.joule.2018.03.017
6. H. Michaels, M. Rinderle, R. Freitag, I. Benesperri, T. Edvinsson, R. Socher, A. Gagliardi and M. Freitag; *Dye-sensitized solar cells under ambient light powering machine learning: towards autonomous smart sensors for the internet of things*. *Chem. Sci.*, 2020, 11, 2895–2906 doi: /2020/sc/c9sc06145b
7. I. Tributsch H, Calvin M. Electrochemistry Of Excited Molecules: Photo-Electrochemical Reactions Of Chlorophylls. *Photochem Photobiol.* 1971;14:95–112. doi: 10.1111/j.1751-1097.1971.tb06156.
8. Tsubomura H, Matsumura M, Nomura Y, Amamiya T. Dye sensitised zinc oxide: aqueous electrolyte: platinum photocell. *Nature*. 1976;261:402–403. doi: 10.1038/261402a0.
9. O'Regan B, Gratzel M. A low-cost, high-efficiency solar cell based on dye-sensitized colloidal TiO<sub>2</sub> films. *Nature*. 1991;353:737–740. doi: 10.1038/353737a0.
10. Nazeeruddin K, Baranoff E, Gratzel M. Dye-sensitized solar cells: A brief overview. *Sol Energy*. 2011;85:1172–1178. doi: 10.1016/j.solener.2011.01.018.
11. Altobello S, Bignozzi C. A, Caramori S, Larramona G, Quici S, Marzanni G, Lakhmiri R; Sensitization of TiO<sub>2</sub> with ruthenium complexes containing boronic acid functions. *J Photochem Photobiol A Chem*. 2004;166:91–98. doi: 10.1016/j.jphotochem.2004.04.029.
12. *A Chem*. 2004;166:91–98. doi: 10.1016/j.jphotochem.2004.04.029.





26th January 2024  
Gliwice, Poland

DEPARTMENT OF ENGINEERING MATERIALS AND BIOMATERIALS  
FACULTY OF MECHANICAL ENGINEERING  
SILESIA UNIVERSITY OF TECHNOLOGY

## INTERNATIONAL STUDENTS SCIENTIFIC CONFERENCE

### Elevator Potential Recovery

Patricia Ayoub

Georgian Technical University, Faculty of Transport Systems and Mechanical Engineering,  
email: ayoub.patricia@hotmail.com  
Supervisor: Associate professor, Dr. Givi Sanadze  
email: givisanadze@yahoo.com

**Abstract:** The article describes the Elevator Potential Recovery. Compensation of power and the sustainability are the main goals for the future projects and should be respected. Many solutions are investigated to decrease the consumption of power in the elevator field like counter-weight project, Otis Regen and hydraulic piston elevator. Every project of these has advantages and disadvantages and based on their disadvantages, a new project with new solutions can be built. EPR (elevator potential recovery) is a mechanical system that consists of a flywheel, clutch and continuous variable transmission that can recover the potential and kinetic energy of the elevator instead of losing it through friction in form of heat. This project can save energy, serve in new job opportunities and doesn't have any relevant negative effects on the environment.

**Keywords:** elevator, potential recovery, shaft design, bearing friction, mechanical system, flywheel, clutch, continuous variable transmission, energy, mechanical battery, counter weight elevator, regenerative elevator drives, hydraulic elevator.

### 1. INTRODUCTION

Sustainable engineering is the process of designing or operating systems such that they consume energy and resources in a sustainable way, in other words, at a rate that does not compromise the natural environment, or the ability of future generations to meet their own needs. Based on sustainability, the discoveries around the world serve the humans and their presence on the earth. The research for saving energy, reducing losses and recovering energy losses are very crucial topics in providing sustainability for the whole world.

The consumption of energy increases rapidly with time and many countries try to reduce it through new inventions, principles and regulations. The energy consumption is multiplied by about 3 times in the last 50 years. Moreover, the U.S. Energy Information Administration's latest International Energy Outlook 2017 projects announces that world energy consumption will grow by 28% between 2015 and 2040. This high consumption of energy must be confronted by new techniques and solutions. Recovering waste energy in different fields

around the world and transforming it into reusable source of energy can take part in saving the situation.

The main objective is to provide a new technology to recover the energy wasted in the elevator system. Converting the heat generated from friction force of the elevator's brakes into reusable energy that is useful to raise the elevator up and therefore reducing the overall energy consumption. This project is based on storing the elevator's potential energy through a mechanical battery-system consisting mainly of a flywheel that stores this energy in form of rotational kinetic energy. The suggested system is called "Elevator Potential Recovery" (EPR) and it positively affects the energy saving and the environmental impact compared to nowadays solutions. EPR is a mechanical system that stores the wasted energy of the elevator in form of kinetic energy into a mechanical battery consisted of rotating flywheel. This energy will be saved and reused to lift up the elevator.

## **2. MECHANICAL BATTERY**

A mechanical battery is an old technique to store energy, way different that the conventional methods like chemical and ultra-capacitor batteries. Recent studies prove that this type of batteries was underestimated and is very promising since it has many advantages like reliability, low maintenance requirements, and high efficiency.

As buildings are becoming taller, more energy consumption is used to lift the elevators up or down, the energy needed in these operations represents a large percentage of the overall energy used in the building (about 15% of the building's energy).

A mechanical battery in form of a rotating flywheel can be introduced to elevator's systems in order to decrease the usage of brakes that cause energy losses and reuse the collected energy to help the motor in lifting back the elevator and therefore reducing the overall power consumption.

Each Elevator consists of some basic components, rarely changed from an elevator to the other, like: machine drive, elevator car, breaking system, landing doors, cables, controls, rails.

## **3. COUNTER WEIGHT ELEVATOR**

Counter weight elevator is a presented solution and is widely used to reduce the consumption of energy through the counter weight. The counter weight represents 40 % of the total mass of the elevator, so it can help in four cases: the counterweight makes the raising and lowering of the elevator easier for the motor; less motor energy, so less friction and less strain on the cables; the counterweight decreases the required forces while moving up or down, therefore the energy used by the motor decreases; the counterweight reduces the amount of breaking needed to stop the elevator.

One may benefit from a counterweight in his elevator system as it is noticed above in two situations: When the cabinet weight is less than the counter weight and the elevator moves up. When the cabinet weight is more than the counter weight and the elevator moves down. Under these two conditions, the counter weight system is beneficial. But in many other conditions, this system consumes more energy to move the counter weight than the cabinet alone.

#### 4. REGENERATIVE ELEVATOR DRIVES

Regenerative drive (Otis Regen) is an efficient energy saving technology. This process is based on an electrical system that benefits from regenerating energy while the elevator moving down. During the cabinet descent, the motor acts as a generator, transforming the mechanical energy to an electrical power, which is fed to the electrical grid of the building. The Otis Regen system is illustrated in Figure 1.

This process has 75% maximum efficiency and in normal case between 20 and 40% efficiency. The system produces more power than it uses when the cabinet is lifted with light load (empty) and down with a heavy load (max load supporting). These small amounts of power can be fed to the building or to the elevator itself (J, 1987).

The high efficiency of the Otis Regen is affected by many factors, like: The height of the building, Weight of the load, Frequency of use, Capacity of the elevator, Whether it's going up or down, Type of equipment, Age of the equipment.

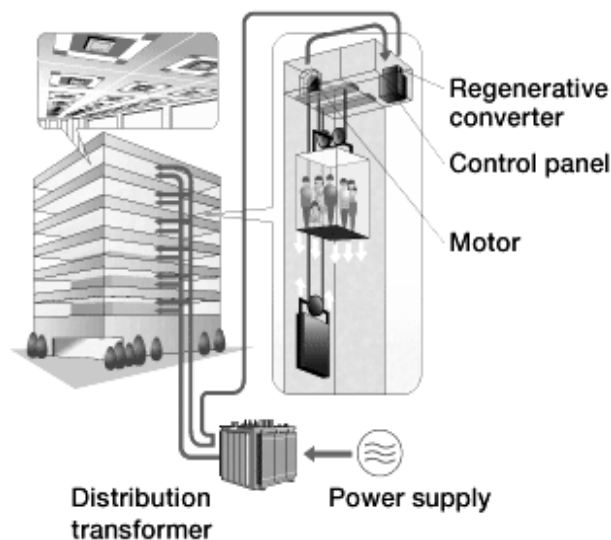


Figure 1: Role of electrical box of Regenerative elevator

#### 5. HYDRAULIC ELEVATOR

Hydraulic elevators, illustrated in Figure 7, are powered by a piston moving inside a cylinder. Through an electric motor, the oil is pumped into the cylinder to move the piston. By moving the piston up, the elevator cab moves up and vice-versa. However, the descending motion needs more breaking due to the weight of the cab. This process is used for five to six stories high buildings only due to the limited power of the pump based on its convenient size.

#### 6. DESIGN OF EPR SOLUTION

Elevator potential recovery (EPR) is a system that recovers the elevator's wasted energy and transforms it to useful energy. The recovery of the wasted energy by this mechanical system

may save power in every building around the world, and thus updates a new environmental system.

EPR is a system installed on the elevator with new concepts under the title of saving energy. The main parts of the elevators are still used as is. Like cab, steel rope wires, motor, and control cabinet. A new system will be added to the elevator and consists of: a continuous variable transmission (CVT) between the flywheel and the gearbox attached by a belt, a multi-plate clutch installed on the flywheel, Mechatronics system with an Arduino code to control the movement of the clutch with numerous sensors, like proximity sensors. Use of a braking system to bring the cab to a complete stop, potentially regenerative braking. No use of counterweight. This system has its maximum efficiency while the cab goes up empty and goes down with full weight (cab weight + max people weight).

As illustrated in figure 2, while the elevator goes down, the clutch is connected to the flywheel that starts to rotate, the CVT controls the cab's acceleration and speed by varying its pulleys ratios, therefore the elevator cabinet doesn't exceed the maximum allowed speed and acceleration that provides comfort and security, while accelerating the flywheel at the maximum possible angular velocity. The CVT is controlled using a stepper motor that precisely changes the ratio as desired. Before the cabinet reaches its final position by 1.8 meters, the breaks work begins to stop the cabinet. Before the braking process begins, the clutch is separated from the flywheel in order to maintain its maximum speed without being affected by the braking process, which allows the flywheel to rotate freely.

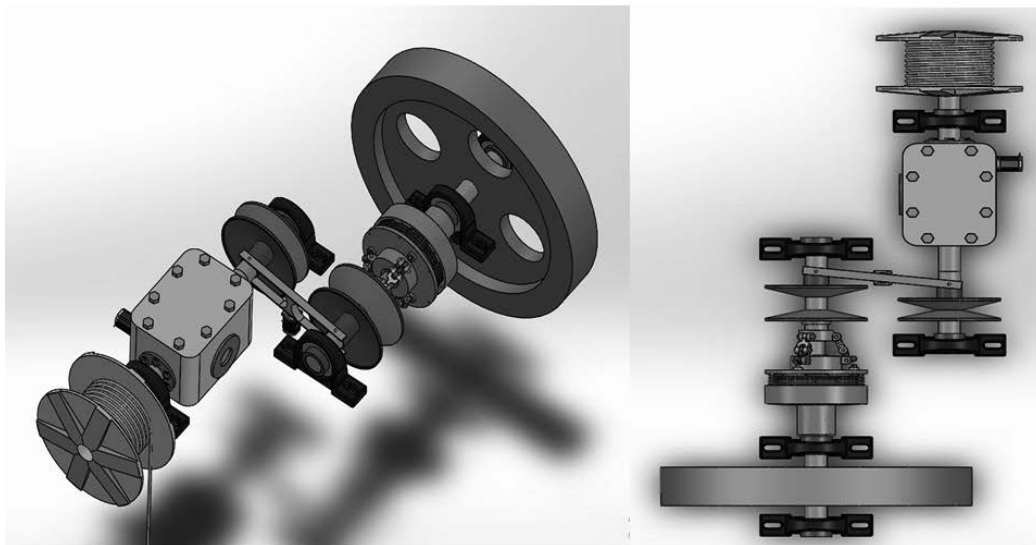


Figure 2. SolidWorks drawing of the system

To lift the elevator, the gearbox controlled by a stepper motor and having the flywheel's shaft as input is set to reverse rotation, thus the elevator's pulley rotates in the direction of lifting the elevator. When the flywheel is able to supply sufficient energy and speed for the cab, it will work to lift the cab otherwise the flywheel is disconnected by the clutch and the motor will complete the mission. An RPM sensor checks the speed of the flywheel to evaluate the quantity of energy in the flywheel. Proximity sensors are used to detect the elevator's position.

## **7. CONCLUSION**

Lebanon has a major problem of energy lag in the majority of its cities. Implementing projects similar to the aforementioned EPR devices in Lebanon could lead to minimize the shortage gap. By implementing EPR on numerous buildings, which doesn't cost a lot with taken into consideration the safety standards and other standards like ASME, energy can be salvaged and reused in a proper way. EPR creates job opportunities in the country and helps Lebanon saving the environment and money at the same time.

## **ACKNOWLEDGEMENTS**

The work was created as a result of the project as part of project based learning - PBL, in the 10th competition under the Initiative of Excellence - Research University, Silesian University of Technology.

## **BIBLIOGRAPHY**

1. D. Vallero and C. Brasier. *Sustainable Design: The Science of Sustainability and Green Engineering*. Publisher: John Wiley & Sons ISBN: 978-0-470-13062-9. 2008.
2. Hydraulic Elevators Basic Components. <http://www.electrical-knowhow.com/2012/04/hydraulic-elevators-basic-components.html>
3. High-speed flywheels cut energy bill. *Railway Gazette International*. 2001-04-01. Retrieved 2010-12-02.
4. Al-Sharif L, Escalator Energy Consumption, Part I: The relationship between escalator power consumption and escalator handling capacity (the ETP method)", London Underground Ltd., Internal Report, January 1996.
5. Evans, Barrie. Fuzzy Logic for Smarter Lifts. *Architect's Journal*, May 18, 1994, pp. 24-25.



26th January 2024  
Gliwice, Poland

DEPARTMENT OF ENGINEERING MATERIALS AND BIOMATERIALS  
FACULTY OF MECHANICAL ENGINEERING  
SILESIA UNIVERSITY OF TECHNOLOGY

## INTERNATIONAL STUDENTS SCIENTIFIC CONFERENCE

### Charging and Maintenance System for Drone Fleet

P. Bartosz <sup>a</sup>, D. Bereta <sup>b</sup>, J. Sarno <sup>a</sup>, D. Myszor <sup>c</sup>

<sup>a</sup> Silesian University of Technology, Faculty of Automatic Control, Electronics and Computer Science, Virtual Flying Student Research Club

<sup>b</sup> Silesian University of Technology, Faculty of Environmental and Energy Engineering, Virtual Flying Student Research Club

<sup>c</sup> Silesian University of Technology, Faculty of Automatic Control, Electronics and Computer Science, Department of Algorithmics and Software  
email: [dariusz.myszor@polsl.pl](mailto:dariusz.myszor@polsl.pl)

**Abstract:** The Charging and Maintenance System for Drone Fleet integrates Universal Charging Smart Modules (UCSMs) with advanced features for intelligent charging. Managed by a Central Management Server, the system ensures efficient and safe charging processes. User-friendly client applications provide manual control, detailed monitoring, and flexible scheduling, contributing to optimal drone fleet performance.

**Keywords:** Drones, Electronics, Server, Charging

## 1. INTRODUCTION

The Charging and Maintenance System for Drone Fleet is conceptualized as an advanced solution in the evolving landscape of unmanned aerial systems. The proposed system envisions the use of Universal Charging Smart Modules (UCSM) with potential functionalities such as voltage control, battery monitoring, and adaptive charging optimization. A core component of this conceptual system is a Central Management Server, which is envisaged to consolidate data and employ sophisticated algorithms for potential data analysis and dynamic management of the UCSM. Additionally, user interfaces in the form of potential client applications are envisioned to provide operators with manual control, detailed monitoring, and flexible scheduling functionalities. This approach aims to explore the potential enhancement of efficiency, reliability, and operational efficacy of drone fleets through a science-inspired framework. This project is being realized by the Virtual Flying Student Research Club of Silesian University of Technology.

## 2. CHARGING MODULES

UCSMs should be engineered with a suite of intelligent functionalities, including precise battery status monitoring and adaptive charging optimization. This sophistication ensures the

optimal charging of drone batteries and contributes significantly to prolonging their overall lifespan. The introduction of UCSMs marks a transformative step towards enhancing the operational efficiency, reliability, and longevity of unmanned aerial systems in a rapidly evolving technological landscape.

### **2.1 Charging Control Module**

Universal Charging Smart Modules (UCSM)[1] should be sophisticated devices designed with advanced sensors specifically dedicated to monitoring the voltage levels of drone batteries during the charging process. Through the implementation of control algorithms, UCSMs should possess the capability to fine-tune charging parameters automatically. This dynamic adjustment would ensure that optimal voltage conditions are consistently maintained throughout the entirety of the charging cycle, contributing significantly to the prolonged overall lifespan of drone batteries.

### **2.2 Battery Status Monitoring**

Intricate sensors employed within the UCSM should meticulously track and record variations in charge levels among individual battery cells. The system would generate comprehensive reports providing a detailed overview of battery conditions. This granular insight would allow for proactive planning of battery replacements before potential failures occur[2], thereby enhancing the overall reliability and readiness of the drone fleet.

### **2.3 Charging Optimization**

UCSMs should be equipped with advanced optimization algorithms that should take into consideration both the real-time energy demands of the drones and the specific requirements of their planned missions. These sophisticated algorithms will dynamically adjust the charging pace based on the system load, effectively minimizing charging time and optimizing energy consumption[3]. The result would be an efficient and effective charging process that ensures the readiness of the drone fleet for operational tasks.

### **2.4 Remote Control**

The central management server, serving as the nerve center of the system, should possess the capability to monitor and exert control over each UCSM through a centralized console. This remote control functionality would empower real-time adjustments to charge parameters, allowing the system to promptly respond to changing field conditions or operational requirements. The ability to manage UCSMs remotely will enhance operational flexibility and adaptability.

## **3. CENTRAL MANAGEMENT SERVER**

The Central Management Server will serve as the nerve center, unifying data from Universal Charging Smart Modules (UCSMs) and leveraging sophisticated algorithms for comprehensive data analysis (see fig. 1). This server should facilitate dynamic UCSM management, ensuring optimal resource allocation and safety protocols. As the backbone of the system, the Central Management Server plays a pivotal role in enhancing operational efficiency, reliability, and overall system intelligence within the context of drone fleet management.

### 3.1 Central Data Storage

The Central Management Server would act as the centralized repository for storing comprehensive data collected from each UCSM. This repository encompasses detailed information on battery status, historical charging patterns, and any reported errors. By centralizing this data, the server would facilitate real-time analysis and informed decision-making, forming the backbone of the system's intelligence. This repository would encompass detailed information on battery status, historical charging patterns, and any reported errors. By centralizing this data, the server will facilitate real-time analysis and informed decision-making, forming the backbone of the system's intelligence.

### 3.2 Data Analysis

The server should employ advanced algorithms to conduct in-depth analyses of the stored data, providing valuable insights into energy consumption trends and predicting charging needs based on historical patterns. These analytical capabilities would allow to optimize the management of charging processes, enhance efficiency, and assist in forecasting maintenance requirements. The server's data-driven decision-making would contribute to the overall operational effectiveness of the drone fleet.

### 3.3 Dynamic UCSM Management

The server would autonomously make decisions regarding the connection and disconnection of individual UCSMs based on the dynamically changing system load. This dynamic management feature eliminates the need for constant human intervention, contributing to operational efficiency. The server ensures that UCSMs will be strategically employed, responding to real-time demands and optimizing the overall performance of the charging system.

### 3.4 Safety and Maintenance

As the overseer of charging processes, the server will ensure strict compliance with safety standards throughout the fleet. Additionally, the system will automatically respond to potential issues, minimizing the risk of equipment damage. This proactive approach to safety and maintenance will enhance the overall reliability and longevity of the drone fleet.

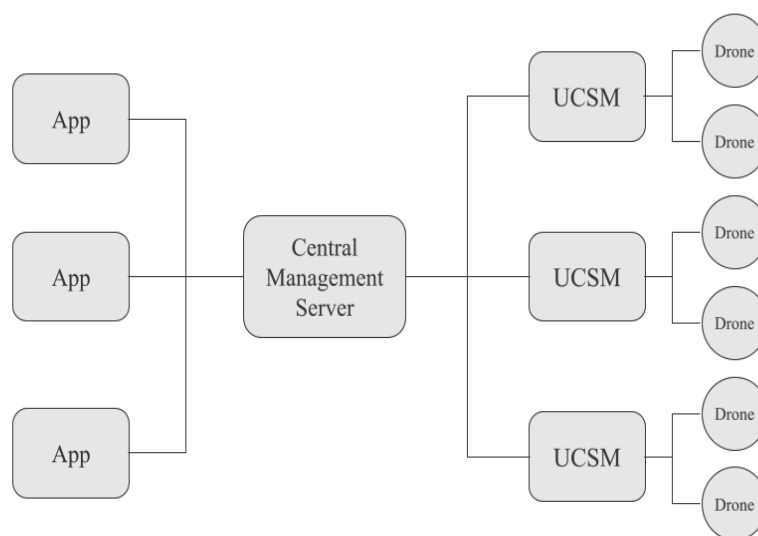


Figure 1. A full system with one Central management server, three UCSMs and six drones



## **4. CLIENT APPLICATION**

Designed to enhance user interaction, the application will offer a user-friendly experience, enabling operators to initiate pre-flight charging procedures, fine-tune charging parameters, and monitor real-time status. The applications will also provide comprehensive insights into battery status, historical performance, and flexible scheduling options. As an integral part of the system, Client Applications will empower users to manage and optimize charging processes actively, contributing to the overall efficiency and readiness of the drone fleet.

### **4.1 Manual Control**

The client applications will provide an intuitive and user-friendly interface that empowers operators to manually initiate pre-flight charging procedures for individual drones. Operators should be able to fine-tune charging parameters based on specific requirements, allowing for a personalized and adaptive approach to meet varying operational needs. The interactive nature of the interface facilitates seamless control over the charging processes.

### **4.2 Monitoring and Management**

Users will have access to detailed reports through the client applications, offering comprehensive insights into battery charge status, planned charging cycles, and historical performance data. The monitoring features will enable users to track the performance of each Universal Charging Smart Module (UCSM) and make informed decisions about the overall health and readiness of the drone fleet. Users should be able to actively manage and optimize charging schedules based on real-time information.

### **4.3 Scheduling**

Client applications will extend the capability to schedule tasks and drone usage well in advance, aligning with operational planning and resource allocation requirements. The flexibility in scheduling features enables users to adapt plans in real-time, ensuring optimal operational efficiency and availability of the drone fleet for various tasks and missions.

## **BIBLIOGRAPHY**

1. H. R. Everett Jr. U.S. Patent US5045769A, 1989.
2. Liao, Linxia; Köttig, Felix. Review of hybrid prognostics approaches for remaining useful life prediction of engineered systems, and an application to battery life prediction. *IEEE Transactions on Reliability*, 2014, 63.1: 191-207.
3. Sulzer, Valentin, et al. The challenge and opportunity of battery lifetime prediction from field data. *Joule*, 2021, 5.8: 1934-1955.



26th January 2024  
Gliwice, Poland

DEPARTMENT OF ENGINEERING MATERIALS AND BIOMATERIALS  
FACULTY OF MECHANICAL ENGINEERING  
SILESIA UNIVERSITY OF TECHNOLOGY

## INTERNATIONAL STUDENTS SCIENTIFIC CONFERENCE

### VR and 3D Tiles as a catalyst for the creation of immersive flight simulators

P. Bartosz <sup>a</sup>, J. Sarno <sup>a</sup>, D. Myszor <sup>b</sup>

<sup>a</sup> Silesian University of Technology, Faculty of Automatic Control, Electronics and Computer Science, Virtual Flying Student Research Club

<sup>b</sup> Silesian University of Technology, Faculty of Automatic Control, Electronics and Computer Science, Department of Algorithmics and Software

email: [dariusz.myszor@polsl.pl](mailto:dariusz.myszor@polsl.pl)

**Abstract:** The article describes the idea of designing a flight simulator based on virtual reality and photorealistic earth recreation. Also presented are implementation attempts by the Virtual Flying Student Research Club.

**Keywords:** VR, Flight Simulators, Photorealism, Immersion

#### 1. INTRODUCTION

With the introduction of new technologies like Photorealistic 3D Tiles by Google [5], allowing to recreate real places in virtual space easily, and improvements in VR technologies bringing higher resolutions and better optimization, the birth of realistic simulators allowing for high levels of freedom is natural. Such simulations can be extremely valuable especially for industries that pose high costs of training and exploitation, by allowing to train personnel as well as conduct tests and research in realistic conditions with fractions of costs. One such industry is aviation. While it already relies heavily on simulations for training and experimentation, those are usually expensive mechanical devices with high maintenance requirements. Simulating flight in virtual reality lowers the hardware requirements and maintenance costs while providing very realistic simulation. Additionally, technologies that allow to recreate accurately realistic environments existing on Earth allow for unparalleled immersion. This paper showcases the approach taken by students from the Virtual Flying Students Research Club to develop such a simulation and the knowledge gained from it.

#### 2. MELT INTO COCKPIT - VIRTUAL REALITY IN FLIGHT SIMULATION

VR (Virtual Reality) headsets are a group of head-mounted devices that allow the user to experience "virtual reality" - the computer-generated environment that can be interacted with in a seemingly real or physical way. VR devices are used in a multitude of industries and are growing in popularity for entertainment purposes. The virtual environment is presented to the user by displaying it on one or many screens located near the user's eyes. Then, lenses are used

to direct the user's gaze at the screen plane properly. The environment can be generated in two ways: by an external system (computer with graphic card) or by self-contained headsets. While using an external system, the VR headset functions as a display and provides tracking data. The self-contained VR headsets provide processing power, memory, and battery packs that allow for mobile use. Such an approach increases the weight and heat generation of the device, while providing less processing power. Recently, some more advanced VR headsets possess advanced tracking capabilities, like eye tracking and face tracking, that help to increase the immersion of the user and allow for more precise controls and interactions with the virtual world. Examples of such VR could be Pico 4 Enterprise, Oculus Pro, or PlayStation VR 2.

Budget flight simulators used to be created with flat screens placed in front of the recreated or repurposed aircraft cockpits. That allowed pilots to learn the aircraft's controls in various scenarios and practice some maneuvers. Still, the experience was not very immersive, and scenarios were limited to a single type of simulated plane.

The VR-based flight simulator allows for much more freedom with scenario design, enables simulation of various aircraft with a single device, and allows for high immersion [1] while requiring a fraction of the costs to run and maintain.

## **2.1 Immersion**

Utilization of virtual reality allows the user to become fully immersed in the virtual world [2]. By seeing the environment around, while having completely synchronized movements and interactions with surroundings, erases the boundary between realities. The advantages of such a solution cannot be understated. The user can interact more naturally and realistically with the world while being capable of better perception and more true reactions. Moreover, the utilization of separate perspectives for each eye allows for unparalleled depth perception that not only adds to realism but also allows the user to perform actions that were very hard with flat screen-based simulators, like judging distances.

## **2.2 Challenges**

The creation of VR applications is a challenge in itself. However, adding motion and realistic graphics takes it to the next level. The biggest problem in VR simulations is motion sickness [3], which occurs due to a difference between actual and expected motion. To mitigate that a specialized platform (yawVr) that allows motion in a limited arc by rolling the user in multiple axes was applied. The solution allowed to semi-realistically recreate quick maneuvers during various phases of the flight. This resulted in decreased motion sickness in flying simulations and an enhanced experience for the pilots.

## **3. FREEDOM OF FLIGHT - RECREATING EARTH IN VIRTUAL SPACE**

Recreation of a virtual environment on a big enough scale for flight simulation, while preserving a good amount of details, used to be tremendously difficult, but the rise of satellite data-powered procedural mesh generation systems like Photorealistic 3D Tiles by Google drastically simplified the entire process. While moving with the speed of an airplane, the user can traverse hundreds of kilometers in the span of an hour, so the environment in which a flight takes place has to be measured in thousands of square kilometers. Handcrafting such environments is impossible while maintaining any level of detail. Thus, procedural mesh generation is the preferred solution, but older generations of such generators provided very

limited detail, depending only on 2D satellite data. New solutions incorporate real-world height into the dataset, which allows them to accurately represent many objects with realistic sizes and shapes and enough detail that even at low altitudes, the environment looks realistic and can be created in a matter of hours. What's more, the usage of real-world environments allows for simulations that can incorporate real scenarios like approaching particular airports or navigating over certain mountains. Examples of graphics utilized in the simulator implemented by Virtual Flight Students Research Group were presented in fig. 1 and fig. 2.



*Figure 1. The Silesian University of Technology generated in Unreal Engine 5.*



*Figure 2. Flight in simulator over Venice.*

### **3.1 Unreal Engine**

To put the entire simulation together Unreal Engine 5 [4] was used. This new generation engine allows for the smooth integration of both VR and Photorealistic 3D Tiles by Google [5]. Additionally, it provides many useful features like dynamic lightning. Moreover, the advanced physics engine included in Unreal Engine 5 was used for the accurate simulation of flight mechanics of various aircraft with fully recreated virtual cockpits. For optimization purposes, the entire simulation was rendered with Nanites, which allowed for extremely good performance, with the Lumen system calculating realistic lighting to improve the visual aspects of the simulation.

## **4. FULL THROTTLE TOWARDS THE FUTURE - TECHNOLOGY APPLICATION AND POTENTIAL**

A combination of used technologies creates a very capable basic flight simulator that is easy to expand or customize to cater to specific needs. Basic principles of the design allow for performing research or utilizing it in pilot training and for entertainment purposes. The creation of such a realistic and immersive simulator allows for an increase in the quality of pilots' training, for example, for navigation in VFR flights. Pilots can fly in a virtual environment in order to become familiar with their typical areas of operation and then during real flights benefit from better orientation in the terrain. Such features are currently being worked on by the students of the Virtual Flying Student Research Club.

Designed flight simulators are not restricted to specialized usage like training or research, they are also a very good option for casual usage. Many people are scared to fly in reality but love to do it in simulators. For them, increased realism and immersion is a great option. It allows for a close-to-real flight while seating safely and comfortably on the ground.

High customizability and ease of plane modification, in combination with real size and immersive environment, create a powerful tool for prototyping cockpit designs. It allows testing designs not only in static conditions but also creates opportunities to test them in simulated flight conditions with pilots and engineers testing them in various changing situations, thus creating valuable insight into their ergonomics and practicality.

## **BIBLIOGRAPHY**

1. Oberhauser, Matthias, et al. What's real about virtual reality flight simulation?. *Aviation Psychology and Applied Human Factors*, 2018.
2. Bowman, Doug A.; McMahan, Ryan P. Virtual reality: how much immersion is enough?. *Computer*, 2007, 40.7: 36-43.
3. Chatta, Umer Asghar, et al. Motion sickness in virtual reality: An empirical evaluation. *IEEE Access*, 2020, 8: 130486-130499.
4. <https://www.unrealengine.com/en-US/unreal-engine-5>
5. <https://developers.google.com/maps/documentation/tile>



26th January 2024  
Gliwice, Poland

DEPARTMENT OF ENGINEERING MATERIALS AND BIOMATERIALS  
FACULTY OF MECHANICAL ENGINEERING  
SILESIA UNIVERSITY OF TECHNOLOGY

## INTERNATIONAL STUDENTS SCIENTIFIC CONFERENCE

### Modification of the machine for double pressing of fuel briquettes

Kakha Beridze; George Taturashvili

Georgian Technical University, Faculty of Transport Systems and Mechanical Engineering,  
Department of Mechanical Engineering

email: Beridzekaxa409@gmail.com; Gtatu2019@agrni.edu.ge

Supervisors: Professor, Dr. Qiria Vaja; Associate professor, Dr. Amkoladze khatuni

email: v.qiria@gtu.ge; k.amkoladze@gtu.ge

**Abstract:** A new scheme for pressing fuel briquettes on a double-acting hydraulic installation has been developed in order to improve the quality of briquettes and work productivity. The parameters of the hydraulic components are calculated.

**Keywords:** hydraulic press, sawdust, briquettes, pellets, pump, cylinder.

### 1. INTRODUCTION

Global warming forced scientists to elaborate new technologies of energy sources amongst which it should be noted the technologies of granulating and briquetting of remnants from reprocessing the biomass. In the West the product received from that kind of technology is called "biofuel!". "Biofuel" is received by drying of 6-10% of bio remnants, by shredding them to homogeneous mass and afterwards by granulating or briquetting of them.

Briquetted "biofuel" to its energetic and techno-economic indicators might be widely used as an alternative to wood (fuel) that will avoid deforestation danger.

According to preliminary evaluations existing raw materials for "biofuel" in Georgia allows to produce at least 300-400 thousand tone of briquettes annually, that will save 1.2-1.6 million cub. M of wood.

All regions are given chance to produce from bio remnants ecologically pure, cheap biofuel and during the winter period to solve not only heating problem, but widely use fuel also for local farming, greenhouses and etc.

Sawdust briquetting (or pelleting) is a process during which the raw material is pressed under strong pressure. Lignin (*lignum- from Latin*), which is contained in the tree, is released under pressure and glues the raw material into a briquette. When the piston presses the raw material, the temperature rises significantly, while the adhesive substances contained in the raw material come out. However, the moisture content of the raw material must be at least 6%. The moisture in the raw material evaporates due to the high temperature. With strong evaporation, steam cavities may form, which will lead to the destruction of the briquette due to expansion. The best moisture percentage for briquetting

depends on the raw materials used, but based on our experience, we recommend between 6% and 16%. Above 16% moisture content, the quality will be significantly reduced until briquetting is not possible at all.

Pellets are recommended for fully automatic domestic boiler with a little storage space.

- Wood chips are recommended for medium-sized and industrial boilers due to the storing conditions and higher damp content (wood chips store is 3-4 times larger in volume than that of pellets).

- Briquettes can be used in fireplaces/boilers of all dimensions and sizes, feeding to the burning chamber in tiny heating units should be accomplished manually.

There are three main types of production of fuel briquettes:

**1. RUF.** Get in a hydraulic press, the finished product comes out in the form of a brick (250×90×60 mm). Requires mandatory packaging in a waterproof film.



**2. Pini Kay.** They look like a bar of a given length (25 ... 40 cm), produced using a screw press. During production, the briquette comes out with a finished sintered film, which partially prevents the absorption of moisture. Products can be packed in plastic bags (big bags).

**3. Nestro.** Cylindrical bars (50...90 mm, length – 50...100 mm) are produced on hydraulic presses

We are considering a double pressing machine designed and manufactured at the Department of Mechanical Engineering and Technology of the Georgian Technical University.

Parameters of this machine are:

- Size of briquettes -70X70X120mm;
- Form of briquettes – rectangular;
- Pressure value 300 bar;
- Pressure of hydraulic power system – 180bar.

Experience with this machine has shown the need for some modifications to improve quality and productivity. Due to the fact that a rectangular shape is used for briquettes the density is not the same, it is smaller in the corners, therefore the quality of the briquettes is generally low. In addition, it has been established that in order to obtain a high-quality product (Density =  $1\text{g/cm}^3$ ), it is necessary that the pressing pressure be at least 700 bar (according experience).

Based on the foregoing, it is possible to determine the desired parameters for the modified press:

**Initial parameters:**

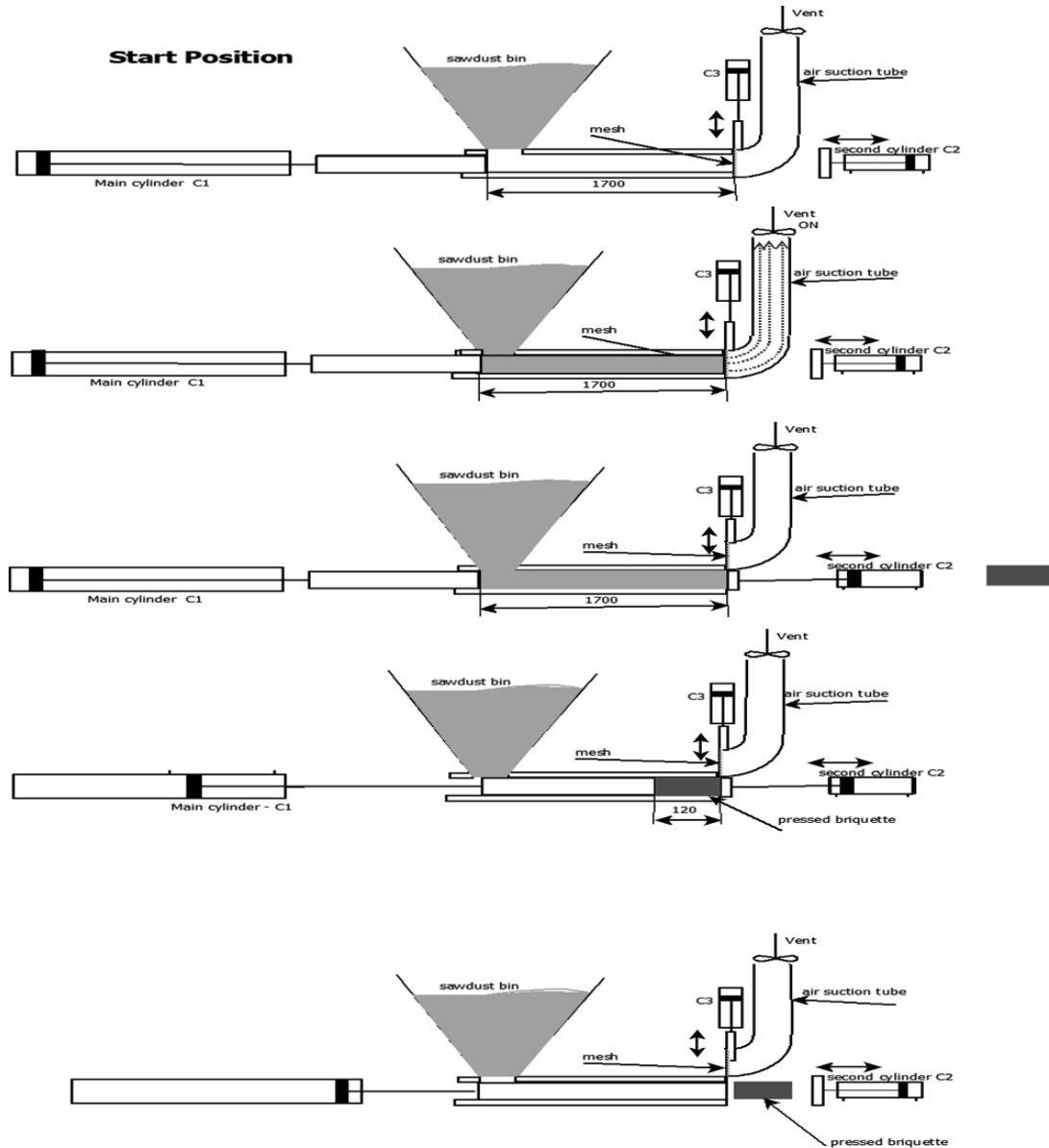
Productivity 300kg/h;

Briquette sizes: Diameter 70mm, Length 120-250mm;

Density of briquettes min.  $1\text{g/cm}^3$ ;

### Double pressing briquetting machine

For our project, we use briquettes with a round section and have changed the principle of briquetting, which is shown in the following figure:

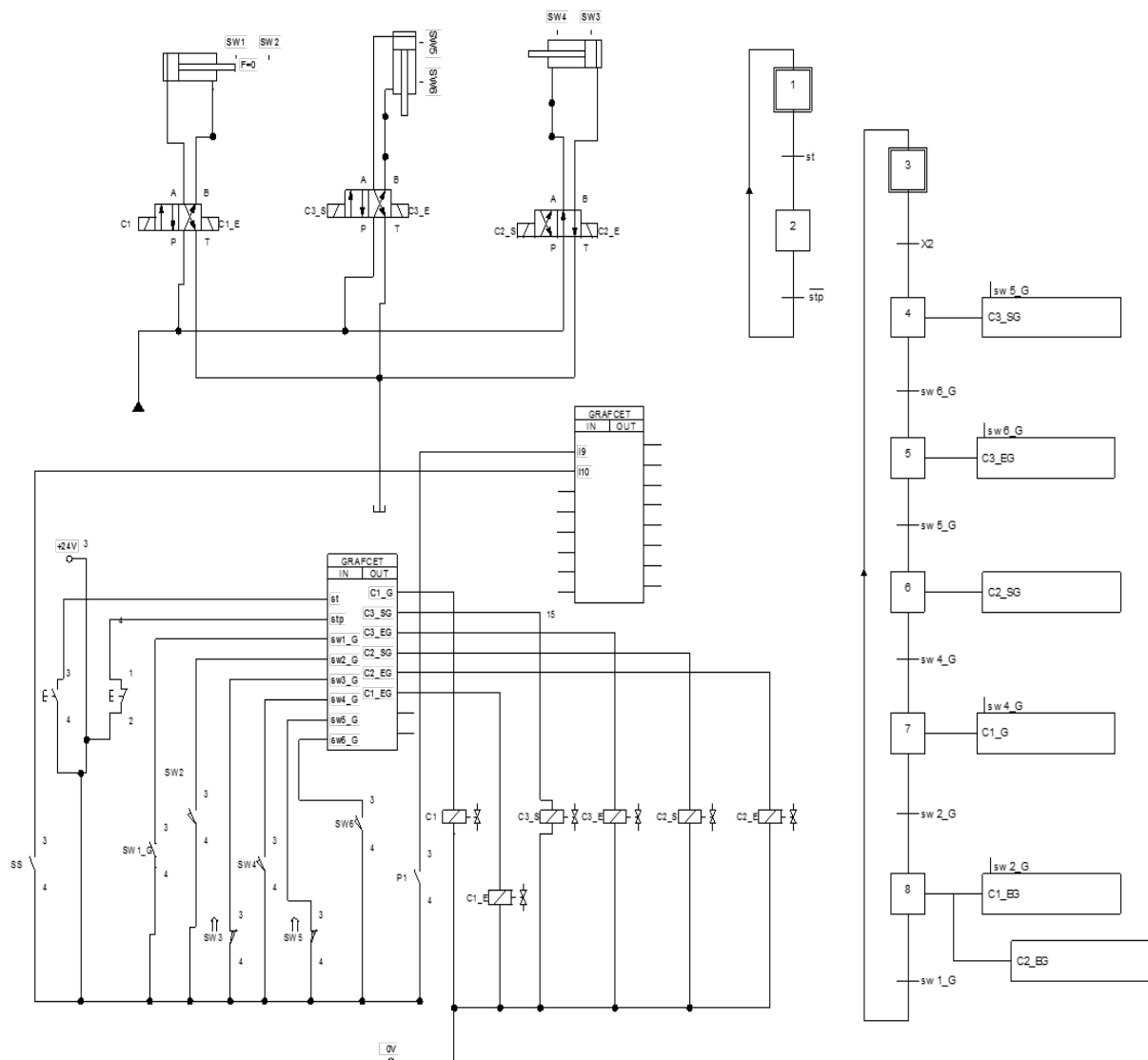


Here we Use 3 cylinders C1, C2 and C3. Filling the mold with sawdust using a suction fan.

The sawdust is in the bunker. In the initial position, by means of a suction fan, the sawdust fills a special cylindrical mold, where the pressing will take place. Then the hydraulic cylinder C3 retracts the suction pipe and the piston of second cylinder C2 closes the mould and cylinder C1 starts the pressing process. When the required pressure value is reached, the second cylinder C2 retracts in the initial position, the cylinder C1 continues to move forward and pushes the finished briquette out.

The hydraulic diagram of our project is shown in Figure below.





## CALCULATIONS

**Cylinder C1.** During of briquetting, the volume of sawdust decreases by 14 times, therefore, to obtain a briquette 120 mm long, the initial pressing volume should be:

$$L = 14 \cdot 120 = 1680\text{mm},$$

i.e. the minimum working stroke of the hydraulic cylinder C1 should be 1680mm.

Typically, the working pressure of the industrial hydraulic system is 160-350 bar.

We are going to use hydraulic components from Diplomatic.

**To select the type of cylinder, we will carry out the following calculation.**

We can calculate the cross section of a briquette as:

$$A_{br} = \frac{\pi \cdot D_{br}^2}{4} = \frac{3,14 \cdot 70^2}{4} = 3848,5\text{mm}^2$$

With a standard pressure in the cylinder of 250 bar, and if we need 700 bar in a briquette, then this means that the piston section must be  $700/250 = 2.8$  times the briquette section and will be:

$$A_{ps} = A_{br} \cdot 2,8 = 3848,5 \cdot 2,8 = 10775,7mm^2,$$

Cross section of piston = 10775.7mm

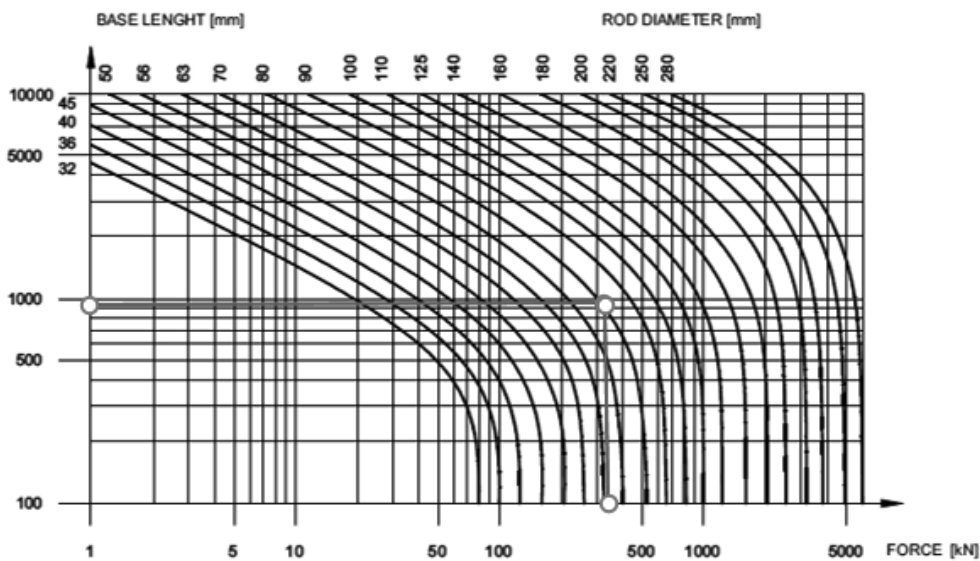
According to the data sheet, it is necessary to select a cylinder with a piston diameter of 125 mm with a piston cross section of 122 72mm<sup>2</sup>.

In addition, according to the manufacturer's recommendation, it is necessary to determine the allowable force of the cylinder depending on the mounting and stroke factor. In our case we have - stroke factor = 0.5.

Table 1

Mounting style	Rod connection	Mounting	Stroke factor
A	Fixed and supported		2
	Fixed and rigidly guided		0.5
	Jointed and rigidly guided		0.7
B	Fixed and supported		4
	Fixed and rigidly guided		1
	Jointed and rigidly guided		1.5
D - F	Jointed and supported		4
	Jointed and rigidly guided		2
L	Jointed and supported		3
	Jointed and rigidly guided		1.5

Diagram 1



We determine the permissible cylinder force according to diagram 1, while multiplying the stroke by the stroke coefficient. Thus, we get a force of approximately 350 kN (see diagram 1). This is acceptable, because with a pressure of 250 we will have:

$$P_{ps} = p \cdot A_{ps} = 250 \cdot 12.272 = 306.08kH$$

So, for cylinder C1 we choose: **HC3A-125 80-1700-M3-0-0-11 2 10**

And for cylinder C2 - **HC3A-125 80-200-M3-0-0-11 2 10**

**Pump.** Based on the dimensions of the cylinders and the desired performance of our machine, we calculate the required pump flow –Q.

For briquette sizes  $\Phi 70$  L120 and density  $1\text{g/cm}^3$  its weight will be

$$W = \frac{1 \cdot 12 \cdot \pi \cdot 7^2}{4} = \frac{1 \cdot 12 \cdot 3,14 \cdot 7^2}{4} \approx 0,462\text{kg.}$$

This means that it is necessary to produce  $300 / 0.462 = 650$  pieces per hour. And the time for making 1 briquette will be:

$$T_{1br} = 3600c / 650pcc \approx 6s.$$

It means that the pump must ensure the movement of all cylinders in order to produce 1 briquette in 6 s. The working volume of the cylinders from the piston side will be:

$$V_{c1} = A_{c1} \cdot L_{c1} = 12272 \cdot 1700 = 20862400\text{mm}^3 \approx 21\text{l}$$

$$V_{c2} = A_{c2} \cdot L_{c2} = 12272 \cdot 200 \approx 2,5\text{l}$$

$$V_{c3} = A_{c3} \cdot L_{c3} \approx 1\text{l}$$

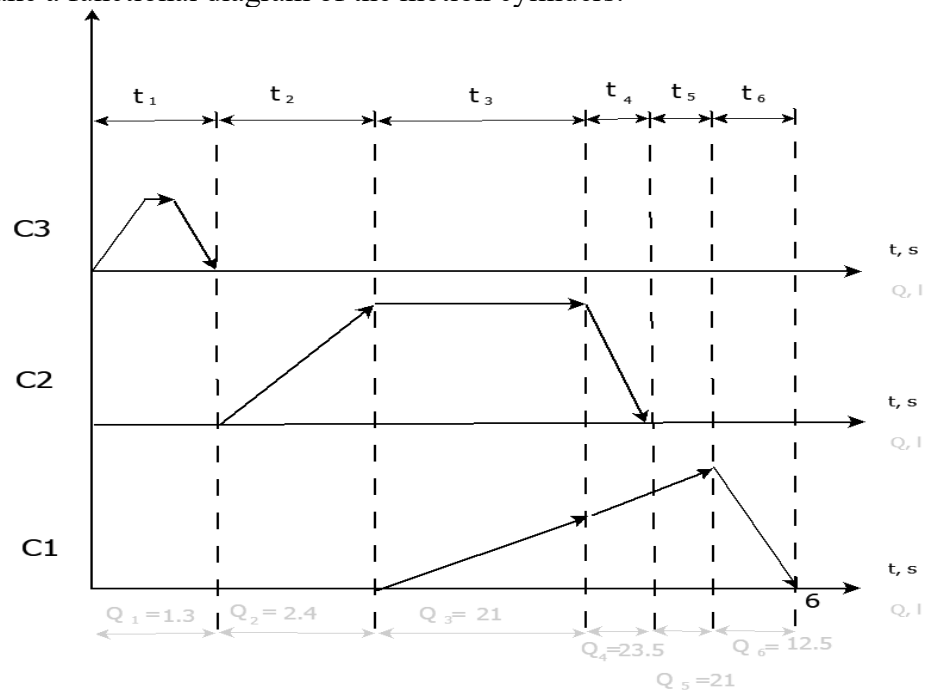
volume of the cylinders from the piston rod side will be:

$$V_{c1} = A_{c1} \cdot L_{c1} = 7245 \cdot 1700 = 207862400\text{mm}^3 \approx 12,5\text{l}$$

$$V_{c2} = A_{c2} \cdot L_{c2} = 7245 \cdot 200 \approx 1,4\text{l}$$

$$V_{c3} = A_{c3} \cdot L_{c3} \approx 0,3\text{l}$$

So let's make a functional diagram of the motion cylinders:



In accordance with this scheme, we make up an equation for calculating the pump flow rate Q:

$$t = t_1 + t_2 + t_3 + t_4 + t_5 + t_6,$$

When

$$t_1 = \frac{q}{q_1}, t_2 = \frac{q}{q_2}, t_3 = \frac{q}{q_3}, t_4 = \frac{q}{q_4}, t_5 = \frac{q}{q_5}, t_6 = \frac{q}{q_6}$$

And here -  $Q_1 \dots Q_6$  are the required flow rate at the corresponding time points.

So

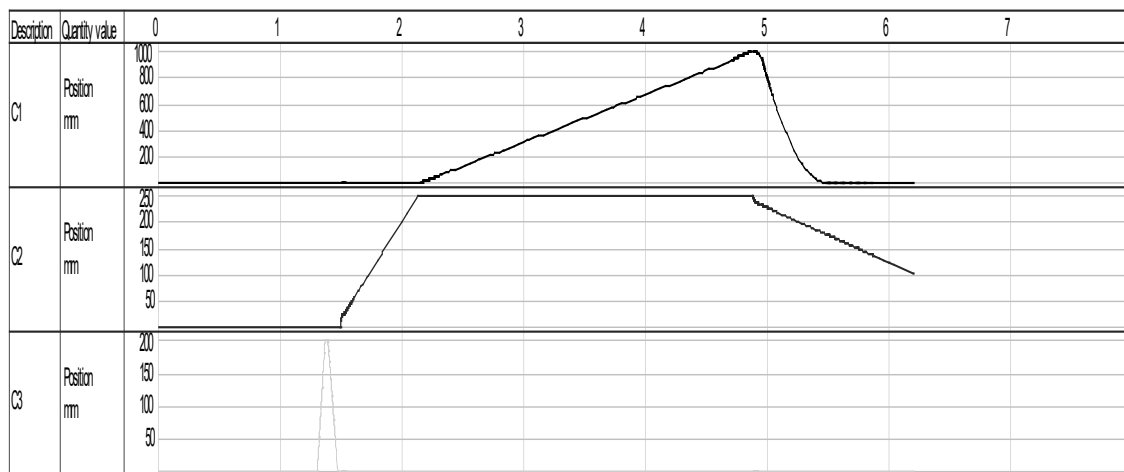
$$\frac{Q}{1,3} + \frac{Q}{2,4} + \frac{Q}{21} + \frac{Q}{23,5} + \frac{Q}{21} + \frac{Q}{12,5} = 6$$

$$Q = 8,3 \text{ l/s} = 498 \text{ l/min.}$$

According to the technical data, we choose double pump IGP7-250 and IGP7-160 with parameters of  $Q_1 = 377 \text{ l/min}$ ;  $p_1 = 210 \text{ bar}$  and  $Q_2 = 241 \text{ l/min}$ ;  $p_2 = 280 \text{ bar}$ ;

Pilot operated valves must be selected for control cylinders C1 and C2: DSP7-S1-D24

We tested the performance of the hydraulic circuit we created using the Fluidsim simulation program. The simulation result is given below as a plot of the position of the cylinders over time.



## CONCLUSION

1. In order to improve the quality of the briquette and the performance of the machine, a modification scheme for the machine for double pressing briquettes has been developed.
2. A suction fan is used to fill the briquetting mold, which significantly reduces the production time.
3. To test the resulting hydraulic system in the Fluidsim environment, a modular program is created and simulation modeling is performed, thereby confirming the correctness of the calculation.

## ACKNOWLEDGEMENTS

The work was created as a result of the project as part of project based learning - PBL, in the 10th competition under the Initiative of Excellence - Research University, Silesian University of Technology.

## **BIBLIOGRAPHY**

1. Renate Aheimer, Christine Löffler, Dieter Merkle, Georg Prede, Klaus Rupp, Dieter Scholz, Burkhard Schrader. Hydraulics, Electrohydraulics. Fundamentals. Textbook. 215p, © Festo Didactic GmbH & Co. KG, 73770 Denkendorf, Germany, 2013.
2. Frank Ebel, Siegfried Idler, Georg Prede, Dieter Scholz. Pneumatics, Electropneumatics. Fundamentals. 212p. © Festo Didactic GmbH & Co. KG, 73770 Denkendorf, Germany, 2010.
3. Alan Hitchcox. FLUID POWER BASICS. 61p. Copyright © 2017 by Penton Media, Inc. All rights reserved.
4. Andrew Parr. Hydraulics and Pneumatics. A technician's and engineer's guide. Third edition. 2011.
5. R.B. Walters. Hydraulic and Electric-Hydraulic Control Systems. Second Enlarged Edition. SPRINGER-SCTENCE+BUSINESS MEDIA. B.V. 2000.



26th January 2024  
Gliwice, Poland

DEPARTMENT OF ENGINEERING MATERIALS AND BIOMATERIALS  
FACULTY OF MECHANICAL ENGINEERING  
SILESIA UNIVERSITY OF TECHNOLOGY

## INTERNATIONAL STUDENTS SCIENTIFIC CONFERENCE

### Wybrane własności stopu $\text{Ni}_{36,3}\text{Co}_{25}\text{W}_{23,7}\text{B}_{15}$ wytworzonego metodą melt-spinning

M. Bigaj<sup>a</sup>, W. Pilarczyk<sup>a</sup>, I. Kredowska<sup>a</sup>, K. Młynarek-Żak<sup>b</sup>

<sup>a</sup> Politechnika Śląska, Wydział Mechaniczny Technologiczny, Katedra Materiałów Inżynierskich i Biomedycznych

<sup>b</sup> Politechnika Śląska, Wydział Mechaniczny Technologiczny, Katedra Automatyzacji Procesów Technologicznych i Zintegrowanych Systemów Wytwarzania  
email: [michal.bigaj@polsl.pl](mailto:michal.bigaj@polsl.pl)

**Abstract:** The following article presents the general characteristics of the  $\text{Ni}_{36,3}\text{Co}_{25}\text{W}_{23,7}\text{B}_{15}$  alloy in the form of ribbons produced by the melt-spinning method. The results of phase analysis based on X-ray diffraction are presented. In addition, differential scanning calorimetry curves recorded during heating process are described. The corrosion resistance of the tested alloy in the form of ribbons cast using the melt-spinning method with the speed of 10 m/s and 20 m/s was characterized based on the results of electrochemical tests.

**Streszczenie:** W poniższym artykule przedstawiono ogólną charakterystykę stopu  $\text{Ni}_{36,3}\text{Co}_{25}\text{W}_{23,7}\text{B}_{15}$  w postaci taśm wytworzonych metodą melt-spinning. Przedstawiono wyniki rentgenowskiej analizy fazowej na podstawie badań dyfrakcji rentgenowskiej. Ponadto, opisano krzywe skaningowej kalorymetrii różnicowej zarejestrowane podczas nagrzewania. Scharakteryzowano odporność korozyjną badanego stopu w postaci taśm odlewanych metodą melt-spinning z prędkością 10 m/s i 20 m/s na podstawie wyników badań elektrochemicznych.

**Słowa kluczowe:** stop Ni-Co-W-B, melt-spinning, skaningowa kalorymetria różnicowa, odporność korozyjna

#### 1. WSTĘP

Częstą przyczyną awarii elementów metalowych jest ich interakcja z otaczającym środowiskiem w wyniku zużycia, korozji, ścierania, zmęczenia materiału, utleniania i pęknięcia. Stopy na bazie Ni-Co zostały opisane w literaturze [1-4] jako materiały charakteryzujące się wysoką wytrzymałością na rozciąganie oraz dużą twardością. Ponadto, wykazują dobrą odporność na zużycie ścierne i korozję [5]. Stopy Ni-Co są stosowane jako powłoki między innymi w elementach czujników oraz cewek indukcyjnych. Costa i in. [6] wskazali, że na poprawę właściwości powłok na bazie niklu wpływa dodatek kobaltu i wolframu. Ponadto, w tej samej publikacji [6], autorzy scharakteryzowali stopy Ni-W o strukturze amorficznej jako materiały charakteryzujące się bardzo dobrą odpornością na korozję, twardością oraz właściwościami magnetycznymi. Dodatek wolframu w stopach na bazie Ni-Co wpływa

na zwiększenie twardości i odporności na wysokie temperatury [6]. Bekish i in. [7] opisali wpływ dodatku boru na właściwości stopów Ni-Co. Autorzy [7] wykazali, że wzrost zawartości tego pierwiastka prowadzi do uzyskania struktury amorficznej. Wraz ze zmniejszeniem wielkości ziarn, powłoki ze stopów Ni-Co-B charakteryzują się większą odpornością na korozję. W przypadku powłok o strukturze amorficznej stopów z dużym udziałem boru zaobserwowano zwiększoną aktywność korozyjną w początkowych fazach testów immersyjnych. W miarę wydłużania się czasu zanurzenia badanych powłok stopów Ni-Co-B o strukturze amorficznej, zaobserwowano stopniowy spadek aktywności korozyjnej, który wynikał z powstania warstwy wodorotlenków niklu i kobaltu. Bekish i in. [7] wykazali również, że dodatek boru w stopach Ni-Co prowadzi do zwiększenia mikrotwardości.

Właściwości fizyczne stopów metali zależą w dużym stopniu od składu chemicznego i mikrostruktury, na którą ma wpływ zastosowana technologia wytwarzania. Melt-spinning jest jedną z najbardziej rozpowszechnionych metod szybkiego chłodzenia stosowaną do otrzymywania stopów o strukturze nanokrystalicznej i amorficznej [8]. Materiał wsadowy umieszcza się w kwarcowym tyglu. Pod wpływem ciśnienia gazu stopiony materiał natryskuje się przez otwór na wirujący miedziany bęben. W metodzie melt-spinning otrzymuje się materiały w postaci cienkich taśm [5].

Ze względu na fakt, że wiele właściwości stopów na bazie Ni-Co-W-B nie zostało jeszcze opisanych, przedmiotem zainteresowania w niniejszym artykule jest zbadanie składu fazowego, własności termicznych oraz odporności na korozję stopów w postaci taśm wytworzonych metodą melt-spinning.

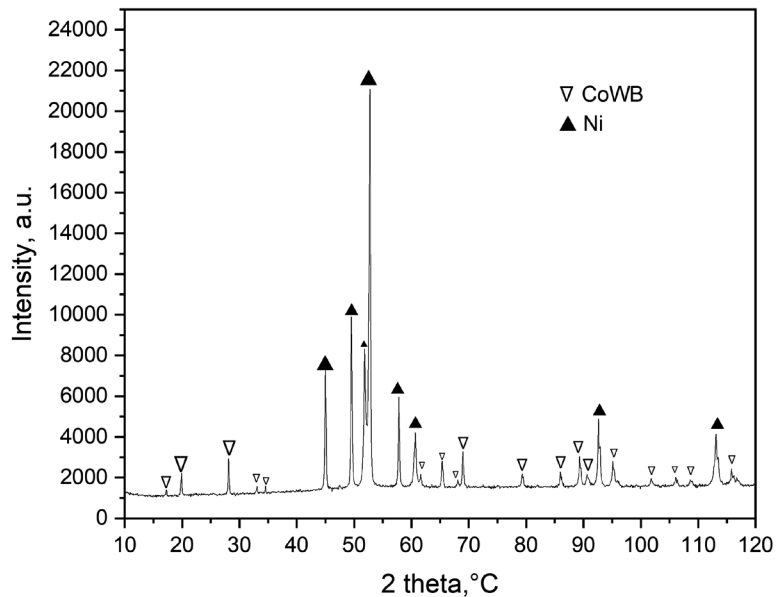
## 2. MATERIAŁ DO BADAŃ I METODYKA BADAWCZA

W artykule materiał badawczy stanowi stop  $Ni_{36,3}Co_{25}W_{23,7}B_{15}$  w postaci taśm. Pierwiastki takie jak Ni, Co, W oraz B, które wchodzi w skład badanego stopu, posiadały czystość powyżej 99%. W pierwszym etapie odważono i przetopiono pierwiastki za pomocą nagrzewnicy indukcyjnej w atmosferze ochronnej. W dalszej kolejności wlewki rozdrobiono i poddano procesowi melt-spinning w celu uzyskania taśm. Dla określenia składu fazowego przeprowadzono badania rentgenowskie przy użyciu dyfraktometru Seifert-FPM model XRD 7. Przemiany cieplne zachodzące w stopie  $Ni_{36,3}Co_{25}W_{23,7}B_{15}$  w postaci taśm odlewanych z prędkością 10 m/s oraz 20 m/s określono na podstawie krzywych nagrzewania skaningowej kalometrii różnicowej, które zarejestrowano przy użyciu urządzenia TGA/SDTA 851 firmy Mettler Toledo. Wykonano również badania elektrochemiczne w roztworze wodnym 3,5% NaCl w temperaturze 25°C przy użyciu potencjostatu. Zastosowano celkę wyposażoną w nasyconą elektrodę kalomelową (NEK) jako elektrodę odniesienia oraz elektrodę platynową jako przeciwelektrodę.

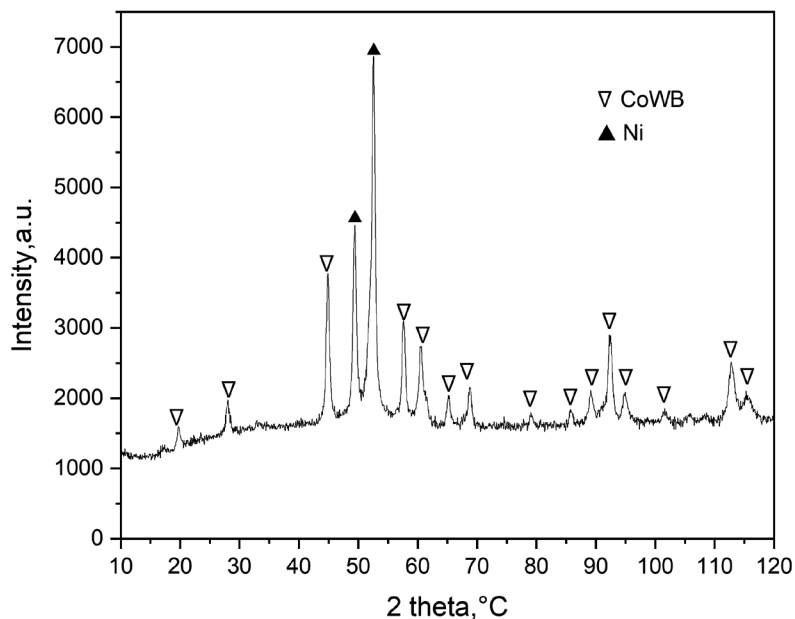
## 3. WYNIKI BADAŃ

Stop  $Ni_{36,3}Co_{25}W_{23,7}B_{15}$  w postaci taśm odlewanych z prędkością obrotową bębna 10 m/s i 20 m/s został poddany badaniu dyfrakcji rentgenowskiej w celu określenia składu fazowego. Dyfraktogramy rentgenowskie badanego stopu w postaci taśm przedstawiono na rysunku 1 dla prędkości 10 m/s oraz na rysunku 2 dla prędkości 20 m/s. Widoczne na dyfraktogramach refleksy świadczą o występowaniu faz krystalicznych. Na podstawie badań rentgenowskich

zidentyfikowano fazy CoWB oraz Ni. Stop  $Ni_{36,3}Co_{25}W_{23,7}B_{15}$  uzyskany przy prędkości chłodzenia równej 10 m/s, charakteryzował się większą ilością wydzieleni fazy Ni w stosunku do stopu odlewanych z prędkością 20 m/s.



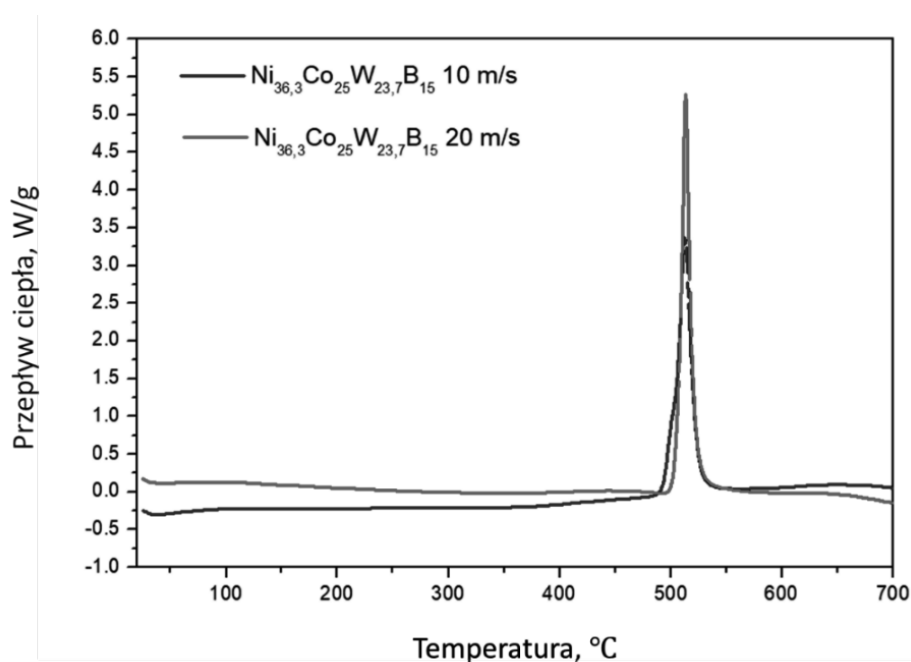
Rys 1. Dyfraktogram rentgenowski taśmy wytworzonej metodą melt-spinning z prędkością obrotową bębna 10 m/s stopu  $Ni_{36,3}Co_{25}W_{23,7}B_{15}$



Rys 2. Dyfraktogram rentgenowski taśmy wytworzonej metodą melt-spinning z prędkością obrotową bębna 20 m/s stopu  $Ni_{36,3}Co_{25}W_{23,7}B_{15}$



Stop  $Ni_{36,3}Co_{25}W_{23,7}B_{15}$  w postaci taśm został poddany badaniom skaningowej kalorymetrii różnicowej (DSC). Krzywe nagrzewania badanych taśm, przedstawione na rysunku 3., charakteryzują się występowaniem efektów egzotermicznych. W przypadku taśmy stopu  $Ni_{36,3}Co_{25}W_{23,7}B_{15}$  otrzymanej przy prędkości chłodzenia 20 m/s dostrzegalny jest ostry efekt cieplny, który świadczy o przemianie fazowej podczas nagrzewania. Ponadto, zachodzi on w porównaniu ze stopem  $Ni_{36,3}Co_{25}W_{23,7}B_{15}$  otrzymanym przy prędkości chłodzenia 10 m/s w węższym przedziale temperaturowym wynoszącym od 500°C do 520°C.



Rys 3. Wyniki badań różnicowej kalorymetrii skaningowej dla stopu  $Ni_{36,3}Co_{25}W_{23,7}B_{15}$  w postaci taśm wytworzonych metodą melt-spinning z prędkością obrotową bębna 10 i 20 m/s

Odporność na korozję oceniono na podstawie wyników krzywych polaryzacyjnych. Na podstawie poniższego równania Sterna-Geary'ego (1) obliczono wartość oporu polaryzacyjnego [9]. W Tabeli 1 przedstawiono wyznaczone parametry elektrochemiczne. Krzywe polaryzacyjne zostały przedstawione na rysunku 4.

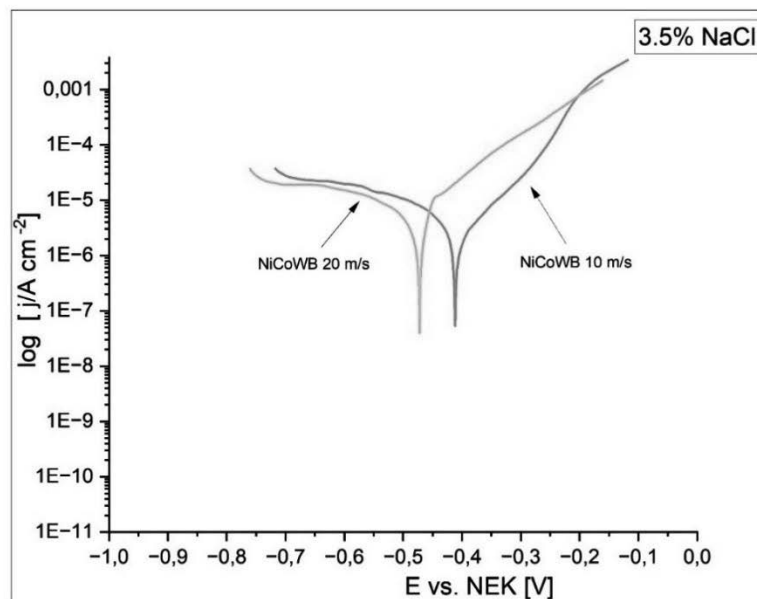
$$i_{corr} = \frac{\beta a |\beta c|}{2,303(\beta a + \beta c)} \frac{1}{R_p} = \frac{B}{R_p} \quad (1)$$

Przeprowadzone badania korozyjne wykazały, że stop  $Ni_{36,3}Co_{25}W_{23,7}B_{15}$  odlewany z prędkością 10 m/s charakteryzuje się lepszą odpornością korozyjną, co wynika z większego oporu polaryzacyjnego  $R_p = 10,52 \text{ k}\Omega \text{ cm}^2$  w porównaniu do stopu  $Ni_{36,3}Co_{25}W_{23,7}B_{15}$  20 m/s  $R_p = 6,66 \text{ k}\Omega \text{ cm}^2$ . Potencjał korozyjny dla stopu  $Ni_{36,3}Co_{25}W_{23,7}B_{15}$  10 m/s jest równy -409,27 mV. Dla stopu  $Ni_{36,3}Co_{25}W_{23,7}B_{15}$  otrzymanego przy chłodzeniu z prędkością 20 m/s potencjał ten wyniósł -486,77 mV. Przedstawiane wartości potencjału korozyjnego dla stopu  $Ni_{36,3}Co_{25}W_{23,7}B_{15}$  10 m/s są przesunięte bardziej w kierunku wartości dodatnich. Można przypuszczać, że stop ten posiada lepszą odporność korozyjną. Kolejnym wskaźnikiem, świadczącym o poprawie własności antykorozyjnych stopu  $Ni_{36,3}Co_{25}W_{23,7}B_{15}$  10 m/s jest mniejsza gęstość prądu korozyjnego. Wartość ta jest równa  $1,84 \mu\text{A}/\text{cm}^2$  a dla stopu

$\text{Ni}_{36,3}\text{Co}_{25}\text{W}_{23,7}\text{B}_{15}$  20 m/s  $5,11 \mu\text{A}/\text{cm}^2$ . Mniejsza wartość  $j_{\text{corr}}$  może świadczyć o lepszej odporności korozyjnej stopu  $\text{Ni}_{36,3}\text{Co}_{25}\text{W}_{23,7}\text{B}_{15}$  uzyskanego przy chłodzeniu z prędkością 10 m/s w środowisku 3,5% wodnego roztworu chlorku sodu w temperaturze  $25^\circ\text{C}$ . W literaturze, udowodniono, że powłoki na bazie stopów Ni-Co charakteryzują się bardzo dobrą odpornością na korozję [10, 11]. W artykule [10] stwierdzono, że stop na bazie niklu z dodatkiem kobaltu 17wt% charakteryzował się najlepszymi parametrami elektrochemicznymi w porównaniu do czystego niklu oraz innych badanych powłok na bazie Ni-Co. Dla powłoki  $\text{NiCo}_{17}$  badanej w środowisku wodnego 3,5% roztworu NaCl zarejestrowano gęstość prądu korozyjnego równą  $2,41 \mu\text{A}/\text{cm}^2$  oraz opór polaryzacyjny wynoszący  $13,24 \text{k}\Omega\text{cm}^2$  [10]. W niniejszym artykule, taśma stopu  $\text{Ni}_{36,3}\text{Co}_{25}\text{W}_{23,7}\text{B}_{15}$  wytworzona metodą melt-spinning z prędkością obrotową bębna 10 m/s charakteryzowała się zatem mniejszą gęstością prądu korozyjnego, jednakże mniejszym oporem polaryzacyjnym w porównaniu do powłoki na bazie stopu  $\text{NiCo}_{17}$  [10].

Tabela 1. Parametry elektrochemiczne wyznaczone dla taśm stopu  $\text{Ni}_{36,3}\text{Co}_{25}\text{W}_{23,7}\text{B}_{15}$  wytworzonych metodą melt-spinning z prędkością obrotową bębna 10 i 20 m/s

$\text{Ni}_{36,3}\text{Co}_{25}\text{W}_{23,7}\text{B}_{15}$ 10 m/s	$\text{Ni}_{36,3}\text{Co}_{25}\text{W}_{23,7}\text{B}_{15}$ 20 m/s
$E_{\text{corr}} = -409,27 \text{ mV}$	$E_{\text{corr}} = -486,77 \text{ mV}$
$j_{\text{corr}} = 1,84 \mu\text{A}/\text{cm}^2$	$j_{\text{corr}} = 5,11 \mu\text{A}/\text{cm}^2$
$R_p = 10,52 \text{k}\Omega\text{cm}^2$	$R_p = 6,66 \text{k}\Omega\text{cm}^2$



Rys 4. Krzywe polaryzacyjne taśm stopu  $\text{Ni}_{36,3}\text{Co}_{25}\text{W}_{23,7}\text{B}_{15}$  wytworzonych metodą melt-spinning z prędkością obrotową bębna 10 i 20 m/s badanych w 3,5% wodnym roztworze NaCl w temperaturze  $25^\circ\text{C}$

## 6. WNIOSKI

1. Badania rentgenowskie stopu  $Ni_{36,3}Co_{25}W_{23,7}B_{15}$  wytworzonych w postaci taśm wykazały, że pomimo zastosowania dużej szybkości chłodzenia otrzymane materiały charakteryzują się strukturą krystaliczną składającą się z faz Ni oraz CoWB.
2. Na podstawie badań elektrochemicznych, stwierdzono, że stop  $Ni_{36,3}Co_{25}W_{23,7}B_{15}$  w postaci taśmy, wytworzony przy prędkości obrotowej bębna 10 m/s charakteryzuje się lepszą odpornością korozyjną w porównaniu do stopu, dla którego zastosowano prędkość 20 m/s, ze względu na większy potencjał korozyjny i opór polaryzacyjny oraz mniejszą gęstość prądu korozyjnego.

## LITERATURA

1. A. Karimzadeh, M. Aliofkhaezai, Frank C. Walsh, A review of electrodeposited Ni-Co alloy and composite coatings: Microstructure, properties and applications, *Surface & Coatings Technology* 372 (2019) 463–498.
2. A. Amadeh, R. Ebadpour, Effect of Cobalt Content on Wear and Corrosion Behaviors of Electrodeposited Ni-Co/WC Nano-Composite Coatings, *Journal of Nanoscience and Nanotechnology* 13 (2013) 1360–1363.
3. G. Chow, J. Ding, J. Zhang, K. Lee, D. Surani, S. Lawrence, Magnetic and hardness properties of nanostructured Ni-Co films deposited by a nonaqueous electroless method, *Applied Physics Letters* 74 (1999) 1889–1891.
4. A. Karpuz, H. Kockar, M. Alper, O. Karaagac, M. Hacıismailoglu, Electrodeposited Ni-Co films from electrolytes with different Co contents, *Applied Surface Science* 258 (2012) 4005–4010.
5. J. Jaworski, E. Dryzek, E. Fleury, Cobalt; Characteristics, Compounds and Applications, Chapter 5: Magnetic properties of Co-based metallic glasses, Nova Science Publishers, Inc. 2011.
6. J. M. Costa, D. G. Portela, A. F. de Almeida Neto, Alloy Materials and Their Allied Applications, Chapter 3: Ni-Co-W Alloys: Influence of Operational Process Conditions on Their Electroplating, Wiley Online Library 2020.
7. Y. N. Bekish, S. K. Poznyak, L. S. Tsybulskaya, T. V. Gaevskaya, V. A. Kukareko, A. V. Mazanik, Electrodeposited Ni-Co-B Alloy Coatings: Preparation and Properties, *Journal of The Electrochemical Society* 161 (2014) 620–627.
8. K. Filipecka, P. Pawlik, J. Wysłocki, P. Gębara, Nowoczesne metody wytwarzania materiałów amorficznych, *Fizyka IX*, Wydawnictwo im. Stanisława Podobińskiego Akademii im. Jana Długosza w Częstochowie, Częstochowa, 2014, 41–51.
9. R. Babilas, M. Spilka, K. Młynarek, W. Łoński, D. Łukowiec, A. Radoń, M. Kądziołka-Gaweł, P. Gębara, Glass-Forming Ability and Corrosion Resistance of  $Al_{88}Y_{8-x}Fe_{4+x}$  ( $x = 0, 1, 2$  at.%) Alloys, *Materials* 14 (2021) 1–12.
10. B. Bakhit, A. Akbari, Nanocrystalline Ni-Co alloy coatings: electrodeposition using horizontal electrodes and corrosion resistance, *Journal of Coatings Technology and Research* 10 (2013) 285–295.
11. Z. Lin, W. Zhang, L. Xu, Y. Xue, W. Lia, Fabrication of Ni-Co/Cu super-hydrophobic coating with improved corrosion resistance, *Materials Chemistry and Physics* 277 (2022) 1–7.



26th January 2024  
Gliwice, Poland

DEPARTMENT OF ENGINEERING MATERIALS AND BIOMATERIALS  
FACULTY OF MECHANICAL ENGINEERING  
SILESIA UNIVERSITY OF TECHNOLOGY

## INTERNATIONAL STUDENTS SCIENTIFIC CONFERENCE

### **The characteristics of the ABS polymer material used for 3D printing filaments**

I. Blumski<sup>a</sup>, L. Gabiga<sup>a</sup>, R. Gabrys<sup>b</sup>, J. Pająk<sup>b</sup>, M. Polok-Rubinić<sup>c</sup>, A. Włodarczyk-Fligier<sup>c</sup>, A. Kania<sup>c</sup>

<sup>a</sup> Students of Students of Mechanical Engineering, <sup>b</sup> Students of Industrial Mechatronics  
email: iwoblum937@student.polsl.pl

<sup>c</sup> Silesian University of Technology, Faculty of Mechanical Technology, Department of Engineering and Biomedical Materials  
email: magdalena.polok-rubinić@polsl.pl

**Abstract:** In the article, a filament made of ABS polymer (acrylonitrile-butadiene-styrene) was characterized in the context of 3D printing. Its advantages and disadvantages were analyzed, and it was compared with other materials used in 3D printing. in terms of costs and physicochemical properties. Unique properties of ABS, such as mechanical strength and chemical resistance were described, while also examining critical aspects like shrinkage during cooling and the emission of odors during printing.

**Keywords:** Polymers materials, ABS, 3D printing

### **1. INTRODUCTION**

3D printing, a modern technology that allows for the rapid creation of three-dimensional structures, has gained immense popularity. One of the most commonly used filaments in 3D printing is ABS, known for its exceptional mechanical properties and versatile applications. ABS stands out for its strength, flexibility, impact resistance, and resistance to chemicals and temperature. Studies have shown the possibility of modifying its properties by adding fillers, such as glass fibers. ABS filament has also been compared with other materials, such as PLA (polylactic acid), PETG (polyethylene terephthalate glycol), and nylon, in terms of costs, physicochemical properties, and potential applications [1]. This perspective allows for a fuller understanding of the context of filament choice, tailored to specific project requirements, production efficiency, and intended use of the printed objects [2]. Compared to PLA and PETG, ABS is characterized by its strength and heat resistance, but it is less environmentally friendly than PLA. The main disadvantages of ABS filament include a tendency to deform and emit harmful fumes [3]

## 2. THE PROPERTIES OF THE ABS POLYMER MATERIAL

The main advantages of the ABS polymer material are its tensile strength (Table 1)  $R_m$  - 24.56-33.78 MPa and  $E$  - 787.68 MPa [4,5]. However, printing with ABS can be problematic due to its tendency to deform and crack when cooled or exposed to UV radiation. In addition, ABS emits harmful fumes during printing, requiring adequate ventilation. ABS is characterized by tensile strength, impact resistance and flexibility. It is also resistant to most dilute acids, e.g. sulfuric acid, hydrochloric acid, nitric acid, salt solutions, alcohols, oils and fats. The temperature range in which it loses mechanical properties is between 80-100°C. May degrade at higher temperatures, especially in the presence of UV light. A characteristic feature of ABS material is its solubility in acetone. The properties of ABS can be modified by adding microscale fillers such as glass fibers or natural fibers [1], which can affect tensile strength and flexibility as well as resistance to deformation and cracking. The use of natural fillers, such as Curauá (*Ananas erectifolius*), improves tensile strength and elasticity  $E = 63.7\text{GPa}$  [6]. Curauá fibers are obtained from a plant originating from the Amazon, these fibers are characterized by high tensile strength  $R_m$  - 543MPa [6]. The use of a filler in the form of Curauá contributes to faster decomposition of the material in the natural environment, which is beneficial for ecological reasons [1]. Fillers reinforce the polymer matrix, which increases the material's resistance to mechanical stress. The filler in polymer matrices also reduces the pore density, which translates into better uniformity and print quality. ABS is susceptible to the phenomenon of processing (linear) shrinkage. In order to minimize the effects of this phenomenon, it is required to compensate it by optimizing printing parameters, which minimizes shrinkage and improves dimensional accuracy [6]. ABS also tends to delaminate when printing large objects or thin, tall walls. To prevent this, a relatively high printing temperature of 200-230°C is used (Table 2) and the worktable is heated to 80-110°C. A good solution that ensures high quality ABS prints are 3D printers with a built-in working chamber where a constant temperature is maintained between 80-110°C, which has a positive effect on the behavior of the material. This ABS filament is often chosen for prototyping, especially in the aerospace and tool industries, due to its tensile strength and dimensional stability [7]. Due to its good impact resistance, ABS is often used to produce mechanical parts such as handles and gears. It is also used in 3D printing in the biomedical field (Fig. 1), including the creation of customized assistive devices such as prostheses and implants and in surgical simulations [8] [9].

Table 1. Mechanical properties of the ABS polymer material [4].

$R_m$ (MPa)	$E$ (MPa)	$R_{p0.2}$ (MPa)	KU ( $\text{Jm}^{-3}$ )
33.78	787.68	25.17	2.83

### 2.1. Comparison of ABS filament with other popular filaments used for 3D printing.

ABS is widely used in 3D printing and prototyping due to its good mechanical properties and ease of printing. However, depending on the intended use of the given model, we may choose a different filament, e.g. PLA (polylactic acid) due to the lack of shrinkage, or nylon, which is characterized by very high tensile strength and flexibility. Table 2 shows a comparison of the properties of ABS filaments with PLA and nylon filaments.

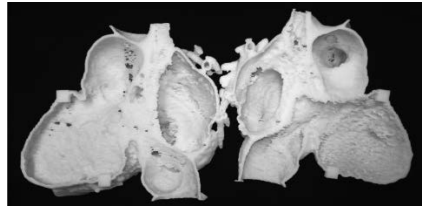


Figure 1. heart model made of ABS, printed on a 3D printer [10].

Table 2. The comparison of selected properties of ABS, PLA and nylon filaments [3,11]

	ABS (Acrylonitrile- Butadiene-Styrene)	PLA (Polylactide)	Nylon
Material composition:	Composed of acrylonitrile, butadiene, and styrene.	Produced from renewable sources such as corn starch or sugar cane.	Polyamide polymer, derived from petroleum or renewable sources.
Printing temperature [°C]	200-230	180-220	230-260
Table temperature during 3D printing [°C]	80+	40-60	110-120
Flexibility	Relatively stiff; not as flexible as Nylon.	Less flexible compared to ABS and Nylon.	Flexible and durable, offers good impact resistance.
Biodegradability	Not biodegradable	Biodegradable under certain conditions, considered more environmentally friendly.	Is not easily biodegradable, but can be recycled
Odor and fumes	May emit unpleasant fumes during printing.	emits minimal odor and is considered safer in terms of fumes.	emits less odor compared to ABS.
Cost Per 1kg spool	20-30\$ ABS is an affordable 3D printing filament, with good rigidity and ease of printing.	20-30\$ Typically, more affordable than Nylon, but prices may vary depending on quality and specifications.	65-75\$ Often more expensive than ABS and PLA
Application in 3D printing	Most often used for prototypes that require strength	Good for general purpose printing, prototypes, and objects with lower mechanical requirements.	Perfect for flexible and durable parts, engineering applications

### 3. SUMMARY

ABS polymer material filament is a commonly used material for 3D printing due to its good impact resistance and flexibility as well as low cost, compared to other materials used for prototyping. The main disadvantages of ABS filaments are its tendency to deform, and release of harmful gases during the printing process.

### BIBLIOGRAPHY

1. A. C. Mendonça, et al. Mechanical Characterization of Filler Modified ABS 3D Printed Composites Made via Fused Filament Fabrication, Federal Center of Technological Education in Rio de Janeiro, Brazil, Vol. 33 (2022) 27-34.
2. L. E. Vendland, et al. Investigating the adhesive properties of polymers for 3D printing, IOP Publishing, Journal of Physics: Conference Series 2057 012106 (2021) 4-6
3. N. Vidakis, M. Petousis, E. Velidakis, M. Liebscher.; V. Mechtcherine, L. Tzounis. On the Strain Rate Sensitivity of Fused Filament Fabrication (FFF) Processed PLA, ABS, PETG, PA6, and PP Thermoplastic Polymers (2020) 5-13.
4. S. K. Selvamani, M. Samykan, S. Subramaniam, W. K. Ngui, K. Kadirgama, G. Kanagaraj, M. Idris, 3D printing: Overview of ABS evolution, AIP Conference Proceedings 2059/1 (2019) 25-26.
5. A. Weiser, B. Kipp, M. Dillon, S. Ralph, K. Rodriguez, A. Young, D. Saikumar, C. Greene, Shrinkage Compensation for FFF Printing for PLA, ABS, and PETG Thermoplastics, A Regional Conference of the Society for Industrial and Systems Engineering, West Point, New York, USA (2021) 1-5.
6. M. E. A. Fidelis, T. V. C. Pereira, O. F. M. Gomes, F. A. Silva, R. D. T. Filho. The effect of fiber morphology on the tensile strength of natural fibers, Journal of Materials Research and Technology, Elsevier 2/2 (2013) 149-157.
7. M. Samykan, S. K. Selvamani, K. Kadirgama, W. K. Ngui, G. Kanagaraj, K. Sudhakar Mechanical property of FDM printed ABS: influence of printing parameters, The International Journal of Advanced Manufacturing Technology, Springer Nature 102 (2019) 2779–2796.
8. A. H. Abdullah, Effects of Printing Parameters on the Mechanical Strength of Thermoplastics 3D Printed Specimens, Journal of Mechanical Engineering 33 (2023) 27-32.
9. L.P.F. Assemany, Rodrigues Junior, O., & Potiens, M.P.A. Reuse of 3D printed materials for dosimetry purposes, Proceedings of the 6th Brazilian congress on ionizing radiation metrology, Brazil: Sociedade Brasileira de Metrologia (2019) 77-84.
10. M. Salmi, Possibilities of Preoperative Medical Models Made by 3D Printing or Additive Manufacturing, Journal of Medical Engineering PMID: 27433470 (2016).
11. M. Lay, N. L. N. Thajudin, Z. A. A. Hamid, A. Rusli, M. K. Abdullah, R. K. Shuib, Comparison of physical and mechanical properties of PLA, ABS and nylon 6 fabricated using fused deposition modeling and injection, Composites Part B: Engineering, Elsevier 176 (2019) 1-7.

**Praca powstała w wyniku realizacji projektu Project Based Learning (PBL) pt. Projektowanie i wydruk 3D modeli anatomicznych pomocnych w przygotowaniu do operacji i wyjaśnieniu procesu leczenia pacjentom.**



26th January 2024  
Gliwice, Poland

DEPARTMENT OF ENGINEERING MATERIALS AND BIOMATERIALS  
FACULTY OF MECHANICAL ENGINEERING  
SILESIA UNIVERSITY OF TECHNOLOGY

## INTERNATIONAL STUDENTS SCIENTIFIC CONFERENCE

### Creating of layers on the surface of the materials

A. Bodnar <sup>a</sup>, K. Jędrzejczyk <sup>a</sup>, M. Szafron <sup>a</sup>, M. Bonek <sup>b</sup>

<sup>a</sup> Student of Silesian University of Technology, Faculty of Mechanical Engineering

<sup>b</sup> Silesian University of Technology, Faculty of Mechanical Engineering, Department of Materials Engineering and Biomaterials

**Abstract:** The article describes examples of layer production methods on the surface of the materials. There are descriptions of Chemical Vapor Deposition and Physical Vapor Deposition with plasma assisted methods. At the end of the article there is a comparison of the properties of the above methods.

**Keywords:** PVD, CVD, Multilayer coatings

### 1. INTRODUCTION

The development of coating technology has allowed the development of many new methods that increase the durability and improve the mechanical and chemical properties of the surfaces of engineering materials. Some of them are frequently used in the industry, like: CVD (Chemical Vapor Deposition), PVD (Physical Vapor Deposition) and hybrid methods that use some of the features of CVD and PVD methods.

#### 1.1. Chemical Vapor Deposition- CVD

The CVD method is carried out by producing layers of carbides and metal nitrides, e.g. chromium, vanadium, titanium, tantalum or zirconium, from components of the gas atmosphere, on the surface of the processed material.

The substrate components participate in the process of producing layers using the CVD method, which is carried out in a sealed reactor as a consequence of heterogeneous chemically and physically catalyzed reactions on the steel surface at a pressure of 1-10÷1.35-10<sup>3</sup> Pa and a temperature of approximately 1000°C.

The best conditions for carrying out this process are gas atmospheres, most often containing vapors of chemical compounds of the metal constituting the main component of the produced layer (carbide, nitride, boride, oxide) at a temperature of 900-1100°C. The most industrial applications are atmospheres composed of a volatile halide of a diffusing element and a hydrocarbon, nitrogen, hydrogen or an inert gas, e.g. argon. As a result of a chemical reaction occurring on the metal surface, atoms (e.g. boron, chromium, titanium, tantalum or aluminum) are released from a compound (e.g. BCl<sub>3</sub>, CrCl<sub>2</sub>, TiCl<sub>4</sub>, TaCl<sub>5</sub>, AlCl<sub>3</sub>). The second component



of the layer is taken from the substrate (e.g. carbon in the case of carbide layers) or from the atmosphere (e.g. nitrogen or oxygen in the case of nitride or oxide layers).

Heat-activated CVD coating deposition can be divided into:

- chemical vapor deposition at atmospheric pressure APCVD (atmospheric pressure CVD),
- chemical vapor deposition under reduced pressure LPCVD (low pressure CVD).

Over recent years, several varieties of CVD processes have been improved, for example PACVD (plasma assisted CVD), leading to a significant reduction in process temperature. By using low-temperature plasma, we can benefit from the positive features of high-temperature CVD processes (high efficiency and quality of the obtained coatings) at a low coating temperature and the beneficial effect of the plasma - the possibility of cleaning the substrate as a result of the plasma action ensures good adhesion of the coating to the substrate.

CVD methods allow the production of surface layers differentiated in terms of phase composition, up to 15  $\mu\text{m}$  thick, and are most often used for machining materials such as sintered carbides, and for machining machine elements where resistance to frictional wear is important. without applying high dynamic loads.

## **1.2 Physical Vapor Deposition- PVD**

The PVD method is based on the use of physical phenomena, such as the evaporation of metals or alloys or cathodic sputtering in a vacuum and the ionization of gases and metal vapors using various physical processes. Their common feature is the crystallization of metal vapors or phases from the plasma. The coatings are applied on a cold or heated to 200÷500°C substrate, which allows the coating of hardened and tempered substrates without reducing their hardness, but the coatings will be very thin and poorly bonded to the substrate. The cleanliness of the surface has a significant impact on the strength of the adhesive coating-substrate bond.

Most often, there are three stages of coating formation in the PVD process:

- Obtaining vapors of the applied material,
- Transport of vapors (neutral or ionized) to the substrate material,
- Condensation of vapors of the applied material on the substrate and growth of the coating.

Changing the process parameters has a significant impact on the structure of the coating when using PVD techniques. The basic parameters are: substrate temperature, gas pressure, energy of bombarding ions, which, together with the characteristics of the substrate: chemical composition, microstructure, topography, determine the mechanical properties of coatings. The intensity of phenomena occurring on the surface is influenced by, among others, density of the energy flux of bombarding ions, the upper value of which is limited by the thermal resistance of the substrate material. At low energy of ion-body collisions, there may be a local increase in temperature and desorption of particles located on the surface (including pollutants) due to solids. When the energy increases, i.e. in processes involving plasma, the phenomena described previously occur, and ion implantation may occur along with the sputtering of atoms from the coated surface. The value of ion energy in PVD processes depends on the change in the intensity of the electric field that accelerates the ions (polarization of the substrate with negative voltage) and on the free path of the ions on which they are accelerated in the electric

field. The changed energy of the bombardment ions determines the nucleation and growth of the coating, surface morphology and adhesion to the substrate.

The concentration of elements in the matrix and coating varies in the transition zone with thickness of 1-2  $\mu\text{m}$  and is stronger the cleaner the coated surface is, which proves that the coating-substrate connection is of a diffusion-adhesive nature. Transition metals most often used for tribological applications are Ti, V, Ta, Zr, Cr, Mo, W, Nb, reactive gases (nitrogen, oxygen) or vapors (e.g. boron, silicon) and elements obtained from various chemical compounds (carbon), forming hard-fusible nitrides, carbides, borides, sulfides and oxides. In PVD processes, one of the most important properties of coatings is the adhesion of the coating to the substrate.

### 1.3. Plasma Assisted Physical Vapor Deposition -PAPVD

PAPVD techniques, unlike PVD techniques without the presence of plasma are increasingly used in the processes of applying thin coatings. This is due to the greater kinetic energy of the particles in the device chamber, which leads to improved adhesion of the applied coating and the substrate, and at the same time the surface is well cleaned thanks to the high energy of the plasma stream. This method allows both to improve the corrosion resistance of steel.

Non-equilibrium processes include PAPVD methods, in which plasma plays an important role during the crystallization of the coating. The use of bombardment of the crystallizing shell with ions with an energy of 1 eV to 1 keV leads, among other things, to an increase in the mobility of adsorbed atoms and provides the energy needed to activate chemical reactions in low-temperature PAPVD methods. The effects of interactions of an ion with a solid depend on the energy of the ions and the method of producing the coating. It is assumed that the ion flux corresponds to the ionic current density on the substrate, while the flux of condensing atoms is proportional to the coating application rate. The chemical and phase composition of coatings obtained using reactive PVD methods depends on the ratio of the density of the reactive gas particle stream to the number of condensing metal atoms.

### 1.4 Multilayer coatings

Multi-layer coatings, which provide much wider possibilities of shaping properties, despite being less popular than single-layer coatings, are indispensably used when the requirements for material properties are higher. A special feature of multi-layer coatings is the ability to smoothen the transition between the properties of the surface layer and the properties of the substrate, which affects the durability of the coating.

Various properties are expected from the produced layers, depending on their location. Layers applied to the ground should have the greatest as possible adhesion, but also the jump in mechanical properties compared to the properties of the substrate should be as low as possible. The outer layers, due to the exposure of atmospheric factors and the effect of friction, should be resistant to corrosion and have low consumption with friction.

The loss of multi-layered construction by mutual mixing of materials forming the layers may take place when the periods of occurrence of layers are insufficient, which may result in not obtaining the intended properties.

## 2. Comparison of PVD and CVD

In both methods, the temperature of the gas phase of atoms or ions deposited on the surface and the temperature of this surface differ. In the PVD method, the substrate temperature is higher than the temperature of the gas phase, while in the CVD method this temperature is lower.

PVD and CVD coatings are used for elements exposed to friction. As is known, the chemical composition of materials, their hardness and surface topography influence friction wear. The influence of surface roughness in this aspect is more significant than the influence of the chemical composition of materials.[9,10,11]

The CVD method, thanks to the dense microstructure and the lack of internal coating defects, allows for greater surface smoothness, which consequently reduces the sliding friction coefficient. In the case of CVD coating, surface irregularities are mainly due to the coating growth process and the resulting crystalline structure, which can be eliminated by polishing. The topography of the CVD coatings after polishing resulted in almost zero material transfer and illustrating stable, low-friction sliding contact conditions. Smooth surfaces, e.g. surfaces with a Ra value of 0.1 mm, can exhibit significant differences in friction and transfer behavior, which is important in many tribological conditions. In the case of metal, the ability of the coating to improve chip flow on the rake face is crucial to the function of the coating, and consequently the topography of the coating surface is important. However, structural defects such as the presence of droplets and craters throughout the entire depth in the PVD coating make it difficult to obtain similar surface roughnesses.

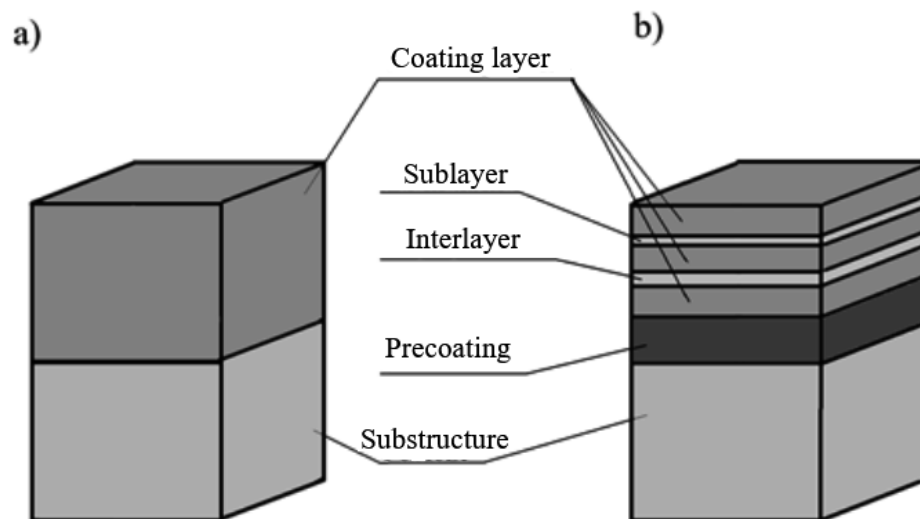


Figure 1. Scheme of the construction of a) single-layer coatings; b) multi-layer; based on[13]

## 3. CONCLUSIONS

Conscious choice among many varieties of coating application techniques is very important due to the differences in the properties of coatings with the same composition depending on the

selected method.

After choosing the technology of creating a layer, attention should be paid to the parameters of its creation, among others due to the significant deterioration of mechanical properties when not ensuring the minimum thickness of the layer

Table 1. Comparison of approximate properties characteristic of PVD and CVD coatings[5]

Properties	PVD	CVD
Coating thickness [ $\mu\text{m}$ ]	4	15
Hardness [HV]	Bigger	Smaller
Roughness Ra [ $\mu\text{m}$ ]	Większa	Mniejsza
Temperature [ $^{\circ}\text{C}$ ]	500-600	900-1100
Adhesion strength	Smaller	Bigger
Defects		
Particles 0,2-3 $\mu\text{m}$	-	$4000 \cdot 10^2 / \text{mm}^2$
Particles >3 $\mu\text{m}$	$28 / \text{mm}^2$	$2 \cdot 10^2 / \text{mm}^2$
Craters 0,2-3 $\mu\text{m}$	-	$500 \cdot 10^2 / \text{mm}^2$
Craters >3 $\mu\text{m}$	-	$2 \cdot 10^2 / \text{mm}^2$

## ACKNOWLEDGEMENT

The work was created as a result of the project of the Student Scientific Circle “Laser Surface Treatment” operating at the Department of Engineering Materials and Biomaterials at the Faculty of Mechanical Engineering, Silesian University of Technology.

## BIBLIOGRAPHY

1. J. Chen, J. Zhang, K. Li, D. Zhuang, Q. Zang, H. Chen, Y. Lu, B. Xu, Y. Zhang, Microstructure and Properties of Laser Surface Remelting AlCoCrFeNi[sub.2.1] High-Entropy Alloy, Metals (Basel ), 2022, Vol.12 (10). T. Suntola, J. Anlson, U.S. Patent 4,058.430, 1977.
2. M.K. Nayak, S. Roy, I. Manna, Effect of substrate surface roughness on the microstructure and properties of laser surface cladding of Tribaloy T-400 on mild steel, Surface & coatings technology, 2023, Vol.455, p.129210, Article 129210. Atomic Layer Deposition, Beneq, <http://www.beneq.com/atomic-layer-deposition.html>, 2013.
3. G. Shi, P. Ding, J. Liu, H. Yin, J. Wang, Microstructure and properties of laser surface hardened M2 high speed steel, Acta metallurgica et materialia, 1995, Vol.43 (1), p.217-223.
4. Sokovic, Mirko, Kopac, J. Dobrzanski, L.A. Mikula, J. Golombek, K. Pakula, D. Cutting characteristics of PVD and CVD - Coated ceramic tool inserts, Tribology in industry, 2006, Vol.28 (1-2), p.3-8
5. Saketi, S. Olsson, M, Influence of CVD and PVD coating micro topography on the initial material transfer of 316L stainless steel in sliding contacts – A laboratory study, Wear, 2017, Vol.388-389, p.29-38.

6. A. Śliwa, J. Mikuła, K. Gołombek, T. Tański, W. Kwaśny, M. Bonek, Z. Brytan, Prediction of the properties of PVD/CVD coatings with the use of FEM analysis, *Applied surface science*, 2016, Vol.388, p.281-287.
7. M. Stoiber, J. Wagner, C. Mitterer, K. Gammer, H. Hutter, C. Lugmair, R. Kullmer, Plasma-assisted pre-treatment for PACVD TiN coatings on tool steel, *Surface and Coatings Technology*, Volumes 174-175, September-October 2003, Page 687-693.
8. C.B. Santos, E. Tentardini, L.A. Piana, D. Carpenteya, T.R. Strohaecker, J. Z. Ferreirif, Corrosion Resistance of PAPVD TiN Coating, on AISI 304 Stainless Steel, *The International Journal of Surfac Engineering and Coatings* Volume 80, 2002.
9. P. Karlsson, A. Gåård, P. Krakhmalev, Influence of tool steel microstructure on friction and initial material transfer, *Wear* 319 (2014) 12–18.
10. J. Heinrichs, M. Olsson, S. Jacobson, New understanding of the initiation of material transfer and transfer layer build-up in metal forming – In situ studies in the SEM, *Wear* 292–293 (2012) 61–73.
11. Westlund, J. Heinrichs, M. Olsson, S. Jacobson, Investigation of material transfer in sliding friction – Topography or surface chemistry, *Tribol. Int.* 100 (2016) 213-223.
12. L.A. Dobrzański, A.D. Dobrzańska-Danikiewicz, *Obróbka powierzchni materiałów inżynierskich*, Open Access Library, Volume 5, 2011.
13. Burakowski T., Wierzchom T.: *Inżynieria powierzchni metali*. Wydawnictwa Naukowo-Techniczne, Warszawa 1995.

## Computer simulation of the welding process of various materials manufactured using SLM methods

W. Borek <sup>a</sup>, K. Elanany <sup>b</sup>, M. Kremzer <sup>c</sup>, S. Ebied <sup>d</sup>

<sup>a</sup> Silesian University of Technology, Faculty of Mechanical Engineering, Department of Engineering Materials and Biomaterials

email: wojciech.borek@polsl.pl

<sup>b</sup> Student of the Silesian University of Technology, Faculty of Mechanical Engineering, Department of Engineering Materials and Biomaterials

email: ke500594@student.polsl.pl

<sup>c</sup> Silesian University of Technology, Faculty of Mechanical Engineering, Scientific and Didactic Laboratory of Nanotechnology and Material Technologies

email: marek.kremzer@polsl.pl

<sup>d</sup> Tanta University, Faculty of Engineering, Department of Production Engineering and Mechanical Design.

email: saad\_ebied@f-eng.tanta.edu.eg

**Abstract:** In this article, a simulation of an experimental study of the welding process of diverse materials fabricated through Selective Laser Melting (SLM) methods was investigated. The approach involved the application of a constant force side by side with the temperature in the same time to the welding direction. Through simulation using specialized software, the distribution of force and temperature was analysed for three distinct cases, each characterized by different force and temperature parameters. The primary objective of the simulation was to elucidate the temperature, deformation and stress distribution within the welding zone, providing valuable insights into the welding behaviour of the materials under consideration.

**Keywords:** welding, simulation, temperature, deformation, stress

### 1. INTRODUCTION

Tool steels are economically advantageous due to their durability and resistance to wear, reducing the need for frequent replacements and maintenance costs [1]. The global tool steel market was valued at US\$ 9081.9 million in 2023, indicating its significant economic importance. The steel sector, including tool steels, is anticipated to experience a moderate rise in profitability. This is attributed to improving demand and a slight increase in prices, creating a favourable environment for steelmakers. Tool steels excel mechanically, providing high hardness, strength, and resistance to deformation, making them ideal for cutting tools and forming dies. In addition to that, they exhibit excellent thermal stability, maintaining their mechanical properties at elevated temperatures, crucial for applications involving heat-intensive

processes. On the other hand, maraging steels offer economic benefits through their longevity and low-carbon composition, contributing to extended service life and reduced material costs [2]. Also, maraging steel is gaining prominence in the global market, with an anticipated growth trajectory till 2030. They are mechanically robust, combining strength and toughness through precipitation hardening, making them suitable for applications requiring high performance [3]. Additionally, maraging steels show thermal resilience, with their low-carbon martensitic structure enhancing resistance to thermal aging and maintaining strength at elevated temperatures [2].

## 2. TEST MATERIAL AND SAMPLE PREPARATION

Two types of steels are used in this test: H13 Tool Steel and M789 Maraging Steel with a chemical composition presented in Table 1, Table 2, respectively [4] [5]. Two identical samples with a length of 54 mm and a diameter of 6 mm. One sample is prepared from H13 Tool steel and the other one is prepared from M789 Maraging steel. In order for both samples to be securely fixed, 4 grippers, which are made from copper alloy are required. In order to enable temperature measurement and control during the welding process, type K thermocouple wires were welded right next to one of the joined surfaces. Then, the samples were welded using the Gleeble 3800 thermomechanical simulator.

*Table 1. Chemical composition of H13 Tool Steel*

Name	Element Content, [wt.%]									
	Cr	Mo	Si	V	C	Ni	Cu	Mn	P	S
H13 Tool Steel	4.75-5.50	1.10-1.75	0.80-1.20	0.80-1.20	0.32-0.45	0.3	0.25	0.20-0.50	0.03	0.03

*Table 2. Chemical composition of M789 Maraging Steel*

Name	Element Content, [wt.%]									
	Fe	C	Si	Mn	Cr	Mo	Ni	Cu	Ti	Al
M789 Maraging Steel	Bal.	0.01	0.44	0.03	12.25	1.04	10.45	<0.02	1.00	0.62

## 2. SIMULATION PARAMETERS

Using ANSYS software, we have done a Coupled Field Transient Analysis with all required joints and contacts so that we can apply force with temperature in the same time and find out the behavior of the sample during the welding process. In all three tests, the applied force is constant at 2.5 KN and applied to H13 Tool Steel sample, but the temperature is ranging from 900°C to 1100°C. The duration of application of force and temperature may change slightly in the three tests, as shown in Table 3.

Table 3. Simulation parameters

Time	Force (kN)	Temperature (°C)
00:05.00	0.0	10
00:05.00	-1.0	10
01:30.00 for temperature 900°C 01:40.00 for temperature 1000°C 01:50.00 for temperature 1100°C	-2.5	900 or 1000 or 1100
01:00.00	-2.5	900, 1000, 1100
00:10.00	-2.5	20

### 3. RESULTS

After the end of the test, we were able to obtain an illustration of the temperature, deformation, and stress distributions resulting from the welding process at the moment when the largest amount of deformation occurred, as shown in Fig. 1. In order to be able to monitor the change in temperature, deformation, and stress during the test, we were able to obtain a curve showing the distributions of the three parameters over time, which is presented in Fig. 2.

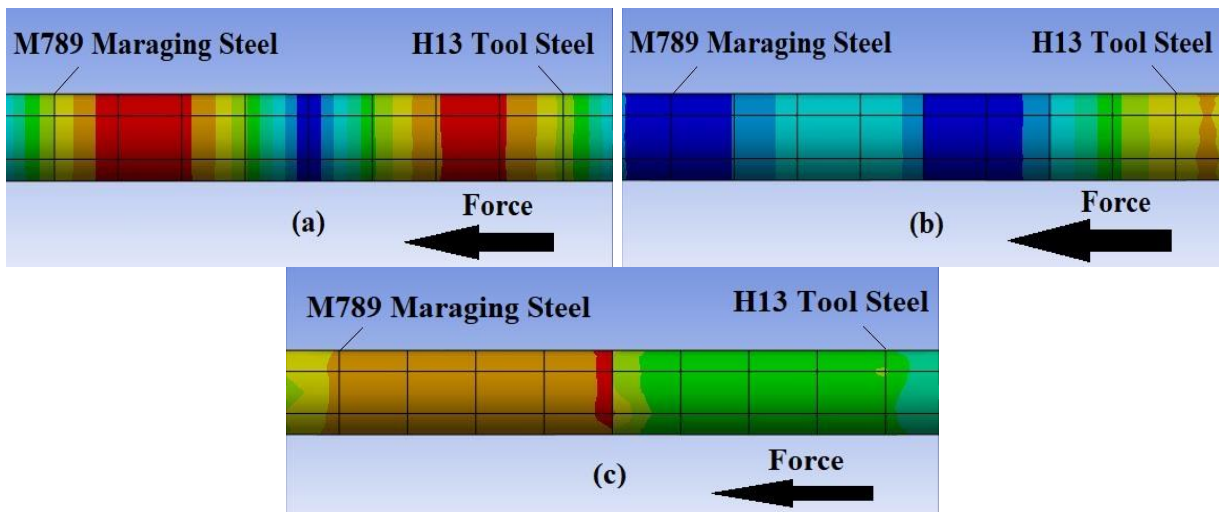


Figure 1. Distributions of deformation zone: (a) Temperature, (b) Deformation, (c) Stress

In addition to that, by the end of the simulation, we managed to find out the maximum values of the three different parameters, as shown in Table 4.

Table 4. Maximum values of simulation parameters

Parameter	Deformation temperature		
	900°C	1000°C	1100°C
Max. Temperature (°C)	903.29	1003.6	1104
Max. Deformation (mm)	0.14	0.16	0.17
Max. Stress (MPa)	3443.4	3835.5	4227.3



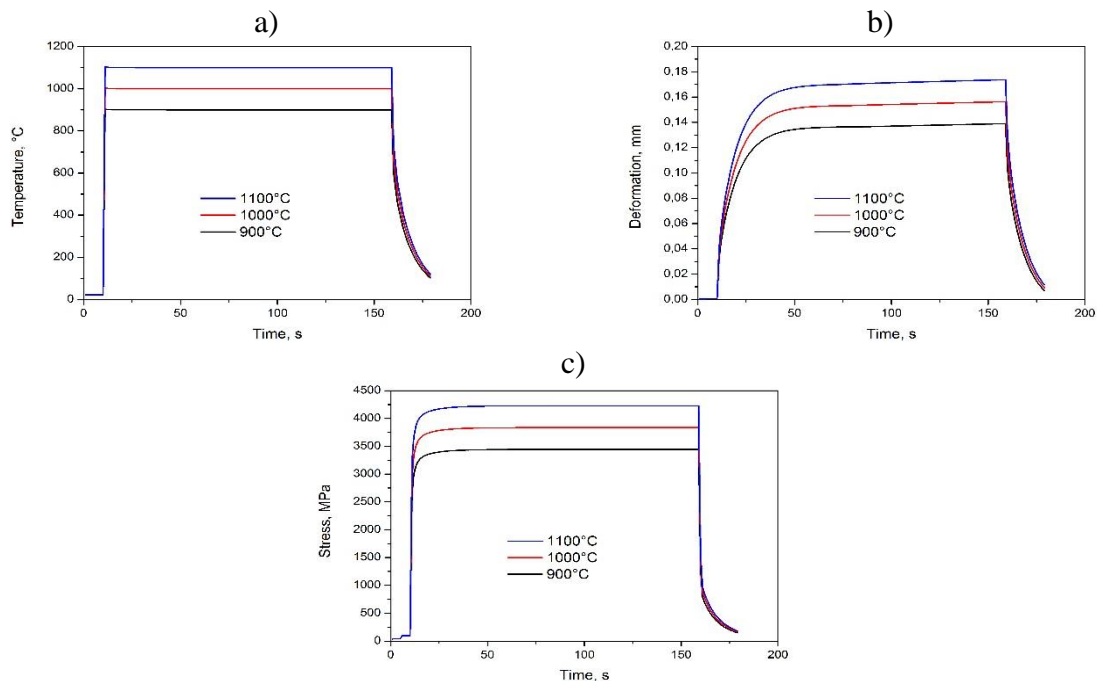


Figure 2. Distributions VS Time: (a) Temperature, (b) Deformation, (c) Stress

#### 4. CONCLUSIONS

The final results of the simulation indicate that the higher the temperature of deformation of the welding process, the greater the deformation and the equivalent stress, which in turn reach their maximum value at the end of the process. This simulation is mandatory as it can be considered as an introduction to real welding test of the samples on the Gleeble 3800 thermo-mechanical simulator. The results obtained allowed us to optimize the process and select the best welding temperature for this type of materials, and depending on our three cases, the temperature of 1100°C was selected in the final tests. Such these simulations enable you to perform several factors such as temperature and force, etc., at the same time and see what effect it will have on the deformation of this type of welded joint in real tests.

#### 5. BIBLIOGRAPHY

- [1] A. HAYES, "Economics Defined with Types, Indicators, and Systems," 31 December 2023. [Online]. Available: <https://www.investopedia.com/terms/e/economics.asp>.
- [2] N. M. W.M. Garrison Jr., "Hydrogen embrittlement of high strength steels," in *Gaseous Hydrogen Embrittlement of Materials in Energy Technologies: The Problem, its Characterisation and Effects on Particular Alloy Classes. Volume 2*, WOODHEAD PUBLISHING, 2012, pp. 421-492.
- [3] M. K. B. Warren M. Garrison, "Martensitic Non-Stainless Steels: High Strength and High Alloy," *ScienceDirect*, 30 November 2015.
- [4] "H13 Tool Steel - Chromium Hot-Work Steels," 10 July 2013. [Online]. Available: <https://www.azom.com/article.aspx?ArticleID=9107>.
- [5] Seung-Chang Han, at all, "Effect of Heat Treatment on Corrosion and Mechanical Properties of M789 Alloy Fabricated Using DED," *Metals*, 29 June 2023.



26th January 2024  
Gliwice, Poland

DEPARTMENT OF ENGINEERING MATERIALS AND BIOMATERIALS  
FACULTY OF MECHANICAL ENGINEERING  
SILESIA UNIVERSITY OF TECHNOLOGY

## INTERNATIONAL STUDENTS SCIENTIFIC CONFERENCE

### Wirtualna symulacja próby lejności odlewniczych materiałów inżynierskich

S. Borowski, R. Dąbrowski, M. Dudzik, R. Honysz<sup>a</sup>

<sup>a</sup> Silesian University of Technology, Faculty of Mechanical Engineering, Department of Engineering Materials and Biomaterials  
email: rafal.honysz@polsl.pl

**Streszczenie:** Przedstawiona w tym artykule symulacja ma zapoznać użytkownika z podstawowymi informacjami na temat próby lejności odlewniczego stopu inżynierskiego, stosowanej w odlewnictwie. Użytkownik wirtualnej symulacji ma możliwość zapoznania się z podstawowymi stopami odlewniczymi, i ich własnościami. Dzięki dostępnym w symulacji opcjom użytkownik może samodzielnie przeprowadzić własną symulację, samodzielnie zbadać lejność wybranych materiałów odlewniczych i zapoznać się z podstawowymi parametrami procesu odlewania.

**Abstract:** The simulation presented in this article is intended to familiarize the user with basic information about the castability test of a casting engineering alloy used in foundry. The user of the virtual simulation has the opportunity to become familiar with the basic casting alloys and their properties. Thanks to the options available in the simulation, the user can independently conduct his own simulation, examine the castability of selected casting materials and become familiar with the basic parameters of the casting process.

**Keywords:** Komputerowa nauka o materiałach, Próba lejności, Odlewanie, Symulacja, Wirtualna rzeczywistość,

### 1. WSTĘP

Przez lejność rozumie się zdolność ciekłego metalu do płynięcia przez kanały układu wlewowego formy odlewniczej, wypełniania jej wnęki i dokładnego odtwarzania jej kształtu (konturów). Na lejność wpływają:

- a) czynniki związane ze składem chemicznym, a więc temperatura początku krzepnięcia, zakres temperatury krzepnięcia, ciepło właściwe, przewodność i pojemność cieplna, gęstość, lepkość, napięcie powierzchniowe, ilość i rodzaj rozpuszczonych w metalu tlenków oraz innych wtrąceń niemetalicznych
- b) czynniki związane z formą odlewniczą, a więc ukształtowanie układu wlewowego i wnęki formy, rodzaj i właściwości materiału formy, jej temperatura i jakość powierzchni itp.,
- c) czynniki związane z warunkami odlewania, a mianowicie temperatura odlewania, stopień przegrzania, szybkość i czas zalewania formy odlewniczej. Z wymienionych czynników

do najistotniejszych zalicza się skład chemiczny, stopień przegrzania i temperaturę zalewania, tj. temperaturę metalu w chwili zalewania do formy odlewniczej.

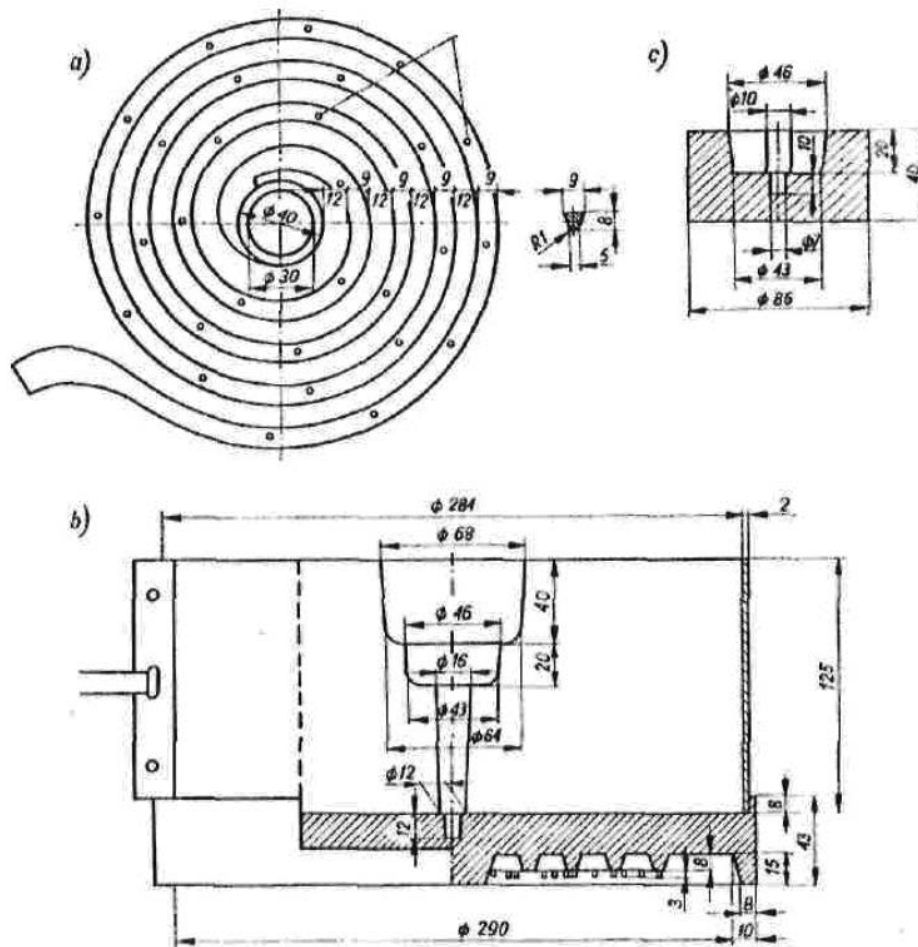
Z wymienionych czynników do najistotniejszych zalicza się skład chemiczny odlewanej materiału, stopień przegrzania i temperaturę zalewania, tj. temperaturę materiału w chwili zalewania do formy odlewniczej. Największy wpływ na lejność materiału odlewanej wywierają węgiel, krzem i fosfor. Ich łączny wpływ można scharakteryzować za pomocą równoważnika węglowego Ce, lub stopnia nasycenia eutektycznego Sc, ze wzrostem których lejność ulega polepszeniu. Ilościowy wpływ składu chemicznego można przedstawić za pomocą tzw. równoważnika lejnościowego węgla

$$Ce,l = C + 0,35 Si + 0,5 P \quad (1)$$

Ze wzoru wynika, że na wartość Ce,l wpływ fosforu jest dwukrotnie, a krzemu trzykrotnie mniejszy od wpływu węgla. Pozostałe pierwiastki występujące w żeliwie, tj. Mn i S są zawarte w ilościach nie wywierających istotnego wpływu na lejność żeliwa. Inne pierwiastki stopowe przejawiają natomiast swój wpływ na lejność poprzez ich wpływ na temperaturę początku krzepnięcia i stopnia przechłodzenia stopu, na tworzenie tlenków i ich błonek, jak również na położenie punktu eutektycznego w stosunku do układu Fe-C. W praktyce wyznaczanie lejności odbywa się za pomocą odpowiednich prób technologicznych, których cechą wspólną jest pomiar długości drogi strugi metalu w kanale o małym przekroju poprzecznym w okresie całkowitej jeszcze ciekłości metalu. Najpowszechniej stosowanym rodzajem próby technologicznej lejności jest próbka typu spiralnego, której kształt zgodnie z BN-80/4051-17 został pokazany na rysunku 1. Schemat i wymiary pokazuje rysunek 2a, model spirali i układ wlewowy pokazuje rysunek 2b, a zbiornik wlewowy wraz z filtrem z jednym otworem wlewowym o średnicy 10 mm pokazuje rysunek 2c [1-6]. Przykładowe spirale powstałe w wyniku przeprowadzonych badań pokazuje rysunek 3.

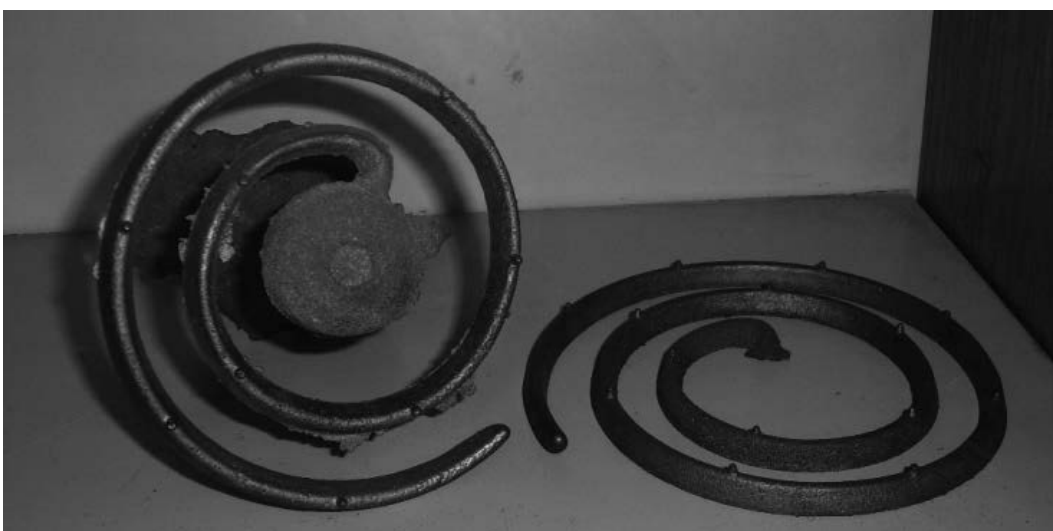


Rysunek 1. Zdjęcie formy do przeprowadzenia próby lejności  
*Figure 1. Photo of the mold for castability testing*



Rysunek 2. Wymiary formy dla próby lejności zgodnie z BN-80/4051-17

Figure 2. Mold dimensions for castability test in accordance with BN-80/4051-17



Rysunek 3. Przykładowe spirale z przeprowadzonych prób lejności

Figure 3. Examples of spirals from conducted castability tests

## 2. PRZEBIEG SYMULACJI

Po uruchomieniu symulacji przechodzimy przez ekran tytułowy klikając w przycisk „ROZPOCZNIJ”. Zostaniemy przeniesieni do okna wyboru materiału do próby lejności. Do wyboru mamy trzy rodzaje materiału

- stop miedzi,
- staliwo,
- żeliwo.

Obok nazw w tabeli znajdują się podstawowe informacje na ich temat. Klikając na sztabkę znajdującą się po prawej stronie ekranu wybieramy materiał. Ekran wyboru materiału został pokazany na rysunku 4.



Rysunek 4. Okno początkowe symulacji umożliwiające wybór materiału

*Figure 4. The initial simulation window for material selection*

Po wybraniu interesującego nas materiału przechodzimy do ekranu wyboru parametrów do przeprowadzenia próby lejności. Ekran wyboru parametrów procesu jest okazany na rysunku 5. W zależności od wybranego materiału możemy tu wybrać temperaturę w której będzie próba przeprowadzana poprzez kliknięcie na przycisk wyboru temperatury, lub przegrzanie materiału, z jakim ma być przeprowadzona próba. Przycisk „START” umożliwia nam przeprowadzenie próby przy użyciu wybranych parametrów.

Jeżeli się pomyliły przy wybieraniu parametrów i chcemy je zmienić możemy kliknąć w przycisk „RESET” i przywrócić ustawienia próby do warunków początkowych, a jeżeli wciśniemy jeszcze raz przycisk „RESET” wtedy wrócimy do ekranu wyboru materiału. Jeżeli chcemy jeszcze raz przeprowadzić próbę przy użyciu tych samych paramentów należy kliknąć w przycisk „POWTÓRZ”. Przycisk „POMOC” umieszczony u góry ekranu umożliwia nam szybki wgląd do opisu przycisków programu i wyjaśni ich działanie. Przycisk w kształcie domku znajdujący się u dołu ekranu pozwala na powrót do początku symulacji.

Po kliknięciu przycisku „START” rozpoczyna się symulowane przeprowadzanie próby lejności. Na wyświetlaczu po lewej stronie oznaczonym „TEMP” mamy podaną temperaturę w stopniach Celsjusza w jakiej jest przeprowadzana próba. Na wyświetlaczu oznaczonym „LEJNOŚĆ” mamy podawany wynik z przeprowadzanej próby w milimetrach. Po prawej stronie ekranu pokazywany jest postęp symulacji.

Na rysunku 6 pokazane są przykładowe ekrany z przeprowadzonych prób lejności dla różnych materiałów.



Rysunek 5. Ekran początkowy wprowadzania parametrów symulacji próby lejności dla wybranego materiału

Figure 5. Initial screen for entering the castability test simulation parameters for the selected material



Rysunek 6. Przykładowe ekrany pokazujące przebieg symulacji próby leżności  
Figure 6. Sample screens showing the course of the material castability test simulation

**BIBLIOGRAFIA**

1. L. A. Dobrzański, Podstawy nauki o materiałach i metaloznawstwo: materiały inżynierskie z podstawami projektowania materiałowego, Wydawnictwo Naukowo-Techniczne WNT 2006,
2. R. Honysz, L. A. Dobrzański, Virtual laboratory methodology in scientific researches and education, *Journal of Achievements in Materials and Manufacturing Engineering*, 84/2, (2017), 76-84.
3. *Odlewnictwo Współczesne Poradnik Odlewnika*, Pod redakcją Jerzego J. Sobczaka, Wydawnictwo Stowarzyszenia Technicznego Odlewników Polskich, 2013
4. Badania technologiczne żeliwa - Próba lejności BN-80/4051-17 = [https://www.europeana.eu/pl/item/0940444/\\_nn8W6xW](https://www.europeana.eu/pl/item/0940444/_nn8W6xW)
5. Z. Pirowski, S. Pysz, Computer simulation of castability trials, *Journal of Research and Applications in Agricultural Engineering*, 2013, Vol. 58(1), 151.
6. T. Wachelkc, M. S. Soiński, Porównanie wyników próby lejności zmodyfikowana metodą spirali i metodą zasysania, Instytut Technologii Metali Politechniki Częstochowskiej, 1975.





26th January 2024  
Gliwice, Poland

DEPARTMENT OF ENGINEERING MATERIALS AND BIOMATERIALS  
FACULTY OF MECHANICAL ENGINEERING  
SILESIA UNIVERSITY OF TECHNOLOGY

## INTERNATIONAL STUDENTS SCIENTIFIC CONFERENCE

### Co-sensitization of titanium dioxide layers for photovoltaic applications with dyes

J. Budzynowski<sup>a</sup>, K. Tyczyński<sup>a</sup>, S. Bielec<sup>a</sup>, J. Sobolewski<sup>b</sup>, A. Drygala<sup>c</sup>, J. Wyrwał<sup>d</sup>, S. Leszc<sup>e</sup>, E. Tillová<sup>e</sup>, P. Palček<sup>e</sup>

<sup>a</sup> Student, Silesian University of Technology, Faculty of Mechanical Engineering, Konarskiego 18a Str., 44-100 Gliwice, Poland

<sup>b</sup> Student, Silesian University of Technology, Faculty of Automatic Control, Electronics and Computer Science, Akademicka 16 Str., 44-100 Gliwice, Poland

<sup>c</sup> Silesian University of Technology, Faculty of Mechanical Engineering, Department of Engineering Materials and Biomaterials, Konarskiego 18a Str., 44-100 Gliwice, Poland

<sup>d</sup> Silesian University of Technology, Faculty of Automatic Control, Electronics and Computer Science, Department of Measurements and Control Systems, Akademicka 16 Str., 44-100 Gliwice, Poland

<sup>e</sup> University of Zilina, Faculty of Mechanical Engineering, Department of Materials Engineering, Univerzitná 1 Str., 010 26 Zilina, Slovak Republic  
email: aleksandra.drygala@polsl.pl

**Abstract:** Dye is one of the most important components of dye-sensitized solar cell (DSSC) whose photoabsorption properties are directly related to device effectiveness. It can produce higher efficiency if covers a broad range of light spectrum. In this work, the influence of titanium dioxide co-sensitization with N719 and N749 dyes on the optical properties of the deposited layers and the electrical properties of the produced dye-sensitized solar cells was determined.

**Keywords:** dye-sensitized solar cells, photoanode, titanium dioxide, co-sensitization, N749 black dye, N719 dye

## 1. INTRODUCTION

Given the current state and degradation of the natural environment, the use of alternative energy sources has become a necessary condition in today's times. According to the latest analysis (2021) from the Central Statistical Office, the consumption of solar energy by photovoltaic devices in 2021 was 23.8 times higher compared to 2017 [1]. This indicates a growing interest in this technology, and consequently, in dye-sensitized solar cells (DSSCs) [2].

DSSCs belong to the third generation of solar cells and consist of a photoanode, cathode, and electrolyte. The substrate for the photoanode and cathode is a glass plate onto which a thin layer of conductive fluorine-doped tin oxide (FTO) is applied. The cathode, also known as the counter electrode, catalyses the reduction reactions of the redox mediator in the electrolyte,

enabling the regeneration of the dye. It is made of materials with high conductivity of electric charges, characterized by chemical stability and corrosion resistance. Platinum is the most commonly used catalytic material. On the other hand, the photoanode, responsible for absorbing photons and transporting electrons, consists of a nanocrystalline semiconductor layer (usually  $\text{TiO}_2$  or  $\text{ZnO}$ ) coated with a photosensitive dye. The space between the photoanode and the cathode is filled with an electrolyte containing a redox couple  $I^-/I_3^-$ . Under the influence of radiation, electrons in the dye are excited from the ground state and transferred to the conduction band of the semiconductor. Subsequently, they move to the FTO conductive layer. Through the external circuit of the DSSC, electrons flow to the cathode and are transferred to the  $I_3^-$  ion in the electrolyte, reducing it to form  $I^-$ . The  $I^-$  ion reduces the excited state of dye molecules and is oxidized back to  $I_3^-$  [2-5].

Appropriate selection of sensitizer responsible for absorbing solar radiation enables achieving high efficiency of DSSCs. The dye should possess light absorption ability in the whole visible spectrum as well as in the ultraviolet and near-infrared regions. The dye's energy levels should maintain the correct match with the energy levels of the metal oxide and the electrolyte [6,7]:

- LUMO (lowest unoccupied molecular orbital) of dye must be higher than the conduction band edge of metal oxide,
- HOMO (highest occupied molecular orbital) of the dye must be lower than the HOMO level of the electrolyte.

The dye should be stable both in its ground state and the excited state. There must be some anchoring groups in the photosensitizer to guarantee that the dye is adsorbed on the surface of semiconductor nanoparticles [6-8].

Dye-sensitized solar cells use:

- dyes with metal complexes - the most commonly used dyes from this group are ruthenium complexes, e.g. *cis*-bis(isothiocyanato)bis(2,2'-bipyridyl-4,4'-dicarboxylato) ruthenium (II) marked as N3 and its tetrabutyl ammonium salt, referred to as N719 due to their effective charge transfer and absorption of light in the entire visible range. These substances are expensive due to the synthesis time and the difficulty of the purification process. Recent record DSSCs efficiencies of over 11.9 % were documented using dye N719 [9-11].
- organic dyes devoid of metal complexes, which include, among others, squaraine, cyanine, merocyanine, and hemicyanine dyes. They are characterized by high absorption for visible light and near-infrared (NIR), so they can be used for co-sensitization DSSCs. In addition, they are much cheaper than dyes with metal complexes, their molar absorption coefficient is high, and the redox reaction is easy to control. DSSCs using one of the above sensitizers have an efficiency of 5 to 9% [9, 10].
- natural dyes, which are divided into four groups: chlorophylls, anthocyanins, carotenoids, and betalains. They are obtained from plants, e.g. leaves, fruits, inflorescences, or tubers. To obtain them, the chemical synthesis used in synthetic dyes is replaced by a simple extraction process. Obtaining them is much easier and cheaper, and naturally occurring dyes do not pose a threat to the environment. Nevertheless, the efficiency of DSSCs does not exceed 1.5% [6,9-12].

Various attempts have been made to improve the efficiency of DSSCs, including the use of different sensitizers. Among them, co-sensitization with multiple dyes seems to be a promising method to enhance their effectiveness due to the possibility of expanding the absorption spectrum. The drawback of using a single sensitizer is the inability to utilize photons from the

near-infrared (NIR) or visible light range. Through co-sensitization, it is possible to create a DSSC photoanode containing two or more different dyes with complementary optical absorption properties. Co-sensitization ensures higher light-harvesting efficiency and minimizes energy losses resulting from the recombination of electrons and holes, thereby increasing the ability to passivate the TiO<sub>2</sub> surface. There are two main methods of co-sensitizing DSSCs [13,14]:

- cocktail method,
- sequential dyeing.

The first one involves dissolving two different dyes in the same solvent and then sensitizing the photoanode in their mixture. This method is less frequently used due to the different densities of dyes and the variety of solvents, which makes uniform sensitization of the photoanode much more difficult. Sequential dyeing is based on immersing the substrate with a printed TiO<sub>2</sub> layer in one solution and then, after a specified time, in another one. This is the most frequently used method for co-sensitization of DSSCs due to the greater possibility of controlling the sensitizer concentration and the use of dyes soluble in various substances [13-16].

In this work, two types of dyes, N719 and N749, were used for co-sensitization of titanium dioxide. N719 dye (Di-tetrabutylammonium cis-bis(isothiocyanato)bis(2,2'-bipyridyl-4,4'-dicarboxylato) ruthenium (II)) is one of the most commonly used dyes in the production of DSSC photoanode. It is caused by the wide absorption spectrum of visible light (maximum absorption occurs for wavelengths 313, 393, and 534 nm) [16], fast generation of electron-hole pairs, good and stable adhesion to titanium dioxide, and facility in dissolution (the most commonly used solvent is ethanol). Moreover, dye-sensitized solar cells using the N719 dye exhibit higher efficiency and more stable operation compared to DSSCs sensitized with the "twin" N3 dye [18, 19].

To extend the absorption of solar radiation towards longer wavelengths by DSSCs, N749 black dye was used for co-sensitization. N749 black dye (Ruthenizer 620-1H3TBA, triisothiocyanato-(2,2':6',6''-terpyridyl-4,4',4''-tricarboxylato) ruthenium (II) tris(tetrabutylammonium)) belongs to the dye family with ruthenium complexes. It is known for the high efficiency of TiO<sub>2</sub> photosensitization in a wide range of wavelengths up to ~920nm. This sensitizer is used to prepare dyeing solutions (usually with ethanol 0.35mM), so it can be used for co-sensitization with the cocktail method together with the N719 dye due to the same solvent. It is chemically and physically stable in various environmental conditions, thanks to which DSSCs with this dye achieve an efficiency of 9.1% [20,21]. In this work, the influence of titanium dioxide co-sensitization with N719 and N749 dyes on the optical properties of the deposited layers and the electrical properties of the produced dye-sensitized solar cells was determined.

## 2. MATERIALS AND METHODS

In the present work, the dye-sensitized solar cells in a structure of glass/TiO<sub>2</sub>/dye/electrolyte/platinum/ glass were produced. Materials were purchased from:

- Sigma Aldrich - FTO coated glass, platinum paste, EL-HPE high performance electrolyte,
- Greatcell – titanium dioxide paste,
- Solaronix - N719 and N749 dyes.

Fluorine doped tin oxide coated glass with a resistivity of 7 Ω/sq and a surface area of 25x25mm was used as the substrate.

Two solutions of the individual dyes and one solution of the dye mixture in ethanol were

prepared at the following concentrations: 0.35 mM N719, 0.35 mM N749, 0.35 mM N719, and 0.35 mM N749 (in the volume ratio of 1:1). Both the cocktail and sequential methods of sensitizing the DSSCs photoanode were used. Depending on the type of co-sensitization, three photoanodes were prepared:

- cocktail method – the electrode was sensitized in a mixture of dyes N719 and N749 for 24h,
- sequential method – the electrode was first sensitized in N719 dye for 12h and then in N749 dye for 12h,
- sequential method – the electrode was first sensitized in N749 dye for 12h and then in N719 dye for 12h.

In addition, two reference photoanodes were prepared, each sensitized in individual dyes, the first one in N719 for 24 h and the second one in N749 for 24 h.

The absorbance of produced photoanodes was measured by Thermo Scientific Evolution 220 spectrophotometer in the wavelength range from 190 nm to 850 nm. The dye-sensitized solar cells were characterized by their illuminated I-V characteristic under AM 1.5 solar radiation spectrum and 1000 W/m<sup>2</sup> irradiance. For each DSSC, ten measurements of current-voltage characteristics were made.

### 3. RESULTS

Figure 1 presents the dependence of light absorption on wavelength for TiO<sub>2</sub> layers deposited on FTO-coated glass sensitized with various dyes and methods. It was observed that the highest light absorption for the generated photoanodes occurs for ultraviolet radiation. When considering the visible radiation range, electrodes with adsorbed single dyes N719 and N749 absorbed the most light in the ranges from 460 to 582 nm and above 615 nm, respectively.

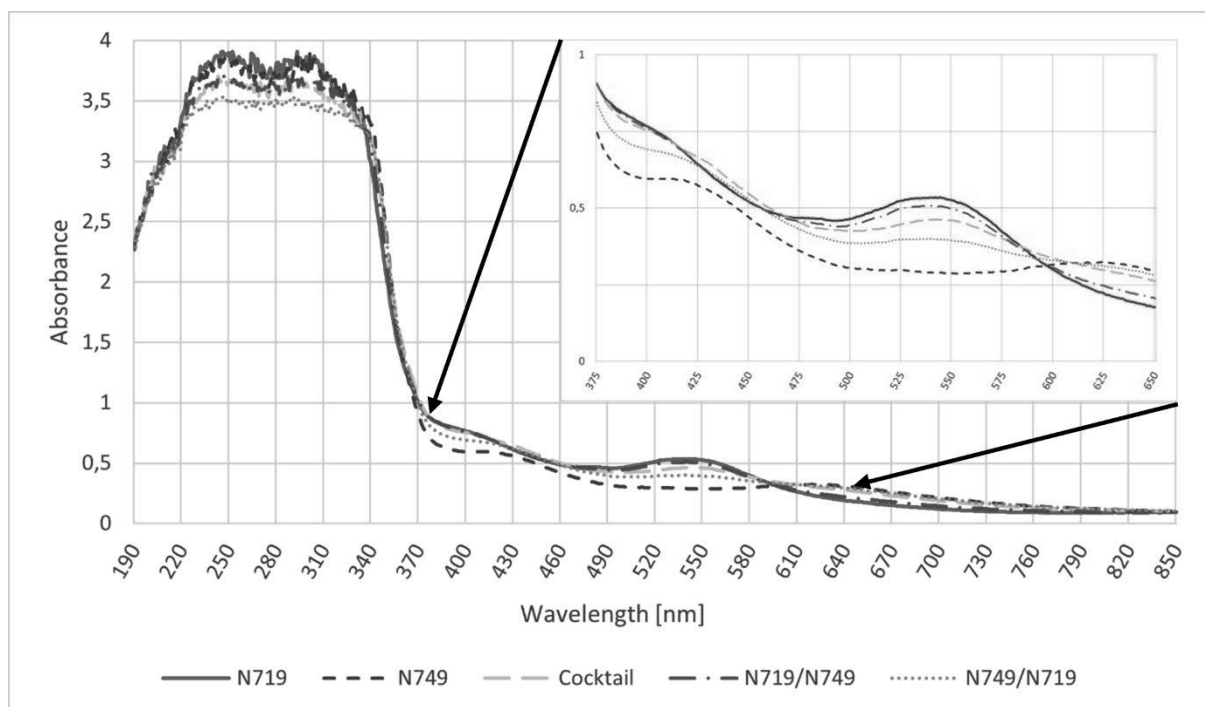


Figure 1. UV-Vis spectra of dye-sensitized photoanodes in various configurations

In the range of 368-593 nm, all co-sensitized photoanodes achieved higher absorption compared to the electrode sensitized only with the N749 dye. However, in the range of 610-850 nm, their light absorption is higher than that of the photoanode sensitized with the N719 dye. It was observed that the absorption for the photoanode sensitized with a mixture of dyes in the ranges of 368 to 582 nm and 582 to 850 nm is similar to the absorption of electrodes containing the N719 and N749 dyes in their structure, respectively. The curve shape for the photoanode dyed sequentially with N719/N749 throughout the entire wavelength range is comparable to the curve for the anode that used the N719 dye. Meanwhile, the electrode sensitized first with the N749 dye and then with N719 absorbs more light in the range of 370-610 nm compared to the photoanode sensitized with N749.

Based on the measured current-voltage characteristics (Figure 2), the electrical properties of DSSCs sensitized with dyes in different configurations were determined. Short-circuit current ( $I_{sc}$ ), open-circuit voltage ( $V_{oc}$ ), fill factor (FF), and efficiency ( $E_{ff}$ ) are compiled in Table 1. It was observed that co-sensitized solar cells exhibit a higher fill factor compared to devices sensitized with a single dye. Its value is 0.57, 0.55, and 0.57, respectively, for cocktail co-sensitization, N719/N749, and N749/N719 co-sensitization. Additionally, the sequentially dyed N719/N749 solar cell shows the highest efficiency (4.52%) and short-circuit current (5.07 mA). In the range of 0-480mV, the N719/749-sensitized DSSC is characterized by the highest current, while the highest open-circuit voltage is obtained for the device with a photoanode sensitized with the N719 dye. The DSSC with an electrode sensitized with a single N749 dye exhibits the lowest electrical properties.

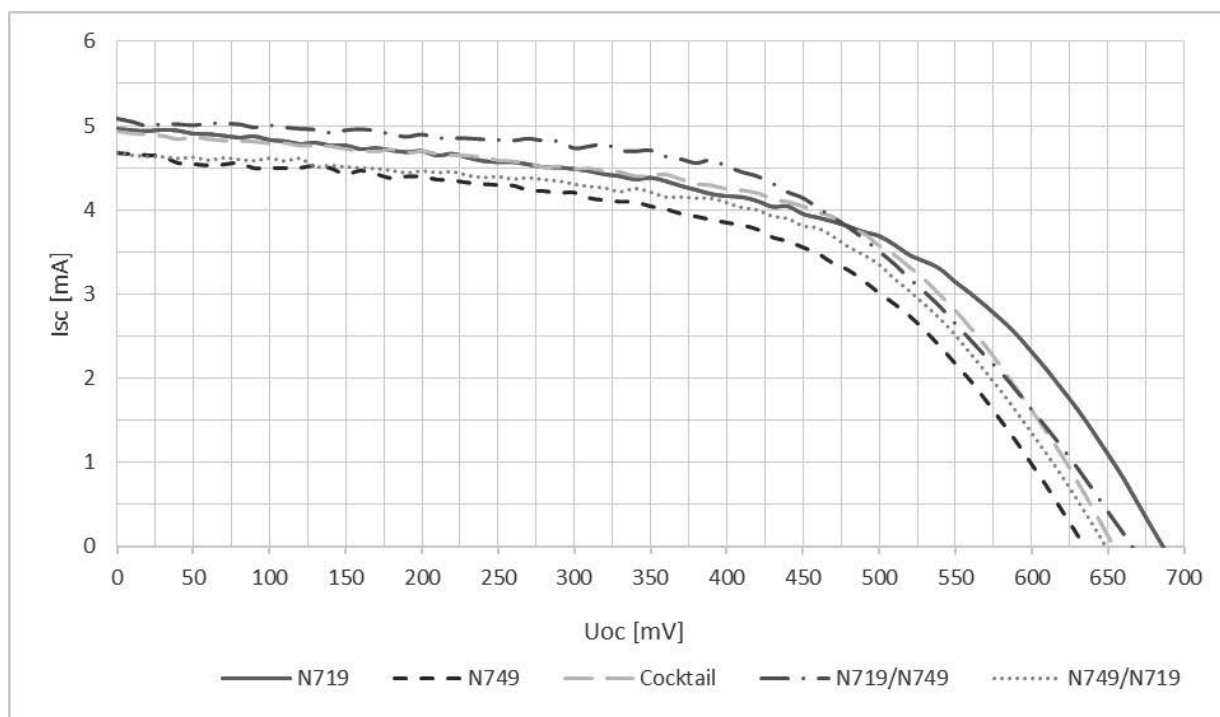


Figure 2. Current-voltage characteristics of solar cells based on dye-sensitized photoanodes in various configurations

Table 1. Electrical properties of solar cells based on dye-sensitized photoanodes in various configurations

	<b>I<sub>sc</sub> [mA]</b>	<b>V<sub>oc</sub> [mV]</b>	<b>FF [-]</b>	<b>E<sub>ff</sub> [%]</b>
<b>N719</b>	5.04	682.17	0.53	4.36
<b>N749</b>	4.66	634.44	0.54	3.89
<b>Cocktail</b>	4.94	652.81	0.57	4.42
<b>N719/N749</b>	5.07	668.83	0.55	4.52
<b>N749/N719</b>	4.70	648.59	0.57	4.19

#### 4. CONCLUSIONS

Photovoltaics is one of the most promising and environment friendly sources of energy. It does not generate noise, or vibrations, and, most importantly, does not emit toxic gases. Third-generation solar cells are still in the research phase, with results indicating significant potential. Various attempts are being made to improve the efficiency of solar cells. In this study, co-sensitization with N719 and N749 dyes was applied in different configurations on the photoanode of the dye-sensitized solar cells. Based on the conducted research, it was found that the highest efficiency was achieved for the DSSC with a sequentially dyed N719/N749 photoanode. Its efficiency is 0.10 and 0.16 percentage points higher compared to DSSCs dyed with cocktails and a single N719 dye, respectively. The differences in efficiency are not significant, hence the obtained research results serve as a basis for further work in this area.

#### ACKNOWLEDGMENTS

The work was created as a result of the project PBL (Project Based Learning) - 10th edition – of the Excellence Initiative - Research University, Silesian University of Technology.

#### BIBLIOGRAPHY

1. G. Berent-Kowalska, A. Jurgaś, J. Kacprowska, I. Moskal, K. Kapica, Energia ze źródeł odnawialnych w 2021 r., Analizy Statystyczne, Główny Urząd Statystyczny, Warszawa, 2022.
2. K. Siuzdak, M. Klein, K. Łapiński, A. Cenian, Barwnikowe ogniwa słoneczne, Rynek energii 5 (2015) 75-83.
3. M. Klein, W. Stampor, Barwnikowe ogniwa słoneczne, Instrukcja do ćwiczenia laboratoryjnego, Politechnika Gdańska, Gdańsk, 2016.
4. K. Barczak et al., Wpływ grubości warstwy półprzewodnikowej na własności optoelektryczne barwnikowych ogniw fotowoltaicznych, TalentDetector2023\_Summer: International Students Scientific Conference, Brenna, Poland, 26th June 2023, Bonek

- Mirosław (*red.*), Prace Katedry Materiałów Inżynierskich i Biomedycznych, 2023, Gliwice, Politechnika Śląska, (2023) 41-48.
5. D. Czutył et al., Obserwacje makro- i mikroskopowe fotoanody barwnikowego ogniwa słonecznego, TalentDetector2023\_Summer: International Students Scientific Conference, Brenna, Poland, 26th June 2023, Bonek Mirosław (*red.*), Prace Katedry Materiałów Inżynierskich i Biomedycznych, 2023, Gliwice, Politechnika Śląska, (2023) 184-192.
  6. K. Siuzdak, Energia elektryczna z kwiatów – ogniwa fotowoltaiczne wykorzystujące naturalne barwniki, Fizyka w szkole 1 (2014) 29-34.
  7. A. Sen M.H. Putra, A.K. Biswas, A.K. Behera, A. Groß, Insight on the choice of sensitizers/dyes for dye sensitized solar cells: A review, Dyes and Pigments 213 (2023) 111087.
  8. A.S. Najm, SA. Alwash, N.H. Sulaiman, M. S. Chowdhury, K. Techato, N719 dye as a sensitizer for dye-sensitized solar cells (DSSCs): A review of its functions and certain rudimentary principles, Environmental Progress and Sustainable Energy (2023); 42: e13955.
  9. S. Rahman et al., Research on dye sensitized solar cells: recent advancement toward the various constituents of dye sensitized solar cells for efficiency enhancement and future prospects, RSC Advances 13 (2023) 19508-19529.
  10. S. Kaliramna et al., A review and comparative analysis of different types of dyes for applications in dye-sensitized solar cells, Brazilian Journal of Physics 52 (2022).
  11. C.A. Peñuelas et al., Synthesis of a new dinuclear Cu(I) complex with a triazine ligand and diphenylphosphine methane: X-ray structure, optical properties, DFT calculations, and application in DSSCs, Inorganics 11 (2023) 376.
  12. O. Adedokun, K. Titilope, A.O. Awodugba, Review on natural dye-sensitized solar cells (DSSCs), International Journal of Engineering Technologies IJET, 2 (2016) 34-41.
  13. D. Kharkwal, N. Shrama, S.K. Gupta, C.M.S. Negi, Enhanced performance of dye-sensitized solar cells by co-sensitization of metal-complex and organic dye, Solar Energy 230 (2021) 1133-1140.
  14. S. Ananthakumar et al., Role of co-sensitization in dye-sensitized and quantum dot-sensitized solar cells, SN Applied Sciences 1 (2019).
  15. Y. Ooyama et al., A new co-sensitization method employing D- $\pi$ -A dye with pyridyl group and D- $\pi$ -Cat dye with catechol unit for dye-sensitized solar cells, Dyes and Pigments 122 (2015) 40-45.
  16. S. Reddy, A. Sambandam, M. Ashokkumar, Cosensitization strategies for dye-sensitized solar cells, Rational Design of Solar Cells for Efficient Solar Energy Conversion (2018) 15-60.
  17. N719 dye, Sigma-Aldrich, <https://www.sigmaaldrich.com/PL/pl/product/aldrich/703214>, 2023
  18. G. Shrama et al, Revealing the photophysics of N719 dye based dye-sensitized solar cell, Optical Materials 142 (2023) 114113.
  19. N719 dye, Greatcellenergy, <https://www.greatcellenergy.com/materials/n719>, 2023.
  20. Ruthenizer 620-1H3TBA, Solaronix, [https://www.solaronix.com/notes/Note\\_Ruthenizer\\_620-1H3TBA.pdf](https://www.solaronix.com/notes/Note_Ruthenizer_620-1H3TBA.pdf), 2023.
  21. M. Tahir et al, Thin films characterization and study of N749-black dye for photovoltaic applications, Coatings 12/8 (2022) 1163.



26th January 2024  
Gliwice, Poland

DEPARTMENT OF ENGINEERING MATERIALS AND BIOMATERIALS  
FACULTY OF MECHANICAL ENGINEERING  
SILESIA UNIVERSITY OF TECHNOLOGY

## INTERNATIONAL STUDENTS SCIENTIFIC CONFERENCE

### The application of surface layers in the construction of photovoltaic cells

P. Bułka<sup>a</sup>, G. Latacz<sup>b</sup>, D. Pakuła<sup>c</sup>, M. Staszuk<sup>c</sup>

<sup>a</sup> Silesian University of Technology, Faculty of Automatic Control, Electronics, and Computer Science

email: piotbul246@student.polsl.pl

<sup>b</sup> Silesian University of Technology, Faculty of Mechanical Engineering and Technology

email: grzelat830@student.polsl.pl

<sup>c</sup> Silesian University of Technology, Faculty of Mechanical Engineering and Technology, Department of Engineering and Biomedical Materials

email: daniel.pakuła@polsl.pl , marcin.staszuk@polsl.pl

**Abstract:** The article provides a description and analysis of the structures and surface layers present in the construction of silicon solar cells, along with a comparison of methods used to obtain the required types of surface layers.

**Keywords:** Monocrystalline silicon, polycrystalline silicon, front and rear electrodes, surface layers, PVD (Physical Vapor Deposition), ALD (Atomic Layer Deposition), texturization, screen printing

## 1. INTRODUCTION

The technology of photovoltaic cells has been advancing for many years, leading to the development of cells with increasingly higher efficiency. Surface layers are one of the essential components of photovoltaic cells construction. They are crucial for the functioning of cells, and their improvement contributes to enhancing the functional properties of cells [1].

Currently, the market is dominated by cells produced using polycrystalline and monocrystalline silicon. Monocrystalline cells show higher efficiency (20%-22%) compared to the efficiency of polycrystalline cells (16%-18%) [2].

## 2. TYPES OF PHOTOVOLTAIC CELLS

Silicon solar cells consist of the following elements [3]:

- silicon wafer with a formed p-n junction, which can have a monocrystalline or polycrystalline structure and a textured surface,
- electrical contacts (both back and front electrodes),



- passivation layer,
- anti-reflective layer.

Monocrystalline cells - this type of cell is based on the utilization of a monocrystalline silicon crystal. Additionally, selective layers are applied with the purpose of filtering the light spectrum and transmitting desired wavelengths. These operations aim to reduce losses in the form of reflected radiation energy [3].

Polycrystalline cells - are more economical alternative to monocrystalline silicon cells. They are produced from silicon blocks, and typically have lower efficiency in comparison to monocrystalline cells (up to 6 percentage points less), but they are significantly more cost-effective [3,4].

Thin-film cells - are considerably cheaper to produce than typical silicon cells, due to the reduced use of production materials, which also impacts the weight of the panels. These cells are manufactured using amorphous silicon [5].

### 3. STRUCTURE OF PHOTOVOLTAIC CELLS

Currently majority of utilized photovoltaic cells are silicon-based [6]. The construction scheme of a silicon photovoltaic cell is presented below (*Figure 1*).

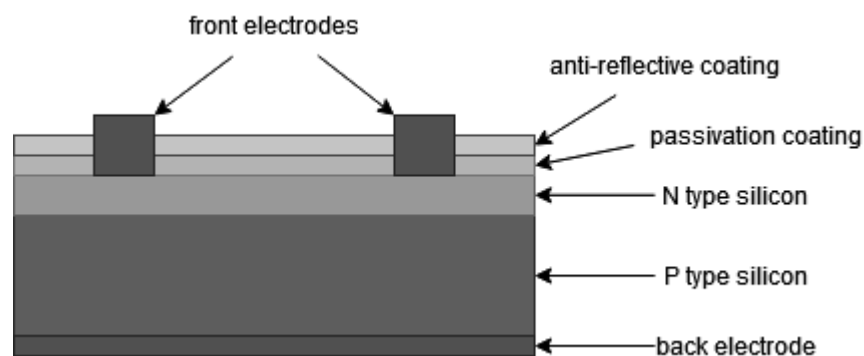


*Figure 1* Diagram of the structure of a silicon-based photovoltaic cell [7]

In the construction of a photovoltaic cell, individual components can be distinguished [2]:

- back electrode,
- P-type silicon,
- N type silicon,
- passivation layer,
- anti-reflective layer,
- front electrodes.

N-type silicon is a doped semiconductor material where the carriers of energy are electrons. On the other hand, P-type silicon is a semiconductor material with hole conductivity [2]. At the junction of N-type silicon and P-type silicon, a semiconductor p-n junction is formed. This junction enables the the photovoltaic effect to occur, which means generating current under the influence of incident light [2].

The front and rear electrodes allow the collection of the charge generated by the semiconductor p-n junction to power an external circuit. The front electrode should cover the

surface of the cell as little as possible to minimize the obstruction of light energy reaching the p-n junction [2].

#### 4. SURFACE LAYERS IN THE CONSTRUCTION OF PHOTOVOLTAIC CELLS

##### Passivation layer

This coating is designed to prevent processes that decrease the efficiency of converting light into electrical energy by photovoltaic cells. Passivation layers are applied to either the front or rear surface of the cell. The most popular solution involves a passivation layer located between the electrode and the silicon layer [8,9]. These layers are commonly made from chemical compounds such as silicon oxides and aluminum [10].

##### Anti-reflective layer

Reflection of light from the surface of the cell layer reduces the amount of light reaching the active layer. To minimize the impact of this phenomenon anti-reflective layers are applied to the cells. These layers are typically applied to the top layers of the cells [9].

Additionally, this layer serves the function of protecting the cell from contamination during the electrodes firing process. The anti-reflective layer is most commonly made from titanium dioxide, silicon nitride, tin oxide, zinc sulfide, magnesium fluoride, or tantalum oxide [9].

##### Types of coatings based on composition

Various types of coatings are used in the production of photovoltaic cells. These coatings can also be categorized based on the chemical compounds from which they are made. The mentioned layers can be divided into [7]:

- oxide coatings – anti-reflective (silicon dioxide  $\text{SiO}_2$ , titanium dioxide  $\text{TiO}_2$ ), electron-conducting (zinc oxide  $\text{ZnO}$ ), protective (aluminum oxide  $\text{Al}_2\text{O}_3$ ),
- nitride coatings – anti-reflective (silicon nitride  $\text{Si}_3\text{N}_4$ , titanium nitride  $\text{TiN}$ ),
- metallic coatings – electrode materials (aluminum, copper, silver, gold),
- organic coatings – active layers (semiconductor polymers, organic dye-sensitized solar cells – DSSC).

##### PVD

The technological process of PVD (Physical Vapor Deposition) allows for the deposition of thin films onto various materials using material vapors in a gaseous phase. This process is widely used in the industry and in the production of photovoltaic cells [11].

The PVD process is divided into [11]:

- evaporation - the first stage of the process involves using high temperatures to generate material vapors, which can be achieved, for example, by using an electric arc,
- transport and deposition - material vapors are transported to the area where deposition is intended on the target surface, where material particles condense, forming a thin layer on the substrate,
- layer deposition - a thin film is formed, the thickness of which can be controlled and adjusted according to the application's requirements. This process is conducted in a vacuum, eliminating the influence of external factors on the quality of the layer.

Layers produced in the PVD process include [11]:

- anti-reflective layers - by depositing thin dielectric layers on the surface of photovoltaic cells, energy losses caused by light reflection can be minimized,
- conductive layers - the PVD process allows for the deposition of conductive layers, such as copper layers, which benefit the efficient collection of current generated in photovoltaic cells,
- protective layers - adding protective layers can safeguard photovoltaic cells from external factors such as moisture, corrosion, or UV radiation, therefore extending the lifespan of the cells.

### **ALD**

ALD (Atomic Layer Deposition) is a method of chemical deposition from the gaseous phase. It has a pulsating character, meaning that at any given time, only one precursor, serving as the source for at least one component of the deposited material, is present in the working chamber. Additionally, the dosing of individual precursors is separated by rinsing the working chamber, often using argon or another inert gas. The ALD process can be divided into cycles, and in the case of using two precursors, it proceeds as follows [12]:

- placement of the first precursor,
- rinsing with argon or another inert gas,
- introduction of the second precursor,
- repeat rinsing with an inert gas.

ALD is a time-consuming method, but the quality of the deposited layers and the versatility of the used materials compensate for this inconvenience. Coatings produced using the ALD method have very good quality, low porosity, and good conformality [12]. ALD operates over a wide temperature range, from 25°C to even 500°C, allowing for coating deposition on materials resistant to high temperatures. Therefore, ALD is ideal for applying anti-reflective coatings on silicon cells [12].

### **Applying electrodes to photovoltaic cells using the screen-printing method**

The deposition of the front and rear electrodes, known as metallization, is carried out using methods such as screen printing, vacuum evaporation, chemical deposition, or Selective Laser Sintering (SLS) [13]. However, screen printing is the cheapest and most commonly used method [14].

Electrodes are made of materials with low electrical resistance and good mechanical properties. To achieve these characteristics, silver, aluminum, or copper pastes are commonly used. In the case of screen printing, the printing is achieved by forcing the ink through a mesh with a specific pattern, providing a durable deposition method. The paste is applied to the screen and then spread across the entire surface of the mesh using a squeegee [14].

### **Surface texturing of the silicon solar cells**

To further improve the efficiency of photovoltaic cells, a process called surface texturing is applied to the active (front) surface of the cell [8]. This process involves modifying the microstructure of the surface to minimize light reflection from the cell's surface (*Figure 2*).

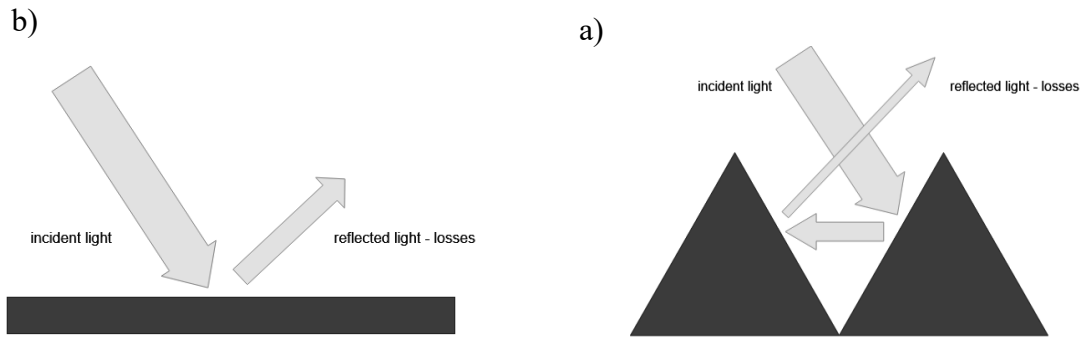


Figure 2 The amount of light reflected from: a) a flat surface b) a textured surface

Surface texturing is carried out using various techniques [15]:

- chemical texturing involves applying acids or bases to the surface of photovoltaic cells, causing corrosion and creating microstructures on the surface,
- mechanical texturing is achieved by employing mechanical surface treatment processes, such as sandblasting,
- laser texturing involves using a laser to precisely apply micro-protrusions or micro-grooves on the surface of photovoltaic cells,
- plasma texturing utilizes a gas plasma to modify the surface structure of cells.

As a result of the described process, a pyramidal structure is formed on the surface of silicon (Figure 3), enhancing the efficiency of the conversion of light energy into electrical energy [15].

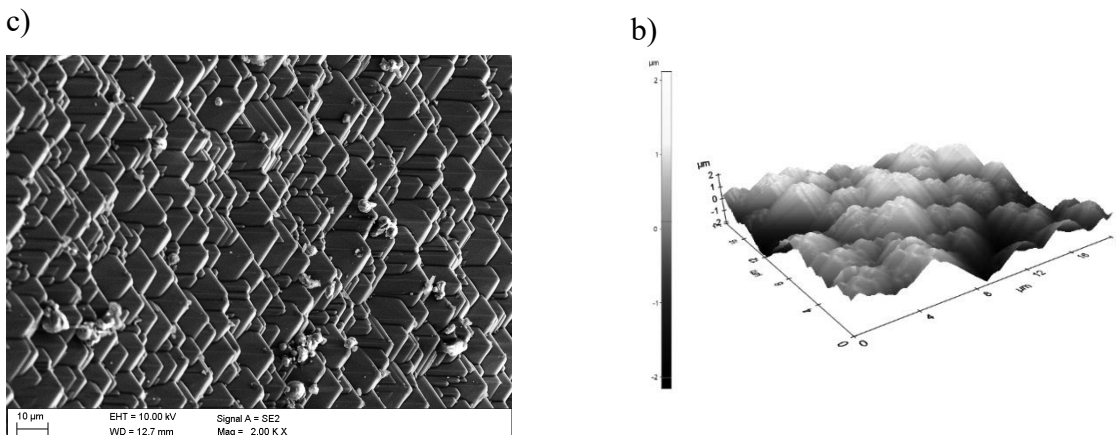


Figure 3 Topography of monocrystalline silicon surface subjected to the texturing process: a) obtained using SEM [16] b) obtained using AFM [17]

## ACKNOWLEDGEMENT

This work was produced as part of the project implemented within the framework of project-oriented education – PBL, in the X competition under the Excellence Initiative – Research University program, at the Silesian University of Technology.

## **BIBLIOGRAPHY**

1. H. Hoppe, N. Serdar Sariciftci, Organic solar cells: An overview, Linz Institute for Organic Solar Cells, 2004
2. K. Siuzdak, M. Klein, M. Szkoda, Badania i rozwój technologii ogniw PV, Czysta Energia, nr 2, 2014
3. W. Zientarski, R. Figura, Analiza pracy modułu fotowoltaicznego, Wydawnictwo Instytut Naukowo-Wydawczy „SPATIUM”, 2016, strony 602-611
4. <https://fotowoltaikaonline.pl/panele-monokrystaliczne-czy-polikrystaliczne>
5. K. Marszałek, T. Stapiński, Rozwój cienkowarstwowych ogniw fotowoltaicznych, Prace Instytutu Elektrotechniki, zeszyt 266, 2014
6. S. Nowak, M. Musztyfaga, Krystaliczne ogniwa słoneczne i ich praktyczne zastosowanie, PSKN, zeszyt 28, 2014, Gliwice
7. M. Musztyfaga-Staszuk, Nowe kompozyty na bazie miedzi w zastosowaniu do wytwarzania krzemowych ogniw fotowoltaicznych, Wydawnictwo Politechniki Śląskiej, Gliwice, 2019
8. S. W. Glunz, F. Feldmann, SiO<sub>2</sub> surface passivation layers – a key technology for silicon solar cells, Solar Energy Materials and Solar Cells, 2018
9. R. Figura, W. Zientarski, Analiza parametrów pracy modułu fotowoltaicznego, Efektywność transportu, 2016, strony 602-611
10. T. Kruk, Mikroskopia Sił Atomowych, Nanonauka, nr 1, 2018, strony 46-50
11. N. Selvakumar, H. C. Barshilia, Review of physical vapor deposited (PVD) spectrally selective coatings for mid- and high-temperature solar thermal applications, Solar Energy Materials and Solar Cells, volume 98, march 2012, pages 1-23
12. P. Boryło, M. Szindler, M. M. Szindler, Metoda atomowego osadzania cienkich warstw optycznych, PSKN, zeszyt 30, 2014, Gliwice (ALD)
13. [https://en.wikipedia.org/wiki/Selective\\_laser\\_sintering](https://en.wikipedia.org/wiki/Selective_laser_sintering)
14. M. Prokopiuk vel Prokopowicza, A. Tomiczek, A. Drygałae, Nanoszenie elektrod ogniwa słonecznego metodą sitodruku i ich wypalanie, PSKN, zeszyt 30, 2014, Gliwice
15. G. Kulesza, Chemiczna teksturyzacja powierzchni krzemu krystalicznego do zastosowań w fotowoltaice, sympozjum, Krynica, 2013
16. [https://en.wikipedia.org/wiki/Scanning\\_electron\\_microscope](https://en.wikipedia.org/wiki/Scanning_electron_microscope)
17. [https://en.wikipedia.org/wiki/Atomic\\_force\\_microscopy](https://en.wikipedia.org/wiki/Atomic_force_microscopy)



26th January 2024  
Gliwice, Poland

DEPARTMENT OF ENGINEERING MATERIALS AND BIOMATERIALS  
FACULTY OF MECHANICAL ENGINEERING  
SILESIA UNIVERSITY OF TECHNOLOGY

## INTERNATIONAL STUDENTS SCIENTIFIC CONFERENCE

### Scanning, modelling, and printing in 3D technology

D. Celeban<sup>a</sup>, G. Pośpiech<sup>a</sup>, P. Kruczyński<sup>a</sup>, M. Szczypiór<sup>b</sup>, A. Kania<sup>c</sup>, A. Włodarczyk-Fligier<sup>c</sup>,  
M. Polok-Rubinić<sup>c</sup>

<sup>a</sup> Students of Mechanical Engineering at the Faculty of Mechanical Engineering at the Silesian University of Technology

<sup>b</sup> Student of Automation and Robotics at the Faculty of Automatic Control, Electronics and Computer Science at the Silesian University of Technology

email: dc307597@student.polsl.pl

<sup>c</sup> Silesian University of Technology, Faculty of Mechanical Engineering, Department of Engineering Materials and Biomaterials

email: aneta.kania@polsl.pl

**Abstract:** This paper presents an innovative approach to the design and fabrication of orthopedics and insoles by leveraging advanced computational modeling techniques and 3D printing technology. Traditional orthopedic solutions often rely on generic designs that may not fully address the unique anatomical characteristics of individual users. In this study, we propose a method that combines 3D scanning of specific body parts, such as the foot, with computational modeling to create personalized and precise orthoses and orthopedic insoles. The paper describes the process of scanning, modeling and the process of printing presented examples.

**Keywords:** 3D scanning, 3D modelling, printing in 3D technology.

## 1. INTRODUCTION

3D printing, often referred to as additive manufacturing, stands as a transformative technological process that not only revolutionizes conventional manufacturing methods but also provides an avenue for the cost-efficient and expeditious production of intricately shaped objects. The intrinsic capabilities of 3D printing empower the creation of complex structures with unparalleled precision, all while maintaining a cost-effective and time-sensitive approach. Within this innovative manufacturing, the domain of insoles and orthotics has undergone a remarkable paradigm shift through the seamless integration of 3D printing technology. This evolution has ushered in a new era where these indispensable products are no longer bound by mass production constraints but can instead be meticulously tailored to the unique anatomical intricacies of each individual. This paper explores the profound impact of 3D printing technology on the fabrication of insoles and orthotics, elucidating how this transformative approach not only ensures individualized production but also significantly

expedites and simplifies the manufacturing process. The amalgamation of precision, efficiency, and customization marks a fundamental shift in the insole and orthotic production, underscoring the potential for widespread advancements in personalized healthcare solutions.

## 2. SCANNING AND MODELLING PROCESS

For scanning purposes EinScan PRO HD SHINING 3D camera was used, as this method was not invasive, very precise and enabled creating personalised insoles and orthotics swiftly and efficiently (Fig. 1).

The camera operates based on the display of a special structural grid, from which, following distance and sensitivity configuration, it scans the object. To ensure optimal scanning conditions, it is advisable to have subdued lighting or covered blinds in the room. Additionally, providing ample space around the scanned object is essential to allow for freedom of movement throughout the entire scanning process.



Figure 1. 3D EinScan Pro HD scanner [1]

Software used for scanning and processing the scan was EXScan Pro\_v3.7.4.0 [2].

The scans that will be performed will be utilized to create models, upon which customized stabilizers will be designed.

The sequence of scanning operation was following:

1. Choosing mode

Due to the necessity of scanning challenging areas, we utilized the Handheld Rapid Scan option (Fig. 2). Its quality proved to be sufficiently good, and additionally, the file with the finalized model occupied significantly less space on the disk and within the modelling software.

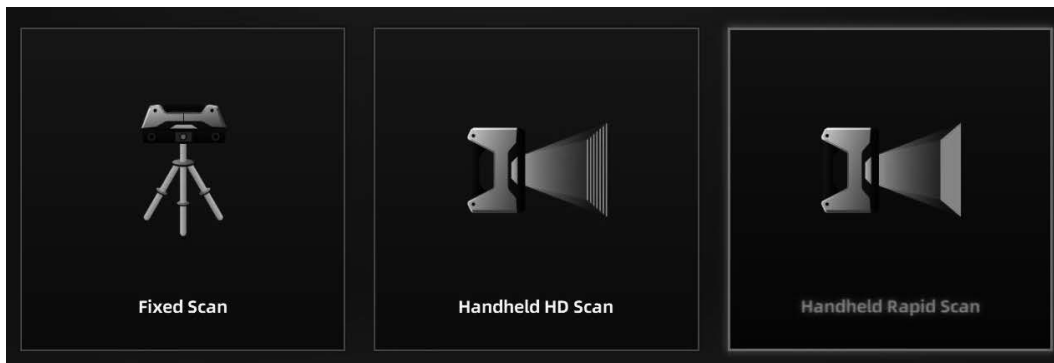


Figure 2. Choosing mode in scanning process

## 2. Adjustment of brightness and distance

Upon initiating the scanner, we received a real-time image of the scanning area from the camera (Fig. 3). To ensure accurate scanning, it was necessary to adjust the brightness slider so that the elements indicating the device being too close to the object were barely visible.



Figure 3. Adjustment of brightness and distance in the scanning process

## 3. Scanning execution

The crucial step of scanning required a slow and meticulous approach, constantly considering:

- the distance between the scanner and the object,
- the angle at which we scanned to avoid sudden loss of camera position,
- maintaining the object in a consistent position,
- scanning every section of the object to avoid leaving gaps.

## 4. Image processing

The example of obtained foot scan is shown in Figure 4.



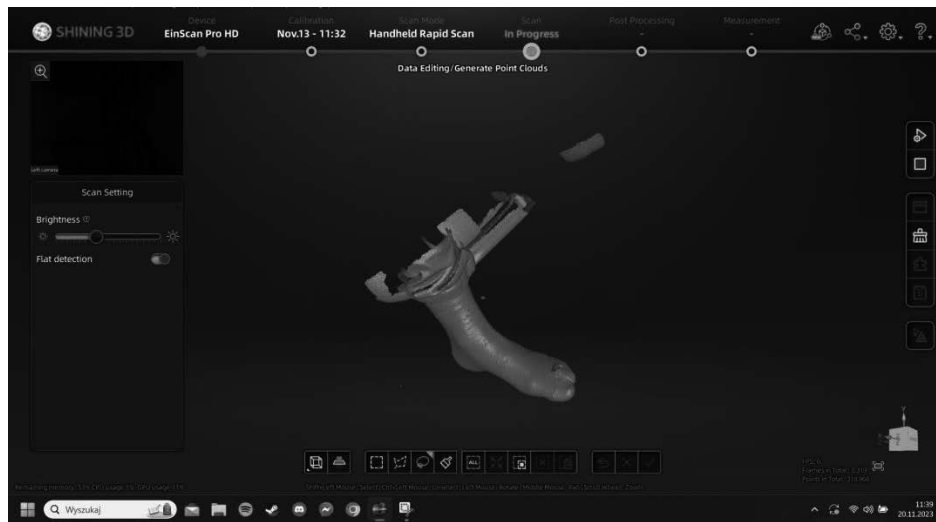


Figure 4. Example of foot scan

As seen in Figure 4, there are several imperfections in the scan, including an unnecessary pant leg, a portion of the table, and an unclosed model in the toe area. Model optimization is achieved by adjusting specific values in the ‘Mesh Optimization’ menu (Fig. 5).

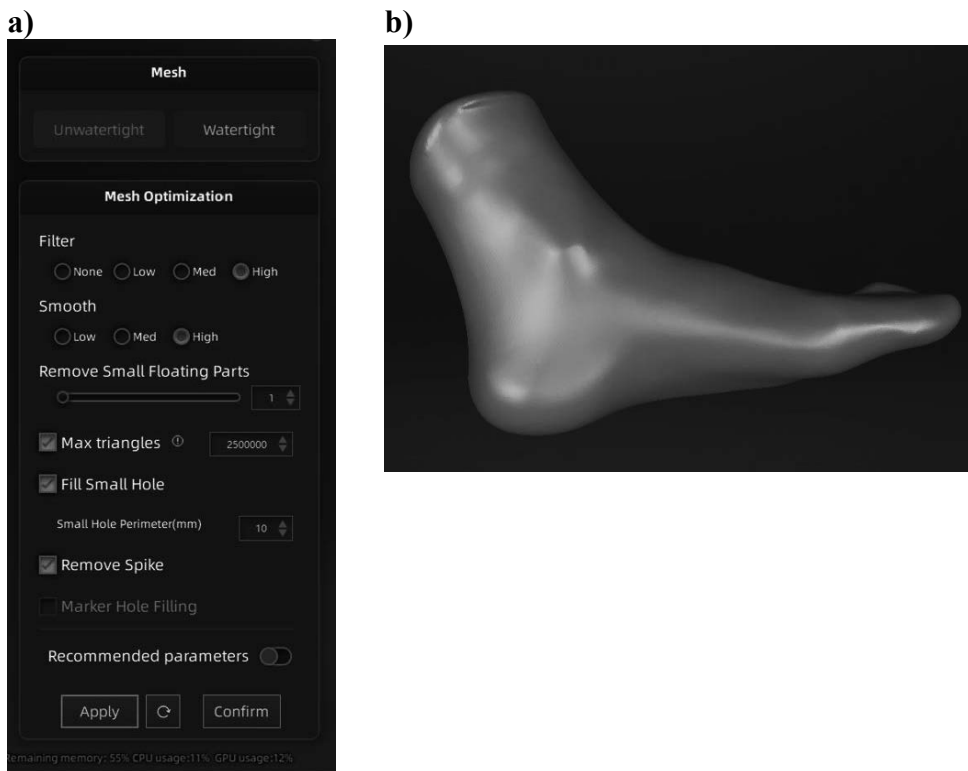


Figure 5. ‘Mesh Optimization’ menu (a) and improved model (b)

## 5. Final Optimization

At that point, we could perform additional optimization, including hole filling, smoothing, and simplification of the model.

In ‘Manual Hole Filling’, we selected specific areas to be filled using the curvature, flat, or tangent function, thereby restoring previously missing sections. In cases where the perimeter of the hole is open, as shown in Figure 6 below, filling cannot be completed. Therefore, precise scanning from all sides is crucial.

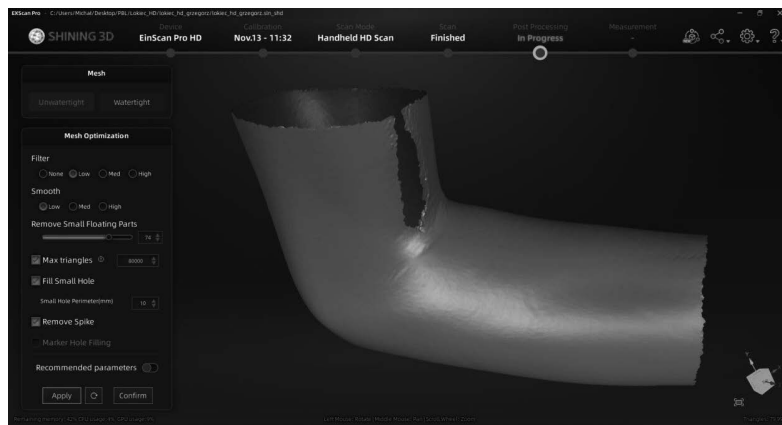


Figure 6. Uncompleted elbow scan

The scan conducted for the elbow stabilizer yielded an unsatisfactory final result, despite using both Automatic and Manual filling. Given the intended purpose of the scan for the elbow stabilizer, it was necessary to repeat the process with greater precision.

In the ‘Simplification’ and ‘Smooth’ tabs, we were able to smooth out protruding ‘cones’, such as those occurring in areas where we artificially filled holes (Fig. 7).

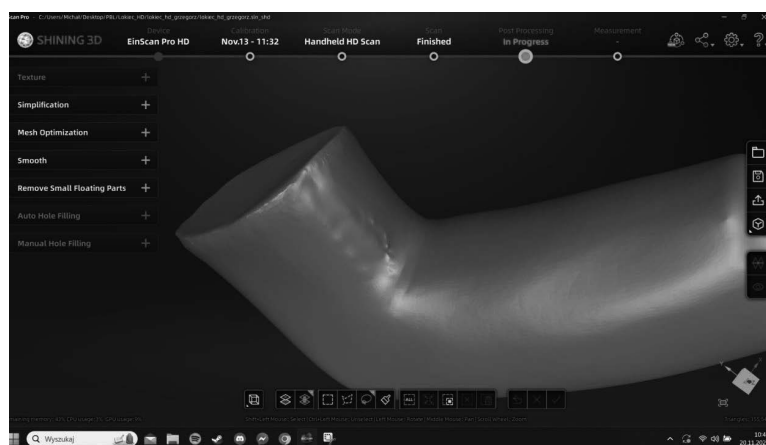


Figure 7. Optimized elbow scan model

During scanning, it is essential to avoid leaving ‘holes’ or incomplete areas. Such gaps may lead to errors in the model, ultimately impacting the effectiveness and comfort of wearing orthopaedic stabilizers. Incorrectly filling these areas in the software may result in improper fitting or discomfort for the patient. Therefore, ensuring the accuracy of the scanning process is

crucial, aiming to navigate and cover all areas of the limbs. Systematically checking scanning results and eliminating any gaps or errors becomes a crucial step in creating precise models of orthopaedic stabilizers. Efficient scanning with the camera minimizes the possibility of errors and guarantees high-quality final orthopaedic products. Additionally, this process is considerably faster than creating molds, and adjustments can be made in real-time.

### **3. 3D PRINTING**

The first step is to obtain a 3D model through scanning or other means. In this case, limbs are scanned for creating orthoses. Then software, like Blender or Fusion 360 is used to refine the model, then save it in a format compatible with the 3D printer, typically STL (Standard Tessellation Language).

#### **1. Slicing**

Specialized slicing software was employed, to divide the model into layers of a specified thickness. G-code file containing instructions for the printer was generated, including head movement, temperature, speed, layer height, and other parameters.

#### **2. Printer setup**

The appropriate material (commonly polymers, like: PLA, ABS, TPU, PET, PET-G) was loaded onto the printer spool. Print settings were adjusted according to the chosen material to enhance the final product's properties.

#### **3. Layer building**

The FDM printer deposits thin layers of material on top of each other until a complete object is formed. Support structures are added to maintain the geometry of the print as it solidifies.

#### **4. Completion of printing**

It is necessary to allow the printed object to cool before removing it from the print bed to prevent deformations.

#### **5. Adding Details and Finishing**

Depending on requirements, detailed cleaning and smoothing of the printed object is performed. Additional processes like painting or sanding may be applied. In this case, grinding and chemical smoothing are conducted for user comfort.

The accuracy of scanning and meticulous attention to printing parameters contribute to the production of precise orthopaedic models using FDM technology.

### **4. CONCLUSIONS**

This paper outlines an efficient workflow for creating personalized orthotics using handheld scanning, parametric modelling, and FDM 3D printing. The process starts with precise limb scanning, followed by tailored parametric modelling to design orthotics, and concludes with FDM printing, optimizing materials and structural parameters. The research explores challenges related to the mechanics of the body and material considerations, providing valuable insights into the effectiveness of this integrated approach for tailoring orthopedic solutions to individual needs.

**LITERATURE**

1. Skaner 3D EinScan Pro HD, [https://vpi-polska.pl/skanery-3d/skaner-3d-einscan-pro-hd/?gad\\_source=1&gclid=CjwKCAiAmZGrBhAnEiwAo9qHiRfmuxL](https://vpi-polska.pl/skanery-3d/skaner-3d-einscan-pro-hd/?gad_source=1&gclid=CjwKCAiAmZGrBhAnEiwAo9qHiRfmuxL), 2023.
2. EXScan Pro\_v3.7.4.0, <https://www.einscan.com/einscan-software/exscan-pro-software-download/>, 2023.

**Praca powstała w wyniku realizacji projektu Project Based Learning (PBL) pt. Opracowanie spersonalizowanych stabilizatorów i wkładek ortopedycznych z wykorzystaniem technologii druku 3D.**



26th January 2024  
Gliwice, Poland

DEPARTMENT OF ENGINEERING MATERIALS AND BIOMATERIALS  
FACULTY OF MECHANICAL ENGINEERING  
SILESIA UNIVERSITY OF TECHNOLOGY

## INTERNATIONAL STUDENTS SCIENTIFIC CONFERENCE

### **Consolidation of 18Ni300 maraging steel powder in the Gleeble 3800 simulator**

J. Chudy<sup>a</sup>, M. Kremzer<sup>b</sup>, W. Borek<sup>c</sup>, B. Tomiczek<sup>b</sup>

<sup>a</sup> Student, Silesian University of Technology, Faculty of Mechanical Engineering, Department of Engineering Materials and Biomaterials

email: julichu884@student.polsl.pl

<sup>b</sup> Silesian University of Technology, Faculty of Mechanical Engineering, Scientific and Didactic Laboratory of Nanotechnology and Material Technologies

email: marek.kremzer@polsl.pl, blazej.tomiczek@polsl.pl

<sup>c</sup> Silesian University of Technology, Faculty of Mechanical Engineering, Department of Engineering Materials and Biomaterials

email: wojciech.borek@polsl.pl

**Abstract:** The paper presents a method of consolidating maraging steel powders in the Gleeble 3800 plastic deformation simulator. A consolidation device for hot pressing of the steel powder was designed as part of the work. The pressing pressure and temperature of the sintering process were optimized. The obtained results constitute the basis for developing an innovative technology for producing steel elements using powder metallurgy methods.

**Keywords:** materials, consolidation, powder metallurgy, Gleeble 3800

## 1. INTRODUCTION

Developing new methods of powder consolidation has become a crucial element in various industries, especially in the production of ceramic materials, powder metallurgy, and materials engineering. In recent years, advanced technologies such as process simulators have begun to play a significant role in refining these processes. One of the most promising tools in this field is the Gleeble 3800 simulator.

### 1.1. Maraging steels

Maraging steel is a high-strength steel alloy belonging to the maraging steel family. Maraging steels are known for their exceptional strength and toughness, achieved through a specialized aging process. The term maraging is a portmanteau of martensitic and aging, describing how this steel gains its unique properties. The steel is initially subjected to a heat treatment to form a supersaturated solid solution. Following this, it undergoes an aging process, which involves low-temperature heat treatment to allow the formation of intermetallic

compounds. This aging process significantly enhances its strength. Maraging steels typically contain nickel, cobalt, molybdenum, and titanium. These alloys offer outstanding strength, hardness, and toughness, making them suitable for applications requiring high-strength materials, like aerospace components, missile casings, high-performance shafts, and structural parts in industries where toughness and durability are crucial [1 - 3].

Due to their exceptional mechanical properties, maraging steel grades are often used in many applications where other materials might fail under extreme conditions, balancing strength, and toughness [4].

## 1.2 Simulator Gleeble 3800

The Gleeble 3800 simulator is an advanced laboratory device that simulates various heat treatment conditions of metals and other materials. A thermo-mechanical simulator allows controlled temperature and mechanical loading manipulation, enabling the study of material behavior under different thermal and mechanical conditions [5].

The Gleeble system is used to conduct various tests, such as [6 - 8]:

- Simulating heat treatment processes: It can replicate different thermal processes like quenching, annealing, aging, and cyclic hardening to examine their impact on material properties.
- Studying material behavior under different temperatures and loading conditions: It helps analyze how materials behave under extreme conditions, such as high temperatures, to understand their properties in various environments.
- Fatigue and cyclic testing: The Gleeble system enables the simulation of cyclic mechanical and thermal loads, examining material durability and fatigue resistance.

The use of the Gleeble simulator is crucial in scientific research, materials engineering, and the development of new metal alloys and materials. It allows for precise examination of material properties under controlled conditions, leading to a better understanding of their behavior in different environments and applications.

## 2. Practical research

Based on advanced computer models, the Gleeble simulator enables the analysis and simulation of powder consolidation processes. Its main advantage lies in accurately reproducing conditions and material behaviors during consolidation. The ability to model various parameters such as temperature, pressure, and time allows for a better understanding of the processes occurring during consolidation. Classic powder consolidation methods, such as sintering or pressing, often generate uneven material density, which affects its mechanical and thermal properties. By using the Gleeble simulator, we can experiment with different scenarios and process parameters, potentially leading to the optimization of the consolidation process [9].

Developing a new powder consolidation method using the Gleeble simulator has the potential to reduce production costs and improve the quality of the final product. This could open new applications for producing materials with increased durability, strength, and thermal properties [10,11].

The examination material was 18Ni300 maraging steel, which chemical composition is presented in Table 1.

Table 1. Chemical composition of test material (MS300 maraging steel), wt. % [12].

C	Mn	Si	P	S	Ni	Co	Mo	Ti	Al <sub>met</sub>
0,015	0,12	<0,05	0,010	0,010	17,8	9,4	4,5	0,74	0,11
<0,008	<0,05	<0,05	<0,01	<0,010	17,9	9,3	5,0	0,70	0,13

In order to perform the simulation, a test system was developed consisting of steel tube, quartz tube, tantalum foil caps and thermocouple. The detailed configuration of the consolidation device is shown in Figures 1 and 2.

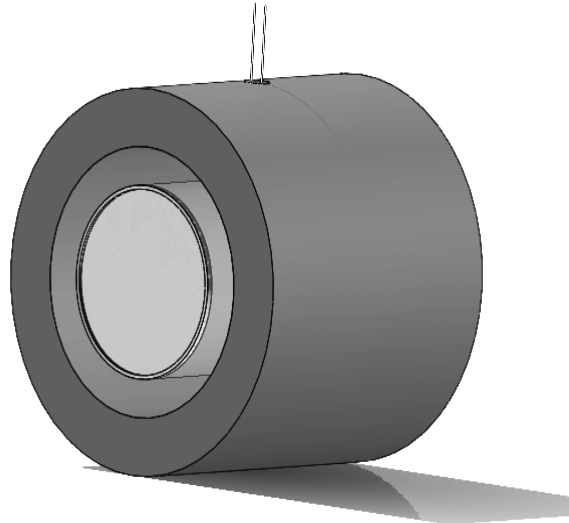


Figure 1. Consolidation device

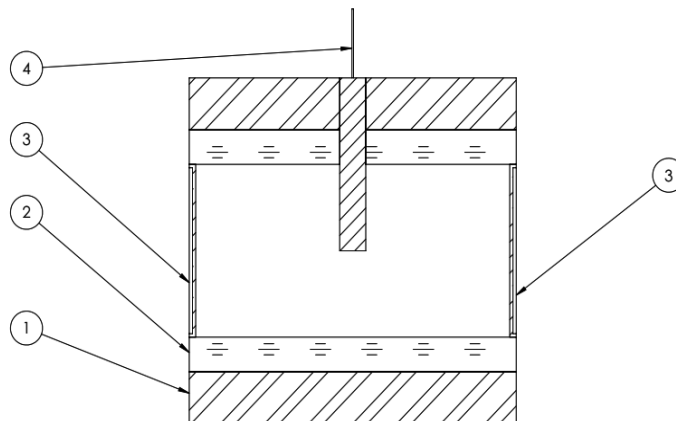


Figure 2. Cross-section of the consolidation device: 1- steel tube with hole, 2- quartz tube with hole, 3- tantalum foil, 4- thermocouple.

The purpose of using a quartz tube was to electrically isolate the powder from the outer steel part of the die, because the material was heated using the resistive method (the current should flow through the punch/powder system and not through the die). A thermocouple installed inside the powder enabled direct control of its temperature. The use of tantalum foil was aimed at better separating the sample from the steel stamps used.

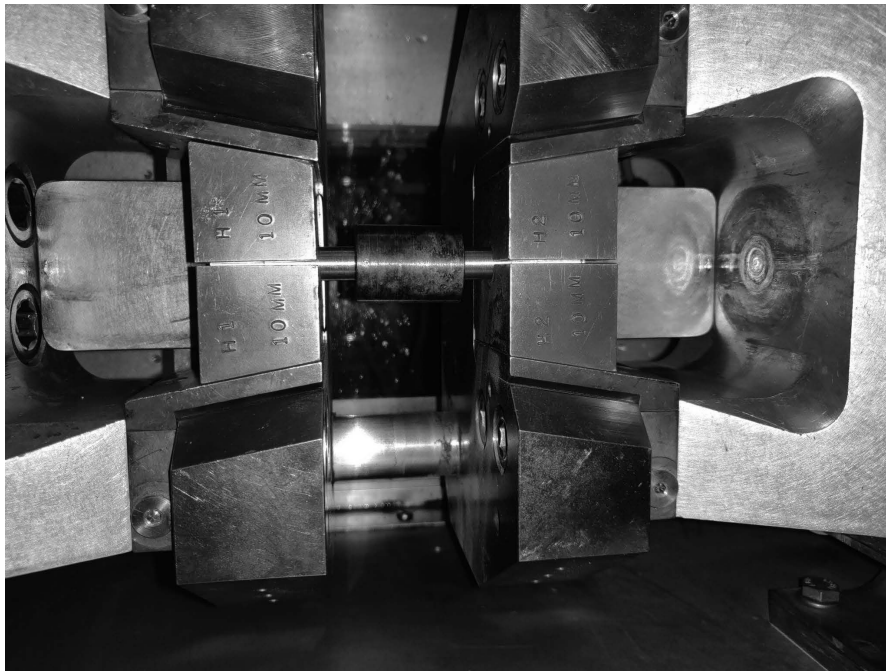


Figure 3. View of the consolidation device installed in the Gleeble simulator.

The previously weighed 3 grams of maraging steel powder were placed in this system. The system was then placed in the Gleeble simulator and tested (Fig. 3). The powder was first pre-pressed at 1kN force, then heated to 900°C at 10°C/s and at that time, the force value was also increased proportionally to 3kN. Then, the sample was soaked for 60 seconds at 900°C and cooled freely to ambient temperature. As a result of the test, consolidated samples of maraging steel powder were obtained (Fig 4.) The microstructure of the manufactured sample was analyzed using a scanning electron microscope, a Supra 35, ZEISS. As seen in the microscopic pictures (Fig. 5), the structure of the sample made of maraging steel powder is not fully compacted. Therefore, the hot consolidation process parameters should be refined, especially the temperature, time, and pressure.

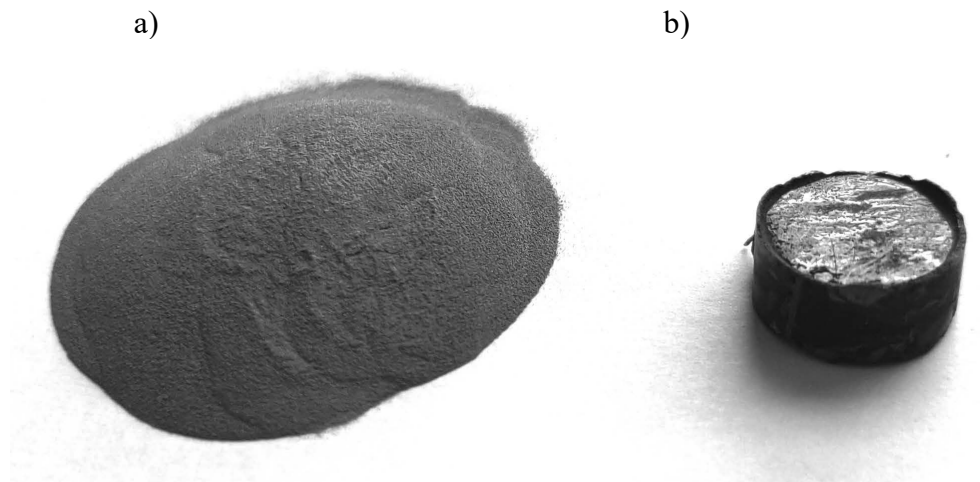


Figure 4. View of a) maraging steel powder and b) compacted maraging steel



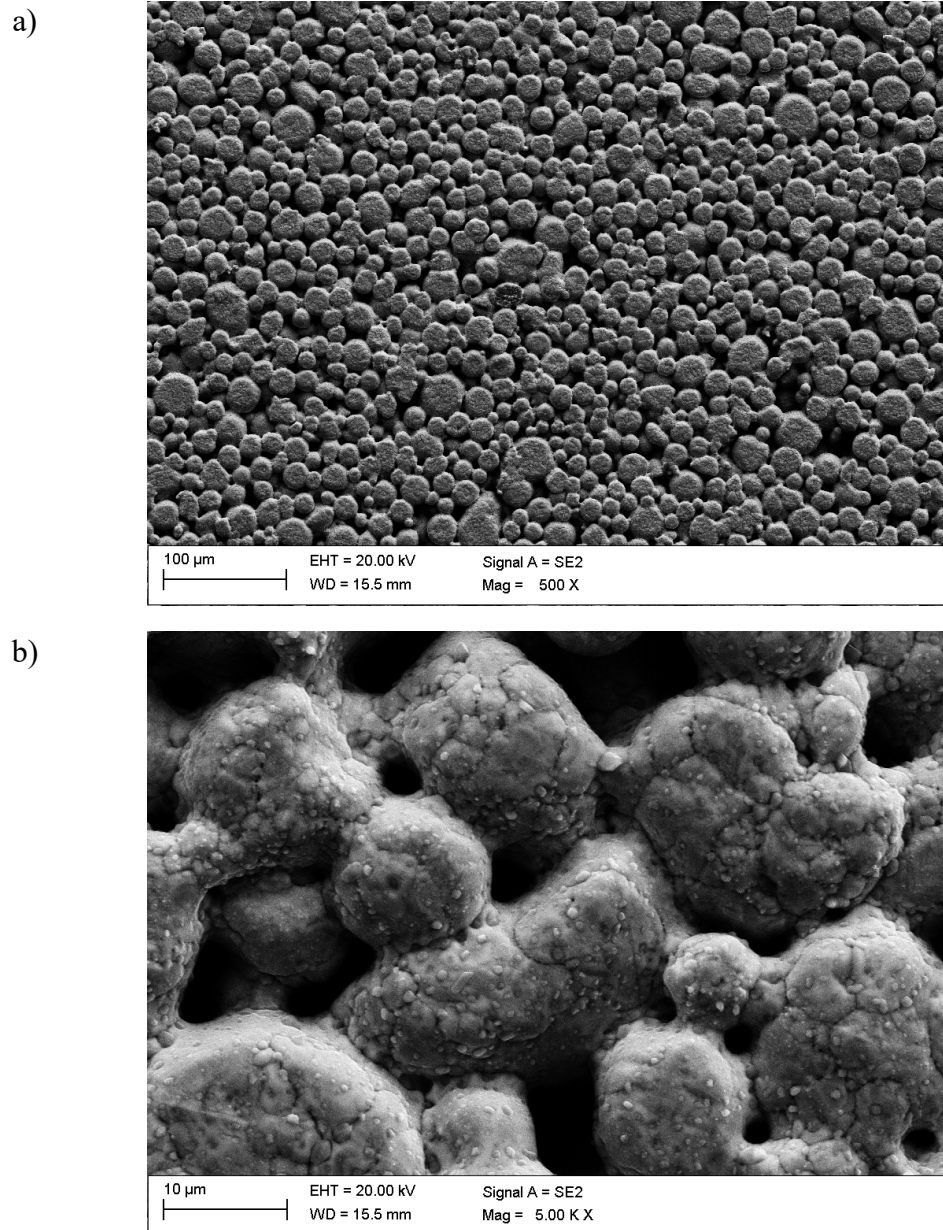


Figure 5. Microstructure of consolidated maraging steel powder, SEM

#### ACKNOWLEDGMENT

The work was created as a result of the implementation of a project within the framework of oriented education project - PBL, in competition X within the framework of the Excellence Initiative – University programme Research, Faculty of Mechanical Engineering, Silesian University of Technology.

**BIBLIOGRAPHY**

1. Marcisz, J., Burian, W. i Adamczyk, M. (2013). Właściwości mechaniczne stali maraging MS300 po starzeniu krótkotrwałym.
2. R. Tewari, S. Mazumder, I.S. Batra, G.K. Dey, S. Banerjee. (2000) Precipitation in 18 wt% Ni maraging steel of grade 350. Volume 48, Issue 5, ( pages 1187-1200).
3. Kurt Rohrbach, Michael Schmidt, Maraging Steels, Properties and Selection: Irons, Steels, and High-Performance Alloys, Vol 1, ASM Handbook, By ASM Handbook Committee, ASM International, 1990, (pages 793–800)
4. Piekło Jarosław , Garbacz-Klempka Aldona (2022) Analysis of Failure Process of Maraging Steel Produced by Selective Laser Melting (SLM)
5. M. Hojny, M. Głowacki, R. Kuziak, and W. Zalecki (2011). Development of Dedicated Computer System for Gleeble 3800 Thermo-Mechanical Simulator.
6. Borek, W. (2015) Application of the thermo-mechanical symulator. *Stal, Metale & Nowe Technologie*, (pages 82-84).
7. Czaja, M. i Borek, W. (2014). Kształtowanie struktury i własności materiałów inżynierskich z wykorzystaniem symulatora obróbki cieplno-plastycznej Gleeble 3800. Bonek Mirosław (red.): Sesja Okolicznościowa Studenckich Kół Naukowych "SO-KÓŁ'14", *Prace Studenckich Kół Naukowych, Instytut Materiałów Inżynierskich i Biomedycznych. Politechnika Śląska*, vol. 30, 2014, Politechnika Śląska, (pages 31-40). Gliwice.
8. Kwapisz, M. (2016). Numeryczne modelowanie próby jednoosiowego ściskania testu systemu Gleeble 3800. *Hutnik, Wiadomości Hutnicze* ,Vol. 83, nr 11 (pages 504—506)
9. Kuczek, Ł. (2014). Praca doktorska. Wpływ intensywnych odkształceń plastycznych na warunku zagęszczania i konsolidacji plastycznej proszków metalicznych. Kraków.
10. E.I. Galindo-Nava, W.M. Rainforth, P.E.J. (2016) Rivera-Díaz-del-Castillo, Predicting microstructure and strength of maraging steels: Elemental optimisation, *Acta Materialia*.
11. Ciszewski, B. Stan i perspektywy rozwoju metalurgii proszków. *Polska Akademia Nauk - IV Wydział*.
12. Sha, W., Cerezo, A. & Smith, G.D.W. (1993) Phase chemistry and precipitation reactions in maraging steels: Part IV. Discussion and conclusions. *Metall Trans A* 24, (pages 1251–1256)



26th January 2024  
Gliwice, Poland

DEPARTMENT OF ENGINEERING MATERIALS AND BIOMATERIALS  
FACULTY OF MECHANICAL ENGINEERING  
SILESIA UNIVERSITY OF TECHNOLOGY

## INTERNATIONAL STUDENTS SCIENTIFIC CONFERENCE

### **The influence of wood waste on the mechanical properties of cast epoxy resin**

N. Ciemala<sup>a</sup>, S. Mason<sup>a</sup>, W. Kala<sup>a</sup>, K. Konopka<sup>a</sup>, K. Świerczok<sup>a</sup>, Ł. Wantuch<sup>a</sup>, M. Szymiczek<sup>b</sup>,  
M. Chomiak<sup>b</sup>

<sup>a</sup> Silesian University of Technology, Faculty of Mechanical Engineering

<sup>b</sup> Silesian University of Technology, Faculty of Mechanical Engineering, Department of Theoretical and Applied Mechanics, email: malgorzata.szymiczek@polsl.pl

**Abstract:** This article presents the results of strength tests on epoxy resin samples with wood waste filler. Wood waste from elm, larch, pine and alder was used. Static tensile tests and flexural tests were carried out.

**Keywords:** epoxy resin, wood waste, tensile test, flexural test

### **1. INTRODUCTION**

Epoxy resins are widely used in the electronics, automotive and furniture industries, among others. They are characterized by many desirable properties, including good mechanical properties, chemical resistance and resistance to high temperatures. They are also characterized by low shrinkage during curing, high hydrophobicity and very good adhesion to various substrates. Epoxy resins are synthetic materials that belong to the group of polymeric synthetic resins. These resins can be one-component or two-component and contain substances such as polyphenols or polyglycols and epichlorohydrin's or oligomers in their composition. Depending on the molecular weight, the resin has a viscous or liquid structure. Cured epoxy resin has versatile applications [1,4].

Wood materials are found in the form of sawn timber, veneer, chipboard, fiberboard, plywood, pulp, paper and cardboard. The products are widely used in the furniture industry, construction industry, as auxiliary materials, insulation, as furniture components, walls or countertops. Wood waste is largely generated in the furniture and construction industry and as post-consumer wood waste from households. Wood waste can have different properties due to its origin and use. Often, waste wood is used for decoration, combined with epoxy resin, which has a bonding function with waste wood. For example, furniture is made from waste wood and resin. In this case, the waste wood has a protective function. The shape, type of wood or colour of resin can be freely mixed. An example of a table made of oak waste and black dyed resin is shown in figure 1. Other properties of wood waste are also being investigated, and the aim of this study is to assess the effect of wood waste in the form of powder, chips and chunks on the performance properties of composites made of epoxy resin and wood waste. It was assumed that transparent resin and wood waste from larch, alder, pine and elm would be used in the

project in percentages of 5%, 10% and 15%. The effects of these fillers on the performance properties were assessed by static tensile testing and flexural tests [5 – 8].



Figure 1. An example of a table made from epoxy resin, oak waste and steel sections.

## 2. RESEARCH METHODOLOGY

### 2.1 Materials

EPOXED products, shown in figures 2a) - 2c), were used in the project. The epoxy resin used is EPOXED CLEAR ECO, the hardener is EPOXED CLEAR ECO +, the dye is BLACK TRANSPARENT EPOXY DYE. Table 1 shows the properties of the resin and hardener separately, as well as the final properties and hardener, as well as the final properties of the resin-hardener system used. The optimum working conditions for the resin-hardener system are 20°C and a relative humidity of 70%. A higher resin temperature can increase the curing time, but

a higher temperature results in a lower resin viscosity. Protective clothing, gloves and goggles had to be worn during the work. Table 2 shows the basic working parameters, such as the working and crosslinking time of the resin and the weight ratio of resin and hardener. Tools additionally used were a gas torch to blow over the surface of the poured resin to remove any blockages. Additionally, acetone was used to dissolve resin residues [11].

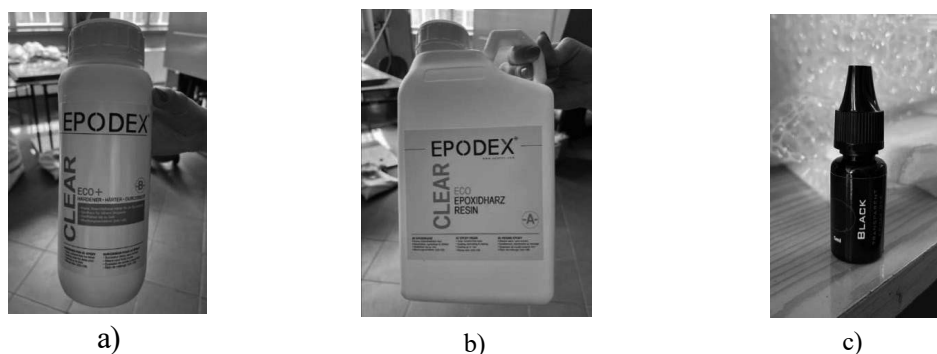


Figure 2. Materials intended for research: a) hardener, b) resin, c) pigment

Table 1. Properties of the resin and hardener [9-10]

Properties	ECO	ECO +	RESIN +HARDENER
Density	1,1 g/cm <sup>3</sup>	1,1 g/cm <sup>3</sup>	1,1 g/cm <sup>3</sup>
Viscosity	700 mPas	350 mPas	350 mPas
Max. heat resistance up to *	60°C	60°C	60°C
Min. heat resistance to	-30°C	-30°C	-30°C
Shore hardness after curing (D1)	87	80	80
Resistance to chemicals	yes	yes	yes

\* Heat resistance indicates the temperature to which the cured epoxy resin system remains mechanically stable. The cured epoxy resin can become softer at higher temperatures. Heat resistance can be increased by (curing at higher temperatures >60°C) [9-10].

Table 2. Operating parameters of the resin and hardener system [9-10]

Properties	RESIN +HARDENER
Work time	in 20°C do 240 min
Pre-hardening	in 20°C po 48-72h
Full-hardening	in 20°C po 14 day
Resin+Hardener	100:50 (weight)

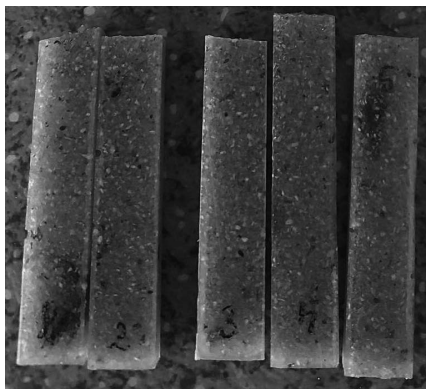


Figure 3. Samples before flexural testing

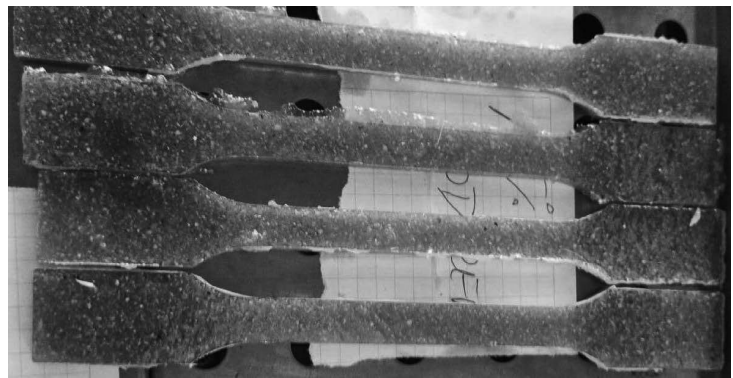


Figure 4. Samples before the static tensile test

## 2.2 Preparation of test samples

In order to analyse the influence of the type of wood on the final properties of the composite made of from wood waste and epoxy resin, specimens were made for static tensile testing and bending tests. The specimens were cast in the silicone moulds shown in figure 5. The moulds were treated with the release agent shown in figure 6. Wood waste from larch, alder, pine and elm were used for the analysis. Their properties were compared on the basis of wood species as well as the amount of filler used. For each type of wood, samples were prepared in which the percentage composition of filler in the composite was 5%, 10% and 15%. The properties of these composites were compared together with the resin material alone and the resin coloured with a black dye.



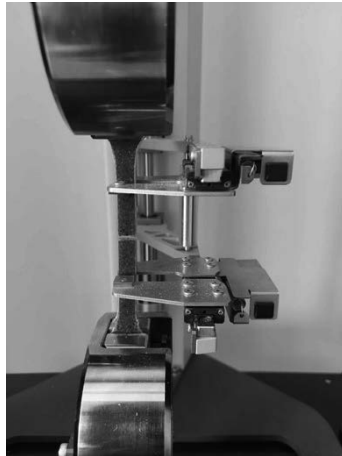
Figure 5. Moulds for casting samples



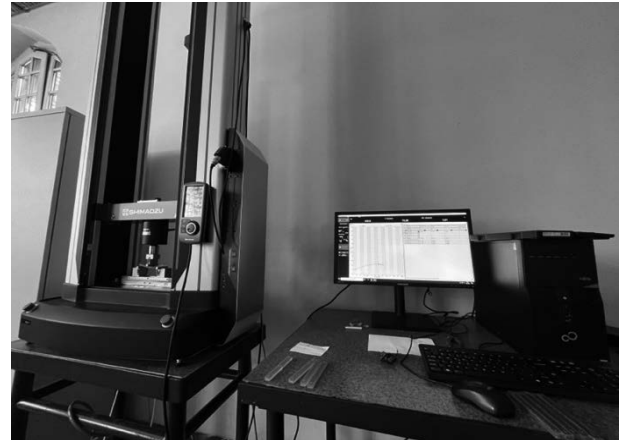
Figure 6. Release agent

## 2.3 Research methodology

Static tensile tests according to ISO-527-2 and three-point bending tests according to ISO 178 were carried out. The test rig for both tests can be seen in figure 7(a) and (b). The tests were carried out on a Schimadzu KN 10 machine collaborating with a Trapezium X software.



a)



b)

Figure 7. Photo of an example specimen undergoing a tensile test a), testing station for tensile and bending tests b)

Tensile testing is the most commonly performed strength test. The test specimens are standardised. The tensile test consists of subjecting a specimen of suitable shape to a tensile force in the axial direction until it breaks. This test is carried out under the constant speed of the machine's moving jaws. The bend test involves bending the specimen to a suitable angle at three points. This test aims to determine the plastic deformation capacity of the test material.

## 3. RESULTS

### 3.1 Static tensile test

The static tension test results are presented in Figures 8 - 11. The static tension test results are tabulated (Table 3). The test specimens are shown in Figures 12 - 15.

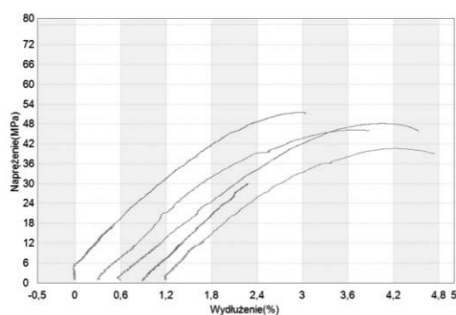


Figure 8. Stress-strain diagram and elongation of a resin specimen during a static tensile test

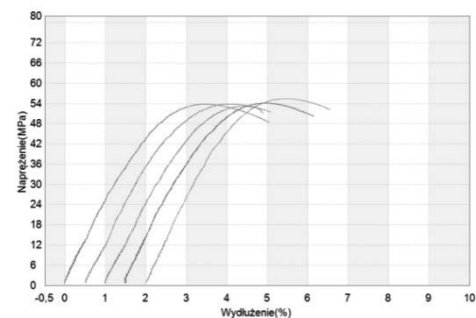


Figure 9. Stress-strain diagram and elongation of a colored resin specimen during a static tensile test

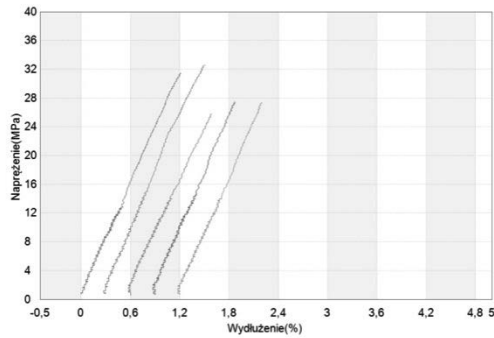


Figure 10. Stress-strain diagram and elongation of a composite specimen filled with 5% pine

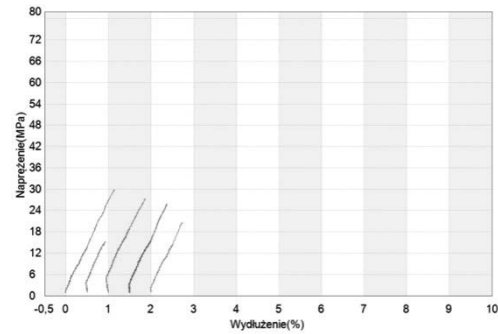


Figure 11. Diagram of the stress-strain relationship and elongation of a composite specimen filled with 15% pine

Table 3. Results of the tensile test

	Tensile strength [mpa]		Deformation for maximum strength [%]		Maximum strength [N]	
	Arithmetic mean	Standard deviation	Arithmetic mean	Standard deviation	Arithmetic mean	Standard deviation
Resin	43,28	8,42	2,84	0,85	2122,9	367,65
Resin with dye	54,05	0,81	3,48	0,06	2631,5	112,56
Larch 5%	38,072	1,39	1,71	0,07	1753,3	154,8
Larch 10%	31,80	6,06	1,39	0,18	1664,9	115,9
Larch 15%	24,39	15,97	0,84	0,62	917,6	643,9
Alder 5%	32,61	3,9	1,24	1,50	1368,5	178,0
Alder 10%	36,34	3,3	1,51	0,14	1675,6	279,4
Alder 15%	32,39	4,5	1,07	0,12	986,8	79,8
Pine 5%	28,91	2,9	1,08	0,11	1476,5	103,1
Pine 10%	18,78	7,4	0,61	0,18	707,6	309,3
Pine 15%	23,72	5,9	0,8	0,25	929,0	258,7
Elm 5%	36,80	2,4	1,50	0,29	2014,3	201,7
Elm 10%	32,85	1,9	1,67	0,2	1602,5	177,3
Elm 15%	26,51	2,0	0,99	0,1	974,4	220,0

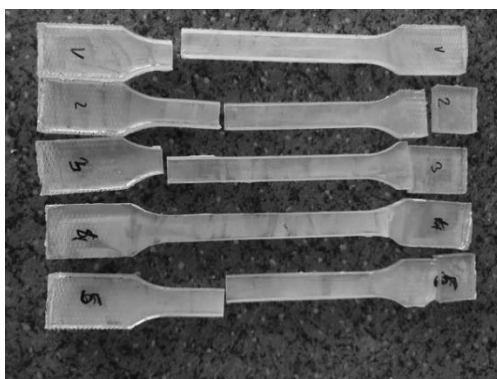


Figure 12 The photo of reference specimens made of cured epoxy resin



Figure 13. The photo of specimens of epoxy resin with added dye



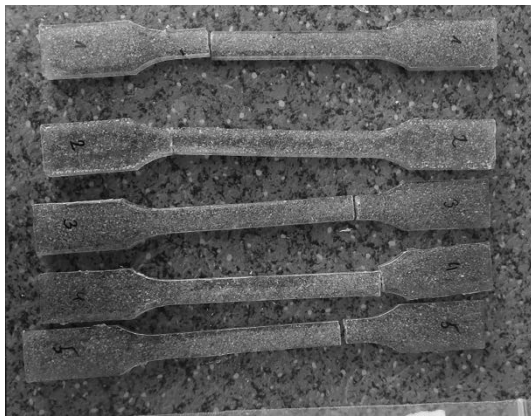


Figure 14. Composite with larch 5%

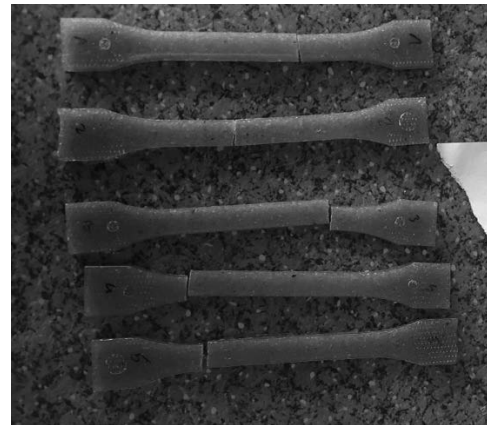


Figure 15. Composite with larch 10%



Figure 16. Composite with larch 15%



Figure 17. Composite with alder 5%



Figure 18. Composite with alder 10%



Figure 19. Composite with alder 15%

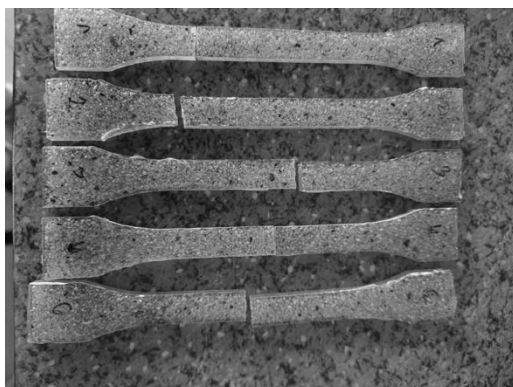


Figure 20. Composite with pine 5%

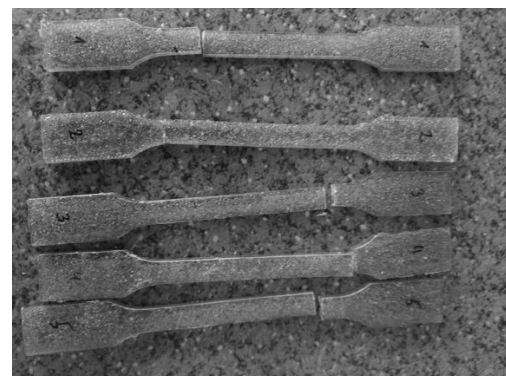


Figure 21. Composite with pine 10%

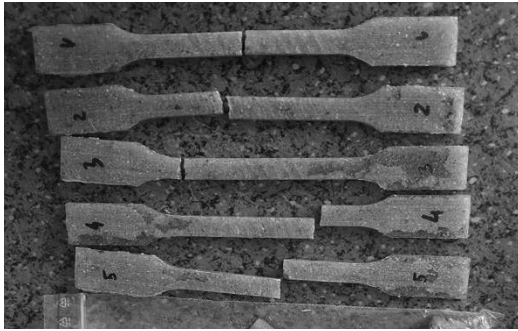


Figure 22. Composite with pine 15%

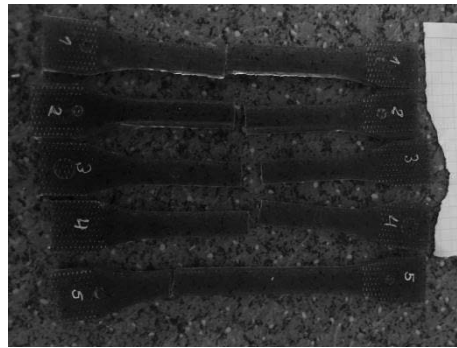


Figure 23. Composite with elm 5%

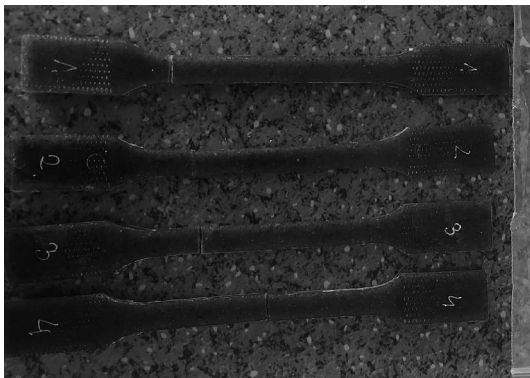


Figure 24. Composite with elm 10%

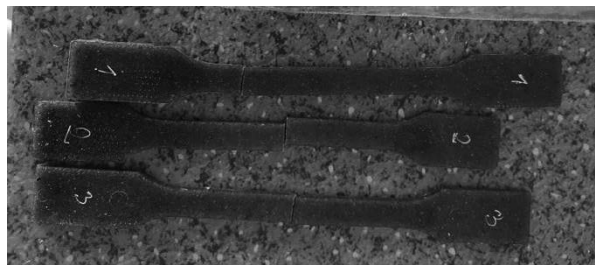


Figure 25. Composite with elm 15%

The tensile test specimens are shown in figures 12 to 25. From the images shown, it can be seen that the majority of the specimens did not fracture in the gauge zone. The majority of the specimens cracked close to where the specimens were fixed, but it is possible to distinguish specimens with a 5% elm content, where four specimens cracked in the gauge zone. From the test results shown in table 3, it can be concluded that the highest tensile strength is found in the unfilled resin, specifically the one that was dyed black. In the case of deformation for maximum force and maximum force, the highest values are also achieved by the sample without filler.

It can be concluded that the addition of the filler reduces the properties of the tensile strength values. Comparing the samples where filler was used, it can be seen that the highest tensile strength is found in the larch sample with a filler content of 5%. The results of the samples with filler vary, but it was observed that as the percentage of filler content increases, the tensile strength, strain for maximum force and maximum force decrease.

### 3.2 Flexural test

The results of the flexural test are shown in Figures 26-29. The results of the flexural test are shown in the Table 4. The test specimens are shown in Figures 30-37.

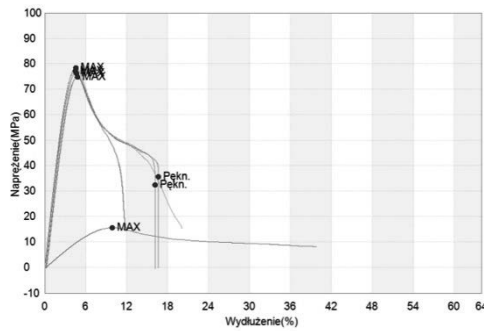


Figure 26. Stress-strain diagram and elongation of the resin sample during the flexural test

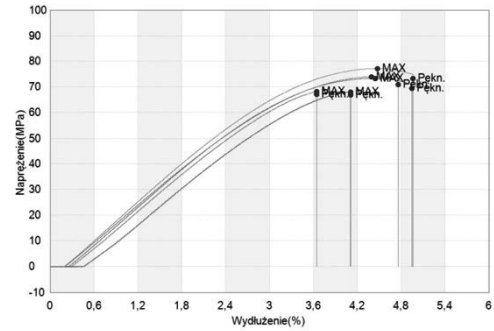


Figure 27. Stress-strain diagram and elongation of the coloured resin sample during flexural test

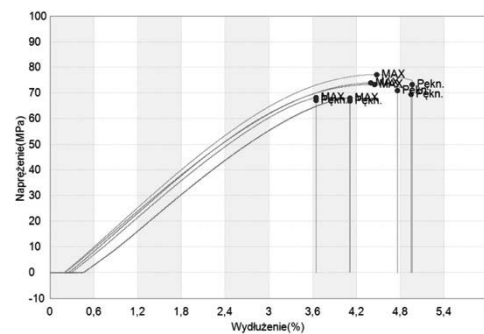


Figure 28. Stress-strain diagram and elongation of a specimen filled with 5% elm during a flexural test

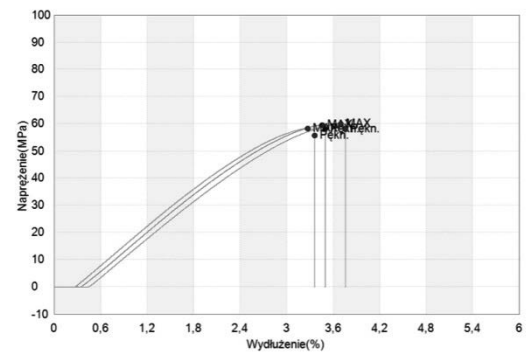
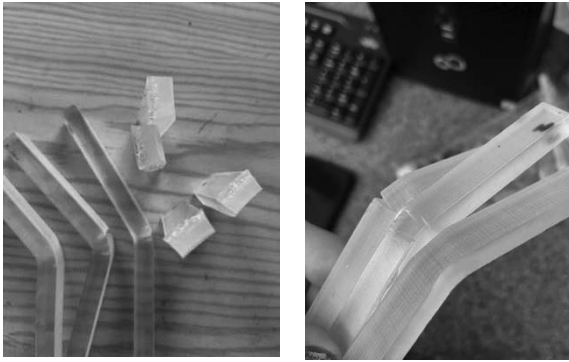


Figure 29. Stress-strain diagram and elongation of a specimen filled with 10% elm during a flexural test

Table 4. Results of the flexural test

	Bending strength [mpa]		Deformation for maximum strength [%]	
	Arithmetic mean	Standard deviation	Arithmetic mean	Standard deviation
Resin	76,64	1,81	4,61	0,11
Resin with dye	76,07	1,68	4,63	0,104
Larch 5%	67,24	5,13	3,78	0,474
Larch 10%	55,58	2,90	2,43	0,017
Larch 15%	48,28	0,83	2,49	0,105
Alder 5%	70,76	1,35	4,31	0,078
Alder 10%	58,08	9,67	2,57	0,54
Alder 15%	58,83	2,18	2,41	0,21
Pine 5%	46,64	7,69	2,27	0,5
Pine 10%	48,44	3,57	2,14	0,151
Pine 15%	40,94	6,62	2,29	0,302
Elm 5%	72,17	3,94	4,22	0,351
Elm 10%	59,23	0,93	3,48	0,213
Elm 15%	48,43	1,16	2,75	0,405



*Figure 30. The photo of reference specimens made of cured epoxy resin*



*Figure 31. The photo of specimens of epoxy resin with added dye*

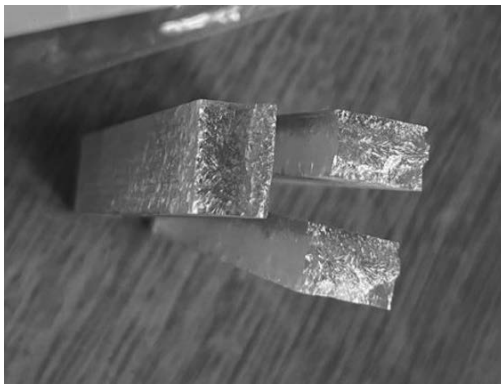


*Figure 32. Place of fracture of the filled composite larch 5%*

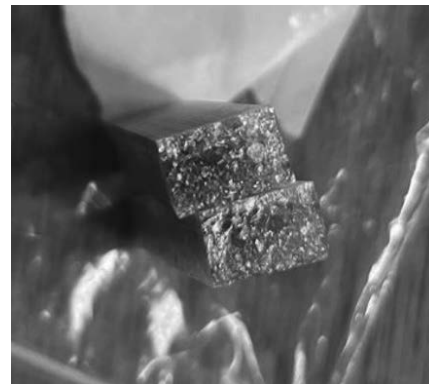


*Figure 33. Place of fracture of the filled composite larch 10%*



*Figure 34. Place of fracture of the filled composite larch 15%*



*Figure 35. Place of fracture of the filled composite alder 5%*



*Figure 36. Place of fracture of the filled composite alder 10%*



*Figure 37. Place of fracture of the filled composite alder 15%*

The specimens after the bending test are shown in Figures 30 to 37. It can be seen from the photographs that often, at low filler concentrations, the filler settled to the bottom of the specimen, which may have affected the test results. Figures 30 and 31 show characteristic fractures in which some of the material fractured plastically and some brittle. From the results shown in Table 4, it can be concluded that the resin without any fillers shows the highest flexural strength. It can also be seen that the dye did not affect the properties of the resin. However, the fillers have an effect on reducing the flexural strength. Samples using wood waste fillers show different flexural strengths. When comparing the properties of samples with the same filler, the highest resistance is shown by samples with 5% wood waste and the lowest by 15% in each case. The highest flexural strengths are characterised by combinations of epoxy resin with elm, alder and larch, while pine shows slightly poorer properties. Comparing the deformation of the samples for maximum force, the resin samples without fillers showed the highest deformation. For samples with fillers, it can be seen that the lower the filler content, the higher the strain. Only in the case of the pine tree was the deformation very similar for all three samples.

#### **4. CONCLUSIONS**

Based on the strength tests carried out, it can be concluded that:

- The highest values in the static tensile test are characterized by the sample without the filler additive hence it is concluded that the wood waste adversely affects the results in the static tensile test.
- The test specimen without filler has the highest values in the bend test, so it is concluded that the wood waste has an unfavorable influence on the flexural strength.
- The developed composites were characterized by specific properties and design and in the final stage were the basis for the design and manufacture of a table with oak lumber obtained from waste wood.

**BIBLIOGRAPHY**

1. Kajda-Szcześniak M., Evaluation of the basic properties of the wood waste and wood based wastes, Archives of Waste Management and Environmental Protection, vol. 15 issue 1 (2013).
2. Resin in the furniture industry - how to use it? 2017  
[https://www.biznesmeblowy.pl/produkcja\\_mebli/116/zywica\\_w\\_przemysle\\_meblarskim\\_jak\\_ja\\_stosowac,10087.html](https://www.biznesmeblowy.pl/produkcja_mebli/116/zywica_w_przemysle_meblarskim_jak_ja_stosowac,10087.html) (accessed on day 20.06.2023)
3. Drózdź K.: The dynamics of timber market in Poland between 2000 and 2020. Academic Review of Business and Economics, 2022 | 2(1) | 1-19. DOI 10.22367/arbe.2022.02.01
4. Kaputa V.: Wood materials market in Poland, Intercathedra, 2004, 20, pp. 74 – 78. (in Polish)
5. Wasilewski R., Hrycko P.: Energy and emission effect of the wood board waste combustion in the small boiler. Archives of Waste Management and Environmental Protection, 12/1, 2010, pp. 27 – 34.
6. Belay Taye Wondmagegnehu & Addisalem Adefris Legesse (2023) Experimental Investigation of Mechanical and Physical Properties on Epoxy Resin with Wood Timber for Furniture Application, Journal of Natural Fibers, 20:2, DOI: 10.1080/15440478.2023.2286327
7. Çiftçi S, Ciritcioglu HH, As N, Tankut N. Determination of epoxy resin usability for mass production of reinforced laminated veneer lumber. *Proceedings of the Institution of Mechanical Engineers, Part E: Journal of Process Mechanical Engineering*. 2022;0(0).
8. Dengkang Guo, Nai Guo, Feng Fu, Sheng Yang, Gaiyun Li, Fuxiang Chu, Preparation and mechanical failure analysis of wood-epoxy polymer composites with excellent mechanical performances, Composites Part B: Engineering, Volume 235, 2022, 109748, ISSN 1359-8368, <https://doi.org/10.1016/j.compositesb.2022.109748>
9. Technical data sheet for epodex eco+ resin [https://www.epodex.com/en/product/eco-system-resinhardener/?1=Transparent-colourless-\(clear\)](https://www.epodex.com/en/product/eco-system-resinhardener/?1=Transparent-colourless-(clear)) (accessed on day 29.06.2023)
10. Basic properties of the resin with EPODEX CLEAR ECO + hardener <https://www.modelarnia24.pl/strona-glowna/671-epodex-clear-eco-eco-zalew-do-5cm.html> (accessed on day 29.06.2023)
11. <https://www.ateliersstaub.com/follow-the-step-by-step-manufacturing-of-tables-in-epoxy-resin-and-solid-oak-en8925.html> (accessed on day 20.06.2023)



26th January 2024  
Gliwice, Poland

DEPARTMENT OF ENGINEERING MATERIALS AND BIOMATERIALS  
FACULTY OF MECHANICAL ENGINEERING  
SILESIA UNIVERSITY OF TECHNOLOGY

## INTERNATIONAL STUDENTS SCIENTIFIC CONFERENCE

### Improvement of the functional properties of the top layer of tool steel after laser processing

P. Cisowski<sup>a</sup>, S. Szeja<sup>b</sup>, J. Badora<sup>a</sup>, A. Kłapsia<sup>a</sup>, J. Muszyńska<sup>a</sup>, E. Krajewska<sup>a</sup>, M. Bonek<sup>c</sup>, U. Ozdemir<sup>d</sup>

<sup>a</sup> Student of Silesian University of Technology, Faculty of Mechanical Engineering, Department of Engineering Materials and Biomaterials

<sup>b</sup> Student of Silesian University of Technology, Faculty of Electrical Engineering

<sup>c</sup> Silesian University of Technology, Faculty of Mechanical Engineering, Department of Engineering Materials and Biomaterials

<sup>d</sup> Gazi University, Faculty of Technology, Metallurgical and Materials Engineering Department, Ankara, Turkey

email: mirosław.bonek@polsl.pl

**Abstract:** In the theoretical part of the work was characterized by its high-speed steels heat treatment, the principle of operation of the laser, and their types. The aim of the study was the melting of the surface layer of high-speed steel with laser power: 0,7kW, 1.4 kW, 1,7kW, 2,1kW. We made an analysis of the chemical composition, the change in the structure of HSS HS6-5-3-8. Hardness measurements were made, as well as the roughness of the microstructure of the material was examined.

**Keywords:** High-speed steel, laser processing, surface treatment

### 1. INTRODUCTION

The tool steels that are the subject of our research belong to a group of materials that are characterized by high wear resistance, high hardness and low ductility. Depending on their chemical composition, their characteristics can vary. Thanks to various alloying additives, the properties of steels can take on different parameters depending on demand.

The word LASER stands for Light Amplification by Stimulated Emission of Radiation. The operation of laser is based on the passage of a laser beam from the laser to work piece which, by falling on the top of metal, causes the formation of continuous metal lake because of the emitted heat. The laser had found applications in many areas of materials engineering, including heat treatment, remelting, laser alloying and fusion, surfacing, laser Rapid Prototyping methods, laser marking, laser ablation, cutting and laser technology in medicine. The laser can be used for surface processing of materials such as cast iron, titanium alloys, copper and aluminium, high-speed steels, spring steels, structural steels, corrosion-resistant steels, low-carbon steels and bearing steels.

The laser processing method is characterized by high reliability, precision, as well as speed of execution. It makes it possible to obtain the optimal shape and size of metal work piece by repeatedly processing the material. Due to its ability to cut organic and inorganic materials, it is an ideal method to meet the ever-growing demand for high-quality products [1-3].

## 2. PURPOSE AND SCOPE OF WORK

The aim of the study was to melt the surface layer of high-speed steel using different laser powers, measure hardness and roughness, investigate the material's microstructure, and analyse its chemical composition.

### 2.1 Material for testing

Experiments were conducted on cobalt high-speed steel with elevated carbon concentration, specifically HS6-5-3-8, in accordance with the PN-EN ISO 4957:2002 standard. The chemical composition is presented in Table 1.

Table 1. Chemical composition of steel.

Steel grade	Average concentration of elements, %								
	C	Cr	W	Mo	V	Co	Si	P	S
HS6-5-3-8	1,28	4,2	6,3	5,0	3,0	8,4	1,09	0,015	0,010

### 2.2 Heat treatment of HS6-5-3-8 steel

The heat treatment of HS6-5-3-8 steel involved austenitizing the samples in a salt bath furnace and tempering them in a chamber furnace with an argon protective atmosphere. The samples were gradually heated to the austenitizing temperature, with isothermal stops at 650 and 850°C for 15 minutes. The austenitizing time was 30 minutes at a temperature of 1180°C, followed by quenching in hot oil. After hardening, the samples were tempered twice, each time for 2 hours at a temperature of 560°C. After heat treatment, the samples were sanded and machined on a magnetic grinder.

### 2.3 The process of remelting high-speed steel with a laser

A high-power diode laser, specifically the HPDL Rofin DL 020 with technical specifications outlined in Table 4, was employed for the melting of the tested steel. The utilized laser is a high-power, versatile device commonly used in materials engineering for various applications such as cladding, welding, melting, and surface enrichment.

The melting and alloying of surface layers were performed within a power range of 0.7 to 2.1 kW. Melting paths were created on each sample surface, each with a length of 55 mm. The dimensions of the laser beam focused on the material surface were 1.8×6.8 mm. The working focal length (measured from the protective glass surface in the head) was 92 mm. The melting was carried out perpendicular to the longer side of the focused beam with a multimode energy distribution, ensuring the attainment of a wide bead face.

During preliminary investigations, it was determined that the maximum speed at which the process remains stable is 0.5 m/min. Subsequent trials were conducted at a constant melting



speed, varying the laser beam power within the range of 0.7-2.1 kW during the melting of the surface layer of the samples. It was observed that complete protection of the melting area is ensured by argon blowing with a flow rate of 20 l/min through a circular nozzle with a diameter of  $\varnothing$  12 mm, directed opposite to the melting direction [4].

Table 2. Technical data of the HPDL Rofin DL 020 LED laser

Wavelength of laser radiation, nm	808 $\pm$ 5
Output power of the laser beam (continuous radiation), W	2300
Power range, W	100-2500
Focal length of the laser beam, mm	82 / 32
Dimensions of the laser beam focal point, mm	1,8 $\times$ 6,8 / 1,8 $\times$ 3,8
Power density range in the plane of the laser beam focus, kW/cm <sup>2</sup>	0,8-36,5

## 2.4 Sample preparation

Samples of HS6-5-3-8 steel, subjected to standard heat treatment, and melted using a laser, were cut in a plane perpendicular to the melting direction using a Struers Discotom-2 device. The cutting disk was cooled with water. The cut samples were hot-embedded in thermosetting resin for 12 minutes, with 7 minutes dedicated to heating the resin and 5 minutes to cooling the samples. Specimens were prepared by grinding on abrasive papers and mechanically polishing with diamond pastes using Struers equipment. Subsequently, they were etched in solutions as outlined in Table 3. The etching time was experimentally adjusted for each form of the surface layer of the examined material.

Table 3. Chemical compositions of reagents used

L.p.	Chemical composition of the etchant and conditions for etching or polishing	Application of the etchant
1.	5 cm <sup>3</sup> of nitric acid and 100 cm <sup>3</sup> of ethyl alcohol; temperature 20°C, time 5-20 s	Chemical etching of specimens; reveals the structure and boundaries of primary austenitic grains
2.	490 cm <sup>3</sup> of orthophosphoric acid, 50 g of chromic anhydride, and 5 cm <sup>3</sup> sulfuric acid; temperature 20°C, time 2-4 s, voltage 30 V, and current density approximately 6 A/cm <sup>2</sup>	Electrolytic polishing of thin foils using the modified Bolmann method.
3.	50 cm <sup>3</sup> of perchloric acid and 1000 cm <sup>3</sup> of glacial acetic acid; temperature 12°C, time 5-15 s, voltage approximately 20 V, and current density approximately 3 A/cm <sup>2</sup>	Electrolytic polishing using the stream method of 3 mm diameter disks in the Tenupol device.

## 2.5 Metallographic analysis

Metallographic examinations were conducted using a Leica MEF4A metallographic microscope, equipped with the Leica-Qwin computer image analysis system, at magnifications ranging from 100 to 1000 $\times$ . Additionally, scanning electron microscopy was performed using an Opton DSM-940 scanning electron microscope. A computer image analysis system, Leica-Qwin, was employed for the assessment of the thickness of individual zones in the surface layer

and the measurement of grain surface area. The recorded results regarding the average grain size and dendrite length in distinct zones were subjected to statistical analysis.

## 2.6 Rockwell hardness test

Hardness measurements were conducted in accordance with the PN-EN ISO 6508-1:2002 standard. The examination was carried out using the C scale on the Shimadzu DUH 202 dynamic microhardness tester, with 10 measurements taken for each condition and their average values calculated. The measurements were performed with a 0.1 N load, creating the necessary number of impressions across the cross-section of each tested sample, corresponding to the depth of structural changes in the surface layer of the material. The research results were statistically analysed. Hardness was measured on ground and mechanically polished frontal surfaces of the samples. Microhardness measurements were taken along lines perpendicular to the sample surfaces, along the axis of the bead face. The experimental conditions are detailed in Table 4. The purpose of the hardness measurements was to determine the hardness distribution on the sample surface [5].

Table 4. Test conditions for dynamic micro-hardness of the tested steel

Indenter type	Vickers
Load	100 mN
Loading and unloading time	6,62 mN/s
Load resistance time	10 s

## 3. RESEARCH FINDINGS

### 3.1 Examination of the top layer of the molten sample

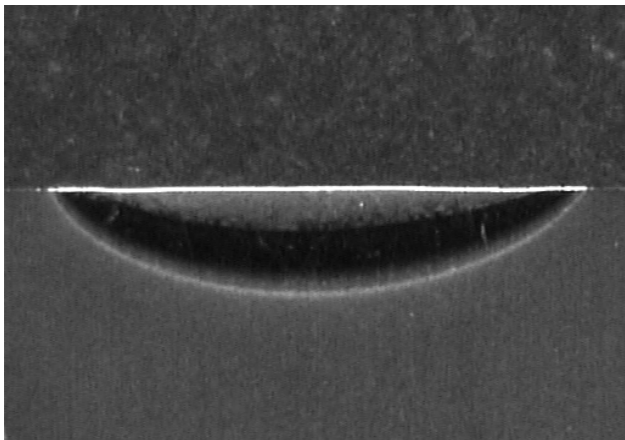


Figure 1. Surface layer of HS6-5-3-8 steel after melting with the following parameters: scanning speed – 0.5 m/min, beam power – 1.7 kW.

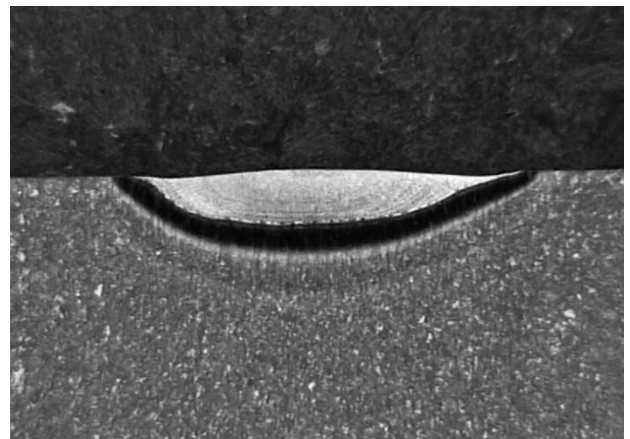


Figure 2. Surface layer of HS6-5-3-8 steel after melting with the following parameters: scanning speed – 0.5 m/min, beam power – 2.1 kW.

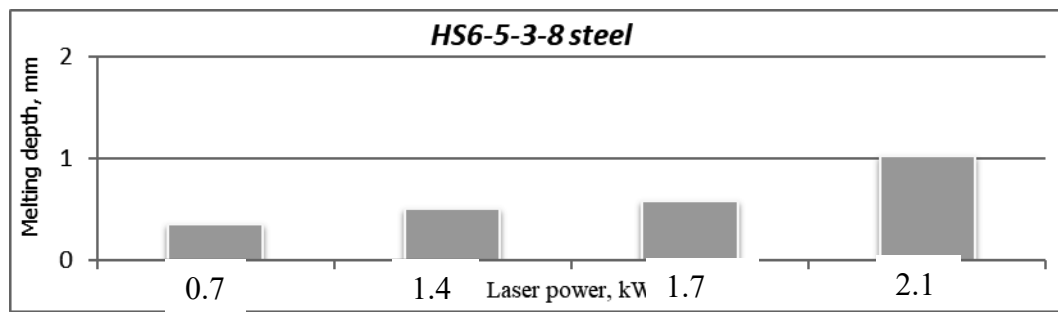


Figure 3. Influence of laser power on the depth of the melted surface layer zone of HS6-5-3-8 steel after laser melting with laser powers of 0.7 kW, 1.4 kW, 1.7 kW, 2.1 kW, at a constant melting speed of 0.5 m/min.

### 3.2 Examination of the transformed layer of the molten steel sample HS6-5-3-8

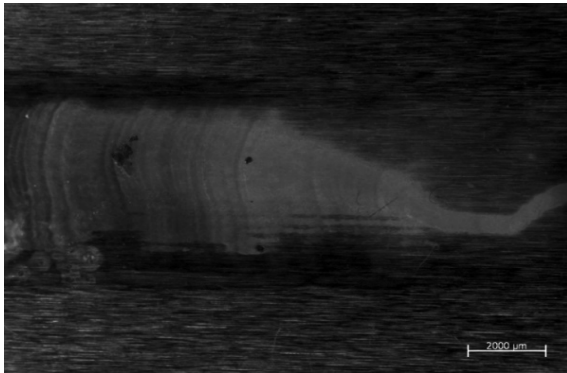


Figure 4. View of the transformed layer after melting HS6-5-3-8 steel, laser power 0.7 kW.

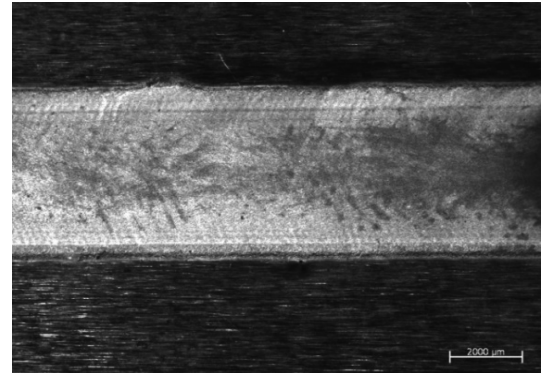


Figure 5. View of the transformed layer after melting HS6-5-3-8 steel, laser power 1.4 kW.

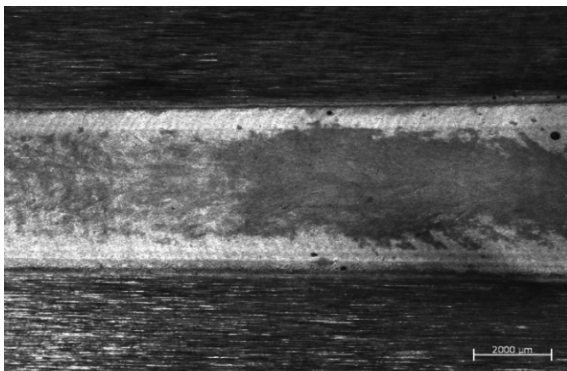


Figure 6: View of the transformed layer after melting HS6-5-3-8 steel, laser power

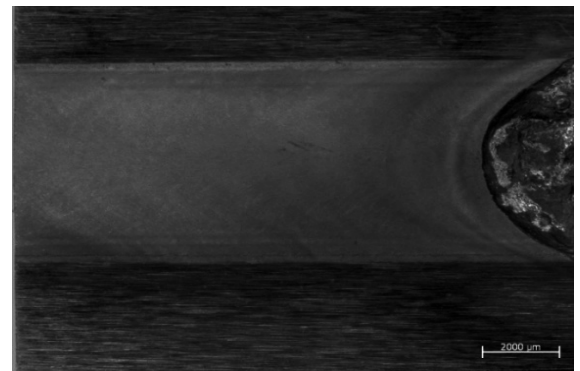


Figure 7: View of the transformed layer after melting HS6-5-3-8 steel, laser power 2.1 kW.

As a result of laser surface remelting, a path with a cross-sectional profile corresponding to the energy distribution in the laser beam was obtained. Surface layer melting was carried out within a power range of 0.7 to 2.1 kW. Melting paths were created on each sample surface, each with a length of 55 mm.

The dimensions of the laser beam focused on the material surface were  $1.8 \times 6.8$  mm. The working focal length (measured from the surface of the protective glass in the head) was 92 mm. The melting was performed perpendicular to the longer side of the focused beam with a multimode energy distribution, ensuring the attainment of a wide bead face.

In Figure 7, it can be observed that paths obtained with higher laser power exhibit a smoother surface and a distinct melting boundary compared to the sample melted at lower laser power.

### 3.3 High-speed steel top layer roughness test

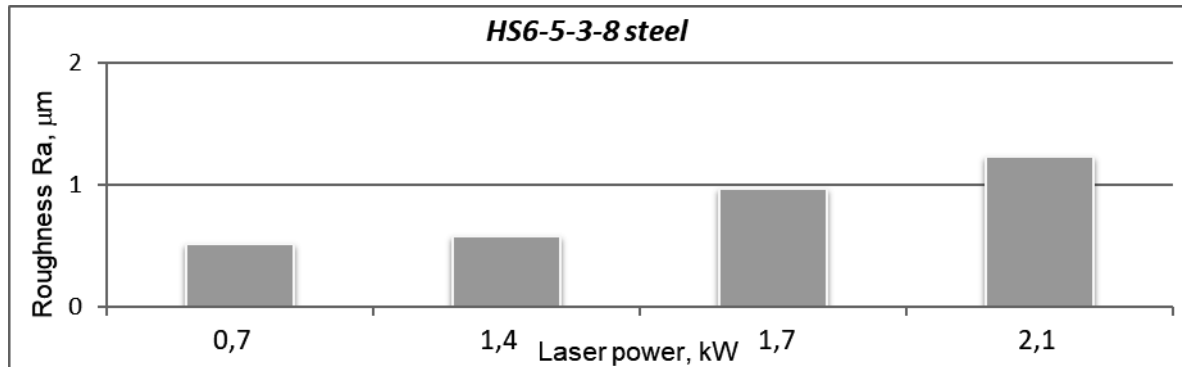


Figure 8: Influence of laser power on the surface roughness parameter value of the HS6-5-3-8 steel surface layer after laser melting with laser powers of 0.7 kW, 1.4 kW, 1.7 kW, 2.1 kW, at a constant melting speed of 0.5 m/min.

The surface of the sample after laser melting exhibits rough areas. This can be attributed to oxidation and material evaporation from the surface layer, correlating with the melted zones. The steel melted with a 0.7 kW laser displays the smallest roughness, while the 2.1 kW laser-melted steel shows the highest, as depicted in Figure 8. Laser power plays a significant role here, as it is evident that the roughness of the steel increases with the rise in laser beam power. Upon macroscopic observation of the laser heat treatment, it is suggested that the surfaces of the components require additional processing to reduce their roughness. The presence of pores on the surface can be utilized as micro-reservoirs for lubricating fluid. This will help reduce the friction coefficient between interacting elements.

### 3.4 Hardness test of the top layer of high-speed steel

Microhardness measurements were conducted linearly on the cross-sectional plane of the weld, starting from the bead face towards the native material, using the Shimadzu DUH 202 dynamic microhardness tester. Measurements were performed with a 0.1 N load, creating the necessary number of impressions across the cross-section of each tested sample, corresponding to the depth of structural changes in the surface layer of the material. The measurement results were presented in the form of a chart for selected laser beam power density values. In Figure 10, a chart is presented that includes the microhardness of the native material of HS6-5-3-8 high-speed steel, which is approximately 850 HV0.1, and the average microhardness of the surface layer after laser melting with different powers. In the case of significant melting depths, it can be observed that the hardness of the surface layer increases. This is due to the melting of a larger area, leading to a significant refinement of the structure, which positively influences the strengthening of the melted surface. The lowest hardness was achieved in the sample

melted with a 0.7 kW laser power, approximately 1300 HV0.1, while the highest was obtained with a 2.1 kW laser power, reaching around 1400 HV0.1. The difference in hardness between the layer melted with a 0.7 kW beam power and a 2.1 kW beam power is approximately 100 HV0.1. Based on the microhardness measurement results, the relative percentage increase in microhardness was determined for each sample. Compared to the native material, there was an increase in hardness of approximately 30% after melting.

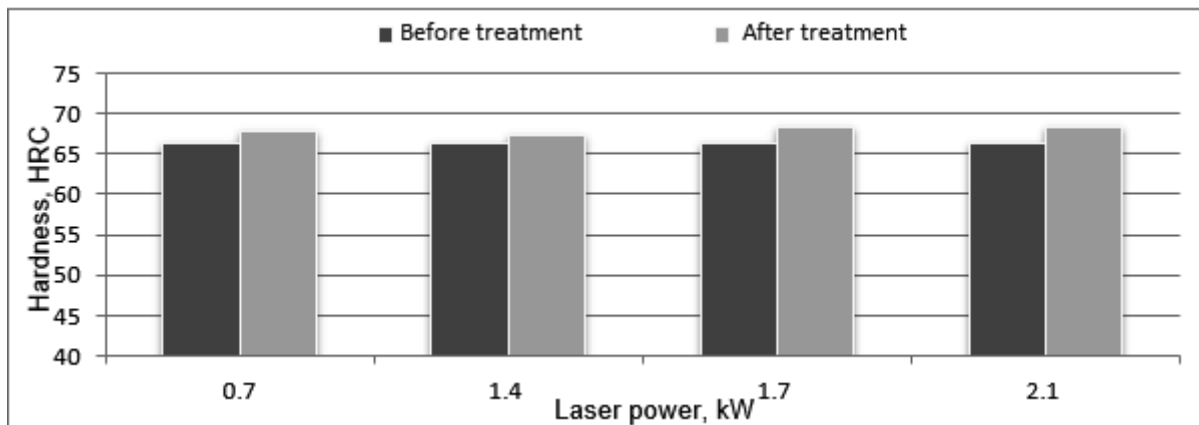


Figure 9: Variation in the average hardness of the surface layer of HS6-5-3-8 steel after laser melting with laser powers of 0.7 kW, 1.4 kW, 1.7 kW, 2.1 kW, at a constant melting speed of 0.5 m/min.

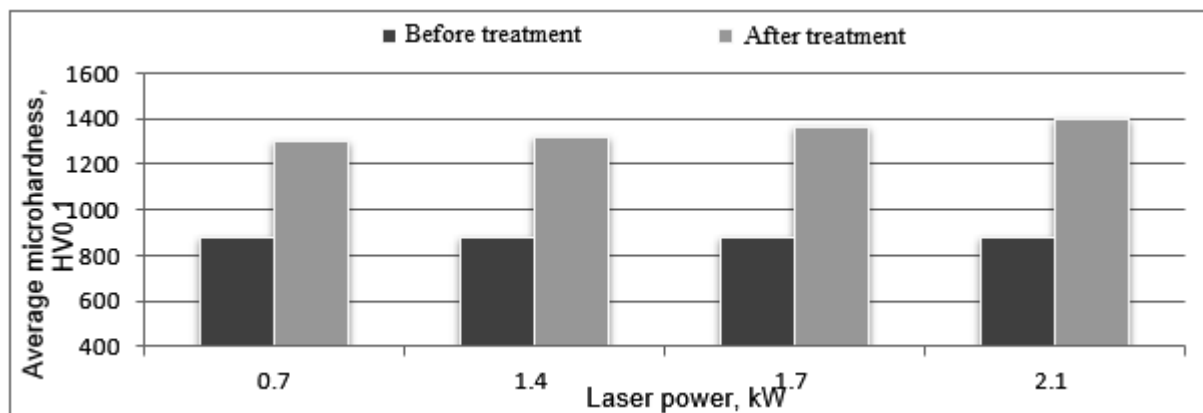


Figure 10: Average microhardness of the surface layer of HS6-5-3-8 steel after laser melting with laser powers of 0.7 kW, 1.4 kW, 1.7 kW, 2.1 kW, at a constant melting speed of 0.5 m/min.

#### 4. CONCLUSIONS

In conclusion, the research highlights the substantial effect of laser power on the formation process of the transformed layer, with laser beam power being of critical impact, influencing the depth of the melt zone. The hardness tests demonstrated the effectiveness of laser melting in enhancing surface hardness, up to approx. 30%. The examination of the transformed layer showcased the significance of laser power in achieving smoother surfaces and distinct melting boundaries. The roughness test underscored the influence of laser power on surface

irregularities, with lower powers exhibiting minimal roughness compared to higher power lasers.

## **ACKNOWLEDGEMENTS**

The work was created as a result of the project as part of project based learning - PBL, in the 10th competition under the Initiative of Excellence - Research University, Silesian University of Technology.

## **BIBLIOGRAPHY**

- 1 L. A. Dobrzański, Podstawy nauki o materiałach i metaloznawstwo, Materiały inżynierskie z podstawami projektowania materiałowego, WNT, Gliwice-Warszawa, 2002.
- 2 F. Staub, J. Adamczyk, Ł. Cieślak, J. Gubała, A. Maciejny, Metaloznawstwo, Wyd. „Śląsk”, Katowice, 1979.
- 3 K. Przybyłowicz, Metaloznawstwo, WNT, Warszawa 2003.
- 4 Norma PN-EN ISO 6507-1, Metale. Pomiar twardości sposobem Rockwella. Część 1, Metoda badań (skale A, B, C, D, E, F, G, H, K, N, T).
- 5 J. Klimpel, Technologie laserowe: spawanie, napawanie, stopowanie, obróbka cieplna i cięcie, Wydawnictwo Politechniki Śląskiej, Gliwice 2012.



26th January 2024  
Gliwice, Poland

DEPARTMENT OF ENGINEERING MATERIALS AND BIOMATERIALS  
FACULTY OF MECHANICAL ENGINEERING  
SILESIA UNIVERSITY OF TECHNOLOGY

## INTERNATIONAL STUDENTS SCIENTIFIC CONFERENCE

### **Effect of spindle rotations and feed speed on energy consumption of milling on a CNC machining centre**

Tomáš Čuchor<sup>1</sup>, Peter Koleda<sup>1</sup>, Richard Kminiak<sup>2</sup>, Miroslava Ťavodová<sup>3</sup>

<sup>1</sup> Department of Manufacturing and Automation Technology, Faculty of Technology, Technical university in Zvolen, T. G. Masaryka 24, 960 01, Zvolen, Slovakia,

<sup>2</sup> Department of Woodworking, Faculty of Wood Sciences and Technology, Technical university in Zvolen, T. G. Masaryka 24, 960 01, Zvolen, Slovakia,

<sup>3</sup> Department of Manufacturing Technologies and Quality Management, Faculty of Technology, Technical university in Zvolen, T. G. Masaryka 24, 960 01, Zvolen, Slovakia,  
email: xcuchor@is.tuzvo.sk

**Abstract:** The main goal of article is to create overview of measurements and evaluation of energy demand of machining process with practical implementation in energy consumption measured during milling process. The energy demand changes with different working parameters of machining centre. The changed parameters are revolution of machine tool and speed of tool. The parameters for revolutions were 14 000, 16 000 and 18 000 rounds per minute. The feed speed of tool were 6, 8 and 10 meters per minute. Then the electricity consumption of the machining center during the milling process was statistically evaluated. Based on the investigated technical-technological parameters, the revolutions of cutting tool have the most statistically substantial effect on electricity consumption and thus have the most energetic impact on the manufacturing process, followed by feed speed of machine tool.

**Keywords:** energy consumption, milling, CNC machining center, electricity consumption, statistical evaluation, revolutions of machine tool, speed of machine tool,

### **INTRODUCTION**

The manufacturing sector is one of the largest electricity consumers in the world, accounting for approximately 33% of total energy consumption. Most of the existing studies on energy reduction in the manufacturing sector focus on the development of the most energy efficient machining processes. The high cost of electricity in the production and processing of materials are among the main factors affecting the final price of products. This is a significant factor underlying the current environmental and economic challenges. While the main focus of scientists in the field of energy efficient production is to achieve minimal overall energy consumption, they also have the opportunity to look for solutions that are beneficial from an other points of view.

In the production process, the energy consumed could be divided into the energy needed to process the material to the required state and the energy consumed by the machine without load. The electrical energy that was consumed by the machine at no load is the energy that is usually consumed by the process unit and its supporting processes. A modern CNC machine tool normally consists of a CNC system, servo control system, feedback communication device, machine bed, lubricant, cooling system, etc. Most machine tools are powered by electricity, where part of the electricity is used to drive the servo systems and the remaining energy is used by the lubrication mechanism, cooling, information display and other auxiliary functions of the machine tool (Figure 1).

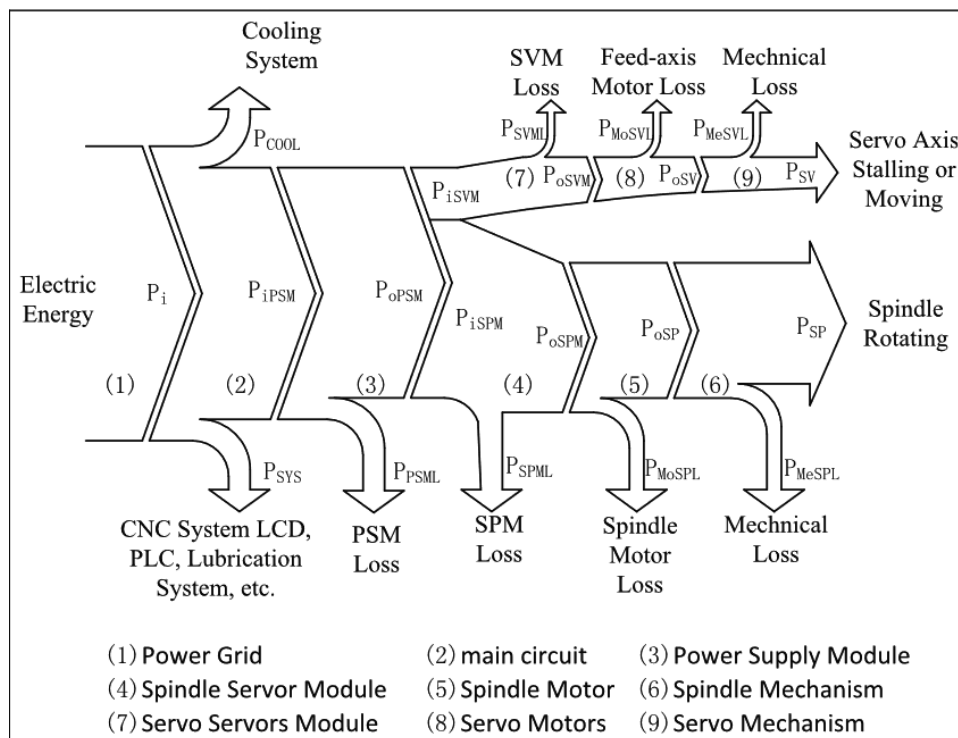


Fig. 1 Energy flow in a CNC production machine (Liu et al. 2017)

1. In the process of machining on the CNC centre, electrical energy enters the input.
2. The electrical energy required for the cooling and lubrication system is taken.
3. Power consumption for the power supply module (PSM).
4. Electrical energy consumed by the spindle amplifier module (SPM) for the servo motor driving the spindle.
5. Part of the electrical energy used to drive the spindle motor
6. Energy required for the spindle mechanism.
7. Energy used by the feed axis amplifier module (SVM).
8. Loss of motor energy that enables movement along the sliding axis.
9. Mechanical loss of the servomechanism.

For most servo systems, the AC input is converted to DC through a power supply module (PSM), then the PSM supplies power to the spindle amplifier module (SPM), or the servo axis amplifier module (SVM), respectively, to drive the motor to rotate spindles and turning, or blocking the motor of the feed axis (Liu et al. 2017).



The consumption of critical raw materials (such as steel, aluminium, copper, nickel, zinc, wood, etc. for industrial use has increased worldwide. The rapid growth in manufacturing has created many economic, environmental and social problems from global warming to local waste disposal (Sangwan 2011).

Manufacturing processes include a wide range of operations from processes such as machining, grinding and polishing, or injection, pressing, chemical treatment and others. All these production processes take material inputs, including work materials and auxiliary materials, and transform them into products and wastes. The flow of the production process together with the material and energy into the process is shown in the Figure 1.

## **ENERGY AND ITS LOSSES**

During machining processes, energy loss occurs through the conversion of electrical energy into wasteful heat. This leads to other problems, the increased temperature of the machining tool reduces its service life, increases cooling costs and in some cases leads to malfunctions that slow down or stop production. In an effort to reduce wasted energy in the production process, it is necessary to use the efficiency of the machine. Exergy is a measure of the energy potential of a material that could be converted into energy. By efficient material processing and replacement of machining elements that convert energy into work during the processing process. By increasing their efficiency and eliminating shortcomings, the amount of operating costs can be reduced (Gutowsky et al. 2006).

In order to create techniques to save energy during machining processes and increase energy efficiency, achieving a credible prognostication of energy consumption of machine tools by analysing the power consumption of their various components is essentially required. Using optimized cutting parameters is an effective technique for controlling energy consumption during manufacturing processes (Moradnazhad et al. 2015).

The total power consumption is the addition of air cutting power and material-removal power. Air cutting power is the power required by a machine tool when cutting tool is ready to cut the material from the workpiece without contacting the workpiece and follows the same tool path as during the material removal. The material removal power is the difference between total power and air cutting power. Based on material removal, the machining processes in machine tools can be classified into constant- material removal rate (MRR) and variable-MRR. In the constant-MRR machining process, all the cutting parameters remain unchanged during the machining for example turning and milling whereas, in variable-MRR, at least one of the cutting parameter changes e.g. end face turning, chamfering and grooving etc. (Pawanr et a. 2021).

This article provides a practical example of measuring machine consumption during machining with a subsequent evaluation of the influence of individual technical-technological parameters on this consumption.

## **METHODS**

The measurement was carried out on the CNC milling centre SCM TECH Z5 from the company SCM – group, Rimini, Italy and was carried out in the laboratories of the Technical University in Zvolen. Technical parameters of machining centre can be seen in Table 1 below.

*Table 1 Parameters of the 5-axis CNC machining centre SCM TECH Z5*

Axes		
Working area along X-Y-Z axes	mm	3050 – 1550 - 160
Panel length along Y axis	mm	1550
Panel length (for alternated work process)	mm	1390
Vectorial speed X-Y axes	m.min <sup>-1</sup>	83
Electrospindle		
Std motor power	KW (Hp)	11(15)
Max. speed	rpm	20 000

By correctly modifying the technical parameters and geometry of the machining tool, it is possible to save considerable finances. Incorrect geometry of the tool leads to an increase in costs, most often it leads to a reduced lifespan of the machining tool.

During the experimental milling, the tools shown in Fig. 2a and 3a with technical parameters in Table 2 and 3 were used. The dimensions of tools and chips direction are shown in the Fig. 2b and 3b for better comprehensibility.

*Table 2 Technical parameters of milling tool spiral cutter*

Tool length	$L = 157.8$ mm
Tool diameter	$D = 20$ mm
Working length of tool	$B = 75$ mm
Maximum feed	$f_{\max} = 20$ m min <sup>-1</sup>
Minimum feed	$f_{\min} = 6$ m min <sup>-1</sup>
Maximum speed	$n_{\max} = 20\ 000$ rpm
Standard speed	$n = 18\ 000$ rpm
Chip direction	positive

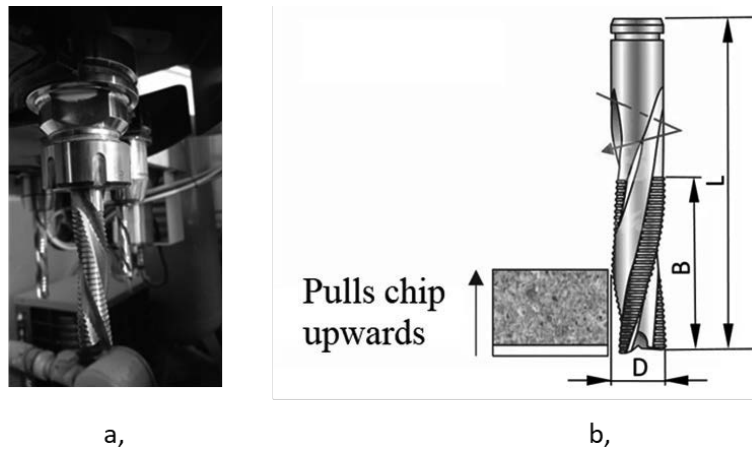


Fig. 2 Roughing tool (a.); Diagram of the positive roughing cutter tool,  $D$  – tool diameter,  $B$  – tool working length,  $L$  – tool length (b,) (www.freudtools.com)

Table 3 Technical parameters of finishing tool spiral cutter

Tool length	$L = 213.26 \text{ mm}$
Tool diameter	$D = 20 \text{ mm}$
Working length of tool	$B = 110 \text{ mm}$
Maximum feed	$f_{\max} = 20 \text{ m min}^{-1}$
Minimum feed	$f_{\min} = 6 \text{ m min}^{-1}$
Maximum speed	$n_{\max} = 20\,000 \text{ rpm}$
Standard speed	$n = 18\,000 \text{ rpm}$
Chip direction	negative

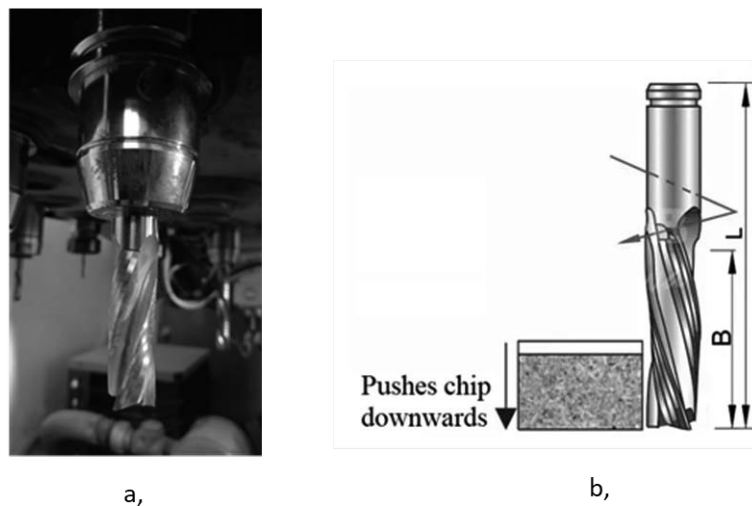


Fig. 3 Finishing tool (a.); Diagram of the negative finishing cutter tool,  $B$  – tool working length,  $L$  – tool length (b,) (www.freudtools.com)

The power measuring instrument was connected to the electrical power supply of the CNC machining centre. It was connected with the help of current probes and voltage clamps. The voltage clamps were connected to the phase conductors, zero and protective conductor using the installed socket 32 A5P. The current probes were connected in the direction of the current flow, in the case of the opposite connection, the values measured on the terminals would be negative. After the connection of measuring circuit, a test measurement of the signal was realized on the phases.

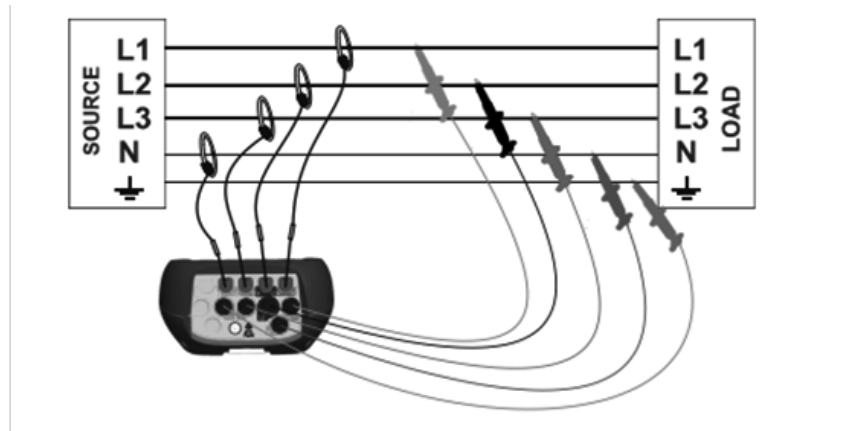


Fig. 4 Connecting the Metrel measuring device

The CNC program was programmed as linear movement from point A to point B. Technological parameters of milling process are in Table 4.

Table 4 Technological parameters of milling

Technological parameters of milling			
Revolutions (n) [1000rpm]	14	16	18
Feed (f) [m.min <sup>-1</sup> ]	6	8	10

The measured data had to be processed, to access the measured data the Metrel Power View program was used, which then opened each measurement separately. The measurements contained all the information on the measurement values that the device allowed us to measure. For our purpose, the required data was manually transcribed into Excel. We calculated amount of energy by processing the measured data under milling load and without load. Subsequent evaluation of effect of rotations and feed speed on cutting power was realised in the program Statistica.

## RESULTS AND DISCUSSION

Description statistics of measured and calculated values of power during milling is described in the Table 5.

Table 5 Description statistics of cutting power

Parameter	Value	Average P [kW]	St. Dev. [kW]	-95,0 % [kW]	+95,0 % [kW]
n [rpm]	14000	3.36	0.23	3.26	3.46
	16000	3.68	0.28	3.56	3.80
	18000	4.07	0.39	3.91	4.24
f [m.min <sup>-1</sup> ]	6	3.68	0.43	3.50	3.86
	8	3.66	0.44	3.47	3.84
	10	3.78	0.40	3.61	3.95

F-statistic and the corresponding p-value of ANOVA are in the Table 6. When analyzing all the combinations, it was found that mainly the revolutions of cutting toll, have a significant influence on the consumption of electricity. It is assumed that the consumption of electrical energy by the feed of the tool will increase if the speed of the cutting tool increases. It was predicted that with increased revolutions of cutting tool the energy consumption rises.

Table 6 Statistical method of ANOVA

Effect	One dimensional results for each dependent. variable				
	Degrees of freedom	P [kW] (SS)	P [kW] (MS)	F	p
Abs. member	1	987.56	987.56	9973.39	0.000
Revolutions (n)	2	6.0922	3.0461	30.763	0.000
Feed (f)	2	0.2041	0.1021	1.031	0.363
n .f	4	0.0895	0.0224	0.226	0.922
Error	63	6.2383	0.099		
Total	71	12.6241			

SS means "the sum of squares due to the source."

MS means "the mean sum of squares due to the source."

F means "the F-statistic."

p means "the P-value."

Duncan's test (method of more detailed evaluation) shows a mutual comparison of averages with each other. From the values presented in the table, it can be noted that there is a difference between the speed of rotation of spindle in terms of electricity consumption and they have a statistically significant difference. It can concluded that with an increase in revolutions, the overall consumption of energy is also increased, that means that this factor has a statistically significant effect.

Table 7 Duncan's test for revolutions

revolutions [1000 rpm]	14 M = 3,360	16 M = 3,679	18 M = 4,072
14		0.000159	0.000063
16	0.000159		0.000122
18	0.000063	0.000122	

The graphic interpretation is shown in more detail on the speed chart in Fig. 5. In the graph, it can be also seen how the consumption of electricity increases linearly with the increase in the speed of the machining tool.

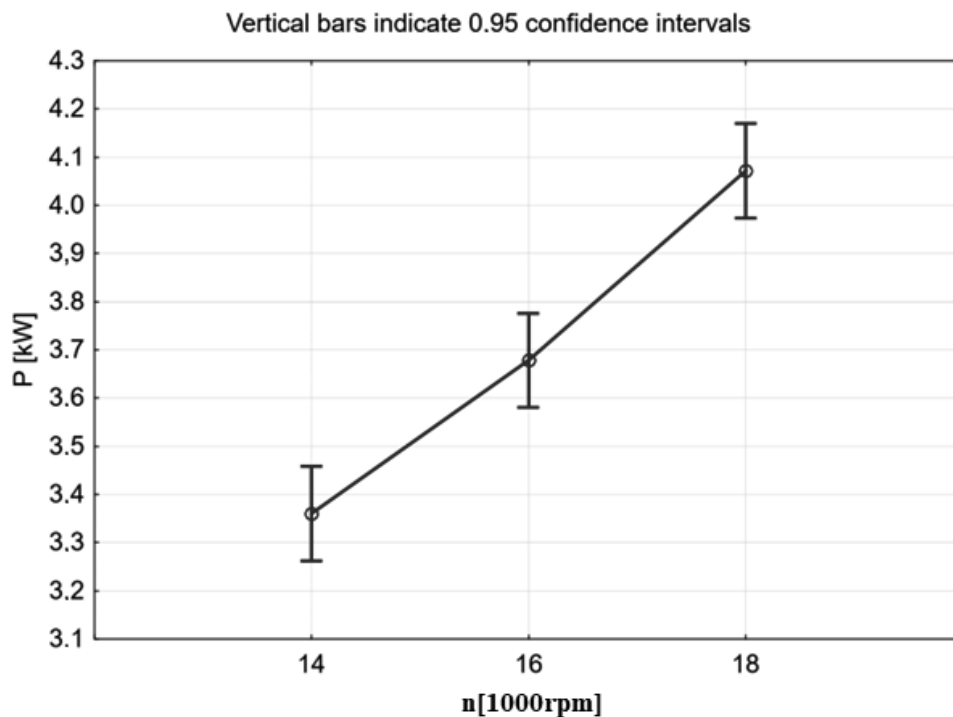


Fig. 5 Dependence of the consumption of electricity on the revolutions of the milling tool

On the basis of the experiments carried out and their evaluation through analysis of dispersion followed by post-hoc test, it can be concluded that with increasing revolutions of spindle of machine centre, the electrical output also increased almost linearly from value of 3,36 kW and speed of 14 000 rpm to the value of 4.07 at speed of 18 000 rpm. This increase is caused by the increase in the values of currents flowing through the windings of the electric drive for spindle and also by the increased volume of removed material pre unit of time. The increase in power required to remove material is also confirmed by the authors (Sedlecký et a. 2017) who examined power consumption during edge milling of MDF and edge-glued panel and also (Barčík et a. 2010) who examined the effect of various feed rates and cutting speed on power consumption during the surface milling of beech wood. The change in revolutions had a statistically significant effect on the change in the consumed electrical energy (parameter  $p < 0.05$ ). With Duncan's test shows a mutual comparison of the averages of electricity consumption by the spindle revolutions speed. From the values presented in the table, it can clearly pointed out that the speed of the tool movement of the machining centre does not

confirm a statistically significant dependence to current consumption of electricity. It can be concluded that the energy consumption is not significantly increased with the acceleration of the movement of machining tool, this factor does not have a statistically significant effect.

Table 8 Duncan test for feed speed

Feed speed [m.min <sup>-1</sup> ]	6 M = 3,678	8 M = 3,655	10 M = 3,778
6		0.743	0.151
8	0.743		0.097
10	0.151	0.097	

The graphical interpretation is shown in more detail on the shift graph in Fig. 6. From the graph, it can be seen that the largest consumption was precisely when the tool was moved 10 meters to the right. Acceleration of the machining tool will not significantly increase our consumption of electrical energy.

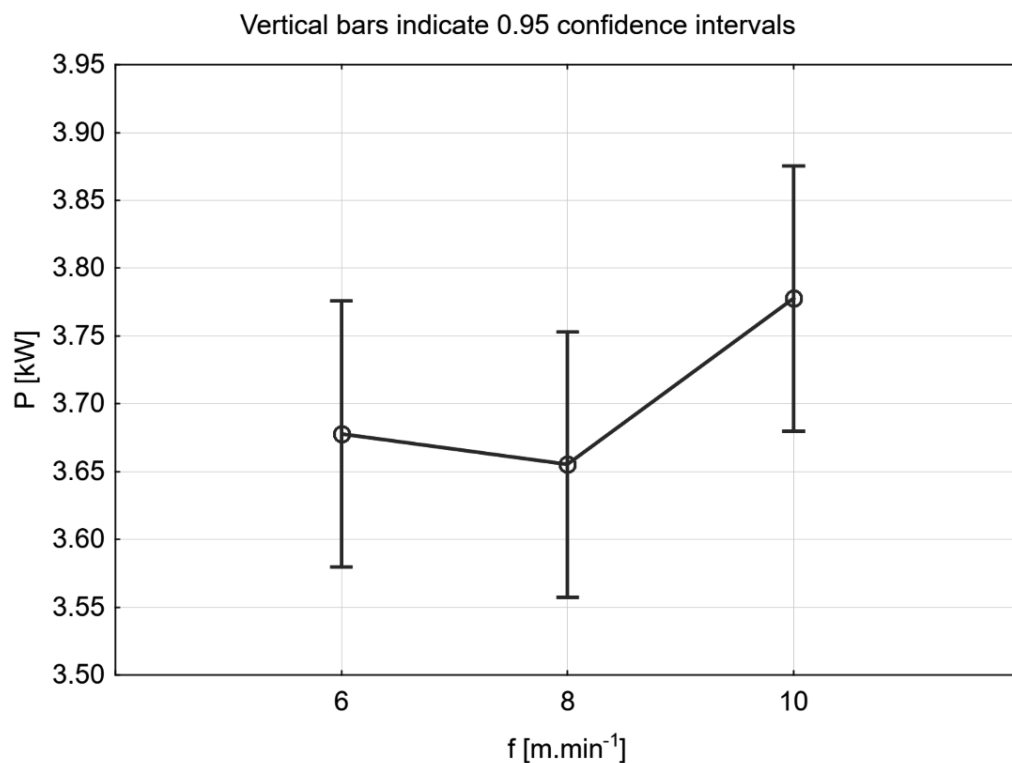


Fig. 6 Dependence of electrical power consumption on feed speed

When the feed speed changed from 6 to 8 m.min<sup>-1</sup>, the cutting power decreased from 3.38 to 3.66 kW, when it changed to 10 m.min<sup>-1</sup>, it increased to 3.78 kW. Small increase of milling output with increase of feed speed also stated (Sedlecký et al. 2017) and also (Atanasov and Kovatchev 2019) who examined cutting power during milling of wood based materials as MDF and plywood. However, Duncan's post hoc test did not show statistical significance of this change.

## CONCLUSION

Reducing the energy demand of not only processes in the manufacturing industry is one of the current challenges of society for more sustainable production. This also includes analysing the factors that have the greatest influence on energy consumption and which are modifiable, while other economic and material parameters must also be taken into account. The results of the experiment confirmed that the greatest influence on the energy consumption of milling are revolutions of the tool, or cutting speed. The effect of feed speed did not show statistical significance. These findings will be further expanded and deepened in further research.

## BIBLIOGRAPHY

1. ATANASOV, V., KOVATCHEV, G. 2019. Determination of the cutting power during milling of wood-based materials. *Acta Facultatis Xylogiae*. 61. 93-101. 10.17423/afx.2019.61.1.09.
2. BARCÍK, Š., KMINIAK, R., ŘEHÁK, T., KVIETKOVÁ, M. 2010. The influence of selected factors on energy requirements for plain milling of beech wood. *Journal of Forest Science*. 56. 243-250. 10.17221/119/2009-JFS.
3. www.freudtools.com page of Freud®. [online] [cit. 2023-10-31]. Available on: <<https://www.freudtools.com/public/catalog/freud-catalog/>>.
4. GUTOWSKI T, DAHMUS J, THIRIEZ A 31.05.2006 Electrical Energy Requirements for Manufacturing Processes [online]. [cit. 2023-10-12]. Available on: <<http://web.mit.edu/2.813/www/readings/Gutowski-CIRP.pdf>>
5. HORTOBÁGYI, A. 2023. Analýza vibrácií obrobku ako potenciálneho parametra preadaptívne riadenie CNC stroja. PhD-thesis. Zvolen: Technická univerzita vo Zvolene. Fakulta techniky. 2023. 113 s.
6. LIU, Z. ZHANG, W., LIU, L., XIAO, Z. 2017 Measuring and calculating the computer numerical control lathe's cutting power and total electric power consumption based on servo parameters [online]. [cit. 2023-10-12]. Available on: <<https://journals.sagepub.com/doi/pdf/10.1177/1687814017723293>>
7. MORADNAZHAD M, UNVER H.O. 2015 Energy Efficiency of machining operations: A Review. *Proc IMechE Part B J Engineering Manufacture*, 1–19
8. PAWANR, S., GARG, K.G., ROUTROY, S. 2021 Modelling of Variable Energy Consumption for CNC Machine Tools Department of Mechanical Engineering, Birla Institute of Technology and Science, Pilani, Rajasthan, INDIA –333031
9. SANGWAN, K. S., 2011. Development of a multi criteria decision model for justification of green manufacturing systems. *Int. J. Green. Econ.* 5, 285-305
10. SEDLECKÝ, M., GAŠPARÍK, M. 2017. Power consumption during edge milling of medium-density fiberboard and edge-glued panel. *Bioresources*. 12. 7413-7426. 10.15376/biores.12.4.7413-7426.





26th January 2024  
Gliwice, Poland

DEPARTMENT OF ENGINEERING MATERIALS AND BIOMATERIALS  
FACULTY OF MECHANICAL ENGINEERING  
SILESIA UNIVERSITY OF TECHNOLOGY

## INTERNATIONAL STUDENTS SCIENTIFIC CONFERENCE

### **Exploring the potential of duplex stainless steels in additive manufacturing: composition, corrosion, and challenges**

Mengistu Jemberu Dagnaw<sup>a\*</sup>, Zbigniew Brytan<sup>a</sup>

<sup>a</sup> Silesian University of Technology, Faculty of Mechanical Engineering, Department of Engineering Materials and Biomaterials, 18a Konarskiego Street, 44-100, Gliwice, Poland

\*Corresponding author: Mengistu.Jemberu.Dagnaw@polsl.pl

**Abstract:** Duplex stainless steels (DSS) are two-phase alloys that have an equal number of ferritic and austenitic phases in their microstructure. These alloys offer a combination of the corrosion resistance of austenitic stainless steels and a higher level of strength. In comparison to austenitic stainless steels and ferritic stainless steels, DSS have a higher strength and a greater resistance to stress, pitting, and crevice corrosion. DSS are also more resistant to corrosion in crevices. Altering the alloying elements of DSS, such as chromium, nickel, molybdenum, nitrogen, copper, tungsten, rare earth, and so on, can result in improvements to the mechanical properties and corrosion resistance of the steels. There is still a phenomenon known as corrosion that has a significant impact on the performance of the materials that are exposed, and it is imperative that special attention be made when dealing with this.

**Keywords:** Duplex Stainless Steel, Composition, Corrosion, Additive Manufacturing

### **1. DUPLEX STAINLESS STEELS**

Duplex stainless steels are becoming more commonly utilized as structural materials in chemical and petrochemical applications, as well as in power plants and other industries. Their exceptional resistance to localized corrosion, combined with their remarkable strength and toughness, primarily accounts for this phenomenon. DSS exhibit distinct mechanical characteristics and coefficients of thermal expansion in their two phases. These disparities can lead to significant stress gradients during straining or following different surface treatments. The corrosion resistance of both individual phases and the overall metallic alloy can be influenced by the presence of significant stress gradients. Oil reserves provide significant challenges for metallic materials due to their highly corrosive nature. Venezuela, Saudi Arabia, and Canada are the dominant nations in this sector, while Mexico now ranks 17<sup>th</sup>. Consequently, it is essential to update, maintain, and safeguard all infrastructure due to the presence of harmful elements in petroleum [1]. Given that corrosion is a critical concern in the oil and gas company, there is a constant need for steel that can resist corrosion.

Stainless steels, particularly martensitic and duplex ones, are very suitable for these applications, specifically in the oil and gas industry, where hydrogen sulphide poses the greatest risk on the outside platform [2].

DSS lack resistance to chloride ions. Similarly, when exposed to specific temperature conditions and concentrations of S, stainless steels exhibit a decline in their ability to resist corrosion and begin to experience mechanical failure [3]. The petrochemical industry is increasingly interested in this material because of its ability to enhance component performance and generate cost savings. Additionally, it offers hidden savings by reducing maintenance requirements, thereby improving overall industrial efficiency. Hruska et al. conducted a study for the biomass industry where they applied coatings to stainless steels, leading to enhanced corrosion resistance [4]. Stainless steels are a collection of high-alloy steels that are mostly composed of the Fe-Cr, Fe-Cr-C, and Fe-Cr-Ni systems. To be classified as stainless, the material must contain at least 10.5% chromium. These steels belong to a broad category of specialized alloys principally designed to withstand corrosion [5]. Additional notable attributes of these materials encompass exceptional malleability, resilience to extreme hot and cold temperatures, and durability against oxidation and fracturing under elevated temperatures [6]. Despite the well-established resistance of DSS to classical sensitization caused by chromium carbide precipitation, it is now recognized that sensitization can occur in DSS due to the formation of intermetallic compounds such as  $\sigma$  (sigma) or  $\chi$  (chi), as well as other particles or phases like  $\text{Cr}_2\text{N}$  (chromium nitrides) or  $\alpha'$  (alpha prime). The primary factor responsible for significantly lowering the resistance to stress corrosion cracking (SCC) in this material is the production of  $\sigma$ .

Duplex stainless steels can be classified into various categories based on their chemical composition and performance characteristics ( Fig.1). The main classifications are duplex (DSS), lean duplex (LDSS), super duplex (SDSS), and hyper duplex (HDSS).

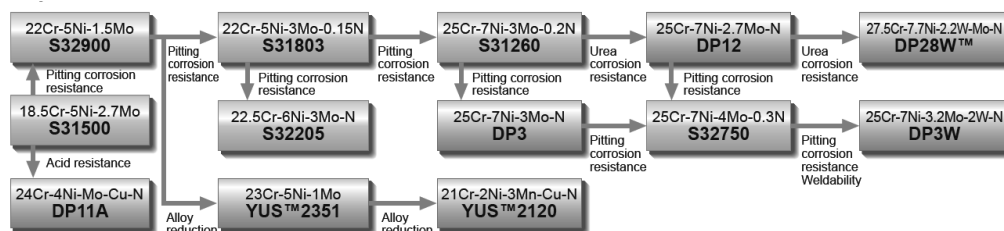


Figure 1. Duplex stainless-steel grades, correlation between chemical composition [6].

Standard DSS typically contain about 22% Cr, 5% Ni, and 3% Mo. This composition ensures a balanced mix of ferrite and austenite, providing a good combination of strength and corrosion resistance, particularly against chloride stress corrosion cracking. The presence of Cr and Mo in significant amounts imparts notable resistance to corrosion, while Ni aids in maintaining an austenitic structure. Lean duplex stainless steels (LDSS) are formulated with less Ni and Mo – usually around 21% Cr, 1.5% Ni, and 0.3% Mo. This reduced content makes them more cost-effective while still maintaining higher strength and satisfactory corrosion resistance compared to standard austenitic stainless steels. Super duplex stainless steels (SDSS), have higher levels of these alloying elements – typically around 25% Cr, 7% Ni, and 4% Mo. This enhanced composition results in exceptional resistance to pitting and crevice corrosion, along with higher strength. Hyper duplex stainless steels (HDSS) push the envelope

further with even higher levels of Cr, Ni, and Mo. This category is designed for the most demanding applications that require the utmost corrosion resistance and strength.

The Pitting Resistance Equivalent Number (PREN) is a widely recognized metric used to classify and compare the corrosion resistance of DSS. PREN is calculated using a formula that considers the key alloying elements in the steel: Cr, Mo, and Ni. Specifically, the formula is usually represented as  $PREN = \%Cr + 3.3 \times \%Mo + 16 \times \%N$  [8]. When addition of wolfram is considered, then the formula is presented as:  $PRE(W) = \%Cr + 3.3 \times \%Mo + 0.5 \times \%W + 16 \times \%N$ . This calculation provides a numerical value that correlates with the material's resistance to pitting corrosion, a common and aggressive form of corrosion in stainless steels. Higher PREN values indicate a greater resistance to pitting corrosion, making this number a crucial factor in selecting the appropriate grade of DSS for specific environments, especially those involving chloride exposure or other corrosive elements.

### 1.1 Molybdenum effect

Molybdenum is a powerful ferrite-stabilizing element that enhances the development of ferrite and widens the zone where ferrite is present [9]. The addition of Mo can improve the resistance to corrosion by the formation of a stable passive film on the surface of the stainless steel. In particular, its ability to improve the pitting and crevice corrosion resistance is 3.3 times that of Cr [10]. In DSSs, Mo significantly improves the chloride-induced corrosion resistance (pitting, crevice corrosion, and stress-corrosion cracking) [11]. This is because Mo can keep the passive film stable and promote the recovery of the passive film, thereby improving the pitting resistance and repassivation performance of DSSs as a whole. Mo is more potential stable than single-phase stainless steel. This means that it stops the activity of alloy elements and helps to stabilize passive film, which is why DSSs have a passive film that is almost completely unpenetrated [12].

Upon absorption of  $Mo^{6+}$  by the damaged surface, the functionality of the passive film is restored, resulting in the formation of an undamaged surface. On the other hand, the partially shielded single-phase stainless steel is vulnerable to corrosive substances and experiences pitting. However, the addition of Mo encourages the formation of detrimental intermetallic compounds like  $\sigma$  phase and  $\chi$  phase. This expands the range of time and temperature in which precipitation occurs, while also reducing the time it takes for precipitation to happen. As a consequence, the steel becomes more prone to embrittlement and cracking, making it challenging to work with [13]. As a ferrite former, Mo increases the yield strength of DSSs but decreases their ultimate tensile strength [14]. Meanwhile, Mo also enhances the high-temperature strength, creep strength, and high-temperature fatigue properties of austenite stainless steels, improving the intergranular corrosion resistance of austenite [15].

### 1.2 Chromium effect

Chromium is a common element that forms ferrites. Cr is the most important and crucial element in DSS, since it can increase the ferrite phase region and stabilize the ferrite structure [16]. Cr can generate a dense oxide protection film on the surface of stainless steel, boosting the ability of the damaged passivation film to repair and repassivated. The Cr concentration of the stainless steel must be at least 10.5 wt.% in order to generate a stable passive film. The higher the Cr content, the stronger the corrosion resistance of the stainless steel [17]. However, in strong oxidizing acids and some reducing environments, the passivation of Cr alone is

insufficient to maintain the stainless steel's corrosion resistance. To play a good role in corrosion resistance, some elements that hinder anode dissolution, such as Ni, Mo, Si, and other elements with Cr, must be included. To achieve a two-phase composition in DSSs, Cr must be at least 18 wt.%. Cr and Fe can combine to form a continuous solid solution, which can operate as a solid solution strengthening agent. In addition, Cr can improve high-temperature oxidation resistance [18].

Chromium improves the performance of duplex stainless steel's oxidation resistance medium and acid chloride medium; under the combined action of nickel, molybdenum and copper, chromium improves the resistance of DSS to some reducing media, organic acid, urea, and alkaline media; chromium also improves the resistance of DSS to localized corrosion, such as intergranular corrosion, pitting corrosion, crevice corrosion, and stress performance under certain conditions. In addition to having an important influence on the corrosion resistance of negative-number austenitic stainless steel, chromium can also significantly improve the oxidation resistance, sulfidation resistance and resistance to melting salt corrosion of such steels. The presence of chromium in duplex stainless steel significantly enhances its corrosion resistance, making it a versatile and durable material for various applications in corrosive environments. The specific performance of the alloy depends on the overall composition, including the amounts of chromium, nickel, molybdenum, and other alloying elements.

### 1.3. Nitrogen effect

Nitrogen is a strong austenite stabilizing element that is 30 times stronger than nickel in stabilizing austenite. As a result, it can partially or entirely replace the costly austenite stabilizer Ni in stainless steel. In general, N exists as an interstitial solid solution in austenite, which can improve its strength. The N content of the austenite in the DSSs influences the relative mechanical characteristics of the constituent phases to some extent. When the N concentration of austenite is less than 0.12 wt.%, for example, ferrite is harder than austenite. Austenite, on the other hand, develops a harder phase when it exceeds 0.12 wt.%. However, N's solubility in steel is limited. When combined with Mn, the solubility of N in austenite can be enhanced. Under normal pressure, adding 3 wt.%-10 wt.% Mn can increase the N content of austenitic stainless steel to 0.5 wt.%. Austenite stabilized by N is metastable and consequently has a distinct deformation behavior. Unlike in classic Cr-Ni-Mo DSSs, where dislocation slip is the primary method of deformation, the austenite in Mn-N-type LDSSs will undergo martensite transition or twinning. TRIP enabled a high-performance LDSS to attain an excellent mix of strength and ductility above 1 GPa-60%, which was problematic for traditional Cr-Ni-Mo DSSs. The volume percentage and mechanical stability of austenite (dominated by stacking fault energy) are determined by minor variations in N concentration [19].

It was shown that the austenite composition increases linearly with N content, delaying the appearance of the TRIP effect. The strain-induced martensite that creates the TRIP effect nucleates at austenite grain borders and annealing twin boundaries as well as in-grain - martensite band intersections. The deformation mechanism of the LDSSs is relatively complicated and difficult. In this case, austenite controls the deformation process, and stacking fault energy (SFE) is the most important factor in separating the austenite deformation mechanism. The TRIP effect is easily observed in low-SFE austenite. In summary, the mechanism of strain-induced plasticity is that the part of the deformation process with the greatest strain first induces martensitic transformation and/or mechanical twinning, which increases local strength and makes it difficult to continue the deformation, leading to

deformation to transfer to other regions and delaying necking. This effect improves work hardening and uniformly expands the strain range for plastic deformation [20].

## **2. ADDITIVE MANUFACTURING OF DUPLEX STAINLESS STEEL**

In comparison to traditional approaches, additive manufacturing (AM) processes provide a viable alternative method for fabricating DSS, especially when complex and irregular shapes are required in addition to the density of the materials. However, high cooling rates and process control are critical to minimize the precipitations of harmful secondary phases that might impair mechanical properties and corrosion resistance. Local temperature cycles, for example, that occur within AM processes might result in the formation of unique microstructural characteristics with tiny grain structures. The development of unmelted powders, microcracks, porosities, and balling has an impact on the corrosion mechanism and performance of AM components. As a result, the unique microstructural properties of the metallic structures define their longevity [21].

There are a number of factors that affect the corrosion resistance of AM duplex stainless steels. The following factors are crucial for AM DSS qualifications and reliability: The quality of the starting material, such as powder feedstock, has a considerable impact on the corrosion resistance of AM DSS. Gas atomization (GA), which includes atomizing a molten alloy with a high-pressure flow of argon or nitrogen gas, is the most common method for creating commercial stainless-steel powder. The GA process and its characteristics, such as atomization gas pressure, melt delivery tube diameter, and melting temperature, have a significant impact on powder properties. Furthermore, the temperature of the atomization gas influences particle size and form. When hot gas is used for atomization, the sound velocity of the atomization gas increases, as does the relative velocity between droplets and gas during breakdown. As a result, smaller droplets are formed that retain their spherical shape under the influence of surface tension. At the same time, due to the influence of gas compressibility, the atomization gas flow rate reduces. Meanwhile, the process gas type influences the atomization process, resulting in powders of varying chemistry and quality. Nitrogen pickup in the steel melt may occur if steel is melted in a nitrogen environment. If argon is used to atomize the steel melt, the argon can become contained in the droplets during droplet deformation and breakage, resulting in hollow particles. The aforementioned process parameters and process conditions may have a significant impact on the powder properties and, as a result, on the quality of the LPBF component [26]. GA powder particles typically have spherical and dimpled forms, as well as some surface roughness from smaller satellite particles. Shape and size distributions might differ between manufacturers and lots, influencing powder packing density (LPBF) and nozzle flowability (DED) during the build. This, in turn, contributes to the part's porosity and surface roughness, and hence to its corrosion resistance. Furthermore, entrapped atomization gas porosity in GA powders can convert into gas porosity in the consolidated LPBF or DED material. Heat treatment can impact the microstructure and mechanical properties of AM DSS, which in turn can affect its corrosion resistance. Heat treatment after printing is commonly used to reduce residual stress, modify mechanical properties, and homogenize microstructure. Because of variations in the initial microstructure and stored strain energy, the thermal stability and evolution of AM SS microstructures differ significantly from those of traditional thermomechanical treated counterparts.

AM of DSS has received little attention. When employing ordinary DSS like 1.4462 or 1.4410, it is not possible to achieve a duplex microstructure with roughly the same quantity of ferrite and austenite. Because of the high cooling rates ( $\sim 10^6$  K/s), the as-built parts have a mostly ferritic microstructure, which suppresses the change from ferrite to austenite during cooling in laser AM. Because nitrogen doesn't dissolve easily in ferrite, chromium nitrides are precipitation. This changes how these steels react to corrosion and their mechanical properties. Heat treatment (solution annealing) can be used to achieve the duplex microstructure and eliminate undesirable phases from the parts. During heat treatment, austenite is believed to occur at sub grain boundaries or lattice flaws. The solution treatment, on the other hand, reduces the density of dislocations, making the annealed sections less robust and hard [22].

DSS have a complex precipitation behavior due to the significant number of alloying components. The different distribution of alloying elements in the ferritic and austenitic phases enhances this. Intermetallic precipitations in DSS have a significant impact on both mechanical and corrosive properties. When brittle phases precipitate, the toughness rapidly decreases, and low-alloy tertiary austenite develops, making them more prone to rust [23]. The presence of too much nitrogen (N) in the ferrite matrix leads to the precipitation of chromium nitride. This makes LPBF DSS stronger but less flexible than wrought DSS. Ferrite is the dominant phase in SDSS in the as-built condition, and to restore the balance between austenite and ferrite and therefore regain desired ductility, high-temperature annealing at approximately 1100°C followed by water quenching are common post-processing steps. The austenitic phase contributes to toughness and resistance against corrosion, while ferrite improves strength but decreases crack susceptibility and toughness. The benefit of alloy development by powder mixing and screening is the reduction of potential uncertainties and expenses connected with their manufacturing. These uncertainties, which are mostly related to the atomization process, include aspects such as the feasibility of atomizing a novel alloy, process yield, powder morphology conformity with LPBF process parameters, and powder batch compositional consistency. Adopting an accelerated alloy screening methodology allows for a better understanding of the complex link between process-driven events and material structure. This, in turn, offers information on how these interactions influence component performance while permitting the development of a comprehensive testing matrix for novel materials, allowing the determination of robust AM parameters suited to yield desirable material properties [24].

Powder characteristics are recognized to play a major influence in LPBF processability. To develop good-quality powder layers during powder spreading, powder properties such as particle size distribution, particle shape, powder flowability, and apparent density should be examined and improved. Spherical powders offer good flowability and spreadability in general, leading to high density powder layers and as-built objects with low porosity. Because of interlocking mechanisms, particles with uneven shapes have poor flowability. Very tiny particles, on the other hand, cause particle agglomeration and a lack of flowability because interparticle forces, such as van der Waals forces between particles, can exceed gravitational forces [25].

## 2.1. Challenges in the AM of duplex stainless steels

Additive manufacturing of DSS poses several significant challenges. The first is related to phase imbalance and phase instability. The balance between austenite and ferrite is critical for optimal mechanical and corrosion resistance properties. However, during AM this balance can be disturbed by rapid heating and cooling cycles. These cycles can lead to excessive growth of

one phase at the expense of the other, potentially forming undesirable phases such as sigma and chi, which can degrade the mechanical properties and corrosion resistance of the material [21].

The next challenge is related to microstructural heterogeneity. The rapid solidification in AM processes can lead to non-uniform microstructures in DSS. This heterogeneity often manifests as micro-segregation of alloying elements, leading to localised variations in phase composition and properties. This heterogeneity can be detrimental to both the mechanical strength and corrosion resistance of the manufactured parts. Järvinen et al. (2015) investigated these microstructural variations and their impact on material properties in their study of AM duplex stainless steels [22].

The next important issue in AM of DSS is related to porosity and defect formation typical of AM technology. AM processes, particularly those involving powder bed fusion, are prone to the introduction of defects such as porosity, lack of fusion and cracks. These defects result from improper melting and solidification, variations in energy input and inconsistencies in powder properties. In DSS, such defects can significantly affect mechanical integrity and corrosion resistance. Research has shown that optimising process parameters is critical to minimising these defects, but achieving consistency remains a challenge. Residual stress and distortion are also important aspects of AM of DSS. The localised and rapid heating and cooling associated with AM can introduce significant residual stresses into DSS components. These stresses, if not properly managed, can lead to distortion and warping of the printed parts, as well as reduced fatigue life. Post-processing, such as heat treatment, is often required to relieve these stresses, adding complexity and cost to the manufacturing process [21-23].

Post-processing and surface quality is the next important issue to be resolved in AM of DSS. AM often results in rougher surface finishes compared to traditional manufacturing methods. For DSS this can be a significant issue as the surface finish plays an important role in corrosion resistance. Post-processing techniques such as machining or polishing are required to achieve the desired surface finish, which can be challenging and costly. The final challenging issue relates to AM process parameters. The quality of AM duplex stainless-steel parts is highly dependent on the precise control of process parameters such as laser power, scan speed and layer thickness. Small variations in these parameters can lead to significant changes in microstructure and properties. However, achieving and maintaining this level of control is challenging, especially given the variability in material properties and environmental conditions [21-25].

### **3. CONCLUSION**

The application of DSS in additive manufacturing presents distinct challenges, largely due to the complexity of their chemical composition and the demands of AM processes. The intricate balance of alloying elements in DSS, crucial for their superior strength and corrosion resistance, is often disrupted during AM, leading to phase instability and microstructural irregularities. Addressing these issues is key to harnessing the full potential of DSS in AM, making it a focal point for future research and technological advancements in this field.

### **BIBLIOGRAPHY**

- [1]. Hou, Y.; Nakamori, Y.; Kadoi, K.; Inoue, H.; Baba, H. Initiation mechanism of pitting corrosion in weld heat affected zone of duplex stainless steel. *Corros. Sci.* 2022, 201, 110278.

- [2]. Gennari, C.; Pezzato, L.; Simonetto, E.; Gobbo, R.; Forzan, M.; Calliari, I. Investigation of Electroplastic Effect on Four Grades of Duplex Stainless Steels. *Materials* 2019, 12, 1911.
- [3]. Hruska, J.; Mlnarik, J.; Cizner, J. High-Temperature Corrosion of Nickel-Based Coatings for Biomass Boilers in a Chlorine-Containing Atmosphere. *Coatings* 2022, 12, 116.
- [4]. Hu, Y.; Shi, Y.; Shen, X.; Wang, Z. Microstructure, pitting corrosion resistance and impact toughness of duplex stainless steel underwater dry hyperbaric flux-cored arc welds. *Materials* 2017, 10, 1443.
- [5]. Practical guide to using duplex stainless steels, Nickel Institute, Second Edition, published in 2020, <http://www.nickelinstitute.org/>
- [6]. Nippon Steel Corporation, <https://www.tubular.nipponsteel.com/>.
- [7]. 20-ENG. 0 .2009 – Sandvik duplex stainless steels. <https://www.materials.sandvik/link/>
- [8]. Sun Y-T, Tan X, Lei L-L, Li J, Jiang Y-M. Revisiting the effect of molybdenum on pitting resistance of stainless steels. *Tungsten*. 2021;3(3):329.
- [9]. Schweitzer PA. *Metallic materials: physical, mechanical, and corrosion properties*. Florida: CRC Press; 2003.
- [10]. Roberge PR. *Corrosion engineering handbook*. Florida: CRC Press; 1996.
- [11]. Tian H, Cheng X, Wang Y, Dong C, Li X. Effect of Mo on interaction between  $\alpha/\gamma$  phases of duplex stainless steel. *Electrochim Acta*. 2018; 267:255.
- [12]. Martins M, Casteletti LC. Heat treatment temperature influence on ASTM A890 GR 6A super duplex stainless-steel microstructure. *Mater Charact*. 2005;55(3):225.
- [13]. Sieurin H, Sandström R. Sigma phase precipitation in duplex stainless steel 2205. *Mater Sci Eng, A*. 2007;444(1–2):271.
- [14]. Jiménez JA, Frommeyer G, Carsí M, Ruano OA, Superplastic properties of a  $\delta/\gamma$  stainless steel. *Mater Sci Eng, A*. 2001;307(1–2):134.
- [15]. Clayton C, Lu Y. A bipolar model of the passivity of stainless steel: the role of Mo addition. *J Electrochem Soc*. 1986;133(12):2465.
- [16]. Lee J-B. Effects of alloying elements, Cr, Mo, and N on repassivation characteristics of stainless steels using the abrading electrode technique. *Mater Chem Phys*. 2006;99(2–3):224.
- [17]. Brooks A, Clayton C, Doss K, Lu Y. On the role of Cr in the passivity of stainless steel. *J Electrochem Soc*. 1986;133(12):2459.
- [18]. Fujisawa M, Kato Y, Ujiro T. Mechanical properties, and stress corrosion cracking receptivity of metastable Cr-Mn-N duplex stainless steels. *CAMP-ISIJ*. 2009;22:1163.
- [19]. Herrera C, Ponge D, Raabe D. Design of a novel Mn-based 1GPa duplex stainless TRIP steel with 60% ductility by a reduction of austenite stability. *Acta Mater*. 2011;59(11):4653.
- [20]. Cui, C.; et al., Laser Additive Manufacturing of Duplex Stainless Steel via Powder Mixture. *Journal of Manufacturing and Materials Processing* 2022, 6.
- [21]. Pohl, M.; Storz, O.; Glogowski, T. Effect of Intermetallic Precipitations on the Properties of Duplex Stainless Steel. *Mater Charact* 2007, 58, 65–71.
- [22]. Gargalis, L.; et al., Novel Powder Feedstock towards Microstructure Engineering in Laser Powder Bed Fusion: A Case Study on Duplex/Super Duplex and Austenitic Stainless-Steel Alloys. *Metals (Basel)* 2023, 13, doi:10.3390/met13091546.
- [23]. Vock, S.; Klöden, B.; Kirchner, A.; Weißgärber, T.; Kieback, B. Powders for powder bed fusion: A review. *Prog. Addit. Manuf*. 2019, 4, 383–397.
- [24]. Fritsching, U. Droplets and particles in sprays: Tailoring particle properties within spray processes. *China Particuology* 2005, 3, 125–133.
- [25]. Cui C, et al., Gas Atomization of Duplex Stainless-Steel Powder for Laser Powder Bed Fusion. *Materials (Basel)*. 2023 Jan 3;16(1):435. doi: 10.3390/ma16010435.





26th January 2024  
Gliwice, Poland

DEPARTMENT OF ENGINEERING MATERIALS AND BIOMATERIALS  
FACULTY OF MECHANICAL ENGINEERING  
SILESIA UNIVERSITY OF TECHNOLOGY

## INTERNATIONAL STUDENTS SCIENTIFIC CONFERENCE

### **Modern technologies for welding polymers - thermoplastics - review of research and techniques**

K. Dziedzic <sup>a</sup>, A. Kleszcz <sup>a</sup>, M. Bentkowski <sup>a</sup>, M. Bonek <sup>b</sup>

<sup>a</sup> Student of Silesian University of Technology, Faculty of Mechanical Engineering

<sup>b</sup> Silesian University of Technology, Faculty of Mechanical Engineering, Department of Engineering Materials and Biomaterials  
email: mirosław.bonek@polsl.pl

**Abstract:** The article describes various methods of welding thermoplastic polymer materials. It covers welding techniques such as ultrasonic, laser, extrusion, and spin welding. It also illustrates potential applications of each method, along with their advantages and limitations. The article focuses on the practical application of welding methods in the industry, emphasizing the benefits and areas where they can be particularly effective.

**Keywords:** materials, laser treatment, polymers

### **1. INTRODUCTION**

Polymeric material consists of long chains or networks of polymers. Polymers are chemical compounds composed of repeating units called monomers. The process in which monomers join to form long chains or networks is called polymerization. Polymer materials can exhibit different physical and chemical properties depending on the type of polymer, processing methods, and additives used during production. They can be rigid or flexible, transparent, or opaque, thermoplastic, or thermosetting. Polymers are widely used in various applications, ranging from everyday products like packaging, bottles, to advanced industrial applications such as automotive components, construction materials, and even in medicine.

Joining methods such as welding are used to connect elements made of thermoplastic materials when durable, high-performance, and high-quality connections are necessary. The use of welding techniques allows for the rapid and cost-effective production of end products while ensuring specific functional parameters.

Thermoplastic materials bond very well using modern techniques such as welding and fusion in various forms. Easily weldable (weldable and fusible) materials include polyvinyl chloride PVC (plasticized - soft - PVCP and rigid PVC), polypropylene PP, low-density polyethylene LDPE, high-density polyethylene HDPE, polyamide PA, polystyrene PS, acrylonitrile-butadiene-styrene copolymer ABS, polymethyl methacrylate PMMA (organic glass - plexiglass), and polycarbonate PC.

### 1.1. Welding of polymer materials

In welding of polymer materials, various techniques are distinguished, such as manual shuttle and traction welding, extrusion welding, laser welding, and ultrasonic welding. This process primarily involves similar principles to traditional metal material welding, which entails filling a weld groove to create a joint. To execute the connection correctly, it is essential to heat the material to its plasticization temperature while ensuring not to exceed a temperature that might cause its degradation. Conversely, too low a temperature is also undesirable because it might prevent a durable bond between the base material and the additional material.

### 1.2 Laser welding

Laser welding can be performed in two fundamental ways. In the first scenario (Fig. 1a), the laser beam is directed directly at the junction of materials, creating edge bonding by absorbing laser radiation. The second case (Fig. 1b), known as laser transmission welding, involves the laser beam being directed perpendicular to the join. The radiation passes through a transparent part, reaching the area where the absorbing material is located, resulting in the bonding of the surfaces at the junction of these two parts. Laser welding technology for polymers offers several advantages. Firstly, it enables precise and controlled bonding of elements without introducing additional substances, which can be crucial in applications requiring cleanliness, such as in medicine. Secondly, the process is fast and efficient, making it attractive for mass production. Moreover, due to the precision of welding, it is possible to achieve strong, durable connections of high quality.

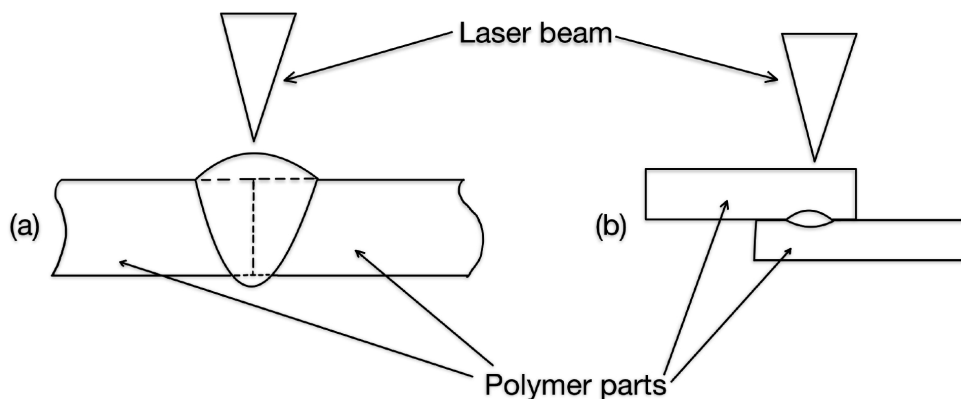


Fig. 1 Scheme of direct laser welding a) and transmission welding b) based on [3]

### 1.3 The principle of operation of transmission welding

The laser beam penetrates through the upper transparent polymer part and is absorbed by the absorbing lower part. The portion of the laser beam not reflected penetrates the material. The dispersed laser light absorbed by the material gradually transfers its energy in the form of heat. The generated heat leads to the melting of the material, creating a connection between the parts. Welding using this method is challenging because most polymer materials are transparent to

the laser beam. Hence, dyes and fillers enhancing the absorption of laser radiation are employed.

#### 1.4 Ultrasonic welding

Ultrasonic welding utilizes high-frequency sound to soften or melt thermoplastic materials at the joining point. The components to be joined are pressed together and subjected to ultrasonic vibrations typically at frequencies of 20 or 40 kHz. The mechanism generating heat at the junction is not fully understood, and the heating effect of ultrasonic waves varies depending on the material's crystalline structure. The effectiveness of welding depends on equipment design, material mechanical properties, and component design. Due to its rapidity (welding times are usually below 1 second) and ease of automation, ultrasonic welding is widely employed. To ensure successful welding, precise design of components and fixtures is necessary, making this technique best suited for mass production.

Ultrasonic waves can be generated by harnessing the piezoelectric effect in certain ceramic materials. These materials, with lead zirconate titanate (PZT) being the most used, form the basis for most commercially available ultrasonic transducers. The system comprises a high-frequency power supply, transducer, booster horn, and pressure application system (Fig. 2). The power supply converts mains electricity into high-frequency electric power that drives the transducer. Within the transducer, a disk of piezoelectric material is placed between two metallic sections and tightly clamped together, maintaining constant pressure. Piezoelectric transducers can convert electrical energy to mechanical energy with efficiencies exceeding 95%. Most ultrasonic welders operate at a frequency of 20 kHz, typically above the highest frequency detectable by the human ear.

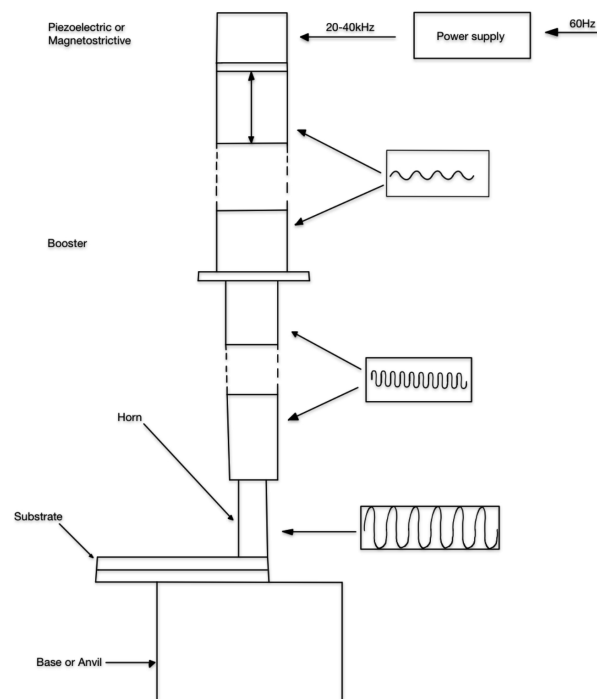


Fig. 2 Scheme of ultrasonic welding device based on [1]

### 1.5 Wire welding

Wire is the term used for the connecting material, usually made of the same material as the elements being joined, with a circular or triangular cross-section ranging from 3 to 7 mm in transverse dimensions. In the wire welding process, the surfaces being joined and the filler material in the form of wire or rod become plastic under the influence of hot gas. Subsequently, the weld is laid manually or using a welding nozzle. To join thicker elements, it is necessary to lay a greater number of stitches.

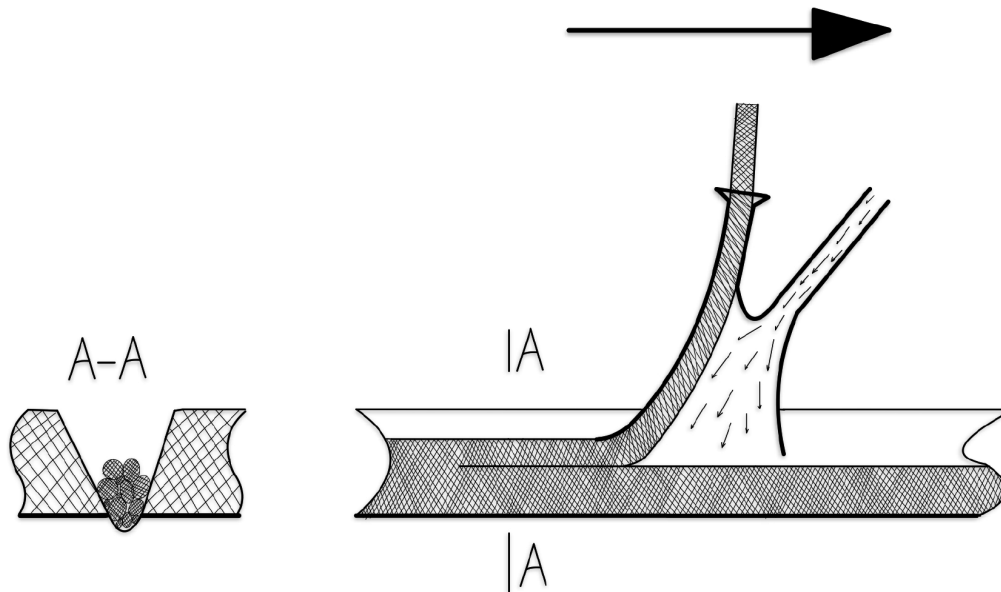


Fig. 3 Scheme of wire welding based on [4]

### 1.6 Extrusion welding

In the extrusion welding process, a plastic binder material is pushed out from an extruder. The weld is formed using a specialized head that separates the plastic material from the surfaces being joined by means of hot gas. This process constitutes a partially mechanical joining method for most materials of significant thickness, where achieving a uniform and high-volume weld is necessary. The depth of plasticization typically ranges from 0.5 to 1.0 mm, resulting in reduced welding time. Due to the excellent weld quality, high mechanical strength and minimal internal stresses are attained. These properties significantly impact the overall system's integrity. A characteristic feature of extrusion welding is the application of only a single filler bead, further emphasizing its efficiency and precision. This process finds extensive use in industries, particularly where durable, tight, and robust polymer connections are required, such as in the production of tanks, pipes, or other structural plastic components. It is an effective method for joining various polymer materials, enabling the creation of strong and enduring connections in numerous applications.

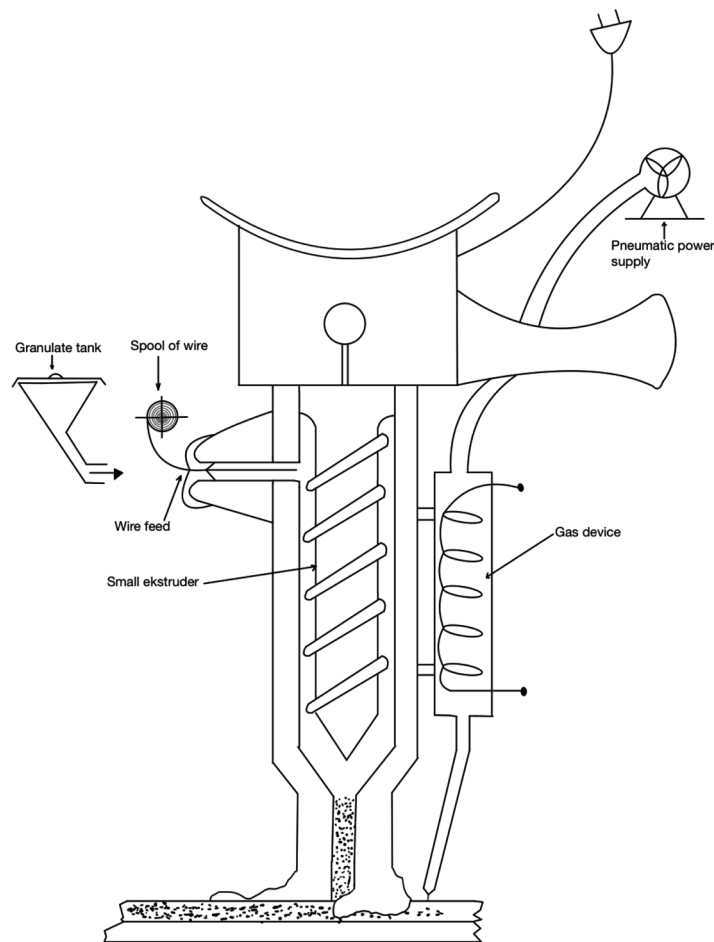


Fig. 4 Scheme of the extrusion welding device based on [4]

### 1.7 Spin welding

Thermoplastic components having rotationally symmetric joining surfaces are rubbed together under pressure in a single-directional circular motion to create spin welding. Usually, one component is rotated while the other is kept stationary. The plastic at the contact melts due to the heat produced during this process, and when it cools, a weld forms. Because there is no surplus heat produced, spin welding is an easy and very energy-efficient technique with quick cooling times. Because of this, the procedure is ideal for automated assembly line uses.

It is possible to create strong, hermetic junctions that are often stronger than the parent pieces. Unlike solvent welding or adhesive bonding, no external components are incorporated into the weld and no environmental concerns need to be taken into account. The earliest documented use of spin welding was in the production of fluid-filled compasses, where the liquid's surface was penetrated during the welding process. Thus, the procedure can be applied to the sealing of a liquid within a container. Aerosol cylinders, floats, truck lights, check valves, and fuel filters are among more uses. In addition, spin welding is utilized to weld container tops and bottoms, join ventilation pipes to blow-molded fuel tanks, and assemble structural components. Spin welding is a method that can be used to attach any thermoplastic.

## 2. CONCLUSIONS

The article presents various techniques for joining polymers, each of which has its own set of advantages and disadvantages. Methods such as ultrasonic and laser welding provide fast and strong bonding, whereas hot tool welding may be more cost-effective but time-consuming. The choice of the most suitable welding method depends on the specific context. For instance, in the automotive sector where durability is of paramount importance, advanced technological approaches may be preferred, whereas in industries such as packaging, cost efficiency and speed might hold greater significance.

## ACKNOWLEDGEMENT

The work was created as a result of the project of the Student Scientific Circle “Laser Surface Treatment” operating at the Department of Engineering Materials and Biomaterials at the Faculty of Mechanical Engineering, Silesian University of Technology.

## BIBLIOGRAPHY

1. R. J. Wise, Thermal welding of polymers
2. Handbook of Plastics Joining (Second Edition), William Andrew Publishing, 2009
3. Laser transmission welding of polymers – A review on process fundamentals, material attributes, weldability, and welding techniques, Bappa Acherjee, Department of Production Engineering, Birla Institute of Technology: Mesra, Ranchi, 835215, India
4. [https://ztp.zut.edu.pl/fileadmin/Instrukcje\\_laboratoryjne/12\\_13\\_14\\_v1](https://ztp.zut.edu.pl/fileadmin/Instrukcje_laboratoryjne/12_13_14_v1)
5. <https://pspaw.pl/pspaw/article/view/523/528>



26th January 2024  
Gliwice, Poland

DEPARTMENT OF ENGINEERING MATERIALS AND BIOMATERIALS  
FACULTY OF MECHANICAL ENGINEERING  
SILESIA UNIVERSITY OF TECHNOLOGY

## INTERNATIONAL STUDENTS SCIENTIFIC CONFERENCE

### Improvement of work organization in a selected manufacturing company

M. Dziubanowska<sup>a</sup>, M. Spilka<sup>b</sup>

<sup>a</sup> Student, Silesian University of Technology, Faculty of Mechanical Engineering, Department of Engineering Materials and Biomaterials, Management and Production Engineering  
email: marzdz564@polsl.pl

<sup>b</sup> Silesian University of Technology, Faculty of Mechanical Engineering, Department of Engineering Materials and Biomaterials  
email: monika.spilka@polsl.pl

**Abstract:** The article presents the application of the methodology used to improve work organization at a selected position. The 5S method and the Spaghetti diagram were used to improve the work organization and the production process. The drilling workplace was analyzed and a proposal for its improvement was presented. The workflow has been streamlined and the time needed to perform tasks related to preparing the workplace has been shortened. The wastefulness, which in this case included unnecessary movements, was eliminated and work efficiency at the analyzed workplace was increased.

**Keywords:** 5S method, Spaghetti diagram, wastefulness, unnecessary movements, work efficiency

### 1. INTRODUCTION

In the modern world, the use of the 5S method and the Spaghetti diagram to improve efficiency in enterprises is becoming more and more common. Regardless of the size of the company, these methods bring many benefits because they allow for improvement of quality indicators.

The 5S method is one of the management tools that is increasingly used on the market. Thanks to it, companies are more competitive and acquire a large number of customers. It also allows to create a positive image of the company on the global market because it promotes order and organization in the workplace. Moreover, the 5S method makes it possible to minimize errors, which has a positive impact on the financial situation in the enterprise [1].

Another tool supporting improvement in the production process is the Spaghetti diagram. Using a diagram to identify, visualize and analyze the flow of people, resources and materials within the enterprise allows to reduce the occurrence of inefficiency and wastefulness. The effectiveness of this tool depends mainly on the information detail that can be collected while observing the work of employees in the workplace. The degree of employee involvement during the implementation of changes is also important [2].

## **2. RESEARCH METHODOLOGY**

In order to improve the work organization at the drilling workplace, the 5S method and the Spaghetti diagram were used.

### **2.1. 5S method**

The 5S method is an approach to organizing, cleaning, tidying up and standardizing the workplace. It can be implemented in any enterprise where it will be necessary to improve the work organization at the workplace. It enables the company to improve efficiency and productivity. The name of the 5S method comes from five Japanese words that start with the letter S [3, 4]:

- Seiri – Sort;
- Seiton – Straighten;
- Seisou – Shine;
- Seiketsu – Standardize;
- Shitsuke – Sustain.

In the 5S method, the first three rules: sorting, systematics and cleaning help implement improvements, while the last two: standardization and self-discipline help maintain changes [5].

### **2.2 Spaghetti diagram**

The easiest and most frequently used tool for assessing movements made by employees and materials is the Spaghetti diagram. The lines presented in the diagram represent the paths of movement of people and materials and may intertwine or cross each other. The diagram shows how complicated an incorrectly planned production process can be. When there are too many lines on the diagram that make it impossible to read it correctly, should create as many diagrams as necessary to properly plan the working space [6].

## **3. CHARACTERISTICS OF THE WORKPLACE**

In order to detect the workplace causing the greatest losses in a small carpentry enterprise, the entire production process was subjected to direct observations. Observations showed that the drilling workplace would be analyzed and improved. An interview with employees was conducted at the workplace, which showed that tools and devices did not have a clearly designated place where they should be put away after work. The lack of a clearly defined storage location and the lack of a system for identifying tools and devices meant that the employee spent a significant amount of time at work finding appropriate equipment and drills, which resulted in delays in starting the production process. The lack of systematicity in the position resulted in a decrease in the efficiency and quality of the employee's work. It contributed to situations in which the employee made mistakes, which at later stages of production generated losses in the form of waste materials and longer waiting times.

During the job evaluation, the employee's transition path was also analyzed. Observation of the employee's movements allowed to notice the wastefulness of unnecessary movements.



#### 4. IMPLEMENTATION OF THE 5S METHOD

After collecting information and defining an action plan, the implementation of the 5S method at the workplace began.

##### Sort

The introduction of changes began with sorting things into useful and unhelpful ones. Tools, devices and protective equipment that were considered necessary to perform work during segregation remained at the workplace. Items marked with a red 5S card (Figure 1) have been removed from the workplace and moved to another place where they will be used. The stage of categorization in terms of usefulness allowed to minimize unnecessary items at the workplace.

<b>5S RED TAG</b>	
No.....	
Date:	
Item Description:	
Quantity:	
Reason for Red Tag:	
<input type="checkbox"/> No longer used	
<input type="checkbox"/> Damaged	
<input type="checkbox"/> Unnecessary at the workplace	
<input type="checkbox"/> Other.....	
DECISION:	
<input type="checkbox"/> Throw away	
<input type="checkbox"/> Sell	
<input type="checkbox"/> Keep (provide the place where the item will be stored)	
.....	.....
Date of removal	Signature

Figure 1. 5S red card (based on [4,5])

##### Straighten

The next stage that was carried out when introducing the 5S method is systematics. A shadow board was used on which tools and work equipment that remained at the workplace after the inventory were hung. There are additional descriptions above the items, which make them easier to identify and allow to quickly put them away after finishing work.

At this stage, a place to store personal protective equipment was also designated. The place where they should be put away has also been carefully described, so that every employee has quick and easy access to them.

##### Shine

In order to ensure safe and hygienic working conditions, a workplace cleaning schedule has been developed. Every day after finishing work at the station, it is necessary to clean up any wood residues and dust. Machines and tools must be thoroughly cleaned of dust and oil after work. At the end of the day, it is necessary to clean the floor to remove wood chips.

### Standardize

In order to document changes after the implementation of the 5S method, documents were created describing the benefits that appeared after the introduction of 5S at the workplace. The documentation includes photos showing the state before and after the changes, which shows the effects of the changes introduced.

A cleaning schedule was also systematized, including when and what activities should be performed. Deadlines for daily and weekly cleaning have been established, along with a description of the tasks that need to be carried out.

### Sustain

After three weeks, an on-the-job assessment was carried out and it was noticed that the employees were complying with the changes introduced. There was a noticeable improvement in the efficiency of activities performed and the quality of products manufactured. The adopted standards regarding order in tools and cleanliness at the workplace are systematically observed by employees.

## 5. IMPLEMENTATION OF THE SPAGHETTI DIAGRAM

In order to check the cause of the wastefulness that is unnecessary movements, a Spaghetti diagram was prepared, which allowed a visual representation of the path an employee takes when moving material between workplaces.

The Spaghetti diagram (Figure 2) starts from the drilling workplace, then the employee moves to the saw station, where he collects 10 pieces of cut materials and returns with them to his workplace. The pass cycle is repeated 4 times because the employee needed to move 40 pieces of material. After cutting, the prepared amplifiers are placed loosely on the table, which makes it difficult for the employee to take everything in one go. Then the employee performs the same activity three times, but this time taking the material (30 pieces) from the second workplace with the circular saw. The black lines in Figure 2 represent the paths taken by the employee when moving the material. Each transition between workplaces increases the time needed to start work. Analyzing the lines, it can be noticed that the employee spends most of his time transferring materials from the table located next to the first saw.

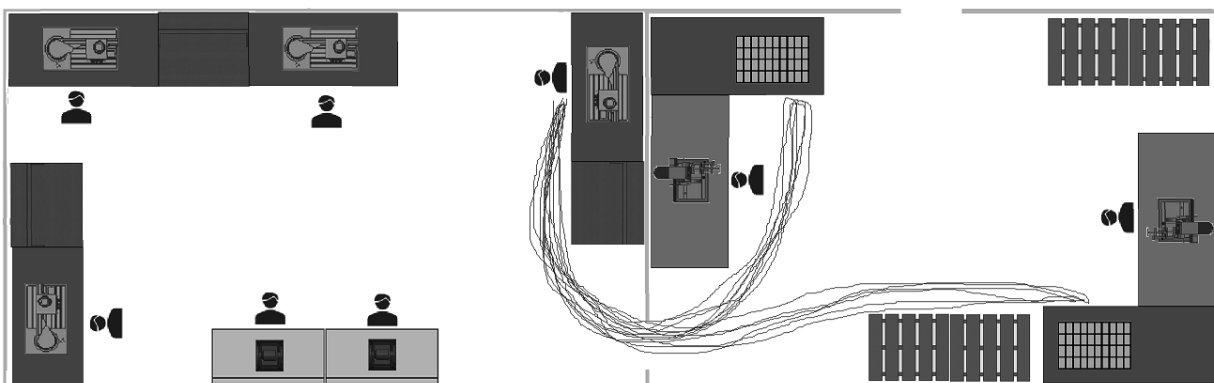


Figure 2. Spaghetti diagram flow before changes were made

In order to optimize the movements performed by the employee, changes were introduced,

which are visible in the Spaghetti diagram (Figure 3). The number of passes between workplaces has been reduced thanks to the use of packages in which the material is packed immediately after cutting and the addition of an additional table on which the worker can freely place even larger amounts of material than in the previous example. The previously prepared packages are carried by the employee in two passages back and forth to the workplace.

This diagram allowed for the detection and removal of inefficiencies in the process and contributed to shortening the employee's transition time between workplaces.

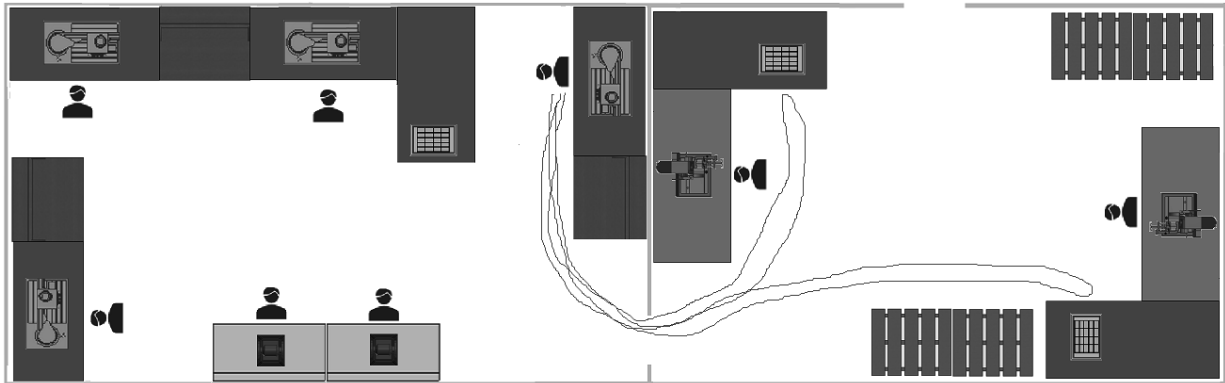


Figure 3. Spaghetti diagram flow after making changes

## 6. SUMMARY

The use of the 5S method and the Spaghetti diagram allowed for a significant improvement in working conditions at the drilling workplace. The 5S method made it possible to effectively manage the space at the workplace by eliminating unnecessary items and developing permanent standards that had a positive impact on maintaining order at the workplace. The Spaghetti diagram made it possible to identify and eliminate unnecessary movements made by the employee. The diagram contributed to reducing the number of routes an employee makes between workplaces. Thanks to the use of the 5S method and the Spaghetti diagram, it was possible to create a safe and more ergonomic workplace. These methods contributed to improving the production process.

## BIBLIOGRAPHY

1. S. Wani, D. Shinde, Study and Implementation of '5S' Methodology in the Furniture Industry Warehouse for Productivity Improvement, *International Journal of Engineering Research & Technology* 10 (2021) 184-191.
2. N. Moro, Set in Order—Fundamental Stage for 5S Methodology, *International Conference Knowledge-Based Organization* (2020) 238-244.
3. J. Michalska, D. Szewieczek, The 5S methodology as a tool for improving the organization, *Journal of Achievements in Materials and Manufacturing Engineering* 24/2 (2007) 211-214.

4. R.S Agrahari, P.A. Dangle, K.V. Chandratre, Implementation of 5S methodology in the small scale industry: a case study, *International Journal of Scientific and Technology Research* 4/4 (2015) 180-187.
5. M. Krasieński, *Kulturowe uwarunkowania wykorzystania japońskich koncepcji, metod i technik zarządzania*, Wydawnictwo Uniwersytetu Ekonomicznego we Wrocławiu, Wrocław, 2014.
6. K. Senderska, A. Mareš, Š. Václav, Spaghetti diagram application for workers' movement analysis, *UPB Scientific Bulletin, Series D, Mechanical Engineering* 79/1 (2017) 139-150.



26th January 2024  
Gliwice, Poland

DEPARTMENT OF ENGINEERING MATERIALS AND BIOMATERIALS  
FACULTY OF MECHANICAL ENGINEERING  
SILESIA UNIVERSITY OF TECHNOLOGY

## INTERNATIONAL STUDENTS SCIENTIFIC CONFERENCE

### Analysis of stress distribution in the bottle opener

A.R. Dziwis<sup>a</sup>, P. Bzdon<sup>a</sup>, A. Dziwis<sup>b</sup>, W. Mikolejko<sup>b</sup>, A. Śliwa<sup>b</sup>

<sup>a</sup> II Liceum Ogólnokształcącym im. Romualda Traugutta w Częstochowie

email: aleksanderdziwis@gmail.com, paszczal2@wp.pl

<sup>b</sup> Silesian University of Technology, Faculty of Mechanical Engineering, Department of Engineering Materials and Biomaterials

email: amadeusz.dziwis@polsl.pl, Wojciech.mikolejko@polsl.pl, agata.sliwa@polsl.pl

**Abstract:** This work contains a MES computer simulation of stress distribution in a bottle opener made of stainless steel. Geometrical model of the bottle opener and analysis were made in SolidWorks software. Applied boundary conditions simulated strength that an average adult man has in his hand.

**Keywords:** SolidWorks, stresses, opener, bottle, computer simulation, FEM, stainless steel.

### 1. INTRODUCTION

A bottle opener is a device that allows you to remove metal corks closing glass bottles, the so-called caps. The metal cap is attached to the edge of the bottle neck using one of two methods: pleating or crown closure. A bottle opener is a specialized lever located beneath a pleated metal surface that uses a point on the bottle lid as a fulcrum. The first bottle opener was patented by Alfred Louis Bernardin in 1893. It was an opener that was permanently attached to the tabletop (Fig. 1). There are several types of bottle openers. They are presented in Figures 2 – 5.

From here in every home and in public places you can find a bottle opener, which greatly facilitates the removal of bottle caps from drinks. Openers can be found in many sizes and shapes. From the typical ones found in restaurants to even those that double as a keychain.



*Fig. 1 Table bottle opener*



*Fig. 2 Church key bottle opener*



*Fig. 3 Simple bottle opener*



*Fig.4 Speed Bottle Opener*



*Fig. 5 Wall – mounted opener*

## 2. MODEL PROPERTIES

The purpose of the computer simulation was to present the distribution of stresses in the opener when opening a bottle. The analysis allowed to demonstrate the resistance of a given material and object to pressure and resistance. A computer simulation was performed for a traditional opener with the dimensions shown in Figure 6 and the geometry presented in Figure 7. The model was fixed in the place of contact with the cap, and the place where the pressure force will be applied is the handle (Fig. 8, 9). The applied force is 250 [N], which corresponds to the force that an average adult man has in his hand. 70% of openers are made of austenitic stainless steel, less popular materials used for the production of openers are aluminum and chrome stainless steel.

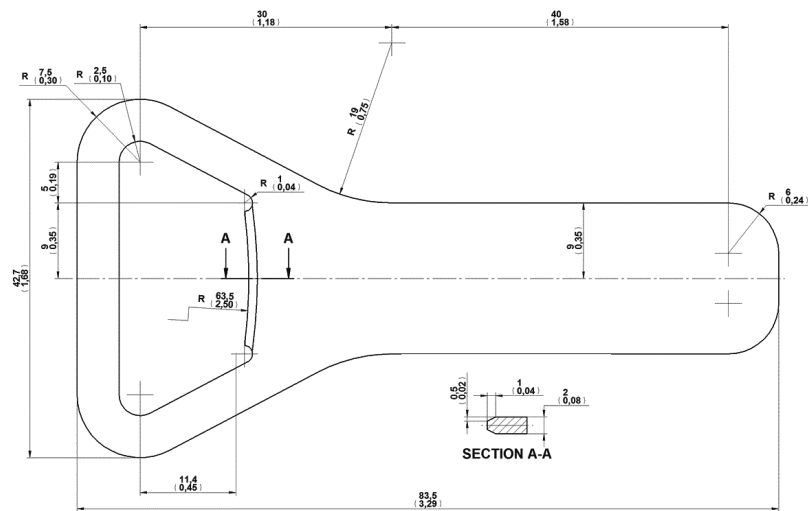


Fig. 6 Dimensions of bottle opener



Fig. 7 Example of bottle opener



Fig. 8 Bottle opener with applied mesh

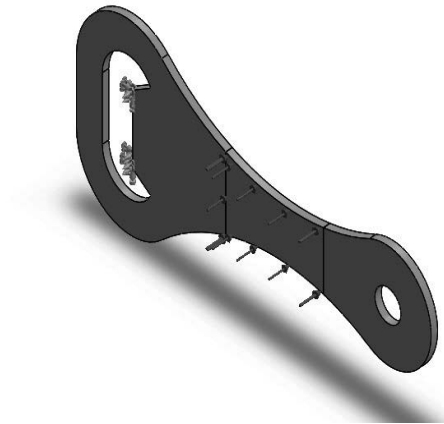


Fig. 9 Bottle opener with applied boundary conditions

Table 1. Properties of aluminum

Properties	Aluminum	Unit
Young's modulusprężystości	69000	[N/mm <sup>2</sup> ]
Poisson's ratio	0.33	[n.d]
Shear stress	27000	[N/mm <sup>2</sup> ]
Thermal expansion coefficient	2.4e-005	[/K]
Thermal conductivity coefficient	230	[W/(m*K)]
Tensile strength	82.7227	[N/mm <sup>2</sup> ]
Yield strenght	27.5742	[N/mm <sup>2</sup> ]
Density	2700	[Kg.m <sup>3</sup> ]
Specific heat capacity	1000	[J/(kg*K)]

Table 2. Properties of stainless chrome steel

Properties	Chrome steel	Unit
Young's module	200000	[N/mm <sup>2</sup> ]
Poisson's ratio	0.28	[n.d]
Shear stress	77000	[N/mm <sup>2</sup> ]
Thermal expansion coefficient	1.1e-005	[/K]
Thermal conductivity coefficient	18	[W/(m*K)]
Tensile strength	413.613	[N/mm <sup>2</sup> ]
Yield strenght	172.339	[N/mm <sup>2</sup> ]
Density	7800	[Kg.m <sup>3</sup> ]
Specific heat capacity	460	[J/(kg*K)]

### 3. COMPUTER SIMULATION

Computer simulations are based on the finite element method, or FEM. It is a tool that is increasingly used for engineering calculations. These calculations involve transforming a set of differential equations that describe the behaviour or properties of the analysed element into a system of nonlinear equations. Systems of equations are solved using a computer. When the first ENIAC computer was created in 1946, the first calculations using finite element methods were made. The calculations concerned elements or objects characterized by simple shapes, described by linear differential equations. Thanks to the development of techniques and the



increase in computing power, the finite element method was used to solve nonlinear problems for objects with simple shapes, one and two dimensions. For over 30 years, FEM has been used to solve nonlinear problems for objects of arbitrary three-dimensional shapes.

Three results were obtained in the computer simulation: stress, strain and displacement. Two simulations were performed (Figs. 10 – 15) for different materials with the same parameters in order to compare the results. The analysed materials were aluminum and chrome steel, the applied force was 250 [N]. The figures show analyses for three parameters. Fig. 10 shows stress analysis (Fig. 10), displacement analysis (Fig. 11) as well as strain analysis (Fig. 12). The second simulation was based on the same analyses but for a different material, i.e. chrome steel. Fig. 13 shows, as in the previous case, the stress analysis, while Fig. 14 shows the displacement analysis and strain analysis (Fig. 15). The forces were applied on the handle, i.e. in the place where the hand is placed to grab the opener. The second place to which forces were applied during the simulation is the area that is in direct contact with the cap when opening the bottle. Both simulations were successful. In the displacement analysis, however, in the case of aluminum and chrome stainless steel, there was a slight bend at the end of the handle.

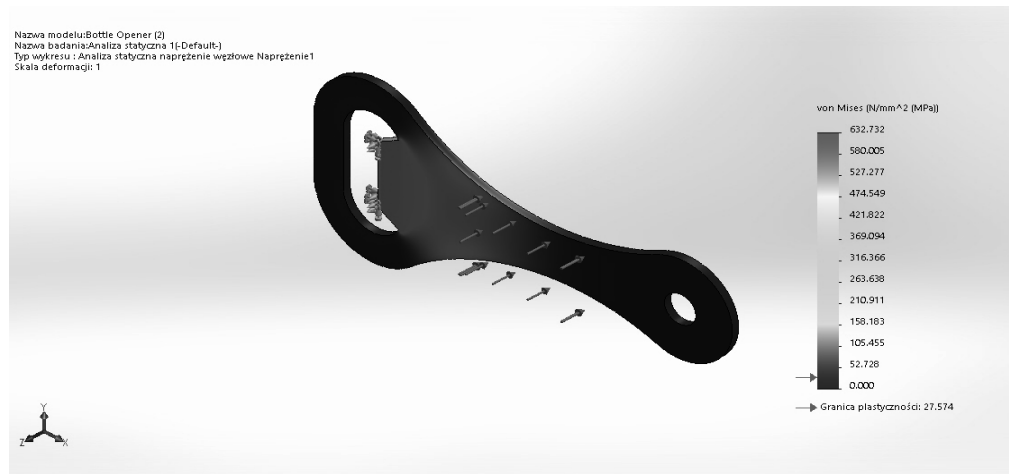


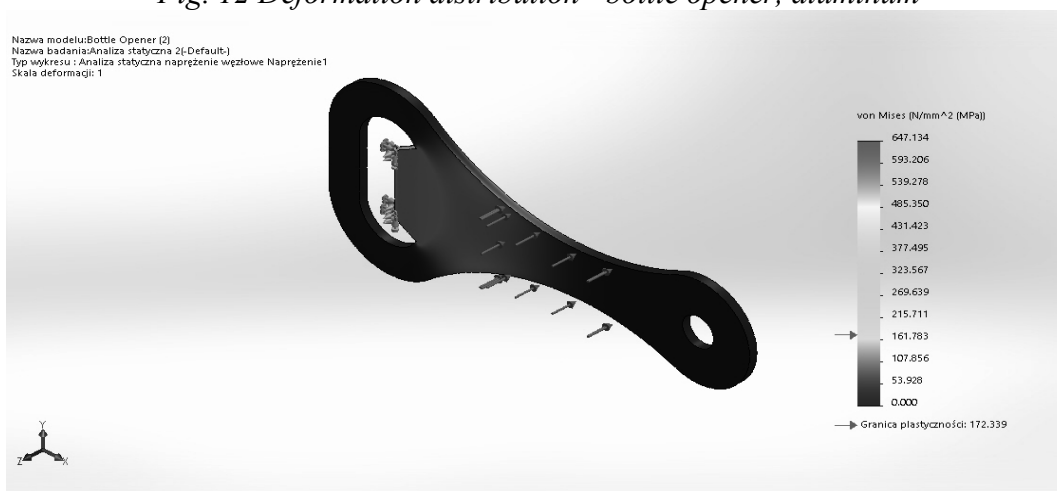
Fig. 10 Stress distribution – bottle opener, aluminum



Fig. 11 Displacement distribution - bottle opener, aluminum



*Fig. 12 Deformation distribution - bottle opener, aluminum*



*Fig. 13 Stress distribution – bottle opener, stainless chrome steel*

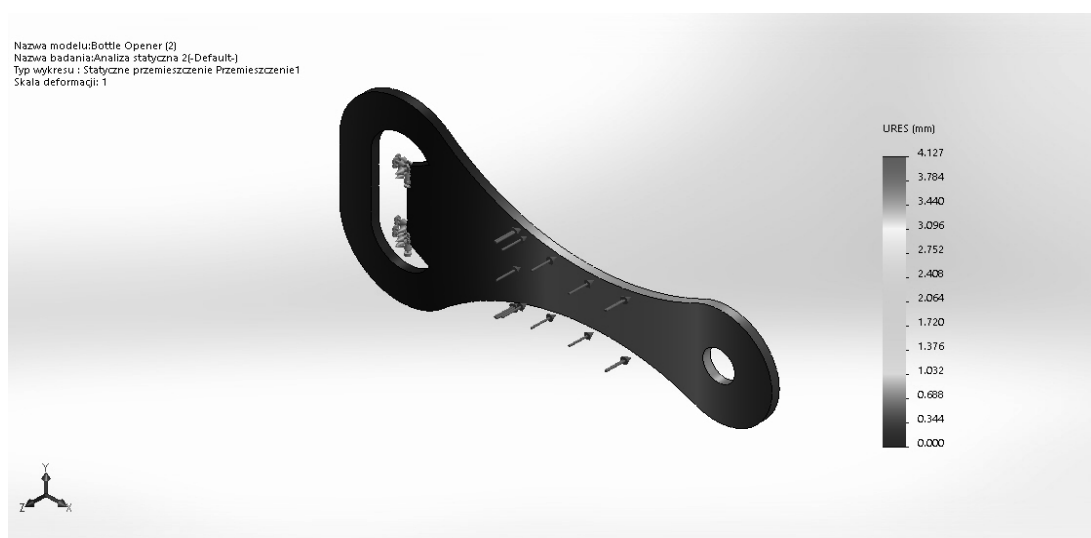


*Fig. 14 Displacement distribution - bottle opener, stainless chrome steel*



Fig. 15. Deformation distribution - bottle opener, stainless chrome steel

#### 4. SUMMARY

The project presents an analysis of FEM computer simulation, which was carried out in SolidWorks. The materials selected for analysis do not belong to the types of materials often used in the production of openers. The model of the opener, made of aluminum and chrome stainless steel, was analysed. Both models were subjected to a force of 250 [N] which was applied on the handle, and the model was additionally secured at the point of contact with the cap. In the case of aluminum, the yield strength is: 27.574 [N], the imposed forces did not result in exceeding the maximum value of the yield strength: 623.732 [MPa]. Chrome stainless steel also performed well, its yield strength is: 172.339 [MPa], where the value of the maximum yield strength is: 632.732 [MPa]. The displacement values for both materials are the same. Aluminum as well as chrome steel meet the stress conditions that make it possible to use them in the production of bottle openers. The condition is the maximum applied force (on which the analysis was carried out as an example) when opening drinks with a cap, amounting to a maximum of 250 [N].

#### LITERATURE

1. L.M. Wiseman, The Bottle Opener, Red Dashboard, 2014.
2. Z. Brytan, Vademecum Stali Nierdzewnej, Stowarzyszenie Stal nierdzewna, Katowice 2014.
3. Pod red. M. Głowacka, Metaloznawstwo, Praca zbiorowa, Gdańska, 1996
4. S. Rudnik, Metaloznawstwo, Wyd. 2, PWN Warszawa, 1996
5. Baza materiałowa SolidWorks



26th January 2024  
Gliwice, Poland

DEPARTMENT OF ENGINEERING MATERIALS AND BIOMATERIALS  
FACULTY OF MECHANICAL ENGINEERING  
SILESIA UNIVERSITY OF TECHNOLOGY

## INTERNATIONAL STUDENTS SCIENTIFIC CONFERENCE

### **Tribological properties of the surface layer of tool steels after laser remelting**

A. Dzwonek<sup>a</sup>, K. Malon<sup>a</sup>, M. Paluch<sup>a</sup>, M. Świącicka<sup>a</sup>, M. Volkmer<sup>a</sup>, O. Więcek<sup>a</sup>, M. Bonek<sup>b</sup>, E. Tillova<sup>c</sup>

<sup>a</sup> Student of Silesian University of Technology, Faculty of Mechanical Engineering, Department of Engineering Materials and Biomaterials

email: matepal541@student.polsl.pl

<sup>b</sup> Silesian University of Technology, Faculty of Mechanical Engineering, Department of Engineering Materials and Biomaterials

<sup>c</sup> University of Zilina, Faculty of Mechanical Engineering, Department of Materials Engineering, Slovak Republic

email: mirosław.bonek@polsl.pl

**Abstract:** This research delves into the comprehensive exploration of tribological properties inherent in laser-remelted surface layers of tool steels. Employing advanced high power diode laser (HPDL) technology, the study meticulously investigates structural modifications and performance enhancements specifically within high-speed steel alloys. A nuanced examination is undertaken to underscore the profound influence of varying laser power levels on the tribological characteristics of the surface layer, with a particular focus on discernible improvements in hardness, resistance to abrasive wear, and surface roughness. The intricate findings not only shed light on the multifaceted interactions occurring during laser remelting but also provide invaluable insights for the strategic optimization of tool surfaces. Through the judicious application of laser technology, this research aims to elevate and refine the tribological performance of tool surfaces in industrial applications.

**Keywords:** tool steel, laser remelting, laser treatment, surface properties

## **1. INTRODUCTION TO LASER TREATMENT**

### **1.1 Laser processing, its history and automation**

Modern laser technology has become an extremely important factor transforming various industrial sectors and research fields. Its use in the modification of the outer layer of materials is becoming increasingly popular, due to the laser's unique ability to precisely focus power into a specific area while remaining completely non-contact, making it an invaluable tool for engineers and researchers.

Initial applications of laser processing included cutting and welding metals, but it proved so effective that it began to be used to process other materials as well. In the 1990s, developments in the technology enabled new processing methods to be implemented, such as marking,

engraving and machining non-metallic materials such as wood and glass. As it progressed, the process was automated by incorporating automation, with the help of which processing became automatic through the use of robots and control systems. [1-4]

The development of the laser, which began in the 1950s, was originally focused on research purposes, but soon found its practical application in industry, particularly in materials processing. The origins of the laser are linked to Albert Einstein's work on the phenomenon of electromagnetic radiation emission and the generation of laser radiation. These discoveries gave rise to the idea of developing microwave generators (masers - Microwave Amplification by Stimulated Emission of Radiation), as well as electromagnetic wave generators in the light wave range (lasers). In 1960, the first laser was built, which was a ruby laser generating red visible radiation (wavelength  $\lambda=0.694\mu\text{m}$ ). The construction of the ruby laser initiated the development of a series of lasers. [6,9]

Forced emission is one of the three processes of interaction of light with matter, in which it causes a change in the quantum state of an atom, ion or molecule. The other two processes are absorption and spontaneous emission. The former process is always accompanied by absorption and spontaneous emission, because otherwise it would be impossible to achieve thermodynamic equilibrium in the system.

In the context of laser processing, the classification of steels becomes a key aspect, as different types of steel respond differentially to the laser. By properly selecting the laser parameters and fully understanding the properties of the materials, the desired processing results are achieved.

Laser technology is not limited to surface treatment; it is also applicable to remelting and alloying processes. The layers thus created are characterised not only by fine-crystalline structures, but also by a high degree of chemical differentiation and excellent metallurgical purity. Rapid crystallisation, resulting from the rapid cooling of the metal, leads to materials with increased hardness, mechanical strength and excellent tribological properties.

The application of laser technology in surface treatment is not only an industrial tool, but also an open gateway to new possibilities in the design of materials with customised properties. Contemporary research is focusing on optimising laser surface treatment processes and discovering new areas of application for this technology, making it a key area for the development of modern industrial technologies. [2,5,6]

## **1.2 General characteristics of the construction and operation of lasers and their application in materials engineering**

The name LASER is an acronym for the term in English: Light Amplification by Stimulated Emission of Radiation. Laser beam passing from the laser to the workpiece. The workpiece is focused on the area of operation. The fall of the beam onto the metal surface releases heat, causing a puddle of liquid metal to form.

The laser has several unique properties used in the heat treatment of material surfaces. The electromagnetic radiation from the beam of the laser is absorbed inside the first few atomic layers of opaque materials, such as metals. Another important advantage is that the laser beam can be placed on the surface of the workpiece exactly where it is required. [7, 8]

Laser surface processing is currently a rapidly growing field of knowledge due to its ability to save materials and improve surface properties. Such processing also makes it possible to improve corrosion and wear resistance, including increasing the hardness and abrasion resistance of surfaces with relatively small dimensions.

The cost of laser processing is the only limitation for using this method on large surfaces. Covering a large surface for decorative or anti-corrosion purposes using laser techniques is more expensive than traditional methods such as painting or electroplating.

The use of laser surface treatment is justified both from an economic point of view and because laser treatment in many cases provides a higher quality of finish, as well as improving the functionality of, for example, gear teeth or cutting tool blades, the specific properties of which cannot be achieved using standard surface treatment methods. [6,7,9]

### 1.3 Laser ablation

Laser ablation is the most advanced thermo-chemical processing method to improve the properties of surface layers and materials. The process involves the use of a high-power diode laser (HPDL), which uses semiconducting active materials such as silicon (Si) or gallium (Ga) in combination with arsenic (As) or phosphorus (P). The main difference between other lasers and this one is the way the laser beam is produced. Focusing on the diode laser, electrons in the material are stimulated to higher energy levels by the flow of electrical current through the diode. As a result of the electrical energy being supplied to the semiconductor, the electrons move to higher energy levels and, upon returning to their ground state, emit photons of a specific wavelength. The photons pass through a p-n optical region sandwiched between two mirrors, where they are amplified; this type of structure is called an optical resonator. This process continues until the number of photons reaches an appropriate level, beyond which cumulative and coherent laser light is generated. The laser beam is directed out of the resonator through one of the mirrors, which is partially transparent. [2-5,10]

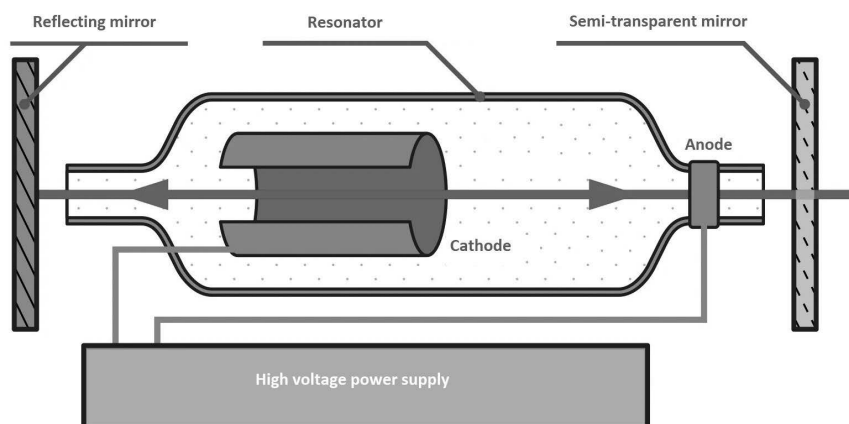


Figure 1 Example of Diode Laser

This technique has found applications in a variety of areas, from laser surgery to material processing in industry. Its precision and ability to focus on selected areas make it invaluable in the field of materials engineering. In recent years, advanced laser technology has gained increasing popularity due to its variety of applications, enabling the modification of material properties, which is an important part of today's manufacturing and research processes.

#### 1.4 Process automation

Process automation in laser machining has become much more efficient through the use of advanced robotic systems that have been precisely integrated with a variety of vision systems, sensors and advanced cooling and suction mechanisms. The implementation of robotics in laser-related processes has brought numerous benefits, not only increasing efficiency but also improving the precision and repeatability of the tasks performed. With precise and repeatable movements that are programmed, robots eliminate errors made by humans, resulting in results with the highest accuracy. Their role during cutting, welding or engraving is to manipulate the laser heads to achieve complex and detailed results. The use of robots has significantly reduced the execution time of the process, eliminating the need to manually move the heads and minimising interruptions to the task.

The integration of various systems, such as sensors or automatic cooling and suction systems, often relies on complex solutions that work in harmony with the overall laser system. In addition, current technological developments make it possible to use robots with gripping tools to handle the material, making it possible to precisely move and position the workpiece without interrupting the process. These state-of-the-art solutions not only streamline processes, but also eliminate the human factor, resulting in increased efficiency and accuracy of the tasks performed. [7,9-11]

## 2. METHODOLOGY FOR THE SELECTION OF LASER PROCESSING PARAMETERS AND THEIR EFFECT ON STRUCTURE AND PROPERTIES

The experimental procedure began with a Rofin DL 020 high-power diode laser (HPDL) for remelting of HS6-5-2 steel. This advanced laser, which is widely used in materials engineering, is capable of a variety of applications such as surfacing, welding, remelting and surface enrichment of materials. The laser system, which consists of a laser head, a rotating work table, a moving table in the X-Y plane, a protective gas nozzle, power and cooling systems, and a computer system to control laser operation and work table positioning, was a key component of the experiment.

Table 1 *Chemical composition of HS6-5-2C steel. [5]*

	Chemical Composition %										
	C:	Mn:	Si:	P:	S:	Cr:	Mo:	Ni:	V:	W:	Co:
ISO	HS6-5-2C										
	0.86					3.8	4.7		1.7	5.9	
	- 0.94	<0.4	<0.45	<0.03	<0.03	- 4.5	- 5.2	-	- 2.1	- 6.7	-

It is worth noting that the rectangular or linear size of the laser spot was an important advantage of this system, in addition to its versatility, reliability and compact size. Melting and alloying of surface layers was carried out in the power range of 0.7 to 2.0 kW, which allowed for varied experimental conditions.

During the experiment, the laser spot, focused on the surface of the material, had dimensions of 1.8 x 6.8 mm, and the working focal length was 92 mm. It is interesting to note that the remelting was performed perpendicular to the longer side of the focused beam, which made it possible to obtain a wide contact surface. This approach was facilitated by the multi-mode energy distribution of the laser beam.

In order to evaluate the structure of the coating and the zone between the matrix material and the coating, as well as the structure of the matrix, micrographs were carried out on cross sections of the test samples. In addition, the hardness of the coatings was examined using an FM-700 microhardness tester. Analysis of the structure of the fabricated coatings was carried out using a SUPRA 25 scanning electron microscope (SEM), which was also equipped with an X-ray energy dispersive spectrometer (EDS).

To sum up, the experimental procedure focused on using a high-power diode laser to remelt and alloy steel using various process parameters. Micrographs, microhardness and structure analysis using an advanced electron microscope provided comprehensive knowledge of the coating structure and its mechanical properties.

### 3. RESEARCH FINDINGS

Based on preliminary examinations, it is evident that coatings applied to the substrate through pressureless forming and laser processing methods effectively fulfill their primary purpose. A metallographic analysis was conducted to scrutinize the structure of the material post-laser alloying, revealing distinctive areas exhibiting gradient morphology linked to the crystallization of steel. This phenomenon is closely tied to the rapid heating of the material surface to 3500°C under the influence of the laser beam, leading to vigorous circulation of molten material and subsequent swift solidification after the laser passes.

These observations underscore the occurrence of exceptionally rapid phase transformations, exerting a significant influence on the structural mechanisms governing the formation of surface layers undergoing laser treatment. The surface layers of the examined steel affirm the existence of both a melted zone and a heat-affected zone, the thickness of which is contingent upon the specific laser processing parameters employed (Fig. 2, 3). Elemental segregation at dendrite boundaries within the melted zone is confirmed, a consequence of fluctuations in chemical composition, particularly at the base of the melt (Fig. 4).

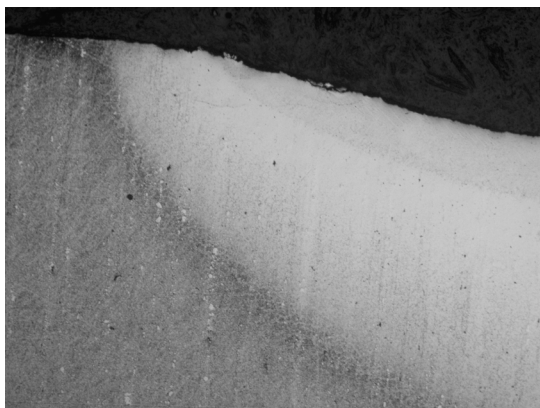


Figure 2 Surface layer of the HS6-5-2 steel, laser power 1,7 kW, 100x

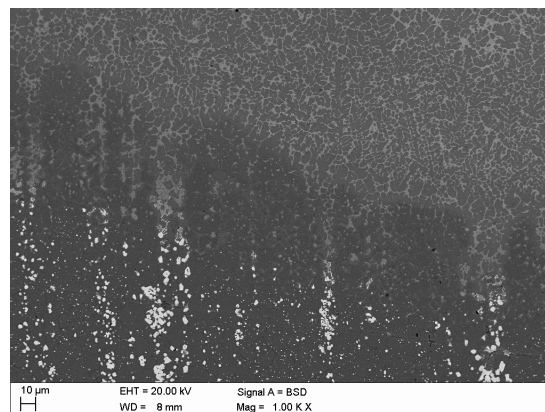
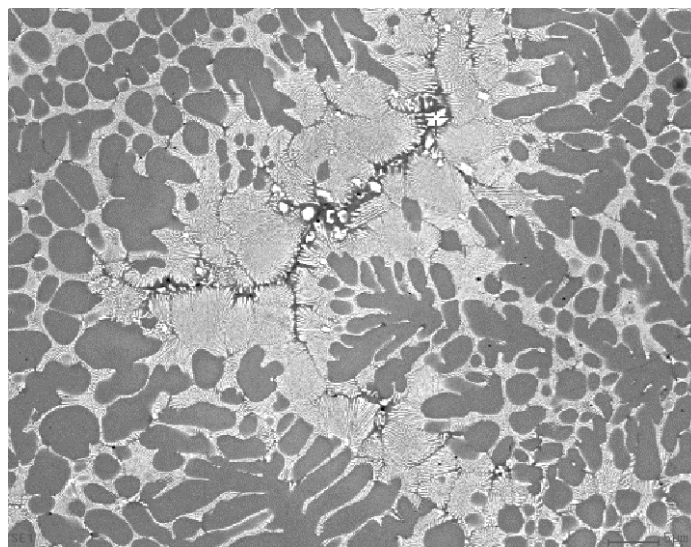


Figure 3 Boundary of the remelted surface layer of the HS6-5-2 steel, laser power 2,0 kW, 500x



As the laser power escalates, capillary lines undergo turbulence, resulting in the maximum thickness of the melted surface layer. However, the bottom of the melt displays undulations due to the intense movements of the molten material. Laser treatment significantly amplifies the surface hardness of all tested steel samples, a transformation achieved through phase alterations intricately connected to the rapid dissipation of heat from the melted zone.

The rate of cooling is primarily dictated by the thickness of the melted layer, a factor reliant on the absorbed energy from radiation and the duration of interaction between the laser beam and the material. Solely the laser power has a discernible impact on the energy supplied to the surface layer, holding a consistent melting rate. Lower laser power leads to a shallower melting depth, resulting in the highest rate of heat removal and, consequently, the occurrence of super-fast phase transformations, ultimately contributing to a fine-grained martensitic structure, known for its heightened hardness.



*Figure 4 Alloying material and small eutectic in the surface layer of the HS6-5-2 steel, laser power 1,7 kW*

The pinnacle of surface hardness is attained at a laser power of 2.0 kW, registering at approximately 66 HRC. Moreover, the highest microhardness among all laser-treated steel specimens, amounting to 830 HV0.1, is achieved at a laser power of 1.7 kW (Fig. 5). Notably, on the microhardness measurement graphs for all samples, an area with markedly reduced hardness, around 680 HV0.1, is discernible. This phenomenon signifies the development of a laser-annealed material zone heated to a temperature surpassing the typical annealing temperature.

Furthermore, an additional layer of complexity is introduced through the process of additive annealing at 570°C, demonstrating a notable enhancement in the average microhardness, reaching 920 HV0.1 (Fig. 6). This multifaceted exploration offers profound insights into the intricate interactions and transformations occurring during laser surface modification, providing a comprehensive understanding of the resulting material properties.

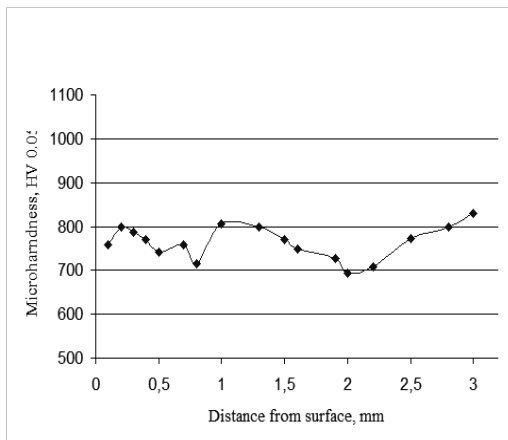


Figure 5 Microhardness changes of the surface layer of the HS6-5-2 steel, laser power 1,7 kW

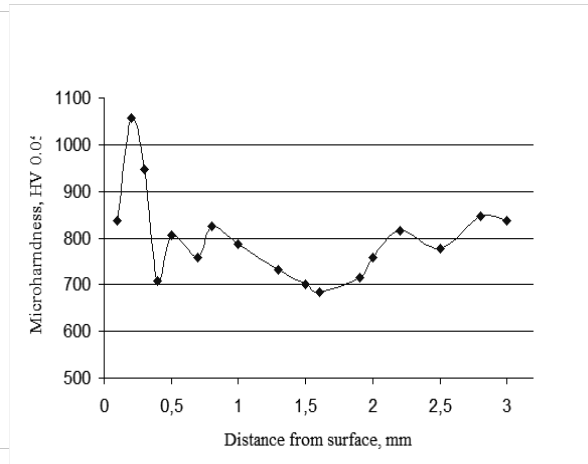


Figure 6 Microhardness changes of the HS6-5-2 steel after tempering at the temperature of 570°C by 2h

#### 4. SUMMARY

This paper investigates the impact of laser remelting on the tribological properties of tool steels, specifically focusing on high-speed steel alloyed with carbides. Utilizing high power diode laser (HPDL) technology, the study explores the structural modifications induced by laser treatment and their influence on hardness, abrasive wear resistance, and surface roughness. The research underscores the importance of adjusting laser power in optimizing the tribological performance of tool steel surfaces. The paper highlights the occurrence of rapid phase transformations during laser treatment, leading to distinctive melted and heat-affected zones. The findings reveal that increasing laser power results in enhanced surface hardness, with the peak hardness achieved at 2.0 kW. The study also introduces the concept of additive annealing at 570°C, demonstrating further improvements in microhardness. The methodology involves using a Rofin DL 020 HPDL for remelting and carbide alloying, with a focus on various laser processing parameters. Micrographs, microhardness testing, and SEM analysis with an X-ray energy dispersive spectrometer contribute to a comprehensive understanding of the coating structure and its mechanical properties. Overall, the research provides valuable insights for optimizing tool surfaces through laser remelting for improved tribological performance in industrial applications.

#### 5. CONCLUSION

In summary, this study highlights the crucial role of laser processing in enhancing the tribological properties of tool surfaces. Utilizing high power diode laser (HPDL) technology, the research focused on structural modifications and performance improvements within high-speed steel alloys. The influence of laser power on surface tribological characteristics, particularly in hardness, abrasive wear resistance, and roughness, was emphasized. These nuanced findings provide valuable insights for strategically optimizing tool surfaces through

laser technology, aiming to elevate their overall tribological performance in industrial applications.

## **ACKNOWLEDGEMENTS**

The work was created as a result of the project as part of project based learning - PBL, in the 10th competition under the Initiative of Excellence - Research University, Silesian University of Technology.

## **BIBLIOGRAPHY:**

- [1] R. Poprawe, „Tailored Light 2 – Laser Application Technology”, Springer Verlag, Berlin, Heidelberg, 2011
- [2] A. Klimpel „Technologie laserowe: spawanie, napawanie, stopowanie, obróbka cieplna i cięcie”, Gliwice, 2012
- [3] H. Klejman „Lasery”, PWN, Warszawa, 1974
- [4] F. Karczmarek, „Podstawy działania laserów” PWN, Warszawa, 1983
- [5] PN-EN ISO 4957:2002
- [6] A. Kalinowski „Tribological properties of textured diamond-like carbon coatings”, Technical Transactions, 2023
- [7] M. Bonek „the investigation of properties of high-speed steel after laser surface treatment”, Institute of Metallurgy and Materials Science of Polish Academy of Sciences, Gliwice, 2018
- [8] K. Labisz „Struktura i własności laserowo przetapianych i stopowanych warstw wierzchnich stali narzędziowej 32CrMoV12-28”, rozprawa doktorska, Gliwice, 2005
- [9] L. Berkowski „Influence of structural state on the effects of laser treatment of steel with different chemical compositions. Part I: Carbon steels”, Poznań, 2018
- [10] L.A. Dobrzański, M. Piec, M. Bonek, E. Jonda, A. Klimpel „Mechanical and tribological properties of the laser alloyed surface coatings”, Silesian University of Technology, Gliwice, 2006
- [11] L.A. Dobrzański, M. Bonek, K. Labisz „Effect of laser surface alloying on structure of a commercial tool steel”, International Journal of Microstructure and Materials Properties (IJMMP), Gliwice, 2013



26th January 2024  
Gliwice, Poland

DEPARTMENT OF ENGINEERING MATERIALS AND BIOMATERIALS  
FACULTY OF MECHANICAL ENGINEERING  
SILESIA UNIVERSITY OF TECHNOLOGY

## INTERNATIONAL STUDENTS SCIENTIFIC CONFERENCE

### Działanie wiązki laserowej na różne typy stali w oparciu o techniki wytwarzania

A. Dzwonek <sup>a</sup>, K. Malon <sup>a</sup>, M. Świącicka <sup>a</sup>, O. Więcek <sup>a</sup>, J. Kuta <sup>a</sup>, J. Osiewała <sup>a</sup>, O. Sobek <sup>a</sup>, N. Tomanek <sup>a</sup>, J. Badora <sup>a</sup>, A. Kłapsia <sup>a</sup>, E. Krajewska <sup>a</sup>, J. Muszyńska <sup>a</sup>, M. Bonek <sup>b</sup>

<sup>a</sup> Student Politechniki Śląskiej, Wydział Mechaniczny Technologiczny, Katedra Materiałów Inżynierskich i Biomedycznych

<sup>b</sup> Politechnika Śląska, Wydział Mechaniczny Technologiczny, Katedra Materiałów Inżynierskich i Biomedycznych  
email: mirosław.bonek@polsl.pl

**Streszczenie:** Studenci biorący udział w projekcie przeprowadzili badania nad poprawą właściwości funkcjonalnych topowej warstwy stali narzędziowej poprzez obróbkę laserową. Obróbka laserowa, charakteryzująca się niezawodnością i precyzją, umożliwia osiągnięcie optymalnych kształtów i wymiarów metalowego przedmiotu. W kontekście przetwarzania laserowego istotne jest sklasyfikowanie różnych typów stali, gdyż reagują one odmiennie na działanie lasera. Badania obejmowały cięcie laserem światłowodowym, wykorzystujące gazy towarzyszące w zależności od rodzaju materiału. Metoda ta oferuje wiele zalet, takich jak duże prędkości cięcia, niskie naprężenia i minimalne deformacje materiału. Niemniej jednak, istnieją pewne ograniczenia, takie jak maksymalna grubość ciętych elementów, promieniowanie elektromagnetyczne generowane w trakcie procesu, koszty urządzeń oraz konieczność środków bezpieczeństwa dla operatorów. Wartościowe jest również zastosowanie różnych rodzajów wiązek laserowych, takich jak ciągła, impulsowa i udarowa, w zależności od konkretnych wymagań procesu obróbki.

**Słowa kluczowe:** tool steel, przetapianie laserowe, obróbka laserowa, techniki wytwarzania, cięcie laserowe

**Abstract:** The students involved in the project conducted research into improving the functional properties of the top layer of tool steel through laser machining. Laser processing, characterised by its reliability and precision, makes it possible to achieve optimal shapes and dimensions of the metal object. In the context of laser processing, it is important to classify the different types of steel, as they react differently to the laser. The research involved fibre laser cutting, using companion gases depending on the type of material. This method offers many advantages, such as high cutting speeds, low stresses and minimal material deformation. Nevertheless, there are some limitations, such as the maximum thickness of the parts to be cut, the electromagnetic radiation generated during the process, the cost of the equipment and the need for safety measures for operators. There is also value in using different types of laser

beams, such as continuous, pulsed and percussive, depending on the specific requirements of the machining process.

**Keywords:** tool steel, laser remelting, laser treatment, manufacturing techniques, laser cutting

## **1. ZNACZENIE TECHNOLOGII LASEROWEJ W OBRÓBCE MATERIAŁÓW METALOWYCH**

Techniki wytwarzania to dziedzina nauki zajmująca się procesami produkcyjnymi jak i obróbką surowców w celu uzyskania wyrobu o określonych własnościach użytkowych.

W branży maszynowej, techniki wytwarzania obejmują wszelkie metody obróbki używane do formowania elementów maszyn i urządzeń, metody łączenia części (spawanie) oraz nadawanie im wcześniej określonych właściwości użytkowych, a także techniki pomiarowe wykorzystywane do kontroli jakości. [2]

Obróbka laserowa charakteryzuje się dużą niezawodnością, precyzyjnością oraz efektywnością czasową. Umożliwia osiągnięcie optymalnego kształtu i wymiarów przedmiotu metalowego dzięki możliwości wielokrotnej obróbki materiału. Jest to preferowana metoda dzięki jej zdolnościom do cięcia zarówno materiałów organicznych, jak i nieorganicznych, co czyni ją odpowiednią dla zaspokajania rosnących potrzeb rynku w zakresie produktów wysokiej jakości. Technologia laserowa pełni także kluczową rolę w rewolucji wielu sektorów przemysłowych oraz naukowych. Wyjątkowa zdolność laserów do precyzyjnego skoncentrowania energii w określonym obszarze, przy jednoczesnym braku bezpośredniego kontaktu, sprawia, że stają się one niezastąpionym narzędziem dla inżynierów i badaczy. Wraz z postępem technologii laserowej, odkrywane są kolejne innowacyjne zastosowania, co tylko potwierdza jej kluczową rolę we współczesnym świecie technologii i nauki.

W kontekście przetwarzania laserowego istotne jest sklasyfikowanie różnych typów stali, gdyż każdy z nich reaguje odmiennie na oddziaływanie lasera. Stale narzędziowe, wykorzystane w badaniach w ramach projektu PBL, zaliczają się do grupy materiałów wyróżniających się wysoką odpornością na ścieranie, dużą twardością jak i małą ciągliwością. Ich właściwości ulegają zmianie w zależności od składu chemicznego. Wprowadzenie różnorodnych dodatków stopowych pozwala na dostosowanie własności stali do konkretnych wymagań. Ponadto, ciągłe badania nad reakcją różnych rodzajów stali na wiązkę laserową przyczyniają się do rozwijania bardziej precyzyjnych i efektywnych metod obróbki, co ma istotne znaczenie w przemyśle i produkcji.

## **2. ZASTOSOWANIE I PARAMETRY I TECHNOLOGII CIĘCIA LASEROWEGO**

Cięcia laserem światłowodowym to metoda cięcia na gorąco, w której głównym źródłem ciepła jest skupiona wiązka lasera o wysokiej gęstości mocy. Obrabiany materiał topi się i odparowuje szybko w miejscu uderzenia wiązki laserowej. Za pomocą szybkiego przepływu powietrza stopiony materiał jest jednocześnie zdmuchiwany. Dzięki ciągłości tego procesu przedmiot jest cięty. Jako technika wytwarzania cięcie laserowe głównie jest stosowane w przemyśle ciężkim oraz maszynowym. Proces ten jest procesem cieplnym, który dąży do rozerwania spójności materiału przez wpływ wiązki lasera na strukturę elementu. Podczas wykorzystywania cięcia laserowego często wymagane jest użycie gazów roboczych

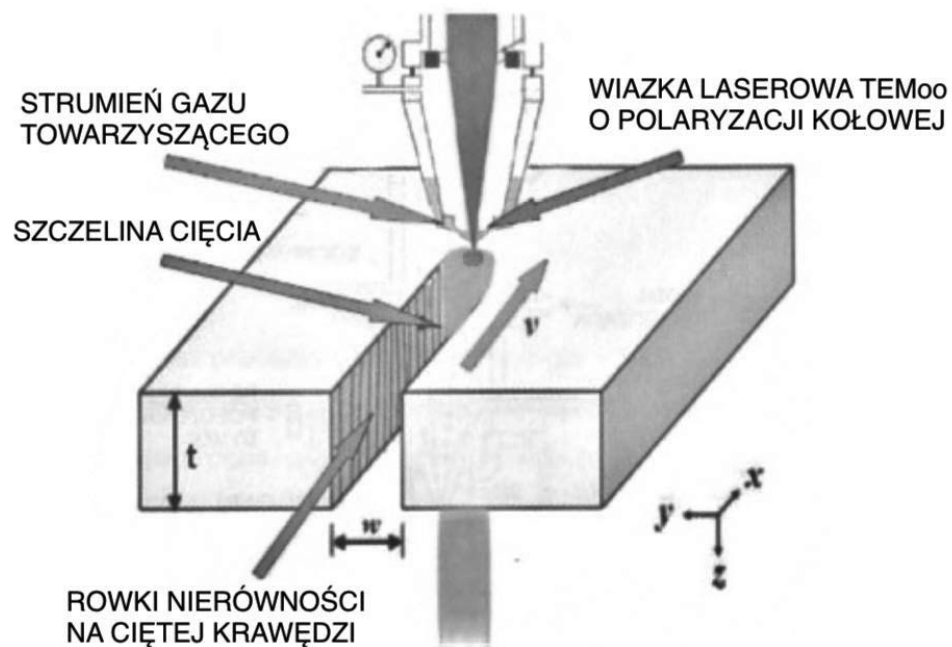
pod ciśnieniem (są to powietrze, tlen, azot oraz argon) zależnie od obrabianego materiału. Powietrze jest używane przy tworzywach, gdzie jakość obróbki nie musi być najwyższej jakości, za to tlen jest stosowany, gdzie precyzja obróbki jest kluczowa. Azot sprawdza się przy wycinaniu laserowym ze stali odpornych na korozję, a argon do stali specjalnych.

Tab. 1: Zalecane gazy towarzyszące do cięcia laserowego różnych materiałów inżynierskich:

Powietrze	Tworzywo sztuczne
	Materiały kompozytowe
	Tlenki glinu
	Szkło
	Guma
	Kwarc
	Drewno
	Aluminium
Tlen	Stale węglowe
	Stale odporne na korozję
	Miedź
	Stale niskostopowe
Argon	Stale specjalne, wysokostopowe i stopy niklu
	Aluminium i stopy aluminium
	Tytan
	Tantal
	Cyrkon
Azot	Stale odporne na korozję
	Aluminium
	Stopy niklu

Korzystając z odpowiedniego urządzenia laserowego do cięcia danego materiału inżynierskiego o określonej grubości, mamy możliwość sterowania jakością i prędkością cięcia poprzez określenie optymalnych parametrów technologicznych cięcia laserowego. Podstawowe parametry, które można dostosować to: moc wiązki laserowej dostarczanej przez laser, co wpływa na zdolność cięcia materiału. Wybór rodzaju wiązki laserowej oraz długość fali promieniowania między promieniowaniem ciągłym, pulsowym lub udarowym oraz długości

fali, co ma wpływ na interakcję z materiałem. Kontrola szybkości przemieszczania wiązki laserowej, wpływającej na jakość i efektywność cięcia. Średnica i głębokość ogniska wiązki laserowej związana z koncentracją energii, wpływająca na detale cięcia. Długość ogniskowa wiązki która jest odległością od soczewki skupiającej do ogniska wiązki laserowej, wpływająca na skupienie energii. Położenie ogniska względem górnej powierzchni ciętego przedmiotu czyli określenie, jak głęboko wiązka przenika w materiał. Rodzaj i ciśnienie gazu towarzyszącego, który może wpływać na proces cięcia poprzez chłodzenie i usuwanie stopionego materiału. Określenie rozmiaru otworu, przez który wypływa gaz pomocniczy. Określenie odległości między dyszą a materiałem, co wpływa na strumień gazu towarzyszącego.



Rysunek 1 - schemat przebiegu procesu cięcia laserowego,  $w$  - szerokość szczeliny cięcia,  $t$  - grubość ciętego przedmiotu,  $V$  - prędkość cięcia

Istotnymi zaletami cięcia laserowego, które powodują, że proces ten jest korzystniejszy w porównaniu do innych metod cięcia termicznego oraz mechanicznego są m.in.: duże prędkości cięcia, niższe naprężenia cząstkowe i mniejsze deformacje ciętego materiału. W tradycyjnych metodach cięcia, takich jak cięcie mechaniczne, generowane są siły i naprężenia, które mogą prowadzić do odkształceń i zmian strukturalnych w materiale., natomiast zastosowanie cięcia laserowego jest skuteczniejsze, szczególnie w przypadkach, gdzie materiały są delikatne bądź podatne na odkształcenia. Wysoka dokładność wymiarowa cięcia oraz gładkość jej powierzchni, wynikają z precyzyjnego sterowania strumieniem światła laserowego oraz bezdotykowego charakteru cięcia. Brak fizycznego kontaktu z materiałem eliminuje ryzyko zarysowań oraz innych niepożądanych czynników na powierzchni materiału. Wysoka niezawodność zautomatyzowanych urządzeń laserowych ze względu na bezkontaktowy charakter procesu cięcia, materiał obrabiany nie jest narażony na zużycie narzędzi, co minimalizuje ryzyko zniszczenia bądź uszkodzenia powierzchni, wąska Strefa Wpływu Ciepła (SWC) i związane z tym oddziaływanie cieplne na cięty materiał,

minimalizacja emisji szkodliwych substancji w stosunku do cięcia tlenem i łukiem plazmowym.

### 2.1. Ograniczenia i wady cięcia laserowego:

**Grubość Materiałów:** Maksymalna grubość ciętych elementów wynosi zazwyczaj 20-25 mm, z wyjątkiem procesu LASOX, który umożliwia cięcie blach stalowych o grubości nawet do 100 mm.

**Promieniowanie Elektromagnetyczne:** Proces cięcia generuje niewidzialne promieniowanie elektromagnetyczne, wymagające środków ochrony dla operatorów.

**Koszty Urządzeń:** Urządzenia laserowe dużej mocy, emitujące wysokiej jakości wiązkę, są kosztowne, co może być istotnym wyzwaniem finansowym dla przedsiębiorstw.

**Bezpieczeństwo Operatorów:** Konieczne są środki bezpieczeństwa dla operatorów, aby zminimalizować ryzyko związane z promieniowaniem laserowym.

**Wymagania Materiałów:** Proces ten stawia specjalne wymagania dotyczące stanu powierzchni, składu chemicznego i właściwości fizycznych materiałów.

Sposób, w jaki wiązka laserowa oddziałuje na przedmiot obrabiany, decyduje o przebiegu procesu obróbki. Do podstawowych zaliczamy proces spawania, napawania, przetapiania, cięcia, przebijania lub proces obróbki cieplnej. Krótkie, ale bardzo energiczne impulsy promieniowania laserowego są stosowane do spawania punktowego lub perforacji, podczas gdy w przypadku procesów napawania, stopowania, przetapiania i obróbki cieplnej wymagana jest wiązka ciągła.

### 2.2 Rodzaje wiązki laserowej:

W praktycznych zastosowaniach wykorzystuje się trzy rodzaje wiązki laserowej:

*Wiazkę ciągłą - CW,*

*Wiazkę impulsową - PM,*

*Wiazkę udarową - GP.*

Dobór wiązki i jej zastosowanie w procesie spawalniczym zależy od tego jak skonstruowany jest laser. W laserach, które emitują wiązkę ciągłą medium laserujące napełniane jest w sposób ciągły, czego rezultatem jest emitowanie wiązki ciągłej. Emitują one promieniowanie o stałym natężeniu od kilku watów do ponad 10,0 [kW]. Lasery, które emitują wiązkę ciągłą są w stanie wyemitować również wiązkę impulsową, z kolei wiązka impulsowa lub udarowa nie jest w stanie wyemitować wiązki ciągłej. W laserach, które emitują wiązkę impulsową medium laserujące dostarczane jest udarowo, aby wytworzyć krótkie impulsy promieniowania laserowego. Moc impulsu dostarczania jest większa od pojedynczego impulsu. Energia, częstotliwość oraz czas trwania impulsów laserowych określają średnią moc wiązki. W nowoczesnych laserach impulsowych dochodzi do wytwarzania mocy do 60[kW]. W laserach, które emitują wiązkę udarową medium laserowe dostarczane jest w sposób ciągły, przy małej mocy, czego rezultatem jest wytworzenie udarowego impulsu wiązki laserowej. Impulsy udarowe charakteryzują się mocą kilkuset kilowatów w bardzo krótkim czasie trwania, który mierzony jest w nanosekundach lub pikosekundach. [1]



### **3. PODSUMOWANIE**

Badania przeprowadzone w ramach projektu PBL potwierdziły, że obróbka laserowa stanowi innowacyjne narzędzie w udoskonalaniu właściwości funkcjonalnych topowej warstwy stali narzędziowej. Wykorzystanie cięcia laserem światłowodowym pozwoliło na osiągnięcie optymalnych kształtów i wymiarów metalowego przedmiotu, co ma kluczowe znaczenie w branży maszynowej. Jednakże, analiza różnych typów stali i ich reakcji na działanie lasera jest niezbędna dla skutecznego przetwarzania laserowego.

W trakcie badań skoncentrowano się na stalach narzędziowych, które charakteryzują się wysoką odpornością na ścieranie, dużą twardością i małą ciągliwością. Dodatki stopowe pozwalają dostosować ich właściwości do konkretnych potrzeb, co potwierdza istotę ciągłych badań nad reakcjami różnych rodzajów stali na wiązkę laserową.

Cięcie laserowe światłowodowe, oparte na zastosowaniu różnych gazów towarzyszących w zależności od rodzaju materiału, oferuje szereg zalet, takich jak duże prędkości cięcia, niskie naprężenia i minimalne deformacje materiału. Jednakże, istnieją pewne ograniczenia, takie jak maksymalna grubość ciętych elementów, generowane promieniowanie elektromagnetyczne, koszty urządzeń oraz konieczność zastosowania środków bezpieczeństwa dla operatorów.

Warto podkreślić, że kluczową rolę w procesie obróbki laserowej odgrywa różnorodność zastosowanych wiązek laserowych, takich jak ciągła, impulsowa i udarowa. Ich elastyczne dostosowanie do konkretnych wymagań procesu obróbki umożliwia wszechstronne zastosowanie w różnych dziedzinach przemysłu. Dalszy rozwój technologii laserowej i ciągłe badania nad jej zastosowaniami mają potencjał przyczynienia się do jeszcze bardziej precyzyjnych i efektywnych metod obróbki. Ten postęp odgrywa kluczową rolę w kontekście postępu w przemyśle i produkcji, wprowadzając nowe standardy efektywności, jakości i zrównoważonego rozwoju, co stanowi kluczowy krok w kierunku przyszłościowej, zaawansowanej produkcji.

### **PODZIĘKOWANIE**

Praca powstała w wyniku realizacji projektu w ramach kształcenia zorientowanego projektowo - PBL, w konkursie X w ramach programu Inicjatywa Doskonałości – Uczelnia Badawcza, Politechnika Śląska.

### **BIBLIOGRAFIA**

1. A. Klimpel, Technologie Laserowe Spawanie, Napawanie, Stopowanie, Obróbka Ciepła i Cięcie, Wydawnictwo Politechniki Śląskiej, Gliwice 2012
2. P. Boś, D. Chodorowska, R. Fejkiel, Z. Wrzask, Podstawy Konstrukcji Maszyn 2, Techniki Wytwarzania i Maszynoznawstwo, Wydawnictwo Komunikacji i Łączności, Warszawa 2012
3. Dubik, Zastosowanie Laserów, Wydawnictwo Naukowo-Techniczne, Warszawa 1991
4. L.A. Dobrzański, Podstawy Nauki o Materiałach i Metaloznawstwo. Materiały Inżynierskie z Podstawami Projektowania Materiałowego, Wydawnictwo Naukowo-Techniczne, Gliwice-Warszawa 2002



26th January 2024  
Gliwice, Poland

DEPARTMENT OF ENGINEERING MATERIALS AND BIOMATERIALS  
FACULTY OF MECHANICAL ENGINEERING  
SILESIAAN UNIVERSITY OF TECHNOLOGY

## INTERNATIONAL STUDENTS SCIENTIFIC CONFERENCE

### **Materials and technologies used in 3D printing in production of organ prototypes and implants**

R. Gabryś<sup>a</sup>, J. Pająk<sup>a</sup>, K. Krochmal<sup>b</sup>, I. Blumski<sup>c</sup>, L. Gabiga<sup>c</sup>, M. Polok-Rubinić<sup>d</sup>, A. Włodarczyk-Fligier<sup>d</sup>, A. Kania<sup>d</sup>

<sup>a</sup> Students of Industrial Mechatronics, <sup>b</sup> Students of Automation and Industrial Robotics, <sup>c</sup> Students of Mechanical Engineering

email: rg302613@student.polsl.pl

<sup>d</sup> Silesian University of Technology, Faculty of Mechanical Engineering, Department of Engineering Materials and Biomaterials

email: magdalena.polok-rubinić@polsl.pl

**Abstract:** 3D printing technology enables the creation of personalized medical implants and tools tailored to the specific needs of patients, utilizing advanced additive manufacturing methods. This significantly enhances the transparency of surgical procedures or rehabilitation, allowing for precise explanations to the patients.

**Keywords:** Polymers materials, 3D printing, medicine, implants, organs

## **1. INTRODUCTION**

3D printing is utilized in medicine, offering the possibility of personalization through the printing of implants and anatomical models for patients. Prototyping involves the creation of internal organs anatomical models or body parts, aiding in the explanation of planned surgical procedures or rehabilitation. Modern additive manufacturing methods such as Stereolithography (SLA), Fused Deposition Modeling (FDM), Electron Beam Melting (EBM), and Selective Laser Melting (SLM) are employed for this purpose. These methods allow the utilization of various material groups, including resins, polymeric materials, and metals, thereby expediting the process from prototype to the final product [1].

## **2. MATERIALS USED FOR 3D PRINTING IN THE PRODUCTION OF ORGAN AND IMPLANT PROTOTYPES**

### **2.1. Polyamides**

Polyamides are characterized by high elongation resistance and excellent mechanical properties (Tab. 1). Various structural variants exist, with significant importance in the technical field for polyamides labeled 6, 6.6, 10, 11, and 12. They find applications in textile production

and the medical sector due to their ability to interact with the human body (biocompatibility) [2-4].

Polyamide 6 (PA6) also known as polycaprolactam, it is a flexible and durable material with chains containing six carbon atoms. Used in prototyping due to ease of processing.

Polyamide 6.6 (PA6.6) Nylon 6.6 with chains of six carbon atoms, differing from PA6 in chemical composition. It exhibits higher thermal, atmospheric and chemical resistance.

Polyamide 10 (PA10) rare type of polyamide with main chains composed of ten carbon atoms, known for good chemical resistance. Primarily used in the medical industry.

Polyamide 11 (PA11) flexible and durable material produced from amino acids derived from rapeseed oil. Its main advantages include resistance to chemical substances and atmospheric conditions.

Polyamide 12 (PA12) flexible material with chains containing twelve carbon atoms, manufactured from lauric acid. It features resistance to oils, greases, and solvents.

Table 1. Physical properties of PA [2-4]

Density[kg/m <sup>3</sup> ]	1130
Melting Temperature [°C]	215
Extrusion Temperature [°C]	270
Glass Transition Temperature [°C]	45
Tensile Strength [MPa]	10
Compressive Strength [MPa]	98

Polyamide for medical applications is primarily available as a powder for SLS (Selective Laser Sintering) 3D printers [2-4]. The SLS technology is a 3D printing process where a laser precisely sinters a layer of thermoplastic powder, creating three-dimensional objects layer by layer. Due to the absence of the need for additional support structures and the ability to print with various materials, SLS enables the production of complex and precise elements. It allows for the creation of custom prosthetics or implants (Fig. 1) that fit the individual needs of the patient perfectly. These could include bone implants, joint prosthetics, and even heart valves [5].



Figure 1. Leg bracing orthosis made of Nylon 12 [6]

## 2.2. Polieteroeterketon (PEEK)

Polyetheretherketone is an exceptional thermoplastic material. Its mechanical properties, such as tensile strength, flexibility, and compression resistance, make it suitable for medical applications as a material for manufacturing implants. It is also highly conducive to sterilization due to its high chemical and temperature resistance (Tab. 2) [7-9].

Polyetheretherketone for medical purposes is available as a filament for FDM/FFF 3D printers, and it is gradually becoming available as a powder for SLS 3D printers [8,9].

Table 2. Physical properties of PEEK [7]

Density[g/m <sup>3</sup> ]	1,31
Melting Temperature [°C]	340
The tensile strength at the yield point [N/mm <sup>2</sup> ]	110
Compressive Strength [MPa]	130

Fused Deposition Modeling (FDM) 3D printing is based on melting and layer-wise deposition of thermoplastic filament by heating nozzles to create three-dimensional objects. This process is characterized by its simplicity, availability of diverse materials, and relatively low costs, making FDM a widely used 3D printing technology. Key features include precise creation of three-dimensional structures, flexibility in material selection ranging from basic polymers to specialized plastics, and the ability to produce complex geometries without the need for traditional tools [10].

## 2.3. Titanium

Titanium and its alloys are among the metals used in medicine for creating various types of implants. In orthopedic implants and dentistry, pure titanium and the titanium alloy Ti6Al4V are most commonly used. They are characterized by high biocompatibility and durability in contact with the human body (Tab. 3). While pure titanium and Ti6Al4V are frequently used in prosthetics, there are other titanium alloys that, due to their cost or specific properties, are applied in more specialized applications. Examples of other titanium alloys used in prosthetics include TiNbZr, Ni-Ti alloys, Ti-(Ta,Nb)-Fe, Ti25Ta, Ti12Mo6Zr2Fe, and Ti6Al7Nb [11,12].

Table 3. Physical properties of titanium [8]

Density[kg/m <sup>3</sup> ]	4.5
Melting Temperature [°C]	1668
Tensile Strength [MPa]	550-1000
Compressive Strength [MPa]	300-550

For 3D printing using titanium, three methods are employed: SLM (Selective Laser Melting), DMLS (Direct Metal Laser Sintering), and EBM (Electron Beam Melting) [13-15].

SLM (Selective Laser Melting), similar to EBM, relies on the melting of metal powders using a high-energy laser. Compared to EBM, SLM offers greater precision but may be slower, making

the choice between these technologies dependent on specific needs and priorities of the application [15].

The DMLS (Direct Metal Laser Sintering) process involves the deposition of thin layers of powdered metal by 3D printers, followed by sintering selected areas using a laser, repeated until complete parts are obtained. It finds extensive use in medicine, especially in the production of complex knee and hip endoprostheses, due to its adaptability to individual patient needs [13].

EBM (Electron Beam Melting) is a manufacturing method where a high-energy electron beam melts powdered metal layer by layer. This technology allows for rapid prototyping of real parts, eliminating the need for traditional processes such as CNC machining and welding [14].

3D printing methods enable the creation of titanium implants, prosthetics, crowns, bridges, bone supplements after accidents or surgeries, simultaneously minimizing production costs and reducing material waste (Fig. 2).



Figure 2. Titanium bone prosthetics [16]

#### 2.4. Epoxy resins

Epoxy resins are compounds containing more than one epoxy group in a molecule. They are characterized by high chemical and corrosion resistance, good mechanical and thermal properties, excellent adhesion to various substrates, low shrinkage after hardening, insulating properties, and the ability to be processed under various conditions [18].

Their versatility makes them useful in various medical fields, including dentistry, prosthetics, and orthotics (Fig. 3). They are well-suited for prototyping due to the capability of 3D printing using the SLA method [18].



Figure 3. Dentures epoxy resin [19]

SLA (Stereolithography) enables the creation of models from a photosensitive liquid polymer that hardens under UV radiation. The process involves layer mapping with a UV laser,

solidification of the model's cross-section, multiple immersion and hardening in a resin bath, and final curing through UV exposure, allowing precise high-resolution printing without the risk of clogging or damaging the model by the nozzle [17].

### 3. SUMMARY

3D printing revolutionizes medicine, enabling personalized solutions. The use of methods such as SLA (Stereolithography), FDM (Fused Deposition Modeling), EBM (Electron Beam Melting), and SLM (Selective Laser Melting), along with materials including polyamides (PA6, PA6.6), PEEK, titanium, and epoxy resins, allows to produce implants and anatomical models, increasing their availability.

### BIBLIOGRAPHY

1. H. Dodziuk, Applications of 3D printing in healthcare, Institute of Physical Chemistry PAS, Warsaw (2016) 283-290 .
2. J. Koszkuł, Polymer materials, Czestochowa: Czestochowa: Czestochowa University of Technology, Publishing House (1999) 88-101.
3. Bortel Edgar, Introduction to polymer chemistry, Cracow, ed. UJ 6-7 (1994) 115-116.
4. PN-EN ISO 527-1, Plastics - Determination of mechanical properties in static tension - Part 1: General principles (2020).
5. S. Lekurwale, T.Karanwad, S. Banerjee, Selective laser sintering (SLS) of 3D printlets using a 3D printer comprised of IR/red-diode laser, Annals of 3D Printed Medicine 6, (2022).
6. 3D printing material Nylon 12 (SLS) CadXpert, <https://cadxpert.pl/materialy-do-druku-3d/formlabs-nylon-12/>, Nylon 12 (2023) 14-25
7. Z. Wang, M. Runzi, M. Gilchrist, H. Gong, Mechanical Properties of High-Performance Plastic Polyether-ether-ketone (PEEK) Printed by Fused Deposition Modeling, Solid Freeform Fabrication Symposium – An Additive Manufacturing Conference (2021).
8. Choosing 3D Printing Materials for Different Medical Applications, Novus Life Sciences, (2023).
9. M.D. Monzón, R. Paz, P. Bordón, Present and future of standardization of additive manufacturing in the medical field, 3D Printing in Medicine (2023) 361–378.
10. F. Madaraka Mwema, E. Titilayo Akinlabi, Basics of Fused Deposition Modelling (FDM), National Library of Medicine (2020).
11. C.N. Elias, J.H.C. Lima, R. Valiev, and M.A. Meyers, Biomedical Applications of Titanium and its Alloys (2008) 46-49.
12. Taylor Juenke, Review on titanium and titanium alloy usage in biomedical implantation applications, University of Washington, Seattle (2021) 36-38.
13. Hendrickson, Joel W., Use of Direct Metal Laser Sintering for Tooling in High Volume Production (2015). All Graduate Plan B and other Reports, Spring 1920 to Spring (2023) 1-3.
14. Miguel Lopez, Mechanical Performance Of EBM TI-6AL-2SN-4ZR-2MO Influenced By The Effects Of Different Hot Isostatic Pressing Treatments, University of Texas at El Paso (2020) 1-5.

15. Finley Marbury, Characterization of SLM Printed 316L Stainless Steel and Investigation of Micro Lattice Geometry 15 (2017) 6-9.
16. MECHANIK 02/2020, Mechanik Editorial Office - SIMP Publishing Agenda, (2022), 23.
17. Dale A. Berry, Composite Materials for Orthotics and Prosthetics, Orthotics and Prosthetics, C.P. The American Orthotic and Prosthetic Association (1987) 41-43.
18. Taylor Wilson, Application of SLA 3D Printing for Polymers, The University of Akron, Spring (2022) 3-10.
19. Formlabs Presents 3D Printed Dentures - iData Research, <https://idataresearch.com/formlabs-presents-3d-printed-dentures/>, Formlabs Presents 3D Printed Dentures (2019).

**Praca powstała w wyniku realizacji projektu Project Based Learning (PBL) pt. Projektowanie i wydruk 3D modeli anatomicznych pomocnych w przygotowaniu do operacji i wyjaśnieniu procesu leczenia pacjentom.**



26th January 2024  
Gliwice, Poland

DEPARTMENT OF ENGINEERING MATERIALS AND BIOMATERIALS  
FACULTY OF MECHANICAL ENGINEERING  
SILESIA UNIVERSITY OF TECHNOLOGY

## INTERNATIONAL STUDENTS SCIENTIFIC CONFERENCE

### **Analysis of the influence of technological parameters of laser cutting of steel on surface quality**

D. Gajczowska <sup>a</sup>, J. Kuta <sup>b</sup>, J. Osiewała <sup>b</sup>, O. Sobek <sup>b</sup>, N. Tomanek <sup>b</sup>, A. Zyzik <sup>c</sup>,  
M. Bonek <sup>d</sup>, O. Polishchuk <sup>e</sup>, B. Gitolendia <sup>f</sup>

<sup>a</sup> Student of Silesian University of Technology, Faculty of Mechanical Engineering, Material Engineering, Gliwice, Poland

<sup>b</sup> Student of Silesian University of Technology, Faculty of Mechanical Engineering, Production engineering and management, Gliwice, Poland

<sup>c</sup> Student of Silesian University of Technology, Faculty of Electrical Engineering, Electrotechnics, Gliwice, Poland

<sup>d</sup> Silesian University of Technology, Faculty of Mechanical Engineering, Department of Engineering Materials and Biomaterials, Gliwice, Poland

<sup>f</sup> Georgian Technical University, Faculty of Transport Systems and Mechanical Engineering, Tbilisi, Georgia

**Abstract:** The article presents a method of laser cutting. It focused on the analysis of technological parameters and their influence on surface quality. A comparison was made between other cutting methods and the laser cutting method.

**Keywords:** materials, laser treatment, laser cutting, surface quality

## 1. INTRODUCTION

Laser cutting can be widely used and used to process many types of organic and inorganic materials. Analyzing the impact of the technological parameters of laser cutting of steel on surface quality is important from both a production engineering and management perspective. From a manufacturing perspective, engineers must precisely control factors such as laser power, cutting speed and type of shielding gas to achieve the expected surface properties. The goal of engineers is to optimize the laser cutting process, who, after analysis, make changes to process parameters to achieve better surface quality and increase production efficiency. Process management involves coordinated activities to control technological parameters, which translates into minimizing defects and production costs. The whole analysis of the influence of technological parameters of laser cutting of steel on the surface quality allows continuous improvement of the production process, which contributes to increasing the competitiveness of the company in the market. Economically, laser cutting by its long life directly affects the reduction of costs associated with the need to replace the blades of classic machining tools that are standing up. An automated workstation using laser cutting significantly saves the time



needed to make a product. In addition, it is characterized by high accuracy in cutting complex geometries, which can often even replace finishing.

Laser cutting uses a phenomenon known as Light Amplification by Stimulated Emission of Radiation (LASER), which creates a thin of visible, ultraviolet or infrared light. Its energy is high enough to burn, melt or cut through chosen materials. There are three main types of laser cutters: CO<sub>2</sub> lasers, Direct Diode laser and Fiber lasers.

Due to its high efficiency, low energy cost and advanced technology the most often used type of laser cutting machine are fiber lasers. The main advantage that fiber lasers have over other types of laser cutting machines is the optical fiber, which is used to transport the emitted light. The fiber is consisted of three main parts: outer layer, inner layer and active core.

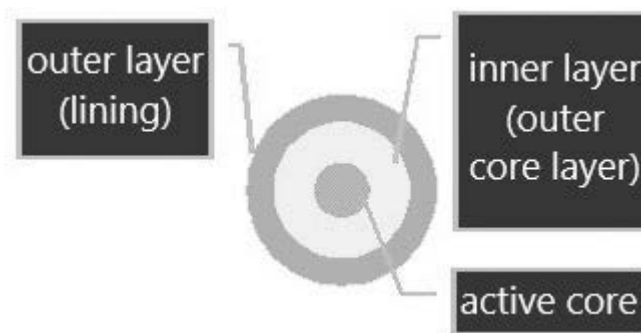


Figure 1 Structure of a laser optical fiber

The three layers use three layers of materials with different refractive index. The lining material should have the lowest refractive index as its main job is to keep the emitted light inside the fiber by reflecting it from its surface inside the fiber. The outer core layer is responsible for focusing the rays of light and initiating the laser action, while providing optimal transfer of energy within the fiber. The last layer of the fiber is its active core has the highest refractive index and it is made out of rare-earth elements.

At the end of the active fiber there are Bragg difference gratings, one of which is a fully reflecting mirror and the other is the output mirror of the optical resonator. Thanks to the high flexibility of the fiber, it can have a very compact structure, creating a long, thin, flexible laser rod. The active optical fiber is terminated on both sides with many connectors that connect and transfer the energy from the pump diodes to the outer layer of the optical fiber. Then, a high-power laser beam emitted from the active core is transmitted via the optical fiber to a collimator, i.e. a system that transforms a beam of laser radiation with high divergence into a beam in which the radiation propagates in parallel. The laser beam prepared in this way then goes to the optical system, where it is focused to a spot of appropriate dimensions, depending on the required technological conditions of laser processing.

Inherent in laser cutting is the use of working gas, the gas stream is blown through a nozzle, giving off the products of the cutting process - liquid and vaporized material. The gas used for cutting can be neutral or chemically reactive to the material. During the laser cutting process, it is very important to choose the right working gas. The gas is selected depending on the material used. For low-alloy or unalloyed steel, oxygen is used, and for tool steels and non-metal materials, nitrogen is used.

When laser cutting, the power density of the laser radiation is important, which should be between  $10^4$  and  $10^6$  [W/mm<sup>2</sup>]. The choice of the appropriate density depends on the material being cut. The laser source delivers continuous energy, melting the material through its total thickness. The polarization of the laser beam is critical to the efficiency of the process and the quality of the cut. The type of polarization, whether linear, random, circular or elliptical, depends on the design of the laser used.

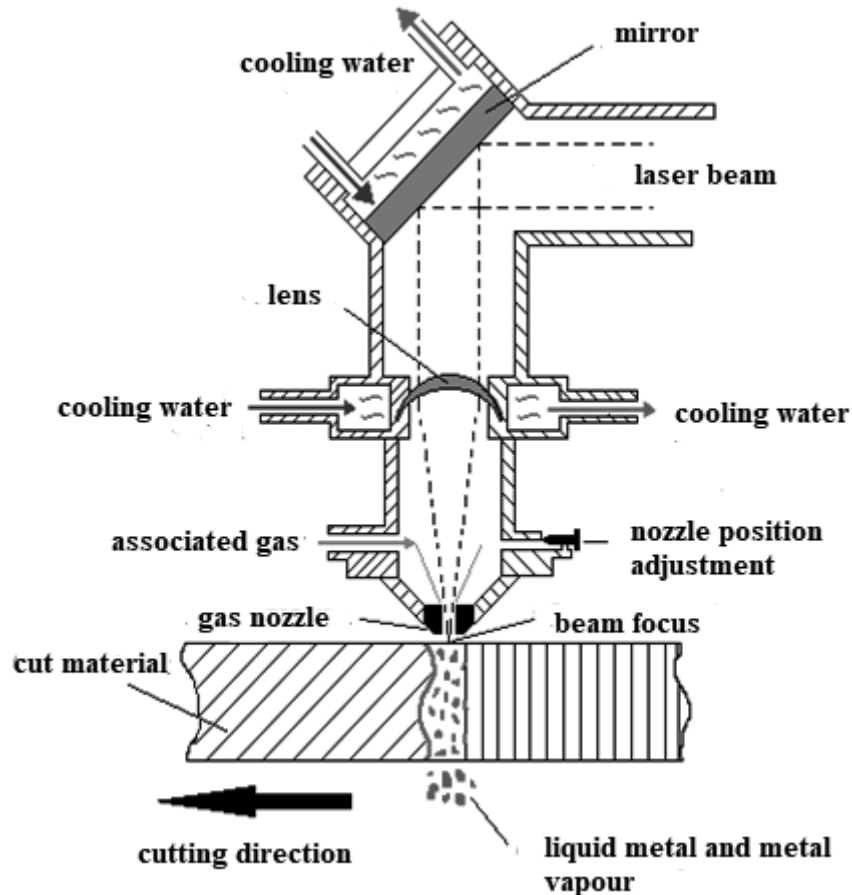


Figure 2. Construction of the laser head [1]

## RESEARCH PART

The research part compared laser cutting with other cutting methods. Then, the material was analyzed in terms of technological properties. Table number 2 shows a comparison of cutting parameters and material characteristics after the process.

Figure 3 and figure 4 shows the macrostructure of the steel after the laser cutting process. The observation was made on a stereoscopic light microscope. The surface of the part after laser cutting showed little roughness. The cutting direction used in the process was noticeable. No cracks, infiltration and surface deformation were observed.

Table 1 Comparison of features and parameters of cutting processes

	Method used	Cut number 1	Cut number 2	Cut number 3
1.	Cutting tool	laser beam	plasma jet	cutters
2.	Character of the cutting	laser cutting	gas cutting	mechanical cutting
3.	Heat affected zone	small	large	no
4.	Impact on the surface layer	low	high	low
5.	Cutting parallelism	high	medium	medium
6.	Surface roughness after cutting	good	medium	medium
7.	Dimensional accuracy	good	medium	medium
8.	Cutting speed	high	medium	low
9.	The need for further processing	seldom	sometimes	seldom
10.	Environmental factors	Minor noise; emissions of harmful radiation and oxides	High noise; emission of harmful radiation and oxides	Medium noise
11.	Amount of waste generated	small	small	small

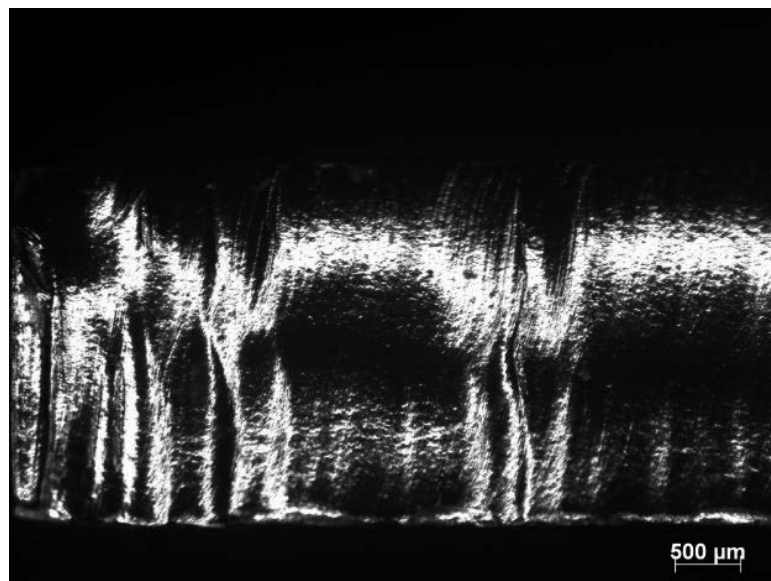


Figure 3 Surface of steel after laser cutting, zoom 25 x

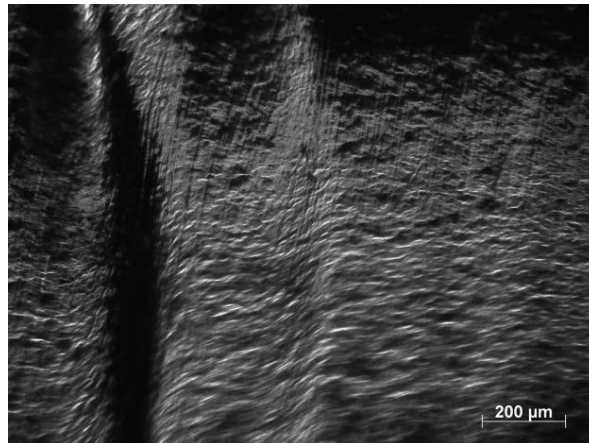


Figure 4. Surface of steel after laser cutting, zoom 100 x

In figure number 4 and figure 5 we see the structure of the material after plasma cutting. As with laser cutting, the surface was not corrugated and the direction of the material cut was noticeable. However, the infiltrations formed during the cutting process were clear. In addition, corrosion foci were observed in figure number 4.

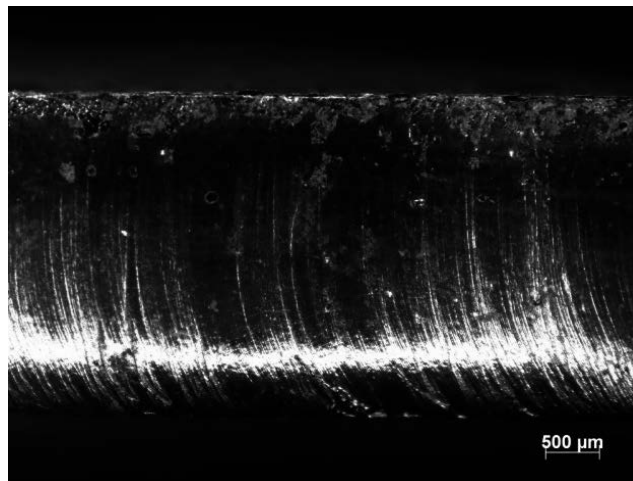


Figure 5. Surface of steel after plasma cutting, zoom 25 x

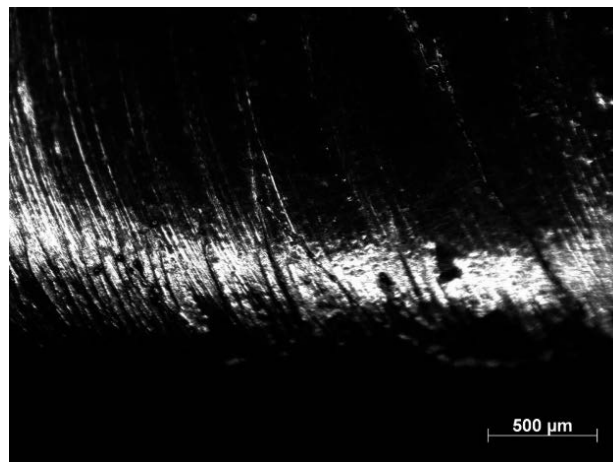
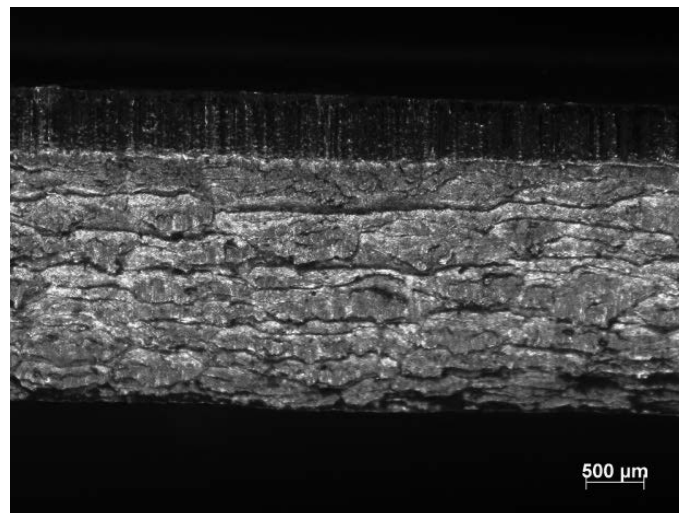
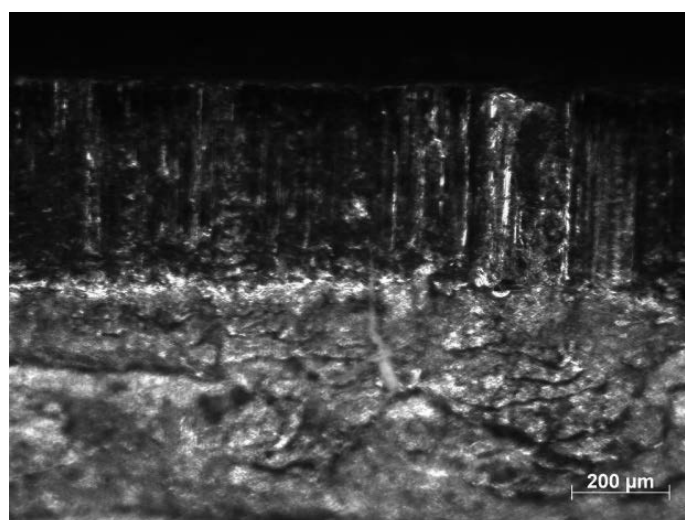


Figure 6. Surface of steel after plasma cutting, zoom 100 x

Observation of the structure of the material after mechanical cutting with a guillotine shear is shown in figure number 7 and figure number 8. In the upper part of the sample, a zone was observed, which was formed during plastic flow of the material. Scratches can be seen there, which are directed according to the direction of the pressure generated by the guillotine shears. Below the zone of plastic flow, we observe the area where the material's continuity was broken. There we can see unevenness and high surface roughness.



*Figure 7. Surface of steel after mechanical cutting, zoom 25 x*



*Figure 8. Surface of steel after mechanical cutting, zoom 100 x*

## **2. CONCLUSIONS**

Since the laser beam made it possible to cut materials, the laser has become a very advantageous and effective tool compared to other cutting methods. Laser-cut parts show low surface roughness and a small heat-affected zone, which is undesirable due to the changes in the material. The impact on the surface layer is negligible because the time the beam affects the material is very short. The laser beam allows cutting accuracy of a few micrometers, which is

currently unattainable for other methods. The small widths of the cutting slots eliminate the finishing process, which reduces material loss, which reduces costs, as does the high cutting speed, which increases the profitability of using this method. Laser cutting equipment also offers a wide range of possibilities when it comes to automating and robotizing the cutting process. One disadvantage of laser cutting is the high cost associated with the purchase of a laser, which is a major obstacle to their use in industry. Summing up the advantages and disadvantages, in the cutting processes of various materials, laser systems offer great opportunities that are not available in conventional methods.

## **ACKNOWLEDGEMENTS**

The work was created as a result of the project as part of project based learning - PBL, in the 10th competition under the Initiative of Excellence - Research University, Silesian University of Technology.

## **BIBLIOGRAPHY**

1. A. Klimpel.: Technologie laserowe: spawanie, napawanie, stopowanie, obróbka cieplna i cięcie, Wydawnictwo Politechniki Śląskiej, Gliwice 2012.
2. J. Kusiński.: Lasery i ich zastosowanie w inżynierii materiałowej, Wydawnictwo Naukowe Akapit, Kraków, 2000.
3. A. Klimpel.: Technologia spawania i cięcia metali, Wydawnictwo Naukowo-Techniczne, Warszawa 1999.
4. J. Pilarczyk.: Poradnik inżyniera. Spawalnictwo, Wydawnictwo Naukowo-Techniczne, Warszawa 2005.
5. A. Klimpel.: Podstawy teoretyczne cięcia laserowego metali. Przegląd spawalnictwa, 2012/6



26th January 2024  
Gliwice, Poland

DEPARTMENT OF ENGINEERING MATERIALS AND BIOMATERIALS  
FACULTY OF MECHANICAL ENGINEERING  
SILESIA UNIVERSITY OF TECHNOLOGY

## INTERNATIONAL STUDENTS SCIENTIFIC CONFERENCE

### **Planning and organization of biopolymers material process for biomedical applications**

M. Gawlas<sup>a</sup>, M. Rzepiela<sup>a</sup>, M. Żydowicz<sup>b</sup>, L. Ochocka<sup>b</sup>, M. Nitszke<sup>b</sup>, S. Bober<sup>b</sup>,  
K. Cesarz-Andraczke<sup>a</sup>, M. Adamiec-Organisciok<sup>b</sup>

<sup>a</sup> Silesian University of Technology, Faculty of Mechanical Engineering, Department of Engineering Materials and Biomaterials

email: mg303333@student.polsl.pl

<sup>b</sup> Silesian University of Technology, Faculty of Automation, Electronics and Computer Science, Department of Engineering and Systems Biology

email: malgorzata.adamiec-organisciok@polsl.pl

**Abstract:** The article presents the plan, concept, and schedule of tasks necessary for the biopolymer's material process to implementation of the potentially applicable as a coating material on zinc alloys in implantology, using production planning and organizing methods.

**Keywords:** planning, material process, biopolymers, Gantt chart, biomaterials

### **1. INTRODUCTION**

Contemporary medicine and biomaterials engineering are constantly focus on innovative solutions that minimize immunological reactions and enhance the biocompatibility of materials used in medical implantology. In the context of this aim, zinc alloys and coating technologies are the subject of intensive research [1]. Zinc with the addition of magnesium is a potentially biocompatible material for absorbable orthopedic implants, owing to the ability of these alloys to undergo gradual biodegradation under biological conditions [2]. In the literature, various groups of scientists point out that zinc alloys with the addition of magnesium are potentially biodegradable materials due to their biocompatible chemical composition, minimizing the need for implant removal and promoting integration with human tissues. The main barrier to the widespread use of zinc alloys as implant materials is their uneven degradation and the excessive release of zinc ions when immersed in solutions simulating human body fluids [3]. The application of polymer coatings on zinc alloys may be a suitable direction for the development of these alloys as a new resorbable biomaterial [2,3].

Biopolymers are organic compounds that occur naturally in living organisms [1]. In the context of medicine and implantology, there is an increasing utilization of these materials due to their characteristic properties, such as low toxicity levels, enabling their safe application [4,5].

The key feature of biopolymers is their biocompatibility, meaning that they are well-tolerated

by the human body and do not induce unwanted immunological reactions or inflammatory states [4]. The important property of biopolymers is their ability to biodegrade, meaning that they can completely break down in living organisms [4]. For the potential use of these materials in implantology, it is necessary that this process occurs in a controlled manner [6].

Currently, synthetic biopolymers such as polylactide (PLA) and natural biopolymers like casein are used in medicine. They are used in medicine as materials for producing implants and drug carriers, thanks to their properties that enable controlled release of active substances and minimize immunological reactions [6-8].







Due to the wide spectrum of applications and the diversity of biopolymers used and potentially applicable as medical materials, it is essential to plan, design, and schedule tasks necessary for the manufacturing process and preliminary biological assessment of new biopolymers for biomedical applications. Material process planning is a holistic process that involves defining steps, resources, and action schedules, as well as planning for control and continuous optimization, leading to the efficient production of a given product [9]. Useful tools for this purpose include production tools such as the Gantt chart, cause-and-effect diagram, also known as the Ishikawa diagram, Pareto analysis, and process maps [10]. The Gantt chart can be particularly helpful in material process planning, enabling a graphical representation of the action schedule, coordination of tasks, project progress tracking, and identification of critical paths. This facilitates resource management, minimizes delays, and optimizes logistical processes [10]. Proper planning of the material process is crucial as it allows for the consideration of all aspects of production and research. It also provides the opportunity to define expectations for the material and determine technical parameters. Starting with a thorough project and defining manufacturing techniques and quality control criteria is fundamental to achieving the goal of the material process project.

## **1.1 Material process planning for biopolymers**

The project's aim was developed a polymer's coating to control the degradation process of a resorbable alloy intended for short-term orthopedic implants. This project encompasses interdisciplinary topics in the fields of materials engineering and biomedical engineering. The biopolymer coatings under investigation in this project aim to reduce the degradation rate and activate or accelerate the formation of new bone tissue at the fracture site. The scientific goal of the project is an attempt to address the issue of a durable coating tasked with controlling or temporarily (during the bone healing period) blocking the degradation of the resorbable alloy for a short-term orthopedic implant. Several types of synthetic polymers and a natural polymer will be used in the study to assess the biological response of cells to the applied biopolymer. The implementation of project tasks will allow the project team members to apply their knowledge and skills in material selection, process parameter selection, biological evaluation of polymeric materials, and the design and execution of scientific research in practice. The research and development project included 16 weeks, conducted from October 2023 to January 2024. The following tasks necessary to achieve the project goal have been identified, and the implementation schedule is presented in Table 1.



*Table 1. Project schedule*

Project schedule		
Lp.	Task	Realization time (days)
1	Evaluation the potential applications of the proposed solution across various fields, identifying potential barriers that may limit its practical implementation, and providing a detailed discussion on the ways to achieve the project goals	1 
2	Evaluation solutions available in the literature, developing a concept, and selecting polymers and manufacturing methods as coating materials for zinc alloys	26 
5	Manufacturing zinc alloys and preparing coating baths. Microscopic observation of the obtained coating structures and their initial selection	16 
7	Evaluation the progress of coating degradation after immersion in Ringer's solution at 37°C for coated samples and reference samples	21 
8	Cytotoxicity studies on selected biopolymers. Performing a comprehensive biological assessment of the produced biopolymers in an environment simulating human body conditions and summarizing the research	5 
10	Analysis of research results and preparation of scientific publications	23 

Based on the determined schedule of performing defined project tasks, an executive plan for the project was established in the form of a Gantt chart (Figure 1). Taking into account the tasks included in the schedule, it should be noted that the implementation of each of the above stages of the project will range from 1 to 6 weeks, depending on the complexity of the task. Some stages will be carried out concurrently. However, after completing each stage, an analysis and summary of the obtained results of project work and research will be conducted, serving as input for the subsequent stages of project implementation.

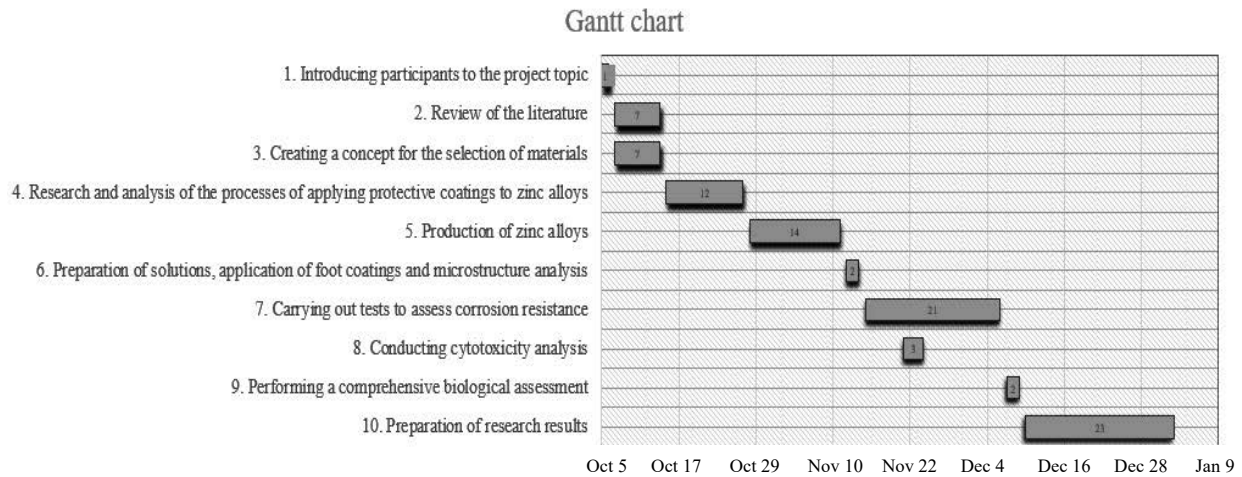


Figure 1. Graphical representation of the task schedule in the form of a Gantt chart.

The risk assessment in the project (Table 2) is an essential step aiming to define predictable events that may act as temporary barriers in achieving the project goals, resulting in an extension of the time required to complete planned activities.

Table 2. Assessment of the likelihood of risk occurrence in the project

Risk factor	Probability of occurrence	Consequences	Action recommended
Unavailability of required materials	low	Delays in initiating the actual project	Finding alternative sources for material acquisition
Issues during the coating manufacturing stage	low	Change in the manufacturing process technology or selection of alternative materials	Detailed literature review and consultations with project supervisors
Failure to meet the deadline for submitting publications	low	Inability to participate in a scientific conference, unpublished research results	Monitoring project progress, systematic work

The execution of tasks outlined in the project is characterized by a low risk of failure, stemming from the extensive experience of the project supervisors in the field of research related to the project's theme. The students participating in the project possess fundamental competencies in management, materials engineering, and biomedical fields, acquired through their education in relevant study programs. They form an interdisciplinary team essential for the implementation of such projects. Additionally, they have access to advanced technological and research laboratories, enabling the completion of project tasks within the designated timeframe.

## 2. CONCLUSIONS

The accurate planning of the engineering materials manufacturing process is the initial and crucial step in commencing research projects. Utilizing project management tools and organizing production processes enables a transparent division of tasks and the achievement of successive milestones. Consequently, reaching the project's goal becomes feasible.

## BIBLIOGRAPHY

- [1] J. Song, B. Winkeljann, O. Lieleg, Biopolymer-Based Coatings: Promising Strategies to Improve the Biocompatibility and Functionality of Materials Used in Biomedical Engineering, *Advanced Materials Interfaces*, 7(17), (2020), 2850.
- [2] C. A. Shahed, F. Ahmad, E. Günister, F.M. Foudzi, S. Ali, K. Malik, W.S. Harun, Antibacterial Mechanism with Consequent Cytotoxicity of Different Reinforcements in Biodegradable Magnesium and Zinc Alloys: A Review, *Journal of Magnesium and Alloys*, 11(9), (2023), 3038–3058.
- [3] R. K. Singh Raman, C. Wen, J.F. Löffler, Human Body-Fluid-Assisted Fracture of Zinc Alloys as Biodegradable Temporary Implants: Challenges, Research Needs and Way Forward, *Materials*, 16(14), (2023), 4984.
- [4] A. Ossowska, S. Sobieszczyk, B. Świeczko-Żurek, A. Zieliński, (ed.), *Biomaterials*, Gdańsk University of Technology Publishing House, Gdańsk, 2014,
- [5] J. B. Park, R. S. Lakes, J. B. Park, *Biomaterials: An Introduction*, Springer Science Business Media, New York, 2007.
- [6] S. Amukarimi, M. Mozafari, Biodegradable Magnesium-based Biomaterials: An Overview of Challenges and Opportunities, *MedComm*, 2(2), (2021), 123–144.
- [7] M. A. Azmah Hanim, R. Calin, D. Jung, PLA-Based Bionanocomposites in Tissue Engineering and Regenerative Medicine, *Bionanocomposites in Tissue Engineering and Regenerative Medicine*, (2021) pp. 481–497.
- [8] A. Kania, K. Cesarz-Andrzejczak, Z. Brytan, Ł. Reimann, P. Smolarczyk, The Influence of Casein Coatings on the Corrosion Behavior of Mg-Based Alloys, *Materials*, 15(4), (2022), 1399.
- [9] H. Kerzner, *Using the Project Management Maturity Model: Strategic Planning for Project Management*, Wiley, Hoboken, New Jersey, 2019.
- [10] R. Knosala, K. Santarek, B. Skołod, A. Kosieradzka, J. Gawlik, J. Plichta, A. Świć, A. Moczala, W. Gierulski, M. Wirkus, A. Szymonik, W. Zielecki, A. Hamrol, Z. Zymonik, W. L. Bojar, J. Duda, A. Maciąg, D. Plinta, E. Górską, J. Lewandowski, J. Matuszek, , (ed.), *Production Engineering: Knowledge Compendium, Vol.1*, Polish Economic Publishing House, Warsaw, 2017.



26th January 2024  
Gliwice, Poland

DEPARTMENT OF ENGINEERING MATERIALS AND BIOMATERIALS  
FACULTY OF MECHANICAL ENGINEERING  
SILESIA UNIVERSITY OF TECHNOLOGY

## INTERNATIONAL STUDENTS SCIENTIFIC CONFERENCE

### Research methods on coatings obtained by vapor phase deposition

J. Glajcar, P. Rucki, D. Pakuła, M. Staszuk

Silesian University of Technology, Department of Engineering Materials and Biomaterials  
email: janglaj695@student.polsl.pl; patruc666@student.polsl.pl, daniel.pakula@polsl.pl;  
marcin.staszuk@polsl.pl

**Abstract:** The article presents selected research methods used for the analysis of coatings obtained through vapor phase deposition (PVD, CVD). The research methods are divided into three main groups: analysis of coating structure (spectroscopic ellipsometry, transmission electron microscopy, scanning electron microscopy, atomic force microscopy, X-ray diffraction), analysis of chemical and phase composition (energy-dispersive spectroscopy, X-ray photoelectron spectroscopy), functional properties of coatings (scratch test method, tribological studies).

**Keywords:** ALD, PVD, CVD, SE, SEM, TEM, AFM, XPS, EDS, EDX, XRD, microhardness, Scratch Test, Pin-on-disc,

### 1. INTRODUCTION

The aim of the article is to present selected research methods performed on coatings obtained by vapor phase deposition. Research on coatings obtained through these methods plays a crucial role in selecting appropriate coatings for given conditions. Industries such as electronics, medical, chemical, and automotive use these studies to assess whether specific coatings meet defined requirements.

In this study, research methods have been divided into three main groups:

- Analysis of coating structure
- Analysis of chemical and phase composition
- Functional properties of coatings

### 2. ANALYSIS OF COATING STRUCTURE

#### Spectroscopic Ellipsometry

Spectroscopic ellipsometry (SE) is an advanced optical technique that allows to investigate properties of thin films. In this method, the change in polarization of light reflected or transmitted through the material is measured and compared with a theoretical model (Fig.1). This method

allows the determination of e.g. coating thickness, refractive index, and extinction coefficient. SE is particularly useful for studying coatings obtained by vapor phase deposition, especially the Atomic Layer Deposition (ALD) method (which allows the production of ultra-thin coatings with thicknesses below 10 nm), as it allows measurements of layer thicknesses even below 10 nm. The advantages of this method are non-invasiveness and non-contact. To obtain reliable results, proper preparation of the investigated surface is necessary, including precise cleaning and drying. [1]

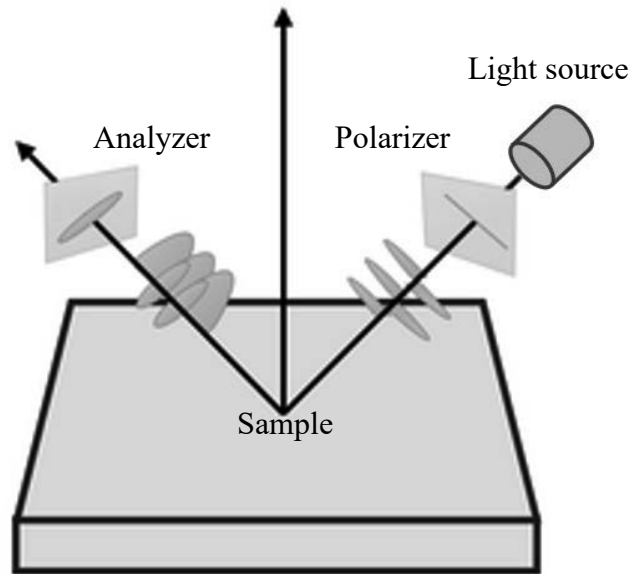


Figure 1. Work principle of Spectroscopic ellipsometry.

### Transmission Electron Microscopy

Transmission Electron Microscopy (TEM) method allows for imaging the internal structure of a material through an electron beam that penetrates the sample. In the case of electron microscopes, studies are conducted under vacuum conditions. Electron beams are emitted by the electron gun, then accelerated and pass through the sample, creating an image on the detector. This method enables the creation of highly detailed images of the examined sample at magnifications of up to several tens of millions of times (Fig.2). The limitation of the TEM method is the ability to study a sample with a maximum thickness not exceeding several tens of nanometers. With the TEM method, it is possible to examine the transition layers between the coating and the substrate material or individual layers within the studied coatings. It also allows the observation of the atomic structure of the examined sample. [2]

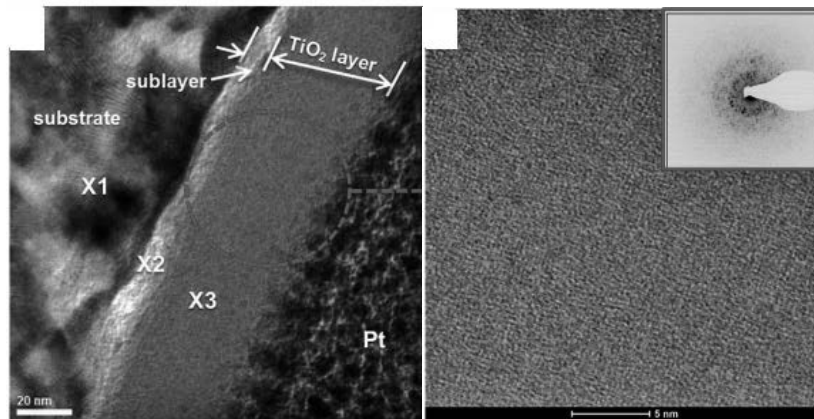


Figure 2. Structure (TEM) of  $\text{TiO}_2$  coating in bright field and with diffraction pattern [3]

### Scanning Electron Microscopy

Scanning electron microscopy (SEM) uses an electron beam to scan the surface of a sample (Fig. 3). In this method, electron beams do not penetrate the sample as in the case of the TEM method, instead, they impact its surface, causing the emission of secondary electrons, which are then analyzed and processed into an image. SEM allows for the observation of the microstructure, morphology, and topography of coatings. Through the SEM method, it is possible to assess the quality of deposition, uniformity of coverage, surface topography, and potential coating defects. In contrast to the TEM method, SEM is not limited by the thickness of the examined sample. Before conducting the study, non-conductive materials should be sputtered, commonly with gold or silver. [2]

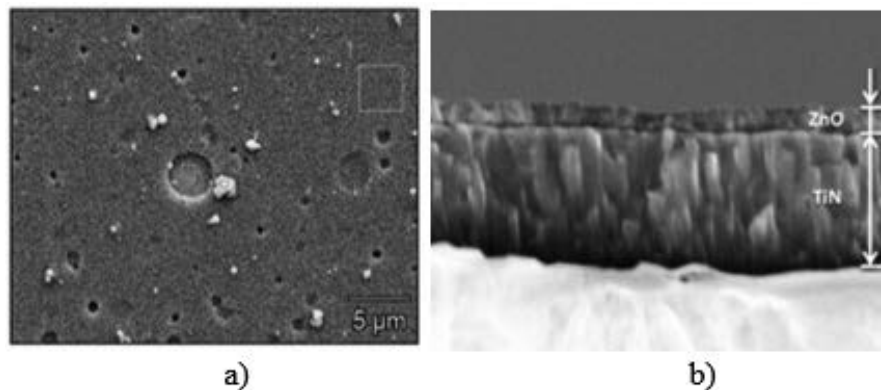


Figure 3. a) Surface topography of the TiN coating deposited on a 316L substrate using a scanning microscope, b) fracture image of the TiN/ZnO(1500) hybrid coating [4]

### Atomic Force Microscopy

Using Atomic Force Microscopy (AFM) and appropriate software, it is possible to obtain a high resolution three-dimensional image of the coating surface (Fig. 4). AFM studies can be conducted in three operational modes:

- Contact mode, where the probe acts with a constant force on the examined surface.
- Dynamic mode (Tapping mode), where the probe vibrates with a constant amplitude.

- Non-contact mode, where Van der Waals forces are used to maintain a constant distance between the probe and the scanned surface.

In addition to surface topography, AFM allows us to investigate changes in the magnetic field on the sample surface and examine local changes in the electric field. An advantage of the AFM method is its capability to study both conductive and non-conductive samples. [5]

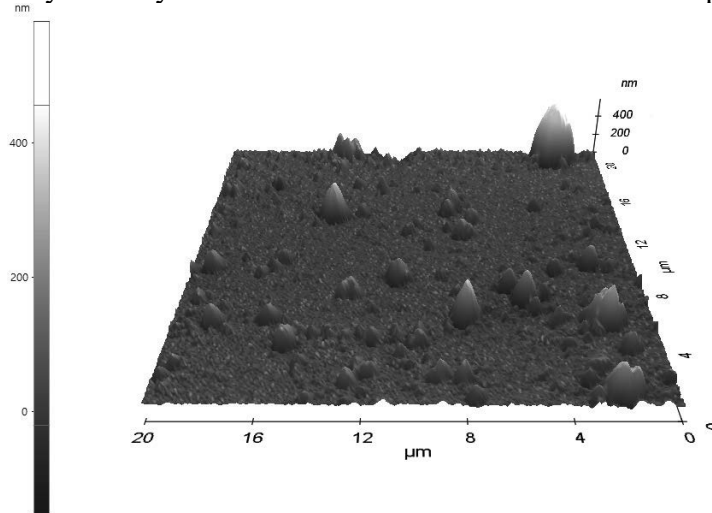


Figure 4. Surface topography (AFM) of  $20 \times 20 \mu\text{m}^2$  of WC-C coating applied on a 316L substrate.

### X-Ray Diffraction

In the X-ray diffraction (XRD), a device is equipped with an X-ray tube and a detector, both of which move in synchronized motion relative to the examined sample. The obtained signal is plotted on a chart (Fig. 5). XRD allows for obtaining information about the dimensions and geometry of the unit cell, as well as the structure of chemical compounds in the examined sample. It also provides information about crystal structure parameters, crystallite size and orientation, residual stresses, Crystallographic defect, and other structural properties. The advantages of XRD are non-invasiveness and non-contact. [6]

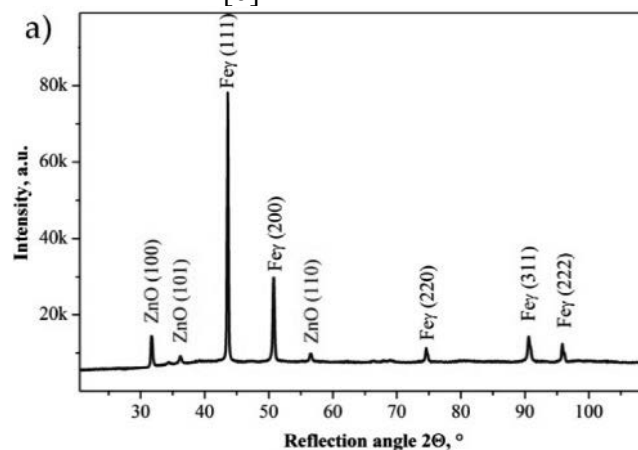


Figure 5. XRD results of ZnO coating deposited on Cr-Ni-Mo steel. [7]

### 3. ANALYSIS OF CHEMICAL AND PHASE COMPOSITION

#### Energy Dispersive Spectroscopy

Energy Dispersive Spectroscopy (EDS/EDX) is a study aimed at determining the chemical composition on the surface of the examined material (Fig. 6). This method involves focusing an electron beam or X-ray beam onto the surface of the sample. As a result, an electron is ejected from the inner atomic shell, following the ejection of the electron. An electron from a higher shell jumps into its place, emitting excess energy in the form of X-ray radiation. Since the amount of emitted energy during the electron jump is characteristic for a specific element, we can determine which element has been scanned by the electron beam. The advantages of this study include non-invasiveness, the ability to scan different areas during a single examination, and easy operation. [2]

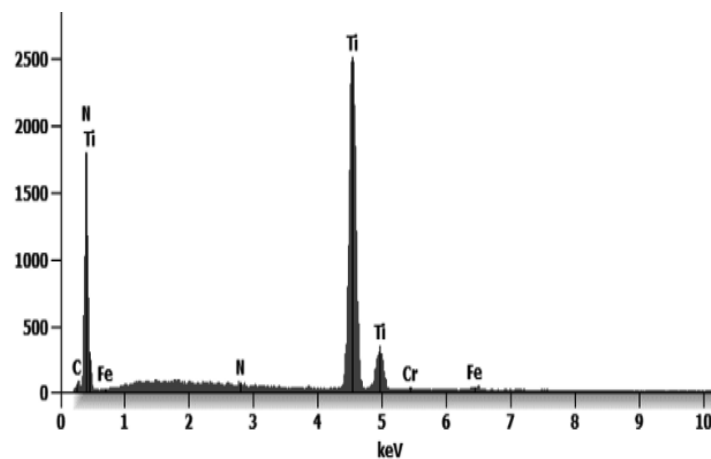


Figure 6. Chemical composition for the TIN coating on a 316L substrate obtained by EDS

#### X-ray Photoelectron Spectroscopy

X-ray Photoelectron Spectroscopy (XPS) is an effective method for identifying elements present on the surface, as well as inside of the analyzed sample, along with their binding energies. This technique is often used in conjunction with ion beam sputtering, allowing for obtaining the spatial distribution of elements and enabling the analysis of multilayer coatings. The method is non-invasive and allows for determining the chemical composition inside of the sample (Fig. 7). [8]

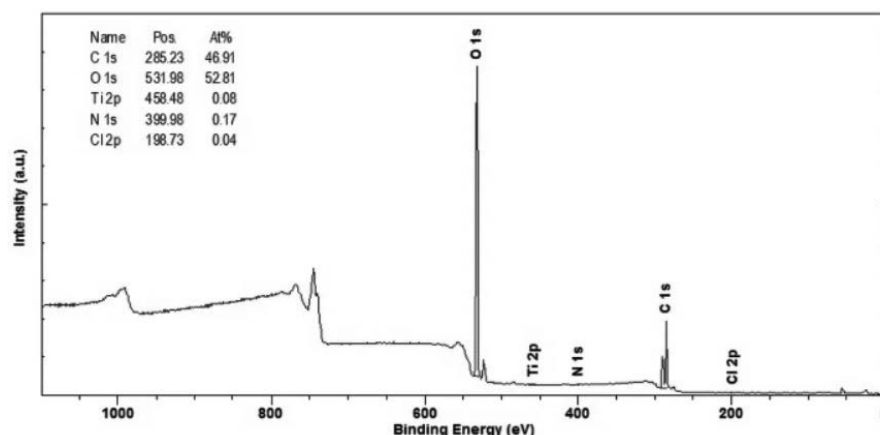


Figure 7. XPS results of Ti + TiO<sub>2</sub>/Al<sub>2</sub>O<sub>3</sub> + TiO<sub>2</sub> coating on LAE442 [7]



#### 4. FUNCTIONAL PROPERTIES OF COATINGS

##### Microhardness testing

Microhardness testing is used to measure the hardness of materials with small indentations. In the microhardness measurement process, the indenter is pressed into the coating under a constantly increasing load until the nominal value  $P_{\max}$  is reached. This allows for the calculation of microhardness and the Young's modulus. Various types of indenters are used in this method, with diamond being the most common, followed by sapphire, quartz, or steel. Indenters can also be categorized based on their shape, with Vickers and Knoop blades being the most popular. Microhardness is defined as the ratio of the applied load  $P_{\max}$  to the surface area of the indentation. [9-11]

##### Scratch Test

The Scratch Test method is used to determine the adhesion of coatings. In this examination, the indenter is in contact with the surface of the sample, during which linear movement occurs between the indenter and the surface under constant or increasing load (Fig. 8). The conducted test results in a graph showing the relationship between force [N], time [s], and distance [mm]. Friction coefficient and acoustic emission functions are also plotted on the graph. This enables the determination of values of  $L_{c1}$  (First cracks in the coating) and  $L_{c2}$ . The measure of adhesion is the critical load  $L_{c2}$ , at which the first chipping of the coating occurs. [12,13]

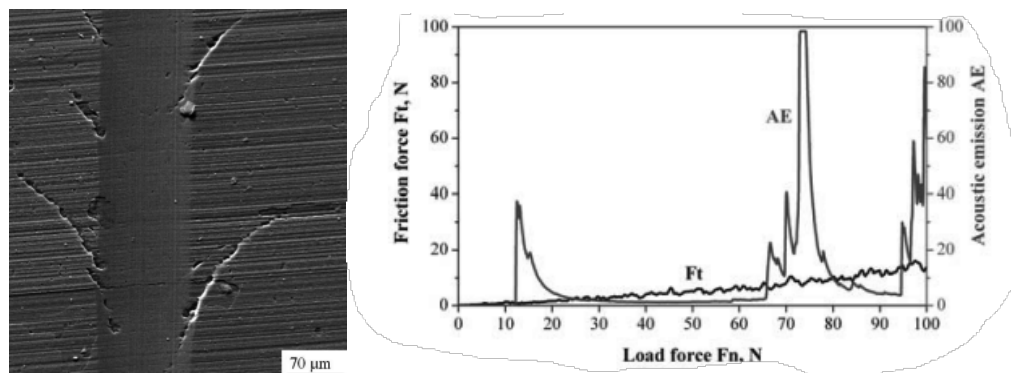


Figure 8. Characteristic failure obtained by scratch test for (Al,Ti)N coating on sialon substrate [14] and acoustic emission (AE) and friction force (Ft) as a function of the load force (Fn) for Ti(B,N) coating surface deposited onto the  $Si_3N_4$  ceramics substrate [15].

##### Wear resistance tests

Wear resistance studies consist of the analysis of surface properties, friction force, material wear, and the impact of lubrication on these processes. They are crucial for understanding the behavior of coatings under operational conditions. These studies enable an analysis of the difference in wear resistance that arises after applying a coating to the tested sample (Fig. 9). The most commonly used method is the pin-on-disc method. In this method, a ball is the pin specimen to which a load is applied. The table on which the sample is placed performs a rotational movement. When conducting the study, attention should be paid to parameters influencing its results, such as: load, speed, number of cycles, and the counter-sample material (typically

carbide, steel, or ceramics). Proper selection of the test parameters allows for a good representation of the real conditions to which the coating may be exposed. [9]

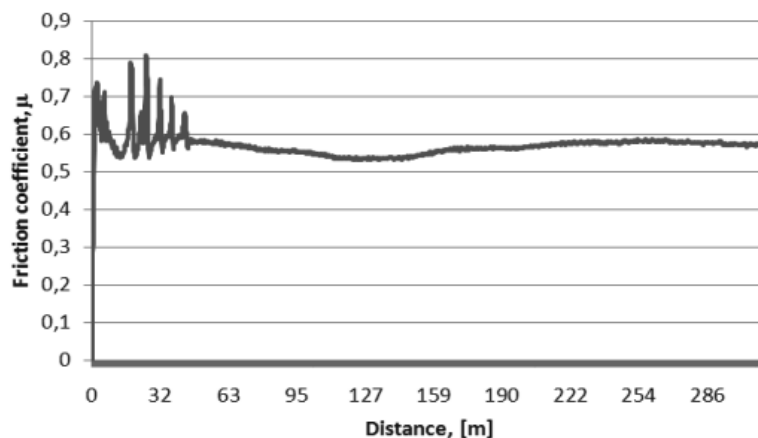


Figure 9. Friction coefficient diagram depending on friction path during the „pin-on-disc” test for Ti(B,N) coating laid on sialon ceramic base [16]

## 5. SUMMARY

The article emphasizes the importance of precise coating research methods for selecting appropriate materials in various industrial applications. When choosing coatings, attention should be paid to their structure, chemical and phase composition, and their functional properties. Precisely defining these criteria will simplify the selection of coatings for specific applications. It is important to note that to obtain reliable results, proper sample preparation is necessary, and also in some methods the correct determination of input parameters. The article does not mention other equally significant methods. In some cases, it is necessary to apply corrosion resistance tests, erosion tests, assessments of the bactericidal properties of coatings, or to analyze the chemical composition using GDEOS spectroscopy.

## ACKNOWLEDGEMENT

This work was produced as part of the project implemented within the framework of project-oriented education – PBL, in the X competition under the Excellence Initiative – Research University program, at the Silesian University of Technology.

## BIBLIOGRAPHY

1. B. Hajduk, P. Jarka, P. Nitschke, Badanie rozkładu grubości powierzchni cienkich warstw metodą elipsometrii spektroskopowej, LAB Laboratoria, Aparatura, Badania, 2019, 24.
2. G. Słowik, Podstawy mikroskopii elektronowej i jej wybrane zastosowania w charakterystyce katalizatorów nośnikowych, Uniwersytet Rzeszowski, 2012.
3. M. Staszuk, Ł Reimann, A. Ściślak, J. Jaworska, M. Pawlyta, T. Mikuszewski, D. Kuc, T. Tański, A. Kříž, Investigations of TiO<sub>2</sub>, Ti/TiO<sub>2</sub>, and Ti/TiO<sub>2</sub>/Ti/TiO<sub>2</sub> coatings produced

- by ALD and PVD methods on Mg-(Li)-Al-RE alloys substrates, *Bulletin of the Polish Academy of Sciences: Technical Sciences*, 2021 e137549-e137549.
4. M. Staszuk, D. Pakuła, Ł. Reimann, A. Kloc-Ptaszna, K. Lukaszewicz, Structure and properties of the TiN/ZnO coating obtained by the hybrid method combining PVD and ALD technologies on austenitic Cr-Ni-Mo steel substrate, *Surfaces and Interfaces*, Volume 37, 2023, 102693
  5. D. Bogdan, I.G. Grosu, C. Filip, How thick, uniform and smooth are the polydopamine coating layers obtained under different oxidation conditions? An in-depth AFM study, *Applied Surface Science*, 2022, 597: 153680.
  6. Q. Luo, S. Yang, Uncertainty of the X-ray diffraction (XRD)  $\sin^2 \psi$  technique in measuring residual stresses of physical vapor deposition (PVD) hard coatings, *Coatings*, 2017, 7(8), 128
  7. M. Staszuk, D. Pakuła, Ł. Reimann, Structure and properties of ZnO coatings obtained by atomic layer deposition (ALD) method on a Cr-Ni-Mo steel substrate type, *Materials (Basel)* 2020, 13: 4223.
  8. Dobrzański, L., Żukowska, L., Kubacki, J., Gołombek, K., & Mikuła, J., XPS and AES analysis of PVD coatings. *Archives of Materials Science and Engineering*, 2008, 32(2), 99-102.
  9. M. Polok-Rubiniec, L.A. Dobrzański, M. Adamiak, Comparison of the adhesion and wear resistance of the PVD coatings, *Journal of Achievements in Materials and Manufacturing Engineering*, 2007, 20.1-2: 87-90.
  10. A. Sliwa, L.A. Dobrzański, W. Kwaśny, M. Staszuk, Simulation of the microhardness and internal stresses measurement of PVD coatings by use of FEM, *Journal of Achievements in Materials and Manufacturing Engineering*, 2010, 43.2: 684-691.
  11. J. Tarnowski, W. Gawędzki, M. Kot, Badanie mikrotwardości warstwy wierzchniej cylindra w aspekcie odporności na zacieranie, *Tribologia*, 2013.
  12. S.J Bull, E.G. Berasetegui, An overview of the potential of quantitative coating adhesion measurement by scratch testing, *Tribology International*, Andhra Pradesh, 2006, 39.2: 99-114.
  13. R.S.R. Kalidindi, R. Subasri, Sol-gel nanocomposite hard coatings. *Anti-Abrasive Nanocoatings*, Woodhead Publishing, 2015, 105-136.
  14. M. Staszuk, T. Tański, L.A. Dobrzański, D. Pakuła, M. Pancielejko, Investigations on wear mechanisms of PVD coatings on carbides and sialons. *Archives of Metallurgy and Materials*, 2017.
  15. D. Pakuła, L.A. Dobrzański, A. Kříž, M. Staszuk, Investigation of PVD coatings deposited on the Si<sub>3</sub>N<sub>4</sub> and sialon tool ceramics. *Archives of Materials Science*, 2010, 54, 54.
  16. D. Pakuła, M. Staszuk, L. Dobrzański, Investigations of the structure and properties of PVD coatings deposited onto sintered tool materials. *Archives of Materials Science and Engineering*, 2012, 58(2), 219-226.



26th January 2024  
Gliwice, Poland

DEPARTMENT OF ENGINEERING MATERIALS AND BIOMATERIALS  
FACULTY OF MECHANICAL ENGINEERING  
SILESIA UNIVERSITY OF TECHNOLOGY

## INTERNATIONAL STUDENTS SCIENTIFIC CONFERENCE

### Investigation of current-voltage relationships of photovoltaic cells

D. Godula<sup>a</sup>, P. Wawrów<sup>a</sup>, M. Bednarski<sup>a</sup>, J. Michlowicz<sup>b</sup>, P. Nowak<sup>b</sup>, S. Markocki<sup>b</sup>,  
M. Musztyfaga-Staszuk<sup>c</sup>, M. Staszuk<sup>d</sup>, W. Filipowski<sup>e</sup>

<sup>a</sup> Silesian University of Technology, Faculty of Automatic Control, Electronics and Informatics, Department of Automatic and Robotics, Poland

<sup>b</sup> Silesian University of Technology, Faculty of Mechanical Technology, Department of Mechanical Engineering and Machine Building, Poland

<sup>c</sup> Silesian University of Technology, Faculty of Mechanical Technology, Department of Welding, Poland

<sup>d</sup> Silesian University of Technology, Faculty of Mechanical Technology, Department of Engineering and Biomedical Materials, Poland

<sup>e</sup> Silesian University of Technology, Faculty of Automatic Control, Electronics and Informatics, Department of Telecommunications and Teleinformatics, Poland

email: [malgorzata.musztyfaga-staszuk@polsl.pl](mailto:malgorzata.musztyfaga-staszuk@polsl.pl)

**Abstract:** The article presents a comparison of several commercial photovoltaic cells based on selected parameters, namely photovoltaic conversion efficiency and fill factor. Photovoltaic cells made from multicrystalline silicon were purchased from a single manufacturer. To conduct the comparison, research for measuring light current-voltage (I-V) characteristics was carried out using a test bench equipped with a solar light simulator. Additionally, a scanning electron microscope (SEM) was employed for microscopic examinations. Using this microscope, the presence of surface texturization on the silicon wafer was confirmed, and the structure of the produced front metallization of the photovoltaic cell was examined. Energy-dispersive X-ray spectroscopy (EDS) was utilized for the analysis of the chemical composition of the selected elements in the photovoltaic cell. The research revealed significant differences in the values of the examined parameters of photovoltaic cells, such as photovoltaic conversion efficiency and fill factor.

**Keywords:** photovoltaic cells, photovoltaics (PV), multicrystalline silicon

## 1. INTRODUCTION

Photovoltaic cells are gaining recognition in connection with the continuous growth of global energy demand and more serious environmental pollution issues. Solar energy, as a readily available, clean, and non-emitting source of energy, is one of the promising sources of energy for the development of civilization [1]. The efficient harnessing of solar radiation attracts the attention of experts, and the analysis of the electrical parameters of photovoltaic

cells plays a crucial role in improving their efficiency, extending durability, and achieving better practical results.

Selected methods for measuring the electrical parameters and conducting microscopic studies of photovoltaic cells are presented in [Fig. 1].

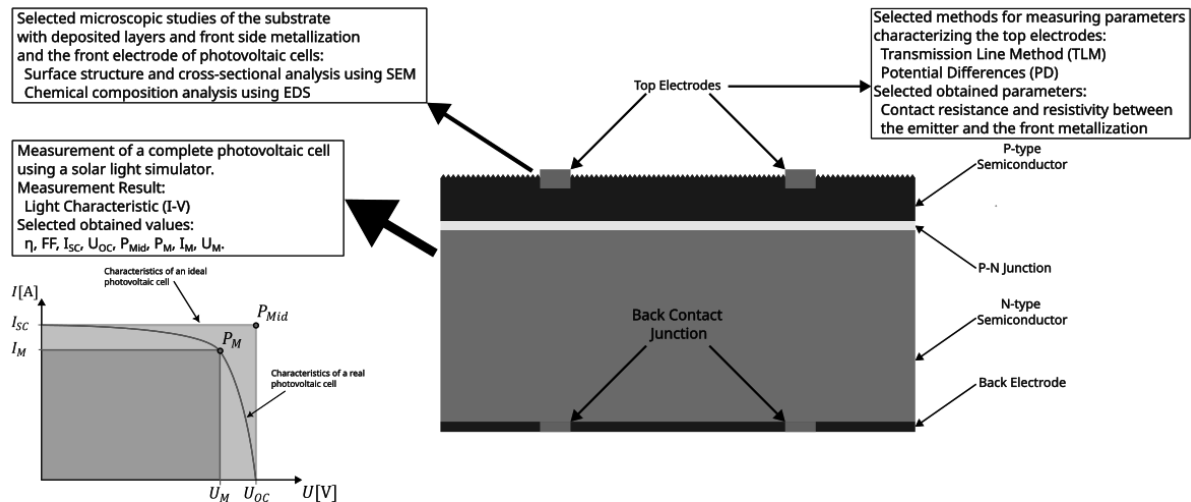


Figure 1. An example of the schematic construction of a photovoltaic solar cell with selected methods of measuring electrical parameters and microscopic examination of photovoltaic cells marked (where:  $U_M$ [V] is the voltage at the point of real maximum power,  $I_M$ [A] is the current at the point of real maximum power,  $U_{oc}$ [V] is the open-circuit voltage,  $I_{sc}$ [A] is the short-circuit current,  $P_M$ [W] is the power at the point of real maximum power, and  $P_{Mid}$ [W] is the power at the ideal point of maximum power)

One of the most commonly chosen methods for measuring the resistance and resistivity of front metallization are the Transmission Line Method (TLM) and Potential Differences (PD) method [Fig. 1]. In the case of the TLM method, the measurement is based on inducing the flow of electrical current between a selected pair of adjacent conducting lines (electrodes) on the front surface of the photovoltaic cell, followed by measuring the voltage drop between the probes. The resistance and resistivity of the front metallization are then determined based on this measurement [2, 3]. In the case of the PD method, local illumination of the photovoltaic cell around the moving measurement probe generates electrical current and, consequently, potential differences, which are measured by the probe. The result of the measurement is a scan of potential differences across the entire surface of the silicon wafer, directly correlated with the resistance and resistivity of the front metallization [2, 3].

The focus of the study was measuring the light current-voltage (I-V) characteristics obtained using a test bench equipped with a solar light simulator. As a result of these measurements, a series of significant parameters [Fig. 1] characterizing individual photovoltaic cells were obtained. The most crucial for practical utility are the fill factor and photovoltaic conversion efficiency, as they determine the effectiveness of photovoltaic cells.

### 1.1. Fill Factor

The Fill Factor (FF) is one of the parameters influencing the efficiency of energy conversion in a photovoltaic cell. FF is calculated using the formula [4]:

$$FF = \frac{U_M I_M}{U_{OC} I_{SC}} 100\% = \frac{P_M}{P_{Mid}} 100\%$$

The formula refers to the current-voltage (I-V) characteristic of photovoltaic cell. The FF value is an indicator of how well the cell transfers the energy generated by the cell to an external electrical circuit. The closer the FF value is to 100%, the better cell transmits the generated energy to an external circuit.

### 1.2. The photovoltaic conversion efficiency

The photovoltaic conversion efficiency ( $\eta$ ) is a measure of the ability to convert solar energy into electrical energy. It expresses what percentage of solar energy is transformed into electrical energy by the photovoltaic cell. The higher the efficiency value, the more efficient the photovoltaic cell is [4]:

$$\eta = \frac{P_{OUT}}{P_{IN}} 100\% = FF \frac{U_{OC} I_{SC}}{P_O A_O}$$

Where  $P_O \left[ \frac{W}{m^2} \right]$  is solar radiation power per unit area,  $A_O [m^2]$  represents the surface area of the photovoltaic cell,  $P_{OUT} [W]$  is the output power of the cell and  $P_{IN} [W]$  is the input power – the power of solar radiation incident on the photovoltaic cell.

The objective of the study is to determine the impact of technological parameters (including, among others, co-firing temperature), selected layers (textured surface) and elements (front metallization) on parameters of the photovoltaic cell.

## 2. STUDY MATERIAL

The study involved the use of six multicrystalline photovoltaic cells [Fig.2] labeled from no. 1 to no. 6. It is presumed that the front metallization was made using commercially available silver paste. According to the manufacturer, the base semiconductor material used is multicrystalline silicon with boron doping of p-type conductivity, with a thickness of  $175\mu m \pm 17.5\mu m$  and surface area of  $166mm \times 166mm \pm 0.25mm$ .

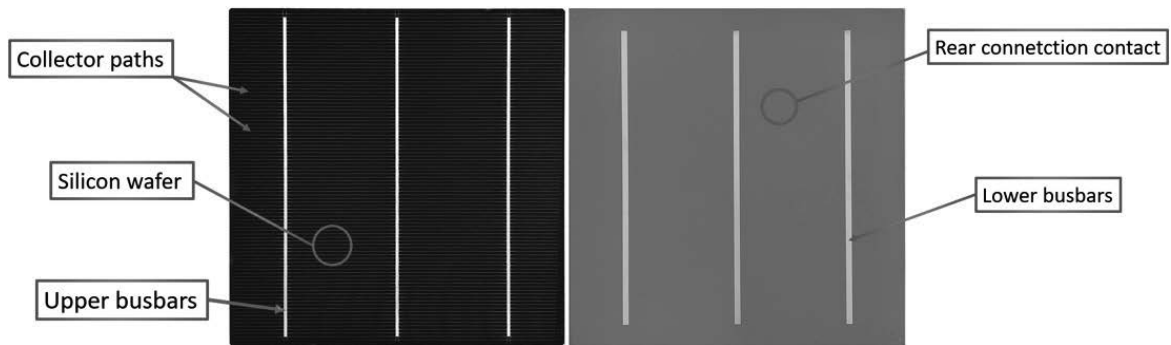


Figure 2. One of the tested photovoltaic solar cells

### 3. RESEARCH METHODOLOGY

The research was conducted using two stations. The station for measuring light current-voltage (I-V) characteristics enabled the examination of electrical parameters such as fill factor and photovoltaic conversion efficiency for individual samples. Meanwhile, the microscopy station was utilized for topography and fractography studies, as well as the chemical composition analysis of selected portions of the examined sample.

#### 3.1. The setup for measurement light current – voltage (I-V) characteristics

The accredited station of the SS200 EM Photo Emission Tech. Inc. class AAA, equipped with the Solar Cells I-V Curve Tracer SS I – V CT-02 PV system (compliant with the European standard IEC 60904 [5]), is located in the Photovoltaics and Electrical Properties Research Laboratory at the Department of Materials Engineering and Biomedical Engineering, Faculty of Mechanical Engineering and Technology at the Silesian University of Technology. Measurements were conducted under STC, meaning they were performed with module illumination using the AM1.5 spectral spectrum, with a radiation intensity of 1000 [W/m<sup>2</sup>] at the temperature of 25 [°C] [6,7]. A Fraunhofer ISE standard photovoltaic cell numbered 005-2013 was used as the reference photovoltaic cell.

The software installed on the measurement control computer allows for the determination of various photovoltaic cell parameters such as:  $\eta$ , FF,  $I_{sc}$ ,  $I_m$ ,  $U_{oc}$ ,  $U_m$ ,  $P_m$ .

#### 3.2. Scanning Electron Microscope (SEM)

The High-Resolution Scanning Electron Microscope Hrsem Supra 35, located in the High-Resolution Scanning Electron Microscopy Laboratory at the Department of Materials Engineering and Biomedical Engineering, Faculty of Mechanical Engineering and Technology at the Silesian University of Technology, is used for studying the surfaces of all groups of engineering materials, both conductive and non-conductive, through a focused electron beam. It is equipped with an attachment for Energy-Dispersive X-Ray Spectroscopy (EDS) [6,7]. The microscope was used to investigate the topography, fractography, and chemical composition of selected portions of the photovoltaic cell. During scanning, the SEM microscope utilized the secondary electron (SE) detection technique, with a constant accelerating voltage of 15kV. Images were obtained in the magnification range from 500x to 20,000x, allowing for a detailed analysis of the sample structure.

#### 4. DISCUSSION OF RESULTS

The photovoltaic cells were investigated in two categories:

- electrical properties [4.1],
- microscopic studies [4.2].

##### 4.1. Electrical properties

In [Fig.3] the current - voltage (I-V) characteristics for cell no. 6 is presented. The depicted I-V curve exhibits a shape close to a rectangle. Parameters for sample 6 such as:  $I_{SC} = 8.44$  [A],  $U_{OC} = 0.61$  [V],  $P_M = 3.74$  [W],  $I_M = 7.98$  [A],  $U_M = 0.47$  [V],  $P_{Mid} = 5.14$  [W]. This characteristic allows for obtaining data necessary for calculating FF and  $\eta$ , which are key parameters reflecting the properties of photovoltaic cells.

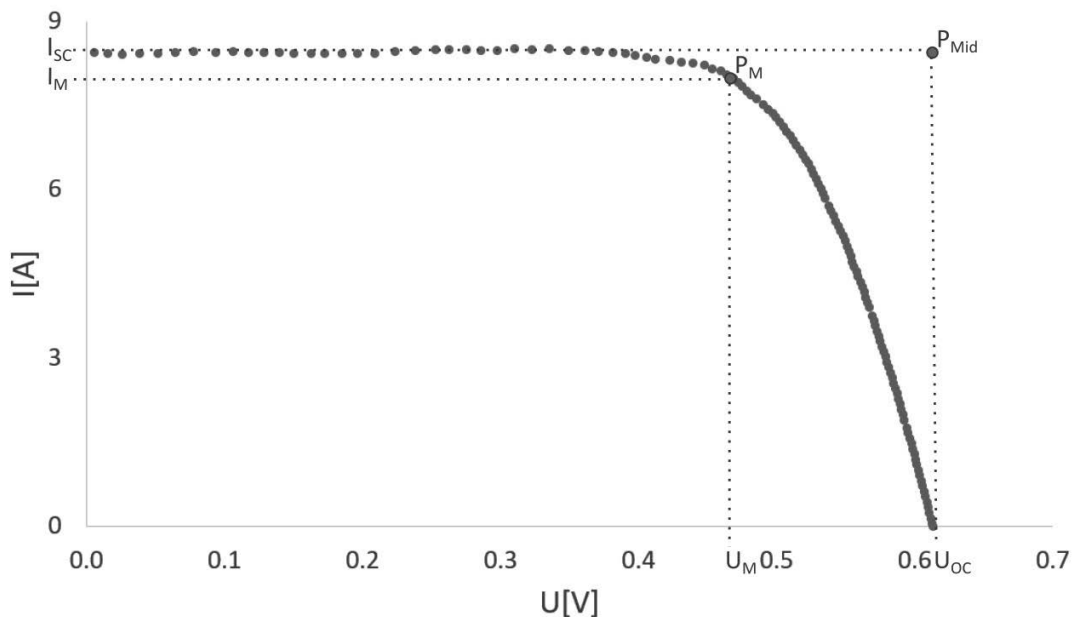


Figure 3. Current-Voltage characteristics for sample no. 6 (selected example)

In [Fig. 4], the values of  $\eta$  and FF for tested samples were presented. Significant differences were observed between samples from the same manufacturer. Values of  $\eta$  were obtained in the range of 4.61% to 15.97%, and FF in the range of 37.20% to 73.30%. Solar cells 1 and 2 achieved the lowest values, approximately  $\eta \cong 5\%$  and  $FF \cong 37\%$ . The remaining cells achieved significantly higher values:  $\eta \cong 16\%$  oraz  $FF \cong 71\%$ .



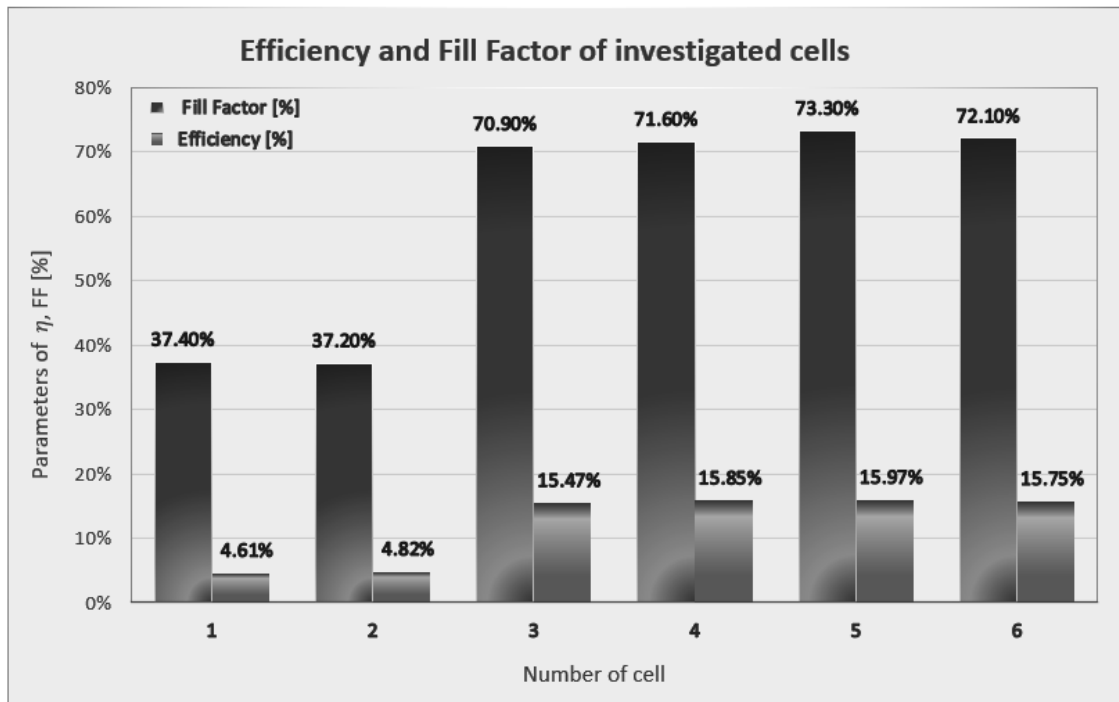


Figure 4. Comparison of photovoltaic cells in terms of FF and  $\eta$

#### 4.2. Microscopic Studies

- Topography Examination of Photovoltaic Cell and Front Electrode (SEM)

In [Fig.5], a scanning electron microscope (SEM) image of the topography of the front electrode is presented. Based on the results obtained from the examinations, a porous and irregular structure of the front metallization was observed, typical for solar cells produced through screen printing using commercial silver paste, as confirmed by the study [8].

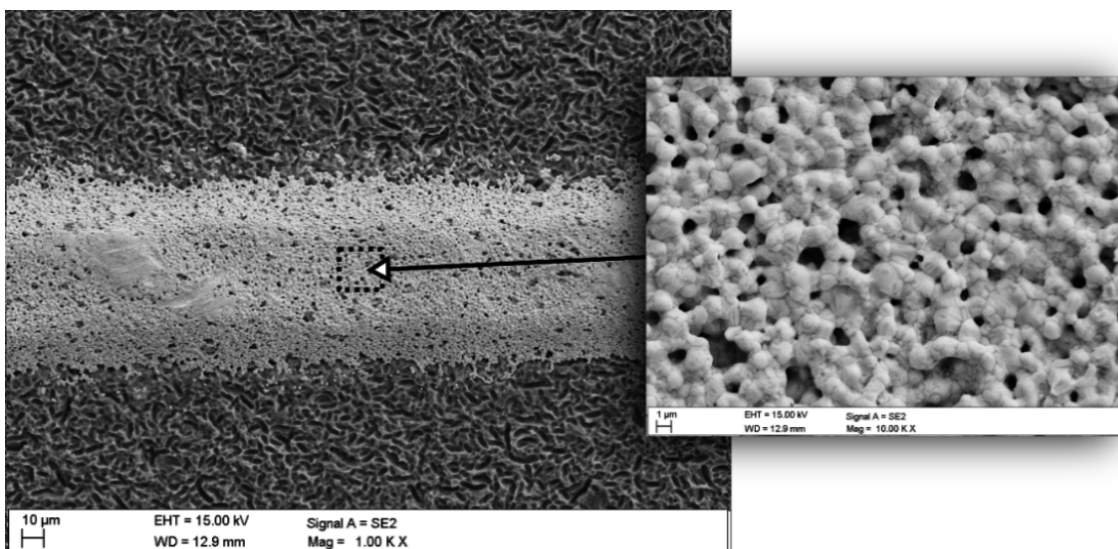


Figure 5. Photo of the topography of the front electrode surface of the photovoltaic cell

In [Fig. 6], an SEM image illustrating the structure of the front surface of a silicon photovoltaic cell is presented. It was observed that this structure is non-uniform and intricate. Analyzing the silicon surface, it was determined that the photovoltaic cell likely underwent a texturing process in an acidic solution with an appropriate concentration and volume ratio, likely utilizing a solvent dedicated for this purpose [9]. A smoothed surface was observed with craters of varying sizes and depths formed on it [10].

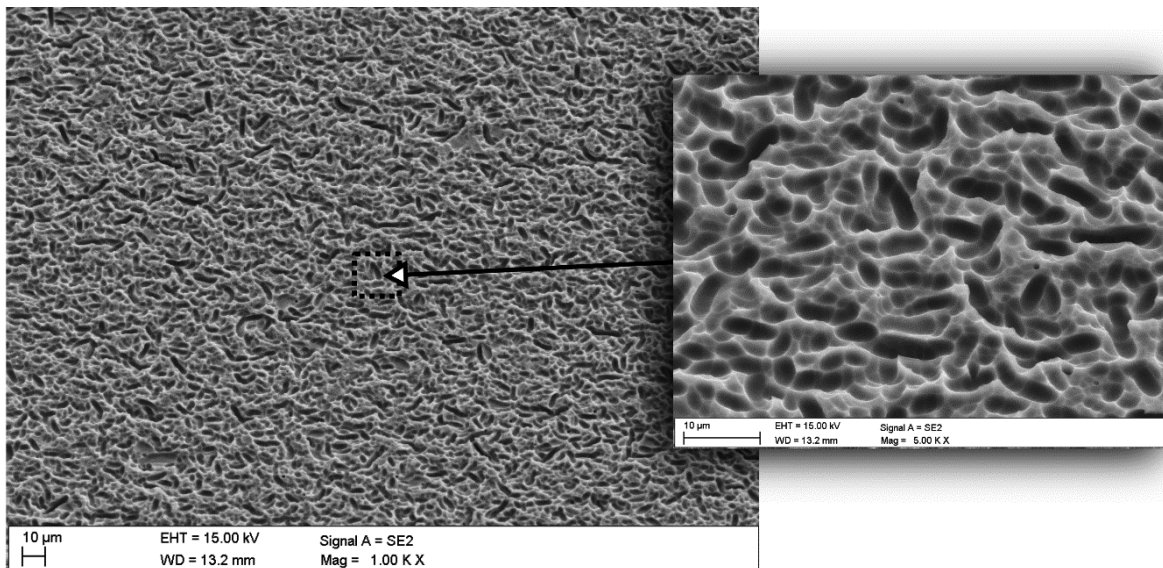


Figure 6. The topography of the silicon surface of the photovoltaic cell

- **Study of Fractography of the Front Electrode of a Photovoltaic Cell (SEM)**

In [Fig. 7], a cross-section of a sample photovoltaic cell is presented. The structure of the cross-section of the front electrode of the photovoltaic cell is porous and irregular. The proper formation of the front electrode on the silicon surface was observed, with a defect in the form of discontinuity at the metal-semiconductor junction likely occurring during the sample preparation process for microscopic examinations.

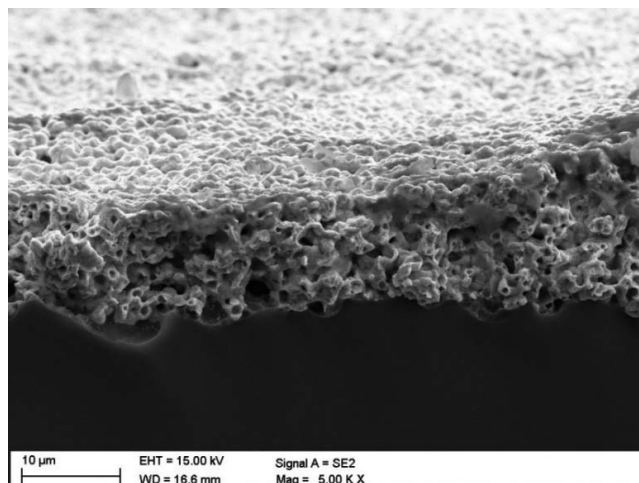


Figure 7. Cross-section of the examined sample

- **Chemical Composition Analysis (EDS)**

In Figure 8, the chemical composition of the collector electrode and the surface of the silicon wafer is depicted. The study confirms the assumptions about the chemical composition of the paste used for producing busbars and collecting tracks - silver, as well as the chemical composition of the silicon wafer surface - silicon.

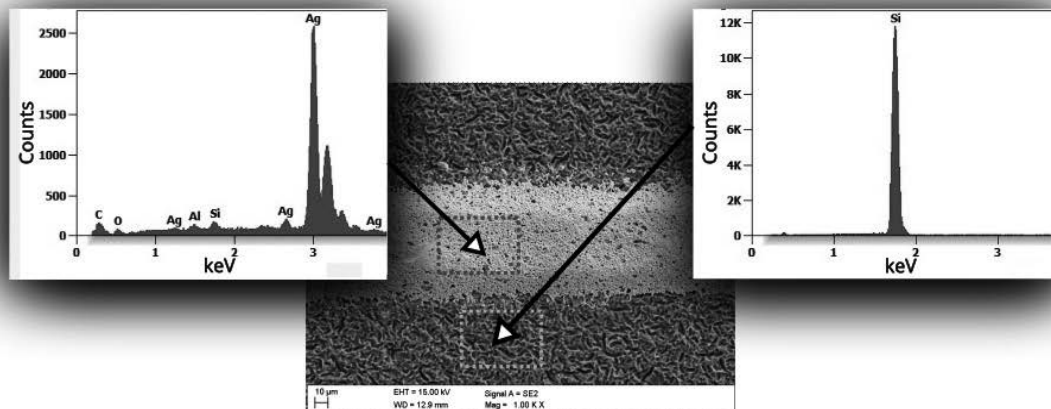


Figure 8. *Chemical composition of a photovoltaic cell*

#### 4. CONCLUSIONS

Based on the obtained research results, an enhanced surface structure of the silicon wafer was identified, which translates into increased light absorption and significantly impacting the efficiency of the photovoltaic cell [9]. The analysis of the topography of the front electrode reveals a porous structure with a dense network of connections between grain agglomerates. Based on this, it is predicted that the electrode was produced using screen printing, with the co-firing temperature likely ranging from 920°C to 930°C, as indicated in the referenced work [8]. During microscopic examinations, the chemical composition of samples (1-6) was also investigated using the EDS method. The studies showed the presence of only silicon on the surface of the silicon wafers and silver on the surface of the front electrode, with negligible amounts of other chemical elements.

Production stages of the photovoltaic cell, such as chemical cleaning processes, doping, layer deposition, and metallization, directly influence the physical parameters of the photovoltaic cell. Negligence and irregularities in the production stage can lead to a deterioration of physical parameters, affecting values such as photovoltaic conversion efficiency and fill factor. It was observed that the examined photovoltaic cells differed in values such as photovoltaic conversion efficiency and fill factor. Measurements of these parameters revealed how much photovoltaic cells from one manufacturer differ from each other. The fill factor for the tested samples (1-6) ranged from 37.20% to 73.30%, with the lowest recorded for sample 2 (37.20%) and the highest for sample 5 (73.30%). The efficiency of the examined photovoltaic cells ranged from 4.51% to 15.97%, with the lowest recorded for sample 1 (4.51%) and the highest for sample 5 (15.97%). Comparing the results of less efficient

to more efficient photovoltaic cells, a correlation between the fill factor and efficiency values was noted, confirming the relationships between analytical formulas.

## 5. ACKNOWLEDGMENT

This work was produced as part of the project implemented within the framework of project-oriented education – PBL, in the X competition under the Excellence Initiative – Research University program, at the Silesian University of Technology.

## BIBLIOGRAPHY

1. M. A. Green, Y. Hishikawa, E. D. Dunlop, et al., Solar cell efficiency tables (Version 53). Progress in Photovoltaics: Research and Applications, 2019.
2. S. Guo, G. Gregory, A.M. Gabor, W.V. Schoenfeld, K.O. Davis, Detailed investigation of TLM contact resistance measurements on crystalline silicon solar cells, USA, 2017.
3. M. Musztyfaga-Staszuk, Comparison of the Values of Solar Cell Contact Resistivity Measured with the Transmission Line Method (TLM) and the Potential Difference (PD), Poland, 2021.
4. T. Rodacki, A. Kandyba, Przetwarzanie energii w elektrowniach słonecznych, Poland, 2000.
5. IEC 60904-1:2020
6. <https://pimib.polsl.pl/pdf/laboratorium-IMIiB-polish.pdf>
7. <https://euslugi.polsl.pl/EUsluga/Aparatura>
8. M. Musztyfaga-Staszuk, Nowe kompozyty na bazie miedzi w zastosowaniu do wytwarzania krzemowych ogniw fotowoltaicznych, Wydawnictwo Politechniki Śląskiej, Gliwice, 2019.
9. G. Kulesza, P. Zięba, Chemiczna teksturyzacja powierzchni krzemu krystalicznego do zastosowań w fotowoltaice, Elektronika: konstrukcje, technologie, zastosowania, vol. 52, nr 4, Poland, 2011.
10. G. Kulesza, P. Panek, P. Zięba, Charakterystyka optoelektroniczna wysokosprawnych ogniw słonecznych na bazie krzemu krystalicznego otrzymywanych w procesie kwasowej teksturyzacji powierzchni, Poland, 2012.



26th January 2024  
Gliwice, Poland

DEPARTMENT OF ENGINEERING MATERIALS AND BIOMATERIALS  
FACULTY OF MECHANICAL ENGINEERING  
SILESIA UNIVERSITY OF TECHNOLOGY

## INTERNATIONAL STUDENTS SCIENTIFIC CONFERENCE

### Static analysis of stainless steel AISI 316L applied in pendulum swings

J. Górny <sup>a</sup>, A. Olszewska <sup>a</sup>, W. Wanczura <sup>a</sup>, A. Śliwa <sup>b</sup>

<sup>a</sup> Student of Silesian University of Technology, Faculty of Mechanical Engineering and Technology, Department of Engineering Materials and Biomedical Engineering  
email: antools020@student.polsl.pl, jakugor296@student.polsl.pl ,  
wiktwan199@student.polsl.pl

<sup>b</sup> Silesian University of Technology, Faculty of Mechanical Engineering and Technology, Department of Engineering Materials and Biomedical Engineering  
email: Agata.Sliwa@polsl.pl

**Abstract:** The purpose of this work is a static analysis of AISI 316L stainless steel for children's swings, comparing the stress, displacement and deformation of the swing with the application of several selected force configurations.

**Keywords:** CAD, simulation, model, force

## 1. INTRODUCTION

In everyday life, one encounters many objects that are often an essential part of simple functioning. It is evident that a series of processes is required to ensure the safe operation of these objects, ranging from selecting the appropriate material to assembling the final product. Equipment intended for use by children is often subject to more restrictive executive frameworks. To achieve this, CAD programs and specialized knowledge are employed to select materials meeting safety standards, design a secure structure, and simulate future usage. This approach significantly aids in predicting potential deviations from design assumptions and mitigating them during the computer simulation phase. The focus of this study is the static analysis of a swing made of AISI 316L steel.

## 2. MATERIAL AND RESEARCH METHODOLOGY

### 2.2 MATERIAL

In the simulation, AISI 316L steel, also known as X2CrNiMo17-12-2 or 1.4404, was used. This stainless steel belongs to the austenitic group, characterized by anti-corrosive properties, resistance to acidic environments, and atmospheric conditions. It also possesses hypoallergenic properties [1]. These characteristics make it safe for skin contact and resistant to

challenging atmospheric conditions (rain, high UV index, etc.). The chemical composition and properties of 316L steel are presented in the tables below (Tab.1-3).

Tab. 1 Chemical composition of AISI 316L steel [2].

C	Si	Mn	P	S	Cr	Mo	Ni	N
≤ 0.03%	≤ 1.0%	≤ 2.0%	≤ 0.045%	≤ 0.015%	16.5-18.5%	2.0–2.5%	10.0–13.0%	≤ 0.11%

Tab. 2 Physical properties of AISI 316L steel [3].

Density	Young's Modulus	Thermal Conductivity	Specific Heat	Specific Resistance
8 [kg/dm <sup>3</sup> ]	200 [GPa]	15 [W/(m.K)]	500 [J/(kg.K)]	0.75 [(Ωxmm <sup>2</sup> )/m]

Tab. 3 Mechanical properties of AISI 316L steel [3].

Yield Strength Re	Tensile Strength Rm	Elongation at Break	Maximum Hardness
Horizontal Direction (XY)	Vertical Direction (Z)	Horizontal Direction (XY)	Vertical Direction (Z)
470-590 [MPa]	380-560 [MPa]	590-690 [MPa]	490-590 [MPa]

## 2.3 RESEARCH METHODOLOGY

Using the Solidworks CAD program for model design, a pendulum swing model for children was prepared (Fig. 1). It consists of a swing arm, two seats, handles at the extremes of the arm, and a spring mount (Fig. 2). The model was meshed with finite elements (Fig. 3), and boundary conditions were applied (Fig. 4). Five static analyses were performed on this model with forces applied to both seats (Table 4).



Fig. 1 A model of a weight swing prepared in the Solidworks.

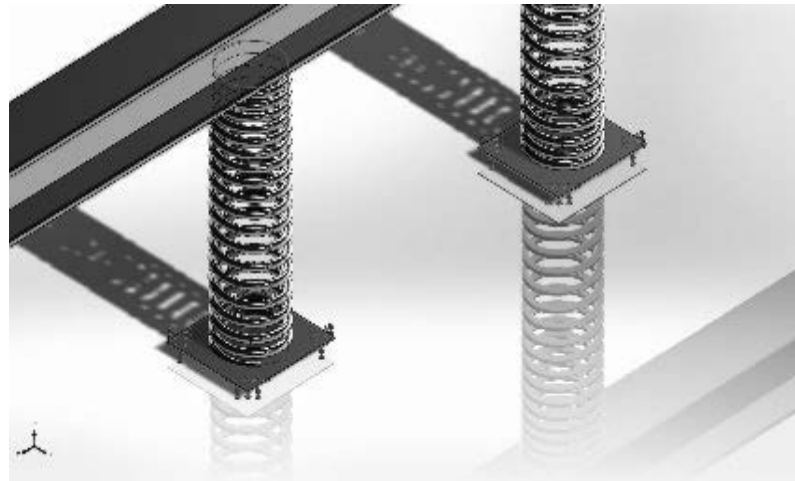


Fig. 2 Spring fastening of the swing.

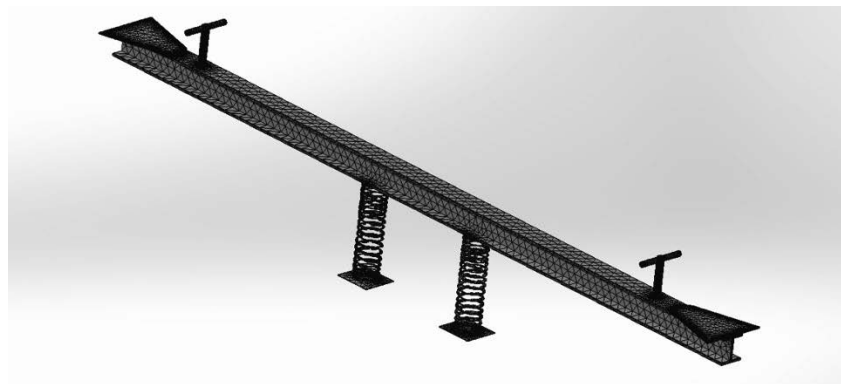


Fig.3 Model of a weight swing with an applied mesh.



Fig. 4 Model of a weight swing with boundary conditions imposed.

Tab. 4 List of forces used during the analyzes.

Analysis 1	Analysis 2	Analysis 3	Analysis 4	Analysis 5
Right Seat	Left Seat	Right Seat	Left Seat	Right Seat
1100 N	900 N	560 N	400 N	400 N

### 3. RESULTS OF COMPUTER SIMULATIONS

As a result of detailed simulations involving various loads of 1100 N, 900 N, 560 N, 400 N, 860 N, 1500 N, 1800 N, and 2000 N, significant conclusions were drawn regarding the deformations of the swing under specific loads. The analysis of the obtained results (Fig. 9 and Fig. 10) revealed noticeable deformations in the swing, closely correlated with the applied loads. Particularly intriguing was the observed minimal deformation during the simulation with a load of 1500 N (Fig. 14-16).

It is noteworthy that the maximum displacement occurred during simulations with loads of 400 N and 500 N (Fig. 9). These results unequivocally indicate the existence of clear relationships between the degree of loading and the deformation of the swing, which is crucial for understanding its behavior under different operating conditions.

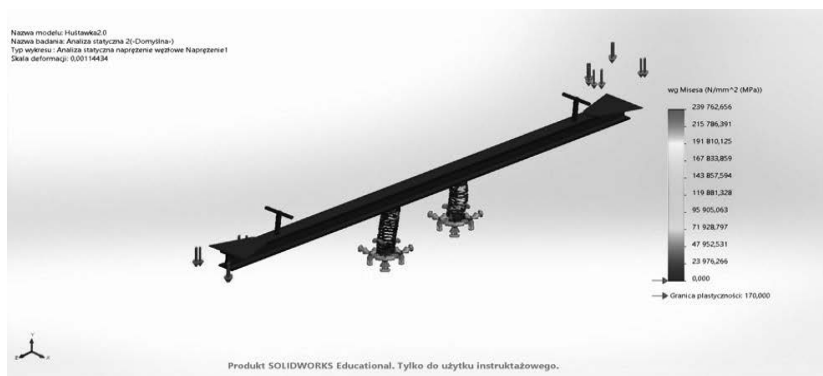


Fig. 5 Stress result for applied forces 1100 N i 900 N.



Fig. 6 Displacement result for applied forces 1100 N i 900 N.

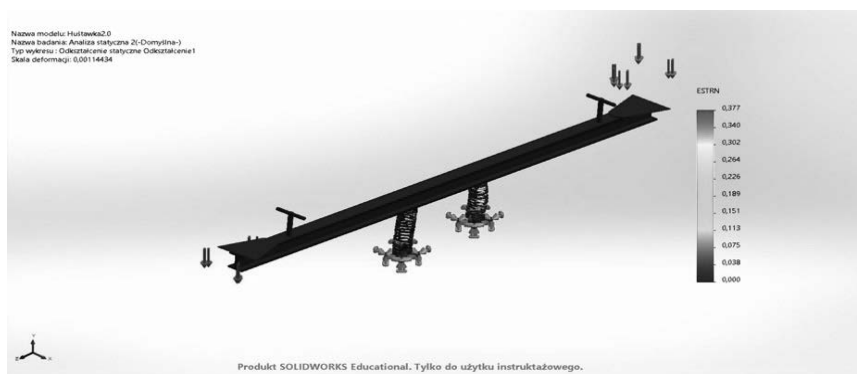


Fig. 7 The result of the deformation for the applied forces 1100 N i 900 N.



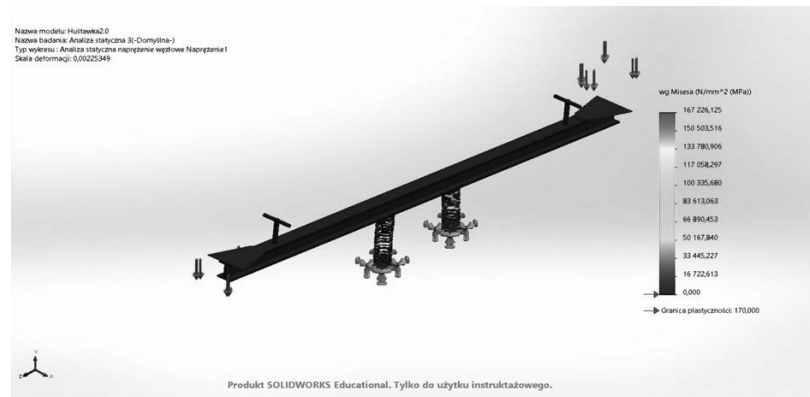


Fig. 8 Stress result for applied forces 560 N i 400 N.

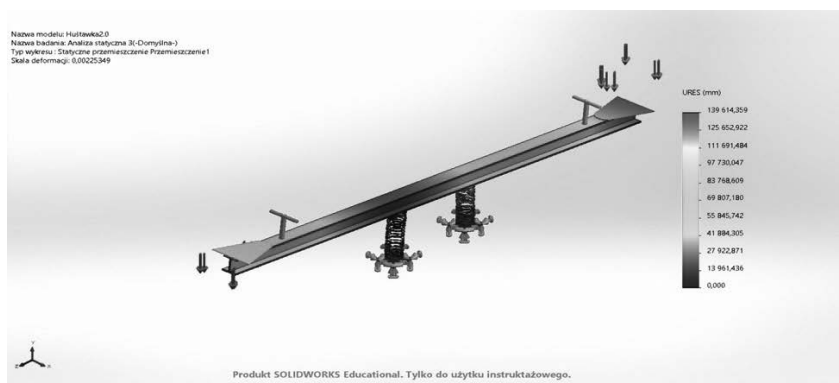


Fig. 9 Displacement result for applied forces 560 N i 400 N.



Fig. 10 The result of the deformation for the applied forces 560 N i 400 N.

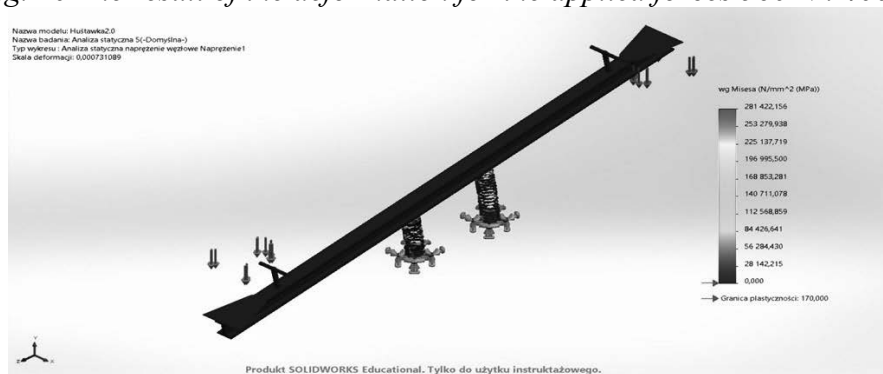


Fig. 11 Stress result for applied forces 400 N i 860 N.

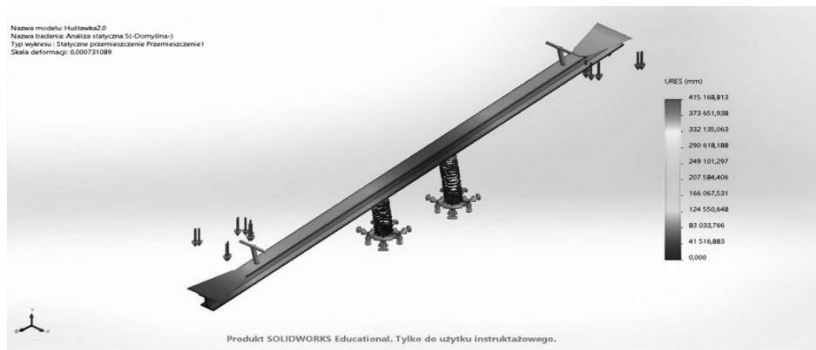


Fig. 12 Displacement result for applied forces 400 N i 860 N.

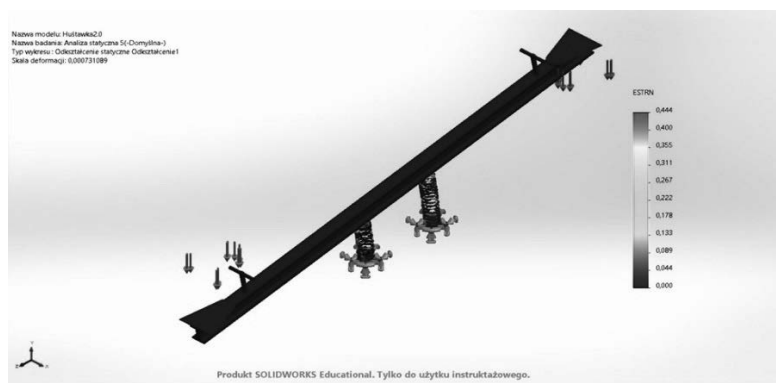


Fig. 13 The result of the deformation for the applied forces 400 N i 860 N.

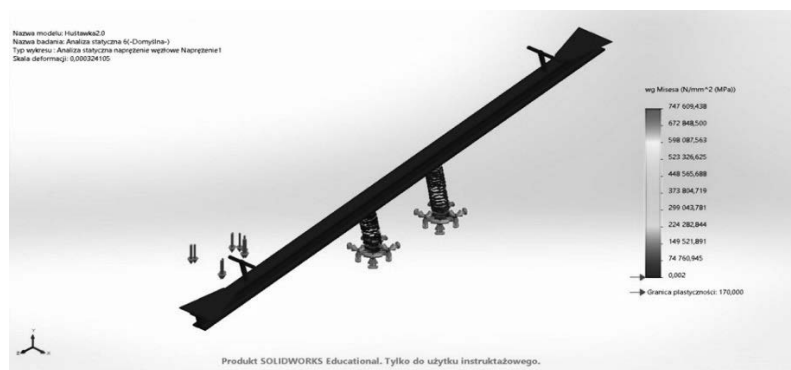


Fig. 14 Stress result for applied forces 0 N i 1500 N.

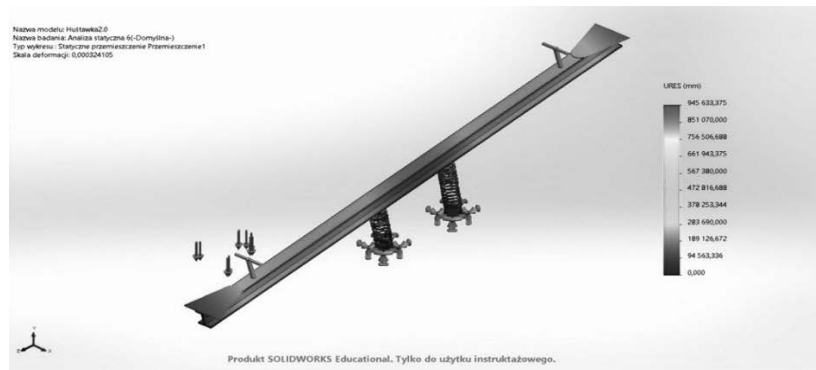


Fig. 15 Displacement result for applied forces 0 N i 1500 N.

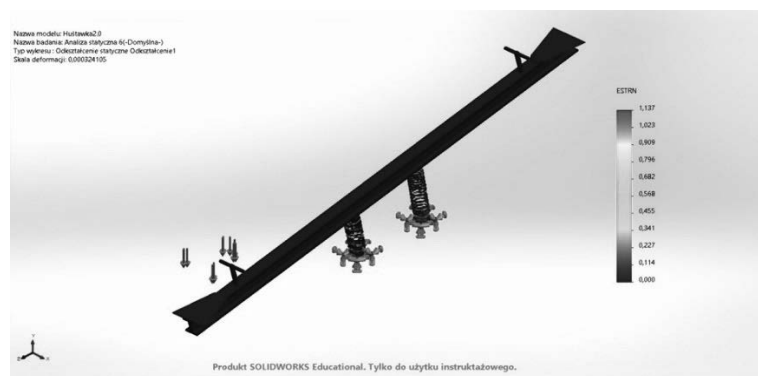


Fig. 16 The result of the deformation for the applied forces 0 N i 1500 N.

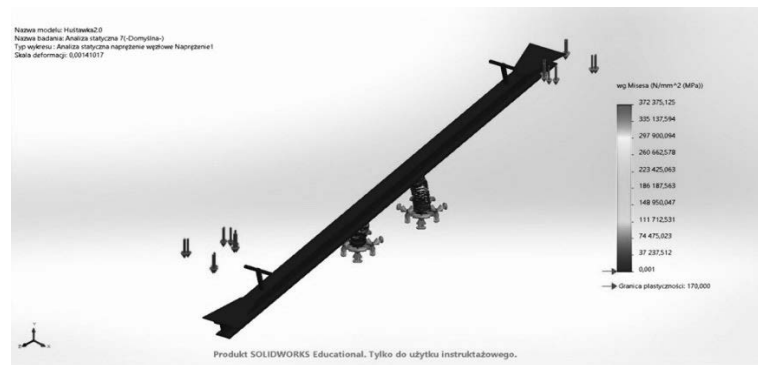


Fig. 17 Stress result for applied forces 1800 N i 2000 N.



Fig. 18 Displacement result for applied forces 1800 N i 2000 N.

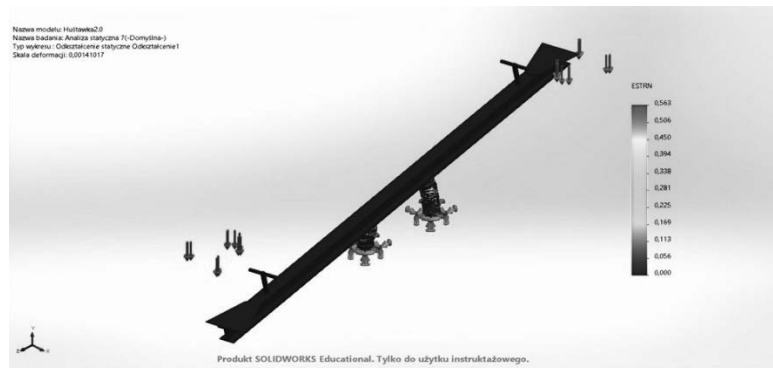


Fig. 19 The result of the deformation for the applied forces 1800 N i 2000 N.

#### 4. SUMMARY

A pendulum swing made of AISI 316L steel was subjected to static simulation, with 5 different force configurations applied. The smallest deformation scale was observed with a force of 1500 N applied to only one side of the swing. The largest deformation scale was exhibited when forces close to each other, 400 N and 560 N, were applied. The strength properties of AISI 316L steel, such as yield strength, tensile strength, and physical properties like the modulus of elasticity, could have influenced these results. The static analysis of the swing, conducted in the SOLIDWORKS program, allowed for verification of whether the material and its construction fulfill their purpose and enable safe usage.

#### 5. BIBLIOGRAPHY

1. <http://www.stalnierdzewne.pl/1092/struktura-i-wlasnosci-stali-316l>
2. <https://www.hempel-metals.pl/pl/gatunki/stal-nierdzewna/316l-14404/>
3. <https://www.ebmia.pl/wiedza/porady/obrobka-porady/stal-316l-1-4404/>



26th January 2024  
Gliwice, Poland

DEPARTMENT OF ENGINEERING MATERIALS AND BIOMATERIALS  
FACULTY OF MECHANICAL ENGINEERING  
SILESIA UNIVERSITY OF TECHNOLOGY

## INTERNATIONAL STUDENTS SCIENTIFIC CONFERENCE

### Implementation of 3D printing in the trade fairs

J. Gryc<sup>a</sup>, A. Kania<sup>b</sup>

<sup>a</sup> Student of Management and Production Engineering at the Faculty of Mechanical Engineering at the Silesian University of Technology

email: jakugry702@student.polsl.pl

<sup>b</sup> Silesian University of Technology, Faculty of Mechanical Engineering, Department of Engineering Materials and Biomaterials

email: aneta.kania@polsl.pl

**Abstract:** The article presents possible ways of implementing 3D printing technology in to the expo industry based on the example of Polish companies in this branch of a market. In the article a specific solution for utilizing 3D printing technology to create a functional part is also presented. This solution has been tested by a collaborating company. Then an analysis was conducted to determine whether the previously set requirements regarding the part were met.

**Keywords:** 3D printing, prototyping, expo industry, trade fairs.

### 1. INTRODUCTION

Trade fairs regardless of their name are mainly meant to promote brands by presenting them to a larger audience. Usually there are not many firms offering direct sales at these types of events. Modern fairs base on exhibiting companies assets and accomplishments in an eye-catching way.

In Poland there are not many establishments providing building such exhibition stands for clients (Fig. 1). Regardless of that, in recent years expo industry in Poland grew significantly. There are many more expo events happening, and their scale is growing rapidly.

Event centers such as District of Culture in Katowice organize hundreds of meetings depending on expo companies a year.

Due to unusual operating of companies providing expo services, there are few fields of their work where implementation of 3D printing could be considered as a possible improvement. The main advantage of using 3D printed parts in building exhibition stands and structures is low time of manufacturing needed part. Because of how many problems and unpredictable changes occur in this line of work, fast prototyping and implementing changes is key to provide a client fine service. On top of that, 3D printing could also be used in:

- Joining modular parts which are widely used in exhibitions.
- Adapting accessories such as lamps to already implemented systems of building stands.

- Visualizing project for clients.
- Creating decorative elements exactly according to costumers requirements.



Figure 1. Omega System promotional stand built with aluminum profiles [1]

## 2. CHARACTERISTICS OF THE INDUSTRY IN RELATION TO 3D PRINTING

Trade fairs are characterized by seasonal occurrence which directly imposes way that companies building exhibition stand works. In most of the cases deadlines are very short, people managing these enterprises need to plan every detail and answer to every possible unplanned obstacle. Mostly it is something doable. But in some cases, especially when the cooperation of many subcontractors is needed it could be very hard [2,3].

Mistakes are made, sometimes at planning phase or directly during the assembly. When those mistakes occur, there is very little time to fix them. This is an opportunity to implement a system which using little time and recourses could fix those problems [4].

3D printing due to it relatively low cost of entry is a perfect solution to test an implementation of that kind of technology. Rapid prototyping using FDM (Fused Deposition Modelling) printers is fast, flexible and precise, which perfectly fits the requirements of solving construction problems in building expo stands. In addition, in most cases, expo companies use some kind of CAD software which give them head start to easily learn how to manufacture 3D printed parts themselves or at least deliver outside company very precise technical description of needed part [5].

## 2. DESIGNING AND CREATING PART FOR COOPERATING COMPANY

During research regarding this work, a company ready for cooperation has been found. It is a company working all around the Poland building fair stands for various clients. They're operating mostly on building stands with lockable aluminum profile system. This system is sold by a company named Elstar with headquarters in Poznan. The system itself is called Opti System. It uses aluminum profiles which can be easily combined in structures using built-in specialized locks.

Horizontal elements in this system have a characteristic groove on the top and bottom side. This groove is placed on the whole length of the profile, and it is used to lock another profile to it (Fig. 2).

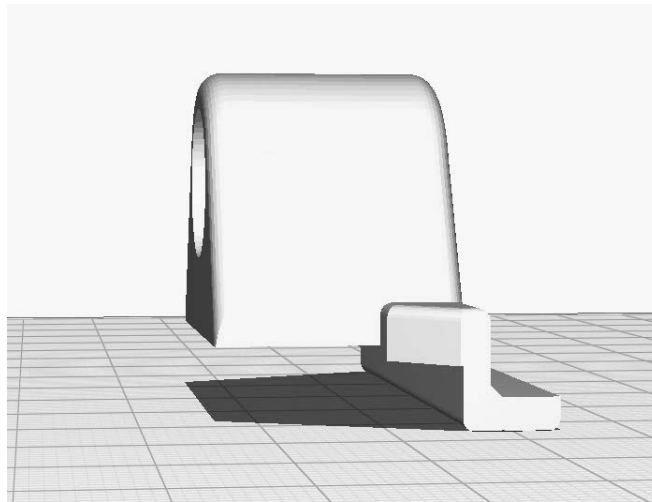


Figure 2. Opti system by Elstar [6]

This project's main goal was to design a 3D printed part which allows attaching a lamp to the wall built with the Opti System. The printed part needed to be strong enough to support the lamp's weight. The following main assumptions were included:

- Part should fit on top of an aluminum profile using the groove as a mounting leverage.
- Lamp mounting hole needs to be narrowed in the middle to lock the lamp in place.
- Part needs to lay flat on top of a profile.
- It needs to be easy to assemble and disassemble.
- Printing time and cost should be as low as possible.

Based on these requirements, a model of a part was made using CAD software, Fusion 360 by Autodesk (Figs. 3, 4).



*Figure 3. Side view showing the mounting lever of the designed part*

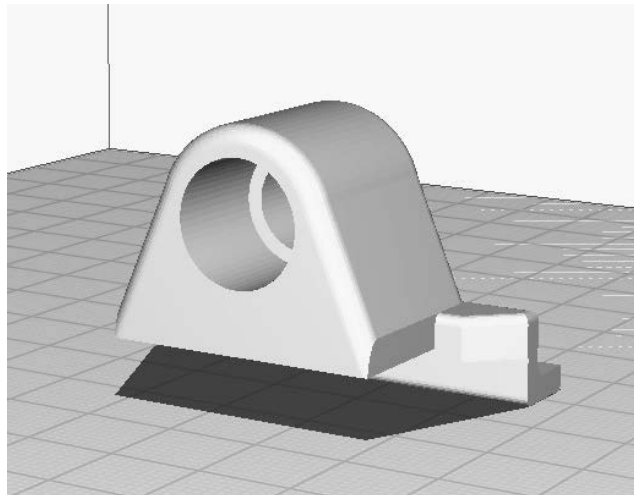


*Figure 4. Front view presenting the mounting hole of the lamp*

Part has been printed using Artillery Hornet 3D printer (Fig. 5). It is relatively budget-friendly printer capable of printing with PLA (Polylactic Acid), PETG (Polyethylene Terephthalate Glycol), or TPU (Thermoplastic Polyurethane). However it is not designed to print with ABS (Acrylonitrile Butadiene Styrene).



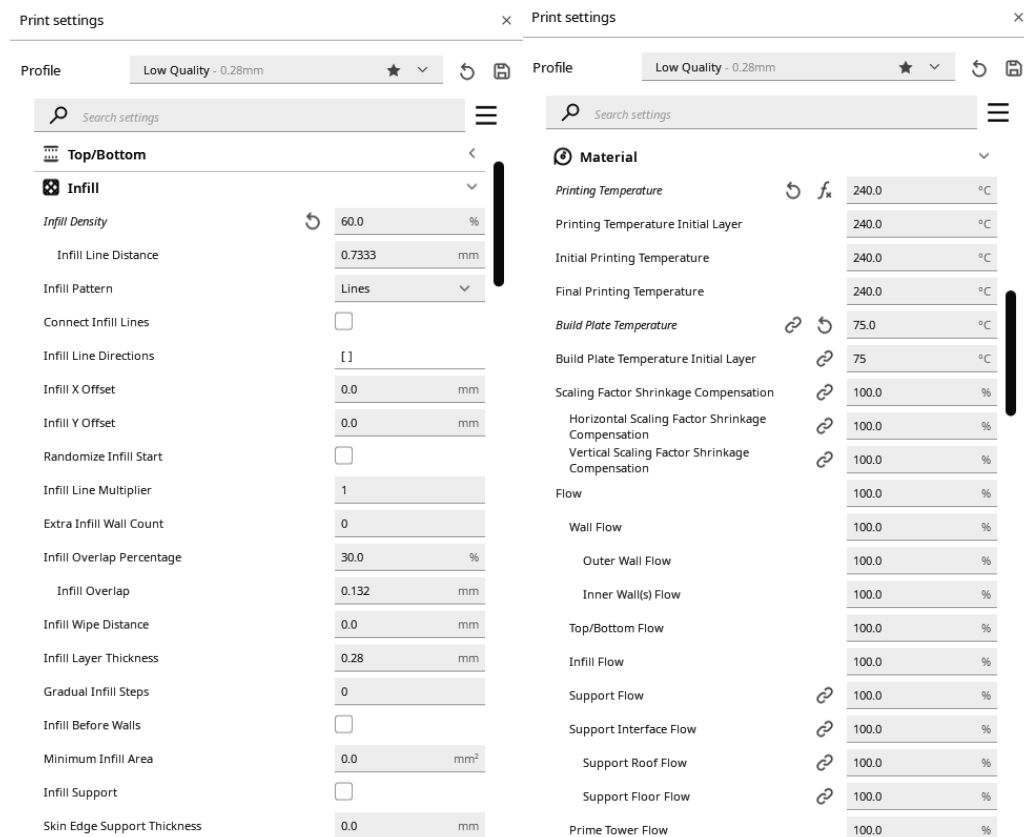


Figure 5. Settings in Cura slicer for the discussed project

Cooperating company needed 30 parts, which took eight hours to print. Parts were printed using PETG filament. This filament is popular alternative for standard PLA. It is affordable and easy to print. It is fairly resistant to stretching and temperature. PETG is mostly used for printing mechanical parts due to its characteristics:

- PETG can be printed using most of FDM printers but they must be equipped with heated bed (bed temperature in this case was set on 75 °C).
- It typically prints within a nozzle temperature range of 230 to 250 °C (in this case was 240 °C).
- PETG works well with a range of layer heights (in this case nozzle 0.4 mm was used with 0.26 mm layer height settings).
- It can be printed much faster than other materials, like ABS.

### 3. CONCLUSIONS

According to associated company, printed parts met their expectations. Lamps were mounted firmly and didn't move at all. Assembly was quick and easy and the customer really liked the design. The only complaint was about removing adapters from profiles groove. Some of the parts broke during the removal. This probably happened due to the small size of a surface connecting leverage holding the whole part and rest of its body. It is easy to repair the problem, all it takes is widening the mentioned connector to increase its durability.

Based on the example provided it can be concluded that even in small exhibition stands building companies there is a place to implement 3D printing technology.

## LITERATURE

1. Exhibition stands, <https://omegasystem.pl/stoiska-targowe-wystawowe/>, 2023.
2. J. Knurek, The role of exhibition fairs in brand management, *Management and Quality* 5/2 (2023) 140-153 (in Polish).
3. A. Drab, Trends and Prospects for the Development of the Trade Fair Industry in Europe. In: H. Mruk (Ed.), *The Significance of Trade Fairs for the Economic Development of the Country*, 2011, 69-88.
4. AHOLA, Eeva-Katri, *Producing experience in marketplace encounters: a study of consumption experiences in art exhibitions and trade fairs*. 2007.
5. D. Bałaga, M. Kalita, M. Siegmund, The application of 3D printing technology for rapid prototyping of misting nozzles, *Mining Machines* 35/3 (2017) 3-13.
6. Elstar, <https://elstar.info.pl/kategorie/opti/>, 2023.



26th January 2024  
Gliwice, Poland

DEPARTMENT OF ENGINEERING MATERIALS AND BIOMATERIALS  
FACULTY OF MECHANICAL ENGINEERING  
SILESIA UNIVERSITY OF TECHNOLOGY

## INTERNATIONAL STUDENTS SCIENTIFIC CONFERENCE

### Comparison of surface topography and electrical properties of crystalline silicon solar cells (part II)

J. Gwozdek<sup>a</sup>, W. Szreter<sup>a</sup>, P. Wilczek<sup>a</sup>, A. Drygala<sup>b</sup>, M. Musztyfaga-Staszuk<sup>c</sup>, J. Budzynowski<sup>d</sup>, M. Staszuk<sup>b</sup>

<sup>a</sup> Pupil, Complex of Communication Schools, Warszawska 35, 44-100 Gliwice, Poland

<sup>b</sup> Silesian University of Technology, Faculty of Mechanical Engineering, Department of Engineering Materials and Biomaterials, Konarskiego 18a, 44-100 Gliwice, Poland

<sup>c</sup> Silesian University of Technology, Faculty of Mechanical Engineering, Welding Department, Konarskiego 18a, 44-100 Gliwice, Poland

<sup>d</sup> Student, Silesian University of Technology, Faculty of Mechanical Engineering, Konarskiego 18a, 44-100 Gliwice, Poland

email: [aleksandra.drygala@polsl.pl](mailto:aleksandra.drygala@polsl.pl)

**Abstract:** Fossil fuel energy is non-sustainable owing to their limited, exhausting resources and the environmental impact. Hence, the demand for alternative energy sources is increasing because they are eco-friendly and sustainable. Solar cell is an electronic device that converts the energy of sunlight directly into electricity. The paper presents the electrical properties of mono- and multicrystalline silicon solar cells and their surface topography.

**Keywords:** photovoltaics, solar cells, crystalline silicon

## 1. INTRODUCTION

Sunlight is a portion of the electromagnetic radiation given off by the Sun, in particular infrared, visible, and ultraviolet light. Solar radiation can be captured and turned into useful forms of energy, such as heat and electricity, using a variety of mechanisms. The amount of solar radiation that reaches Earth's surface varies according to geographic location, time of day, season, regional landscape, and local weather [1].

The maximum power of solar radiation penetrating the outer layers of the atmosphere that can be obtained per 1 m<sup>2</sup> is about 1367 W/m<sup>2</sup>. However, due to the Earth's elliptical orbit, the different angle of inclination of the planet's rotation axis and the thickness of the atmosphere, the maximum flux density of direct solar radiation reaching the Earth's surface is approximately 1000W/m<sup>2</sup> [2].

Because the Earth is round, the sun strikes the surface at different angles, ranging from 0° to 90°. When the sun's rays are vertical, the Earth's surface gets all the energy possible. The more sloped the sun's rays are, the longer they pass through the atmosphere, becoming more scattered and diffuse. Due to climate change and energy shortage in the world today, solar

energy is being used more and more widely as a clean and renewable energy source. The utilization of solar energy is mainly achieved through photovoltaic, photothermal, or photochemical conversions [3,4].

Solar cells use solar radiation, a free and inexhaustible source of energy, to produce emission-free electricity. Silicon is an important material in the photovoltaic industry. According to predictions, it will remain an important and dominant material in photovoltaics over the next 10-30 years, owing to its well-recognized properties and its established production technology [5,6]. The paper presents results of the electrical and microstructural properties of two types of crystalline silicon solar cells.

## 2. MATERIALS AND METHODS

The tests were carried out on crystalline silicon solar cells (Figure 1). Material used as a substrate for solar cells was p-type,  $1\div 3 \Omega\text{cm}$  resistivity, boron-doped mono- and multicrystalline silicon wafers manufactured by Deutsche Solar AG with an area of  $50 \times 50 \text{ mm}$  and thickness of  $200\pm 30 \mu\text{m}$ . The mono- and multicrystalline solar cells were produced using the same technology. The scheme of tested crystalline silicon solar cells is shown in Figure 2.

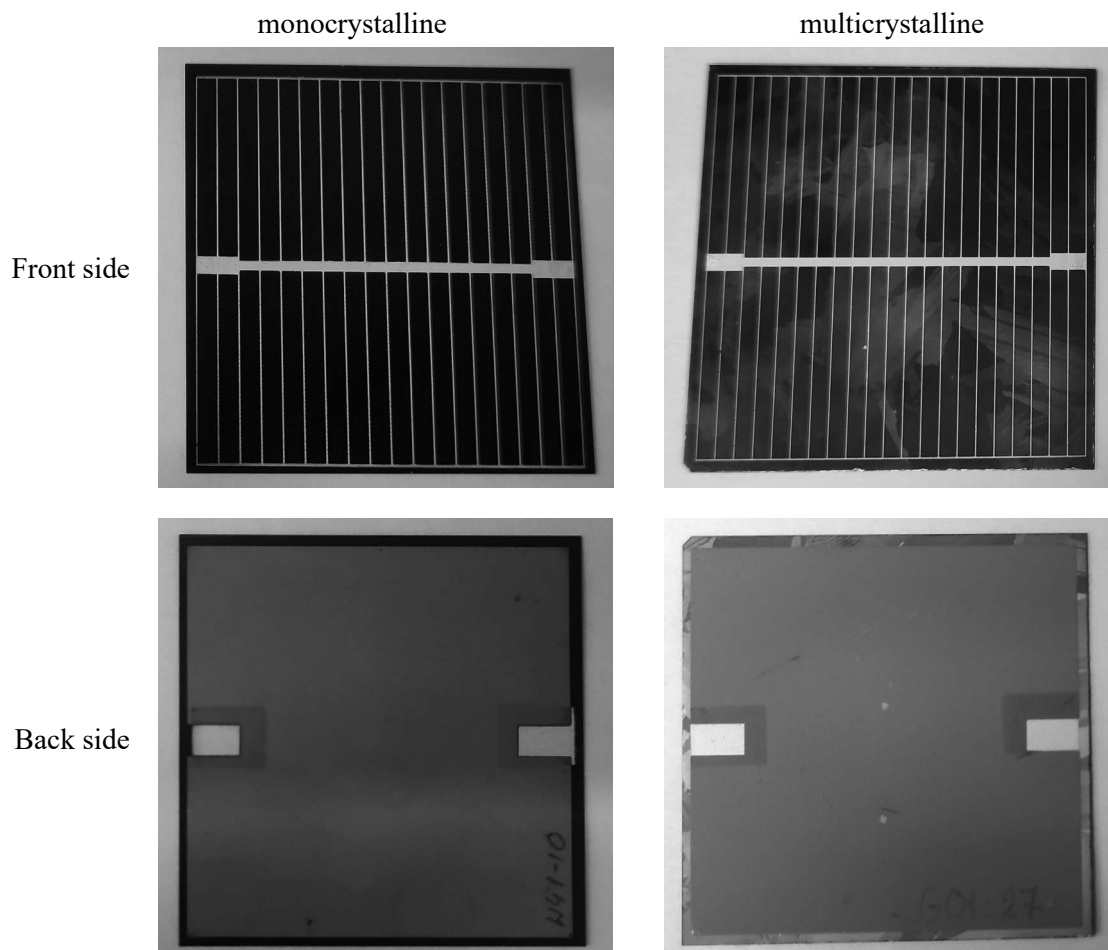


Figure 1. View of tested crystalline silicon solar cells

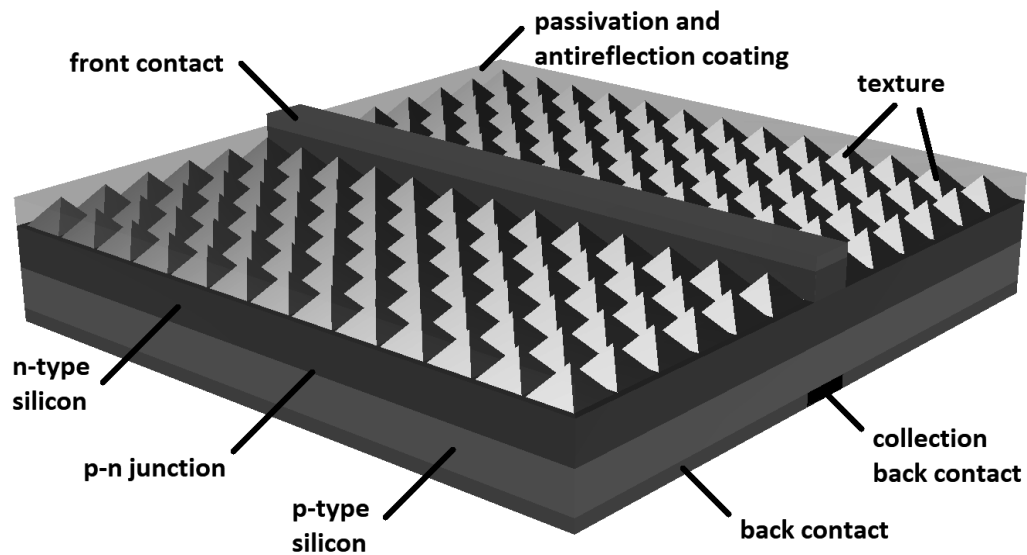


Figure 2. Scheme of tested crystalline silicon solar cells

The topography of mono- and multicrystalline silicon solar cell surfaces was investigated using ZEISS SUPRA 25 scanning electron microscopes. The electrical properties of solar cells were determined using a system for measurement of the current-voltage characteristics SS I V CT 02 made by PV Test Solutions Tadeusz Żdanowicz for solar radiation spectrum AM 1,5, irradiance  $1000 \text{ W/m}^2$  and temperature  $25^\circ\text{C}$ .

### 3. RESULTS

Figure 3 shows the topography of monocrystalline silicon solar cells' surface. To reduce optical losses the front surface of the silicon has been textured. Texturing of monocrystalline silicon (with  $\langle 100 \rangle$  crystallographic orientation) is usually done by etching in alkaline solutions. The anisotropic etching behaviour of KOH mixtures leads to random pyramidal structures on monocrystalline silicon wafers. This reduces light reflection and maximizes light absorption by the material, leading to higher solar cell efficiency.

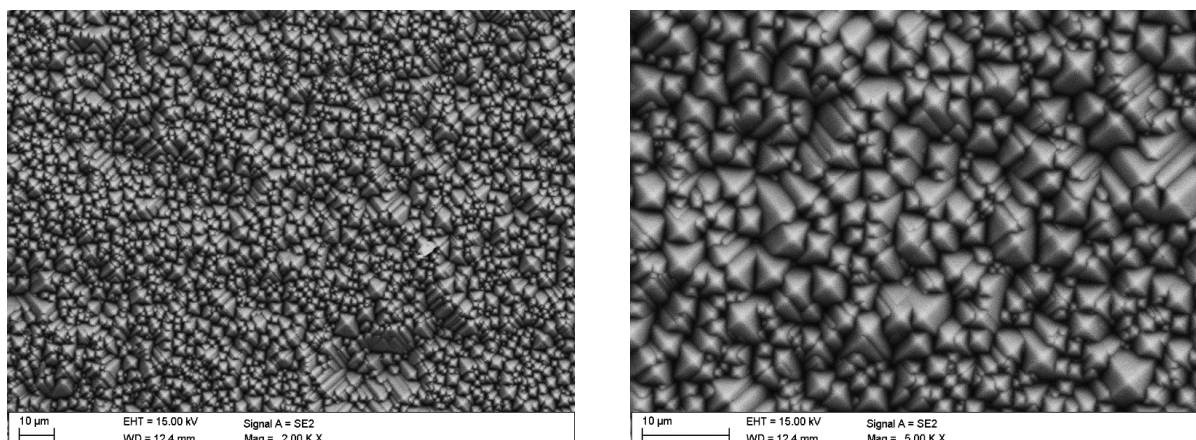


Figure 3. Topography of monocrystalline silicon solar cell surface

Multicrystalline silicon wafers are comprised of many silicon grains which are oriented at varying angles. Figure 4 shows the topography of the multicrystalline silicon surface at the boundary of three grains (each with a different crystallographic orientation) after the alkaline texturing process. Alkaline etching causes different orientations would etch at different rates, leading to non-uniform thicknesses across the surface. For multicrystalline wafers, only a small fraction of the surface has the required orientation of  $\langle 100 \rangle$  and consequently these techniques are not as effective as in the case of monocrystalline silicon.

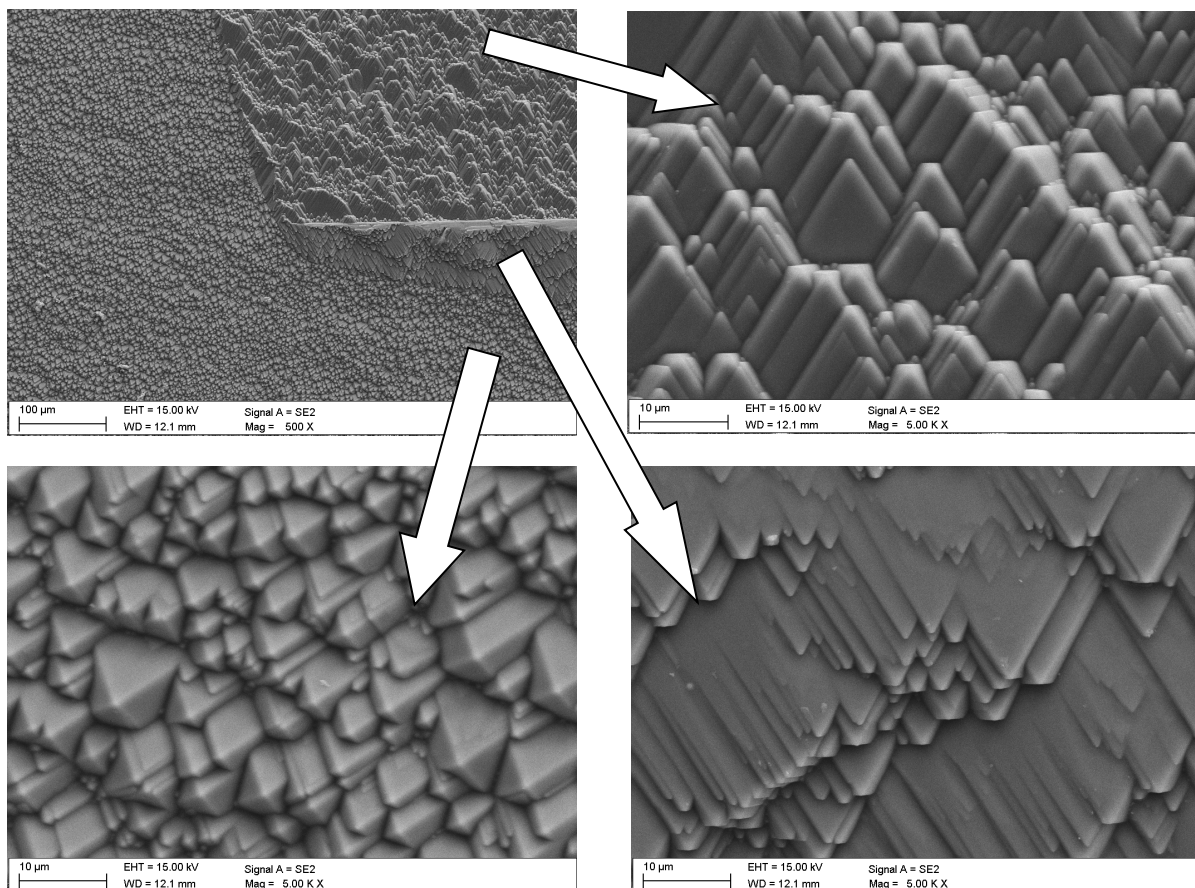


Figure 4. Topography of multicrystalline silicon solar cell surface

The measurement of the current-voltage (I-V) characteristics is the most important step for quality control and optimization of the fabrication process in research and industrial production of solar cells [7]. A comparison of the selected I-V characteristics of mono- and multicrystalline silicon solar cells is shown in Figure 5. The electrical properties such as short-circuit current density ( $I_{sc}$ ), open-circuit voltage ( $V_{oc}$ ), fill factor (FF), and power conversion efficiency ( $E_{ff}$ ) of solar cells are summarized in Table 1. In this study, for each solar cell ten measurements of current-voltage characteristics were made. The table lists the average values of electrical parameters and their standard deviation. Solar cells manufactured from mono- and multicrystalline silicon wafers demonstrate efficiency of 13.13 % and 10.29 %, respectively. The electrical parameters  $I_{sc}$ ,  $V_{oc}$ , and FF of monocrystalline silicon solar cells are higher compared to devices made of polycrystalline silicon by 145.9 mA, 12.0 mV, and 0.01, respectively.

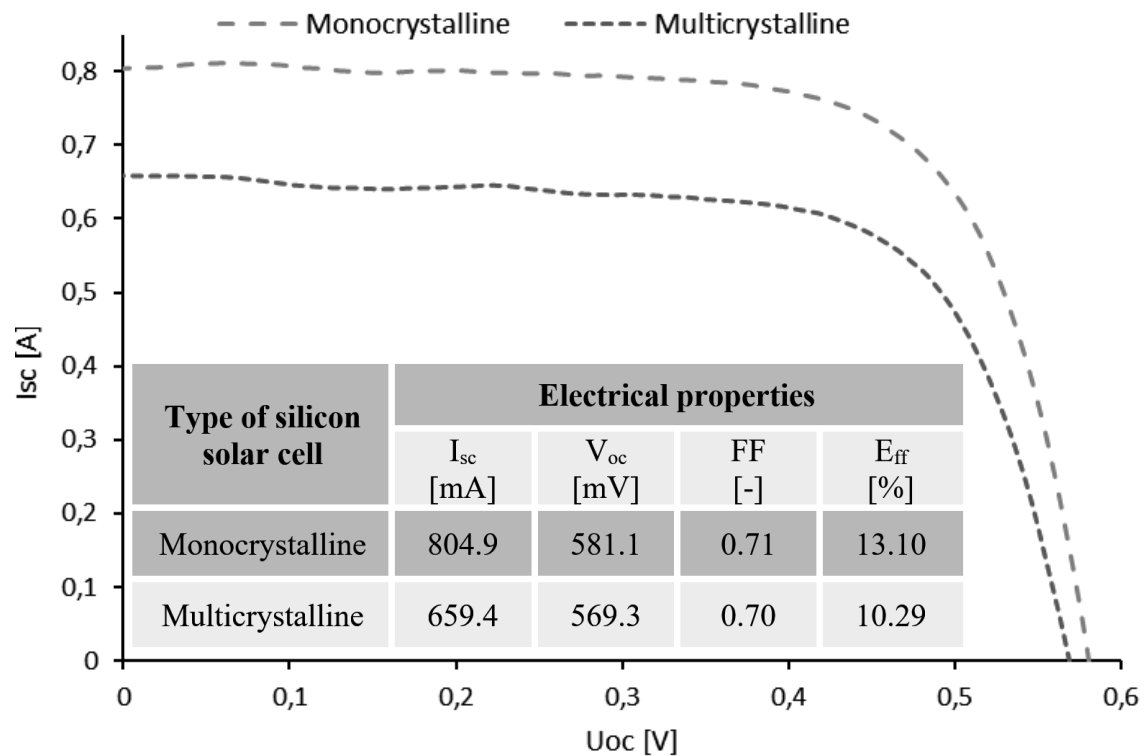


Figure 5. Selected current-voltage characteristics and electrical properties of mono- and multicrystalline silicon solar cells

Table 1. Average electrical parameters of solar cells mono- and multicrystalline silicon solar cells (with their standard deviation)

Type of silicon solar cell	Electrical properties			
	I <sub>sc</sub> [mA]	V <sub>oc</sub> [mV]	FF [-]	Eff [%]
Monocrystalline	804.3 ± 4.2	581.1 ± 0.3	0.71 ± 0.01	13.13 ± 0.04
Multicrystalline	658.4 ± 4.1	569.1 ± 0.6	0.70 ± 0.01	10.29 ± 0.02

#### 4. CONCLUSIONS

Solar radiation is one of the biggest energy sources. The total solar radiative energy delivered over the whole Earth's surface exceeds by many times the amount of energy currently needed worldwide. One of the most direct ways to convert the energy of sunlight into electricity is photovoltaics. In this paper, we present the comparison of the electrical and microstructural properties of mono- and multicrystalline silicon solar cells. Silicon is an important material in the photovoltaic industry. Crystalline silicon is currently the dominant solar cell material for commercial application because it is non-toxic and abundantly available in the Earth's crust. Silicon photovoltaic devices have shown their long-term stability over decades in practice. Based on the obtained results it was found that the electrical properties of

monocrystalline silicon solar cells are higher compared to devices made of polycrystalline silicon. The lower electrical properties of multicrystalline silicon solar cells are probably due to the ineffective texturing process of the material surface. Texturing of monocrystalline silicon is usually done by etching in alkaline solutions. These methods are inefficient for multicrystalline silicon due to the presence of random crystallographic grain orientations and high selectivity of etching along specific directions [6]. The efficiency of the monocrystalline silicon solar cell is 2.84 percentage points higher compared to the device based on polycrystalline silicon.

## ACKNOWLEDGEMENTS

The work was created as a result of a project carried out with secondary school pupils as a part of the Excellence Initiative - Research University program, Silesian University of Technology.

## BIBLIOGRAPHY

1. S.C. Bhatia, Solar radiations. *Advanced Renewable Energy Systems* 2014, 32-67.
2. C.A. Gueymard, 1.10 - Solar Radiation Resource: Measurement, Modeling, and Methods, Editor(s): T. M. Letcher, *Comprehensive Renewable Energy (Second Edition)*, Elsevier (2022) 176-212.
3. N.A. Kelly, T.L. Gibson, Improved photovoltaic energy output for cloudy conditions with a solar tracking system 83/1 (2009) 2092-2102.
4. T. Zhu, Q. Li, A. Yu, Analysis of the solar spectrum allocation in a spectral-splitting photovoltaic-thermochemical hybrid system. *Solar Energy* 232/15 (2022) 63-72.
5. A.O.M. Maka, J.M. Alabid, Solar energy technology and its roles in sustainable development. *Clean Energy* 6/3 (2022) 476-483.
6. L.A. Dobrzański, A Drygała, Surface texturing of multicrystalline silicon solar cells. *Journal of Achievements in Materials and Manufacturing Engineering* 31/1 (2008) 77-82.
7. A. Drygała, Z. Starowicz, K. Gawlińska-Nęcek, M. Karolus, M. Lipiński, P. Jarka, W. Matysiak, E. Tillová, P. Palček, T. Tański, Hybrid Mesoporous TiO<sub>2</sub>/ZnO Electron Transport Layer for Efficient Perovskite Solar Cell. *Molecules* 28 (2023) 5656.





26th January 2024  
Gliwice, Poland

DEPARTMENT OF ENGINEERING MATERIALS AND BIOMATERIALS  
FACULTY OF MECHANICAL ENGINEERING  
SILESIA UNIVERSITY OF TECHNOLOGY

## INTERNATIONAL STUDENTS SCIENTIFIC CONFERENCE

### Korózia horčíka a jeho zliatin

E. Halimovič<sup>a</sup>, M. Uhrčík<sup>a</sup>

<sup>a</sup> Žilinská univerzita v Žiline, Strojnícka fakulta, Katedra materiálového inžinierstva, Univerzitná 8215/1, 010 26 Žilina, Slovak Republic  
email: halimovic@stud.uniza.sk; milan.uhrick@fstroj.uniza.sk

**Abstrakt:** Článok sa zaoberá základným popisom korózneho správania horčíka a jeho zliatin v podmienkach elektrochemickej korózie - teda za prítomnosti elektrolytu a elektrických veličín.

**Kľúčové slová:** horčík, zliatiny horčíka, korózia, elektrochemická korózia

**Abstract:** This article describes the corrosion behavior of magnesium and magnesium alloys in electrochemical corrosion conditions - in the presence of electrolyte and electrical quantities.

**Keywords:** magnesium, magnesium alloys, corrosion, electrochemical corrosion

### 1. ÚVOD

V technologickej praxi je možné sledovať trend ekologických požiadaviek a to nielen na recykláciu napr. polymérnych materiálov, ale práve aj na kovové materiály a ich zliatiny. Preto prichádzajú do úvahy materiály, ktoré svojimi vlastnosťami zodpovedajú súčasným požiadavkám ako ekologickým tak aj konštrukčným, či technologickým.

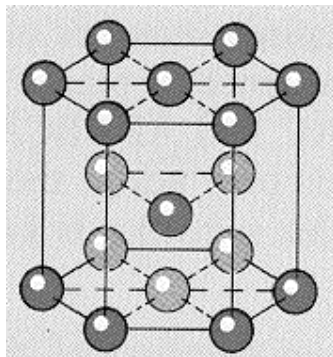
Práve kvôli požiadavkám na znižovanie ekologickej stopy je nutné znižovať hmotnosti vozidiel, ktoré spaľujú palivá na báze uhl'ovodíkov - čím nižšia hmotnosť vozidla, tým je potrebné menšie množstvo pohonných látok. Pre zníženie hmotnosti existuje niekoľko alternatív a to použitie hliníka a jeho zliatin, titánu a jeho zliatin a v neposlednom rade aj horčíka a jeho zliatin, po prípade použitie kompozitných materiálov, nakoľko tieto materiály majú nízku mernú hmotnosť a súčasne majú pomer pevnosti v ťahu k mernej hmotnosti veľmi priaznivý.

Horčík a jeho zliatiny nachádzajú uplatnenie nielen v automobilovom a leteckom priemysle, ale aj biomedicínskom prostredí. Zliatiny horčíka sa v súčasnosti používajú pre rôzne biomedicínske aplikácie, napr. ako dočasné implantáty v ľudskom tele. Keďže sa horčík nachádza v ľudskom tele ako minerál, je voľba horčíkových zliatin značne opodstatnená.

V prírode sa bežne vyskytuje v podobe rôznych zlúčenín, kde nadobúda formu dvojmocného iónu ( $Mg^{2+}$ ). Táto skutočnosť nie je priaznivá z pohľadu na jeho koróznou odolnosť. Nie je termodynamicky ušľachtilý, čo znamená, že má vysokú reaktivitu s prostredím. Z tohto dôvodu sa mnohé výskumné tímy po celom svete venujú práve koróznemu správaniu sa horčíka a jeho zliatin a po prípade hľadaniu spôsobov ako predísť korodovaniu týchto materiálov.

## 2. HORČÍK A JEHO ZLIATINY

Horčík (Mg) je kov kryštalizujúci v hexagonálnej tesne usporiadanej mriežke (Obr. 2). Je veľmi silne zastúpeným prvkom v zemskej kôre ako aj v morskej vode, čo ho činí veľmi dostupným a hlavne recyklovateľným [1].

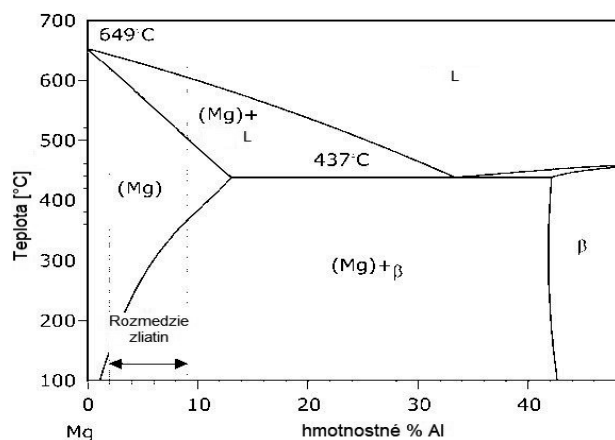


Obr. 1 Hexagonálna tesne usporiadaná mriežka  
Figure 1. Hexagonal close-packed lattice

Horčík, tak ako väčšina kovov používaných v technickej praxi, sa ako čistý kov nepoužíva. Hlavnými dôvodmi sú jeho nepriaznivé mechanické vlastnosti, ako aj korózna odolnosť, ktorá je veľmi nízka. Jeho merná hmotnosť je  $1740 \text{ kg}\cdot\text{m}^{-3}$  a teplota tavenia  $650^\circ\text{C}$ . Veľmi zle sa tvárni, čo zhoršuje zvýšenie jeho pevnosti plastickým pretvorením [1,2]. Horčík je dobre elektricky aj tepelne vodivý a má dobrú zlievateľnosť [1,2,3].

Horčík ako samostatný kov nevyhovuje požadovaným aplikáciám. Z tohto dôvodu sa zlieva s inými kovmi [1]. Horčíkové zliatiny sú prednostne používané na odliatky, avšak existujú aj zliatiny pre tvárnenie [2].

Medzi bežne dostupné zliatiny horčíka patria zliatiny na báze horčík - hliník [1]. Pre bežné zliatiny sa používa približne od 2 hm. % do 10 hm. % Al (Obr. 2) [4].



Obr. 2 Časť binárneho diagramu Mg-Al [4]  
Figure 1. Part of Mg -Al binary diagram [4]

V súčasnosti sa do tejto bázy pridáva aj zinok (Zn). Takéto zliatiny sú podľa ASM normy označované ako AZXX (XX predstavujú orientačné hodnoty hm. % jednotlivých prvkov, kde prvá číslica označuje hm. % prvého prvku, druhá druhého). Hliník a zinok v týchto zliatinách zvyšujú pevnosť, tvrdosť ako aj koróznú odolnosť. Zinok je pridávaný v množstvách okolo 1 hm. %. So zvyšovaním hm. % Zn dochádza k poklesu zvariteľnosti a koróznej odolnosti [5]. Medzi ďalšie prvky s ktorými sa horčík zlieva sú kovy vzácnych zemín (ozn. RE). Tieto zliatiny nachádzajú uplatnenie predovšetkým v automobilovom priemysle, nakoľko sú žiarupevnejšie ako ostatné zliatiny. Používajú sa hlavne po tepelnom spracovaní, po ktorom nadobúdajú požadované vlastnosti. Nepriaznivou skutočnosťou je však ich cena [5,6].

V súčasnosti sa zliatiny horčíka zlievajú s rôznymi inými kovmi ako napr. Mg-Zn, Mg-Al-Zr, Mg-Zr-Y, Mg-Zn-Zr, Mg-Li, Mg-Ca-Zn, atď. V mnohých prípadoch sa jedná o vývojové zliatiny - teda o zliatiny, ktoré sú z hľadiska ich budúcej aplikácie veľmi perspektívne [2,3,6,7]. Vplyv vybraných prvkov na výslednú zliatinu je uvedený v Tab. 1.

Tab. 1 Vplyv vybraných prvkov v zliatinách horčíka [7]

Table 1. Influence of selected elements on magnesium alloy [7]

Vplyv/prvok	Al	Ca	RE	Si	Zn
Tvrdosť	Zvyšuje	-	-	-	-
Pevnosť	Zvyšuje	-	-	Zvyšuje	-
Ťažnosť	Znižuje	-	-	-	-
Oxidácia	-	Znižuje	-	-	-
Korózna odolnosť	Zvyšuje	-	Zvyšuje	Zvyšuje	Zvyšuje
Odolnosť proti tečeniu	-	-	Zvyšuje	-	-

## 2. KORÓZIA HORČÍKOVÝCH ZLIATIN

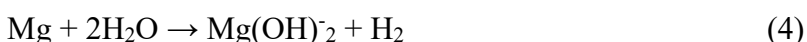
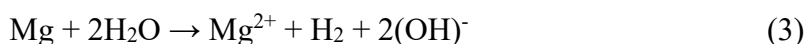
Jedným z najrozhodujúcejších faktorov, prečo sa horčík v technickej praxi nevyužíva je jeho nízka termodynamická stabilita v bežných prostrediach. Jedným zo základných ukazovateľov termodynamickej stability akéhokoľvek materiálu je štandardný elektródový potenciál  $E^0$ . Čím je jeho hodnota kladnejšia, tým je materiál stabilnejší.  $E^0$  horčíka je oproti iným materiálom veľmi záporný (Tab. 2) [1,3,6].

Tab. 2 Štandardné elektródové potenciály vybraných prvkov [8]

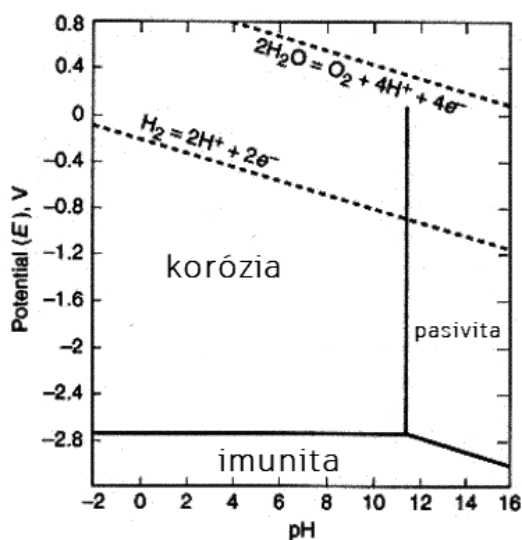
Table 2. Standard electrode potentials of selected elements [8]

Tvorba katiónov	Štandardný elektródový potenciál $E^0$ [V]
$\text{Cu} \rightarrow \text{Cu}^{2+} + 2\text{e}^-$	+ 0,35
$2\text{H} \rightarrow 2\text{H} + 2\text{e}^-$	0
$\text{Fe} \rightarrow \text{Fe}^{2+} + 2\text{e}^-$	- 0,44
$\text{Zn} \rightarrow \text{Zn}^{2+} + 2\text{e}^-$	- 0,76
$\text{Mn} \rightarrow \text{Mn}^{2+} + 2\text{e}^-$	- 1,1
$\text{Zr} \rightarrow \text{Zr}^{4+} + 4\text{e}^-$	- 1,53
$\text{Al} \rightarrow \text{Al}^{3+} + 3\text{e}^-$	-1,69
$\text{Mg} \rightarrow \text{Mg}^{2+} + 2\text{e}^-$	- 2,37

Z termodynamického hľadiska sa teda jedná o materiál, ktorý má vysokú reaktivitu a náchylnosť k odovzdávaniu elektrónov, teda k vytvoreniu kladne nabitého iónu -  $Mg^{2+}$  (1). Takto kladne nabitá častica na seba nabaľuje záporne nabité atómy zo vzduchu, alebo vody - prevažne kyslík, alebo skupiny (napr. hydroxidová skupina) (3). Následne vznikne korózný produkt (4) [9].



Dôležitú informáciu o koróznom správaní sa materiálu podávajú aj tzv. Pourbaixove diagramy. Vykresľujú závislosť medzi pH a potenciálom, ktorý vzniká medzi materiálom a prostredím s daným pH. Horčík koroduje takmer vo všetkých prostrediach, jedine pri nízkych potenciálových napätiach sa správa imúnne (teda nekoroduje) a pri vysokých pH sa správa pasívne (vytvorí sa vrstva ochranných oxidov) (Obr. 3).



Obr. 3 Pourbaixov diagram pre čistý horčík [4]

Figure 3. Pourbaix diagram for pure magnesium [4]

Z rovníc a z Pourbaixovho diagramu (Obr. 3) je zrejmé, že horčík sa vie nachádzať v rôznych stavoch. Každý tento stav má určitý chemický potenciál, ktorý vo všeobecnosti podáva informáciu o tom, ako veľmi je daný prvok, ión, či zlúčenina, stabilný. Najstabilnejšou zlúčeninou je hydroxid horečnatý (Tab. 3). Avšak táto zlúčenina nedokáže byť v bežných podmienkach stabilnou natoľko, aby povrch chránila.

Povrch takéhoto skorodovaného materiálu je porézny, čo umožňuje vznik rôznych kapilárnych efektov, v ktorých korózia môže prebiehať intenzívnejšie, ako pri nenapadnutom povrchu [1,3,11].

Tab. 3 Chemický potenciál rôznych stavov horčíka [1]

Table 3. Chemical potential of different states of magnesium [1]

Zložka	Chemický potenciál [kcal/kmol]
Mg	0
Mg <sup>2+</sup>	-109
MgO	-139
Mg(OH) <sub>2</sub>	-199

Avšak nakoľko v praxi sú využívané zliatiny horčíka je zrejme, že významný vplyv na koróziu odolnosť majú aj prísadové prvky v zliatinách. Väčšina prvkov je ušľachtilejších, ako horčík. V matici zliatiny teda vznikajú mikrogalvanické účinky, ktoré majú za následok rozpad materiálu. Horčík ako menej ušľachtilý kov sa prirodzene stane anódou voči zložke, ktorá je s ním zliata [1,3,6,11].

Jednotlivý vplyv na koróziu odolnosť horčíkových zliatin je už pomerne známy a vo všeobecnosti každý legujúci prvok z časti aj koróziu odolnosť zlepšuje. Nie je však možné zabezpečiť dostatočnú koróziivzdornosť a to práve kvôli mikrogalvanickému účinku, ktorý spôsobuje vznik galvanických trhlín a následne koróziu (niekedy korózne-únarový) lom. Riešením sú prvky ako chróm, alebo titán - tieto prvky sú schopné vytvárať oxidy na povrchu, ktoré sú homogénne a zamedzujú tak ďalšiemu korodovaniu. Z dôvodu ich vysokej mernej hmotnosti sa ale stráca zmysel zlievať horčík s týmito prvkami, keďže hmotnosť takýchto odliatkov by sa pohybovala výrazne vyššie, ako sú napr. hmotnosť zliatin Al, ktorých korózia odolnosť je postačujúca [1,3,5,6].

Jedným z ďalších faktorov, ktoré sú perspektívne, sú povrchové úpravy horčíkových zliatin. Jedná sa buď o rôzne typy povlakovania, vrstvenia, alebo mechanického opracovania. Z rôznych výskumov je zrejme, že niektoré úpravy povrchu ako napr. konvenčné brúsenie, alebo leštenie môže zvýšiť koróziu odolnosť oproti bežne frézovanému, alebo odliatemu povrchu [13,14]. Bežne dostupné metódy síce zlepšujú koróziu odolnosť horčíkových zliatin, avšak nie natoľko, aby to postačovalo pre konkrétne aplikácie. Jednou z ďalších možností sú laserové, poprípade shot peeningové možnosti opracovania povrchu. Výsledky experimentov v súčasnosti však nie sú priaznivé - korózia odolnosť po ovplyvnení povrchov týmito metódami výrazne klesá [3,8]. Ďalšou možnosťou sú možnosti vytvárania vrstiev. Existuje už niekoľko spôsobov ako na povrchu vytvoriť vrstvu, ktorá je nevodivá, takže sa zníži možnosť prúdenia elektrónov a tým sa zamedzí elektrochemickej korózii. Jeden z takýchto typov vrstiev sú vrstvy vytvorené plazmovou elektrolytickou oxidáciou (PEO). Tieto vrstvy dokážu zvýšiť odpor povrchu voči elektrickým veličinám aj o dvojnásobok [8,11].

### 3. ZÁVER

Predkladaný článok sa zaoberá základnými poznatkami v oblasti korózie horčíka a jeho zliatin. Na základe týchto poznatkov je možné vysloviť nasledovné závery:

- Horčík je ako čistý kov v praxi nevyužiteľný - je nutné ho zlievať s inými prvkami, pri čom v súčasnosti majú najavšie využitie zliatiny horčíka na báze Mg-Al-Zn
- Korózia odolnosť čistého horčíka je veľmi slabá. Najstabilnejší korózný produkt, ktorý by mohol materiál chrániť je hydroxid horečnatý (Mg(OH)<sub>2</sub>), ktorý však v bežných prostrediach nie je stály natoľko, aby zliatinu chránil.

- Zliatiny horčíka je možné korózne chrániť aj vplyvom legujúcich prvkov, ktoré by mali nie len vytvárať oxidy, ale taktiež dvíhať celkový štandardný elektródový potenciál zliatiny. Vo všeobecnosti je ale tento efekt často potlačený mikrogalvanickými účinkami, kedy horčík koroduje na úkor legujúceho prvku.
- Možnosťou zlepšenia koróznej odolnosti horčíkových zliatin sú taktiež povrchové úpravy. Okrem konvenčných metód ako brúsenie a leštenie existujú nové progresívne metódy úprav povrchu, ktoré sú v súčasnosti predmetmi skúmania. Mnohé z nich ako napr. PEO majú na koróznú odolnosť významný vplyv - odpor vrstiev vytvorených touto metódou vzrastá až o dvojnásobok alebo trojnásobok.

## POĎAKOVANIE

Príspevok vznikol v rámci riešenia spoločného slovensko-poľského projektu TalentDetector 2023 ako výsledok spolupráce medzi Politechnikou Slaskou (Poľsko) a Žilinskou univerzitou v Žiline a projektov KEGA č. 004ŽU-4/2023 a KEGA č.009ŽU-4/2023.

## BIBLIOGRAPHY

1. G. L. Song. Corrosion of Magnesium Alloys. Elsevier, 2011, ISBN 978-0-85709-141-3.
2. P. Skočovský et al. Náuka o materiáli. EDIS, Žilina, 2014, ISBN 978-80-554-0871-2.
3. Ľ. Halimovič. Vplyv nekonvenčných úprav povrchu na korózne charakteristiky horčíkových zliatin, Bakalárska práca. Žilinská univerzita v Žiline, 2023.
4. Part of Mg-Al binary diagram, [www.researchgate.net/publication/265168745\\_Design\\_with\\_Magnesium-Alloys\\_properties\\_and\\_casting\\_processes/figures?lo=1](http://www.researchgate.net/publication/265168745_Design_with_Magnesium-Alloys_properties_and_casting_processes/figures?lo=1)
5. Ę. Koç, et al. Influence of zinc on the microstructure, mechanical properties and in vitro corrosion behaviour of magnesium-zinc binary alloys, Journal of Alloys and Compounds, vol 648 (2015). ISSN 0925-8388. DOI: 10.1016/j.jallcom.2015.06.227.
6. B. Hadzima. Korózia zliatin Mg-Al-Zn. Dizertačná práca. Žilinská univerzita v Žiline, 2003.
7. D.S. Kumar, et al. Magnesium and Its Alloys in Automotive Applications - A Review, American Journal of Materials Science and Technology, vol 4. 2015. DOI: 10.7726/ajmst.2015.1002.
8. F. Pastorek, B. Hadzima, D. Kajánek. Preparation and corrosion properties of structural materials with refined grain structure. Person, 2019. ISBN 978-8396-1054-7.
9. A. Atrenset al. Review of Recent Developments in the Field of Magnesium Corrosion. In Advanced Engineering Materials, vol 17, 2015 DOI: 10.1002/adem.201400434.
10. Pourbaix diagram for pure magnesium [https://www.researchgate.net/figure/Magnesium-in-water-Pourbaix-diagram-at-25-C\\_fig4\\_289256819](https://www.researchgate.net/figure/Magnesium-in-water-Pourbaix-diagram-at-25-C_fig4_289256819).
11. D. Kajánek. Štúdium mechanizmov korózneho napadnutia povrchovo upravených horčíkových zliatin. Dizertačná práca. Žilinská univerzita v Žiline, 2019.
12. M.A.F Romzi, J. Alias, M.I.M. Ramli. Effect of Zinc (Zn) on the microstructure and corrosion behaviour of Magnesium (Mg). In. Materials Today: Proceedings, vol 48, part 6, 2022. ISSN 2214 - 7853. DOI: 10.1016/j.matpr.2021.09.261
13. U. Reddy et al. Effect of Surface Roughness Induced by Milling Operation on the Corrosion Behavior of Magnesium Alloys. In. Journal of Materials Engineering and Performance, vol 30, 2021. DOI: 10.1007/s11665-021-05933-8, 2021

## Life cycle assessment (LCA) methodology

W. Hankowska<sup>a</sup>, A. Kania<sup>b</sup>

<sup>a</sup> Student of Management and Production Engineering at the Faculty of Mechanical Engineering at the Silesian University of Technology

email: wikthan297@polsl.pl

<sup>b</sup> Silesian University of Technology, Faculty of Mechanical Engineering, Department of Engineering Materials and Biomaterials

email: aneta.kania@polsl.pl

**Abstract:** The aim of the work is to present the LCA requirements and methodology. The article describes LCA goals and scope, inventory analysis, environmental impact assessment and interpretation of LCA results.

**Keywords:** Life Cycle Assessment (LCA), LCA methodology, LCA goals and scope, environmental impact.

## 1. INTRODUCTION

LCA (Life Cycle Assessment) is an environmental management tool. Its aim is to compare the environmental consequences of performing the same function by alternative product systems throughout their life cycle. The life cycle is from the extraction of raw materials through production, usage and its final disposal (Fig. 1) [1-6].

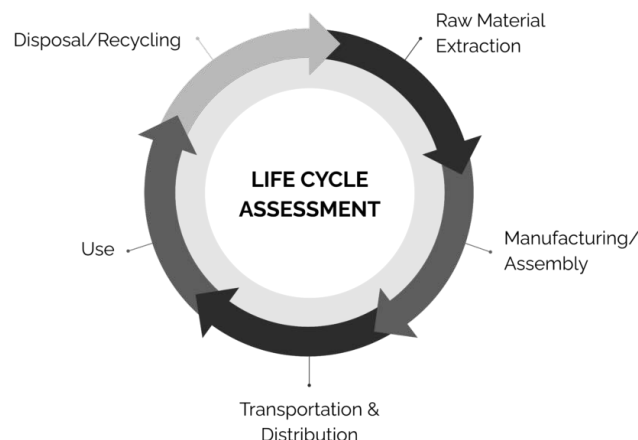


Figure 1. Stages of LCA [1]

Each phase of LCA methodology is divided into different stages, in which energy, natural resources, materials are consumed, wastes are generated, wastewater are produced, as well as many pollutants are released into the environment components. LCA is physical in nature, but defined through the prism of a product's function and its process approach to the subject.

Life cycle assessment makes it possible to analyze the effects of different resource management options as part of creating a sustainable system. In addition, it is an important tool needed for environmental decision-making in a company.

The purpose of LCA is to solve identified problems, as well as to suggest more sustainable forms of consumption and production. Accordingly, LCA is a process that [2-6]:

- identifies and quantifies all environmental emissions associated with the entire life cycle of a product,
- estimates the size of environmental impacts,
- implements all possible modernizations that contribute to reducing the studied negative environmental impacts.

## 2. LCA METHODOLOGY

According to the requirements, environmental life cycle assessment consists of four phases: definition of the goal and scope, analysis of the set of inputs and outputs (inventory analysis), assessment of life cycle impacts and interpretation (Fig. 2) [7,8].

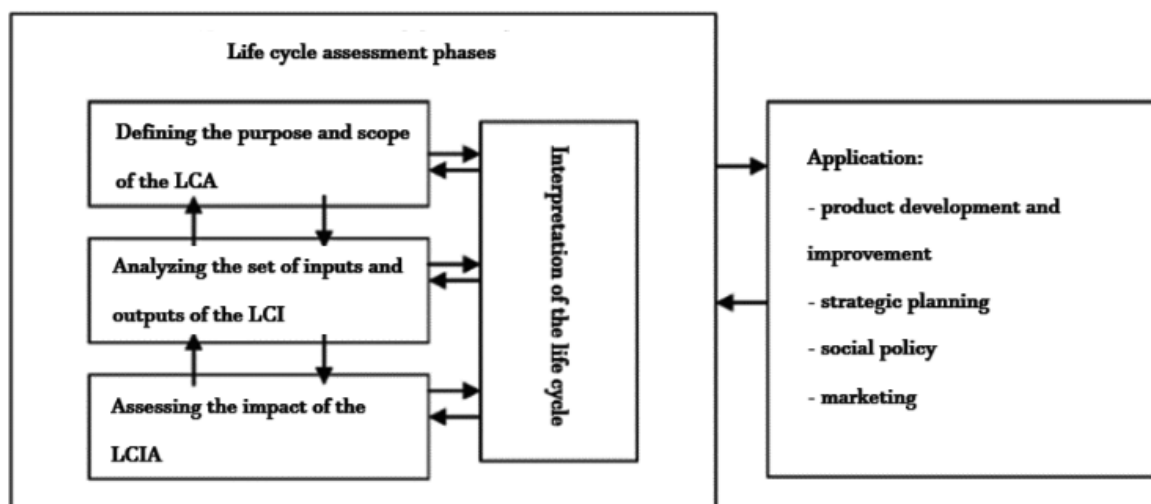


Fig. 2. Life cycle assessment phases according to ISO 14040 standard [7]

In the first step of the study – definition of the goal and scope of the LCA – it is required to determine the consistent boundaries of the system (system boundaries determine which unit processes should be included in the LCA) and the identical functional unit (a functional unit is the reference unit for all inputs and outputs from a product system), the choice of which, as it were, is already determined at the time of defining the goal and scope of the study. The purpose of a LCA is to define why you are conducting a life cycle analysis. You can do it to identify areas where a product or process can be environmentally improved, compare two products or



processes in terms of their environmental impact, create an environmental label for a product [7,8].

The scope of the LCA determines which environmental aspects will be included in the analysis. You can include raw materials consumption, emissions of pollutants, waste production, etc.

Life cycle inventory (LCI) analysis involves collecting data on what goes into a product or process (inputs) and what comes out of it (outputs). According to ISO 14040, the data for individual unit processes within a product system can be, among others [7,8]:

- input data: energy inputs, raw material inputs, auxiliary and other data,
- output data such as products, intermediates and waste,
- release of pollutants into air, water and soil,
- other environmental factors.

You can collect input and output data from various sources such as technical documentation, data from databases, data from your own studies.

These data are recorded in the form of inventory tables, which task is to quantify all natural resources consumed, waste generated, as mentioned above, as well as intermediate products. However, it should be remembered that an important aspect is to check the quality of this data and whether it is complete.

According to PN-EN ISO 14044:2006 [7,8], the entire process of data transfer and its appropriate selection should be carried out with great accuracy and without making errors. The most important data is the result of private and own research. If there is no such data, the standard allows the possibility of using data from the literature or available databases of data and knowledge.

An important feature of LCA is its iterative nature, which means that continuous data adjustments must be made while the assessment is being conducted [8].

The purpose of the life cycle impact assessment (LCIA) stage is to identify the environmental dependencies of all inputs and outputs included in the scope of the LCA, and to estimate their environmental impact. At this stage, the results of the LCI analysis are classified into appropriate impact categories based on the adopted environmental priorities, taking into account regional and local conditions. The impact categories are weighted according to environmental aspects and are weighted according to their degree of environmental impact.

LCIA can be divided into two groups [8]:

**1. Mandatory:**

- selection of impact categories, classification indicators and characterization models,
- assigning LCI results to impact categories (classification),
- calculating the value of category indicators (characteristics).

**2. Optional:**

- normalization,
- grouping,
- weighting,
- data quality analysis.

The choice of impact classification should take into account the goal and scope of the analysis. In this section, data from the inventory table are assigned to the corresponding categories of environmental impacts. The following categories of impacts are often considered:

resource depletion, energy consumption, soil acidification, toxicity to humans and ecotoxicity to soil, water, global warming and many others. During the classification process, each component of the inventory list is classified, so it effects on one or more environmental problems.

The impact characteristics attempts to determine the causes of identified environmental problems. Equivalent values used here analyze and determine what is the contribution of the analyzed substance to the generation of the corresponding environmental hazard compared to the reference component.

Impact valuation, on the other hand, is an attempt to compare environmental problems and assign a weight to each of the identified impacts. In this step, it is necessary to determine if a particular environmental impact plays a primary role or, rather a secondary one. The results of valuing environmental problems can be repeated and tested using the weighted sum method.

The final stage of the LCA procedure is interpretation, which is to evaluate, as well as check the results obtained, present them in the clearest possible way, and draw up conclusions, recommendations and final reports.

The LCA analysis ends with preparation and presentation of a report on the research conducted [8].

### 3. CONCLUSIONS

Product life cycle assessment is an important tool for identifying environmental aspects required in environmental management systems. Methodologically, it can be said that LCA is an 'input-output' analysis, identifying the way a product takes from design to full disposal. A properly conducted life cycle assessment, regardless of the type of procedure, enables both the saving of raw materials and energy, the elimination of toxic raw materials, and the reduction of the amount and harmfulness of all waste discharged into the environment.

### LITERATURE

1. M. Eckelmann, S. Nunberg, Life Cycle Assessment Explained, <https://stich.culturalheritage.org/life-cycle-assessment-explained/>, 2023.
2. K. Santarek, J. Duda, S. Oleszek, Management of life cycle of a product, Polish Economics Publishers, Warsaw, 2022.
3. Z. Kowalski, J. Kulczycka, M. Góralczyk, Ecological life cycle assessment of manufacturing processes (LCA), Polish Scientific Publishers, Warsaw, 2007.
4. I. Samson-Bręk, Application of the LCA life cycle assessment method to estimate the environmental impact of biogas fuel production for internal combustion engines, [https://bg\\_utp\\_edu\\_plartarchiwum20motoryzacji2011samson-brek2.pdf](https://bg_utp_edu_plartarchiwum20motoryzacji2011samson-brek2.pdf), 2023.
5. R. Nowosielski, M. Spilka, A. Kania, Environmental management and environmental management systems, *Publishing House of Silesian University of Technology, Gliwice, 2010.*
6. A. Barański, B. Gworek, A. Bojanowicz-Bablok, Life cycle assessment: Theory and practice, Publishing House of the Institute of Environmental Protection, Warsaw, 2011.
7. ISO 14040:2006. Environmental management. Life Cycle Assessment. Principles and framework.
8. ISO 14044:2006. Environmental management. Life Cycle Assessment. Requirements and guidelines.



26th January 2024  
Gliwice, Poland

DEPARTMENT OF ENGINEERING MATERIALS AND BIOMATERIALS  
FACULTY OF MECHANICAL ENGINEERING  
SILESIA UNIVERSITY OF TECHNOLOGY

## INTERNATIONAL STUDENTS SCIENTIFIC CONFERENCE

### Structure and selected properties of oxide ALD coatings for biomedical applications

M. Herman <sup>a</sup>, M. Rapacz <sup>a</sup>, Ł. Reimann <sup>b</sup>, D. Pakuła <sup>c</sup>, M. Staszuk <sup>c</sup>

<sup>a</sup> Silesian University of Technology, Faculty of Mechanical Engineering; e-mail: mh307613@student.polsl.pl, e-mail: mr307671@student.polsl.pl

<sup>b</sup> Silesian University of Technology, Faculty of Mechanical Engineering Technology, Materials Research Laboratory, e-mail: lukasz.reimann@polsl.pl

<sup>c</sup> Silesian University of Technology, Faculty of Mechanical Engineering, Department of Engineering Materials and Biomaterials, e-mail: daniel.pakula@polsl.pl, e-mail: marcin.staszuk@polsl.pl

**Abstract:** The aim of this article is to present and investigate the electrochemical properties of titanium dioxide (TiO<sub>2</sub>) coatings deposited on 316L stainless steel using the Atomic Layer Deposition (ALD) method. The coating was deposited at a constant temperature of 200°C with 200 cycles. The effects of titanium oxide deposition conditions on the structure, properties, and corrosion resistance of the coatings were investigated. Structural studies were conducted using scanning electron microscopy (SEM) and atomic force microscopy (AFM). The electrochemical properties of the titanium dioxide-coated sample and the uncoated sample were studied using the potentiodynamic method in Ringer's solution to ensure accurate reflection of the conditions within the human body. Based on microscopic analyses, a link was established between the structure of the tested coating and its electrochemical properties, thereby highlighting the effect of deposition conditions on corrosion resistance.

**Keywords:** 316L stainless steel, ALD, TiO<sub>2</sub> coatings, corrosion resistance.

### 1. INTRODUCTION

One area that is the focus of research in biomedical engineering is the development of implants. Dynamic advances in implantology are resulting in increasingly sophisticated requirements for these advanced implants. Any implant that is to be successfully implanted in the human body must meet a number of key criteria, such as biofunctionality, biocompatibility, biotolerance, certain mechanical properties, and above all high corrosion resistance. Modern materials, used for the manufacture of implants, achieve the required corrosion resistance by forming oxide layers on their surface, which act as an inhibitor of corrosion processes [1-3]. One of the commonly used materials for implants is 316 L steel, which meets all the previously mentioned criteria [1]. It is characterized by particularly high corrosion resistance, but is nevertheless liable to pitting and crevice corrosion, especially in the presence of Cl<sup>-</sup> ions, which occur in the environment of the human body [1]. Therefore, to improve corrosion resistance, various modifications to the surface of implants are being carried out increasingly. The most commonly used method is the application of thin layers,

characterized by low solubility, which stops the penetration of unfavorable ions from the material into the human body. Among the various surface layers that are applied by different techniques are those such as  $\text{TiO}_2$  or  $\text{SiO}_2$ , applied using the ALD technique.

The ALD method is based on applying surface layers using a thermo-chemical process. It is classified as one of the variations of chemical vapor deposition, known as CVD. The similarities between CVD and ALD are numerous, but there are significant differences between the technologies, allowing more reactive compounds to be used and more subtle layers to be obtained with the ALD method, compared to CVD [5].

The process of applying surface layers is carried out in special reactors that allow precise control of parameters. The individual elements are applied as a result of a self-limiting chemical process, separately, layer by layer, for each cycle. The coatings are formed from precursors, which can be present in the gas, liquid or solid phase. The precursors form strong chemical bonds with the substrate placed in a heated chamber.

The cycle in the ALD method consists of several steps. First, a small amount of the first precursor is introduced into the reaction chamber using a pulse, then the reactor chamber is purged with an inert gas. The next step is the dosing of the second precursor, and the process is repeated cyclically. The ALD method makes it possible to improve the functional properties of the coated material. Obtaining an amorphous structure on the coating, and getting rid of microstructural defects is crucial to improve not only the functional properties, but also the corrosion resistance.

$\text{TiO}_2$  is an important material commercially used in various industrial sectors such as paint manufacturing, biomedical engineering, food industry, pharmaceuticals, cosmetics, etc. In optical preparations, its high refractive index and good visible light transmission are important properties.

In addition, titanium dioxide also exhibits excellent insulating properties in electronic devices, thanks to its high dielectric constant. Its activity is used in chemical and electrochemical sensors, as well as in solar cells. In addition,  $\text{TiO}_2$  is a widely used catalyst.

Titanium oxide, as a component of biocomposites, exhibits antimicrobial activity against strains of *E. coli* (*Escherichia coli*), *Staphylococcus aureus* and *Candida albicans* fungi.  $\text{TiO}_2$  is also used for its disinfecting properties, which are used to clean surgical instruments [7, 8].

In the field of oncology, the combination of  $\text{TiO}_2$  with UV radiation or ultrasound is used in anti-cancer therapies, resulting in the destruction of cancer cells [10]. The design of  $\text{TiO}_2$  nanoparticles makes it possible to use them in targeted therapies, thus increasing the effectiveness of cancer therapy and reducing side effects. Particles with sizes of 100-800 nm allow access to tumor tissues, bypassing healthy cells (which are 2-6 nm in size).  $\text{TiO}_2$ -based carriers can also deliver larger amounts of drug to the target sites, leading to a reduction in the required drug dose [9, 10]. Titanium oxide coatings are used to protect against pitting corrosion, which is corrosion that occurs only in certain areas in the form of spots or pits often reaching deep into the material.  $\text{TiO}_2$  coatings are applied using a variety of methods. The ALD method is commonly chosen due to the characteristic features of the process. The properties of  $\text{TiO}_2$  coatings are strongly related to the parameters of the coating process (coating growth temperature, precursors used, number of cycles), this will also be elaborated later in the article. [4].

## 2. MATERIALS

The coated substrate was 316L alloy steel, which is classified as an austenitic steel that is corrosion-resistant. This is the group of metal materials that were first introduced in the implantation in the human body. About 70% of hip joints in the United States are made with 316L steel [3,6]. A steel rod with a diameter of  $\Phi = 14$  mm was cut into discs with a thickness of  $g = 5$  mm. The specimens were prepared by grinding and polishing. Grinding was done on

coarse sandpaper, starting with a gradation of 220, later 500, 800 and 1200. Then the samples were polished on a polishing cloth disc starting with a gradation of 9 to 1 $\mu$ m. Between each step, the samples were rinsed in an ultrasonic scrubber in distilled water with detergent, degreased in acetone and dried with a hot air blower.

Table 1. Chemical composition of 316L steel

Elemental Concentration [%]							
C	Cr	Ni	Mn	Mo	N	P	S
0.006	18.3	10.7	1.67	2.11	0.07	0.04	0.02

The substrates prepared in this way were coated with TiO<sub>2</sub> titanium dioxide coating. The coating was performed using the ALD method. The deposition temperature of TiO<sub>2</sub>, which was 200°C, was chosen based on the known ALD temperature window and the studies already conducted on the subject [4]. Two types of samples were tested, one was TiO<sub>2</sub>-coated, applied by ALD at 200 cycles. While the other was plain uncoated material. The coating was applied using a Picosun R200 reactor. The titanium source was TiCl<sub>4</sub>, and the oxygen source was high-purity (distilled) water.

Table 2. Deposition condition of ALD coating

Temperature (°C)	Reagent Feed Time(s)		Cleaning time (s)		Number of Cycles
	TiCl <sub>4</sub>	H <sub>2</sub> O	TiCl <sub>4</sub>	H <sub>2</sub> O	
200	0.1	0.1	4	5	200

### 3. METHODOLOGY

Surface structure and morphology studies were carried out using a Zeiss high-resolution scanning electron microscope (SEM) SUPRA 35 at magnification: 50-150 thousand times, using secondary electron detection. The study of coating morphology was carried out using an AFM XE-100 atomic force microscope delivered by Park Systems. The non-contact mode was used in the study. The scanned area was 1×1 - 20×20  $\mu$ m. In order to evaluate the electrochemical properties of the titanium dioxide-coated samples and the uncoated sample, potentiodynamic tests were conducted in Ringer's solution at 37°C. In the first step, the open circuit potential was determined under current-free conditions, and then potentiodynamic polarization curves were recorded.

### 4. RESULTS

The structure of titanium oxide layers depends on the conditions of its deposition, in particular, on the number of ALD cycles. At a low number of cycles, an amorphous structure of the titanium oxide layer is obtained, which reduces charge transport and affects the reduction of corrosion current. At 500 cycles, the coating is the most resistant, as it is thicker and at the same time maintain an amorphous structure (Fig 1.a). Coatings obtained at the number of cycles in the range from 200 to 500 exhibits an amorphous structure. The morphology of such coatings is characterized by high smoothness without the presence of grains characteristic of a crystalline structure [11]. At 1000 cycles, areas of nanocrystalline structure were noted (Fig 1.b). The process of formation of TiO<sub>2</sub> crystalline structures under the conditions performed in the study [11] consists of two stages: separation of crystallites from the amorphous phase through phase transformation and grain growth. The driving force behind the phase

transformations occurring during the growth of the coating in the deposition process is the difference in free energy of the individual structural components of titanium oxide. In general, it can be assumed that these transformations follow the Ostwald-Lussac law [12]. According to this law, anatase is considered a transitional phase and less stable than rutile. Therefore, it can be expected that in the case of  $\text{TiO}_2$  coating with a large number of cycles (or increased temperature of the deposition process), the rutile phase will gradually dominate, considered more stable than anatase. Comparing the morphology made in the study of [11] (Fig. 1) and the morphology performed in this article (Fig. 2), it can be concluded that  $\text{TiO}_2$  coatings at the number of cycles in the range of 200 to 500 have an amorphous structure.

Table. 3 Potentiodynamic polarization parameters for samples in Ringer's solution.

Sample	$E_{ocp}$ , V	$j_{corr}$ ; $\text{nA}/\text{cm}^2$	$E_{corr}$ ; mV	$R_{pol}$ ; $\text{k}\Omega \cdot \text{cm}^2$
316L uncoated	-0,29	37	-119	110
$\text{TiO}_2(200)$	-0,73	18	-148	648

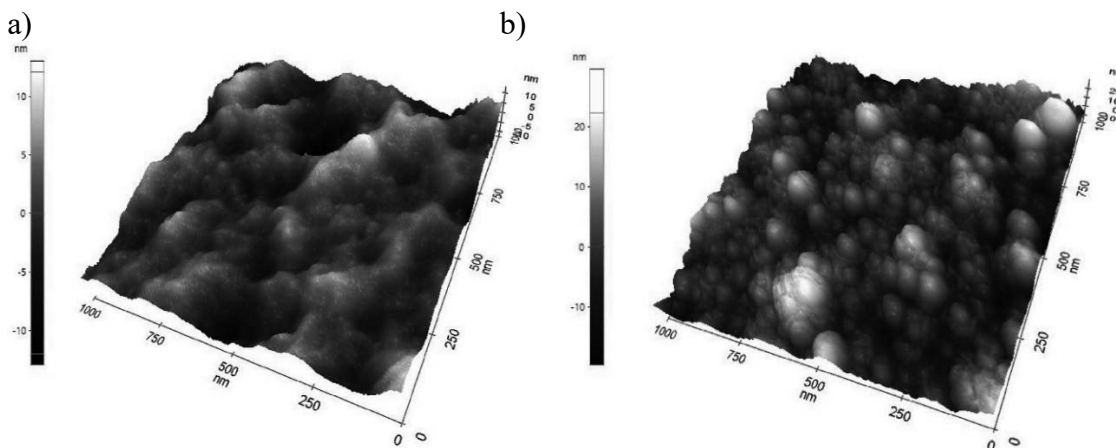


Figure 1. Morphology made in the study [11]: coating topography SEM: a)  $\text{CrN} + \text{Cr}_2\text{O}_3/\text{TiO}_2(500)$ , b)  $\text{CrN} + \text{Cr}_2\text{O}_3/\text{TiO}_2(1000)$ .

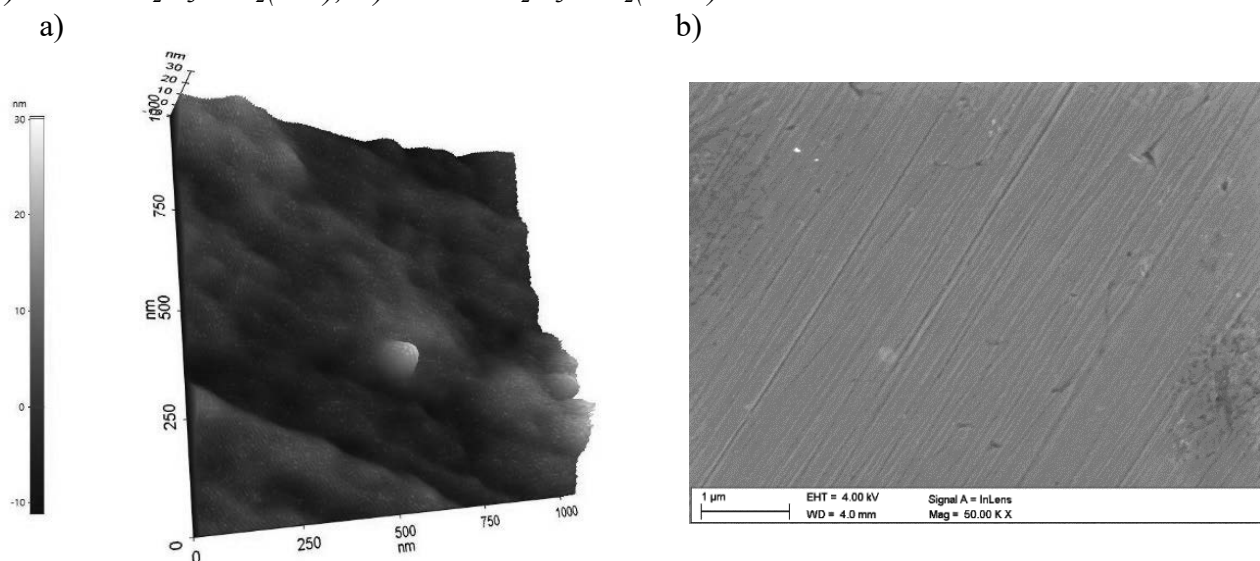


Figure 2.  $\text{TiO}_2$  coating topography a) AFM, b) SEM

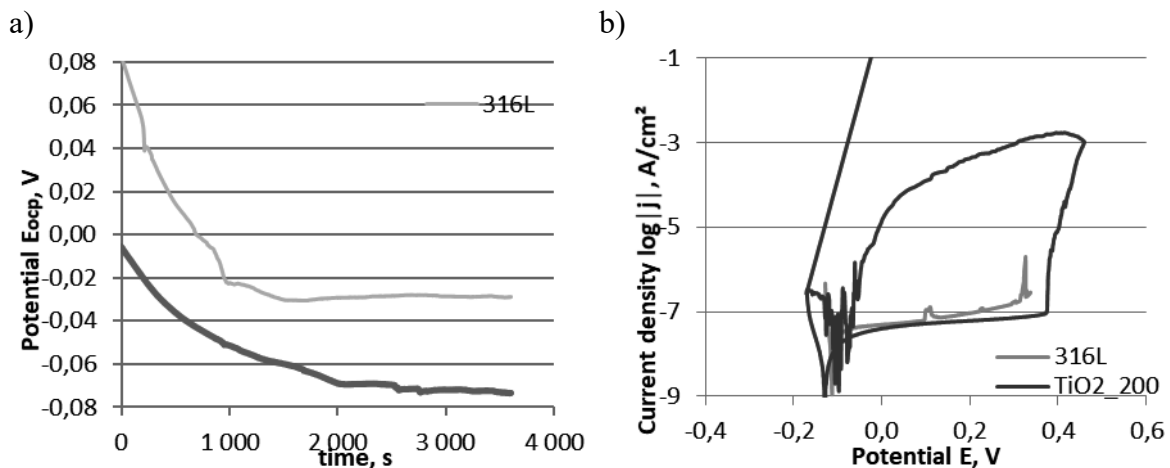


Figure 3. Electrochemical test curves of uncoated substrate and ALD coating: a) open circuit potential, b) anodic polarization curves.

After electrochemical testing (Table. 3), the samples were subjected to microscopic observations to evaluate any corrosion changes. Figure 4 shows the results obtained using a scanning electron microscope (SEM). The analysis revealed the presence of pits in the samples, which were characterized by irregular shapes and varying sizes. Their structure resulted from the etching processes of the grain boundaries of the base material. The highest number of pits was observed in the uncoated sample.[13]

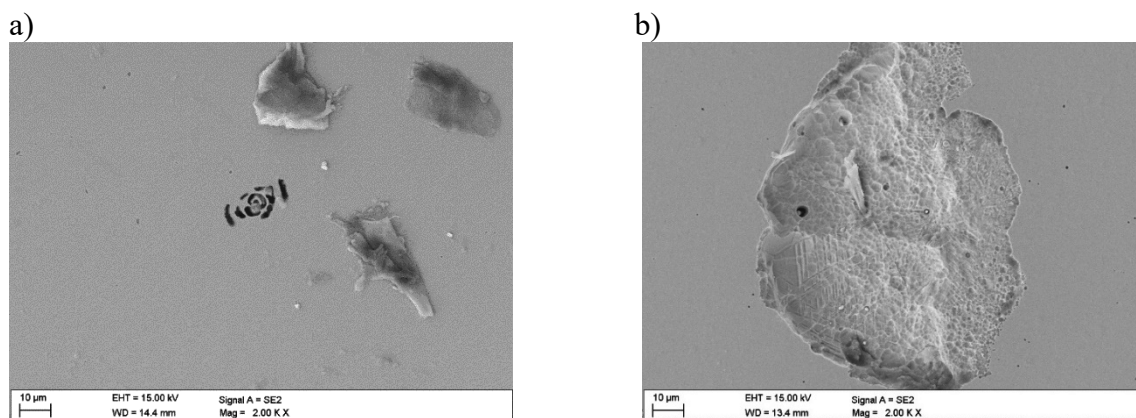


Figure 4. Surface morphology after an electrochemical examination of the sample: (a) uncoated; (b) with a  $\text{TiO}_2$  coating deposited in 200 cycles.

## 5. CONCLUSIONS

Based on the research, the following conclusions were confirmed:

- The amorphous structure of titanium oxide is a key factor in achieving the optimal electrochemical properties.
- $\text{TiO}_2$  layers applied on 316L steel substrates contribute to the improvement of electrochemical properties.

- In the conducted tests, the highest corrosion resistance is shown by coatings with the number of cycles being 500.

## ACKNOWLEDGEMENTS

This work was produced as part of the project implemented within the framework of project-oriented education – PBL, in the X competition under the Excellence Initiative – Research University program, at the Silesian University of Technology.

## REFERENCES

1. J. Marciniak: Biomateriały, Wydawnictwo Politechniki Śląskiej, Gliwice, 2013.
2. K. Wnętrzak, M. Basiaga: Wpływ parametrów nanoszenia warstw TiO<sub>2</sub> metodą ald na ich adhezję do metalicznego podłoża, Aktualne Problemy Biomechaniki 10 (2016) 85-90.
3. B. Świczko-Żurek: Biomateriały, Wydawnictwo Politechniki Gdańskiej, Gdańsk, 2009
4. D. Wilczeka, K. Kopeć, D. Pakuła Własności mechaniczne i elektryczne wybranych tlenkowych powłok ALD, Materiały studenckiej konferencji naukowej Talent Detector, 25 czerwca 2021.
5. P. Boryło, M. Szindler, M. M. Szindler: Metoda atomowego osadzania cienkich warstw optycznych, Prace studenckich kół naukowych Sokół 30 (2014) 3-8.
6. M. Lelis, S. Tuckute, S. Varnagiris, M. Urbonavicius, G. Laukaitis, K. Bockute: Tailoring of TiO<sub>2</sub> film microstructure by pulsed-DC and RF magnetron cosputtering, Surface and Coatings Technology 377 (2019) 124906. <https://doi.org/10.1016/j.surfcoat.2019.124906>.
7. Ł. Wachnicki, S. Gieraltowska, B. S. Witkowski, M. Godlewski, Antimicrobial coatings grown by the atomic layer deposition technique, 2015 IEEE 15th International Conference on Nanotechnology (IEEE-NANO), 27-30 July 2015. doi 10.1109/NANO.2015.7388745
8. Website: <https://zpe.gov.pl> (Access: 5th January 2024).
9. Mohammad Ali Behnam, Farzin Emami, Zahra Sobhani, Amir Reza Dehghanian The application of titanium dioxide (TiO<sub>2</sub>) nanoparticles in the photo-thermal therapy of melanoma cancer model, Iran J Basic Med Sci. 21(11) (2018) 1133–1139, doi 10.22038/IJBMS.2018.30284.7304
10. Ma, Wang; Yi, Shengen; Lin, Liangwu; Huang, He; Peng, Tao; Liu, Zhongtao; Liu, Zhipeng; Pei, Dongni; Miao, Xiongying; Wen, Yu; Chen, Wei; Xiong, Li: Anticancer Effect of Photodynamic Therapy with Photosan-Loaded Titanium Dioxide Nanoparticles on Panc-1 Pancreatic Cancer Cells In Vitro, Science of Advanced Materials, 8 (5) (2016), 1145-1153, doi <https://doi.org/10.1166/sam.2016.2343>
11. M. Staszuk: Investigations of CrN+Cr<sub>2</sub>O<sub>3</sub>/TiO<sub>2</sub> coatings obtained in a PVD/ALD hybrid method on austenitic 316L steel substrate, Vacuum 207 (2023) 111653. <https://doi.org/10.1016/j.vacuum.2022.111653>
12. W. Ostwald, Studien über die Bildung und Umwandlung fester Körper. 1. Abhandlung: Übersättigung und Überkaltung, Z. Phys. Chem. 22 (1897) 289-330.
13. M. Staszuk, D. Pakuła, Ł. Reimann, M. Król, M. Basiaga, D. Mysłek, A. Kríž: Structure and Properties of ZnO Coatings Obtained by Atomic Layer Deposition (ALD) Method on a Cr-Ni-Mo Steel Substrate Type, Materials 13(19) (2020) 4223. <https://doi.org/10.3390/ma13194223>





26th January 2024  
Gliwice, Poland

DEPARTMENT OF ENGINEERING MATERIALS AND BIOMATERIALS  
FACULTY OF MECHANICAL ENGINEERING  
SILESIA UNIVERSITY OF TECHNOLOGY

## INTERNATIONAL STUDENTS SCIENTIFIC CONFERENCE

### Zváranie a zvariteľnosť hliníka a jeho zliatin

E. Illichmanová<sup>a</sup>, M. Uhrčík<sup>a</sup>

<sup>a</sup> Žilinská univerzita v Žiline, Strojnícka fakulta, Katedra materiálového inžinierstva, Univerzitná 8215/1, 010 26 Žilina, Slovak Republic  
email: illichmanova@stud.uniza.sk milan.uhricik@fstroj.uniza.sk

**Abstrakt:** Článok sa zaoberá popisom hliníka a jeho zliatin a porovnaním vlastností s oceľou. Ďalej je práca zameraná na opis zvariteľnosti a metód zvárania vhodných pre Al a jeho zliatiny.

**Abstract:** The article deals with the description of aluminium and its alloys and the comparison of properties with steel. Further, the work is focused on the description of weldability and welding methods suitable for Al and its alloys.

**Kľúčové slová:** hliník a jeho zliatiny, zváranie

**Keywords:** aluminium and Al-alloys, welding

### 1. ÚVOD

V súčasnej dobe nájdeme v rôznych odvetviach priemyslu hliník a jeho zliatiny, ako najčastejšie používaný neželezný kovový materiál. Vyznačuje sa skvelými vlastnosťami pre široké využitie, najmä dobrým pomerom pevnosti k hustote, vynikajúcou koróznou odolnosťou, fyzikálnymi, chemickými a metalurgickými vlastnosťami.

Uplatnenie nachádza v automobilovom, námornom, leteckom, potravinárskom, elektrotechnickom a vesmírnom priemysle. Al a jeho zliatiny, v porovnaní s oceľou, nám ponúkajú rovnako množstvo výhod ako aj nevýhod. Pre rad problémov, ako sú slabá zvariteľnosť, predstavuje zváranie hliníka pre technológa určitú výzvu. Zabránenie vzniku chýb vo zváranom kove si vyžaduje nielen správny výber technológie zvárania, ale aj presný výber parametrov zvaracieho procesu. Pri zváraní treba tiež počítať so znížením mechanických vlastností hliníka v teplom ovplyvnenej oblasti [1].

### 2. HLINÍK A JEHO ZLIATINY

Čistý hliník sa vyznačuje nízkou mernou hmotnosťou ( $2700 \text{ kg}\cdot\text{m}^{-3}$ ), nízkou teplotou tavenia ( $658^\circ\text{C}$ ), dobrou koróznou odolnosťou, vysokou elektrickou ( $38 \text{ MS}\cdot\text{m}^{-1}$ ) a tepelnou vodivosťou ( $209 \text{ W}\cdot\text{m}^{-1}\cdot\text{K}^{-1}$ ). Je to nepolymorfny kov s kubickou plošne centrovanou mriežkou.

Veľmi dobre sa tvaruje za tepla, ale aj za studena. Značnou nevýhodou tohto materiálu je nízka pevnosť a veľkosť zmrastenia pri prechode z kvapalného skupenstva na pevné, ktoré dosahuje až 6% [2].

Pre zlepšenie vlastností hliníka sa používajú legujúce prvky, deformácia za studena alebo tepelné spracovanie. Ako legujúce prvky pre zvýšenie mechanických vlastností sa využíva meď, horčík, mangán, kremík a zinok. Prísady ako sú chróm, titán a nikel sa používajú na zjemnenie štruktúrneho zrna. Legujúce prvky by nemali v súčte presiahnuť 10%. Výrazné zvýšenie pevnosti je možné doceliť vytvrdzovaním, avšak nie všetky zliatiny hliníka sa dajú vytvrdzovať. Nevytvrditeľné zliatiny je možné spevniť tvárnením za studena [1].

## 2.1. Rozdelenie Al zliatin

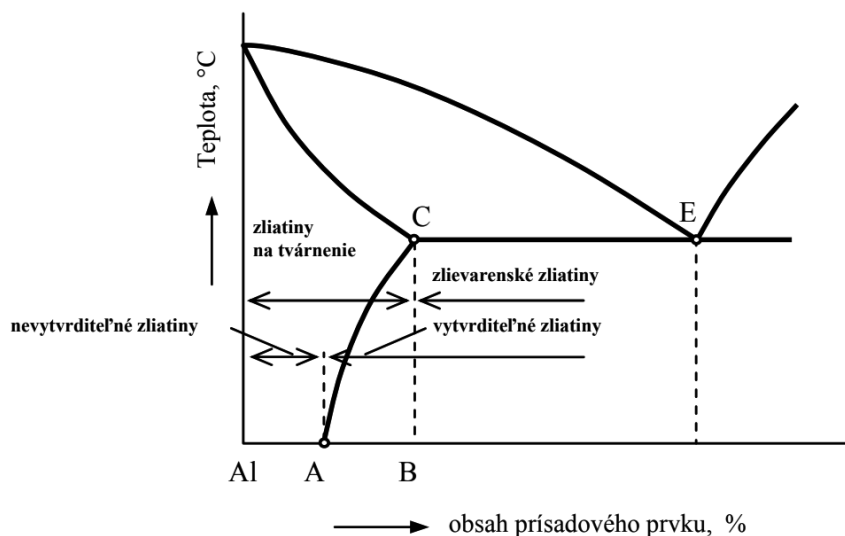
Zliatiny hliníka prevyšujú svojimi mechanicko-fyzikálnymi vlastnosťami vlastnosti čistého hliníka a je možné ich roztriediť na základe dvoch hľadísk (Obr.1):

Z hľadiska možnosti zvýšenia ich pevnostných vlastností cestou tepelného spracovania ich delíme na:

- nevytvrditeľné,
- vytvrditeľné.

Z hľadiska technológie spracovania ich delíme na:

- zliatiny na tvárnenie,
- zliatiny na odlievanie [3].



Obr. 1 Schéma rozdelenia hliníkových zliatin podľa možností zvýšenia ich mechanických vlastností a podľa technológie spracovania [4]

Figure 1. Schematic diagram of aluminium alloys according to the possibilities of increasing their mechanical properties and according to the processing technology [4]

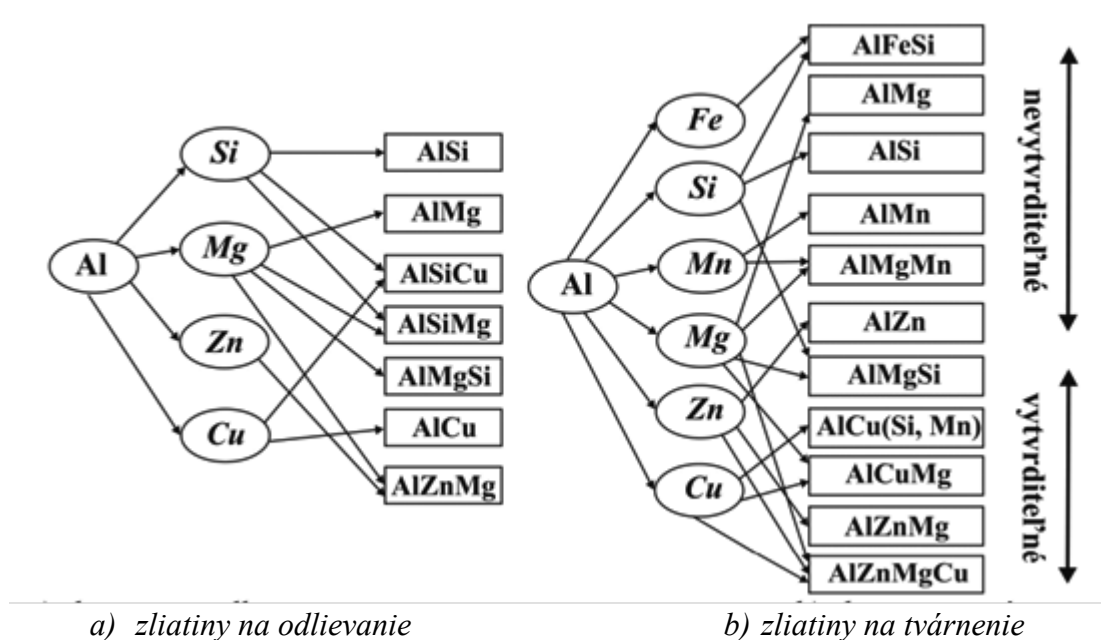
**Nevytvrditeľné zliatiny** obsahujú 5 až 20 % Si a ďalšie prísady, z ktorých najdôležitejší je Mn, ktorý eliminuje vplyv prímеси Fe. Zvýšenie ich pevnosti nie je možné pomocou tepelného spracovania - vytvrdzovania. Spevnenie je možné tvárnením za studena, pričom sa deformuje kryštálová mriežka a aj jednotlivé kryštály, ktoré sa predlžujú a orientujú podľa smeru a

intenzity tvárnenia. Pri tvárnení nastávajú väčšie poruchy a napätia v mriežke, čo spôsobuje sťažený pohyb dislokácií v ďalších sklzových systémoch. Výsledkom je spevnenie zliatiny (od 200 MPa do 300 MPa).

**Vytvrdiviteľné zliatiny** sú zliatiny, pri ktorých je možné zvýšiť mechanické vlastnosti vytvrdzovaním. Vytvrdiviteľnosť týchto zliatin je podmienená prítomnosťou Mg alebo Cu. Po tepelnom spracovaní nastáva zvýšenie medze pevnosti  $R_m$  (na viac ako 300 MPa) pri súčasnom poklese ťažnosti  $A$ .

**Zliatiny na odlievanie** majú vyšší obsah prísadových prvkov, tuhnú preto ako heterogénne. Vo výslednej štruktúre sa vyskytuje eutektikum. Najlepšie zlievarenské vlastnosti majú zliatiny s obsahom prísady v okolí eutektickej koncentrácie (bod E), tieto sa tiež najčastejšie používajú.

**Zliatiny na tvárnenie** (Obr. 2), sem patria hlavne zliatiny na báze Al-Mn a Al-Mg. Sú charakteristické menším obsahom prísad (do 10%), sú veľmi dobre tvárniteľné za studena aj za tepla, čím sa dosiahne zvýšenie pevnosti. Nevytvrdzujú sa z dôvodu malého efektu vytvrdzenia (zliatiny typu Al-Mn) a taktiež preto, lebo malé zvýšenie pevnosti by bolo sprevádzané veľkým znížením ťažnosti (zliatiny typu Al-Mg). Zliatiny na tvárnenie Al-Mg a Al-Mg-Si sa využívajú aj pre výrobu plechov, rúr, tyčí a profilov valcovaním, pretlačovaním a ťahaním [4].



Obr.2 Schematické znázornenie používaných hliníkových zliatin [4]

Figure 2. Schematic representation of aluminium alloys [4]

Pri nižšom obsahu prísadového prvku ako je hodnota udávajúca jeho rozpustnosť v hliníku za normálnej teploty, nemôže vzniknúť presýtený tuhý roztok, ktorý je predpokladom tepelného vytvrdzovania a takéto zliatiny sa nedajú tepelne vytvrdzovať. Vytvrdzovať sa nedá čistý hliník, ktorý neobsahuje žiadnu prísadu a zliatiny Al-Mn, pretože mangán je iba veľmi málo rozpustný v hliníku. Zliatiny typu Al-Mg nie je vhodné tepelne vytvrdzovať, aj keď sa to dá, pretože sa môže nepriaznivo ovplyvniť jej odolnosť voči korózii. Zo zliatin používaných v strojárskom priemysle sa vytvrdzujú zliatiny typu Al-Mg-Si, Al-Zn-Mg a duraly Al-Cu-Mg. Pevnosť nevytvrditeľných zliatin je možné zvýšiť iba tvárnením [1].

## 2.2. Číselné označenie hliníkových zliatin

V dnešnej dobe sa využíva veľké množstvo hliníkových zliatin. Tento trend si vyžiadala jednotné medzinárodné označovanie. Rozlišujeme dva systémy označovania a to číselný, alebo na základe chemických značiek. Pri hliníkových zliatinách pre tvárnenie sa v medzinárodnej praxi prijal spôsob označovania používaný organizáciou Aluminium Association (AA) vo Washingtone, USA. Číselné označenie zliatiny je zložené z písmen EN označujúcich, že ide o európsku normu, písmen AW (Aluminium Wrought - označuje zliatinu na tvárnenie), štvorčíslia, z ktorého prvé číslo udáva hlavný legujúci prvok a označenia v akom stave sú zliatiny dodávané (Tab.1). [1]

Tab. 1. Triedy hliníkových zliatin podľa legujúcich prvkov [5]

Tabela 1. Classes of aluminium alloys according to alloying elements [5]

Označenie	Hlavný legujúci prvok	Vlastnosti a aplikácia
1XXX	čistý hliník Al 99,9 % a viac	Sú málo pevné, ale vysoko odolné voči korózii. Používajú sa na vedenie elektriny alebo prepravu chemikálií.
2XXX	meď - Cu	Na zvýšenie pevnosti sa často pridávajú ďalšie legujúce prvky, ako je Ni, Ti, Mn. Pri zváraní sú náchylné na praskanie. Často sa používajú v leteckých aplikáciách.
3XXX	mangán - Mn	Táto séria zliatin je iba stredne pevná, takže nepracuje dobre v štruktúrnych aplikáciách. Je to však veľmi dobre na ohýbanie a tvarovanie. Najčastejšie sa používa vo výmenníkoch tepla a klimatizáciách.
4XXX	kremík - Si	Sú vysoko zvárateľné, ale častejšie sa používajú ako výplňové materiály pre iné triedy (napr. pre triedu 5XXX).
5XXX	horčík - Mg	Majú veľmi vysokú pevnosť. Používajú sa v konštrukčných a ťažkých aplikáciách ako je stavba lodí, mostov, či budov.
6XXX	horčík a kremík - Mg + Si	Najčastejšie používané na zváranie. Majú vysokú pevnosť a dobre reagujú na tepelné spracovanie. Sú bežne extrudované a používané ako konštrukčné diely.
7XXX	zinok - Zn	Sú extrémne pevné. Používané v leteckých aplikáciách. Počas zvárania sú náchylné na praskanie a menej odolné voči korózii.
8XXX	iný prvok (napr. cín - Sn)	

## 2.3. Porovnanie vlastností hliníka s oceľou

Hliníkové zliatiny predstavujú pevný a ťažný kov a majú podobné vlastnosti ako oceľ. Tie s vyššími pevnosťami sú porovnateľné s oceľou, sú však menej ťažné. Hliník, na rozdiel od ocele je nemagnetický. [1]

**Medzi výhody použitia hliníkových zliatin patria:**

- *nízka hmotnosť* - hliník je veľmi ľahký kovový materiál s hustotou len  $2,7\text{g/cm}^3$ , čo je asi 36 % hustoty ocele. Použitie hliníkovej zliatiny na výrobu mechanických častí môže výrazne znížiť hmotnosť a dosiahnuť efekt nízkej hmotnosti, úspory energie a zníženia emisií;
- *odolnosť voči korózii* - hliník nekoroduje a za normálnych podmienok môže zostať bez ochrany náterom. Vysokú odolnosť hliníka voči korózii zabezpečuje povrchová oxidická vrstva  $\text{Al}_2\text{O}_3$ . V agresívnych prostrediach však korodujú aj najpevnejšie hliníkové zliatiny a teda môžu vyžadovať ochranu;
- *spájanie lepením* - spájanie je možné používať aj v konštrukčných spojoch;
- *použitie pri nízkych teplotách* - na rozdiel od ocele nie je náchylný na krehký lom pri nízkych teplotách. Jeho vlastnosti sa s klesajúcou teplotou zlepšujú;
- *recyklovateľnosť* - pri recyklovaní hliníka sa ušetrí až 95 % energie potrebnej na výrobu nového hliníka z bauxitu.

**Medzi nevýhody použitia hliníkových zliatin patria:**

- *deformácie pri zváraní* - sú spôsobené v dôsledku 3-krát menšieho modulu pružnosti;
- v hliníkovom prvku vznikajú 3-krát väčšie deformácie ako v ocelovom prvku;
- *stabilita konštrukcii* - hliník má 3-krát menší modul pružnosti v ťahu E ako oceľ, a preto kritické napätie štíhlych prvkov a stien je 3- krát menšie. Je citlivejší na stratu stability vybočením, skrútením, vydúvaním atď. [1].

### 3. ZVARITEĽNOSŤ HLINÍKOVÝCH ZLIATÍN

#### 3.1. Problémy pri zváraní hliníka a Al-zliatin

Ovplyvnené fyzikálnymi a chemickými vlastnosťami hliníkových zliatin existujú určité ťažkosti v procese zvárania. Súčasné zváranie hliníkových zliatin má hlavne tieto problémy: tepelné namáhanie, ablačné vyparovanie, pevné inklúzie, kolaps pórov atď.:

**Tepelný stres.** Zliatiny hliníka majú vyšší koeficient tepelnej rozťažnosti a nižší modul pružnosti. Počas procesu zvárania je v dôsledku veľkej deformácie a veľkého koeficientu lineárnej rozťažnosti hliníkovej zliatiny miera zmršťovania objemu počas tuhnutia približne 6 percent a rýchlosť ochladzovania a rýchlosť primárnej kryštalizácie roztaveného kúpeľa sú rýchle, čo vedie k vnútornému napätiu zvaru a tuhosť zvarového spoja. Ak je veľký, je ľahké generovať veľké vnútorné napätie v spoji z hliníkovej zliatiny, čo spôsobuje veľké napätie pri zváraní a deformáciu a vytvára defekty, ako sú praskliny a deformácia vln [5].

**Ablatívne odparovanie.** Teplota topenia hliníka je  $660^\circ\text{C}$  a bod varu je  $2\,647$  stupňov, čo je menej ako u iných kovových prvkov, ako sú meď alebo železo. Počas procesu zvárania, ak je teplota zvárania príliš vysoká, môže ľahko explodovať a vytvárať rozstreky, najmä pri zváraní vysoko energetickým lúčom. Okrem toho niektoré legujúce prvky pridávané do hliníkovej zliatiny majú nízky bod varu, ktorý sa ľahko odparuje a horí pri okamžitej vysokej teplote zvárania a rozstrekovanie spôsobené výbuchom tiež odoberie niekoľko kvapiek, čo nevyhnutne zmení oblasť zvaru. Chemické zloženie neprispieva k regulácii výkonu zvarových spojov. Preto sa na kompenzáciu vysokoteplotnej ablácie pri zváraní často používajú zvaracie drôty alebo iné zvaracie materiály s vyšším bodom varu ako základný kov.

**Pevné inklúzie.** Chemické vlastnosti hliníka sú veľmi aktívne a ľahko oxidujú. Počas procesu zvárania sa povrch hliníkovej zliatiny oxiduje na  $\text{Al}_2\text{O}_3$  s vysokou teplotou topenia (asi

2050 stupňov, zatiaľ čo teplota topenia hliníka je 660°C, čo je veľmi rozdielne). Oxidy sú husté a majú vysokú tvrdosť a sú zmiešané v roztavenej zliatinovej kvapaline s nízkou hustotou v oblasti roztaveného bazéna, čo ľahko vytvára malé pevné troskové inklúzie, ktoré sa nedajú ľahko vyprázdniť, čo ovplyvňuje nielen mikroštruktúru zvaru, ale je náchylný aj na elektrochemickú koróziu, ktorá spôsobí pokles mechanických vlastností zvarových spojov a  $\text{Al}_2\text{O}_3$  prekryje roztavený kúpeľ a drážku, čo vážne ovplyvňuje zváranie zliatin a znižuje mikroštruktúru a vlastnosti zvarových spojov.

**Pórovitosť.** Pôsobením okamžitého vysokého výkonu zdroja zváracieho tepla sa v zliatinovej kvapaline rozpustí veľké množstvo vodíka. Po ukončení zvárania, keď teplota roztaveného kúpeľa klesá, rozpustnosť plynu sa postupne znižuje, čo sa stáva hlavnou príčinou pórov počas procesu zvárania. Tieto póry sa budú počas procesu zvárania naďalej hromadiť a rozširovať, prípadne vytvoria viditeľné póry a znížia štruktúrne vlastnosti spoja. Samozrejme, tvorba pórov sa nemusí nevyhnutne vytvárať počas procesu zvárania. Vplyvom technológie odlievania bude samotný základný kov vytvárať póry aj počas procesu odlievania. Pri zváraní neustála zmena vneseného tepla a vnútorného tlaku spôsobuje, že pôvodné póry v základnom kove sa teplom rozťahujú alebo sa navzájom spájajú a vytvárajú zvarové póry. So zvýšením tepelného príkonu zvárania sa zväčšia aj póry. Preto, aby bolo možné kontrolovať zdroj vodíka, zvárací materiál musí pred použitím prejsť prísny sušením. Počas zvárania by sa mal prúd primerane zvýšiť, aby sa predĺžila doba existencie roztaveného kúpeľa a umožnil sa dostatočný čas na vyzrážanie vodíka, čím sa reguluje tvorba pórov [5].

### 3.2. Metódy zvárania hliníka a Al-zliatin

Zváranie hliníka a jeho zliatin je známe niekoľko desiatok rokov. Napriek tomu hliník má niektoré špecifické vlastnosti, ktoré doteraz spôsobujú zváranie nie malé problémy. Hliník má nízky bod tavenia (cca 660 °C) a jeho farba sa nemení pri prechode do tekutého stavu. Má veľmi vysokú tepelnú vodivosť, čo znamená, že pre natavenie potrebuje vysokú koncentráciu energie. Podobne ako u iných neželezných kovov sú hliník a jeho zliatiny zvárané mnohými spôsobmi v závislosti od použitia spájaných komponentov. Okrem tradičného zvárania tavením, odporovým zváraním, zváraním plynom môžu tiež ľahko zvärať zliatiny hliníka ďalšie metódy zvárania. Zvárač vyberie príslušnú metódu podľa tried, hrúbky, štruktúry výrobku a požiadaviek na zváranie [6].

**Plynové zváranie.** Zváranie pomocou kyslíka a acetylénu má nízku tepelnú energiu plameňa, tepelné rozptyľovanie, deformáciu zvárania a nízku produktivitu. Predhriatie je potrebné pre hrubé hliníkové zvary, zvary kovových zrn sú silné a voľné, čo je ľahké, pokiaľ ide o tvorbu oxidu hlinitého, pórovitosť, praskliny a ďalšie chyby. Táto metóda sa používa iba na zváranie nekritických hliníkových častí a odliatok s hrúbkou od 0,5 do 10 mm.

**Zváranie volfrámovým argónom.** Tento spôsob sa prevádzkuje pod ochranou argónu, ponúka relatívne koncentrované teplo, stabilné spaľovanie oblúkom, získava sa hustý zvarový kov a vyššia pevnosť a plasticita zváraného spoja. Zváranie TIG je široko používaná metóda zvárania pre zliatiny hliníka, ale nie je vhodná pre vonkajšie a vonkajšie podmienky pre zváracie zariadenia TIG.

**Zváranie roztaveným argónom.** Oblúkový výkon automatického a poloautomatického zvárania argónovým oblúkom je veľký, teplo je koncentrované a ovplyvnená oblasť je malá, jeho výrobná účinnosť je 2 až 3-krát väčšia ako manuálne zváranie argónovým volfrámovým oblúkom. Oblúkové zváranie roztaveným argónom je vhodné pre zváranie s hrúbkou menej ako 50 mm čistého hliníka a platne z hliníkovej zliatiny. Napríklad predhrievanie nie je potrebné

pre zváranie hrúbky hliníka s hrúbkou 30 mm, iba hladký povrch a dobrú kvalitu je možné získať iba pri zváraní pozitívnych, negatívnych vrstiev. Poloautomatické zváranie v tenkom oblúku je vhodné na lokalizáciu zvarov, prerušovaných krátkych zvarov a zváraných častí s nepravidelným tvarom štruktúry. Poloautomatický zvárací horák TIG sa dá použiť na pohodlné a flexibilné zváranie, ale jeho priemer drôtu je malý a pórovitosť citlivosti zvarov je veľká.

**Pulzné argónové oblúkové zváranie.** Poznáme 2 spôsoby:

- *Zváranie pulzným argónom s volfrámovým zváraním* - tento spôsob môže samozrejme zlepšiť stabilitu procesu nízko prúdového zvárania, ktorý je vhodný na reguláciu oblúkového výkonu a formovania zvaru úpravou rôznych parametrov. Je charakterizovaný malou deformáciou a malou oblasťou ovplyvňovanou teplom, vhodný pre tenkú dosku, všestrannú polohu zváranie a iné príležitosti, ako aj zváranie kovaného hliníka, duralu a superduralu so silnou tepelnou citlivosťou.
- *Pulzné zváranie elektrónovým oblúkom s tavením elektród* - metóda ponúka malý priemerný zvárací prúd a veľký rozsah nastavenia parametrov, môže dosiahnuť malú zváraciu deformačnú a tepelnú nárazovú zónu, vysokú produktivitu, dobrú odolnosť voči pórovitosti a trhlinám, vhodné pre zváranie plechov z hliníkovej zliatiny 2 ~ 10 mm.

**Odporové zváranie (bodové, švové).** Tento spôsob sa môže použiť na zváranie dosiek z hliníkových zliatin s hrúbkou menšou ako 4 mm. Výrobky s vysokými požiadavkami na kvalitu môžu používať bodové zváranie pomocou jednosmerného prúdu, zváranie zvarových švov. zložitú zváraciu zariadenie a veľký prúd, zvlášť vhodné pre hromadnú výrobu hliníka a jeho častí zliatiny hliníka [6].

### 3.3 Požiadavky na ochranné atmosféry.

Pri zváraní hliníka a jeho zliatin primárne ochranná atmosféra slúži ako ochrana zvarového kúpeľa pred okolitým vzduchom. Sekundárne, ochranná atmosféra vplýva aj na vývoj a prenos tepla v oblúku.

Plyn z nízkym ionizačným potenciálom (argón) vytvorí oblúk s nízkou teplotou. V oblúku vznikne plazma s nízkou tepelnou vodivosťou, čo spôsobí nízku entalpiu v oblúku a tým malý prievar. Ak sa použije plyn s vysokým ionizačným potenciálom (hélium), tepelná vodivosť je vysoká s priaznivým vplyvom na vytváranie zvaru. Problémom je zlé štartovanie oblúka. Tieto nedostatky obidvoch typov plynov sa riešia zmesami s rôznym podielom Ar+He. Je to kompromis medzi zapalovaním oblúka, prievarom a schopnosťou zvárača udržať kúpeľ v pracovnej polohe. Stačí pridať 5 % He do argónu a zváracia rýchlosť sa zvýši o 15 %, prievar o 10 % a zvárač dokáže veľmi dobre ovládať zvarový kúpeľ. Pri manuálnom zváraní sa používa max. obsah He v Ar 50 %. Pre automatické zváranie je vhodné cca 70 % He v Ar. Dosahuje sa vysoká zváracia rýchlosť, veľký prievar, zapalovanie je automatické a nižšia teplota predohrevu.

Na zváranie hliníka a hliníkových zliatin tavnou elektródou sa už pred niekoľkými rokmi začala používať ochranná atmosféra argónu s prímiesou kyslíka 1 až 2 %. Výhodou je veľký prievar pri konštantných mechanických hodnotách spoja. Negatívnou stránkou je v tomto prípade vzhľad spoja, na ktorom sa vytvárajú čierne oxidy. Tie sa dajú odstrániť s malými nákladmi, ale nie všade sú tieto oxidy prijateľné.

Mikroprídavky plyných prvkov sa začali používať v 70. rokoch minulého storočia. Mikroprímies alebo mikroprídavok je obecné menší ako 0,5 %. Prvé mikroprímiesi do Ar sa používali na zníženie emisií O<sub>3</sub>. Boli to prímiesi CO a NO a obsah bol medzi 150 až 300 ppm, čo je 0,015 až 0,03 %.

V prípade mikroprímesí nehrajú fyzikálne či chemické vlastnosti jednotlivých prímesí žiadnu rolu. Tepelná vodivosť, entalpia alebo elektrická vodivosť a ionizačný potenciál nemajú vplyv na chovanie oblúku. Vlastnosti pridaných plynov sa posudzujú z hľadiska interakcie medzi plynnou zložkou a roztaveným materiálom.

Monoatomárne plyny sú chemicky inertné voči metalurgii a interakcii pri zváraní. A teda nie sú zaujímavé. Zaujímavejšie sú atómové plyny, lebo molekula sa vo vnútri oblúka rozdelí na jednotlivé prvky, ktoré reagujú buď na taveninu, alebo s voľnými radikálmi. Energia uvoľnená v priebehu rozpadu je pre zlepšenie výkonu zanedbateľná. Z ponuky viacatómových plynov sú kvôli vplyvu na tavenie najzaujímavejšie: CO<sub>2</sub>, O<sub>2</sub>, N<sub>2</sub>, NO, ďalšie NO<sub>x</sub>, CO, H<sub>2</sub>, H<sub>2</sub>O.

#### 4. ZÁVER

Hliník a jeho zliatiny majú v rôznych odvetviach priemyslu významné postavenie. Vďaka svojim špecifickým vlastnostiam sa radia ako jedny z najčastejšie využívaných konštrukčných materiálov. Napriek mnohým výhodám, ako je jeho nízka hmotnosť, existujú faktory, ktoré môžu komplikovať zváranie, ako napr. vysoká tepelná vodivosť alebo nízka teplotná húževnatosť materiálu. S rozvojom pokročilých technológií a metód zvárania sa však tieto problémy postupne eliminujú. Napriek výzvam sú výsledné zvary výnimočné, vďaka svojej pevnosti a odolnosti voči korózii. Celkovo možno povedať, že správna voľba legujúcich prvkov a zváracej technológie môže výrazne ovplyvniť úspech zvárania hliníka a jeho zliatin, a umožniť tak väčšie využitie ich vlastností vo viacerých odvetviach priemyslu.

#### POĎAKOVANIE

Príspevok vznikol v rámci riešenia spoločného slovensko-poľského projektu TalentDetector 2023 ako výsledok spolupráce medzi Politechnikou Slaskou (Poľsko) a Žilinskou univerzitou v Žiline a projektov KEGA č. 004ŽU-4/2023 a KEGA č.009ŽU-4/2023.

#### BIBLIOGRAPHY

1. I. Baláž, Eurokód EN 1999 pre navrhovanie konštrukcií z hliníkových zliatin - materiál. EUROSTAV, Bratislava, 2007.
2. P. Skočovský, O. Bokuvka, E. Tillová, R. Konečná, Náuka o materiály pre odbory strojnícke. EDIS, Žilina, 2013.
3. P. Skočovský, P. Palček, R. Konečná, L. Várkoly, Konštrukčné materiály. EDIS, Žilina, 2000.
4. Teória zliatiny Al – Si. [online] 2010 Dostupné na internete: <<http://kmi2.uniza.sk/wp-content/uploads/2010/02/teoria-zliatiny-Al-Si.pdf>>
5. Zvládnite kľúčovú technológiu zvárania hliníkových zliatin. [online] 2022 Dostupné na internete: <<http://sk.dayangwelding.de/news/master-the-key-technology-of-aluminum-alloy-we-62837225.html>>
6. Metódy zvárania hliníka a jeho zliatin. [online] 2019 Dostupné na internete: <<https://sk.lksteelpipe.com/news/the-welding-methods-of-aluminum-and-its-alloys-30817957.html>>





26th January 2024  
Gliwice, Poland

DEPARTMENT OF ENGINEERING MATERIALS AND BIOMATERIALS  
FACULTY OF MECHANICAL ENGINEERING  
SILESIA UNIVERSITY OF TECHNOLOGY

## INTERNATIONAL STUDENTS SCIENTIFIC CONFERENCE

### Wiązka laserowa jako zaawansowane narzędzie w inżynierii powierzchni

B. Jóźwiak <sup>a</sup>, N. Juszczak <sup>a</sup>, M. Bonek <sup>b</sup>

<sup>a</sup> Uczeń V Liceum Ogólnokształcące z Oddziałami Dwujęzycznymi im. Andrzeja Struga w Gliwicach, email: jozwiakbartek50@gmail.com

<sup>b</sup> Politechnika Śląska, Wydział Mechaniczny Technologiczny, Katedra Materiałów Inżynierskich i Biomedycznych  
email: miroslaw.bonek@polsl.pl

**Streszczenie:** W pracy omówiono nowoczesne metody inżynierii powierzchni, z uwzględnieniem zastosowania wiązki laserowej. Lasery pozwalają na precyzyjną modyfikację struktury i właściwości materiałów poprzez procesy takie jak cięcie, stopowanie, przetapianie, ablację, spawanie oraz grawerowanie laserowe. Praca podkreśla znaczenie zastosowania parametrów procesu, takich jak moc lasera, czas ekspozycji czy rodzaj gazu osłonowego, dla osiągnięcia optymalnych efektów w obróbce laserowej. Zastosowanie laserów w procesach produkcyjnych zostało uznane za kluczowe dla zwiększenia konkurencyjności produktów dzięki zaawansowanej powtarzalności, wydajności i możliwości automatyzacji.

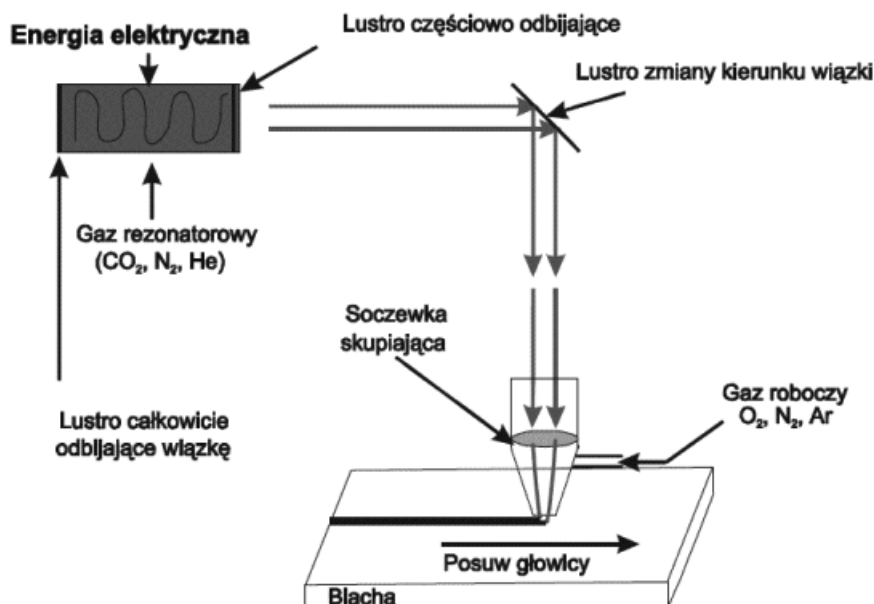
**Słowa kluczowe:** Laser, stopowanie, struktury, inżynieria powierzchni

### WPROWADZENIE

Współczesna inżynieria powierzchni nieustannie poszukuje nowych, skutecznych narzędzi, które umożliwią precyzyjną modyfikację struktury i właściwości materiałów. Jednym z najnowocześniejszych i obiecujących rozwiązań jest zastosowanie wiązki laserowej jako narzędzia inżynierskiego. Wiązka laserowa jest skoncentrowanym promieniem światła o dużej intensywności. W procesie obróbki powierzchni laser może działać na materiał poprzez różne mechanizmy, takie jak topienie, parowanie, ablację czy ogólną modyfikację struktury. Wykorzystanie lasera w obróbce powierzchni otwiera drzwi do szeregu nowych możliwości w dziedzinie produkcji, mikromechaniki, medycyny i wielu innych obszarów technologii. Przy użyciu odpowiednich parametrów, takich jak moc lasera, prędkość skanowania, grubość wiązki czy rodzaj stosowanego gazu osłonowego, można wypracować wysoko ekonomiczny, precyzyjny i wydajny tryb pracy. Ze względu na możliwość automatyzacji procesów laserowych, zastosowanie ich w procesach produkcyjnych pozwala znacznie zwiększyć konkurencyjność produktu na rynku, dzięki zaawansowanej powtarzalności i wysokiej wydajności.

## 1. CIĘCIE LASEROWE

Technologia cięcia laserowego jest procesem, w którym wiązka laserowa jest wykorzystywana do precyzyjnego i skutecznego przecinania różnych materiałów, w tym stali. W procesie tym laser generuje intensywną wiązkę światła o wysokiej energii, która skoncentrowana jest na małej powierzchni, umożliwiając dokładne cięcie w wybranym kierunku. Przy użyciu odpowiednich parametrów, takich jak moc lasera, prędkość cięcia i rodzaj stosowanego gazu osłonowego, można osiągnąć wysoką jakość cięcia, minimalne odkształcenia materiału oraz niską ilość odpadów. Technologia cięcia laserowego pozwala na osiągnięcie niezwykle precyzyjnych linii cięcia, co jest niezwykle istotne w produkcji skomplikowanych elementów.



Rys. 1 Schemat procesu cięcia laserem [1]

W zależności od stosowanego urządzenia (przede wszystkim jego mocy) cięcie przeprowadza się na trzy sposoby: metodą spalania, stapiania lub sublimacji. [2]

### 1.1 Metoda spalania

Metoda ta wykorzystuje zjawisko utleniania materiału rozgrzanego przez promień lasera. Temperatura grzania w szczelinie cięcia wynosi około 1200 st. Celsjusza. Materiał utleniając się pozostawia płynny żużel wydmuchiwany przez ciśnienie gazu technicznego.

### 1.2 Metoda stapiania

Metoda stapiania jest wykorzystywana przy cięciu stali wysokostopowych oraz metali nieżelaznych. Materiał cięty metodą stapiania jest obrabiany przez promień laserowy o dużej intensywności. Stosunkowo duża moc lasera pozwala na doprowadzenie materiału znajdującego się na ścieżce cięcia do postaci płynnej i wydmuchanie go przez gaz techniczny o dużej energii kinetycznej. Ponieważ nie zachodzi tutaj zjawisko spalania (utleniania z wydzielaniem energii) dodatkowa energia musi pochodzić z mocniejszego promienia laserowego lub wspomaganie

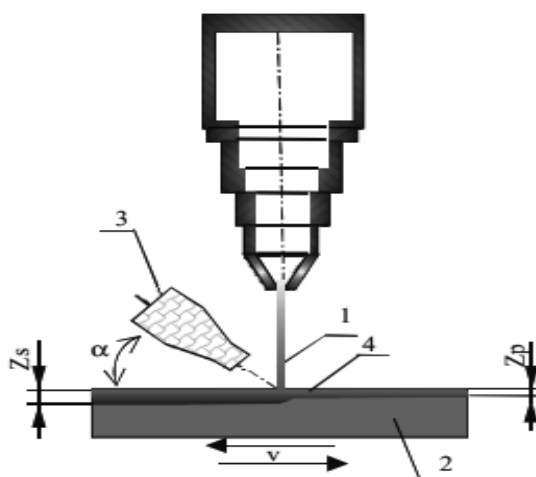
elektrycznego. Brak reakcji utleniania powoduje powstawanie powierzchni wolnych od tlenków co ma istotne znaczenie szczególnie przy obrabianiu stali wysokostopowych.

### 1.3 Metoda sublimacji

Zastosowanie laserów dużej mocy pozwala na doprowadzenie części obrabianego materiału (ścieżki cięcia) do stanu gazowego. Rozgrzany materiał jest wydmuchiwany pod bardzo wysokim ciśnieniem i zamieniany w parę. [1-2]

## 2. STOPOWANIE LASEROWE

Stopowanie laserowe (Laser Surface Alloying – LSA) to proces, w którym pierwiastki stopowe są wprowadzane do warstwy wierzchniej obrabianego przedmiotu podczas topienia powierzchni za pomocą wiązki laserowej. Po stwardnieniu powstaje warstwa o innym składzie chemicznym, strukturze i właściwościach w porównaniu do materiału wyjściowego. Zastosowanie różnych parametrów obróbki może prowadzić do istotnych różnic w ostatecznym stanie materiału. Istnieje wiele metod kształtowania warstwy wierzchniej w celu dostosowania jej do konkretnego zastosowania. Przetapianie powierzchni laserem powoduje lokalne, intensywne podgrzanie materiału, co skutkuje zmianami w morfologii i właściwościach. Te zmiany są związane z parametrami lasera, takimi jak moc, oraz czasem skanowania. [3].



Rysunek 2 Schemat procesu stopowania laserowego [4]: 1 - wiązka laserowa; 2 - próbka; 3 - nadmuch gazu ochronnego, 4 - materiał stopujący,  $Z_s$  - grubość warstwy stopowanej;  $Z_p$  - grubość nanoszonej powłoki stopującej;  $v$  - prędkość posuwu wiązki lasera

### 2.1 Wtapianie

Wtapianie laserowe to innowacyjna technika, w ramach której wiązka laserowa jest skoncentrowana na obszarze roboczym, a następnie wprowadzane są pierwiastki stopowe w postaci proszku, pasty lub gazu do utworzonego jeziora przetopionego materiału podłoża. Proces ten umożliwia precyzyjne kontrolowanie składu chemicznego warstwy wierzchniej, co prowadzi do uzyskania struktury o unikalnych właściwościach. Po zastygnięciu tworzy się

warstwa charakteryzująca się odmiennym składem, a także nowymi właściwościami i strukturą w porównaniu z materiałem bazowym.

Zaawansowane metody kształtowania warstwy wierzchniej w procesie wtapiania laserowego pozwalają na dostosowanie jej do specyficznych wymagań aplikacyjnych. Dodatkowo, kontrolowane podgrzewanie obszaru roboczego wiązką laserową ma istotne znaczenie, generując lokalne zmiany morfologii materiału, które przekładają się na unikatowe właściwości mechaniczne i termiczne. Parametry procesu, takie jak moc lasera i czas ekspozycji, odgrywają kluczową rolę w kształtowaniu finalnych cech warstwy wierzchniej.

## 2.2. Przetapianie

Proces przetapiania stanowi zaawansowaną metodę modyfikacji powierzchni, zakładając naniesienie warstwy materiału stopującego na podłoże i równoczesne przetopienie obu elementów. Inicjalnie, nanoszony jest cienki film z materiału stopującego, który następnie poddawany jest procesowi stopienia wraz z warstwą wierzchnią materiału podłoża. [5]

## 3. ABLACJA LASEROWA

Ablacja laserowa polega na usuwaniu materiału za pomocą wiązki laserowej o dużej energii. Emitowany promień laserowy zostaje absorbowany przez naświetlaną powierzchnię, przekazując jej energię, aż przekroczy on wartość krytyczną, znaną jako próg ablacyjny. Prowadzi do rozerwania połączeń między cząstkami materiału, skutkując ich oderwaniem od naświetlonej powierzchni. Właściwy materiał zostaje odróżniony od zanieczyszczeń za pomocą różnicy absorpcyjności, która jest współczynnikiem opisującym wartość energii przenoszonej przez światło o konkretnej długości fali, która może zostać pochłonięta przez naświetlaną substancję. Mechanizm ablacji wykorzystuje się do bardzo precyzyjnego i ekonomicznego czyszczenia różnorodnych powierzchni.

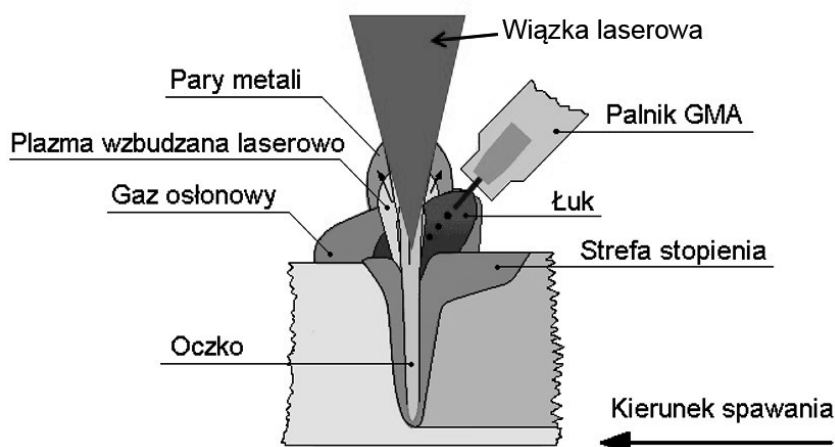


Rysunek. 3. Schemat przebiegu zjawisk podczas wykorzystania ablacji laserowej[6]

## 4. SPAWANIE LASEROWE

Technika spawania oparta na stapianiu obszaru styku przy użyciu wiązki promieni laserowych polega na łączeniu materiałów poprzez skoncentrowane działanie światła laserowego. Proces

spawania jest realizowany w atmosferze gazu obojętnego lub, jeśli materiał spawany nie jest podatny na utlenianie, w powietrzu. Taki sposób spawania gwarantuje wysoką wytrzymałość spoin. Znacząco powszechna w produkcji masowej, szczególnie w przemyśle motoryzacyjnym, ta technika znajduje zastosowanie w łączeniu różnorodnych materiałów, zapewniając efektywne i trwałe połączenia. Spawanie laserowe wykorzystuje wiązkę o dużej gęstości energii (około 1 MW/cm<sup>2</sup>). Efektem spawania laserowego jest mała szerokość strefy wpływu ciepła i niskie oddziaływanie temperatury na konstrukcję, szybkie odprowadzanie ciepła i stygnięcie spoiny



Rysunek 4. Schemat procesu spawania laserowego [7].

## 5. GRAWEROWANIE LASEROWE

Znakowanie laserowe to proces termiczny, gdzie stosowana jest skupiona wiązka światła laserowego, posiadająca duży stopień intensywności w celu dokonania widocznej zmiany na powierzchni danego materiału. Wiązka ta wywołuje wysoką zmianę temperatury na powierzchni, aż do wystąpienia w nim zmian kolorystycznych oraz do usunięcia materiału przez odparowanie. Grawerowanie jest nieusuwalne, a kontrast jest zawsze wysoki. Dodatkowo technologia laserowa umożliwia wykonanie najdrobniejszych szczegółów z maksymalną precyzją. Praktycznie wszystko co może być narysowane, można grawerować i znakować przy użyciu lasera, a przez uniwersalność tego narzędzia grawerować można praktycznie wszystkie powierzchnie i materiały takie jak metale, tkaniny, folie czy nawet kartony. [8].

## 6. PODSUMOWANIE

Przytoczone technologie oparte na laserach doskonale ilustrują wszechstronność ich zastosowań. W tym kontekście, znaczącą rolę odgrywa dział obróbki powierzchniowej, który umożliwia modyfikację struktury materiału, a w konsekwencji wprowadzenie zmian w jego właściwościach. Lasery, dzięki swoim unikalnym właściwościom, znajdują również zastosowanie w spawalnictwie, gdzie wykorzystywane są do precyzyjnego łączenia elementów. Proces cięcia laserowego, charakteryzujący się wyjątkowymi osiągnięciami w porównaniu do tradycyjnych metod cięcia, stanowi kolejne ważne pole zastosowania tej technologii. Wspomniane działy laserowej obróbki materiałów wykazują się niezwykłą różnorodnością

zastosowań w Inżynierii Powierzchni. Od zmiany struktury powierzchni, przez skomplikowane procesy spawalnicze, aż po precyzyjne cięcie i formowanie materiałów, technologie oparte na laserach stanowią kluczowy element postępu w dziedzinie materiałoznawstwa i obróbki materiałów.

## PODZIĘKOWANIE

Praca powstała w wyniku realizacji projektu realizowanego z uczniami szkoły ponadpodstawowej w ramach kształcenia zorientowanego projektowo – PBL, w ramach programu Inicjatywa Doskonałości – Uczelnia Badawcza, Politechnika Śląska.

## BIBLIOGRAFIA

1. Strona internetowa zakładu produkcyjnego BUD-EXPERT: <http://ciecielaserem.info> [dostęp 01/01/2024].
2. B. Józwiak, N. Juszczak, M. Bonek, Zastosowanie nowoczesnej technologii cięcia laserowego stali w przemyśle samochodowym.
3. K. Labisz, W. Banaś, Laserowe stopowanie stali narzędziowej do pracy na gorąco proszkiem ceramicznym NbC
4. J. Bujak, Ocena wpływu wybranych parametrów impulsowej wiązki laserowej na wydajność procesu ablacji tytanu, Instytut Technologii Eksploatacji – PIB, Radom.
5. T. Burakowski, J. Marczak, W. Napadłek, Istota ablacyjnego czyszczenia laserowego materiałów, Prace Instytutu Elektrotechniki w Warszawie, Zeszyt 228, Warszawa, 2006.
6. Strona internetowa dla produkcji.pl [Dostęp: 01.01.2024]
7. Strona internetowa lasitlaeser.pl [Dostęp 01.01.2024]
8. Kotarska A. Stopowanie laserowe. W: Górka J, redaktor. Perspektywy rozwoju technologii spawalniczych : Warsztaty Młodych Spawalników, Istebna, 13-14 czerwca 2017 r. Praca zbiorowa. 2017. s. 51–58. (Górka J. ).



26th January 2024  
Gliwice, Poland

DEPARTMENT OF ENGINEERING MATERIALS AND BIOMATERIALS  
FACULTY OF MECHANICAL ENGINEERING  
SILESIA UNIVERSITY OF TECHNOLOGY

## INTERNATIONAL STUDENTS SCIENTIFIC CONFERENCE

### Implementation guide for the 5S method in a micro-enterprise

M. Kaiser<sup>a</sup>, A. Kania<sup>b</sup>

<sup>a</sup> Student of Management and Production Engineering at the Faculty of Mechanical Engineering at the Silesian University of Technology

email: matykai792@student.polsl.pl

<sup>b</sup> Silesian University of Technology, Faculty of Mechanical Engineering, Department of Engineering Materials and Biomaterials

email: aneta.kania@polsl.pl

**Abstract:** The article serves as a practical guide for micro-entrepreneurs, presenting the steps for implementing the 5S method to improve workplace organization in companies. It focuses on specific stages of implementation and the development of a 5S audit, aiming to enhance operational processes within businesses.

**Keywords:** 5S method, work organization, 5S audit, 5S implementation, workplace management.

## 1. INTRODUCTION

In today's dynamic business environment, effective enterprise management requires not only strategic thinking but also efficient operational functioning. In this context, the key becomes the efficient utilization of resources, process optimization, and maintaining a high level of organization in the workplace. Disorder, lack of standardization, and ineffective workplace management are challenges faced by enterprises of various sizes. These issues not only impact the team's daily work but also the overall operational efficiency. Therefore, the search for effective methods to improve work organization becomes a priority for many companies.

One solution gaining increasing popularity is the philosophy of 5S. This Japanese method of workplace management offers a comprehensive system of improvements aimed at eliminating waste, increasing productivity, and enhancing the overall efficiency of every enterprise.

## 2. PREPARATION FOR 5S IMPLEMENTATION

Before commencing the implementation of the 5S method in a micro-enterprise, meticulous preparation is essential. A crucial aspect of this stage is understanding the full significance of this management philosophy and adequately preparing the team for the upcoming changes.

The 5S method extends beyond simply organizing the workplace. It is a comprehensive philosophy aimed at improving efficiency, eliminating waste, and creating an ergonomic work environment [1].

Effective implementation of 5S begins with a thorough analysis of the current state of the enterprise. Initially, it is necessary to identify areas requiring optimization, both in terms of physical space and business processes. This includes the use of tools that help define the scope of actions [1].

Before initiating the implementation, precise goals and expectations related to the 5S rollout are determined. Whether it's improving efficiency, work quality, or reducing losses, clearly defined goals allow tracking progress and assessing the effectiveness of actions. Prior to implementation, specific goals and expectations are defined. It's worth noting that the implemented 5S system in the enterprise should be supervised by the implementation team, which includes: the plant director, manager, leader, and specialists. Before starting the implementation, all employees of the company must be trained in the 5S method and informed about the schedule of events related to the system implementation. This is a crucial element ensuring the effectiveness and acceptance of changes by the entire team [2].

### 3. STAGES OF 5S IMPLEMENTATION

The implementation of the 5S method in a micro-enterprise is a process consisting of five key stages: Seiri, Seiton, Seiso, Seiketsu, and Shitsuke. Each stage has its unique goals and tasks, which, when effectively accomplished, contribute to efficiency, improvement in workplace organization, and increased discipline in daily practices. Below is a practical guide for each of the stages [3,4]:

#### 1) Seiri (Sort)

Goal: Remove unnecessary items from the workplace.

- Labeling items: Provide employees with red cards and ask them to label all items they consider non-essential in a given area.
- Define a waiting area: Designate a specific place for items marked as unnecessary. This allows for their storage while awaiting a decision regarding their fate.
- Needs analysis: Conduct an assessment of the usefulness of each item, eliminating what is unnecessary while facilitating access to essential items.

#### 2) Seiton (Set in Order)

Goal: Establish order through a well-thought-out arrangement of necessary items.

- Define locations: For each essential item, designate a clear location, typically utilizing visualization techniques such as labels, colors, or arrows.
- Create an organization plan: Develop a plan outlining which items should be stored in specific places. This facilitates quick locating and storing of items for employees.

#### 3) Seiso (Shine)

Goal: Ensure cleanliness and order in the workplace.

- Develop a cleaning schedule: Create a schedule for daily maintenance of cleanliness at the workstation. This should encompass both cleaning the workspace and maintaining the cleanliness of tools and machinery.



- Self-checking: Encourage employees to engage in daily self-checks and upkeep of cleanliness. Providing support in understanding that a clean environment contributes to productivity and workplace safety is crucial.

#### 4) Seiketsu (Standardize)

Goal: Establish standards for the previous three stages.

- Developing procedures: Create standardized procedures for Seiri, Seiton, and Seiso, defining how employees should approach these activities on a daily basis.
- Monitoring and evaluation: Regularly monitor progress and assess whether standards are being adhered to. Adjust procedures as needed to ensure effectiveness.

#### 5) Shitsuke (Sustain)

Goal: Promote the habit of maintaining order and adhering to standards.

- Education and training: Conduct regular education on the benefits of implementing the 5S method and provide training on maintaining the habit of self-discipline.
- Develop 5S audits: Create 5S audits as a tool for assessing and monitoring the effectiveness of maintaining standards. The audit should cover all stages of 5S and be performed regularly.
- Continuation of practice: Integrate 5S as a consistent practice, incorporating it into daily work routines. Emphasize continuous improvement of processes.

In Figure 1, a step-by-step example of the implementation process of the 5S method in a micro-enterprise is presented.



Figure 1. Sample course of the 5S implementation process (own elaboration)

## 4. DEVELOPMENT OF THE 5S AUDIT

For the effective implementation and functioning of the 5S method in improving workplace organization in a micro-enterprise, it is necessary to conduct a systematic audit. To carry out the 5S audit correctly, it is essential to develop a detailed plan covering each stage of the methodology, tailored to the specific characteristics of the enterprise and considering aspects related to safety and occupational health.

The development of the 5S audit should begin with determining its context. First and foremost, define the audit area. Also, create a list of locations and processes to be assessed during the audit. It is advisable to formulate questions that evaluate adherence to 5S principles.

Questions may pertain to sorting, setting in order, cleanliness, standards, and sustainability. Another crucial aspect is scheduling the audit. Set the dates in a way that minimizes disruptions to normal work processes. Organizing training is essential to ensure the audit team understands what to expect during the evaluation.

Table 1 presents sample aspects that can be considered during the audit of the first of the five elements, Seiri (Sort). A detailed specification of what to check will aid in conducting an effective assessment and identifying areas for further optimization.

Table 1. Sample aspects of Seiri (own elaboration)

AUDIT 5S				
Area/Line: Wash Zone				Date: 21.11.2023
A	Sort	2	2	Non-compliance (where and what?)
		YES	NO	
1	At the workplace, only essential items for the job are present: machinery, tools, aids, devices, shelves.		X	Unnecessary platform.
2	At the workplace, only essential materials are present (materials related to tasks, packaging, containers, transport containers, auxiliary materials, etc.).		X	Excess material.
3	At the workplace, only current and required documents are present (e.g., current instructions, forms, etc.).	X		
4	At the workplace, there are no defective, damaged, and/or uncontrolled components, subassemblies, or materials.	X		

## 5. CONCLUSIONS

The article serves as a practical guide for micro-entrepreneurs, detailing the steps of implementing the 5S method to enhance workplace organization. It focuses on specific stages of implementation and the development of the 5S audit, aiming to streamline operational processes in businesses. The guide is a valuable tool for entrepreneurs seeking efficiency and organizational excellence.

## LITERATURE

1. E.V. Crisóstomo, J.C. Jiménez, Application of Lean Manufacturing (5S and Kaizen) to Increase the Productivity in the Aqueous Adhesives Production Area of a Manufacturing Company, *Revista Industrial Data* 24/2 (2021) 249-271.
2. P. Kabiesz, J. Bartnicka, 5S system as a manner for improving working conditions and safety of work in a production company, *Multidisciplinary Aspects of Production Engineering* 2/1 (2019) 496-507.
3. J.S. Randhawa, I.S. Ahuja, 5S – a quality improvement tool for sustainable performance: literature review and directions, *International Journal of Quality & Reliability Management* 34/3 (2017) 334-361.
4. R. Wolniak, Analysis of the 5S method functioning in a production company, *Scientific Papers of Silesian University of Technology – Organization and Management Series, Silesian University of Technology* 146 (2020) 523-531.



26th January 2024  
Gliwice, Poland

DEPARTMENT OF ENGINEERING MATERIALS AND BIOMATERIALS  
FACULTY OF MECHANICAL ENGINEERING  
SILESIA UNIVERSITY OF TECHNOLOGY

## INTERNATIONAL STUDENTS SCIENTIFIC CONFERENCE

### **Influence of Wall Perimeters and Printing Temperature on Tensile Properties of 3D Printed PLA Test Specimens**

P. Karski<sup>a,b</sup>, N. Nokielski<sup>a,b</sup>, J. Krzykawska-Szczepańska<sup>a</sup>, R. Dziembała<sup>c</sup>, M. Dratwiński<sup>c</sup>, J. Banaszkiwicz<sup>c</sup>, M. Rudnicka<sup>b,d</sup>, J. Ptaszny<sup>c</sup>, F. Pawełczyk<sup>b</sup>, M. Kłusek<sup>b</sup>, D.J. Michczyńska<sup>b</sup>, M. Jędrzejowski<sup>b</sup>

<sup>a</sup> Silesian University of Technology, Faculty of Transport and Aviation Engineering

<sup>b</sup> Silesian University of Technology, Institute of Physics – Centre for Science and Education

<sup>c</sup> Silesian University of Technology, Faculty of Mechanical Engineering

<sup>d</sup> Academic Secondary School affiliated to Silesian University of Technology

email: pk308565@student.polsl.pl

**Abstract:** In the article, two series of samples were tested. The first series comprised samples printed exclusively with wall perimeters, while the second series comprised samples printed with 100% rectilinear infill. Both series were printed at three different temperatures: 210 °C, 220 °C, and 230 °C, with each temperature setting replicated four times. Samples from the first series, printed at temperatures of 210 °C and 230 °C, exhibited a higher maximum tensile force than those from the second series. For samples printed at 220 °C, the maximum tensile force was statistically similar. Imperfections occurred during the printing of samples from the first series, making them more susceptible to cracking near the grip section.

**Keywords:** 3D printing settings, wall perimeters, PLA polymer, tensile test specimen

## 1. INTRODUCTION

The 3D printing, or additive manufacturing, is nowadays used very often for prototyping. This is due to its cost efficiency in preparing small series of prototypes, efficient manufacturing time, and the general availability of a broad number of 3D printers and printing materials offered by different manufacturers. These cater to various needs, encompassing specialized areas such as optical elements [1,2], MEMS sensors [3] or even food sector [4].

The model, designed in CAD software, is saved in one of the stereolithography formats, such as STL format (standard tessellation language) [5]. The model is then sliced using specialized software, such as Cura and Slic3r, to produce body cross-sections for each height. A set of these two-dimensional body cross-sections, when assembled, approximates the entire three-dimensional model. Therefore, one of the printing parameters set during slicing is layer height, which is directly proportional to the resolution of the printing and inversely proportional to the printing time.

3D printing technologies can be categorized into solid, liquid, and powder printing [6]. FDM (fused deposition modeling), also known as FFF (fused filament fabrication), is a popular 3D printing technology due to its budget efficiency [7]. During printing, the filament in the form of a wire is pulled from the spool and heated in the printer's extruder head, where the material is melted. The melted material is then deposited on the printing area, called the bed, and due to its molten state, it adheres to the bed (forming the first layer) or to the previous layers.

In this study, the influence of wall perimeters and printing temperature is tested on a series of PLA (Polylactic Acid) samples.

## **2. PRINTING PARAMETERS AND THEIR INFLUENCE ON TENSILE PROPERTIES**

In recent years, numerous studies have been conducted with the primary goal of enhancing the mechanical properties of 3D-printed specimens, specifically focusing on the tensile properties of ABS, PLA, and PET-G. These investigations reflect a concerted effort to improve the tensile strength of these materials in the context of 3D printing technology.

### **2.1. Infill factor**

In summary, recent studies indicate that increasing infill percentage positively correlates with higher yield stress. For instance, in the case of PLA, the yield stress rises from 18.4 MPa at 15% infill to 32.9 MPa at 100% infill [8]. Additionally, the tensile strength can be enhanced by implementing variable infill density. This involves employing dense infill at the outer area of the model and thin infill in the inner area, resulting in improved tensile resistance and flexibility within the inner structure [9].

Furthermore, investigations into the impact of different infill patterns reveal variations in tensile strength. Square and hexagonal infill patterns are found to exhibit the highest tensile strength, as reported in [10]. Conversely, the lowest tensile strength is observed in models with spherical and gyroid infill patterns [11].

### **2.2. Layer thickness**

An increase in layer thickness can result in larger gaps between the extruded filaments, leading to higher porosity in the cross-section of the specimen. Consequently, this increase in porosity is associated with lower mechanical properties, specifically a decrease in tensile strength [12]. For instance, in the case of PLA, a layer thickness of 0.05 mm is reported to yield a tensile strength of 35.5 MPa, whereas a layer thickness of 0.30 mm is associated with a reduced tensile strength of 20.5 MPa [12].

### **2.3. Printing speed**

It has been demonstrated that print speed influences the tensile strength of PLA-printed samples. Comparative analysis was conducted at two distinct speeds: 40 mm/s and 50 mm/s, revealing higher tensile strength at the elevated speed [13]. Conversely, a comparison between substantially different speeds, specifically 20 mm/s and 80 mm/s, indicated that higher tensile strength was achieved at the lower speed [14].

## 2.4. Printing orientation

The tensile properties of printed specimens are influenced by the printing axis. For example, in the case of the BQ Witbox 2 printer, the tensile strength varies with the printing axis: 56.5 MPa in the X-axis, 49.1 MPa in the Y-axis, and 35.6 MPa in the Z-axis [15]. Theoretical model has been developed to describe the ultimate tensile strength of FDM 3D-printed PLA samples with varying printing orientations [16].

## 3. MATERIALS AND METHODS

The samples were 3D-printed using PLA material on the Prusa MK3 printer, following the EN:ISO 527-2:2012 standard with slight modifications tailored to the requirements of this study. The dimensions of the samples are illustrated in Fig. 1.

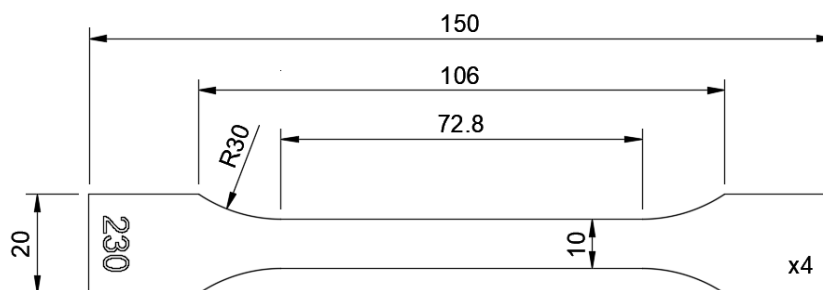


Figure 1. Tensile test specimen used in this study.

The first series comprises samples that were entirely printed with wall perimeters, whereas the second series consists of samples printed using the standard settings of the PrusaSlicer, involving two wall perimeters and 100% infill to match the structure of the samples in the first series. A visual comparison of the sample structures is presented in Fig. 2.

For each series, samples were printed at three different temperatures, 210 °C, 220 °C, and 230 °C, with each temperature setting replicated in four instances. The printing parameters included a nozzle diameter of 0.4 mm, a layer height set to 0.2 mm, and a bed temperature of 60 °C.

The tensile testing was performed using the ZwickRoell Z050 universal testing machine.

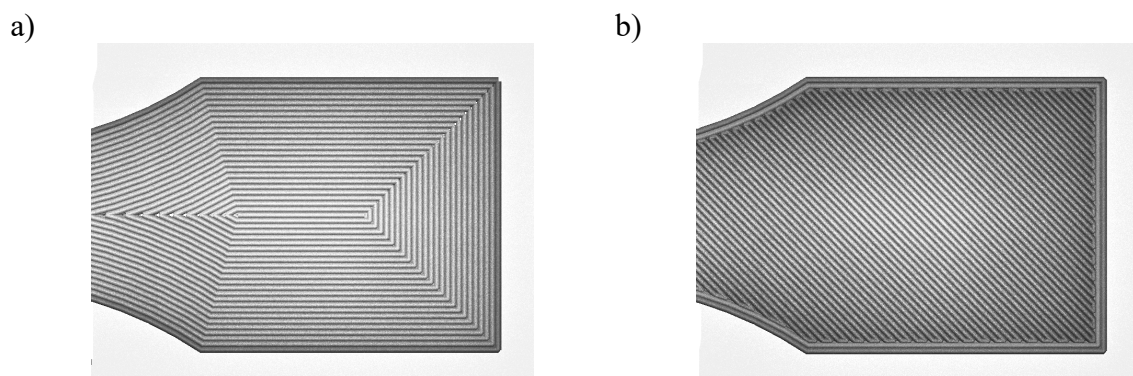


Figure 2. The samples from the: (a) first series with infill consisting of the wall perimeters. (b) second series with the infill consisting of the rectilinear pattern.

## 4. RESULTS AND DISCUSSION

### 4.1. Maximum Tensile Force

The maximum tensile force results obtained in the conducted test are presented in Table 1. For each series, the mean value and its uncertainty were calculated according to the methodology outlined in [17], utilizing Student-Fisher coefficient for the series of four measurements at the  $1\sigma$  level. The force-displacement curves are depicted in Fig. 3 and Fig. 4 for the first and second series, respectively.

Table 1. Results of the maximum tensile force for all types of the samples with the average values.

Printing temperature	Maximum tensile force $F_{\max}$ , N	
	First series <i>Wall perimeters</i>	Second series <i>Rectilinear pattern infill</i>
210 °C	2249 2219 2251 2215 $\bar{F}_{\max} = 2234(11)$	2172 2188 2094 2129 $\bar{F}_{\max} = 2146(24)$
220 °C	2257 2312 2211 2231 $\bar{F}_{\max} = 2253(25)$	2212 2233 2244 2287 $\bar{F}_{\max} = 2244(18)$
230 °C	2314 2323 2344 2266 $\bar{F}_{\max} = 2312(19)$	2237 2256 2228 2170 $\bar{F}_{\max} = 2223(21)$

In the first series of samples, the maximum tensile force at printing temperatures of 210 °C and 220 °C was measured as 2234(11) N and 2253(25) N, respectively. The results were compared using t-Student test, yielding a t-value of 0.70. This indicates that the results are in agreement at the  $1\sigma$  level, suggesting no statistical difference between the maximum tensile forces at these two printing temperatures. Due to this agreement, a weighted mean value of the maximum tensile force can be calculated as 2237(10) N.

Comparing this mean value with the maximum tensile force obtained at 230 °C, which is 2312(19) N, a t-value of 3.5 was obtained. This high t-value suggests that the results are significantly different from a statistical point of view, indicating a notable distinction in maximum tensile force at the 230 °C printing temperature, compared to 210 °C and 220 °C.

For samples printed at 210 °C and 230 °C, printing the test samples with wall perimeters (first series) resulted in a 4% increase in maximum tensile force. The t-values between the first

and second series of the samples are 3.3 and 3.1, at 210 °C and 230 °C, respectively, indicating that this increase is statistically significant.

For samples printed at 220 °C, a very good agreement between the samples from the first and the second series is observed, with a t-value of 0.29. This finding suggests that the samples are in agreement at the  $1\sigma$  level, and it further implies that the change in infill did not influence the tensile properties.

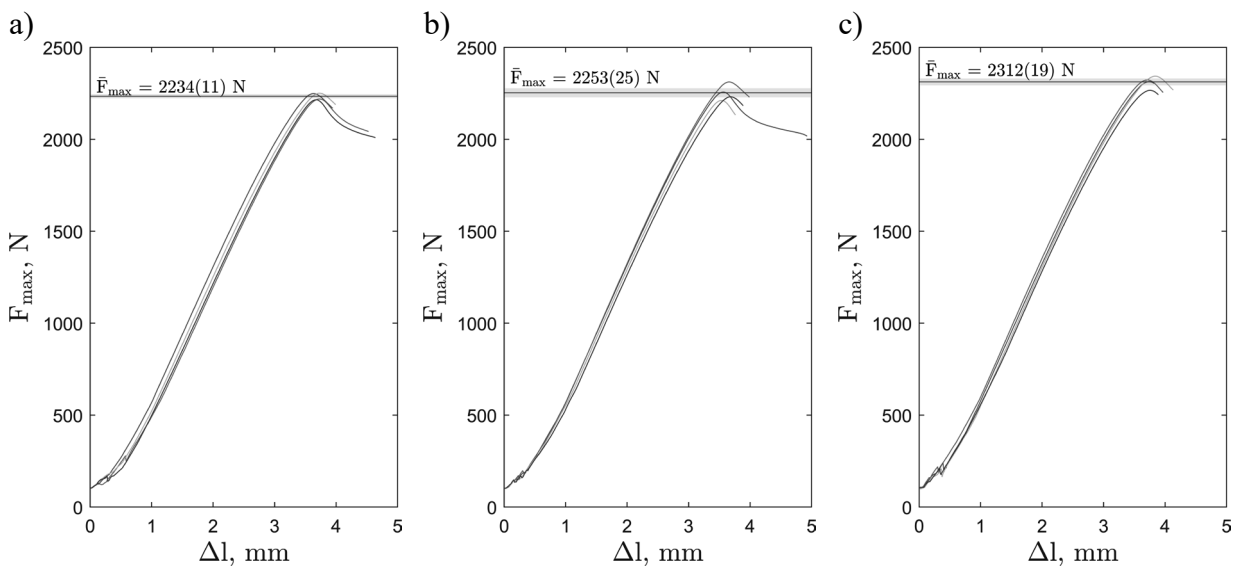


Figure 3. Force-displacement curves for samples from the first series (wall perimeters) printed at temperatures: (a) 210 °C, (b) 220 °C, and (c) 230 °C.

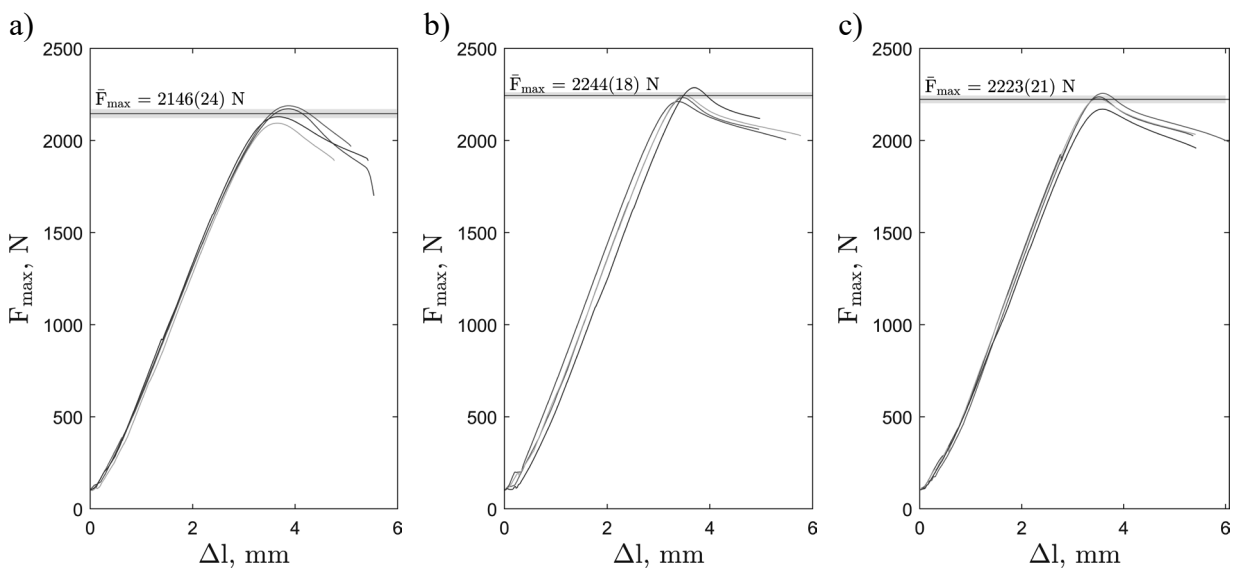
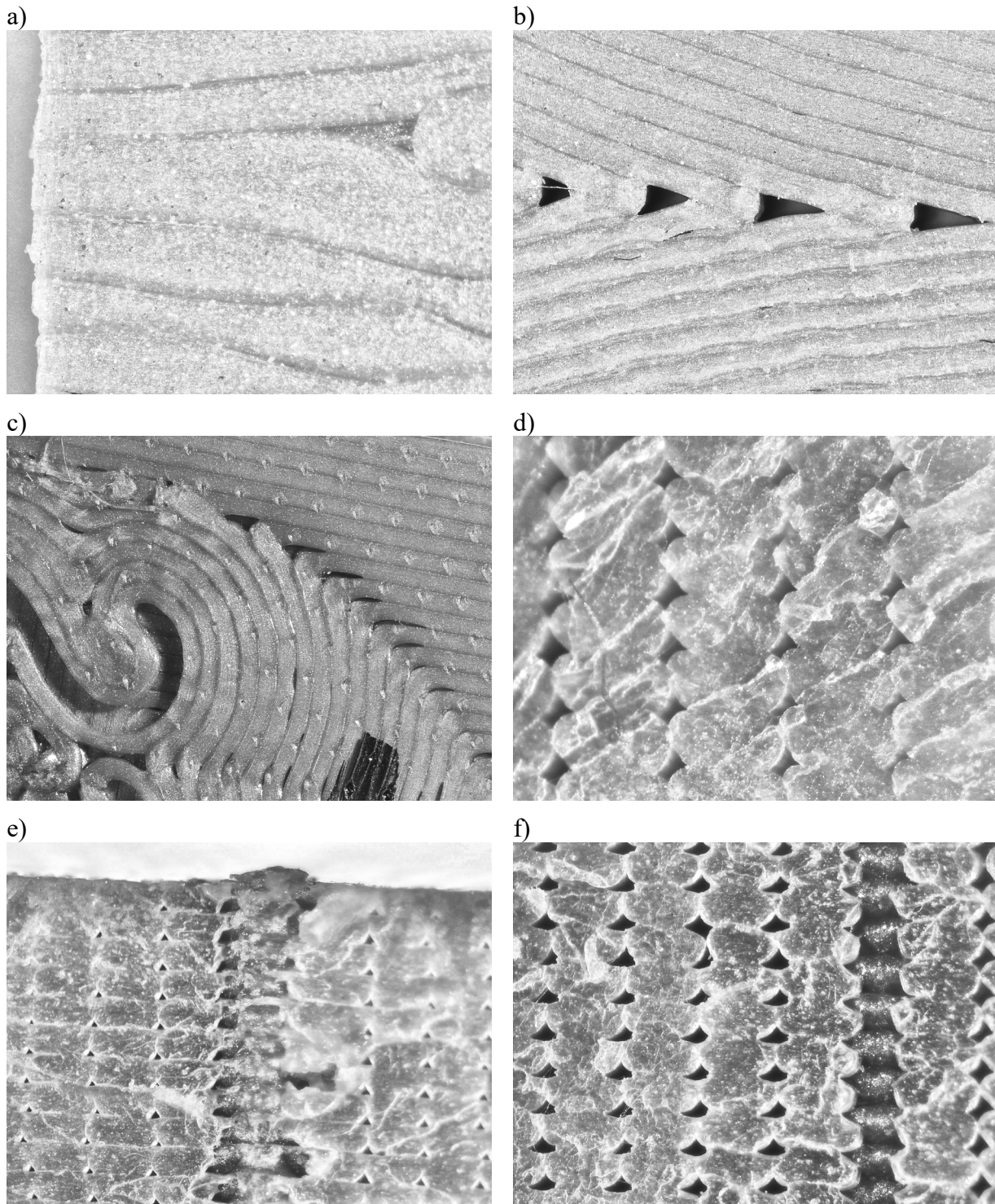


Figure 4. Force-displacement curves for samples from the second series (rectilinear pattern infill) printed at temperatures: (a) 210 °C, (b) 220 °C, and (c) 230 °C.



*Figure 5. Microscopic photographs depicting various artifacts observed in the samples from the first series. (a) A small, triangular absence of filament near the sample border. (b) Illustration of a set-off triangular lack of filament near the enlarged section of the sample, close to the head. (c) Visibility of filament gaps and small spaces between wall perimeters. (d) Exemplary depiction of the porous structure of the sample at the cross-section. (e) Visible deformation of layers in the right part of the photo. (f) Presence of a gap resulting from the slicing process.*



## 4.2. Microscope Photographs of the Specimens

After the tensile tests, microscope photographs of the cross-sections of samples were captured using a ZEISS Stemi 508 optical microscope equipped with an AxioCam 208 Color camera.

For the samples from the first series, an extensive collection of microscope photographs was acquired to pinpoint imperfections in the 3D print. Fig. 5 illustrates typical examples of these imperfections.

In the first series, the samples generally (11 out of 12 times) exhibited fractures near the grip section. In contrast, samples from the second series broke within the gage length in 11 out of 12 instances. This discrepancy is likely attributed to the triangular absence of filament near the grip, which was created by a significant change in the width of the sample (Fig. 5b).

## 5. CONCLUSIONS

The maximum tensile force of samples printed with wall perimeters at 210 °C and 230 °C exceeded that of corresponding samples printed with 100% rectilinear infill. However, for samples printed at 220 °C, the maximum tensile force was statistically the same.

Conversely, specimens printed entirely with wall perimeters exhibited some imperfections visible upon microscopic inspection. It is likely that these imperfections contributed to samples from the first series tending to break near the grip, while samples from the second series were breaking within the gage length.

The presented results may aid in achieving 3D prints with higher tensile properties, particularly in maximum tensile force. Nevertheless, there is a tendency for these prints to break in areas where a significant change in width and infill structure occurs.

## ACKNOWLEDGEMENTS

The analyses were carried out within the project-based learning (PBL) “Inkubator dla roślin i grzybów symulujący skrajne warunki środowiskowe” funded by the Silesian University of Technology.

## BIBLIOGRAPHY

1. C. Schubert, M.C. Van Langeveld, and L.A. Donoso, Innovations in 3D printing: a 3D overview from optics to organs, *British Journal of Ophthalmology* 98 (2) (2014) 159–161.
2. T. Blachowicz, G. Ehrmann, and A. Ehrmann, Optical elements from 3D printed polymers, *E-Polymers* 21 (1) (2021) 549–565.
3. T. Blachowicz and A. Ehrmann, 3D Printed MEMS Technology—Recent Developments and Applications, *Micromachines* 11 (4) (2020) 434.
4. Z. Liu et al., 3D printing: Printing precision and application in food sector, *Trends in Food Science & Technology* 69 (2017) 83–94.
5. N. Ciobota, Standard tessellation language in rapid prototyping technology, *The Scientific Bulletin of “Valahia” University. Materials and Mechanics*. 7 (2012) 81–85.

6. W.S. Tan et al., Comparison of solid, liquid and powder forms of 3D printing techniques in membrane spacer fabrication, *Journal of Membrane Science* 537 (2017) 283–296.
7. O.A. Mohamed, S.H. Masood, and J.L. Bhowmik, Optimization of fused deposition modeling process parameters: a review of current research and future prospects, *Advances in Manufacturing* 3 (1) (2015) 42–53.
8. G.A. Johnson and J.J. French, Evaluation of infill effect on mechanical properties of consumer 3D printing materials, *Advances in Technology Innovation* 3 (4) (2018) 179.
9. Md.Q. Tanveer, A. Haleem, and M. Suhaib, Effect of variable infill density on mechanical behaviour of 3-D printed PLA specimen: an experimental investigation, *SN Applied Sciences* 1 (12) (2019) 1701.
10. C. Lubombo and M.A. Huneault, Effect of infill patterns on the mechanical performance of lightweight 3D-printed cellular PLA parts, *Materials Today Communications* 17 (2018) 214–228.
11. S. Ganeshkumar et al., Investigation of Tensile Properties of Different Infill Pattern Structures of 3D-Printed PLA Polymers: Analysis and Validation Using Finite Element Analysis in ANSYS, *Materials* 15 (15) (2022) 5142.
12. N. Ayrilmis et al., Effect of printing layer thickness on water absorption and mechanical properties of 3D-printed wood/PLA composite materials, *The International Journal of Advanced Manufacturing Technology* 102 (5–8) (2019) 2195–2200.
13. A.A. Ansari and M. Kamil, Effect of print speed and extrusion temperature on properties of 3D printed PLA using fused deposition modeling process, *Materials Today: Proceedings* 45 (2021) 5462–5468.
14. M.R. Khosravani et al., Characterization of 3D-printed PLA parts with different raster orientations and printing speeds, *Scientific Reports* 12 (1) (2022) 1016.
15. M.M. Hanon, R. Marczis, and L. Zsidai, Influence of the 3D Printing Process Settings on Tensile Strength of PLA and HT-PLA, *Periodica Polytechnica Mechanical Engineering* 65 (1) (2020) 38–46.
16. T. Yao et al., A method to predict the ultimate tensile strength of 3D printing polylactic acid (PLA) materials with different printing orientations, *Composites Part B: Engineering* 163 (2019) 393–402.
17. ISO, Guide to the Expression of Uncertainty in Measurement, (1995).



26th January 2024  
Gliwice, Poland

DEPARTMENT OF ENGINEERING MATERIALS AND BIOMATERIALS  
FACULTY OF MECHANICAL ENGINEERING  
SILESIA UNIVERSITY OF TECHNOLOGY

## INTERNATIONAL STUDENTS SCIENTIFIC CONFERENCE

### **Innovative strategies for integrating fibre optic sensors into composite structures for optimized health monitoring of engineering structures**

M. Knutelski<sup>a,b\*</sup>, Z. Brytan<sup>a</sup>

<sup>a</sup> Silesian University of Technology, Faculty of Mechanical Engineering, Department of Engineering Materials and Biomaterials, ul. Konarsiego 18a, 44-100, Gliwice, Poland

<sup>b</sup> Reinbar Sp. z o.o., Przemęczany 76, 32-107 Radziemice

\*email: marcin.knutelski@polsl.pl

**Abstract:** The aim of this publication is to present innovative methods for integrating fibre optic sensors into composite structures, which play a crucial role in Structural Health Monitoring (SHM) of engineering structures. The paper discusses advanced techniques and approaches for incorporating fibre optics into various types of composites, with particular emphasis on their application in concrete structures. Various aspects were analyzed, including material selection, production processes, and challenges and opportunities related to the integration of these sensors. The publication provides a detailed discussion of selected production technologies such as Resin Powder Molding (RPM), vacuum infusion, and pultrusion, evaluating their effectiveness in the integration process of fibre optic sensors. The key aspect of the work is the analysis of the possibilities and limitations associated with the use of fibre optics in composite structures. The outcome of this work is the development of effective strategies for implementing fibre optic sensors in composite structures, which can significantly contribute to the improvement of monitoring and diagnosing the condition of engineering structures. The proposed methods have the potential to revolutionize the approach to structural safety, while also offering new possibilities in the design and operation of engineering structures.

**Keywords:** fibre optic sensor integration, health monitoring systems (SHM), composite structures, resin powder molding, vacuum infusion, pultrusion

## INTRODUCTION

Many engineering structures require a long service life while maintaining safety standards that could affect the health of users. Planning and implementing appropriate measures to inspect or verify the health of a structure is one desirable course of action that can go a long way to dispelling any doubts as to whether an engineering structure can continue to perform its functions safely or should rather be decommissioned. Sometimes structures undergo user changes - retrofitting and/or strengthening - during their lifetime that were not anticipated by the designers, and these should be investigated and analyzed to determine their current

condition. Regardless of whether the structures we exploit are considered 'modern' or, on the contrary, 'archaic', they are continuously exposed to external factors, loads, aggressive environments, the passage of time, seismic shocks in the case of buildings, which can consequently lead to destruction and, in the worst case scenario, endanger the life or death of the exploiter. One example is the building disaster in Riga, where the roof of the "Maxima XX" supermarket collapsed in 2013, in which 54 people were killed [1]. Another example is the collapse of a viaduct in Ponte Morandi, Italy [2]. It was found that the deterioration of the viaduct was contributed to by increasing truck traffic year after year and a significant increase in the weight of the trucks.

The assessment of the condition of engineering structures can be carried out through one-time inspections or continuously. Regardless of the chosen method, collecting data by monitoring key parameters and their analysis is a necessary action that allows for appropriate intervention if necessary. This action, i.e. Structural Health Monitoring (SHM), can be defined as the process of implementing strategies for identifying damage to engineering structures [3].

The successful implementation of Structural Health Monitoring (SHM) systems requires the development of advanced composite material integrated with an embedded sensor. The material should be resistant to damage [4] during assembly or incorporation into concrete structures. Designing and producing such a material requires meticulous selection of constituent materials, strength analysis, and significant modification of existing production technologies. The assumed boundary conditions characterizing the material should be high strength, comparable to traditional steel reinforcement, while providing protection for the embedded fibre optic sensor [5]. In addition to the role of structural reinforcement, the material is also intended to serve as a monitoring element for the tool, combining the dual functionality of reinforcement and measurement in a single, coherent system.

In recent years, there has been a growing interest in structural health monitoring systems for structural assessment of engineering structures in various engineering fields such as civil, mechanical, marine, military, aerospace, or energy engineering. Academic institutions, government agencies, and industry are all drawn to the technological potential of SHM [6-8]. The purpose of this is to provide real-time critical information on structural damage and ensure the expected critical performance of monitored objects during operation.

Despite the increasing interest in SHM due to the growing number of studies and implementations, its original concept can be traced back to the early attempts by humanity to conceptualize, design more demanding structures exposed to damage, and determine their potential reparability. It all boils down to nothing less than the need to maximize the service life of structures, as in engineering, whether it is the type of material, the age of the material, the way it is used or the level of sophistication of the structure has a significant impact on its performance and lifespan. It is undeniable that over time, every structure will lose its original properties.

## 1. MATERIAL SELECTION

Fibre optic is a fundamental component of the SHM measurement system. Available fibre optic cables have been analyzed based on ITU-T (International Telecommunication Union) standards, which describe the geometric and transmission properties of multimode and single-mode fibre optic cables. There are currently several common ITU-T recommendations in force:

- ITU-T G.651.1 - 50/125  $\mu\text{m}$  graded index multimode fibre,

- ITU-T G.652 - Standard single mode fibre for CWDM systems - there are 4 fibre versions: A, B, C, D,
- ITU-T G.653 - Single mode fibre with shifted dispersion characteristics,
- ITU-T G.654 - Single mode optical fibre with staggered dispersion characteristics, ITU-T G.654 - Single mode optical fibre with staggered dispersion characteristics,
- ITU-T G.655 - Single-mode fibre with shifted, non-zero dispersion characteristics,
- ITU-T G.656 - Non-zero dispersion fibre dedicated to data transmission using the widest possible bandwidth of the optical spectrum,
- ITU-T G.657 - Single-mode fibre with reduced bending radius.

Taking the following parameters as criteria: type of optical fibre available, transmission performance categories, construction, chromatic dispersion coefficient, unit attenuation, price, application, the selection was narrowed down to a group of single-mode optical fibres.

The selected fiber optic sensor is characterized by the absence of external braiding. This form exposes it to the influence of moisture and mechanical damage. The premise of the designed material is that it has the dual functionality of enabling accurate measurements and strengthening the concrete structure. With respect to conventional materials used to reinforce concrete, such as bars, meshes or steel mats, it was assumed that the sensor would take the form of a rod or mat/plate, which would facilitate its integration into existing concrete structures. Ensuring that the strength parameters of the SHM rod/mat would match those of traditional structural bars was a key criterion.

Granta Selector software was used for this purpose, guided by criteria such as tensile strength, material density and the ratio of elastic modulus to tensile strength (Figures 1 and 2). From the material base, a group of composite materials suitable for integrating a fiber optic sensor was selected.

Among the constituent materials that serve a protective and reinforcing function, glass fibers in an epoxy/polyester resin matrix, and carbon fibers/mats were selected, which have similar tensile strength to structural steel. Tensile strength parameters correlate with the type of fibers and resin used in the manufacturing process and their proportions in relation to the cross-section of the composite profile.

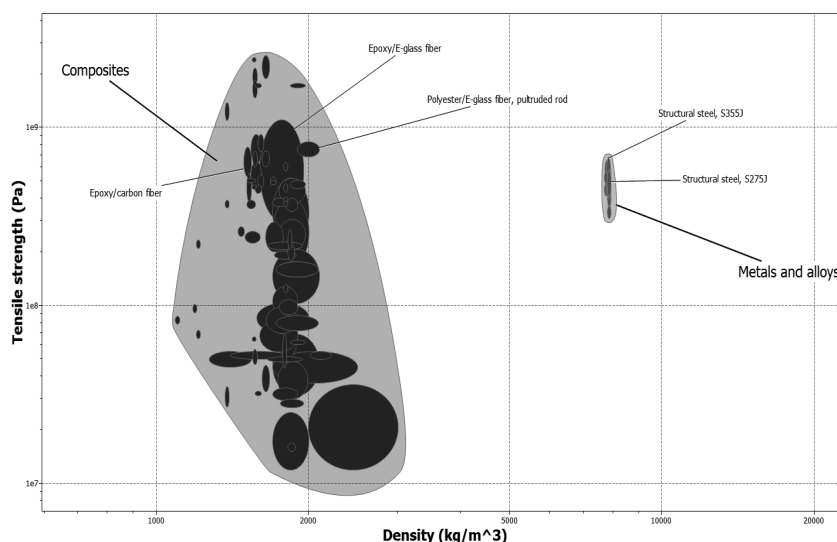


Figure 1. Graph from Granta Selector. Comparison of tensile strength-to-density relationships for structural metals and composite materials.

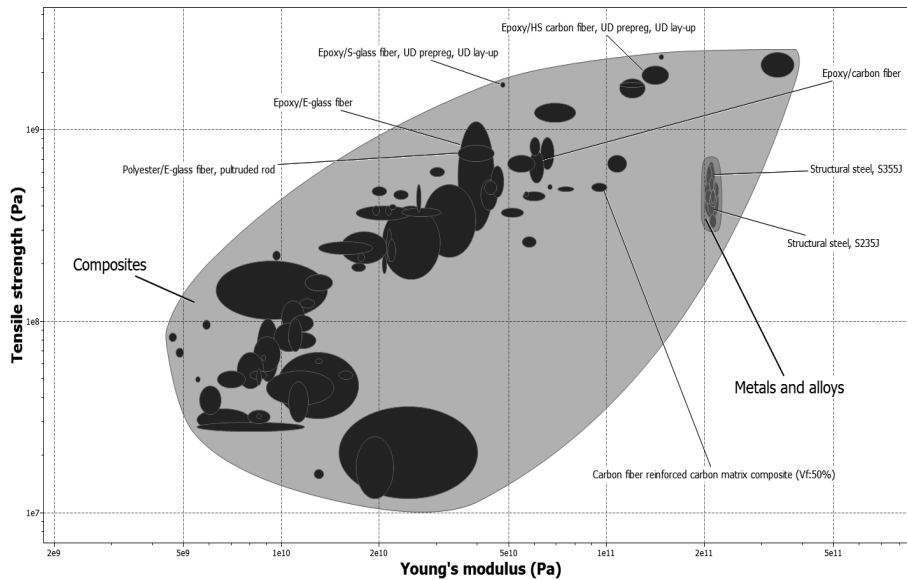


Figure 2. Graph from Granta Selector. Comparison of the relationship of tensile strength to Young's modulus for structural metals and composite materials.

## 2. SHM SENSOR MODELLING

A geometric model of a composite rod (Fig. 3) and a carbon plate with an integrated fiber optic sensor was developed for fabrication and future FEA simulation. The model was made using Solidworks software.



Figure 3. 3D model of composite rod with integrated OS sensor. 1 - fiber optic sensor, 2 - fiberglass, 3 - resin, 4 - double helical glass fiber "notch".

The model assumed a rod diameter of 3 mm. The sensor was embedded along the axis of the rod in the center of the cross-sectional area. The model was simplified and assumed 11 glass roving bundles in its construction, which were treated as elementary, where in fact a single bundle consists of dozens of elementary filaments. A double helix of glass fibre with a diameter of 0.5 mm was designed on the surface along the rod.

### **3. INTEGRATION OF FIBER OPTIC SENSOR**

Due to the similar chemical composition of the optical fiber to glass fibre, it allows the use of optical fibers in almost all glass fiber technologies, but the bending angle and alignment conditions make integration in manufacturing processes difficult. Three potential composite manufacturing technologies have been identified: Resin Powder Molding (RPM), Vacuum Infusion, and pultrusion, and a study of sensor integration in composite materials was conducted.

#### **3.1 Integration of fiber optic sensors in the RPM process**

Two layers of carbon fibre fabric prepared by A.S.SET (Adjustable Simple Thermoset) resin application was used to prepare the samples. The resin has thermoplastic properties in the temperature range between 70-90 °C, with a glass transition temperature of 125 °C. Above the glass transition temperature, the resin is cross-linked giving it duroplastic properties with temperature stability up to 340 °C. In addition, the cross-linking time of the resin was 350 seconds, and depended on the thickness of the composite component produced.

The application of A.S. SET powder to the reinforcement layers was done using powder guns. This allowed an even distribution of the matrix material between the reinforcement layers. In addition, the reinforcement layers were preheated to ~70 °C which ensured good adhesion of the powder, facilitating further manipulation of the semifinished material, and enabling the removal of excess resin even before the main processing.

Between the layers of pre-impregnated carbon fabric, standard 9/125 single-mode telecom optical fibres were placed parallel to the tensile direction of the specimen. The optical fibres were pre-tensioned and then subjected to a pressing process.

#### **3.2 Sensor integration in vacuum infusion technology**

Flat samples were also produced on the laboratory bench using vacuum infusion technology. A plate of glass was used as the mold, onto which a PVA separator was applied each time before the samples were prepared. This prevented the samples from sticking to the substrate. In the next step, butyl tape was applied to the glass mold, marking the boundaries of the system on which the composite parts were made. Inside, 2-5 layers of carbon fibre tape were laid, OS was spread and attached to the substrate.

In the next steps, a PA80 delamination mat and OM70 resin distribution net were laid. The entire system was rigged with a spiral resin distribution line and then sealed with a vacuum bag. A vacuum was created by infiltrating the system with the epoxy resin mixture.

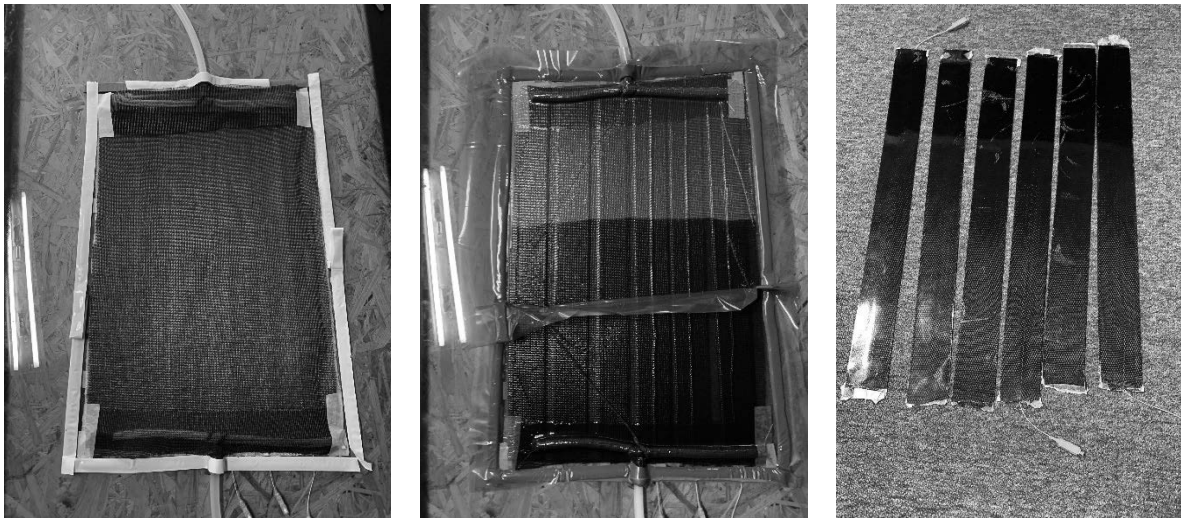


Figure 4. Integration of fibre-optic sensors in vacuum infusion technology. A - resin distribution grid with tubing system. B - infiltration of the system with resin. C - flat samples with integrated fibre optics.

### 3.3 Integration of sensors in pultrusion technology

In the standard pultrusion process (Fig. 5), reinforcement materials such as fibres or fabrics are impregnated with resin, possibly using a separate pre-moulding system, and then drawn through a heated calibrator where the resin polymerises. Impregnation is done either by pulling the reinforcement through a bath or by injecting the resin with a hardener.

Many types of resins can be used in the pultrusion process, including polyester, polyurethane, vinyl ester and epoxy. The resin provides environmental resistance (i.e. corrosion resistance, UV resistance, impact resistance, moisture resistance, etc.), while the fibre provides strength and stiffness while creating protection for the fibre optic sensor.

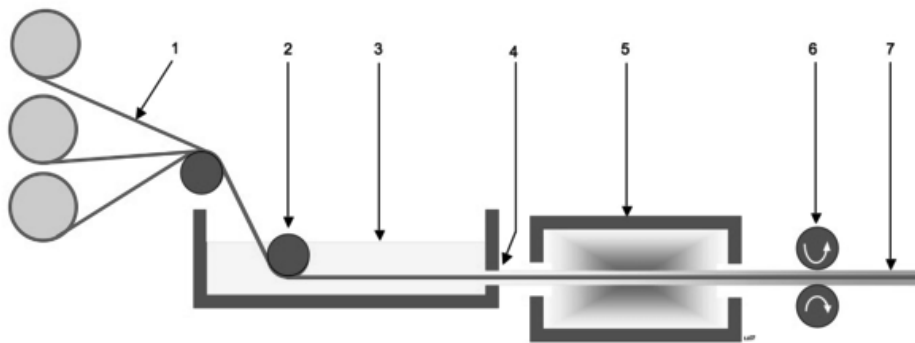


Figure 5. Diagram of the pultrusion process. 1 - Continuous roll of reinforced fibre/woven fibre mat; 2 - Tension roll; 3 - Resin impregnation device; 4 - Resin-impregnated fibre; 5 - Calibrator and heating device; 6 - Pulling mechanism; 7 - Finished cured fibre-reinforced polymer;

For the integration of the fibre optic sensors into the GFRP composite rods, the pultrusion process was modified in order to properly insert the optical sensor guaranteeing less bending.



During the fabrication process, the fabrication speed was adjusted, and the tension was controlled, resulting in rods in which the optical fibre sensor was centrally located in the rod cross-section and continuous throughout the structure.

#### 4. CONCLUSIONS

The research presented in this paper provides a comprehensive overview and analysis of the integration of fiber optic sensors into composite structures, highlighting its significance for the Structural Health Monitoring (SHM) of engineering structures. The study's primary contributions can be summarized as follows:

1. The literature review and studies have demonstrated the feasibility of integrating fibre-optic sensors into high-volume composite component manufacturing technologies.
2. Depending on the technology used, a number of modifications and adaptations to the equipment were necessary to ensure the correct insertion of fibre optics during the process.
3. VARTM technology generated the most problems with the correct integration of fibre optic sensors. This involves time-consuming bench preparation, problems with sensor strain and the formation of leaks in the system, and the relatively expensive materials involved in the system. A much more efficient method for producing flat samples is the RPM method. As both technologies are two-stage, there is also a risk of damage to the sensors during the resin infiltration process. An appropriately prepared infiltration process (appropriately placed resin insertion points, spout, vacuum connection and use of suitable auxiliary materials) greatly reduces the risk of damage to the sensors, guaranteeing a very high repeatability of the process.
4. The possibility of a new application of the technology under development has been noted, namely - the integration of sensors during the production process allows ongoing monitoring of the manufactured composite structure. Performing the monitoring process during the production of a selected number of composite elements will allow to check and supervise the repeatability of the produced elements.
5. Integrating fibre optic sensors into a fully automated pultrusion process without damaging the fibre optic sensors is possible but requires controlling a number of factors such as production speed, resin curing temperature control, pulling roller force. The biggest challenge is to keep the fibre optic in the central part of the rod cross-sectional area along its entire length.

In summary, this study represents a significant advancement in the field of Structural Health Monitoring (SHM) by integrating fiber optic sensors into composite structures. The research successfully demonstrated the feasibility of this integration across various manufacturing technologies, each presenting unique challenges and requiring specific adaptations. The efficiency of Resin Powder Molding (RPM) has been noted in comparison to Vacuum Assisted Resin Transfer Molding (VARTM). Additionally, the potential of integrating sensors during the manufacturing process for continuous monitoring has been highlighted, which could revolutionize quality control in composite manufacturing.

The study highlights the successful integration of fiber optic sensors in an automated pultrusion process. However, it emphasizes the need for meticulous control over various production parameters to ensure optimal sensor integration and functionality.

There is ample scope for further research and development in this field. Future work will focus on refining integration techniques for different composite materials and exploring the potential of these integrated systems in various engineering applications. Furthermore,

developing sensor integration processes with greater automation and precision, particularly in complex manufacturing setups, is a crucial area for further development. The investigation of novel sensor types and their compatibility with various composite materials could provide valuable insights and progress.

## BIBLIOGRAPHY

- [1] Fulcherd M., Design flaws suspected in Riga roof collapse, Architect's Journal, 25 November 2013, <https://www.architectsjournal.co.uk/archive/design-flaws-suspected-in-riga-roof-collapse>,
- [2] Rymysza, J, "Causes of the collapse of the Polcevera Viaduct in Genoa, Italy", Applied Sciences, 11, 8098, doi.org/10.3390/app11178098
- [3] Charles R Farrar, Keith Worden, „An introduction to structural health monitoring”, The Royal Society 2007, 303-315, doi:10.1098/rsta.2006.1928
- [4] Di Sante, R. Fibre Optic Sensors for Structural Health Monitoring of Aircraft Composite Structures: Recent Advances and Applications. Sensors 2015, 15, 18666-18713, doi.org/10.3390/s150818666
- [5] Leng, J., Winter, D., Barnes, R., Mays, G., & Fernando, G. (2006). Structural health monitoring of concrete cylinders using protected fibre optic sensors. Smart Materials and Structures, 15, 302 - 308. doi.org/10.1088/0964-1726/15/2/009.
- [6] Doebling, S.W. & Farrar, Charles & Prime, Michael & Shevitz, D.W.. (1996). Damage Identification and Health Monitoring of Structural and Mechanical Systems From Changes in their Vibration Characteristics: A Literature Review. Technical Report No. LA-13070-MS. 30. 10.2172/249299.
- [7] Raghavan, A.C. & Cesnik, Carlos. (2007). Review of Guided-Wave Structural Health Monitoring. The Shock and Vibration Digest. 39. 91-114. 10.1177/0583102406075428.
- [8] Sohn, H, Farrar, C R, Hemez, F M, and Czarnecki, J J. A Review of Structural Health Monitoring Literature 1996-2001. United States: N. p., 2002. Web.



26th January 2024  
Gliwice, Poland

DEPARTMENT OF ENGINEERING MATERIALS AND BIOMATERIALS  
FACULTY OF MECHANICAL ENGINEERING  
SILESIA UNIVERSITY OF TECHNOLOGY

## INTERNATIONAL STUDENTS SCIENTIFIC CONFERENCE

### **Numerical analysis of the effect of environment and operating conditions on the performance of electric cables**

K. Kojm<sup>a</sup>, Ł. Lomania<sup>a</sup>, C. Zach<sup>a</sup>, J. Polis<sup>a</sup>, Mikołajko<sup>b</sup>, A. Śliwa<sup>b</sup>, A. Dziwis<sup>b</sup>, M. Sroka<sup>b</sup>

<sup>a</sup> Student - Politechnika Śląska, Wydział Mechaniczny Technologiczny, Katedra Materiałów Inżynierskich i Biomedycznych

e-mail: lukalom979@student.polsl.pl, cezazac076@student.polsl.pl, jakupol064@student.polsl.pl, kajekoj367@student.polsl.pl,

<sup>b</sup> Politechnika Śląska, Wydział Mechaniczny Technologiczny, Katedra Materiałów Inżynierskich i Biomedycznych

e-mail: wojciech.mikolejko@polsl.pl, agata.sliwa@polsl.pl, amadeusz.dziwis@polsl.pl, marek.sroka@polsl.pl

**Keywords:** SolidWorks, stresses, computer simulation, FEM, electric cables.

## INTRODUCTION

### Finite Element Method (FEM)

The Finite Element Method (FEM) represents one of the most widely used tools in the field of structural engineering calculations using computer programs. It provides an effective tool for accurately modeling the behavior of structures under the influence of external factors, making it a widely used solution in material strength simulations. The flexibility and intuitiveness of this method contribute to its frequent use in the analysis of systems with complex geometries, making it possible to accurately determine stresses, displacements and deformations of the structure. The reliability of this method makes it extremely useful in engineering, as well as applications where it is crucial to accurately model and analyzing the behavior of structures. [1]

The Finite Element Method (FEM) is based on the conceptual transformation of a model to a discretization grid, which implies the reduction of a given product to a finite number of elements along which stresses are distributed, and their values are calculated at successive nodes of the grid. Analysis using FEM allows obtaining important information on the processes occurring in structures and their response to time-varying force. This method demonstrates high precision when the boundary conditions are properly defined and the mesh is adjusted accordingly, involving the compaction or dilution of elements at the boundaries of different areas of the structure. FEA-enabling programs such as Solidworks, used in this work, allow access to extensive material libraries and the definition of custom structural material parameters. This, in turn, enables the best possible modeling of a given phenomenon and achieves maximum precision in simulations. [2]

## Materials engineering of electric cables

Materials engineering in the context of electrical cables plays a key role in designing, manufacturing and maintaining the performance of these cables. Copper and aluminum are the main materials used for electrical conductivity. Copper is preferred because of its high electrical conductivity, which allows for more efficient current transport. Engineers are working to develop alloys and manufacturing technologies to improve the performance of the conductors thus minimizing energy loss.

However, conductive material alone is not enough, each cable must be protected from the outside. Insulating materials play a key role in protecting conductors from short circuits and energy loss. Various dielectrics are used in materials engineering, such as polyethylene, polypropylene, ethylene propylene diene rubber (EPDM) or silicone rubber, depending on voltage requirements, operating temperature and other factors. Osłony zewnętrzne kabli mają za zadanie chronić przed czynnikami atmosferycznymi, mechanicznymi uszkodzeniami, elektromagnetycznymi zakłóceniami oraz służyć jako ochrona przeciwporażeniowa.

For cables with high electromagnetic interference requirements, aluminum foil or copper mesh screens are used. In this case, the quality of these materials is very important in order to effectively protect the cables from external interference.

Innovation and research in the field of materials engineering for electrical cables is evolving as technology advances. Research into nanomaterials, superconductors and new polymers is aimed at improving the performance, durability and flexibility of electrical cables. In short, materials engineering in electrical cables focuses on optimizing the properties of individual components to ensure safe and efficient power transmission. [3, 4]

## PURPOSE OF THE WORK

The purpose of this study was to simulate the effect of temperature on the displacement of an electrical conductor (Figure 2). Two cases were analyzed, the first where the core is made of copper and the second case where the core is made of aluminum. In addition, the analysis carried out made it possible to assess the influence of the inner and outer coating made of a polymer such as PVC - (Polyvinyl chloride).

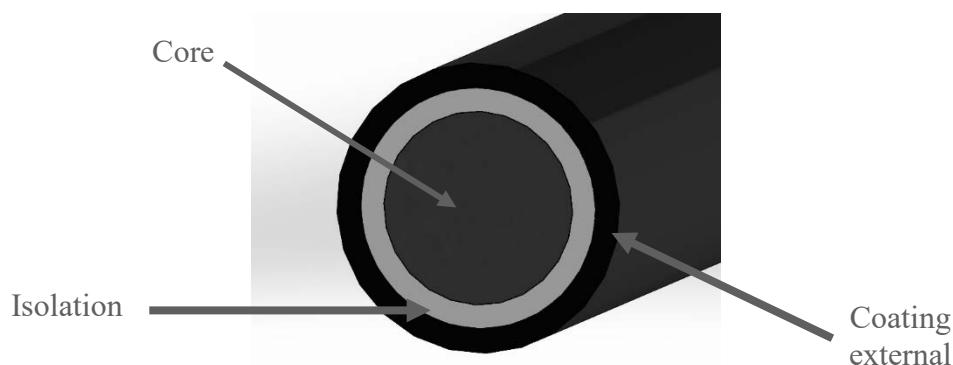


Fig. 2. Diagram of the cable used in the simulation.

## METHODOLOGY

For the analysis, an electrical cable (Figure 2) was modeled in SolidWorks, which allowed the design of the core, insulation and outer sheath. Then the positioning of the components and their joining were performed, resulting in an electrical wire consisting of three models. The next step was to implement the boundary conditions, i.e. the finite element mesh, the fixings, the gravitational force acting on the wire and the thermal load as shown in Figures 3 - 5. The final step was to run the solver. It analyzed the effect of temperature on the displacement of the cable, the type of material used (Table 1 - 3) on the core of the cable, and the effect of the polymer used for the insulation and outer sheath of the cable -. which resulted in eight simulations:

- Solid wire with copper core - temperature 30°C,
- Solid wire with copper core - temperature 100°C,
- Solid wire with copper core - temperature 140°C,
- Solid wire with aluminum core - temperature 30°C,
- Solid wire with aluminum core - temperature 100°C,
- Solid wire with aluminum core - temperature of 140°C,
- Copper core - temperature of 140°C,
- Core made of aluminum - temperature of 140°C.

The height of the temperature was selected according to the optimal operating range of electrical cables from the approximate room temperature, which was inflated to a full number of tens - 30°C up to a temperature of 140 °C, which corresponds to the maximum permissible temperature set by the manufacturer. The assumptions for the analysis assumed the dimensions of the cable such as - the length of the tested cable - 1000mm. The thickness of the outer sheath and insulation is 3mm each. The diameter of the copper or aluminum core is 12mm.

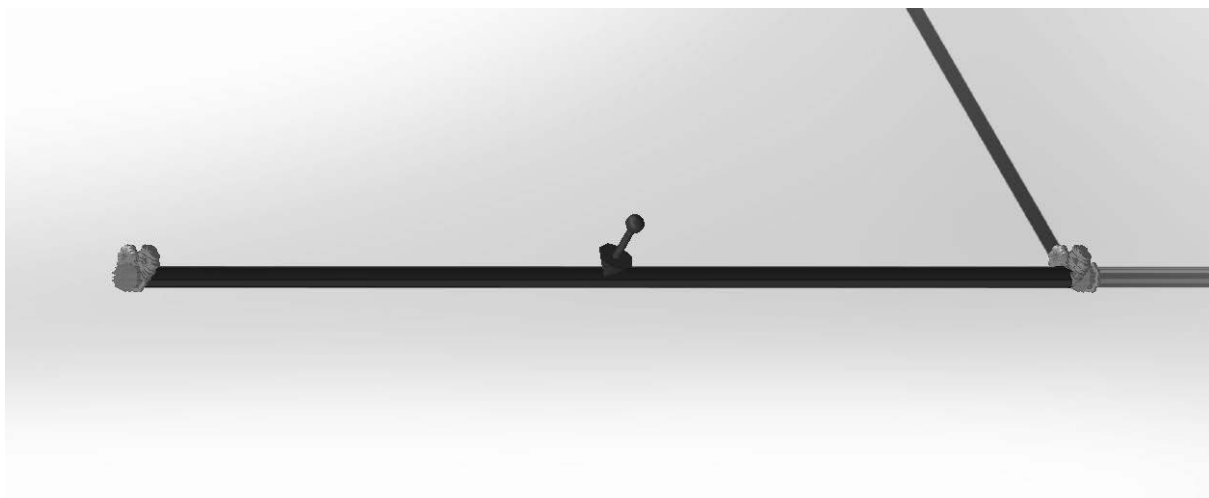


*Fig. 3. Direction of gravitational force and locations of cable fixings.*

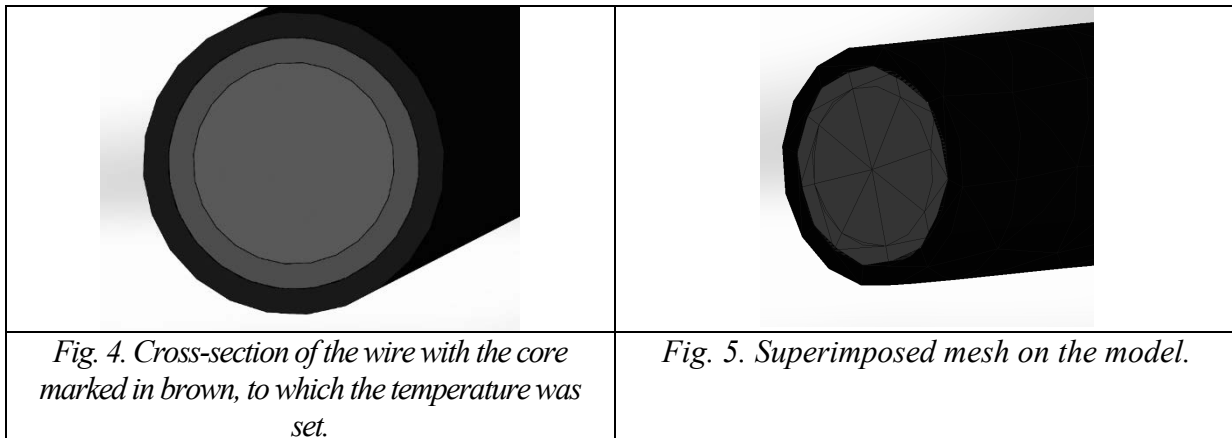


Table 1. Strength properties of PVC.

Properties	Value
Tensile strength	4,07e+07 N/m <sup>2</sup>
Coefficient of longitudinal elasticity	2,41e+09 N/m <sup>2</sup>
Poisson's ratio	0,3825
Specific weight	1 300 kg/m <sup>3</sup>
Transverse elasticity coefficient	8,667e+08 N/m <sup>2</sup>

Table 2. Strength properties of Al.

Properties	Value
Yield strength	2e+07 N/m <sup>2</sup>
Coefficient of longitudinal elasticity	6,8e+10 N/m <sup>2</sup>
Poisson's ratio	0,33
Specific weight	2 699 kg/m <sup>3</sup>
Transverse elasticity coefficient	2,55639e+10 N/m <sup>2</sup>
Coefficient of thermal expansion	2,5e-05 /Kelvin

Table 3. Strength properties of Cu.

Properties	Value
Yield strength	2,58646e+08 N/m <sup>2</sup>
Tensile strength	3,9438e+08 N/m <sup>2</sup>
Coefficient of longitudinal elasticity	1,1e+11 N/m <sup>2</sup>
Poisson's ratio	0,37
Specific weight	8 900 kg/m <sup>3</sup>
Transverse elasticity coefficient	4e+10 N/m <sup>2</sup>
Coefficient of thermal expansion	2,4e-05 /Kelvin

## RESULTS AND SUMMARY

The simulation results made it possible to observe the effect of temperature and the type of cable core material on cable displacements. Figures 6 show a cable whose core was made of copper, while Figures 7 show a cable with an aluminum core. These figures show successively

the results of displacements due to increasing temperatures of 30°C, 100°C and 140°C, respectively. The last two figures 8 and 9 show the displacement results of cores subjected to 140°C. Tables 3 describe the results of these displacements in numerical form.

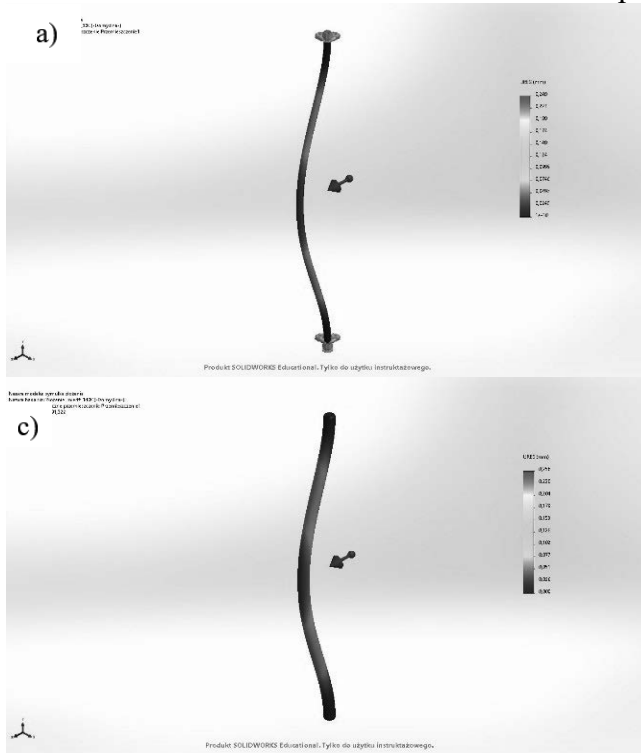


Fig. 6. Displacement of copper cable subjected temperature to:  
 a) 30°C,  
 b) 100°C,  
 c) 140°C.

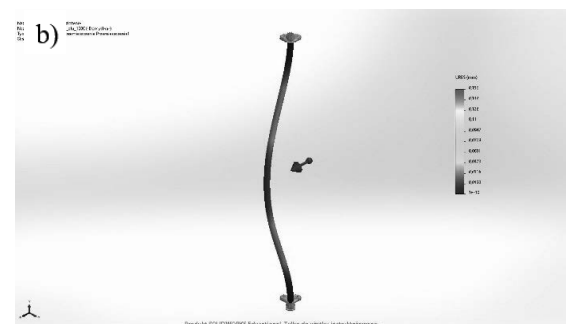
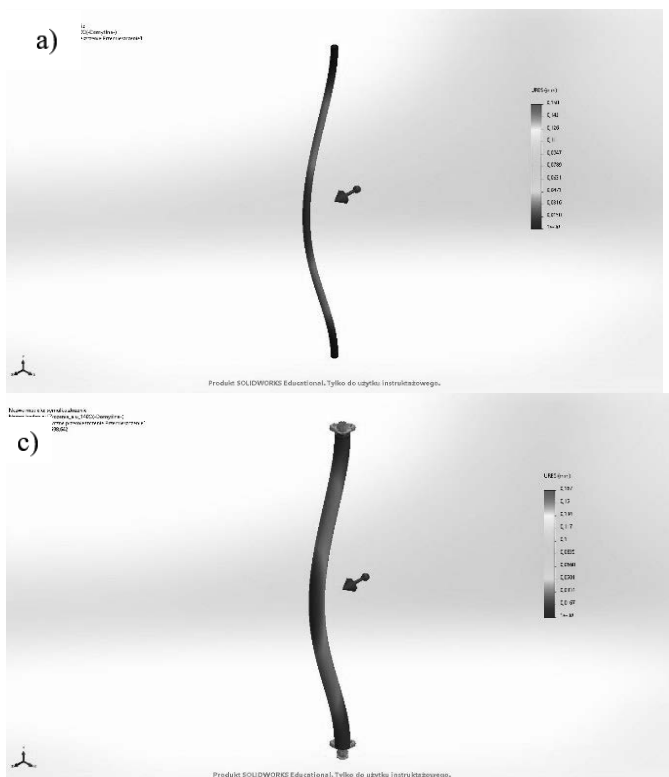


Fig. 7. Displacement of aluminum cable subjected temperature to:  
 a) 30°C,  
 b) 100°C,  
 c) 140°C.



Fig. 8. Displacement of the copper core subjected to a temperature of 140 °C.



Fig. 9. Displacement of aluminum core subjected to 140 °C temperature.

Table 3. Displacement results.

Result	Temperature	Displacements [mm]
Copper wire	30°C	0,249
	100 °C	0,253
	140 °C	0,256
Aluminum wire	30°C	0,158
	100 °C	0,158
	140 °C	0,167
Copper core	140 °C	0,295
Aluminum core	140 °C	0,18

## CONCLUSION

Summarizing the collected results of the analysis of the effect of temperature on the displacement of the electric wire, it can be clearly stated that temperatures as well as the core material have a significant effect on the displacement of wires used in electrical engineering. The best results, and at the same time the smallest displacements are characterized by conductors made of aluminum where at the maximum operating temperature allowed by the manufacturer the displacement was - 0.167[mm]. Worse results are characterized by copper wire, where displacements at the critical temperature amounted to - 0.256[mm]. The use of coating and insulation had a positive effect on the amount of displacement for both copper and aluminum. The difference in displacements between the wire with insulation and the outer coating and the core was - 0.013[mm] and 0.039[mm] for aluminum and copper, respectively.



## **ACKNOWLEDGEMENTS**

The work was created as a result of the student scientific club B@jt part of project based learning - PBL, in the 5th competition under the Initiative of Excellence - Research University, Silesian University of Technology.

## **BIBLIOGRAPHY**

- [1] J. Zielnica, Wytrzymałość materiałów, Wyd. Pol. Poznańskiej, 1996.
- [2] M. Sydor, Podstawy komputerowo wspomaganego projektowania Wprowadzenie do CAD., Warszawa: PWN, 2009
- [3] P. Zydrón, J. Roehrich, Pomiary i modelowanie wpływu parametrów konstrukcyjnych kabli elektroenergetycznych na występujące w nich zjawiska falowe. Wydział Elektrotechniki i Automatyki Politechniki Gdańskiej, 2010
- [4] J. Grobicki, M. Germata, Przewody i kable elektroenergetyczne, PWN, 2019



27th January 2023  
Gliwice, Poland

DEPARTMENT OF ENGINEERING MATERIALS AND BIOMATERIALS  
FACULTY OF MECHANICAL ENGINEERING  
SILESIA UNIVERSITY OF TECHNOLOGY

## INTERNATIONAL STUDENTS SCIENTIFIC CONFERENCE

### Wpływ metody wytwarzania na wybrane własności węglików spiekanych

I. Kredowska<sup>a</sup>, W. Pilarczyk<sup>a</sup>, J. Śliwka<sup>b</sup>, W. Pakieła<sup>a</sup>, M. Bigaj<sup>a</sup>, K. Gajewski<sup>c</sup>

<sup>a</sup> Politechnika Śląska, Wydział Mechaniczny Technologiczny, Katedra Materiałów Inżynierskich i Biomedycznych,

email: inez.kredowska@polsl.pl

<sup>b</sup> Politechnika Śląska, Wydział Mechaniczny Technologiczny, Katedra Budowy Maszyn

<sup>c</sup> Student kierunku Inżynieria Materiałowa, Wydział Mechaniczny Technologiczny, Politechnika Śląska

**Streszczenie:** W artykule przedstawiono wyniki badań laboratoryjnych związanych z wpływem sposobu wytwarzania wybranymi metodami metalurgii proszków — konwencjonalną oraz SPS (Spark Plasma Sintering). Wybrane gatunki węglików spiekanych przeznaczone na badania S30 i S40S należą do węglików przeznaczonych na narzędzia skrawające. Wykonano badania z zakresu pomiaru twardości, tribologii oraz mikroskopii stereoskopowej. Na podstawie otrzymanych wyników wykazano, że zmiana metody wytwarzania spieków z proszków na bazie węgliku wolframu na osnowie kobaltowej poprawia własności wytworzonych spieków. Ponadto wykazano, że zgodnie z przeznaczeniem danego gatunku do rodzaju obróbki, gatunek S30 wykazuje najbardziej obiecujące warunki do zastosowania w potencjalnych badaniach skrawających.

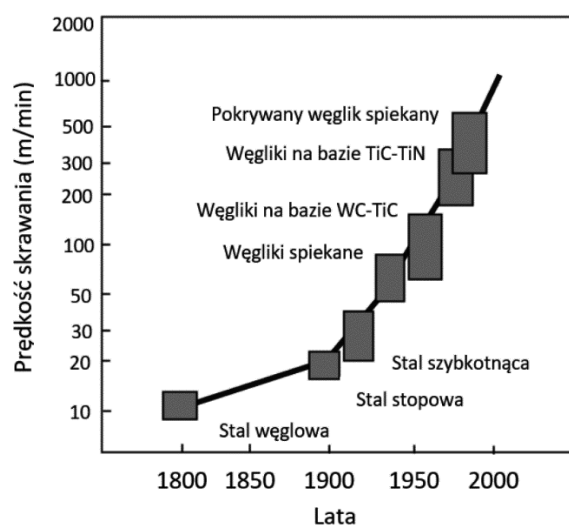
**Abstract:** The article shows results of laboratory tests concerning with the influence of the manufacturing by chosen powder metallurgy methods — conventional and SPS (Spark Plasma Sintering). Selected grades of sintered carbide S30 and S40S, intended for testing, are grades used for tooling in machining. Laboratory tests included measurements of hardness, tribology, density and stereoscopic microscopy. Based on obtained results it was shown that changing the method of cemented carbide on cobalt matrix manufacturing improved the properties of elements. Moreover, it was shown that, according to the typical use of such carbide grades in machining, the S30 grade has the most promising parameters for use in potential machining testing in the future.

**Słowa kluczowe:** metalurgia proszków, Spark Plasma Sintering, obróbka skrawaniem, węgiel wolframu, węgliki spiekane, twardość, tribologia

### 1. WSTĘP

Węgiel spiekany, nazywany żargonowo *widia*, w obróbce skrawaniem zajmuje jedno z najważniejszych miejsc jako materiał przeznaczony na narzędzia. Jest to najczęściej mieszanina proszków węglików pierwiastków wysokotopliwych na osnowie kobaltowej. Na rynku materiał

ten pojawia się jako spieki w formie wymiennych płytek o ustandaryzowanych kształtach oraz wymiarach. Aktualnie najczęściej występuje w formie płytki węglkowej z naniesioną powłoką w celu wzmocnienia własności, które pozwalają na dłuższy czas życia narzędzia podczas pracy przy wyższej temperaturze oraz prędkości (Rysunek 1) [1].

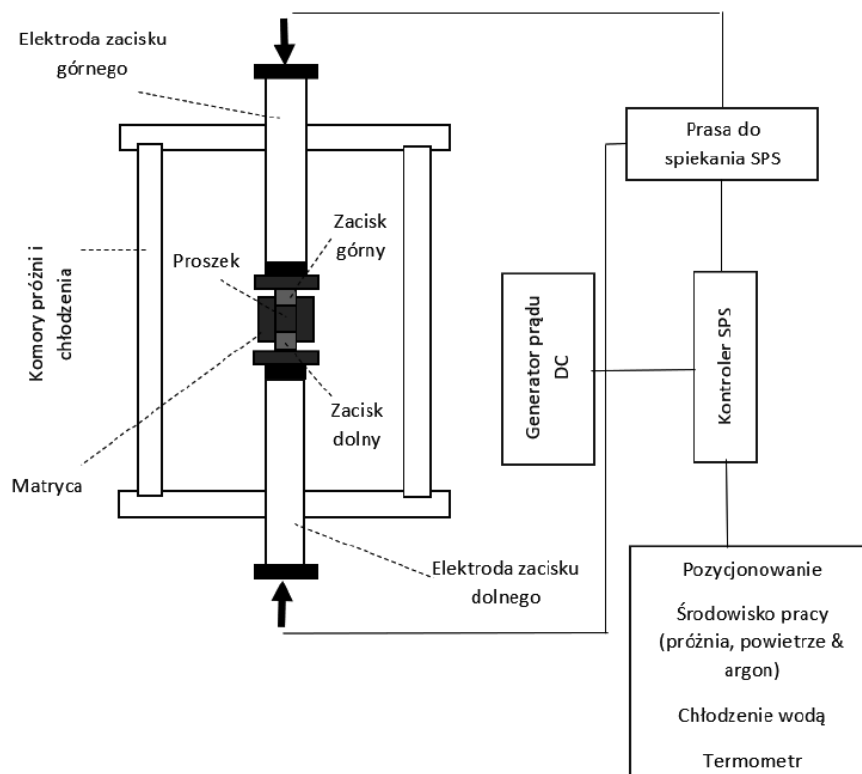


Rysunek 1. Oś czasu przedstawiająca rozwój materiałów na narzędzia skrawające [2]  
 Figure 1. Timeline showing the development of cutting tool materials [2]

Narzędzia dostępne na rynku wykonywane są za pomocą konwencjonalnych metod spiekania. Metalurgia proszków pozwala jednak na zastosowanie innych metod, które nawet jeśli przebadane, nie są szeroko wykorzystywane w danym segmencie przemysłu. Spark Plasma Sintering jest jedną z metod, która uznawana jest za niekonwencjonalną. Jest również jedną z najlepiej przebadanych, szczególnie pod względem możliwości wytwarzania materiałów na bazie węglków. Jej największymi zaletami w porównaniu do spiekania konwencjonalnego, jest skrócenie czasu samego spiekania oraz spajania wsadu, a różnica może wynosić nawet do ok. 30%. W czasie samego procesu w urządzeniu wytwarzana jest wysokotemperaturowa plazma w czasie krótkich interwałów trwających do maksymalnie kilkuset milisekund. Taki proces pozwala zachować plazmę o dużym natężeniu, ale niskim napięciu. SPS służy najczęściej do spiekania materiałów takich jak proszki metali, ceramiki czy cermetali [3-5].

Ważną zaletą związaną z metodą SPS jest zapobieganie rozrostowi ziaren w spieku, co związane jest ze skróceniem czasu do maksymalnie kilkunastu minut (wobec nawet kilkunastu godzin w wypadku spiekania konwencjonalnego) oraz z obniżeniem temperatury. Ma to szczególnie wpływ, jeżeli wytwarzane spieki mają charakteryzować się drobną strukturą ziaren [6, 7].

Najważniejszą wadą metody SPS jest problem z nawęglaniem powierzchni spieków, co jest szczególnie widoczne podczas wytwarzania elementów z proszków na bazie żelaza oraz węglków. Pojawia się również problem z dokładną rejestracją temperatury samego spieku. Aby możliwe było uzyskanie powtarzalnych wyników należy zastosować te same parametry spiekania, ale również i układ wyposażenia w komorze, np. należy zapewnić tą samą liczbę oraz wymiary grafitowych wsporników [8, 9].



Rysunek 2. Schemat urządzenia do spiekania metodą SPS [8]

Figure 2. Scheme of device used for sintering by SPS method [8]

W metodzie SPS wsad w postaci proszku umieszcza się w grafitowej matrycy i poddaje się go grzaniu za pomocą prądu impulsowego (Rysunek 2). Prąd ten przebiega przez matrycę z wsadem. Jednocześnie matryca zostaje poddana obciążeniu za pomocą zacisków pod ciśnieniem, które związane są z prasowaniem. Ważnym etapem jest oczyszczenie powierzchni wsadu z tlenków czy gazów, które mogą się na niej osadzić. Podczas grzania w cząstkach proszku formują się szypki pomiędzy nimi i dochodzi do ich wzrostu. Materiał zagęszcza się w wyniku zachodzących deformacji plastycznych, a po chłodzeniu otrzymuje się gotowy spiek [3,10].

## 2. MATERIAŁ DO BADAŃ I METODOLOGIA

### 2.1 Materiał do badań

Badania wykonano na spiekach przygotowanych za pomocą metody SPS. Są to dwa gatunki mieszanki proszków na bazie węgla wolframu o unormowanych składach S30 (przeznaczony do obróbek średnio-zgrubnych) i S40S (przeznaczony do obróbek wykańczających). Liczba próbek wyniosła sześć, po trzy na każdy skład. Dla każdego zestawu jedna z próbek została zakupiona, dwie kolejne zostały wytworzone metodą SPS. Zastosowano różne wartości temperatury samego procesu.

Proszki do wytworzenia próbek metodą niekonwencjonalną pochodzą z firmy Spiekane Baildonit, która ma swoją siedzibę w Katowicach.

Tabela 1. Składy mieszanek proszkowych

Table 1. Composition of powder mixtures

Oznaczenie	W [%]	C [%]	Ti [%]	Ta [%]	Nb [%]	Co [%]
S30	Resz.	6,23	4,00	-	-	8,00
S40S	Resz.	5,73	3,20	1,64	0,86	14,00

Spiekanie wykonano w Krakowskim Instytucie Technologicznym należącym do Sieci Badawczej Łukasiewicz. Do spiekania zastosowano dostępną aparaturę SPS HP 5 firmy FC. Umożliwia ona spiekanie szerokiego zakresu materiałów. Aparatura ta pozwala na pominięcie operacji wstępnego prasowania oraz izostatycznego dogęszczania. Wsad w formie proszku nagrzewa się bezpośrednio za pomocą przepływającego prądu.

Do spiekania zostały wykorzystane następujące parametry z temperaturą jako zmienną krytyczną.

Tabela 2. Parametry spiekania metodą SPS

Table 2. Parameters of SPS sintering method

l.p.	Temperatura spiekania 1 [°C]	Temperatura spiekania 2 [°C]	Czas [min.]	Obciążenie [kN]
S30	1250	1275	10	25
S40S	1225	1250		

## 2.2 Metodologia

Próbki przygotowano poprzez wytworzenie zglądów metalograficznych za pomocą szlifowania oraz inkludowania.

Szlifowanie wstępne wykonane zostało na urządzeniu STRUERS LaboPol-5 z głowicą LaboForce-3. Proces przebiegał przy prędkości 400 obrotów na minutę oraz wykorzystano papier ścierny o gramaturze 600 g/cm<sup>3</sup>.

Inkludowanie zostało wykonane na urządzeniu STRUERS CitoPress-20. Próbki umieszczano w urządzeniu oraz zasypywano żywicą epoksydową. Inkludowanie płytek o mniejszych wymiarach wykonywano w czasie 5 minut, zaś próbki większe 7 minut.

Szlifowanie końcowe wykonane na urządzeniu STRYERS Tegramin-30. Użyto tarczy diamentowej oraz wody jako medium. Proces trwał ok. 10 minut do uzyskania zadowalającej powierzchni otrzymanych zglądów.

Do badania odporności na zużycie ściernie wykorzystano metodę *pin-on-disc* do wyznaczenia współczynnika tarcia na urządzeniu CSM Instrument w trybie obrotowym. Jako przeciwpróbkę wykorzystano kulkę o średnicy 6 mm wykonaną z Al<sub>2</sub>O<sub>3</sub>. W czasie procesu zmiennymi parametrami są prędkość, siła oraz droga, którą przebyła kulka na powierzchni próbek.

Tabela 3. Parametry do badania tribologicznego  
 Table 3. Parameters for tribological testing

Parametr	Wartość
Średnica wytarcia [mm]	4
Prędkość liniowa [cm/s]	15
Obciążenie [N]	30
Trasa [m]	50
Częstotliwość próbkowania [Hz]	10

Po przeprowadzeniu badania na zużycie ściernie, dokonano pomiaru wskaźnika zużycia za pomocą profilometru Tylor-Hudson Sutronic 25. Pomiar dokonywany jest trzykrotnie na wykonanym wcześniej wytarciu o kształcie okręgu, który dzielony jest na  $120^\circ$ , w celu uzyskania średniego wyniku. Z otrzymanych wyników badań obliczono objętość wytarcia ze wzoru:

$$V = P_{p_{sr}} \cdot obw \left[ \frac{mm^3}{s} \right] \quad (1)$$

Gdzie:

$P_{p_{sr}}$  — średnie pole powierzchni wytarcia po trzech pomiarach;

obw — obwód wytarcia;

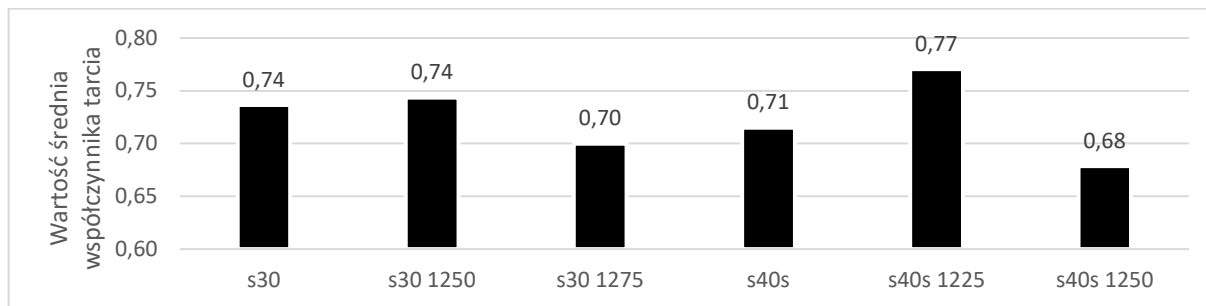
Zdjęcia mikroskopowe wytarc otrzymać na mikroskopie świetlnym stereoskopowym SteREO Discovery firmy ZEISS. Zastosowano powiększenia x10 oraz x50.

Pomiar twardości wykonano za pomocą FUTURE-TECH FM-ARS 9000. Na każdą przygotowaną próbkę wykonane zostało 5 pomiarów, z których wyznaczono wartości średnie zestawione w tabeli. Obciążenie w trakcie badania wyniosło 1 kg, a sam pomiar trwał 15 s.

### 3. WYNIKI BADAŃ I ICH OMÓWIENIE

#### 3.1. Wyniki badań odporności na zużycie ściernie oraz wyznaczania wskaźnika zużycia

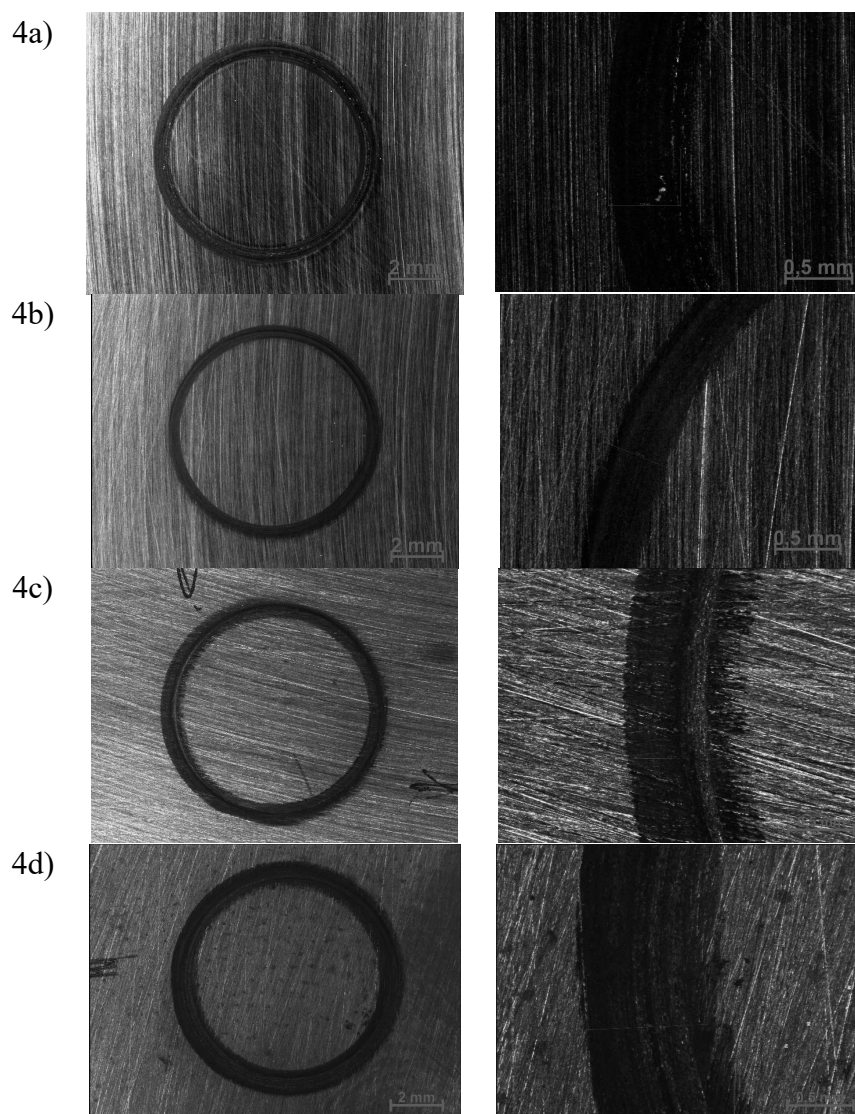
Analiza wyników badań odporności na zużycie ściernie wykazała, że średnia wartość współczynnika tarcia zmienia się. Dla próbki S30 spiekanej w  $1250^\circ\text{C}$  oraz S40S spiekanej w temperaturze  $1225^\circ\text{C}$  wartość nieznacznie się zwiększa. W przypadku próbki S40S można jednak mówić o błędzie w czasie wykonywania pomiarów ze względu na zbyt duże odchylenie, co prezentuje zestawienie na Rys. 3. W przypadku spieków wytworzonych metodą SPS w temperaturze wyższej, współczynnik tarcia zmniejszył się, choć różnica jest niewielka i dla obydwu składów wynosi 0,4.



Rysunek 3. Wykres przedstawiający wartości średnie współczynnika tarcia

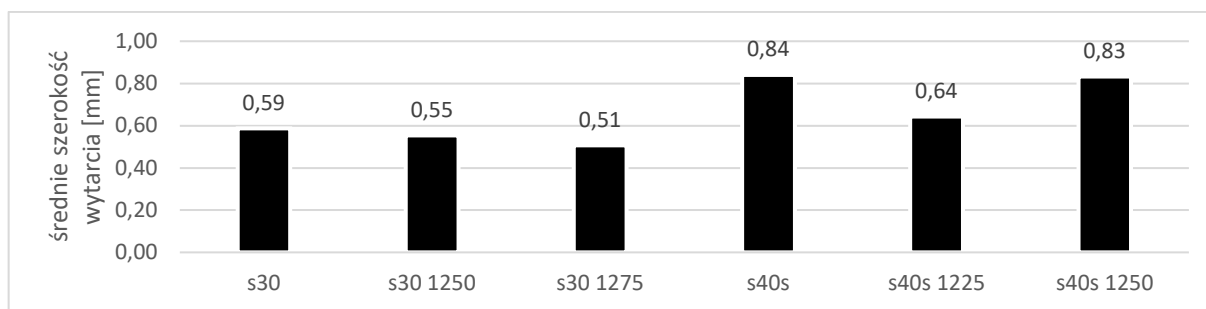
Figure 3. Plot of average values of friction coefficient

Zdjęcia na Rys. 4a-4d pokazują, że szerokości wytarcia mają mniejszą wartość w przypadku próbek spiekanych metodą SPS. Pomiary szerokości również zostały przeprowadzone trzykrotnie dla uzyskania średniego wyniku. Jak widać na zdjęciach, wytarcia dla próbek z gatunku S30 są znacząco węższe.



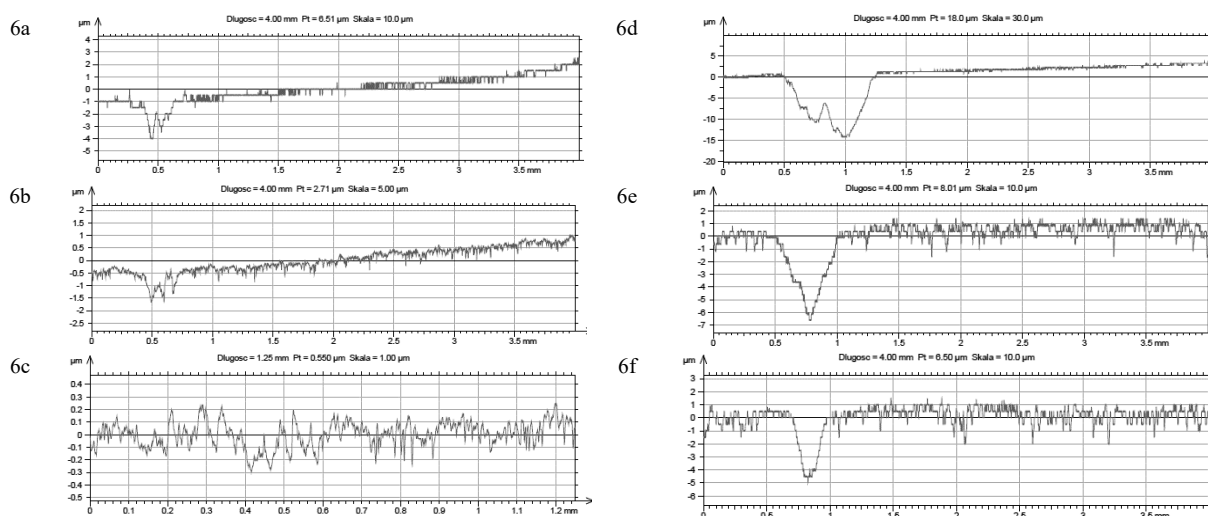
Rysunek 4. a) S30, temperatura spiekana 1250°C, b) S30, temperatura spiekana 1275°C, c) S40S, temperatura spiekania 1225°C, d) S40S, temperatura spiekania 1250°C. (pow. x10, x50)  
Figure 4. a) S30, sintering temperature 1250°C, b) S30, sintering temperature 1275°C, c) S40S, sintering temperature 1225°C, d) S40S, sintering temperature 1250°C. (zoom x10, x50)

Przeprowadzając pomiary szerokości wytarć przedstawionych na Rys. 4a-4d zauważono, że szerokości wytarcia są o ok. 0,3 mm szersze dla próbek z gatunku S40S. Na Rys. 5 widać trend związany ze zmniejszaniem się wartości szerokości wytarcia związany ze zwiększaniem temperatury spiekania. Próbką z gatunku S40S spiekana w 1225°C wykazuje to samo odchylenie, które pojawia się przy współczynniku tarcia.



Rysunek 5. Wykres przedstawiający wartości średnie szerokości wytarcia  
 Figure 5. Plot of average values of wear width

Na Rys. 6a-6f przedstawione zostały geometrie śladów wytarcia, gdzie można zauważyć różnicę w kształcie profili dla poszczególnych próbek. Dla próbek z gatunku węgliku S30 wytarcia są, co więcej dla próbki spiekanej w 1275°C dla tej mieszanki można mówić o tak niewielkim zużyciu, że może zostać ono uznane za obróbkę powierzchni typu szlifowanie czy polerowanie, a nie zużycie. W przypadku próbek z gatunku S40S również dochodzi do zwężenia i spłykania wytarc.



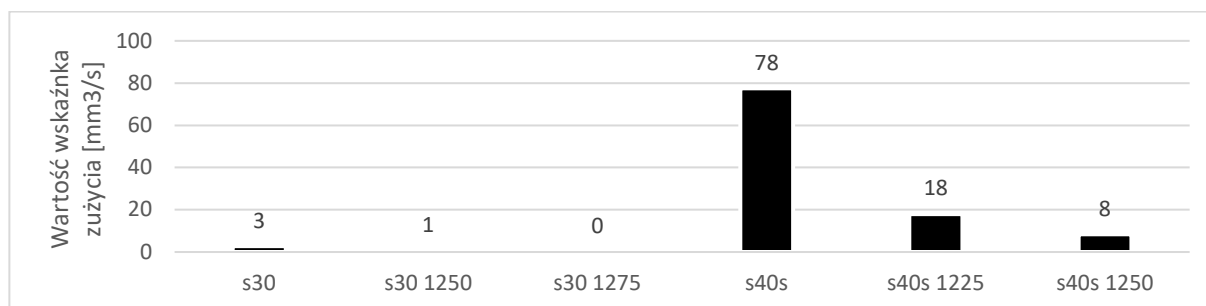
Rysunek 6. Wykresy przedstawiające profile poprzeczne przekroju wytarcia dla: a-6) węgliku spiekane go gatunku S30, d-f) węgliku spiekane go gatunku S40S  
 Figure 6. Plots of cross-sectional profile of the abrasion for: a-c) cemented carbide of S30 grade, d-f) cemented carbide of S40S grade.

Badanie wskaźnika zużycia przyjmowało wykonanie trzech pomiarów i wyliczenie średniej. Dla próbki rynkowej S30 średnia wartości pola powierzchni wytarcia wynosiła  $222 \mu\text{m}^2$ , dla próbki spiekanej w 1250°C —  $58 \mu\text{m}^2$ , a w 1275°C —  $0 \mu\text{m}^2$ . W przypadku próbek z gatunku S40S, próbka rynkowa —  $6175 \mu\text{m}^2$ , próbka spiekana w 1225°C —  $1432 \mu\text{m}^2$ , w 1250°C —  $663 \mu\text{m}^2$ . Na Rysunku 7 przedstawiono graficznie wartości wskaźnika zużycia wyliczone dla wzoru (1), przyjmując  $r=2\text{mm}$  jako połowę ze średnicy wytarcia w czasie badania tribologicznego.

Jak można zauważyć po obliczeniach, potwierdza się, że próbka S30 nie podlega niemal żadnemu wytarciu, wartość wskaźnika dla próbki rynkowej wynosi 3. W przypadku próbek z gatunku S40S wartości zmieniają się gwałtownie, różnica między próbką kontrolną (rynkową) a



spiekany metodą SPS jest ponad czterokrotna.

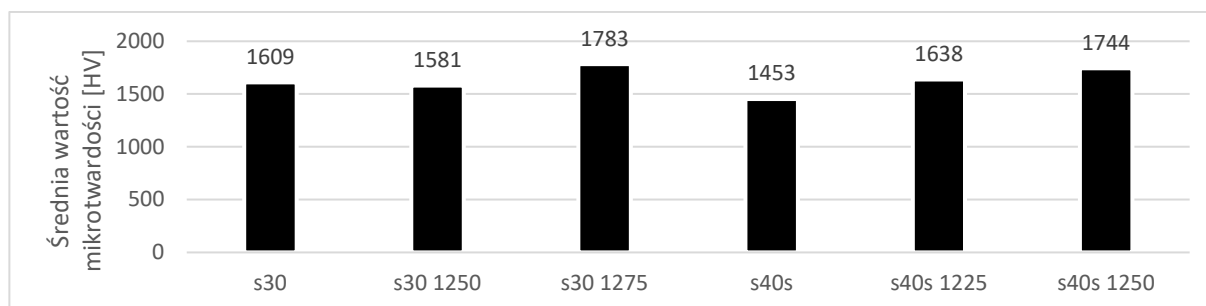


Rysunek 7. Wykres przedstawiający wskaźnik zużycia

Figure 7. Plot of wear factor

### 3.2 Wyniki badań pomiaru mikrotwardości

W czasie badania wykonano pięć pomiarów dla każdej próbki, z których obliczono wartość i zestawiono w formie wykresu na Rys. 8. Średnie wartości mikrotwardości Vickersa pokazują, że spiekanie metodą SPS podwyższa twardość próbek, wobec ich odpowiedników rynkowych. W przypadku próbek z gatunku S30 i dla spiekania w temperaturze 1250°C dochodzi do niewielkiego obniżenia wartości, jednak jest on na tyle znikomy (wynosi około 20HV), że nie wpływa znacząco na wyniki. Być może błędem można dopatrywać się w metodzie badania twardości i wyborze miejsca pomiaru. W przypadku próbek z gatunku S40S widać wyraźnie, że wartość średnia twardości zwiększa się, różnica między próbką rynkową a spiekaną w 1250°C wynosi około 300HV, co jest już różnicą znaczącą.



Rysunek 8. Wykres przedstawiający średnie wartości twardości Vickersa

Figure 8. Plot of average value of Vickers' hardness

## 4. PODSUMOWANIE

Analiza otrzymanych wyników badań pozwoliła na sformułowanie następujących wniosków:

1. Istnieje możliwość zastosowania metody SPS do spiekania wybranych gatunków węgla i wykazanie zmian, które zachodzą we własnościach samych spieków wobec płytek skrawających wykonanych konwencjonalnie.
2. Zmiana (nawet 25°C) temperatura procesu spiekania wpływa na własności wytworzonych elementów.
3. Zastosowanie metody SPS spiekania wpływa na zwiększenie odporności na zużycie ścierne. Zarówno szerokości wytarcia (maksymalnie około 0,1 mm), jak i wskaźniki

- zużycia zmniejszają się. Dla wskaźników zużycia różnica jest znacząca, dla gatunku S40S jest niemal dziesięciokrotna.
4. Analiza pomiarów twardości wskazuje, że metoda SPS ma wpływ na podwyższenie tej właściwości w spiekach. Różnica pomiędzy płytką rynkową a spiekaną wynosi nawet do 200HV.
  5. Metoda SPS może być odpowiednia jako alternatywa do spiekania proszków węgla wolframu na osnowie kobaltowej z przeznaczeniem na płytki skrawające. Wyniki badań oraz znajomość przeznaczenia gatunku danego węgla pozwala jednak stwierdzić, że dla gatunku S40S zmiana metody nie jest krytyczna. Gatunek S40S przeznaczony do obróbek wykańczających nie wymaga tak dużej wytrzymałości z powodu znacząco niższych naddatków oraz sił skrawających. Dla gatunku S30 zmiana metody wytwarzania z konwencjonalnej na SPS ma znaczące uzasadnienie, spieki są odporniejsze na zużycia mechaniczne, co może w przyszłości zostać poparte dodatkowymi badaniami po przeprowadzeniu prób skrawaniowych.
  6. Próbką z gatunku węgla S40S spiekana w temperaturze 1225°C została uznana za niemiarodajną, jeżeli chodzi o część wyników badań. Powód może być związany z błędem w czasie wytwarzania lub też w czasie przeprowadzenia badań trybologicznych.

## LITERATURA

1. R. Kuryjanski, Obróbka skrawaniem i obrabiarki, PW, Warszawa, 2011.
2. K. Tsuda, History of Cemented Carbides and Cermet, SEI Technical Review, 2016.
3. M. Nygren, Z.J. Shen, Spark Plasma Sintering: Possibilities and Limitations. Key Engineering Materials - KEY ENG MAT 264-268 (2004) 719-724.
4. M. Eriksson, M. Radwan, Z. Shen, Spark plasma sintering of WC, cemented carbide and functional graded materials, International Journal of Refractory Metals and Hard Materials. 36 (2013) 31-37.
5. Y.A. Dar, N.A. Sheikh, A review of fabrication and properties of spark plasma sintered tungsten carbide based advanced composites, Proceedings of the Institution of Mechanical Engineers, Part E: Journal of Process Mechanical Engineering, 236(3) (2022) 1216-1228.
6. D. Garbiec: Iskrowe spiekanie plazmowe (SPS): teoria i praktyka, Inżynieria Materiałowa 204(2) (2015) 60-64.
7. V. Aghaali, T. Ebadzadeh, S.M. Zahraee, et al. Microstructure and mechanical properties of WC-TiC-Co cemented carbides produced by spark plasma sintering (SPS) method, SN Appl. Sci. 5 (2023) 285.
8. M. Tokita, Progress of Spark Plasma Sintering (SPS) Method, Systems, Ceramics Applications and Industrialization, Ceramics, 4(2) (2021) 160-198.
9. B. Kumar, S.B. Balashanmuganathan, K. Jerrin, N. Joseph, N. A. Jiss, Review of Spark Plasma Sintering Process, IOP Conference Series: Materials Science and Engineering. (2020) 993.
10. U. Anselmi-Tamburini Spark Plasma Sintering. Encyclopedia of Materials: Technical Ceramics and Glasses, Elsevier (2021) 294-310.



26th January 2024  
Gliwice, Poland

DEPARTMENT OF ENGINEERING MATERIALS AND BIOMATERIALS  
FACULTY OF MECHANICAL ENGINEERING  
SILESIA UNIVERSITY OF TECHNOLOGY

## INTERNATIONAL STUDENTS SCIENTIFIC CONFERENCE

### **The comparison of materials used for 3D printing technology and their environmental impact**

P. Kruczyński<sup>a</sup>, G. Pośpiech<sup>a</sup>, D. Celeban<sup>a</sup>, M. Szczypiór<sup>b</sup>, A. Kania<sup>c</sup>, M. Polok-Rubiniec<sup>c</sup>,  
A. Włodarczyk-Fligier<sup>c</sup>

<sup>a</sup> Students of Mechanical Engineering at the Faculty of Mechanical Engineering at the Silesian University of Technology

<sup>b</sup> Student of Automation and Robotics at the Faculty of Automatic Control, Electronics and Computer Science at the Silesian University of Technology  
email: pk301620@student.polsl.pl

<sup>c</sup> Silesian University of Technology, Faculty of Mechanical Engineering, Department of Engineering Materials and Biomaterials  
email: aneta.kania@polsl.pl

**Abstract:** The article explores possible ways to implement 3D printing technology in the medical industry, discussing the advantages and disadvantages of various materials (filaments) for 3D printing. The importance of material selection is also highlighted in the creation of orthoses and insoles for shoes. This solution was presented by students from the Silesian University of Technology. Subsequently, experiments were conducted to analyze the results, aiming to verify whether the set requirements for the components were fulfilled and, if not, to understand the reasons behind it.

**Keywords:** 3D printing, FDM, filament, PLA, PETG, TPU, environmental impact.

## **1. INTRODUCTION**

3D printing is an innovative technology with potential applications in various fields and industries. Using this technology, a study was conducted on how 3D printing could aid in medicine without harming the planet. Research and experiments were conducted by students from the Silesian University of Technology. The studies aimed to identify the best materials for creating orthotics and insoles that could contribute to society in the near future. Materials such as PLA, PETG, TPU, and ABS will be used in the attempt to create perfect orthotics and insoles. The research utilized FDM (Fused Deposition Modeling) printers and analyzed their environmental impact.

3D printing and the materials used in it represent a great opportunity for environmental protection. There are many pro-ecological solutions that can have a beneficial impact on protecting the Earth. For now, these are quite expensive technologies, representing technical innovations, but over the years they will certainly be widely used [1,2].

3D printing has both advantages and disadvantages. The main argument of skeptics is that objects produced using 3D printing are mainly plastics, so it is another technology that causes littering of the environment. Another issue of concern is the generation of harmful fumes during the printing process. Therefore, you should look for biodegradable or recyclable materials.

## 2. MATERIALS USED FOR 3D PRINTING

There are several materials used for 3D printing, each with different characteristics, properties, and applications. Below are presented details about commonly used materials in 3D printing:

1. PLA (Polylactic Acid) – is a biodegradable and bioactive thermoplastic derived from renewable sources, typically made from cornstarch or sugarcane. It is widely used for prototyping and suitable for general-purpose 3D printing due to its rapid decomposition period of 45-65 days. The properties of PLA [3]:

- Glass Transition Temperature: 45-65°C
- Density: 1.2-1.4 g/cm<sup>3</sup>
- Yield Strength: 40-50 MPa
- Young's Modulus: 2000 MPa
- Elongation at Break: 2-3%
- Shrinkage after Processing: 0.3-0.5%

2. ABS (Acrylonitrile Butadiene Styrene) – is a durable and impact-resistant thermoplastic often used in industrial applications. It has good thermal resistance but may emit fumes during printing, so proper ventilation is recommended. ABS is commonly used for functional prototypes and end-use products, and its advantage includes the ability to be recycled multiple times. The properties of ABS [4]:

- Glass Transition Temperature: 95-100°C
- Density: 1.03-1.05 g/cm<sup>3</sup>
- Yield Strength: 30-40 MPa
- Young's Modulus: 1600-1800 MPa
- Elongation at Break: 4.8-7%
- Shrinkage after Processing: 0.4-0.7%

3. PETG (Polyethylene Terephthalate Glycol) – is a durable and transparent thermoplastic known for its high strength and chemical resistance, as well as its recyclability. However, its drawback is its exceptionally long decomposition period, ranging from 40 to 1000 years [5,6]. The properties of PETG:

- Glass Transition Temperature: 75-85°C
- Density: 1.27-1.35 g/cm<sup>3</sup>
- Yield Strength: 45-65 MPa
- Young's Modulus: 2000-3000 MPa
- Elongation at Break: 140%
- Shrinkage after Processing: 0.2-0.6%

4. TPU (Thermoplastic Polyurethane) – is a flexible thermoplastic characterized by high elasticity and wear resistance. It is often used for 3D printing parts with flexible properties, such as phone cases, watch straps, or damping elements. TPU is known for its good tensile strength and flexibility, making it suitable for various applications, including in the medical field, sports, or the production of insoles for shoes [7,8]. The properties of TPU:
- Glass Transition Temperature:  $\sim 80^{\circ}\text{C}$
  - Density:  $1.1\text{-}1.25\text{ g/cm}^3$
  - Yield Strength:  $45\text{-}65\text{ MPa}$
  - Young's Modulus:  $26\text{-}78\text{ MPa}$
  - Elongation at Break:  $140\%$
  - Shrinkage after Processing:  $--\%$  (not specified)

### 3. SELECTION OF MATERIAL USED AS ORTHOSES AND INSOLE FOR SHOES

The first material selected for the tests was PLA due to its valuable properties; it is biodegradable, but its rigidity caused problems with putting on and taking off the orthosis (Figs. 1,2) [3,9]. As an insole for shoes, this material also did not perform well due to rapid deformation during walking.

The next material selected for the production of orthoses and insoles was ABS [4]. Unfortunately, this material was an incredibly erroneous choice due to its hardness (Shore hardness:  $90\text{-}100\text{ ShD}$ ), which was too uncomfortable to wear as orthoses and insoles.

Before the final material in the test, PETG, performed well as an orthosis, thanks to slight deformations caused by its mild flexibility, allowing it to adapt to the hand of the person for whom it was created [5,6]. However, as an insole for shoes, it remained problematic, as its flexibility was insufficient.

The last material, TPU, proved to be suitable for both orthoses and insoles [7,8]. It is elastic enough, though not biodegradable, it is recyclable, allowing us to save on materials and reduce resources most.

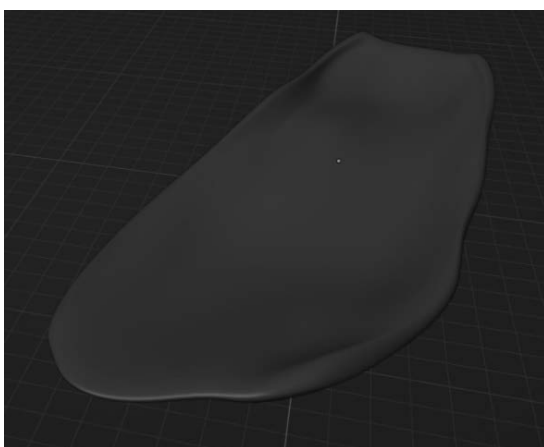


Figure 1. A 3D-printed insole model for use in a 3D printer



Figure 2. A 3D-printed orthosis model made from selected TPU filament

#### 4. CONCLUSIONS

The article discusses a comparison of properties of materials used in 3D printing technology for the production of orthoses and orthopedic insoles. It analyzes the advantages and disadvantages of various materials (filaments) used in 3D printing, with a particular focus on their application in orthopedics [9]. The study presents research results aimed at verifying whether the set requirements for components were met and, if not, understanding the reasons behind it.

Using materials such as PLA, ABS, PETG, and TPU with Fused Deposition Modeling (FDM) technology, the article emphasizes the importance of selecting the right material in terms of its environmental impact [1,2]. The research highlights PLA for its biodegradable and bioactive properties, as well as its rapid degradation period. ABS is dismissed due to significant post-processing shrinkage and challenges in fitting to the body. PETG, despite being durable and recyclable, is characterized by an exceptionally long degradation period. TPU is described as a flexible thermoplastic suitable for medical, sports, and footwear insole applications.

In summary, the article focuses on the significance of choosing appropriate materials for 3D printing in the field of orthopedics, analyzing their characteristics and impact on environmental protection.

#### LITERATURE

1. N. Jaworska, H. Podsiadło, 3D printing technology as an opportunity for the natural environment, [http://www.cobrpp.com.pl/actapoligraphica/uploads/pdf/AP2019\\_2\\_Jaworska\\_Podsiadlo.pdf](http://www.cobrpp.com.pl/actapoligraphica/uploads/pdf/AP2019_2_Jaworska_Podsiadlo.pdf), 2023.
2. Is 3D printing ecological?, <http://www.swiatdruku3d.pl/czy-drukowanie-3d-jest-ekologiczne/>, 2023.
3. PLA filament – properties and printing, <https://3dreaktor.pl/Filament-PLA-wlasciwosci-i-drukowanie>, 2023.
4. ABS plastic – acrylonitrile-butadiene-styrene copolymer, <https://www.resinex.pl/rodzaje-polimerow/abs.html>, 2023.
5. PETG filament – properties and printing, <https://3dreaktor.pl/filament-pet-g-wlasciwosci-i-drukowanie>, 2023.
6. Comparison of PET and PETG plastics, <https://b3d.com.pl/porownanie-tworzyw-pet-i-petg/>, 2023.
7. TPU technical data sheet, <https://sklep.3dl.tech/wp-content/uploads/2017/06/TDS-TPU-95A-v3.010-pol.pdf/>, 2023.
8. What is thermoplastic polyurethane (TPU)?, <https://doapple.pl/pl/blog/co-to-jest-termoplastyczny-poliuretan-tpu-1648634928>, 2023.
9. J. Buckup, R. Hoffmann, Clinical tests in the examination of bones, joints and muscles Examination, symptoms, tests, PZWL Medical Publishing House, Warsaw, 2020.

**Praca powstała w wyniku realizacji projektu Project Based Learning (PBL) pt. Opracowanie spersonalizowanych stabilizatorów i wkładek ortopedycznych z wykorzystaniem technologii druku 3D.**



26th January 2024  
Gliwice, Poland

DEPARTMENT OF ENGINEERING MATERIALS AND BIOMATERIALS  
FACULTY OF MECHANICAL ENGINEERING  
SILESIA UNIVERSITY OF TECHNOLOGY

## INTERNATIONAL STUDENTS SCIENTIFIC CONFERENCE

### **Numerical analysis of the effect of operating conditions on steering components in a passenger car**

Ł. Lomania<sup>a</sup>, C. Zach<sup>a</sup>, K. Kojm<sup>a</sup>, D. Towarnicki<sup>a</sup>, R. Trojnar<sup>a</sup>, M. Musialik<sup>b</sup>, W. Mikołajko<sup>c</sup>,  
A. Śliwa<sup>c</sup>, M. Sroka<sup>c</sup>, A. Dziwis<sup>c</sup>

<sup>a</sup> Student - Politechnika Śląska, Wydział Mechaniczny Technologiczny, Katedra Materiałów Inżynierskich i Biomedycznych

e-mail: lukalom979@student.polsl.pl, cezazac076@student.polsl.pl, kajekoj367@student.polsl.pl, domitow239@student.polsl.pl, radotro676@student.polsl.pl

<sup>b</sup> Zespół Szkół Technicznych i Ogólnokształcących „Mechanik” w Tarnowskich Górach

e-mail: musialmati123321@gmail.com

<sup>c</sup> Politechnika Śląska, Wydział Mechaniczny Technologiczny, Katedra Materiałów Inżynierskich i Biomedycznych

e-mail: wojciech.mikolajko@polsl.pl, agata.sliwa@polsl.pl, amadeusz.dziwis@polsl.pl, marek.sroka@polsl.pl

**Keywords:** SolidWorks, stresses, computer simulation, FEM, steering components.

## **1. INTRODUCTION**

### **Finite Element Method (FEM)**

The Finite Element Method (FEM) is one of the most widely used tools in structural engineering calculations used in computer programs. Its ability to accurately model the behavior of structures under external influences makes it a common tool in material strength simulations. The benefits of this method and its ease of use contribute to its popularity in the analysis of systems with complex geometries, enabling accurate determination of stresses, displacements and strains. [1]

The idea of FEM is to reduce the model to a discretization mesh, which means simplifying the structure to a finite number of elements, where stresses propagate, and their values are calculated at successive nodes of the mesh. Analysis using FEM provides important information about the processes in structures and their response to varying forces over time. The precision of the method depends on the proper definition of boundary conditions and adjustment of the mesh, including the compaction and reduction of elements at the interface of different parts of the structure. Programs that enable FEA, such as Solidworks used in this work, allow the use of extensive material libraries and the definition of custom parameters for structural materials, which makes it possible to simulate a given phenomenon as faithfully as possible and achieve maximum precision. [2]

This, in turn, enables the best possible modeling of a given phenomenon and achieves maximum precision in simulations. [2]

### **FEM in steering analysis**

One of the applications of FEA in materials engineering is the analysis of an automobile's steering system [Fig.1]. The steering system is a key component of any vehicle, from small passenger cars to heavy commercial vehicles. Its role is not limited to providing the driver with directional control, but also includes complex mechanisms that affect stability, safety and comfort. FEA analysis of the steering system is becoming an indispensable tool in the design of modern vehicles, especially in the context of increasing expectations for performance, steering precision and response to changing road conditions.

When designing a structure using Computer Aided Design (CAD), it is possible to simulate various scenarios that may occur during vehicle operation. Theoretical models, responsible for analyzing stress propagation, are approximated using CAE (Computer Aided Engineering) structural engineering calculations. External forces acting on the material are analyzed using numerical methods. The use of these methods makes it possible to obtain results quickly compared to analytical methods, saving time and effort, as well as minimizing the number of product prototypes needed. It is important to predict the appropriate behavior of the structure under different conditions, as improper construction can lead to serious consequences, negatively affecting human life and health, instead of fulfilling the original task of ensuring safety.



*Fig. 1. Example of a steering system [3].*

### **Materials engineering of the steering system**

The rack-and-pinion gear in the steering system consists of a rack-and-pinion bar, also known as a pinion, arranged transversely to the axle of the car [Fig.2]. This pinion gear cooperates with a cylindrical gear, wound onto the vehicle's steering shaft. The main function



of the gearbox is to convert the rotary motion of the steering wheel into the transverse motion of the pinion, allowing precise control of the vehicle. The key benefits of this design solution include simplicity of construction, small size and relatively low weight. The simplicity of this design also carries a low production cost which is a key element for manufacturers. The pinion gear also has a high efficiency in the transmission of torque from the steering wheel to the wheels, efficiency of  $\mu = 0.9$ . Of course, we do not yet know of elements without any disadvantages, one of which of these disadvantages is certainly the high sensitivity to vibration and wheel impacts, due to the low friction in the rack-and-pinion mechanism, is related to the previously mentioned high efficiency, which remains constant in both directions of gear movement. Another disadvantage is certainly the relatively small gear ratios. [4][5]

Materials engineering uses high-strength materials such as steel and aluminum alloys. Manufacturing processes include precision machining, hardening and the application of protective coatings. The choice of materials depends on the application, taking into account power steering systems or high-powered vehicle specifications. The main aspect manufacturers focus on is optimizing weight, strength, and friction and wear analyses. The whole process requires a careful approach, including strength test analyses, precision surface treatments and design optimization studies. As a result, the gearbox must meet stringent requirements for durability, performance and reliability under demanding vehicle operating conditions. [6]



*Fig. 2. Example of a gear wheel [7].*

## **PURPOSE OF THE WORK**

The purpose of the study was to examine the effect of the force applied to the various locations of the gear strip. In the simulations carried out, the stress, displacement and deformation of the component under the effect of the force were checked.

## **METHODOLOGY**

To be able to perform the analysis, a gear strip was designed in SolidWorks. Then the boundary conditions were implemented, i.e. finite element mesh, fixations, gravitational forces acting on the strip. The final step was to run the solver. The effect of the force on the stress,

displacement and deformation of the component depending on where the force is applied was analysed [Fig.3-4]. Table 1 shows the strength characteristics of AISI 304.



Fig. 3. Place of force application for the first simulation.



Fig. 4. The place of force application for the second simulation.

Table 1. Strength characteristics of AISI 304

Yield strength	2,06807e+08 N/m <sup>2</sup>
Tensile strength	<b>5,17017e+08 N/m<sup>2</sup></b>
Coefficient of longitudinal elasticity	1,9e+11 N/m <sup>2</sup>
Poisson's ratio	0,29
Specific weight	8 000 kg/m <sup>3</sup>
Transverse elasticity coefficient	7,5e+10 N/m <sup>2</sup>
Coefficient of thermal expansion	1,8e-05 /Kelvin

## RESULTS AND SUMMARY

The simulation results made it possible to observe the effect of force on the gear strip, which is a component of the vehicle steering system. Figures 5 and 6 show the distribution of stresses [MPa] developed in the modeled component, the next show the results of displacements in millimetres and the results of deformations resulting from forces. Table 2-3 shows the results of tension, displacement and deformation.

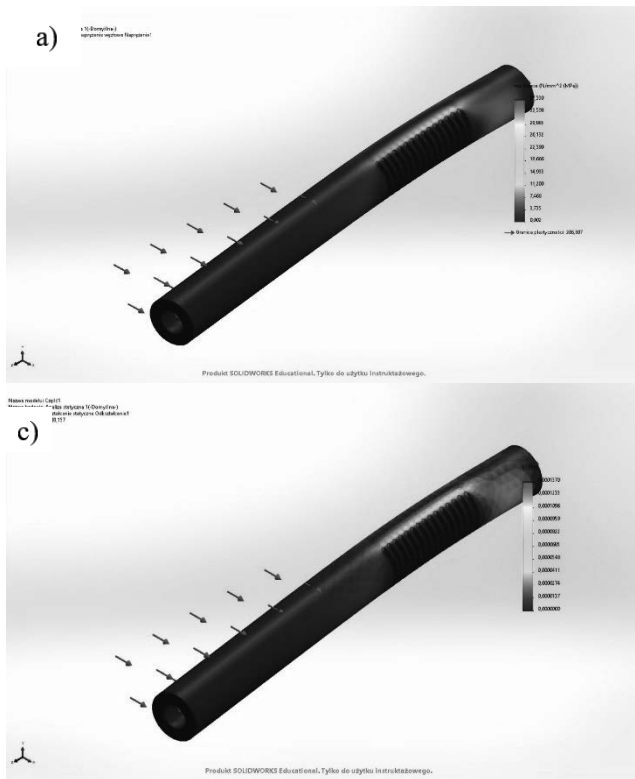


Fig. 5. When a force of 500N is applied to the strip against the notches, the results are shown:  
 a) Tension,  
 b) Displacement,  
 c) Deformation.

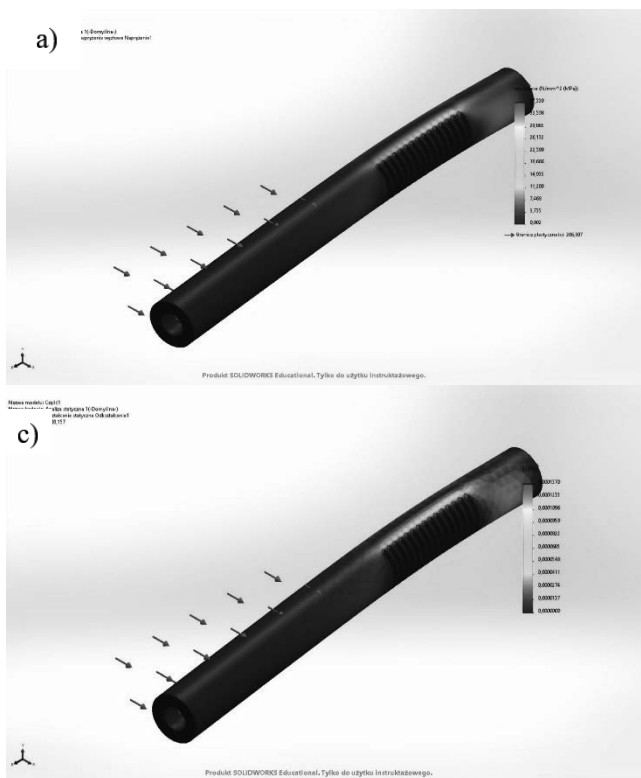


Fig. 6. Under a force of 500N on the strip in the direction of the notches, the results are shown:  
 a) Tension,  
 b) Displacement,  
 c) Deformation.

Table 2. Stress results.

Name	Minimum tension [MPa]	Maximum tension [MPa]
First simulation	0,002	37,330
Second simulation	0,002	37,330

Table 3. Displacement results.

Name	Minimum displacement [mm]	Maximum displacement [mm]
First simulation	0,000	0,329
Second simulation	0,000	0,329

## CONCLUSION

The simulation involved testing the component under applied force. The simulation results confirm that the material exhibits isotropic mechanical properties in the tested load range.

In the case of isotropy, the material's properties are identical in all directions, meaning that the material's responses to force are the same regardless of the orientation of the force relative to the material's structure. The lack of differences between displacement, strain and stress for different force directions suggests that the material is homogeneous and mechanically symmetrical.

The simulation confirms that the analyzed material is isotropic, meaning that its mechanical properties are independent of the direction of forces acting on the on the material.

Symmetry of structure: The lack of differences in results for different force directions suggests, that the structure of the material is symmetrical in terms of mechanical responses.

Homogeneous force responses indicate the homogeneity of the material, meaning that its mechanical properties are the same at all points in the material.

Materials with isotropic mechanical properties are often more useful in practice because their behavior is more predictable and easier to control under different loading conditions.

The findings may be important for material designers and engineers, as they suggest that the analyzed material can be used in applications where uniformity and predictability of mechanical behavior are required regardless of the direction of forces.

## ACKNOWLEDGEMENTS

The work was created as a result of the project as part of project based learning - PBL, in the X competition under the Initiative of Excellence - Research University, Silesian University of Technology.

## BIBLIOGRAPHY

- [1] J. Zielnica, Wytrzymałość materiałów, Wyd. Pol. Poznańskiej, 1996.
- [2] M. Sydor, Podstawy komputerowo wspomaganego projektowania Wprowadzenie do CAD., Warszawa: PWN, 2009

- 
- [3] <https://motofakty.pl/uklad-kierowniczy-jak-jest-zbudowany-i-co-sie-w-nim-psuje/ar/c4-16262345>
- [4] M. Łukasiewicz, Wykonywanie naprawy układów kierowniczych, Wyd. Instytut Technologii Eksploatacji – Państwowy Instytut Badawczy Radom 2007
- [5] S. Orzełowski, Naprawa i obsługa pojazdów samochodowych, Wyd. WSiP, 1969
- [6] G. Gritti, F. Peverada, S. Orlandi, M. Gadola, S. Uberti, D. Chindamo, M. Romano, A. Olivi Advances on Mechanics, Design Engineering and Manufacturing - Mechanical steering gear internal friction, Wyd. Springer, 2016
- [7] <https://www.betkowskiservice.pl/kolo-zebate-przekladni-kierowniczej-john-deere-507,3,39737,46897>



26th January 2024  
Gliwice, Poland

DEPARTMENT OF ENGINEERING MATERIALS AND BIOMATERIALS  
FACULTY OF MECHANICAL ENGINEERING  
SILESIA UNIVERSITY OF TECHNOLOGY

## INTERNATIONAL STUDENTS SCIENTIFIC CONFERENCE

### Measuring the angle of repose of granulates made from automotive waste

V. Mancel<sup>a</sup>, T. Kuvik<sup>a</sup>, J. Krilek<sup>a</sup>, M. Ťavodová<sup>b</sup>

<sup>a</sup> Technical University in Zvolen, Faculty of Technology, Department of Environmental and Forestry Machinery

email: vladimirmancel@gmail.com, t.kuvik14@gmail.com, jkrilek@gmail.com

<sup>b</sup> Technical University in Zvolen, Faculty of Technology, Department of Manufacturing Technologies and Quality Management

email: tavodova@tuzvo.sk

**Abstract:** The article is focused on the evaluation of the repose angles of granulates by measuring the height of the powder cone on a measuring device. The investigated granulates were obtained from waste plastic and rubber parts of cars, specifically painted bumpers, unpainted bumpers, fuel tanks, tires and a mixture of seals and carpets. Plastic granulates were produced in the workshops of the Technical University in Zvolen with a prescribed fraction of 1.0-4.0 mm, and rubber granulates were processed and delivered by the company AVE SK Odpadové hospodárstvo, s.r.o. with a prescribed fraction of 1.0-3.0 mm. The ISO 4324 standard was used to measure the individual angles of repose. The results showed that the angle of repose of individual granulates ranged from 32.99 to 39.62°. Based on the results, we can say that plastic granulates and granulate from tires are included in the "free-flowing" group, and granulate from a mixture of seals and carpets in the "fair to passable flow" group. The output of this work will be utilized to design the equipment's input hopper so that the aforementioned granulates can be applied during the process of producing innovative wood composites.

**Keywords:** angle of repose, granulate, plastic, rubber

## 1. INTRODUCTION

Granular materials including powders, seeds, and soils are inevitably used in industrial and technical applications [1]. Thus, more research and development are currently required to streamline and ease the handling and production of bulk granular materials. These advancements are reliant on the different characteristics and mechanical behavior of these materials being clarified. When granular materials are sheared or disturbed, they behave as non-Newtonian fluids rather than stable, solid materials, which presents difficulties for handling and production [2]. Furthermore, the force chains in granular materials transfer stress in an uneven manner, contingent upon the packing configuration and particle interactions [3]. Several factors influence granule flowability, and the angle of repose is one of them. As such, even while the angle of repose can serve as a gauge for flowability, it is subject to a variety of

influences and has a wide range of definitions, measuring techniques, and uses. Granular materials are second most commonly utilized in industry, with fluid materials being the major material used [1]. A cluster of unique particles that lose energy as they contact with other particles is referred to as granular material [4]. Generally, a material's ability to be classified as granular is determined by its particle size. The particle size range of the granular materials is from 1  $\mu\text{m}$  to 5 mm [5]. One of the most important property of the granular material is angle of repose.

### 1.1. Angle of repose

The angle of repose should be defined according to the particular behavior and application. The many forms (static and dynamic) and definitions of the angle of repose are linked to certain uses and the accompanying characteristics (such as flowability, friction, etc.). Therefore, in order to select a definition that is appropriate and useful in the context of studying and calculating the angle of repose of any granular material, those objectives should be predetermined. According to physical definitions, the angle of repose is the difference in angle between granular material phase transitions [6]. The steepest slope of the unconfined material, measured from the horizontal plane on which the material can be heaped without collapsing, is one of the definitions of the angle of repose that is most frequently employed [7]. The Hausner ratio or the tapped-to-bulk density ratio are commonly used to define the angle of repose for powders, which are defined as small-sized granular materials subject to cohesion and suspension in a gas. Powders will flow at angles greater than the angle of repose. The cohesiveness of the granular material can also be determined by the angle of repose [8], with reference to the Carr categorization of flowability displayed in Table 1.

Table 1. Carr categorization of powder flowability according to repose angle [9]

Description	Repose Angle
Very free-flowing	<30°
Free flowing	30-38°
Fair to passable flow	38-45°
Cohesive	45-55°
Very cohesive	<55°

In general, the static friction coefficient and the angle of internal friction are connected to the angle of repose. The constant volume angle in a critical condition or the residual internal friction angle are frequently taken to be the same as the angle of repose in the literature [10]. Because granular soil behaves very differently under low confining pressure than it does at zero confining pressure, this assumption is not always true [11]. Furthermore, there is no clear correlation between the angles of repose and internal friction for dry, fine granular materials with a short angle of repose and a particle size smaller than 5  $\mu\text{m}$  [12]. The angle of repose can be affected by a wide range of variables, including the mass of the material, the pouring height, the morphology of the material, the pull-out velocity of the hollow cylinder (a measurement tool for the angle of repose), stratification, density, moisture content, interface friction angle, and the addition of solvents. The angle of repose typically falls between 0° and 90° [13].

## 2. MATERIAL AND METHODS

Similar to how the angle of repose is defined, the measurement technique should be chosen with predetermined goals in mind, taking into account the particular material and application.

### 2.1. Granulates processing

Granulates (Figure 1) made from waste painted and unpainted bumpers, fuel tanks, tires and a combination of car seals and carpets were used as material. Painted and unpainted bumpers were made primary of polypropylene (PP), fuel tanks of polyethylene (PE), tires of natural rubber (NR) and styrene butadiene rubber (SBR), and a combination of seals and carpets of nitrile butadiene rubber (NBR) and ethylene propylene diene monomer rubber (EPDM). Plastic granulates were produced in the workshops of the Technical University in Zvolen using a knife shredder (Profing, type: DP 11-240/350) with a prescribed fraction from 1.0 to 4.0 mm. The rubber granulates were processed and delivered by the company AVE SK Odpadové hospodárstvo s.r.o. (Kechnec) with a prescribed fraction from 1.0 to 3.0 mm.

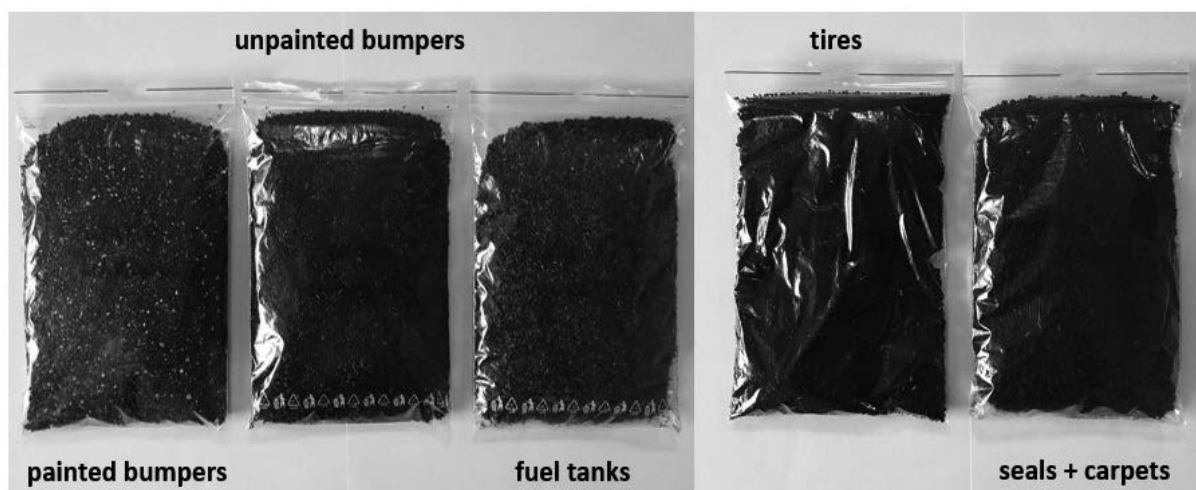


Figure 1. Plastic and rubber granulates

### 2.2. Measurement of the angle of repose

For methodology of repose angle was used international standard ISO 4324 – Surface active agents – Powders and granules – Measurement of the angle of repose [14]. The principle of this measurement is the determination of the angle of repose of the cone obtained by passing a given volume of the product in the form of powder or granules through a special funnel placed at a fixed height above a completely flat and level plate (Figure 2).

The methodology consisted in measuring the height of the bulk material 5 times for each type of granulate. The values were subsequently averaged and used to calculate the angle of repose using the formula [14]:

$$\varphi = \tan^{-1} \frac{2 \cdot h}{100} = \tan^{-1} \frac{h}{50} \text{ [}^\circ\text{]} \quad (1)$$

Where  $h$  is the height of the powder cone (mm).



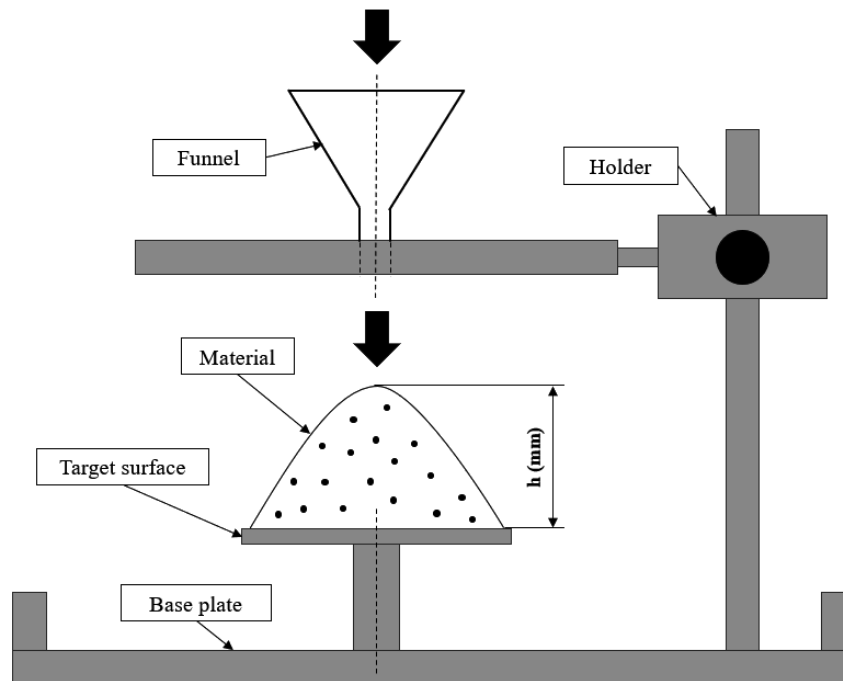


Figure 2. Scheme of the methodology for measuring the angle of repose

### 3. EVALUATION OF RESULTS

The average values of the powder cone heights of individual granulates are shown in the figure (Figure 3).

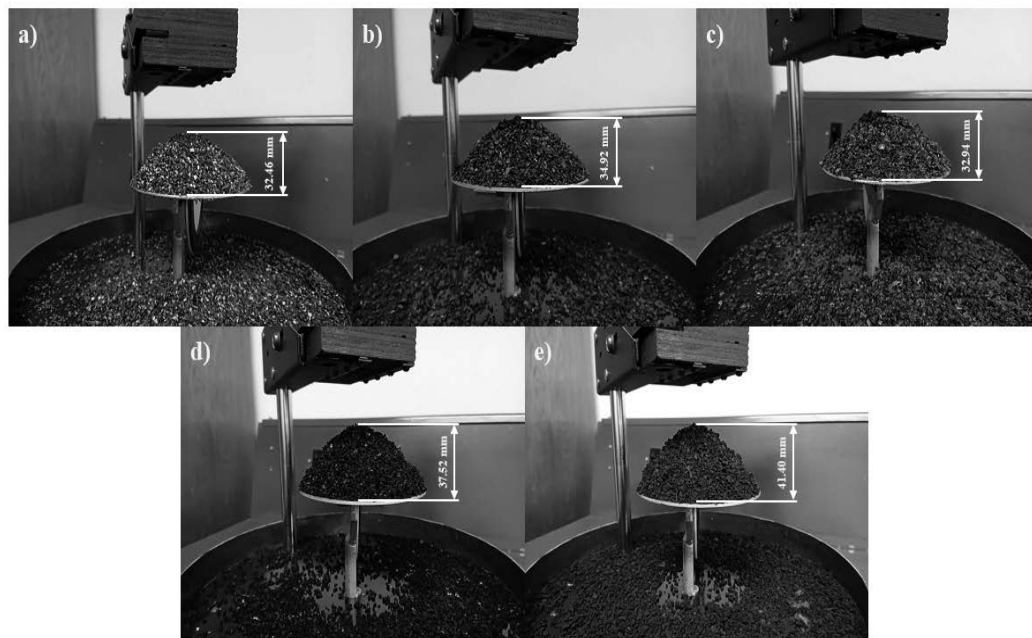


Figure 3. Heights of the powder cones: a) painted bumpers, b) unpainted bumpers, c) fuel tanks, d) tires, e) seals and carpets

From these values, the angles of repose were subsequently calculated according to the formula given in chapter 2.2. The table represents the resulting values of the repose angles of individual plastic and rubber granulates (Table 2).

Table 2. The results of the angle of repose measurements

Material	Measured values of height (mm)					Average value (mm)	Angle of repose (°)
	1.	2.	3.	4.	5.		
Painted bumpers	32.8	33.3	32.7	31.9	31.6	32.46	32.99
Unpainted bumpers	34.7	34.8	35.2	35.1	34.8	34.92	34.93
Fuel tanks	32.9	32.8	33.0	33.1	32.9	32.94	33.38
Tires	37.4	36.9	38.0	37.7	37.6	37.52	36.88
Seals and carpets	40.9	41.5	40.9	41.7	42.0	41.40	39.62

The listed values of the repose angles of individual materials can also be represented by a bar chart (Figure 4).

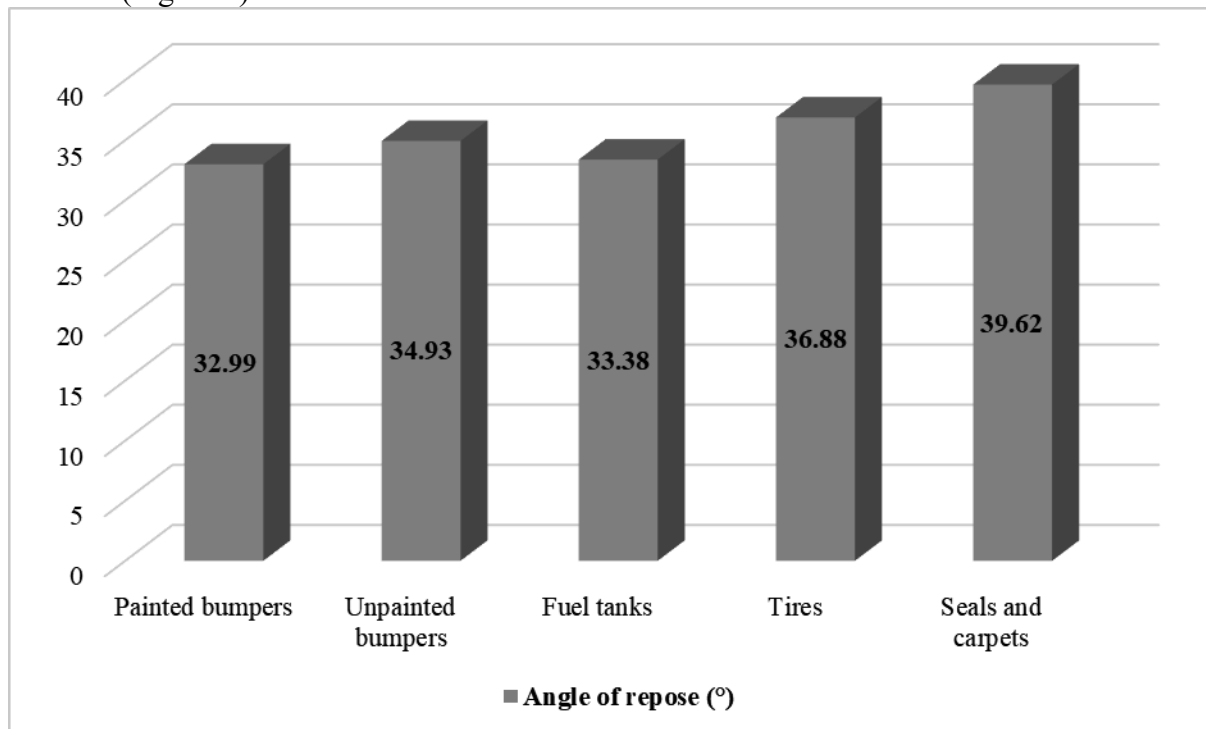


Figure 4. Bar chart of the angle of repose results

Based on the values there can be concluded that granulates made from painted bumpers had the repose angle of 32.99°, granulates made from unpainted bumpers had the repose angle of 34.93°, granulates made from fuel tanks had the repose angle of 33.38°, granulates made from tires had the repose angle of 36.88° and granulates made from seals and carpets had the repose angle of 39.62°. From this point of view, we can say that the granulates from painted bumpers, unpainted bumpers, fuel tanks and tires are “free-flowing” materials and granulate from seals and carpets is “fair to passable flow” material what can be caused by the composition of the granulate.

#### 4. CONCLUSION

This work was focused on measuring the angles of repose of granulates made from waste materials of the automotive industry. In the individual chapters, the angle of repose, the used material, the methodology and the obtained results were described. Overall, in this work was found that plastic granulates have a smaller angle of repose than rubber granulates, namely for plastic granulates from 32.99 to 34.93° and for rubber granulates from 36.88 to 39.62°. Based on the results, it can be concluded that prepared waste plastic and rubber granulates are “free-flowing” respectively “fair to passable flow” materials. Since these are waste materials, the results of this work will be used in the design of the input hopper of the equipment for the application of the mentioned granulates in the production process of innovative wood composites.

#### BIBLIOGRAPHY

1. P. Richard, M. Nicodemi, R. Delannay, P. Ribière, D. Bideau, Slow relaxation and compaction of granular systems, *Nature Materials* 4 (2005) 121-128.
2. B. Kou, Y. Cao, J. Li, C. Xia, Z. Li, H. Dong, A. Zhang, J. Zhang, W. Kob, Y. Wang, Granular materials flow like complex fluids, *Nature* 551 (2017) 360–363.
3. J.F. Peters, M. Muthuswamy, J. Wibowo, A. Tordesillas, Characterization of force chains in granular material, *Physical Review E* 72 (2005).
4. J. Duran, *Sands, Powders, and Grains: An Introduction to the Physics of Granular Materials*, Springer, New York, 2000.
5. J.K. Mitchell, K. Soga, *Fundamentals of Soil Behavior* 3<sup>rd</sup> ed. JohnWiley & Sons, Inc, New Jersey, 2005.
6. Z. Liu, *Measuring the Angle of Repose of Granular Systems Using Hollow Cylinders*, Master thesis, University of Pittsburgh, 2011.
7. A. Mehta, G.C. Barker, The dynamics of sand, *Reports on Progress in Physics* 57 (1994) 383.
8. ASTM-C1444, Standard Test Method for Measuring the Angle of Repose of Free-Flowing Mold Powders, <https://www.astm.org/c1444-00.html>, 2005.
9. R.E. Riley, H.H. Hausner, Effect of particle size distribution on the friction in a powder mass, *International Journal of Powder Metallurgy* 6 (1970) 17-22.
10. E.L. Nicholas, W.S. Franklin, *The Elements of Physics, A College Textbook*, Macmillan, New York, 1896.
11. J.R. Metcalf, Angle of repose and internal friction, *International Journal of Rock Mechanics and Mining Sciences & Geomechanics Abstracts* 3 (1966) 155-161.
12. C. Lanzerstorfer, Dusts from dry off-gas cleaning: comparison of flowability determined by angle of repose and with shear cells, *Granular Matter* 19 (2017) 58.
13. I.S.B. Ferreira, R.S. Peruchi, N.J. Fernandes, P. Rotella, Measurement system analysis in angle of repose of fertilizers with distinct granulometries, *Measurement* 170 (2021).
14. ISO 4324:1977, Surface active agents – Powders and granules – Measurement of the angle of repose.



26th January 2024  
Gliwice, Poland

DEPARTMENT OF ENGINEERING MATERIALS AND BIOMATERIALS  
FACULTY OF MECHANICAL ENGINEERING  
SILESIA UNIVERSITY OF TECHNOLOGY

## INTERNATIONAL STUDENTS SCIENTIFIC CONFERENCE

### A Review on Wear and Friction in Bio-Implants

Abdisa Sisay Mekonnin <sup>a</sup>, Morea Gutu Jiru <sup>b</sup>, M. Bonek <sup>c</sup>, K. Waławiak <sup>d</sup>

<sup>a</sup> Ph.D. Student at the Silesian University of Technology, email: abdisasisay1@gmail.com

<sup>b</sup> Adama Science and Technology University (ASTU), Ethiopia, email: moera.guta@astu.edu.et

<sup>c</sup> Silesian University of Technology, Department of Engineering Material and Biomaterials

<sup>d</sup> Silesian University of Technology, Department of Material Technology

**Abstract:** Bio-implants are an essential component of modern medicine that enhance the lives of millions of people. But the ability of these implants to withstand wear and abrasion in the complex biological environment is what ultimately determines how long-lasting and useful they are. This review aims to identify the primary wear mechanism associated with bio-implants and provide an extensive overview of the challenges, advancements, and possible future advancements related to wear and friction in bio-implants. Several methods are employed to improve the performance of bio-implants and reduce friction. Applying lubricious coatings or textured surfaces can help minimize friction and limit tissue damage. It is also essential to use materials with low coefficients of friction. Bio-implants may occasionally incorporate lubrication systems or self-lubricating materials to further reduce friction. Titanium, stainless steels (SS), cobalt-chromium-molybdenum (CoCr MO), zirconium SS316L, and ultra-high molecular-weight polyethylene (UHMWPE) are the most widely used materials for biodevices with prolonged life in the human body because of their favorable combination of mechanical properties, corrosion resistance, and cost-effectiveness when compared to other metallic implant materials. Wear mechanisms like abrasive, adhesive, and fatigue usually occur in the contact regions. Furthermore, improvements in biomaterial science and manufacturing processes help to minimize wear and friction in these implants. Hence, improving bio-materials tissue reactions and designing bio-implant materials with high biocompatibility, corrosion resistance, resistance to implant wear and aseptic loosening, and appropriate design and manufacturability of implants are necessary.

**Keywords:** wear, friction, bioimplant, self-lubricant

## 1. INTRODUCTION

Bioimplants are deliberately inserted by a surgeon into the human body where it is intended to remain for a significant period to perform a specific function. Biomaterial devices used in orthopedics are commonly called implants [1][2]. The main fundamental requirements that orthopedic devices must fulfill to function adequately are: biocompatibility, corrosion

resistance, resistance to implant wear and aseptic loosening, appropriate design and manufacturability of implants, and biological stability. The friction and wear mechanisms are influenced by the numerous factors that occur at the contact surface interfaces of the tribo-pair. In terms of loading and temperature, wear mechanisms such as abrasive, sticky, and fatigue commonly occur at the contact region. The creation and subsequent migration of wear particles brought on by the combined rolling and sliding between the socket and the ball can be a serious issue with joint replacement implants. In this instance, wear debris can lead to complications like toxicity, inflammation, osteolysis, and implant loosening when it gets into the surrounding tissues. These issues are made more difficult by the possibility that the form and size of the debris produced will alter over the course of an implant. The production of these wear particles can be reduced with better lubrication practices. A capsule that can seal an artificial lubricant inside the joint to lessen wear and friction and stop debris from migrating has been suggested as a potential advantage for joint replacement implants [3-5].

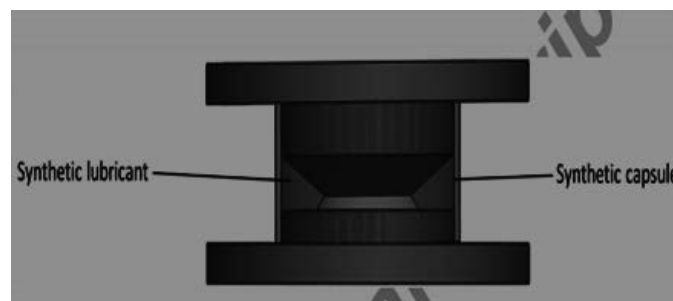


Figure 1. Artificial disc prosthesis with synthetic capsule and lubricant

Low viscosity lubrication is likely to lead to challenging tribological conditions for any spinal implant device that relies on bearing surfaces. If encapsulation is to be successful in spinal implant devices, there will be a need to find an appropriate synthetic lubricant to reduce friction and wear, and increase implant durability [3]. The contact motions like rolling, sliding, transverse and longitudinal, with or without lubrication at ambient and elevated temperatures are have their own consequences for the occurrence of wear. The contact mechanism of these tribo-pair interfaces may differ based on the nature of the material. The metal on ceramic and polymer on ceramic tribo-pairs have better in performance for the total hip-joint replacement. It is very complex in design to reduce the mechanical stress and fatigue due to repetitive load, which leads to wear and dislocates the contact pairs. Metallic materials like titanium alloys, Co–Cr alloys and stainless steels are appropriate choices for implants, by considering their bio and mechanical properties. Regarding metallic implants, Stainless Steel (SS) 316L has all favorable features to be realistic as implants, but its insufficient surface hardness and inadequacy wear resistance, are to be improved for tribological applications. Ti6Al4V alloy is increasingly used as implants in load bearing district, due to its favorable properties such as low density, high strength to weight ratio, high young's modulus, greater corrosion resistance and excellent biocompatibility [5], [8-10]. Nowadays, the most implanted type of hip joint consists of an ultra-high-molecular weight polyethylene (UHMWPE) acetabular cup and metallic or ceramic femoral head. The produced UHMWPE wear particles and the consequent tissue reactions have been known as one of the main sources of osteolysis and implant failure.

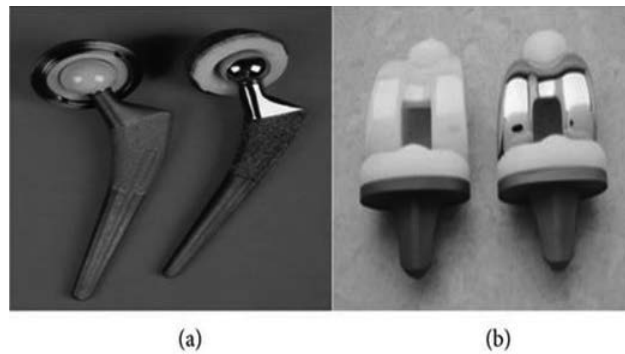


Figure 2. Application of UHMWPE in (a) artificial hip joints, and (b) knee joints

An alternative to improve the wear behavior of the UHMWPE is by using lubricants such as distilled water, saline solution, polyethylene glycol (PEG), sodium hyaluronate, bovine and calf serum as well as hyaluronic acid. Engineered artificial scaffold biomaterials with appropriate mechanical properties, surface chemistry and surface topography are in a great demand for enhancing cell attachment, cell growth and tissue formation at such defect sites. Medical practitioners and engineers since from the yearlong are assessing the mechanical, chemical and biocompatible properties of human bones and implants materials to address a vast area of orthopedic, pathological condition, traumatic injury and some other critical patterns since human bones are considered as natural ceramic composite of several reinforced collagen. Because of this the bioactive coatings are used on some metallic implants for total joint prosthesis, dental implants for bioactive fixation and, fillers for repairing of defective bones [5], [6].

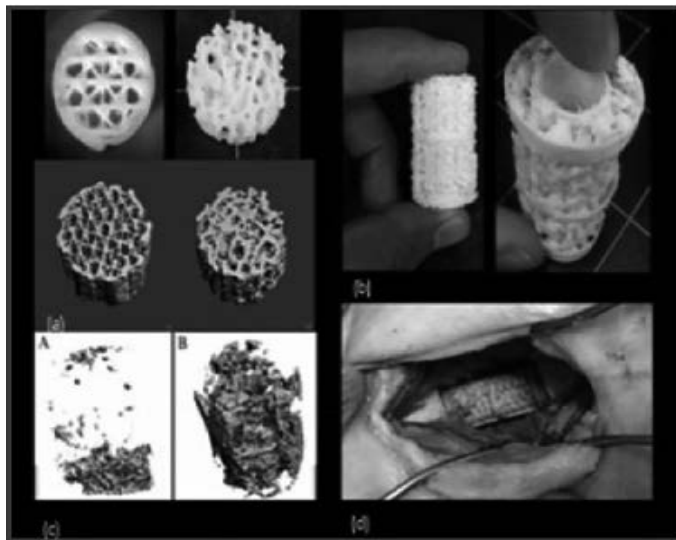


Figure 3. (a) 3D printed simple geometric porous scaffold design and (b) biomimetic porous scaffold design with  $\mu$ CT scans of the bone in growth into each at 6 months in an animal model (c) 3D printed, biomimetic, long segment regeneration scaffolds. (d) Scaffolds implanted into critical sized defect

## 2. LITERATURE REVIEW

A researcher in [6] were aimed on comparative study on tribological behavior of uncoated bio-implant material (SS-316L & Ti6Al4V) while experimented on ball-on-disc wear testing machine. For this purpose, a précised specimen of SS-316L & Ti6Al4V substrate was prepared as per astm standards and were tested with different loadings and wear track diametric length under dry and wet conditions. The findings suggested Ti6Al4V has the lower wear failure compared to SS-316L. According to the results of the wear tests conducted in this study, the examined two alloys can be ranked low to high as Ti6Al4V & 316 L in terms of wear resistance and as Ti6Al4V, and 316 L with respect to the steady state friction coefficient.

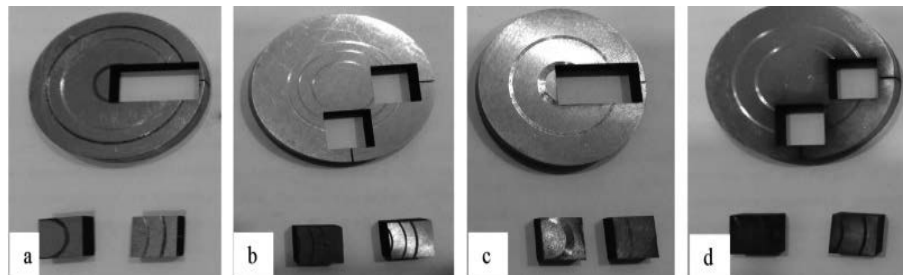


Figure 4. Wear tracks (a) SS 316L – Dry (b) SS 316L – Wet (c) Ti6Al4V – Dry (d) Ti6Al4V – Wet

Researchers in [7] investigated friction and wear behavior of nitrogen ion implanted UHMWPE against ZrO<sub>2</sub> ceramic. The experimental results demonstrate that nitrogen ion implantation enhances the micro surface hardness of UHMWPE. It is found that the friction coefficients of implanted UHMWPE obtain higher values than the untreated one. In plasma lubrication, the friction coefficients of untreated UHMWPE decrease, while the friction coefficients of implanted UHMWPE have little reduction except less fluctuation in wear process. It is shown that the wear rates of nitrogen ion implanted UHMWPE decrease with ion doses in plasma lubrication. Scholar in [8], [9] investigated the torsional wear behaviors of ultrahigh molecular weight polyethylene (UHMWPE) in a ball-on-plate torsional wear device. The alumina femoral head and Ti6Al4V alloy ball were selected as the counter balls in the study. It was found that the torsional fretting running regimes transferred from the partial slip regime (PSR) to the slip regime (SR) were analyzed; however, the mixed fretting regime (MFR) never appeared in this test. In PSR (lower angular displacement amplitudes), slight damage occurred at small angular displacements, and Adhesion appeared at the center zone of all fretting scars in SR. Detachment of particles, ripples, and ploughs was observed under higher angular displacement amplitudes. The UHMWPE/Ti6Al4V pair showed higher contact stiffness, friction torque, wear damage, and material transfer than the presentation of the UHMWPE/Al<sub>2</sub>O<sub>3</sub> pairs.

The wear mechanisms of UHMWPE/Ti6Al4V were combined with abrasive wear and delamination. The generation of radial ripples and micro-cracking were the main damage modes for UHMWPE/Al<sub>2</sub>O<sub>3</sub>. A researcher in [10],[11] investigated the significant factors for the wear mechanism of Ti6Al4V alloy and Ultra High Molecular Weight Poly Ethylene (UHMWPE) hybrid composite on TiN surface. The causes for the material transfer at the tribo-interface are explored in detail. The consequences of the wear phenomenon and their insignificant friction behavior on the tribo-pairs have been illustrated by the evidence of the morphological changes and their projections. The cell viability of the materials makes certain

as suitable for orthopedic implants. Also, researchers in [12] Analysis of wear and friction of total knee replacements. The result showed that Adhesive wear was the dominant mechanism observed with the tibial inserts, manifested as burnishing of the contact area although features indicative of abrasive wear were also observed. Surface profilometry was used to assess the changes in the topography of the components throughout testing and the surface roughness parameters obtained were correlated to the observed wear.

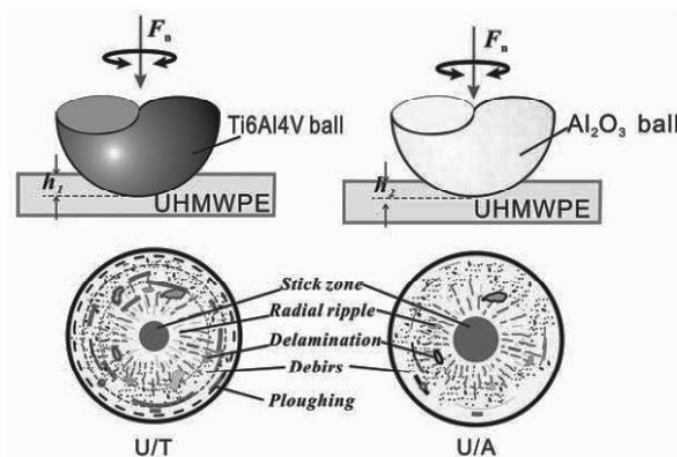


Figure 5. Schematic diagram of the torsional fretting damage progress of the UHMWPE

Scholars in [13] [14], [15] studied the effect of polytetrafluoroethylene (PTFE) encapsulated by polymethylmethacrylate (PMMA) shell on its wear resistance and lubricating properties under reciprocating dry friction was investigated. The experimental results revealed interesting examples of the wear rate of PTFE coating was decreased from  $232 \times 10^6 \text{ mm}^3/\text{Nm}$  to  $1.04 \times 10^6 \text{ mm}^3/\text{Nm}$  and the COF decreased from 0.081 to 0.069. During reciprocating sliding tests, the results show that a continuous, uniform and thin PTFE/PMMA composite film is transferred to the GCr15 steel ball surface. It was demonstrated that the improved lubricating performance was associated with the dispersion effect from core-shell structure, which has a characteristic size in the nanometer range, and composite thus possess a much higher uniformity and higher dispersity of reinforcement phase than do composite obtained by the conventional filling method [16],[17],[18].

### 3. CONCLUSION

The bio-implant materials that used for replacement of injured human bodies such as spinal cases, joints, knee at war, sports and other are gradually debris and finally leads to implant failure due to different wearing action such as adhesion, delamination, abrasive. Several techniques are used to lower friction and enhance the functionality of bio-implants. Applying textured surfaces or lubricious coatings to the surface can assist limit tissue injury and reduce friction. Selecting materials with low coefficients of friction is also crucial. To further reduce friction, bio-implants may occasionally include self-lubricating materials or lubrication systems. Researchers and engineers concentrate on choosing materials with superior wear resistance and low friction coefficients to overcome these issues. Additionally, they use coatings, treatments, and surface changes to improve the wear characteristics of bio-implants.



Furthermore, improvements in biomaterial science and manufacturing processes help to minimize wear and friction in these implants. Bio-implants can give patients more beneficial and long-lasting results by reducing wear and friction.

Wear and friction are the main problems in bio-implant materials. Therefore, improving bio-material tissue reactions and designing bio-implant materials with high biocompatibility, corrosion resistance, resistance to implant wear and aseptic loosening, and appropriate design and manufacturability of implants are necessary and need further investigation.

#### **ACKNOWLEDGMENT:**

We would like to thank the Silesian University of Technology for providing financial support and the Department of Engineering Materials and Biomaterials, Silesian University of technology for preparing such an extraordinary conference.

#### **REFERENCE**

1. H. Basaeri et al., "A Review of Tribological Behavior of Different Bio- Implant Materials," 2022.
2. G. Shen, J. Zhang, C. Kang, and F. Fang, "Surface & Coatings Technology Study on surface texture patterns for improving tribological performance of bioimplants," *Surf Coat Technol*, vol. 422, 2021
3. F. A. Alnaimat, D. E. T. Shepherd, and K. D. Dearn, "Author' s Accepted Manuscript," *Tribology International*, 2016
4. M. Guezmil, W. Bensalah, and S. Mezlini, "Tribology International Effect of bio-lubrication on the tribological behavior of UHMWPE against M30NW stainless steel," *Tribology International*, vol. 94, 2016
5. S. R. Paital and N. B. Dahotre, "Calcium phosphate coatings for bio-implant applications: Materials, performance factors, and methodologies," vol. 66, pp. 1–70, 2009
6. M. M. Sonekar and W. S. Rathod, "Materials Today: Proceedings An experimental investigation on tribological behavior of bio-implant material (SS-316 l & Ti6Al4V) for orthopaedic applications," *Mater Today Proc*, pp. 4–7, 2019
7. S. Ge et al., "Friction and wear behavior of nitrogen ion implanted UHMWPE against ZrO 2 ceramic," vol. 255, pp. 1069–1075, 2003
8. S. Qu and M. Zhu, "Friction and wear behaviour of UHMWPE against titanium alloy ball and alumina femoral head due to torsional fretting Friction and wear behaviour of UHMWPE against titanium alloy ball and alumina femoral head due to torsional fretting Zhen-Bing Cai, Ming-Xue Shen, Jia Yu," 2013
9. S. Gang, F. Fengzhou, and K. Chengwei, "Tribological Performance of Bioimplants: A Comprehensive Review," *Nanotechnology and Precision Engineering*, vol. 1, no. 2. pp. 107–122, Jun. 01, 2018
10. I. Saravanan, A. E. Perumal, and V. Balasubramanian, "Tribology International A study of frictional wear behavior of Ti6Al4V and UHMWPE hybrid composite on TiN surface for bio-medical applications," *Tribology International*, vol. 98, pp. 179–189, 2016

11. S. Mondal and R. Ghosh, "Experimental and finite element investigation of total ankle replacement: A review of literature and recommendations," *Journal of Orthopaedics*, vol. 18, 2020
12. M. Flannery, T. Mcgloughlin, E. Jones, and C. Birkinshaw, "Analysis of wear and friction of total knee replacements Part I. Wear assessment on a three station wear simulator," vol. 265, pp. 999–1008, 2008
13. S. Peng, L. Zhang, G. Xie, Y. Guo, L. Si, and J. Luo, "Friction and wear behavior of PTFE coatings modified with poly (methyl methacrylate)," vol. 172, no. April, pp. 316–322, 2019.
14. D. Gundapaneni, R. T. Laughlin, and T. Goswami, "Characterization of retrieved total ankle replacement liners," *Eng Fail Anal*, vol. 70, pp. 237–254, Dec. 2016
15. G. Shen, J. Zhang, D. Culliton, R. Melentiev, and F. Fang, "Tribological study on the surface modification of metal-on-polymer bioimplants," *Frontiers of Mechanical Engineering*, vol. 17, 2022
16. S. Gang, F. Fengzhou, and K. Chengwei, "Tribological Performance of Bioimplants: A Comprehensive Review," *Nanotechnology and Precision Engineering*, vol. 1, no. 2. pp. 107–122, Jun. 01, 2018
17. B. Elliott and T. Goswami, "Implant material properties and their role in micromotion and failure in total hip arthroplasty," *International Journal of Mechanics and Materials in Design*, vol. 8, no. 1, pp. 1–7, Mar. 2012
18. F. A. Alnaimat, D. E. T. Shepherd, and K. D. Dearn, "The effect of synthetic polymer lubricants on the friction between common arthroplasty bearing biomaterials for encapsulated spinal implants," *Tribol Int*, vol. 98, 2016



26th January 2024  
Gliwice, Poland

DEPARTMENT OF ENGINEERING MATERIALS AND BIOMATERIALS  
FACULTY OF MECHANICAL ENGINEERING  
SILESIA UNIVERSITY OF TECHNOLOGY

## INTERNATIONAL STUDENTS SCIENTIFIC CONFERENCE

### Easily Maneuverable and Portable Cable Reel Design

<sup>1</sup>Meran, C., <sup>2</sup>Aydođan, S., <sup>1</sup>Demirci, İ., <sup>2</sup>Emanet U., <sup>3</sup>Dođan, K., <sup>2</sup>Oztekin, F.

<sup>1</sup>Prof.Dr., Pamukkale University, Faculty of Engineering, Department of Mechanical Engineering, Denizli, Turkey, cmeran@pau.edu.tr

<sup>2</sup>Nexans Turkey Industry, R&D Center, Denizli, Turkey

<sup>3</sup>Student, Pamukkale University, Faculty of Engineering, Department of Mechanical Engineering, Denizli, Turkey, id900624@student.polsl.pl

**Abstract:** The system designed to facilitate the transportation and unwinding of large and heavy cables, while also providing efficient workforce with a single operator, offers an integrated solution that includes a robust flanged transport vehicle, controlled main drum body for unwinding, user-friendly control panel, safety measures, and maintenance convenience. This article outlines the modelling of our design and explains the stages of designing a easily maneuverable and portable reel.

**Keywords:** transportation, single operator, user-friendly

### 1. INTRODUCTION

The deliveries of various cables produced in companies are commonly done by winding them into reels. For the utilization, unloading, and transportation of these heavy cable-loaded reels, rotation is necessary. This process can be challenging for operators. In this article, a solution is presented where the reels are suspended using a single full-reel packaging system, enabling easy movement and rotation in place for operators. The design has been simplified by optimizing previously used components, making it user-friendly.

The Southwire Company has opted for a method, as illustrated below, to connect the movable flanges of the Mobile Milking Reel project to the fixed reel by aligning their axes at the same level, as depicted in **Figure 1**. they also have addressed this issue by vertically adjusting the central axis of the flange using a drill.



Figure 1: *Simpull Flange*

The disadvantages of cable reel transport trailers, such as high costs, storage issues, maintenance requirements, and the need for powerful towing vehicles as illustrated in **Figure 2**, are evident. Therefore, the selection of trailers should be done carefully, and an optimal solution should be found considering operational needs and conditions.



Figure 2: *Cable Transport Trailer and Transport Vehicle*

## 2- DESIGN OF REEL PARTS

### 2.1. Cable Reel Design

The primary goal of the reel design was determined to be the creation of an ergonomic and lightweight design focused on easy transportation and minimal labor for cable reels within the 3500-4000 kg range. This thesis achieved the development of a packaged cable reel, incorporating the bearing and flange design over the 1600 dimensions, enabling effective shipment of cable products with reduced size and effort.

Within the scope of the project, the selection of a central hub with a diameter of 1600 mm was made, aiming to create a suitable design targeting the winding and unwinding speed of the cable reel. In this regard, prioritizing lightweight construction, as seen in **Figure 3** (Detail C), we

achieved the facilitation of unwinding and winding operations at the desired speed by welding 3 mm thick sheets onto 50x30 profiles.

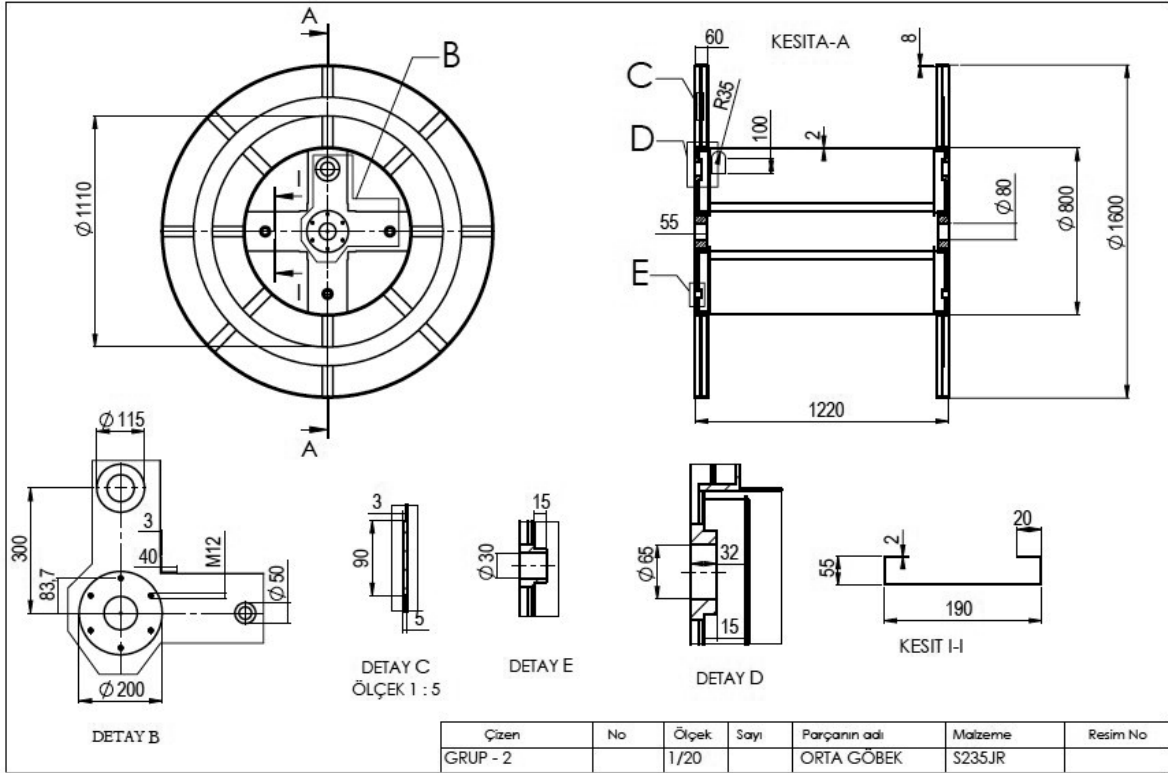


Figure 3: Technical drawing of the central hub design

## 2.2. Flange Design

Among the primary goals in flange design are ensuring the capacity to carry the necessary weight, compliance with occupational safety standards, and facilitating easy assembly, disassembly, and maneuverability. In line with these fundamental objectives, a design has been created with appropriate dimensions.

As seen in Detail C of **Figure 4**, the bearing housing has been constructed with consideration for the required distance criteria, and to provide the necessary strength, 10 profiles of 30x50 have been added between the blades. For winding the produced cables onto the reel and ensuring that the flange, along with the reel, is placed on the machine and rotates at the desired speed, a suitable design has been created with the necessary dimensions, as depicted in Detail B of **Figure 4**

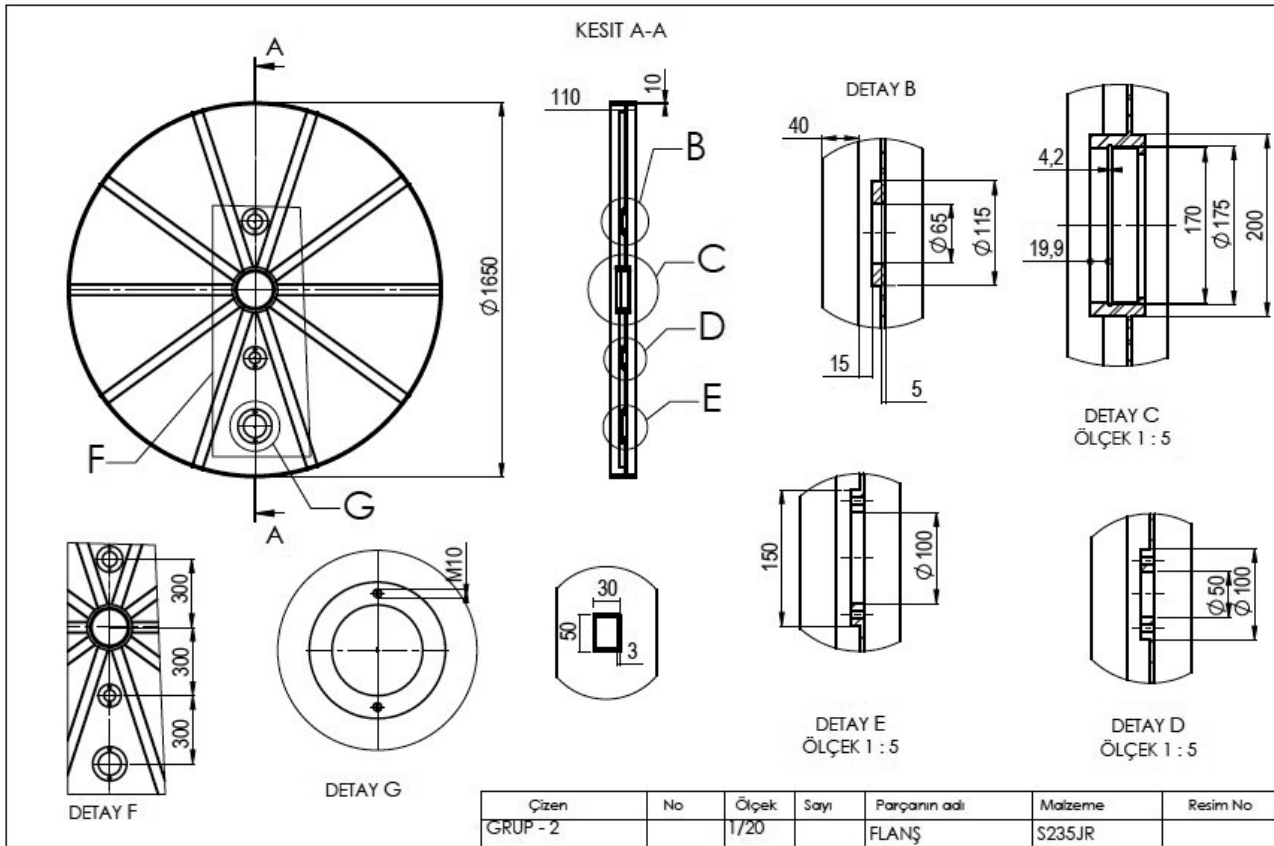


Figure 4: Technical Drawing of the Flange Design

### 2.3 Cover Designs

The cover design in **Figure 5** will be utilized in the operation of the M24 bolt used for securing the flange to the reel. This cover features a threaded hole, which, when the screw is tightened, engages with the socket in the hub, ensuring stabilization.

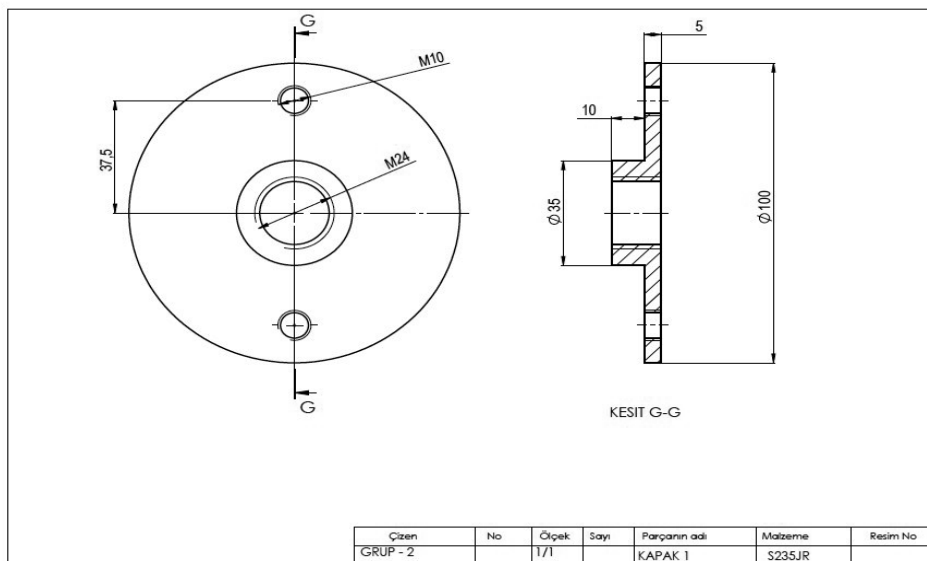


Figure 5: Design of the cover to be used in the fixation mechanism

## 2.4. Flange-Reel Brake Mechanism

The purpose of the brake system between the flange and the reel is to facilitate winding or unwinding at the desired speed on the cable reel. In this context, we aimed to create a system similar to a brake system that would operate between the flange and the reel. This system, as seen in **Figure 6**, works by tightening the M24 bolt, which is welded to the end of this bolt and attached to the hub with friction against the 3mm sheet metal on the reel.

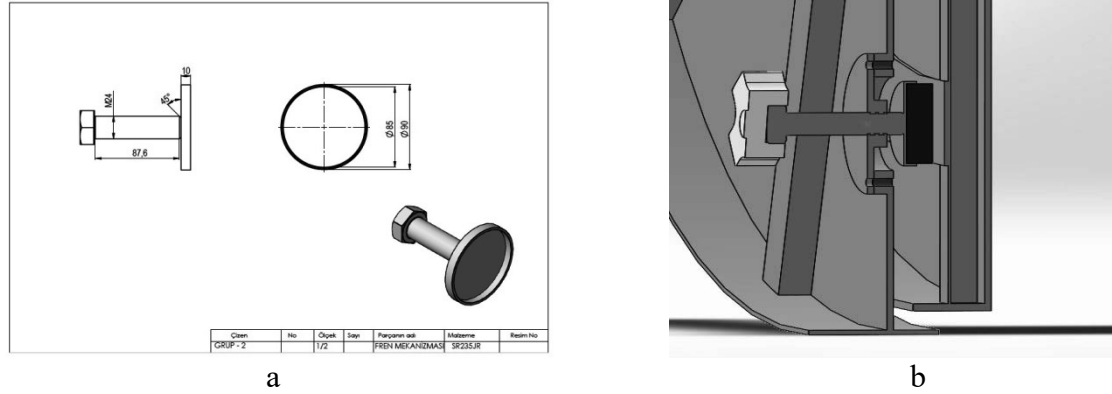


Figure 6: Brake mechanism technical drawing (a) and principle of brake mechanism (b)

## 2.5 Axle-Bearing Design

This component is designed to work in conjunction with the body reel and the outer flange. Its primary function is to keep the body reel and the outer flange concentric. This function is achieved through the bearing housed within the component. The bearing enables the rotation of the body reel and the outer flange, ensuring both components move around the same axis.

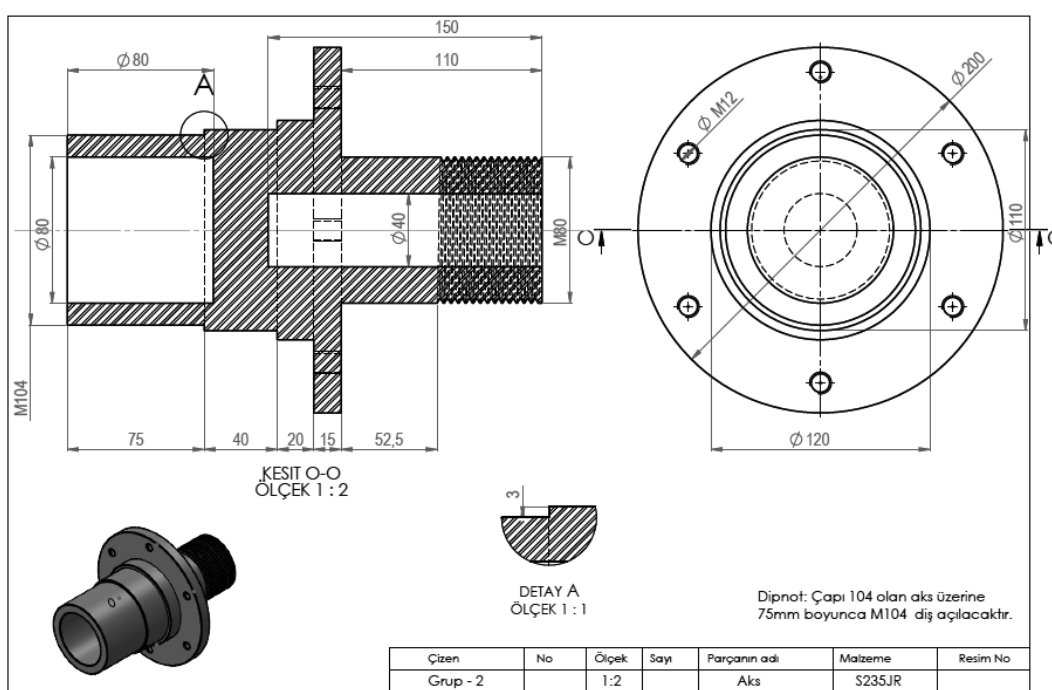


Figure 7: Technical drawing of the axle design

Additionally, this component provides mechanical facilitation for the axial rotations of the reel. Axial rotations involve the rotational movement of an object around its own axis. By fulfilling these two primary functions, this component ensures the harmonious operation of the body reel and the outer flange while optimizing the movements and the manoeuvre of the reel.

In the axle design shown in **Figure 7**, the 3mm step in Detail A is added to facilitate the easy disassembly of the axle. This small gap makes it convenient to quickly replace or maintain the axle. A special gap has been added to support the integration of the 80x80 dimensions of the milking machine element. Additionally, M12 bolts with a diameter of 200mm added to this area ensure a sturdy connection and disassembly of the axle with the body. The design has been carefully planned to provide users with practicality and flexibility, enabling more effective implementation of changes or maintenance procedures in the system. 6022 deep groove ball bearing was chosen.

### 3. ASSEMBLY DRAWING OF CABLE REEL

The assembly drawing is given **Figure 8**, and final rendered view is given **Figure 9**: Firstly, we secure the axle to the reel with 6 M12 bolts, and then we fix the axle to the reel with an M80 nut from within the reel. Next, we place the outer race of the bearing onto the flange's hole, and on the other side of the outer race, we install a circlip. Subsequently, we slide the cover onto the axle, and after aligning the bush with the inner race of the bearing, we secure it with the M108 nut attached to the axle. This bush-nut combination prevents the bearing from shifting outward. Thus, we complete our installation.

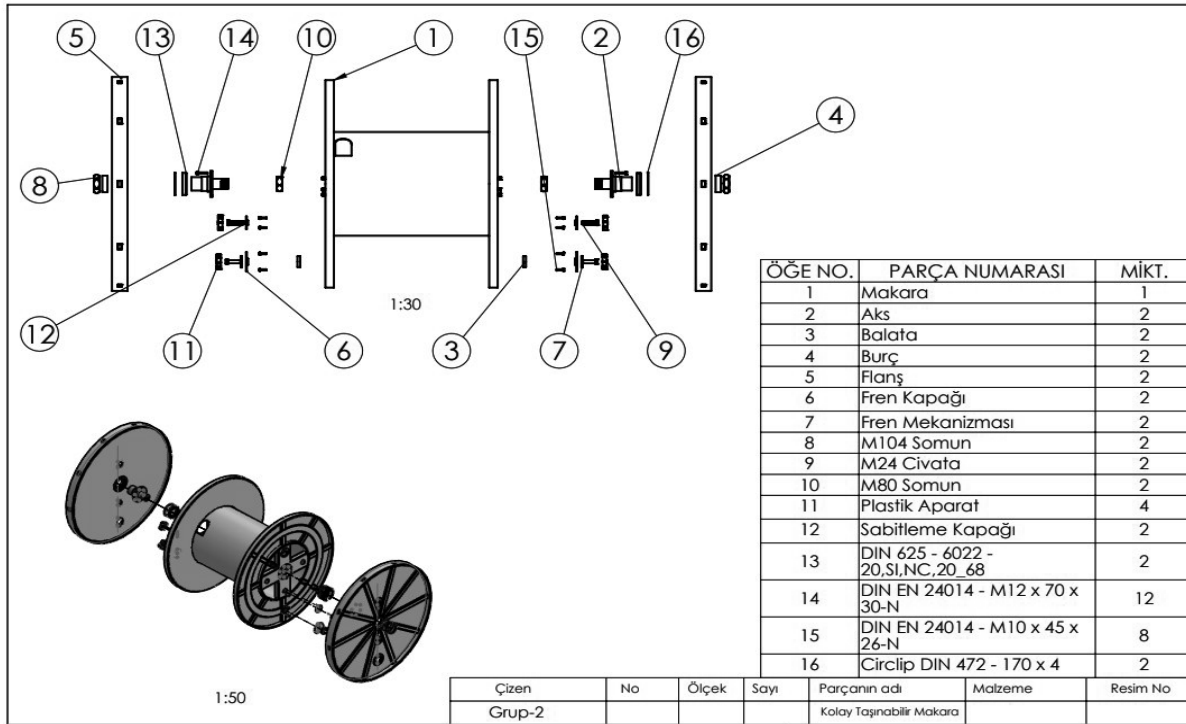
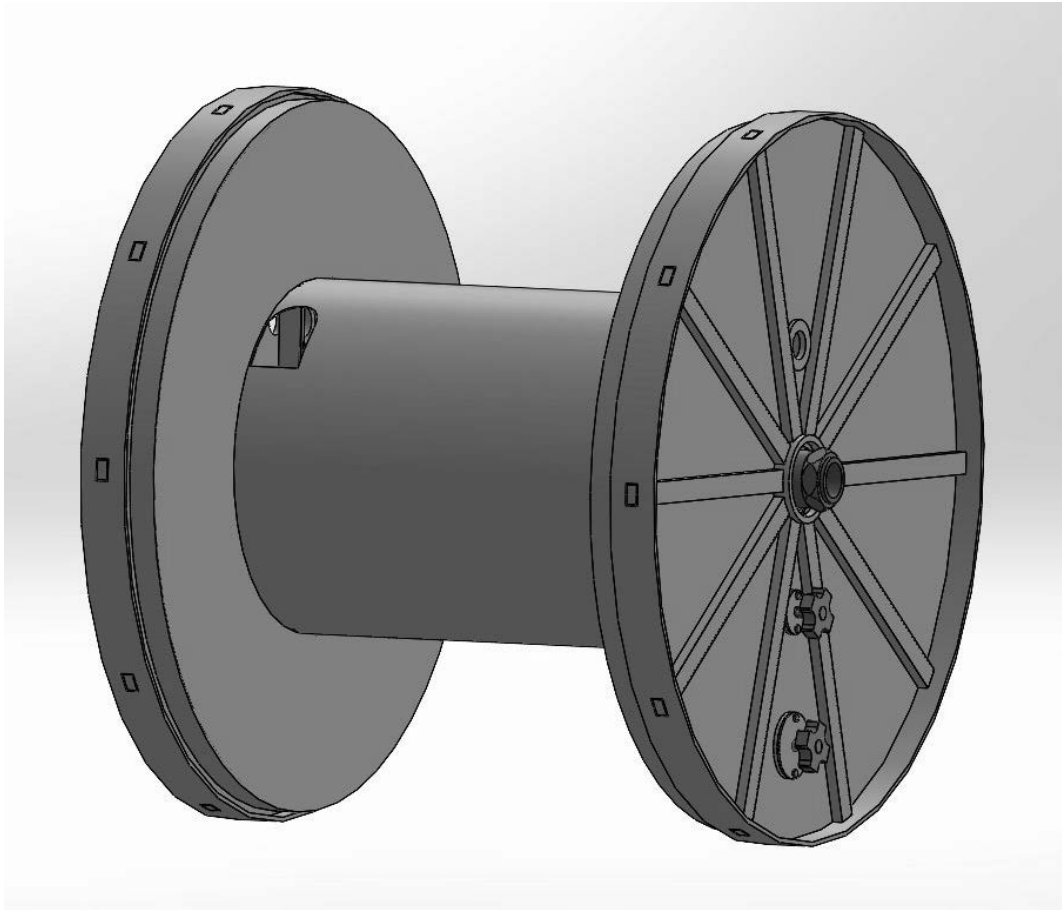


Figure 8: Assembly drawing of cable reel





*Figure 9: Final rendered view*

#### **4. CONCLUSION**

In the reel design, which aims for easy portability and unwinding, a solution has been developed for the transportation, fixation, braking, and easy unloading of cables produced by companies and delivered on reels. This project aims to provide a more economical and user-friendly prototype by reducing the high assembly and manufacturing costs in existing prototypes and designs. It focuses on a single-bearing, slim and durable design, and easy assembly and disassembly.

#### **REFERENCES**

- SOUTHWIRE ‘SIMpull™ Flange Step-by-Step Installation Guide’ YouTube 30 May 2017  
<https://www.youtube.com/watch?v=s8Ji9Gs3fPA> , 20.10.2023 tarihli erişim
- SOUTHWIRE’S SIMpull™ Reel Maneuverable Payoff System Features and Benefits, 20.10.2023 tarihli erişim

[https://www.youtube.com/watch?v=QT-Y5dZXZjY&ab\\_channel=Southwire](https://www.youtube.com/watch?v=QT-Y5dZXZjY&ab_channel=Southwire) SIMpull Wire Reel Demo North Coast Associate spin and move a SIMpull Reel from Southwire to see how it work, 20.10.2023 tarihli erişim.

[https://www.youtube.com/watch?v=Pq0\\_zmsCQZA&ab\\_channel=NorthCoastElectric](https://www.youtube.com/watch?v=Pq0_zmsCQZA&ab_channel=NorthCoastElectric) SKF BEARINGS <https://www.skf.com/group/products/rolling-bearings/ball-bearings/self-aligningball-bearings> 25.10.2023 tarihli erişim

MURAT RULMAN

[http://muratrulman.net/celik\\_dis\\_segman\\_din\\_471\\_4\\_39.html](http://muratrulman.net/celik_dis_segman_din_471_4_39.html) 25.10.2023 tarihli erişim.

SKF TÜRK SANAYİ, 1994, SKF RULMAN BAKIM ELKİTABI, [İSTANBUL]

Meran, C.; 2. Yüksel, M., (2021),Malzeme Bilgisi, Makine Mühendisleri Odası, Ankara

Şekercioğlu, T., (2021), Makine Elemanları Hesap Şekillendirme, Birsen Yayın Evi, İstanbul.

<https://www.runpotec.com/en> 29.10.2023 tarihli erişim



26th January 2024  
Gliwice, Poland

DEPARTMENT OF ENGINEERING MATERIALS AND BIOMATERIALS  
FACULTY OF MECHANICAL ENGINEERING  
SILESIA UNIVERSITY OF TECHNOLOGY

## INTERNATIONAL STUDENTS SCIENTIFIC CONFERENCE

### **Investigation of the Effect of Mechanical Loosening on Vibration Amplitude and Energy Consumption in Cable Production Line Caterpillar Machine**

<sup>1</sup>Meran, C., <sup>2</sup>Eren, O., <sup>3</sup>Alp, A., <sup>3</sup>Irmak, M., <sup>3</sup>Toprak, V., <sup>2</sup>Calhan, B.,

<sup>1</sup>Prof.Dr., Pamukkale University, Faculty of Engineering, Department of Mechanical Engineering, Denizli, Turkey, cmeran@pau.edu.tr

<sup>2</sup>Nexans Turkey Industry, R&D Center, Denizli, Turkey

<sup>3</sup>Student, Pamukkale University, Faculty of Engineering, Department of Mechanical Engineering, Denizli, Turkey

**Abstract:** Maintenance techniques and applications are developing and gaining importance day by day. A breakdown in a machine can lead to production downtime and disruptions. Unplanned downtimes increase operating costs and negatively affect the company's image.

In this study, the effects of mechanical looseness defects that occur in a cable production line caterpillar machine on the causes of failure are investigated. It was examined with two main monitoring techniques, vibration analysis and current analysis. At the end of the study, studies were carried out to correct the mentioned defect. Current analysis was also performed in the tests, and the electrical power difference between the machine that works properly and the machine that works with the detected defect was considered. The cost burden that this difference will bring to the company has been calculated. Ideas for the solution of the problem have been stated. In addition, cost analysis and carbon footprint calculations were also made.

**Keywords:** Predictive Maintenance, Vibration Analysis, Mechanical Looseness, Current Analysis

## 1. INTRODUCTION

Today, with the rapid development of technology, increasing energy demand and changing competitive environment, losses, and stoppages of enterprises during production reduce the efficiency of machines, production processes are disrupted, and operating costs increase.

For the machines to operate continuously and smoothly, they need regular and effective maintenance. Predictive maintenance is a prominent strategy to meet this need and extend the life of the machines.

The understanding of intervening in machines before failure occurs is an understanding developed to get the highest efficiency from a machine and to minimize production losses caused by an incidental downtime or maintenance. This understanding of condition monitoring in operating machines is called predictive maintenance. With the existing predictive maintenance methods, comments are made by analysing the data collected without stopping the running machine. As a result of these interpretations, the occurrence of breakdowns in the

machines in question is predicted and appropriate stops are planned at appropriate times and the machine is intervened. Thus, unnecessary downtime and costs are prevented by intervening in the faulty area of the machine before the breakdown occurs [1].

In this study, mechanical looseness is analysed within the understanding of predictive maintenance method. Vibration and current analyses were performed.

## 2. PREDICTIVE MAINTENANCE

Predictive maintenance approach is the maintenance approach that intervenes in the system after monitoring and analysing the possible failures that may occur without waiting for the machine to breakdown.

This approach predicts the time of occurrence of failures using specific monitoring methods and thus minimises the need to replace parts before they fail. This reduces parts and inventory costs. It aims to minimise downtime due to breakdowns, which in turn minimises production losses. Advantages of predictive maintenance; minimises maintenance costs, minimises unnecessary spare parts and stock parts costs, increases the working life of machine equipment, aims to maximise the efficiency rate of the machines, prevents unplanned downtime and breakdowns.

Few studies have been found in the literature on predictive maintenance. In a study conducted by Sönmez (2003), the inner ring of the bearing in the bearing in the tail of the fan was damaged due to wear and rough operation of the fan shaft and had to work in this way for 8 hours due to the production plan of the enterprise. Looseness was clearly detected in the measurements made. After the welding filling and bearing replacement on the shaft, a decrease of approximately 60% was detected [2]. In the study conducted by Göçülü (2015), an electrical panel was regularly subjected to thermographic testing. In order for the panel to operate under safe conditions, the maximum temperature value was determined as 60 °C and it was determined to intervene at higher temperatures. When the source of the temperature increase observed in the electrical panel, which reached approximately 90 °C after a certain period of use, was investigated, it was observed that the cable connection was loose. Due to the high temperature, the cable lost its properties and the insulator sheath melted and the fault was eliminated by replacing the cable [3]. In a study conducted by Sönmez (2003), vibration was detected in the flue gas fan so as to break the motor foot connection bolts. In the measurements obtained, it was determined that this value was 96 mm/s and 14 mm collapse was detected on the fan side in the laser chassis control. In the vibration measurement made after the collapse was eliminated, it was observed that the peak value decreased to 30 mm/s. It was observed that the measured peak value decreased to 4.67 mm/s with the balance adjustment and eliminated looseness[2].

Unbalance occurs when the axis of rotation and the center of mass do not coincide. This causes high vibration at the first level of the rotational speed in the spectrum. Coupling Misalignment is seen in the horizontal and vertical direction, angularity and parallelism disorders in the coupling connections. This condition manifests itself in the spectrum with high vibration usually at the second floor of the rotational speed. Gear problems manifest themselves at a frequency of (Number of Teeth) x (Shaft Rotational Speed). The occurrence of sidebands of this frequency and the appearance of amplitude modulation in the time plot indicates gear damage. A problem that may occur in the fan blades in machines used in blade passage, fluid transmission, will show itself at the frequency of (Number of Blades) x (Shaft Speed). Bearing

damage produces specific frequencies and the failure frequency of each bearing component is different. The main characteristic produces a harmonic family that is not synchronous to the rotational speed. These frequencies occur at non-integer multiples of shaft speed. Electrical faults usually manifest themselves at the electrical line frequency or  $2 \times$  Line frequency. Failures of mechanical origin, for example, a fracture in the short-circuit bars will manifest itself at a frequency of (Number of Short-Circuit Bars)  $\times$  (Shaft Rotational Speed). Electrical faults require static tests to be carried out along with dynamic tests.

Mechanical looseness is caused by loosening of the structural connections, rotating parts as a result of increased shaft and bearing clearance tolerances, and weaknesses in the structure. Loosening of structural connections manifests itself with a harmonic family up to 8 times the spectrum rotational speed. Loosening in the rotating part produces relatively low peaks at  $0.5x$  harmonics. It can be  $2x, 3x, \dots, 8x$  or  $2x, 3x, 3.5x, 4x, 5x, 5.5x, \dots, 8x$ . Although the first thing that comes to mind when it comes to looseness is the looseness between the fasteners and the machine feet, gaps between the coupling jaws, bearing gaps and gear gaps can also cause serious failures [4]. The dominant harmonic (peak value) may vary in measurements taken horizontally and vertically. Therefore, both horizontal and vertical measurements should be taken and analysed together.

### 3. MATERIAL AND METHODS

Due to the focus of the study, only mechanical looseness defects were dealt with in the measurement, testing and analysis and scenarios were prepared for this. Gaps were created by applying shims to the electric motor legs. The case where the machine has no looseness is considered as the first case and the case where there is looseness is considered as the second case. Two scenarios were set up and measurements were carried out in the light of this idea.

The tests were performed at a constant 50 Hz mains frequency. Measurements were made at engine speeds of  $1400 \text{ min}^{-1}$  in radial (vertical, horizontal) and axial directions and were used as a comparison reference to follow the changes that occurred in the tests. These speeds were specially selected considering the production speed and production limits of the factory in the line.

In the light of the tests carried out, no interpretable data were obtained for the data below  $1400 \text{ min}^{-1}$  due to the low amount of load on the machine and the low number of revolutions. The graphs are based on  $1400 \text{ min}^{-1}$  speed.

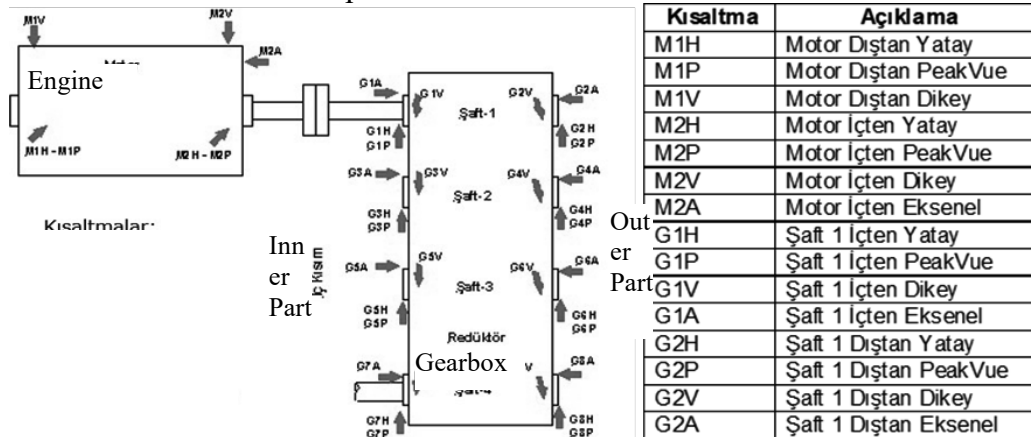
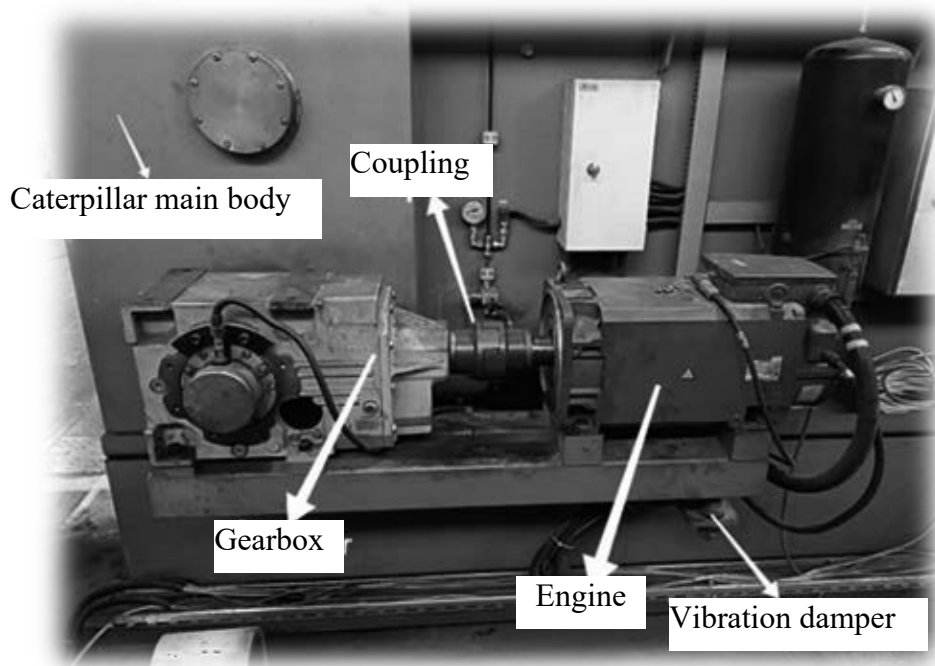


Figure 1: Schematic representation of the measurement directions (M: Engine (Motor), G: Gear, H: Horizontal, V: Vertical, A: Axial, P: PeakVue)

The device used in the vibration analysis is the Emerson 2140. Emerson PeakVue technology is a technology used to monitor and analyse the condition of industrial machines. This technology is used in fault detection and maintenance processes by measuring vibrations in machines. PeakVue is a method generally used for vibration analysis. Unlike other traditional vibration measurement techniques, PeakVue technology analyses the internal state of machines in more depth. This method focuses on the highest values of vibration signals to detect impact or shock conditions in machines.

In order to increase the accuracy of the graphs, measurements were taken from various parts of the setup shown in Figure 1. There are two scenarios, the first measurement with no mechanical looseness and the second measurement with mechanical looseness created. To create mechanical looseness, 1,6 mm shims were placed on the four-foot connections of the motor. Measurements were then taken.



*Figure 2: Machine area where the measurements were made*

The test setup is as shown in Figure 2. It consists of motor, coupling and vibration damper.

#### **4. RESULTS AND DISCUSSION**

The measurement of test results were given Table 1. In the first measurements taken (without mechanical looseness), no intervention was necessary on the motor. Based on the measurements taken on the gearbox, bearing failure was detected in the first stage input bearing. It is recommended to perform bearing maintenance by replacing the bearing at the first planned stop.

In the second measurements taken (when mechanical looseness is created), there are low amplitude mechanical looseness signals on the motor. Values are at traceable level. Based on the measurements taken on the gearbox, bearing failure was detected in the first stage input bearing. It is recommended to perform bearing maintenance by replacing the bearing at the first planned stop.

Table 1: The vibration measurement test results

Machine ID	Meas. ID	Day	Trend Value Scenarioon 1 Current status	Trend Value Scenarioon 2 With looseness
iK32	<u>M1H</u>	19.12.2023	1,311 mm/s	1,374 mm/s
iK32	<u>M1P</u>	19.12.2023	0,125 G's	0,068 G's
iK32	<u>M1V</u>	19.12.2023	0,402 mm/s	0,607 mm/s
iK32	<u>M2H</u>	19.12.2023	1,108 mm/s	1,208 mm/s
iK32	<u>M2P</u>	19.12.2023	0,203 G's	0,223 G's
iK32	<u>M2V</u>	19.12.2023	0,619 mm/s	0,676 mm/s
iK32	<u>M2A</u>	19.12.2023	0,466 mm/s	0,866 mm/s
iK32	<u>G1H</u>	19.12.2023	1,114 mm/s	1,319 mm/s
iK32	<u>G1P</u>	19.12.2023	0,540 G's	0,720 G's
iK32	<u>G1V</u>	19.12.2023	0,489 mm/s	0,839 mm/s
iK32	<u>G1A</u>	19.12.2023	0,279 mm/s	0,639 mm/s
iK32	<u>G3H</u>	19.12.2023	1,119 mm/s	1,249 mm/s
iK32	<u>G3P</u>	19.12.2023	0,125 G's	0,175 G's
iK32	<u>G3V</u>	19.12.2023	0,900 mm/s	1,400 mm/s
iK32	<u>G3A</u>	19.12.2023	0,150 mm/s	0,550 mm/s
iK32	<u>G4H</u>	19.12.2023	1,204 mm/s	1,229 mm/s
iK32	<u>G4P</u>	19.12.2023	0,121 G's	0,181 G's
iK32	<u>B1H</u>	19.12.2023	0,121 mm/s	0,105 mm/s
iK32	<u>B1P</u>	19.12.2023	0,145 G's	0,019 G's

1. Measurements (first scenarioon): Vibration measurements taken when the current situation
2. Measurements (second scenarioon): Vibration measurements taken after mechanical looseness is generated

Measurements were taken at 1400 rpm. The spectrum and wave form graph in **Figure 3** is taken from the engine.

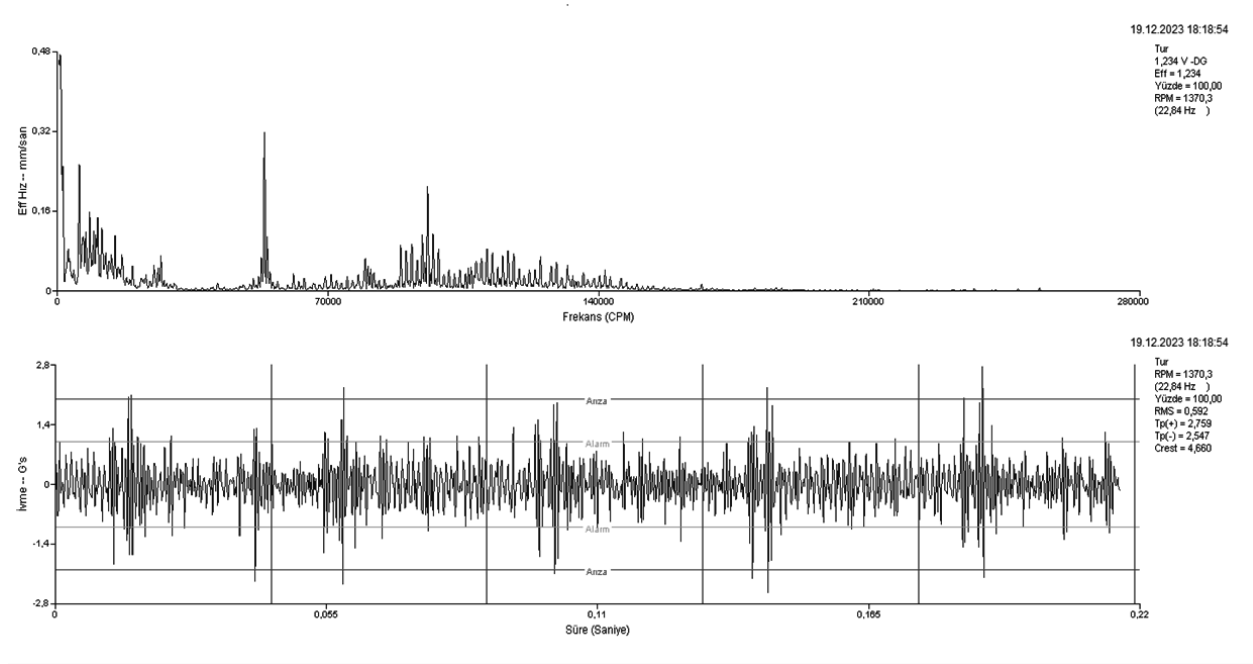


Figure 3: The spectrum and wave form graphs first scenarioon on the gerabox

In the 1st measurements taken, no intervention was necessary on the motor. Based on the measurements taken on the gearbox, bearing failure was detected in the 1st stage input bearing.

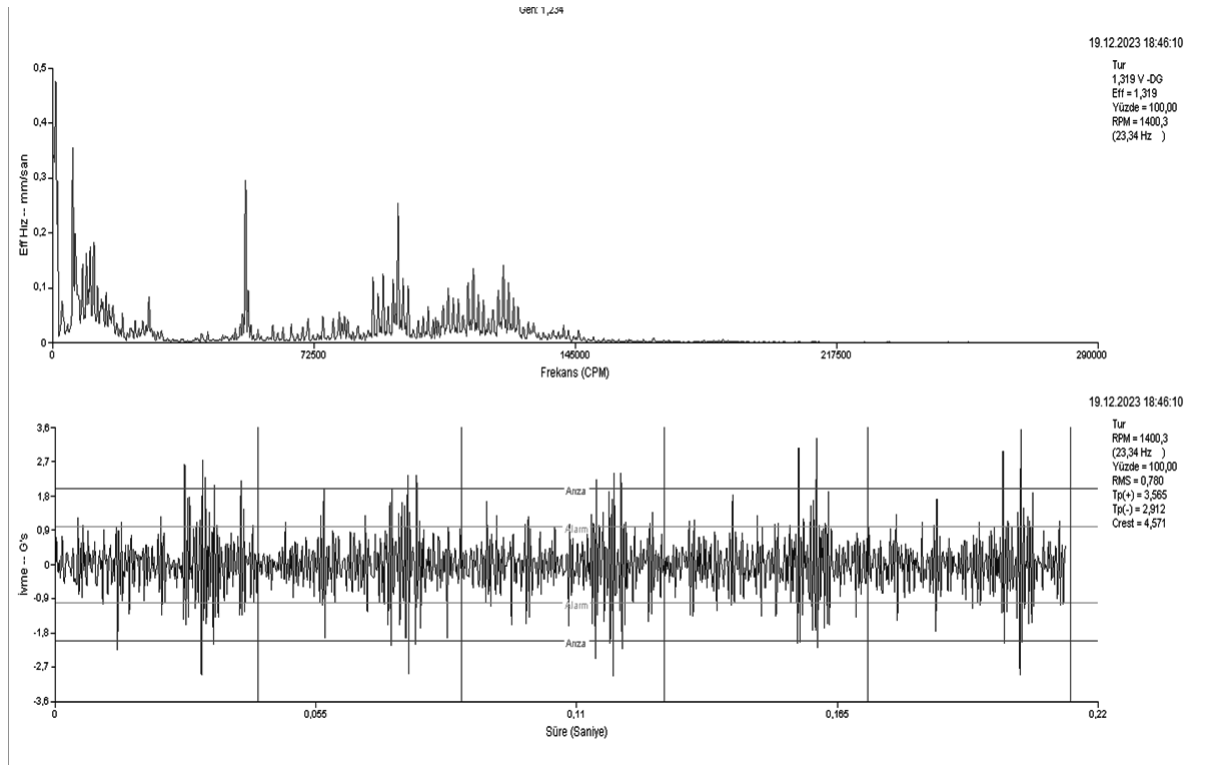


Figure 4: The spectrum and wave form graphs second scenarioon on the gerabox



It is recommended to perform bearing maintenance by replacing the bearing at the first planned stop. As shown in Figure 3, in the gearbox group, the gearbox must be stopped and intervened urgently in a planned manner in case of signals exceeding the red line. In the case of yellow lines, the gearbox should be intervened in the bearing housing after the next planned stop. As can be seen in the Figure 3, the signals have crossed the red line.

In the 2nd measurements taken, there are low amplitude mechanical looseness signals on the motor. Values are at a traceable level. Based on the measurements taken on the gearbox, bearing failure was detected in the 1st stage input bearing. It is recommended to perform bearing maintenance by replacing the bearing at the first planned stop, Figure 4.

Electricity consumption of the line was analysed for both scenarios in four different line speed, Table 2.

Table 2: Comparative of electricity consumption for both scenarios in four different line speed

Line Speed m/min	Amper(A)		Engine revolution min <sup>-1</sup>	
	Scenarioon 1 Current status	Scenarioon 2 With looseness	Scenarioon 1 Current Status	Scenarioon 2 With looseness
30	23	23,5	325	325
60	24	24,3	651	655
100	24.6	24,6	1085	1085
130	24.9	24,9	1400	1400

As can be seen from Table 2, there are not very high differences in terms of electricity consumption in both scenarios. The main reason for this may be that the cable drawn by the catenary is thin. Also, the motor was not fully stressed. However, there was a current increase of 0.005 (five per thousand) when the legs were loose. Even these values should not be ignored. Because if it is ignored for each factory, there may be a serious waste of energy.

## 5. CONCLUSION

Many enterprises continue to produce without checking whether the machines they use in the production line are working properly. Mechanical looseness, coupling misalignment and unbalance in production lines are among the most important factors that need to be monitored frequently. As the system operates with existing mechanical looseness, it can both cause other parts of the machine to fail and reduce product quality. In addition to these, it has been seen in the study that even the slightest mechanical looseness will increase production costs due to significant electricity consumption.

Vibration analysis is of indispensable value today in detecting and controlling machine failures at much earlier stages. In this study, how to detect mechanical looseness, which is one of these faults, with the spectrum and waveform graphs obtained by vibration analysis, is proved practically on a caterpillar machine in a cable production line. What needs to be done is to

monitor the vibration amplitude trends by taking regular measurements and to intervene before exceeding the limit values in the standards.

It should not be forgotten that a healthy working machine will also reduce its carbon footprint by reducing electricity consumption.

## REFERENCES

- [1] Karadayı, H. M. (2011). Titreşim Analizi ile Pompalarda Arıza Tespiti Ve Kestirimci Bakım Uygulamaları (master's Thesis, Balıkesir Üniversitesi Fen Bilimleri Enstitüsü).
- [2] Sönmez, K., "Kestirimci Bakımda Titreşim Analizi Uygulamaları", Bakım Teknolojileri Kongresi ve Sergisi: Bildiriler Kitabı, TMMOB Makine Mühendisleri Odası 16-19 Ekim 2003 / Denizli.
- [3] Göçülü, G., "İşletmelerde Kestirimci Bakım Uygulamaları", Yüksek Lisans Tezi, Mustafa Kemal Üniversitesi Fen Bilimleri Enstitüsü Makina Mühendisliği Anabilim Dalı, Hatay (2015).
- [4] Erol, S. S. (2015). Dinamik Sistemlerin Kestirimci Bakımına Etki Eden Faktörlerin Durum Bazlı İncelenmesi.
- [5] Meran, C. (2023) Bakım Tekniği ve Uygulamaları Ders Notları. [PDF belgesi]. <https://www.pau.edu.tr/cmeran/tr/haber/bakim-teknigi-ve-uygulamaları-ders-notları-07102023> adresinden edinilmiştir.



26th January 2024  
Gliwice, Poland

DEPARTMENT OF ENGINEERING MATERIALS AND BIOMATERIALS  
FACULTY OF MECHANICAL ENGINEERING  
SILESIA UNIVERSITY OF TECHNOLOGY

## INTERNATIONAL STUDENTS SCIENTIFIC CONFERENCE

### **Investigation of the Effect of Unbalance on Vibration Amplitude and Energy Consumption in a Copper Wire Twisting Machine**

<sup>1</sup>Meran, C., <sup>2</sup>Ilhan, K., <sup>3</sup>Dinç, M., <sup>3</sup>Saribay H., <sup>3</sup>Duman, Y., B., <sup>2</sup>Eren, O.

<sup>1</sup>Prof.Dr., Pamukkale University, Faculty of Engineering, Department of Mechanical Engineering, Denizli, Turkey, cmeran@pau.edu.tr

<sup>2</sup>Nexans Turkey Industry, R&D Center, Denizli, Turkey

<sup>3</sup>Student, Pamukkale University, Faculty of Engineering, Department of Mechanical Engineering, Denizli, Turkey

**Abstract:** Unbalance failure, one of the common mechanical faults in machines, is a frequently encountered issue. In today's industry, unbalance problem is a significant concern, often leading to the machine becoming unusable. This study explores the predictive maintenance method and unbalance failure. Additionally, vibration analysis is discussed, and the detection of the unbalance fault, identified through predictive maintenance, is explained using the vibration analysis method. Measurements were taken in two different scenarios, and comparisons were made using temperature, decibel, current, cost analysis, carbon footprint, waveform, circularity, and spectrum graphs. The study concludes that when an unbalance occurs, there is an increase in temperature, current, cost analysis, carbon footprint values.

**Keywords:** predictive maintenance, vibration analysis, unbalance

## 1. INTRODUCTION

In parallel with technological advancements, it becomes possible to predict the condition of mechanical equipment in advance and diagnose faults early. By inspecting machines and machine components, opportunities are provided to preserve or extend the performance of machine elements.

Maintenance methods are widely used in developed countries. By implementing predictive maintenance, one of these methods, the useful life of machines will increase, an improvement in product quality will be achieved, spare part costs and inventory will be reduced, and there will be a decrease in the cost per unit product. In addition to all these benefits, unplanned downtimes and production losses resulting from mechanical failures such as unbalance, misalignment, belt-pulley malfunctions, motor issues, gear, and bearing failures can be prevented. This not only contributes significantly to occupational health and safety but also provides a substantial benefit for sustainability.

In this study, the predictive maintenance method is explained, and the unbalance fault, one of the mechanical faults, is addressed using the predictive maintenance method. The annual energy cost and carbon footprint of the operation are calculated. In the literature, there are not many studies related to 'applying predictive maintenance and unbalance analysis' on copper wire twisting machine. Orhan (2011), in his study, observed the formation of a centrifugal pump rotating at  $1485 \text{ min}^{-1}$  as a sinusoidal graph by first examining a waveform graph and then observing the occurrence of a peak at  $1x$  ( $24.75\text{Hz}$ ) by examining the spectrum graph, indicating the occurrence of unbalance. When investigating the unbalance in the subsequent processes, it was observed that the measured vibration amplitude on the spectrum graph was  $6 \text{ mm/s}$  at  $1x$  while it increased to  $10 \text{ mm/s}$ , and the  $1x$  amplitude remained at the same level. It was observed that by balancing the pump, the vibration value was reduced to  $4 \text{ mm/s}$  in the spectrum graph. As a result, it was concluded that the unbalance condition was monitored, and it was observed that the unbalance increased day by day, and if not intervened, the problem would grow. Meran and his colleagues (2019), in their study, determined vibration amplitudes and energy consumption for different unbalance conditions using vibration and energy analyzer devices based on data taken four times per second. The experiments were conducted on a radial fan with a motor power of  $55 \text{ kW}$ . To create an unbalance in the experimental setup, weights of  $5.9034 \text{ g}$  and  $17.6685 \text{ g}$  were added individually to the fan blades, and finally, a weight of  $10.433 \text{ g}$  was added next to these two loads, and measurements were made under a total load of  $34 \text{ g}$ . In the first experiment, the fan was operated at  $2400 \text{ min}^{-1}$  ( $40 \text{ Hz}$ ) without adding any load, and it was accepted as a reference for the other experiments. When examining the vibration measurements, although there was a small amount of inherent unbalance in the fan, no dominant vibration amplitude was observed. As the experimental weights causing the unbalance increased, it was observed that the energy consumed in the system increased, and the system behaved unusually with the increase in vibration amplitude.

In this study, the effects of balancing in an in copper wire twisting machine main motor and its elimination by predictive maintenance methods were investigated.

## 2. PREDICTIVE MAINTENANCE

Predictive maintenance method is increasingly gaining popularity in the industry each year, solidifying its place. The logic behind the predictive maintenance method is based on the hypothesis that every occurring or potential failure is a precursor. Predictive maintenance, unlike other maintenance methods, is a maintenance approach applied only at real need moments, without waiting for any equipment to fail or adhering to a predetermined plan. In this maintenance approach, a plan is made, taking into account the characteristic features of the machine, working conditions, and operation. When necessary, the machine is briefly stopped, but specific parameters are measured without disrupting production. These measured parameters are interpreted, and if there is a suspected failure, the changes in these parameters are monitored. When a change indicating a potential failure is observed, this fault is identified. After identifying the fault, necessary actions such as part replacement, repair, etc., are taken to eliminate the fault, and efficient production continues.

The advantages of predictive maintenance generally focus on reducing the financial burden of the business, obtaining high-quality products, and ensuring uninterrupted production. Since predictive maintenance is periodically monitored, intervention to the machine is made in case of an alarm situation before a breakdown occurs, allowing production to continue without

interruption. Regular monitoring of the machine's operating settings leads to a decrease in energy consumption, along with a reduction in the carbon footprint. This situation is the desired state for every business. Predictive maintenance helps predict breakdowns through the interpretation of vibration analysis, resulting in shorter maintenance periods and intervention before other faults occur. Another significant advantage is the favorable working environment it brings in terms of occupational safety. The main disadvantages introduced by predictive maintenance are the high initial investment costs (required equipment) and the need for specialized personnel.

Balancing refers to the equilibrium of all forces created by rotating elements in machines. The absence of balance in these forces results in unbalance. Unbalance is one of the most common forms of vibration encountered in machines. Most machines are, to some extent, in an unbalanced state. Although theoretically every machine may appear to be perfectly balanced, such a situation is not practical. Causes of unbalance include the non-homogeneous distribution of material, lack of geometric symmetry in the part, corrosion due to harsh operating conditions, substance accumulation (increased weight, dust, etc.), and the eccentric mounting of sliding bearings, resulting in rotation around a center outside the geometric center. Basic operations performed to address this mechanical issue include mass addition or reduction processes.

The unbalance fault is dominant at the 1x RPM frequency in radial measurements taken from the spectrum graph. In the waveform graph, the unbalance fault is identified when a sinusoidal wave shape is observed, and a single impact is seen in one period. Finally, in the circular form graph, the unbalance is observed as deviations from the reference circle, indicating a disruption in circularity.

### 3. MATERIAL AND METHODS

The unbalance issue of the wire twisting machine, as depicted in **Figure 1**, has been examined, focusing on the machine's vibrational operation. The measurement points on the engine and gearbox for the sample coupling connection are also given in **Figure 1**.

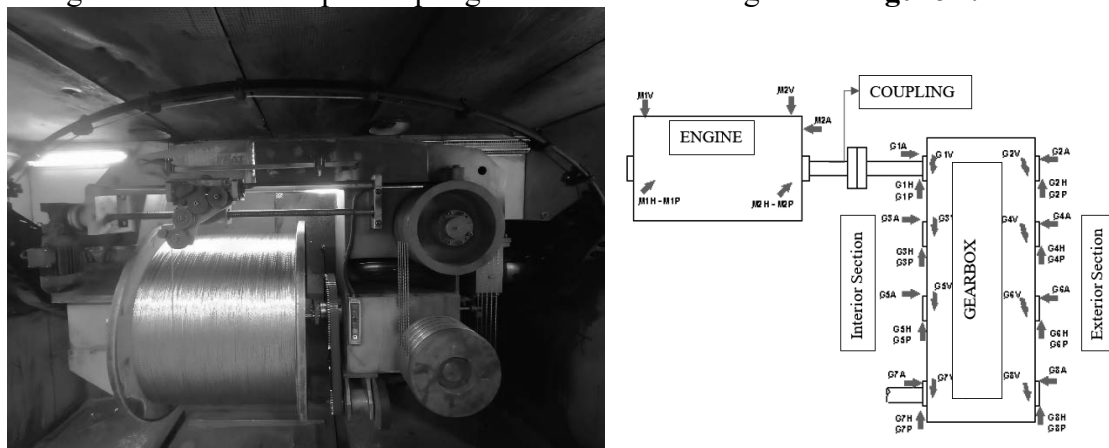


Figure 1: The view of the copper wire twisting machine and measurement points

The first phase of the study aimed to detect and eliminate unbalance in the wire bending machine using predictive maintenance methods. This study consists of two phases. The first phase involves the current condition of the machine, and the second phase deals with the unbalance created by the removed weight from the machine.

In the first phase, measurements were taken while the machine was in production and operating at 550 rpm (14.57 Hz). Temperature, vibration, noise, and current measurements were collected from the machine. Vibration measurements were obtained horizontally from three different points near the bearings using an AMS 2140 device from Emerson. The collected data were converted into spectrum, waveform, and circular form graphs.

**4. RESULTS AND DISCUSSION**

In the conducted study, it was not initially presumed that there was an unbalance issue before measurements. However, through the vibration analysis measurement used in predictive maintenance, it was determined that there was an unbalance problem in the machine during the first measurement. This unbalance issue was found to be of very low amplitude in the upper right bearing of the machine. Despite the low values, it was monitored to prevent any potential issues in the future.

When looking at the spectrum graph in **Figure 2**, we can observe that the resulting velocity reached 2.536 mm/s, and this situation manifests itself at 0.627x magnitude.

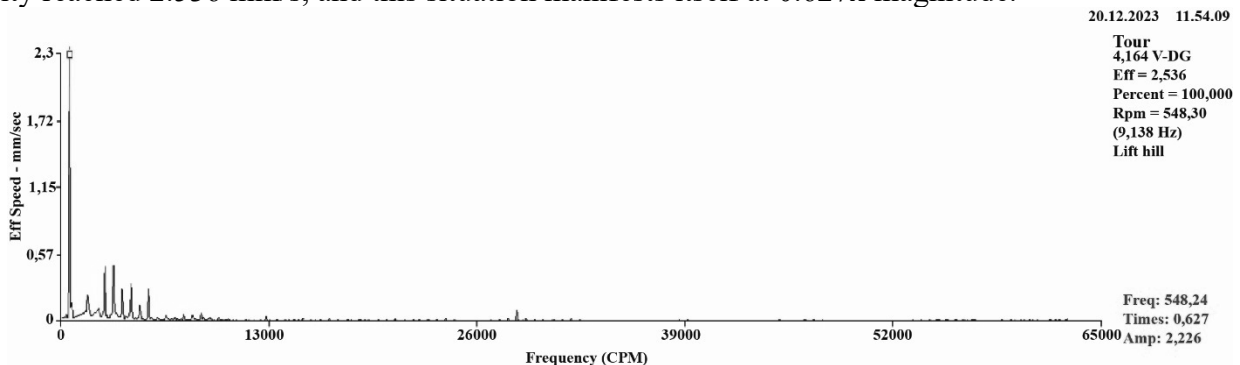


Figure 2: Spectrum graph of the scenario 1 current status

In the waveform graph in **Figure 3**, it can be observed that the generated sinusoidal wave varies between a maximum value of 0.425 and a minimum of -0.385, and no alarm condition is triggered.

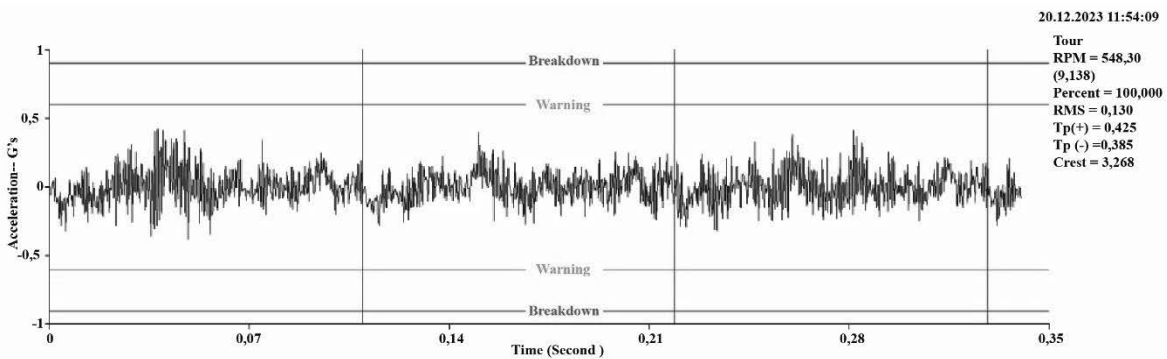


Figure 3: Wave form graph of the scenario 1 current status

The measured current is 138 A and temperature is 26 °C values taken from the machine. These measurements can be later compared with the measurements in the second condition to better understand the machine's condition. In the second stage, measurements were taken by reducing the total weight of the wire bending machine by 3.7112 kg. The aim here is to increase the unbalance and examine the effects of the increased unbalance on the machine. The

current 141 A, and temperature is 28 °C at second stage condition. **Figure 4** shows the spectrum graph obtained through vibration measurements.

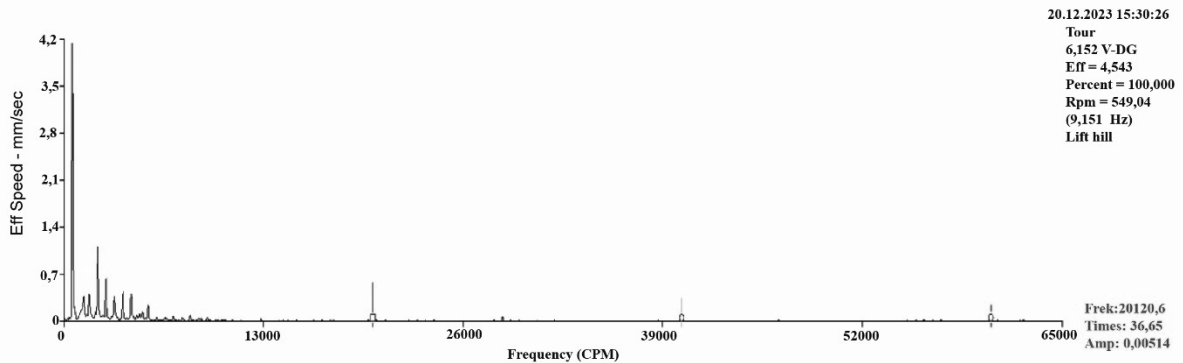


Figure 4: Spectrum graph of the scenario 2 with balanced

When the look at the spectrum graph, it can be observed that, with the created scenario, the speed at 549.04 RPM and 7.151 Hz, that is, at 1X, reaches a value of 4.543 mm/s.

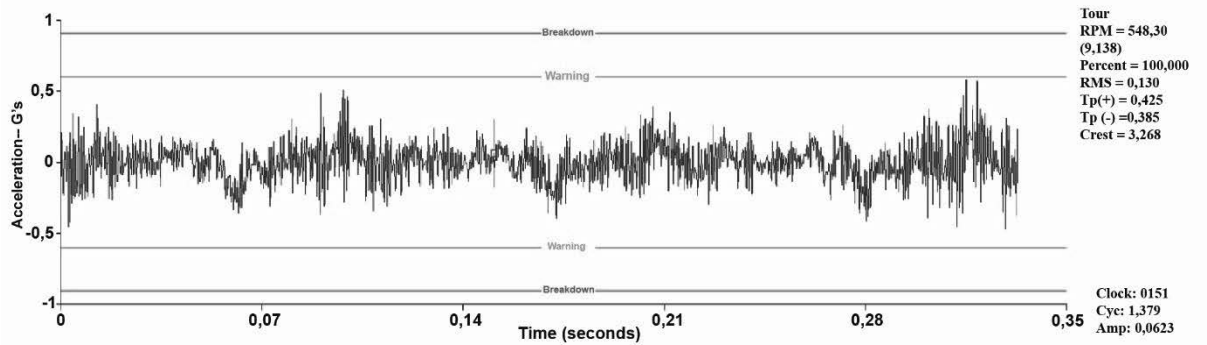


Figure 5: Wave form graph of the Scenario 2 with balanced

At the waveform graph, **Figure 5**, it shows that in the created unbalance scenario, the acceleration value varies between a maximum of 0.583 G and a minimum of -0.469 G, indicating that the machine has entered the alarm state.

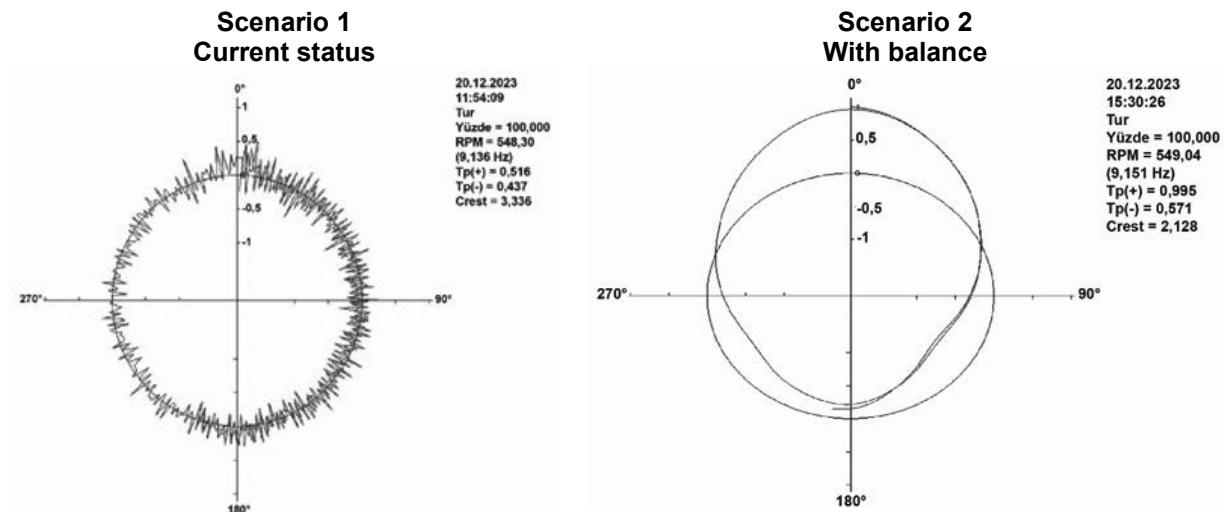


Figure 6: Comparison of two different condition circular form graph of the scenario 1 and 2

In the circularity graph in **Figure 6**, it can be seen that the circularity is disrupted, indicating a balance issue. It can be observed a significant deterioration in circularity at 549.04 rpm and 9.151 Hz, indicating that axial misalignment has even occurred in Scenario 2. This situation indicates a substantial increase in unbalance. The situation that has arisen is a serious issue for the machine because it implies that a breakdown can occur at any moment. This is an undesirable situation. The unbalance created by removing weight indicates that the machine operates with excessive vibrations and is well-balanced. However, the machine triggering an alarm state may lead to future malfunctions and even production stoppages.

The measurement results from each point are given in **Table 1**. The measurement points were remarked as shown in **Figure 1**.

*Table 1: The vibration measurement test results*

Machine ID	Meas . ID	Day	Trend Value Scenario 1 Current status	Trend Value Scenario 2 With unbalance
TB29	<u>B4P</u>	20.12.2023	0,114 G's	0,324 G's
TB29	<u>M1H</u>	20.12.2023	2,141 mm/s	4,977 mm/s
TB29	<u>M1P</u>	20.12.2023	0,486 G's	0,574 G's
TB29	<u>M1V</u>	20.12.2023	1,114 mm/s	1,540 mm/s
TB29	<u>M2H</u>	20.12.2023	2,961 mm/s	3,925 mm/s
TB29	<u>M2P</u>	20.12.2023	0,471 G's	0,576 G's
TB29	<u>M2V</u>	20.12.2023	1,455 mm/s	2,087 mm/s
TB29	<u>M2A</u>	20.12.2023	2,116 mm/s	3,371 mm/s
TB29	<u>B1H</u>	20.12.2023	1,610 mm/s	1,754 mm/s
TB29	<u>B1P</u>	20.12.2023	0,419 G's	0,169 G's
TB29	<u>B3H</u>	20.12.2023	4,982 mm/s	5,427 mm/s
TB29	<u>B3P</u>	20.12.2023	0,410 G's	0,443 G's
TB29	<u>B4H</u>	20.12.2023	4,125 mm/s	6,152 mm/s
TB29	<u>B4P</u>	20.12.2023	0,147 G's	0,324 G's

As evident from **Table 2**, increases in energy costs and carbon footprint are observed in the second measurement. It has been identified that the unbalance fault causes both financial harm to the operation and environmental damage.

In the measurement taken after removing a weight of 3.7112 kg, it was concluded that the unbalance condition in the upper right bearing increased approximately fourfold. This situation is considered to be at an alarm level, indicating a visually noticeable unbalance issue with the machine. The spectrum graphs of the 1x RPM frequency values for both conditions are provided in **Figure 7**.

In addition, the experiment was carried out by increasing the resin ratio. The resin ratio was increased by 40%, but no difference was observed in the strength of the product formed.



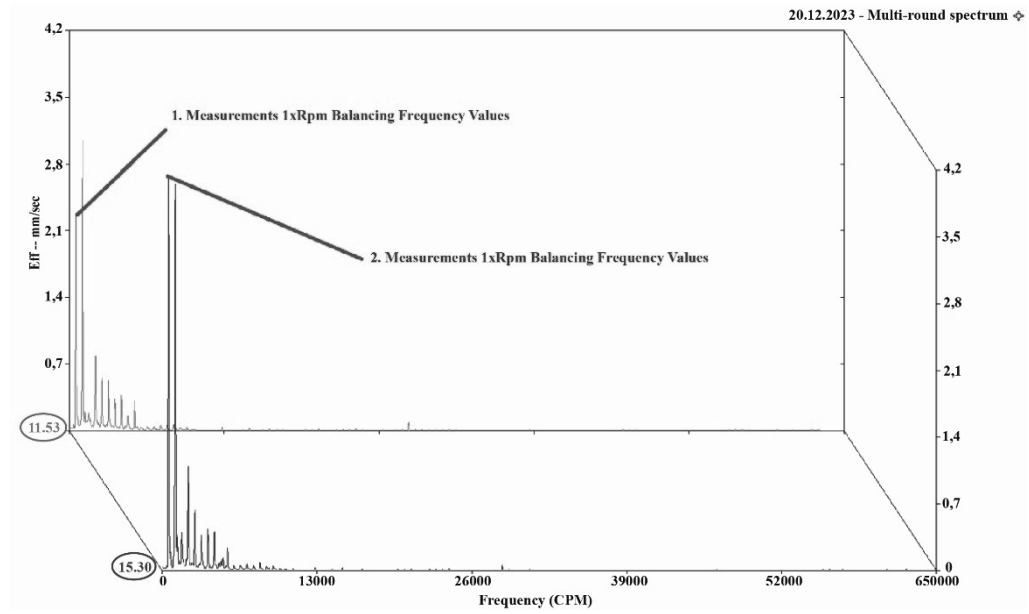


Figure 7: Spectrum form comparison of two different balance condition

Table 2: Energy cost and carbon footprint comparison of two different balance condition

	Scenario 1 Current status	Scenario 2 With unbalance
Energy Cost	91.041 ₺	93.020 ₺
Carbon Footprint	2.050.231,993 kg.CO <sub>2</sub>	2.094.801,672 kg.CO <sub>2</sub>

The Comparison vibration levels for two different balance condition is given in **Figure 8**.

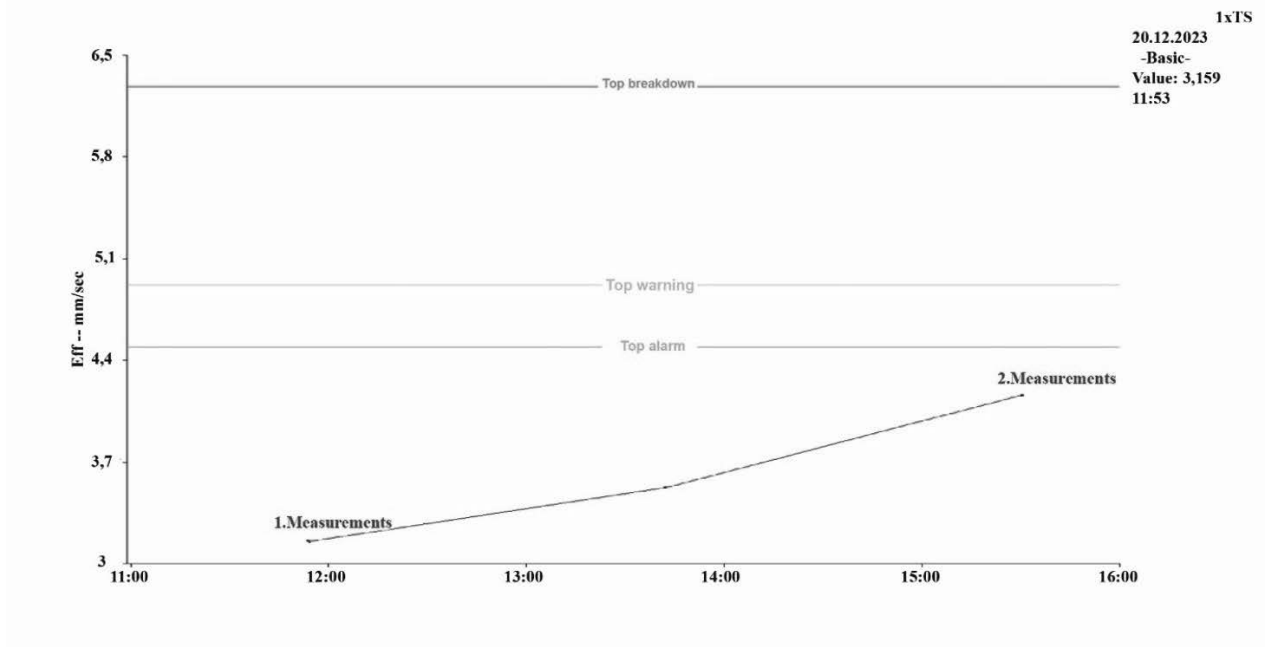


Figure 8: Comparison vibration levels for two different balance condition

## 5. CONCLUSION

Many enterprises continue to produce without checking whether the machines they use in the production line are working properly. Mechanical looseness, axial misalignment and unbalance in production lines are among the most important factors that need to be monitored frequently. As the system operates with unbalanced, it can both cause other parts of the machine to fail and reduce product quality. In addition to these, it has been seen in the study that even the slightest unbalancing will increase production costs due to significant electricity consumption.

Vibration analysis is of indispensable value today in detecting and controlling machine failures at much earlier stages. In this study, how to detect unbalancing, which is one of these faults, with the spectrum and wavm Machine. What needs to be done is to monitor the vibration amplitude trends by taking regular measurements and to intervene before exceeding the limit values in the standards.

In the measurements made with the current balance condition in the study, very low amplitude unbalance signals were detected in the output bearing on the equipment. The values are approximately 2.3mm/s and are at a traceable level.

In the 2nd scenario, the balance was deliberately disturbed. The balancing force on the output bearing creates a vibration of about 4,3mm/s. It is not recommended to operate the machine in this way.

## REFERENCES

1. Erol, S. S., "Dinamik Sistemlerin Kestirimci Bakımına Etki Eden Faktörlerin Durum Bazlı İncelenmesi " Pamukkale Üniversitesi Fen Bilimleri Enstitüsü, Makina Mühendisliği Ana Bilim Dalı, Doktora Tezi, 2015.
2. Meran, C., "Bakım Tekniği ve Uygulamaları" Pamukkale Üniversitesi Mühendislik Fakültesi, Makina Mühendisliği Bölümü, Ders Notları, 2023.
3. Orhan, S., "Balanssızlık ve Rulman Arızası Saha Örnekleri", Yıldırım Beyazıt Üniversitesi Mühendislik ve Doğa Bilimleri Fakültesi Makine Mühendisliği Bölümü, 5. Bakım Teknolojileri Kongresi ve Sergisi, 2011.



26th January 2024  
Gliwice, Poland

DEPARTMENT OF ENGINEERING MATERIALS AND BIOMATERIALS  
FACULTY OF MECHANICAL ENGINEERING  
SILESIA UNIVERSITY OF TECHNOLOGY

## INTERNATIONAL STUDENTS SCIENTIFIC CONFERENCE

### **Investigation of the Effect of Axial Misalignment on Vibration Amplitude and Energy Consumption in Plastic Granule Production Machine Main Motor**

<sup>1</sup>Meran, C., <sup>2</sup>Koksal, I., <sup>3</sup>Baş, A. O., <sup>3</sup>Bozdağ, B., <sup>3</sup>Kerimoğlu, B. N., <sup>2</sup>Oztekin, F.

<sup>1</sup>Prof.Dr., Pamukkale University, Faculty of Engineering, Department of Mechanical Engineering, Denizli, Turkey, cmeran@pau.edu.tr

<sup>2</sup>Nexans Turkey Industry, R&D Center, Denizli, Turkey

<sup>3</sup>Student, Pamukkale University, Faculty of Engineering, Department of Mechanical Engineering, Denizli, Turkey

**Abstract:** The article covers the effects of coupling misalignment on a machine and the elimination of the alignment problem by predictive maintenance methods. An extruder machine with a power of 440 kW was selected for the studies. The coupling of the machine was deliberately breakdowned. The vibration, temperature, noise and electric current values between the ideal state and the initial state of the machine were observed and cost and zero carbon calculations were made as a result.

**Keywords:** predictive maintenance, couplings, vibration, zero carbon footprint.

#### **1. INTRODUCTION**

Machines consist of many different mechanical elements. Every movement of the elements brings vibration. Vibration is the oscillation movement around the reference position. When vibration is not controlled, it can cause damage to the machine. Mechanical problems in the machine cause the machine to operate at higher temperature and noisier and consume more electricity. These effects shorten the life of the machine and increase production costs. In addition, more electricity consumption may cause more carbon emissions.

Few studies have been found in the literature related on prediction maintenance with vibration analysis. In a study conducted by Denli (2007) at Çukurova Construction Machinery Inc. the cost of performing predictive maintenance activities on a CNC machine was analysed. The findings of the research revealed that the average cost of damages that occur when predictive maintenance activities are not carried out on the machine is equal to 5.5 times the money spent for predictive maintenance. DMT Makina (2004) observed that coupling misalignment causes high energy costs. In the studies carried out on this, the current drawn by a motor with 0.5 mm misalignment was 12.2 amps, while it decreased to 11.8 amps after the laser coupling adjustment process was performed. It shows that energy savings amounting to 3% of the total annual energy cost is achieved in an enterprise with a different power of 2000 kW and operating 365 days.

Dereoglu (2020) carried out a study at Hayat Kimya Yeniköy Paper Mill facilities. When the plant was established, the investment cost for predictive maintenance was \$30,000 for devices and training of personnel. This investment provided 56 days of production gain (\$2,419,200) and \$30,000 of material storage gain in only cylinder bearing replacement. Alcelik and Kam (2020) carried out vibration analyses on the shaft bearing system. As a result, it was seen that misalignment causes additional static and dynamic loads on the bearings. The relationship between misalignment and misalignment and the vibration caused by them is explained.

In this study, the effects of coupling misalignment in an in plastic granule production machine main motor and its elimination by predictive maintenance methods were investigated.

## 2. MAINTENANCE METHODS

The history of maintenance dates back to the first invention of machines and equipment. It has always been linked to technological and industrial development. The strategy of letting the device work until it fails is the first strategy that man naturally applies. Before the industrial revolution, machines were repaired only when they broke down. With the industrial revolution, machines and equipment became more complex and maintenance needs increased. The tendency of steam engine boilers to explode required periodic inspection and maintenance of the machines to ensure that the boiler was operating in safe working conditions. The main focus of maintenance is to ensure the safe operation of machines and equipment.

In this study, predictive maintenance methods are utilised to bring the machine to an ideal condition. Predictive maintenance is a condition-based maintenance method performed following a prediction derived from repeated analyses or from known characteristics and evaluation of important parameters related to the deterioration of the part.



*Figure 1 : Reciprocal laser coupling adjustment device.*

By using predictive maintenance methods, you can detect many faults in advance and eliminate them before they cause machine breakdown. There is a vibration caused by the mechanical failure. If we can evaluate these machine vibrations, we can detect faults. Bearing failures,

mechanical looseness, unbalance, electric motor failures, gear failures and coupling misalignment are some of the failures that can be detected by predictive maintenance. Among the coupling adjustment options, the devices that provide the most precise and reliable adjustment are laser coupling adjustment devices. The use of high-tech devices during the adjustment process makes this method very safe. The most commonly used correction method is to align the coupling by adding a shim on the motor side. The device used in the study is given in **Figure 1**.

### 3. MATERIAL AND METHODS

The machine studied is powered by a 440 kW electric motor. It has a structure consisting of different modules for granule production. The raw material is sent from the silos to the extruder through the gravimetric dosing unit and the mixture is formed according to the material recipe. General view of the plastic granule production machine was given **Figure 2**.



Figure 2: General view of the plastic granule production machine

The measurement points on the engine and gearbox for the sample coupling connection are given in **Figure 3**.

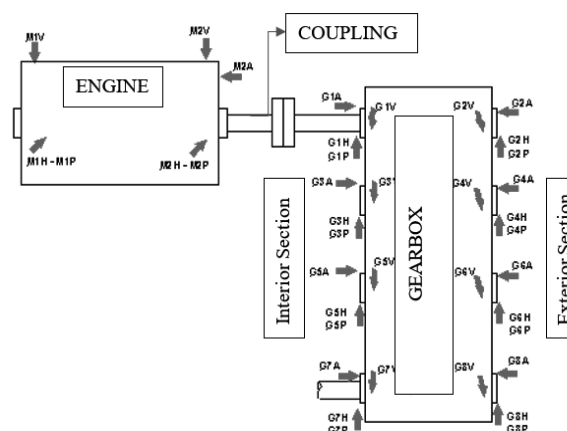


Figure 3 : Engine – gearbox measurement points

Three different devices were used for the experiment. Firstly, Emerson AMS2140 was used for

vibration monitoring and analysis. Emerson A0760GP branded accelerometer was connected to this device and collected data from the machine through sensors. In the detection of machine breakdowns, measurements were taken from the bearing points of the motor and gearbox in three different axes in order to observe the problems completely. For the motor, measurements were taken from 2 different points in total, input and output side. In the gearbox, measurements were taken from only one bearing point, the gearbox input bearing where the coupling is connected to the gearbox. Measurement directions were determined according to vertical, horizontal and axial axis **Figure 4**.



a ) Engine Outboard Horizontal Axis



b ) Engine Outboard Vertical Axis

*Figure 4. The measurement points on the engine*

The last and third device used to eliminate coupling misalignment is rotalign touch | Pruftechnic. This device works wirelessly and transmits the data received from the sensors to the screen. It can be adjusted live during measurement and has the ability to generate reports if desired.

The Emerson AMS2140 device stores the data received and is then transferred to an Emerson computer programme by authorised personnel via USB data cable.

#### 4. RESULTS AND DISCUSSION

In the experiment, 4 different measurements were taken from the extruder machine coded PL-03. First measurements, vibration measurements taken when first arriving at the factory in the current situation. Second measurements, vibration measurements taken after coupling adjustment. Third measurements, vibration measurements taken after coupling misalignment. Fourth measurements, vibration measurements taken after coupling adjustment.

The first measurement was carried out to determine the current condition of the machine in normal operation without any intervention. At this time, the current drawn by the machine was measured as 370 A, the temperature at the motor output side was 33°C and the temperature at the gearbox input side was 40°C. In all measurements, it was observed that the ambient temperature was approximately 23°C. In the noise measurement, the determined value was determined as 86 dB.

The second stage of the experiment was aimed at eliminating the inconsistencies in the coupling and bringing it to an ideal state. At this stage, the temperature value was measured as 27°C at the motor output and 49°C at the reducer side. The electric current value was determined as 360 Amperes. In addition, the noise value was measured as 84 dB, 2 dB less than the first measurement.

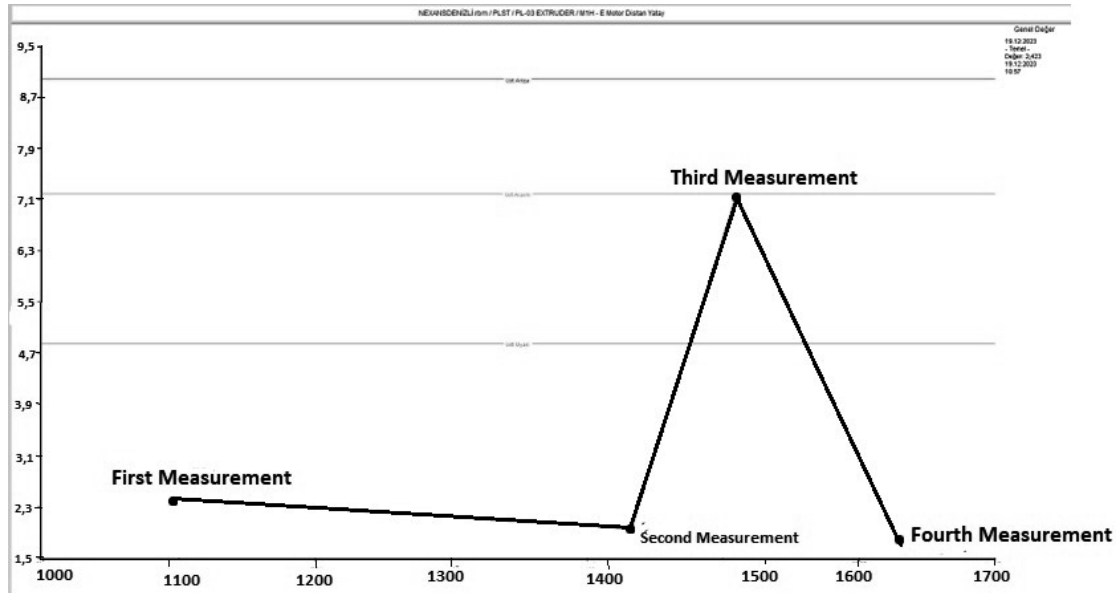


Figure 5 : 4-way spectrum analyse results

In the third measurement phase, the healthy coupling was deliberately misaligned. In this process, 2.5 mm thick shim pieces were removed from both legs at the rear of the engine. As a result of this scenario, it was observed that the electric current increased to 380 Amperes. The noise value was 105 dB, the temperature on the motor side was 35°C and the temperature on the gearbox side was 52°C.

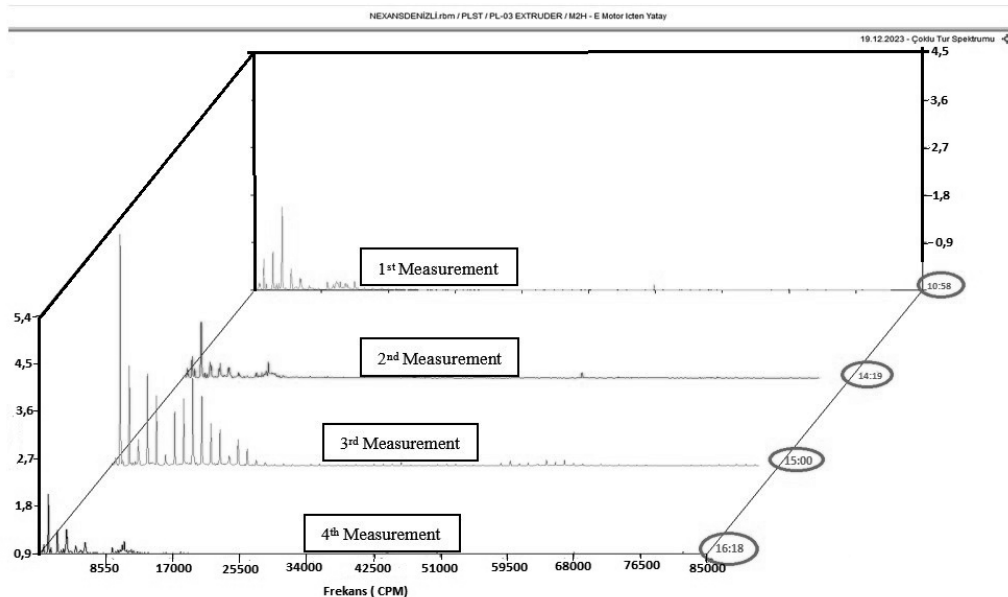


Figure 6 : Trend analyse results

In the last measurement, the temperature value on the motor side was measured as 32°C and the temperature on the gearbox side was measured as 43°C; the noise value was 84 dB and the electric current value was determined as 350 Amperes. The effects of coupling misalignment on the current, the cost caused by the changes in the current and the effects on the carbon footprint. 4-point spectrum analysis visuals are shown in **Figure 5**. In order to compare 4 measurements together, the trend analysis result is given in **Figure 6**. The measurement results from each point are given in **Table 1**. The measurement points were remarked as shown in **Figure 3**.

Table 1: The vibration measurement test results

Machine ID	Point ID	Trend Value 1.Status	Trend Value 2.Status	Trend Value 3.Status	Trend Value 4.Status
PL-03	M1H	2,427 mm/san	1,961 mm/s	7,176 mm/s	1,707 mm/s
PL-03	M1P	0,643 G's	0,523 G's	1,315 G's	0,513 G's
PL-03	M1V	1,167 mm/s	1,020 mm/s	2,650 mm/s	0,819 mm/s
PL-03	M2H	2,337 mm/s	1,985 mm/s	6,635 mm/s	1,593 mm/s
PL-03	M2P	0,663 G's	0,654 G's	0,884 G's	0,843 G's
PL-03	M2V	1,097 mm/s	1,007 mm/s	2,887 mm/s	0,912 mm/s
PL-03	M2A	0,787 mm/s	0,697 mm/s	1,657 mm/s	0,653 mm/s
PL-03	G1H	1,527 mm/s	1,487 mm/s	2,577 mm/s	1,147 mm/s
PL-03	G1P	0,461 G's	0,468 G's	0,744 G's	0,461 G's
PL-03	G1V	1,228 mm/s	1,210 mm/s	1,853 mm/s	1,152 mm/s
PL-03	G1A	1,171 mm/s	0,992 mm/s	1,107 mm/s	0,973 mm/s
PL-03	G2H	1,243 mm/s	1,183 mm/s	1,523 mm/s	1,137 mm/s
PL-03	G2P	0,179 G's	0,192 G's	0,852 G's	0,233 G's
PL-03	G2V	0,738 mm/s	0,711 mm/s	2,714 mm/s	0,659 mm/s
PL-03	G2A	0,888 mm/s	0,755 mm/s	1,795 mm/s	0,696 mm/s
PL-03	G3H	1,511 mm/s	1,421 mm/s	2,722 mm/s	1,131 mm/s
PL-03	G3P	0,431 G's	0,421 G's	0,451 G's	0,430 G's
PL-03	G3V	1,224 mm/s	0,999 mm/s	1,789 mm/s	0,951 mm/s
PL-03	G3A	0,556 mm/s	0,511 mm/s	1,741 mm/s	0,481 mm/s
PL-03	G4H	1,202 mm/s	1,119 mm/s	1,989 mm/s	1,081 mm/s
PL-03	G4P	0,184 G's	0,171 G's	0,879 G's	0,169 G's
PL-03	G4V	0,668 mm/s	0,629 mm/s	0,999 mm/s	0,550 mm/s
PL-03	G4A	0,623 mm/s	0,608 mm/s	0,618 mm/s	0,532 mm/s

Mechanical problems in machines lead to more energy consumption. This causes the machine in which the breakdown occurs to draw more energy and therefore productivity decreases. Such a situation leads to both waste of energy resources and shortening the life of the machines.



Electrical current value measurements to be carried out at regular intervals can be an explanatory observation about the condition of the machine. However, it should be ensured that the machine is in the same condition during the measurements.

*Table 2 : Energy consumption and CO<sub>2</sub> emission calculate*

Status	Energy Consumption (kWh/year)	CO <sub>2</sub> Emission (tCO <sub>2</sub> /year)
First Status	1.204.718	519
Last Status	1.139.743	491

The coupling adjustment performed in the project has an observable effect on energy consumption, **Table 2**. It has been observed that these adjustments carried out within the scope of predictive maintenance have positive results such as reduction in energy consumption and reduction in carbon emissions.

Working time is calculated based on the time from January to the last working day of November from the relevant unit of PL-03. December is not included in this calculation as it was not completed. The machine has worked 5961 hours in total at the end of November. The emission factor used for carbon dioxide emission was calculated as 431 tCO<sub>2</sub>e based on the relevant institution data. It was observed that the intervention made by the coupling adjustment of the predictive maintenance reduced the carbon rate to be released to nature by 5%. Compared to the initial situation, after the adjustments made, the amount of CO<sub>2</sub> that 127 trees could absorb was reduced to 120 trees. In balancing carbon emission, 7 trees were saved. In the first case, the electrical energy used for the lighting of 301 houses per year, as a result of the adjustments made, an energy saving equivalent to the lighting of 16 houses per year was achieved. In addition, it should not be forgotten that energy costs are also an important expense item. In the cost calculations, the unit price of electricity valid in October 2023 was taken as 3.7 Turkish Liras. In this way, 240,408 Turkish Liras were saved by achieving an annual energy saving of 5%. Based on the 29 December 2023 CBRT Euro rate, a waste of € 7367.7 was prevented.

As a result of four measurements, it was found that the temperature value at the inlet of the gearbox was higher than the outlet of the motor in all cases and the difference between them increased over time. While the operating time of the machine is determined as the most important factor among the factors affecting the temperature measurement, the temperature of the plant in which the machine is located, the ambient temperature and the temperatures of other equipment in the plant should also be considered.

## 5. CONCLUSION

Many enterprises continue to produce without checking whether the machines they use in the production line are working properly. Mechanical looseness, axial misalignment and unbalance in production lines are among the most important factors that need to be monitored frequently. As the system operates with existing axial misalignment, it can both cause other parts of the machine to fail and reduce product quality. In addition to these, it has been seen in the study that even the slightest misalignment will increase production costs due to significant electricity consumption.

Vibration analysis is of indispensable value today in detecting and controlling machine failures at much earlier stages. In this study, how to detect axial misalignment, which is one of these faults, with the spectrum and waveform graphs obtained by vibration analysis, is proved practically on in Plastic Granule Production Machine Main Motor. What needs to be done is to monitor the vibration amplitude trends by taking regular measurements and to intervene before exceeding the limit values in the standards.

This study on estimating the current condition of the machine by measuring the noise levels of the machines represents an important application of acoustic-based condition monitoring and estimation. Noise levels of machines are often considered as an important indicator of their operating condition. Therefore, measuring and analysing this parameter provides important information about the overall health of the machine. This study shows that the measurement of noise levels can be a powerful tool to estimate the current state of the machine. Noise measurements can be used to prevent unexpected breakdowns and optimise maintenance processes.

## REFERENCES

1. Denli, H., “Kestirimci Bakım ve Uygulamalarının İyileştirilmesi”, Mersin Üniversitesi Fen Bilimleri Enstitüsü, P 34-64, 2007.
2. DMT Makina, “Vibrasyon”, Teknik Bülten, Issue: 1, P 2, 2004.
3. Dereoğlu, F., “Kağıt Üretim Sistemindeki Kurutucu Silindir ve Sirkülasyon Fanının Kestirimci Bakım Tekniği İle Arıza Takibi ve Titreşim Analiziyle Tespiti”, Kocaeli Üniversitesi Fen Bilimleri Enstitüsü, P 70-71, 2020.
4. Alçelik, N, Kam, M., “Dönen Makinelerde Eksenel Kaçıklık ve Dengesizliğin Titreşim Analizi”, BŞEÜ Fen Bilimleri Dergisi, Volume: 7, P 258-266, 2020.



26th January 2024  
Gliwice, Poland

DEPARTMENT OF ENGINEERING MATERIALS AND BIOMATERIALS  
FACULTY OF MECHANICAL ENGINEERING  
SILESIA UNIVERSITY OF TECHNOLOGY

## INTERNATIONAL STUDENTS SCIENTIFIC CONFERENCE

### Aplikácia DLC povlakov na valivé ložiská

M. Murín<sup>a</sup>, M. Vicen<sup>a</sup>

<sup>a</sup> Žilinská univerzita v Žiline, Strojnícka fakulta, Katedra materiálového inžinierstva, Univerzitná 8215/1, 010 26 Žilina, Slovak Republic  
email: murin2@stud.uniza.sk martin.vicen@fstroj.uniza.sk

**Abstrakt:** Táto práca sa zaoberá analýzou DLC povlakov a ich aplikáciou v oblasti valivých ložísk. Popísané sú ocele, ktoré sa používajú na výrobu valivých ložísk, vznik, štruktúra a metódy vytvárania DLC povlakov a na záver ich využitie u valivých ložísk.

**Abstract:** The thesis focuses on analysis of DLC coatings and their application in the field of rolling bearings. The steels that are used for the production of rolling bearings, the origin, structure and methods of creating DLC coatings are described, and finally their use in rolling bearings.

**Kľúčové slová:** ocele na valivé ložiská, DLC povlaky, trenie, PVD

### 1. ÚVOD

Neustále sa zvyšujúce nároky na ekológiu a ekonomiku prevádzky, vyžadujú aj väčšie požiadavky na životnosť a odolnosť strojných súčastí a zariadení. Postupom času sa však ukazuje, že vytvárať neustále nové materiály, ktoré by mohli spĺňať tieto predpoklady, nie je jedinou cestou vývoja. V mnohých aplikáciách je kľúčový práve povrch súčastí a s jeho úpravou tak môžu materiály získať výnimočné vlastnosti a zachovať si nízku cenu. Jednou z možností, ako vyhovieť týmto požiadavkám, je použitie tvrdých a oteruvzdorných povlakov.

Dnes sa na vytváranie povlakov čoraz viac využívajú nové technológie povlakovania metódami PVD a CVD. Jedny z najrozšírenejších povlakov, vytvárané prevažne metódou PVD, sú povlaky DLC (Diamond-Like-Carbon). DLC povlaky sa stále viac používajú pre zníženie trenia a predĺženia životnosti vysoko namáhaných súčastí, vďaka svojim vynikajúcim tribologickým vlastnostiam. Vykazujú taktiež vysokú tvrdosť, odolnosť voči korózii a nachádzajú uplatnenie aj v medicíne, ako biomateriály.

Medzi jedny z najdôležitejších strojných súčastí nepochybne patria valivé ložiská. Nachádzajú sa takmer v každom zariadení, kde sa vyskytujú pohyblivé komponenty a podliehajú neustálemu procesu inovácie. Často sa na povrch valivých ložísk deponujú práve povlaky DLC, ktoré výrazne predlžujú ich životnosť a zvyšujú ich odolnosť hlavne voči únavovému opotrebeniu.

## 2. OCELE NA VALIVÉ LOŽISKÁ

Medzi základné požadované vlastnosti, ktoré by mali vykazovať ložiskové materiály patrí napr. vysoká tvrdosť a pevnosť, vysoký stupeň čistoty chemického zloženia, alebo vysoká medza únavy pri kontaktnom namáhaní v mieste valivého vztyku. Hlavný dôraz sa však kladie na odolnosť voči opotrebeniu, keďže v bežných aplikáciách sú ložiskové materiály vystavené nepretržitému pohybu a kontaktu s inými komponentami zvyčajne pod veľkým tlakom. V súčasnosti bezpochyby tvoria prevažnú časť celkovej produkcie výroby ložísk na svete práve ložiská vyrobené z ocele. Ocele, ktoré sa používajú na výrobu ložísk patria do skupiny ocelí na menovité použitie, čo je špeciálna skupina konštrukčných ušľachtilých zliatinových ocelí. Sú to ocele, ktoré boli špeciálne vyvinuté na výrobu konkrétnych konštrukčných častí. Z tejto skupiny ocelí boli na výrobu ložísk vyvinuté ocele, ktoré nazývame ocele na valivé ložiská. Ocele na valivé ložiská sú zaradené medzi konštrukčné ocele, no ich chemické zloženie (tab. 1) a tak aj ich vlastnosti sú viac príbuzné nástrojovým oceliam. Sú to nadeutektoidné ocele legované 1,5% chrómom s obsahom uhlíka okolo 1% [1].

Tab.1 . Chemické zloženie vybraných ocelí na valivé ložiská

Table 1. Chemical composition of selected rolling bearing steels

Označenie	Chemické zloženie [%]					
	C	Mn	Si	Cr	Mo	Iné
14 209	0,9 -1,10	0,9 -1,20	0,35 - 0,65	1,30 -1,65	-	Ni max 0,30 Cu max 0,25
14109	1,10	0,50	0,35	1,30 - 1,65	-	Ni max 0,30 Cu max 0,25
100Cr6	1,10	0,45	0,35	1,35 - 1-65	-	-
100CrMo7	1,05	0,45	0,40	1,65 - 1,95	0,20 - 0,40	-

Jednou z najdôležitejších častí spracovania ložiskových ocelí je tepelné spracovanie. Tepelné spracovanie u ložiskových ocelí pozostáva zo žihania na mätko, čoho cieľom je dosiahnutie čo najmensej tvrdosti a tým čo najlepšiu obrábatelnosť. Ďalej nasleduje samotná výroba ložiskových komponentov, ktoré sa ďalej tepelne spracovávajú kalením a nízkoteplotným popúšťaním na dosiahnutie požadovaných mechanických vlastností. Potom môže nasledovať povrchová úprava ložiskových komponentov, kde jednou z možností môže byť práve nanášanie rôznych povlakov [1].

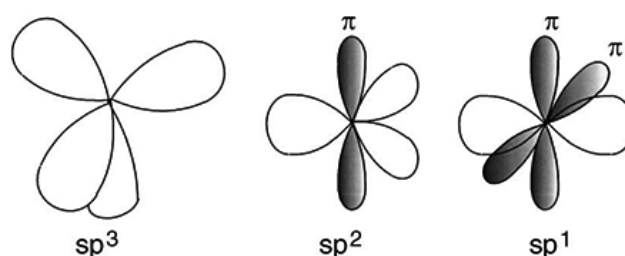
## 3. DLC POVLAKY

Väčšina degradačných mechanizmov vzniká na povrchu komponentov a z povrchu sa šíri ďalej do materiálu. Jednou z najúčinnějších možností zníženia účinnosti degradačných mechanizmov je ošetrovanie povrchu kvalitnými nátermi alebo povlakmi. V dnešnej dobe sa v priemysle čoraz viac využívajú nové technológie nanášania povlakov metódami PVD (Physical-Vapor-Deposition) a CVD (Chemical-Vapor-Deposition), ktoré umožňujú vytváranie širokého spektra tenkých povlakov. Medzi veľké množstvo povlakov vytvorených metódou PVD, patrí aj väčšina DLC povlakov (Diamond-Like-Carbon). Skratka DLC v preklade môže znamenať „diamantu podobné vrstvy“, kedy sa na povrch súčiastok deponujú tenké vrstvy povlakov tvorené rôznymi štruktúrami uhlíka. Povlaky DLC vykazujú vysokú tvrdosť, sú chemicky inertné, majú veľmi nízky koeficient trenia, čiže majú vynikajúce tribologické

vlastnosti, vysokú životnosť a s tým spojenú vysokú odolnosť voči opotrebeniu, vysokú korozivzdornosť a dajú sa deponovať aj na nekovové materiály [2,3].

### 3.1. Štruktúra DLC povlakov

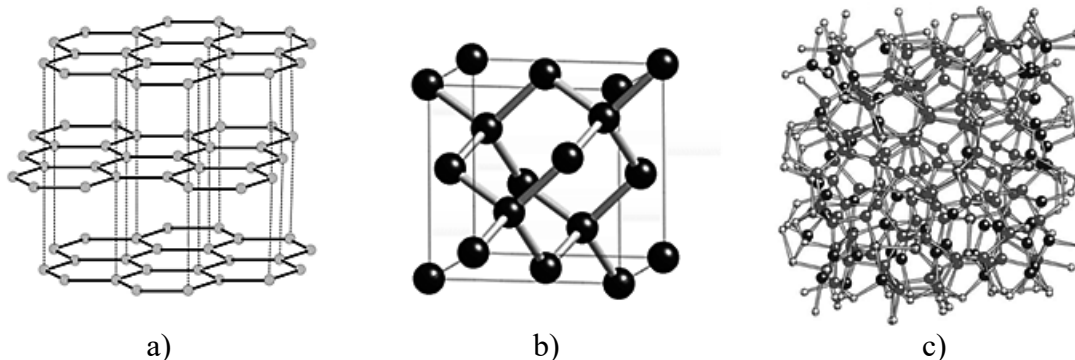
Pri charakterizácii tenkých vrstiev DLC povlakov je dôležité si uvedomiť, že sú tvorené amorfnou štruktúrou, čo znamená, že častice týchto vrstiev sú nepravidelne usporiadané. Amorfná štruktúra DLC povlakov je tvorená vodíkom a rôznymi štruktúrami uhlíka v určitom pomere. Uhlík je základom obrovského množstva rôznych štruktúr, ktorých výsledné vlastnosti závisia od druhu väzieb medzi atómami uhlíka. Väzby medzi atómami uhlíka môžu byť diamantového typu alebo grafitického typu. S typom väzby úzko súvisí hybridizácia atómu uhlíka, čiže usporiadanie orbitálov jednotlivých valenčných elektrónov. Atóm uhlíka obsahuje štyri valenčné elektróny a môže sa vyskytovať celkom v troch hybridizáciách a to v takzvanej  $sp^3$  hybridizácii,  $sp^2$  hybridizácii a  $sp^1$  hybridizácii, ktoré sú zobrazené na obr. 1. V prípade  $sp^3$  hybridizácie smeruje každý orbitál valenčného elektrónu do vrcholu pravidelného štvorstenu a vytvára s ďalším atómom pevnú  $\sigma$  väzbu. Atómy uhlíka v  $sp^3$  hybridizácii tvoria kryštalovú štruktúru diamantu. Hybridizácia  $sp^2$  je typická pre grafit, kedy pevnú  $\sigma$  väzbu medzi atómami tvoria len tri valenčné elektróny, ktorých orbitály smerujú do vrcholov rovnostranného trojuholníka. Posledný valenčný elektrón leží v p-orbitáli, ktorý sa nachádza nad a pod rovinou tvorenou  $sp^2$  orbitálmi a vytvára slabšiu  $\pi$  väzbu. V hybridizácii  $sp^1$  ležia dva valenčné elektróny v p-orbitáloch a ďalšie dva v sp-orbitáloch [2,3,6]



Obr. 1 Zobrazenie orbitálov valenčných elektrónov pre  $sp^3$ ,  $sp^2$  a  $sp^1$  hybridizáciu atómu uhlíka  
Figure 1. Showing the valence electron orbitals for  $sp^3$ ,  $sp^2$  and  $sp^1$  hybridization of a carbon atom

Diamant je najpevnejší a najtvrdší prírodný materiál a jeho extrémne fyzikálne vlastnosti vychádzajú zo silnej  $\sigma$  väzby medzi jednotlivými atómami. Usporiadaná diamantová kubická štruktúra sa vyznačuje najhustejším atómovým usporiadaním a jeho vysokú tvrdosť vytvárajú atómy uhlíka v  $sp^3$  hybridizácii. Grafit je tvorený jednotlivými vrstvami uhlíka so silnou  $\sigma$  väzbou, kde medzi jednotlivými vrstvami pôsobí slabá Van der Waalsova väzba. Takéto rovinné usporiadanie spôsobuje  $sp^2$  hybridizácia atómu uhlíka a práve absencia  $sp^3$  väzieb v grafitě ho radí medzi najmäkšie známe materiály. V DLC povlakoch je dôležitý práve podiel viazaných atómov uhlíka v  $sp^3$  hybridizácii, ktorý je kľúčový pre vytvorenie vlastností podobných diamantu. Rozdiel medzi diamantom a DLC povlakom je v usporiadaní. DLC vrstvy dosahujú vlastnosti podobné diamantu, ale jedná sa o neusporiadanú (amorfnú) štruktúru. Na obr. 2 môžeme vidieť rozdiel medzi amorfnou štruktúrou DLC povlaku

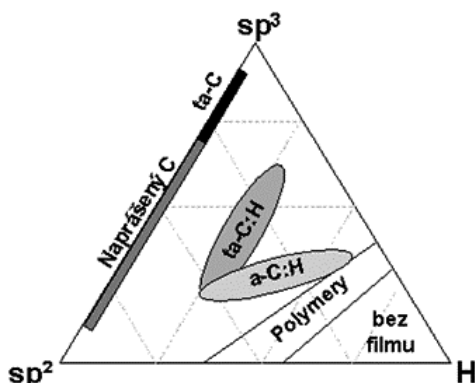
a usporiadanými štruktúrami diamantu a grafitu. Výslednú štruktúru DLC povlaku vytvárajú atómy uhlíka v rôznych hybridizáciách [2,3].



Obr. 2 Porovnanie štruktúry grafitu (a), diamantu (b) a amorfnej uhlíkovej štruktúry DLC povlaku (c)

Figure 2. Comparison of the structure of graphite (a), diamond (b) and amorphous carbon structure of DLC coating (c)

Ako už bolo spomenuté, amorfná štruktúra DLC povlakov je zložená z grafitického uhlíka, z diamantového uhlíka a z vodíka v určitom pomere v závislosti na danom procese. Hlavným parametrom, od ktorého sa odvíjajú vlastnosti vrstiev DLC povlakov, je podiel  $sp^3$  a  $sp^2$  uhlíkových väzieb, čiže pomer grafitickej a diamantovej štruktúry. Práve kvôli širokému spektru DLC vrstiev s rôznym zastúpením pomeru uhlíkových väzieb a vodíka sa vytvorilo základné delenie DLC vrstiev. Veľké množstvo metód prípravy DLC vrstiev využíva ako vstupný zdroj uhl'ovodíky a vo výslednej vrstve sú zakomponované aj atómy vodíka. Takto vzniklo základné rozdelenie vrstiev DLC povlakov, ktoré môžeme vidieť na obr. 3. Obr. 3 zobrazuje ternárny fázový diagram DLC vrstiev, ktorý sa obvykle používa pre znázornenie širokého spektra zloženia DLC povlakov. Tento obrázok predstavuje hlavné možné skupiny pre DLC vrstvy, v rozdelení podľa obsahu vodíka a podľa väzby uhlíkových atómov. Bod  $sp^2$  odpovedá grafitovému typu väzby atómov a bod  $sp^3$  potom odpovedá diamantovému typu väzieb medzi atómami uhlíka [3,6].



Obr. 3 Ternárny fázový diagram DLC povlakov

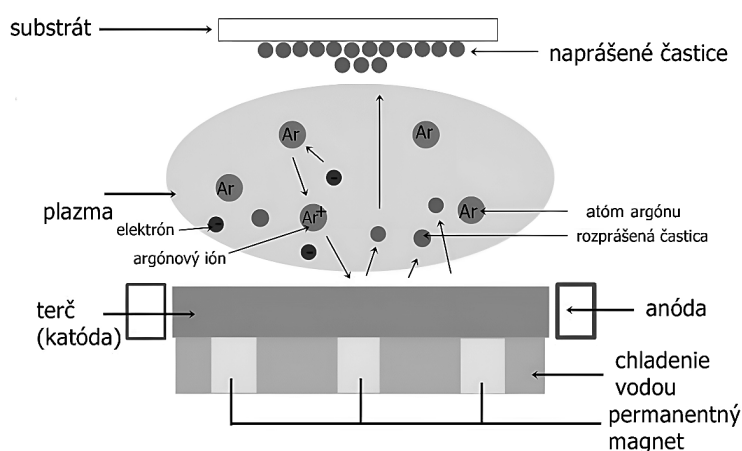
Figure 3. Ternary phase diagram of DLC coatings

V ľavej spodnej časti diagramu sa vyskytuje skupina neusporiadaných grafitických materiálov od čistého grafitu až po naprášený uhlík s vysokým podielom  $sp^2$  väzieb. Pravú spodnú časť charakterizujú uhl'ovodíkové polyméry, ktoré tvoria určitú hranicu, za ktorou sa dané atómy vyskytujú len v molekulárnej forme. Základné rozdelenie DLC vrstiev je teda nasledovné:

- **ta-C** bezvodíkové amorfné vrstvy s vysokým obsahom  $sp^3$  väzieb (takmer 90%). Majú najväčšiu podobnosť diamantu. Majú vysokú tvrdosť a veľký modul pružnosti.
- **ta-C:H** vrstvy s obsahom vodíka (25%-30%) s vysokým obsahom  $sp^3$  väzieb (cca 70%).
- **a-C:H** vrstvy s vysokým obsahom vodíka (40%-60%). Môžu obsahovať aj 70%  $sp^3$  väzieb, avšak nie len medzi atómami uhlíka, ale aj medzi atómami uhlíka a vodíka [3]

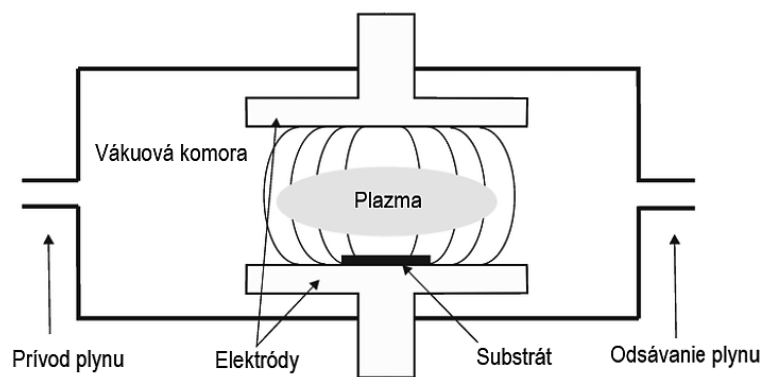
### 3.2. Metódy vytvárania DLC povlakov

Samotné metódy deponovania rôznych tenkých povlakov môžeme rozdeliť na dva základné druhy a to na metódy PVD (Physical-Vapor-Deposition) a CVD (Chemical-Vapor-Deposition). Pri metódach deponovania PVD dochádza k fyzikálnej depozícii vrstvy z plynnej fázy a pri metódach CVD dochádza k chemickej depozícii vrstvy z plynnej fázy. Na deponovanie DLC povlakov sa využívajú rôzne metódy v závislosti od druhu DLC povlaku. DLC povlaky využívané v praxi sa delia na už spomínané dva základné druhy a to bezvodíkové DLC povlaky (ta-C) a hydrogénové DLC povlaky (ta-C:H, a-C:H). Prvá skupina DLC povlakov sa zvyčajne nanáša metódou PVD s využitím uhlíkovej plazmy. V prípade hydrogénových DLC povlakov sa tieto bežne získavajú pomocou plazmového nanášania chemických pár a uhl'ovodíkových plynov, čiže metódou CVD.. Väčšina procesov, na ktorých je založená depozícia DLC vrstiev je fyzikálnej povahy (PVD), pretože na vytváranie väzieb  $sp^3$  majú hlavný vplyv ióny uhlíka. PVD procesy na nanášanie tenkých vrstiev DLC zahŕňajú napríklad nanášanie iónovým lúčom (IB), nanášanie katódovým oblúkom (CVA), ale najčastejším industriálnym depozičným procesom DLC vrstiev je magnetronové naprašovanie pomocou rozprašovania uhlíkoveho terča v Ar atmosfére (Obr. 4). Princíp spočíva v rozprašovaní uhlíkoveho terča v Ar plazme, kedy je povrch substrátu „bombardovaný“ atómami uhlíka. Na obr. 4 môžeme vidieť, že magnety sú umiestnené za terčom, aby spôsobili špirálový pohyb elektrónov a zväčšili dĺžku ich dráhy, a tým zvýšili stupeň ionizácie plazmy, ktorá „bombarduje“ povrch súčiastky iónmi uhlíka [2,3,6].



Obr. 4 Princíp magnetronového naprašovania  
Figure 4. Principle of magnetron sputtering

Chemická plazmová depozícia z pár (PACVD - Plasma Assisted Chemical Vapour Deposition) PACVD metóda deponovania DLC povlakov (Obr. 5) je vlastne CVD metóda povlakovania s tým, že sa celý proces zefektívňuje použitím plazmy. Základným princípom CVD metódy je, že tenká deponovaná vrstva sa na povrchu substrátu vytvára v dôsledku chemických procesov medzi chemickými zlúčeninami, ktoré sú v plynnom stave privedené k substrátu pri vyšších teplotách okolo 1000°C. Takýto plazmou aktivovaný CVD proces umožňuje zníženie teploty potrebnej pre vznik vrstvy na povrchu substrátu na približne 500°C. Pri tejto metóde sa používajú len prekurzory obsahujúce uhlík v plynnom stave, ako je napríklad acetylén. Ten je privedený v plynnom stave k povrchu substrátu, kedy vysoko energetické častice plazmy predávajú časť svojej energie jeho molekulám. Týmto spôsobom je získaná dostatočná energia potrebná pre priebeh chemickej reakcie vedúcej k depozícii povrchovej vrstvy. Využitie plazmy namiesto vysokej teploty, ako zdroja energie pre iniciáciu chemickej reakcie, prináša mnoho výhod. V prvom rade depozícia prebieha pri nižšej teplote a umožňuje rovnomerné nanášanie vrstvy aj v dutinách súčiastok bez nutnosti ich rotácie. Povlaky vytvorené metódou PACVD dosahujú hrúbku 2-3  $\mu\text{m}$  a obsahujú približne 70 % väzieb  $\text{sp}^3$  čo zabezpečuje ich vysokú tvrdosť [2,3,6].



Obr. 5 Schéma PACVD depozície  
Figure 5. Scheme of PACVD deposition

#### 4. Aplikácia DLC povlakov na valivé ložiská

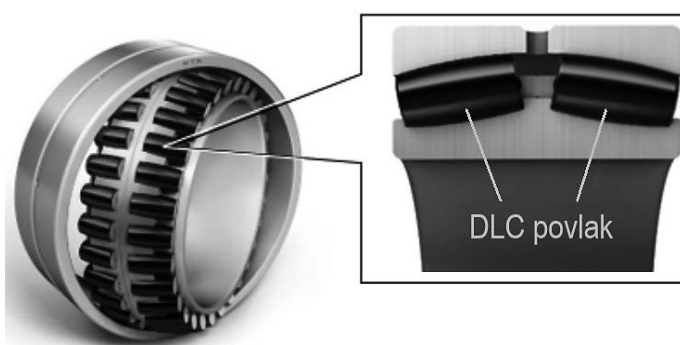
Tendenciou vývoja valivých ložísk je zvyšovanie ich kvality, pričom sa veľký dôraz kladie na znižovanie strát energie trením a s tým súvisiacu životnosť ložísk. Vzhľadom na to, že najnamáhavejšia časť ložiska je jeho povrch, vývoj sa sústreďuje hlavne naň. Aby sme vlastnosti ložísk ešte zlepšili, začali sa na valivé ložiská deponovať rôzne nátery a povlaky, ktoré disponujú ďaleko lepšími tribologickými vlastnosťami ako základný materiál ložiska. Jedny z najpoužívanejších povlakov, ktoré sa deponujú na valivé ložiská sú práve povlaky DLC. Ich tvrdý povrch s veľmi nízkou drsnosťou prispieva k potlačeniu oteru a iným prejavom opotrebenia, a teda k podstatnému predĺženiu životnosti ložiska. Spojením odolnosti a pevnosti bežnej ložiskovej ocele s výnimočne nízkym trením a vysokou tvrdosťou povlakov DLC vznikne ložisko, ktoré sa vyznačuje vysokou tvrdosťou povrchu s nízkym koeficientom trenia. Typické hodnoty tvrdosti DLC povlakov deponovaných na ložiskových oceliach sa rádovo pohybujú okolo 1200 HV, zatiaľ čo tvrdosť bežnej ložiskovej ocele je 650 až 850 HV. Avšak aby nedochádzalo k opotrebovaniu, samotná tvrdosť povrchu nestačí, preto je tiež dôležitou vlastnosťou koeficient trenia. Koeficient trenia valivých ložísk opatrených DLC povlakom



závisí od prostredia, v ktorom budú pracovať, nakoľko povlakom môžu byť opatrené buď všetky súčasti ložiska, ako na obr. 6, alebo len valivé telieska ložiska (obr. 7). Je zrejmé, že najnižšie hodnoty koeficientu trenia sa dosiahnu u valivých ložísk, ktorých všetky funkčné plochy sú ošetrené DLC povlakom[4,5].

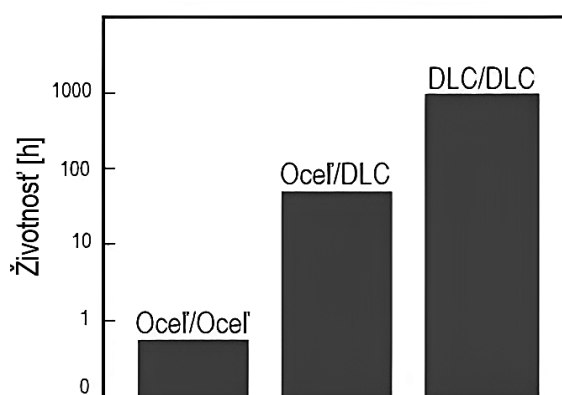


Obr. 6 Valivé ložisko s DLC povlakom  
Figure 6. Rolling bearing with DLC coating



Obr.7 Valivé telieska s DLC povlakom  
Figure 7. Rolling elements with DLC coating

Túto teóriu znižovania koeficientu trenia a predĺženia životnosti valivého ložiska pri ošetrení DLC povlakom všetkých súčastí ložiska, potvrdzuje aj výskum medzinárodnej spoločnosti SKF, ktorá je zameraná na výrobu a vývoj valivých ložísk. Autori Hultman a Sjöström (1998) vo svojom vedeckom článku pre spoločnosť SKF uvádzajú graf (Obr. 8), ktorý porovnáva životnosť jednotlivých trecích dvojíc vzhľadom na to, či ich povrchy boli alebo neboli ošetrené DLC povlakom [5].



Obr.8 Porovnanie životnosti trecích dvojíc vzhľadom na použitie DLC povlaku  
Figure 8. Comparison of the service life of friction pairs with regard to the use of DLC coating

Doteraz sa valivé ložiská ošetrené DLC povlakom prevažne používali v zariadeniach, ako sú kompresory a hydraulické motory. V týchto zariadeniach DLC povlak úspešne prispieva k ochrane proti poškodeniu ložísk takzvaným „rozmazaním“, čo je druh poškodenia ložiska, ktorý vzniká pri valcovom kontakte, keď sa rozdelí olejový film medzi valivými telieskami a ložiskovým krúžkom. Podobným problémom sa zaoberala vo svojom vývoji valivých ložísk

ďalšia spoločnosť s názvom NTN Corporation. Táto spoločnosť využila DLC povlaky na ošetrovanie valivých teliesok ložísk pre hlavný hriadeľ veternej turbíny. Pre ložiská hlavného hriadeľa veternej turbíny sa používajú súdkové telieska, ktoré pracujú pri extrémne nízkych prevádzkových rýchlostiach a pri vysokom kontaktnom zaťažení v dôsledku veľkej hmotnosti komponentov. Tieto ložiská majú problém s opotrebovaním povrchu obežnej dráhy, kde dochádza k jeho odlupovaniu a praskaniu. Spoločnosť NTN uvádza, že odolnosť ložísk ošetrovaných DLC povlakom výrazne stúpla, dokonca aj pri tak náročných prevádzkových podmienkach. Výskum a vývoj v tejto oblasti postupuje veľmi rýchlo a neustále sa objavujú nové koncepcie a nové typy DLC povlakov, ktoré majú stále širšie uplatnenie práve aj u valivých ložísk [4,5]

## 5. ZÁVER

Cieľom tejto práce bolo opísať súčasný stav poznatkov o DLC povlakoch, ich štruktúre, metódach vytvárania a ich využívaní v technickej praxi na povlakovanie valivých ložísk. Na základe tejto teoretickej analýzy môžeme tvrdiť, že DLC povlaky môžu efektívne zvyšovať povrchovú tvrdosť komponentov, ich odolnosť voči opotrebeniu a znížiť trenie v mnohých aplikáciách. Využitie DLC povlakov na valivé ložiská taktiež vykazuje výrazné zlepšenie ich odolnosti voči opotrebeniu, zníženie trenia a nárast životnosti. Na záver možno konštatovať, že DLC povlaky predstavujú sľubný nástroj na optimalizáciu funkčnosti valivých ložísk a mnohých iných strojných súčastí, kde dochádza k treniu.

## POĎAKOVANIE

Príspevok vznikol v rámci riešenia spoločného slovensko-poľského projektu TalentDetector 2023 ako výsledok spolupráce medzi Politechnikou Slaskou (Poľsko) a Žilinskou univerzitou v Žiline a projektov KEGA č. 004ŽU-4/2023 a KEGA č.009ŽU-4/2023.

## LITERATÚRA

1. KONEČNÁ, R., TILLOVÁ, E., VAŠKO, A., MARKOVIČOVÁ, L. 2020. Materiály II Návod na cvičenia. Žilinská univerzita v Žiline/EDIS-vydavateľstvo ŽU, 2020, 26 s., ISBN 978-80-554-1708-0
2. ROBERTSON, J. Diamond-like amorphous carbon. In Materials Science and Engineering: R: Reports, vol 37, 2002. ISSN 0927-796X. DOI: [https://doi.org/10.1016/S0927-796X\(02\)00005-0](https://doi.org/10.1016/S0927-796X(02)00005-0)
3. KROKER, M. 2016. Vývoj průmyslové technologie přípravy diamantu podobných vrstev. Bakalárska práca. Masarykova univerzita 2016. 1-5s.
4. ŠKOVIERA, J. 2017. Návrh systému pro testování valivých ložisek s proměnnými parametry mazání. Diplomová práca. Vysoké učení technické v Brně 2017. 1s.
5. Hard coating for heavy bearing duty [Online]. Anna Hultman a Hans Sjöström 1998 [cit. 2023.22.02] Dostupné na internete: <https://evolution.skf.com/hard-coating-for-heavy-bearing-duty/>
6. AINSWORTH, S., UHURE, N. 2007. Diamond like carbon coatings for tribology: Production techniques, characterisation methods and applications. International Materials Reviews. 52. 153-174. DOI: 10.1179/174328007X160272



26th January 2024  
Gliwice, Poland

DEPARTMENT OF ENGINEERING MATERIALS AND BIOMATERIALS  
FACULTY OF MECHANICAL ENGINEERING  
SILESIA UNIVERSITY OF TECHNOLOGY

## INTERNATIONAL STUDENTS SCIENTIFIC CONFERENCE

### Brain-Computer-Interface-based screen numeric keyboard

D. Myszor <sup>a</sup>, M. Lasak <sup>b</sup>, S. Sadza <sup>b</sup>

<sup>a</sup> Silesian University of Technology, Faculty of Automatic Control, Electronics and Computer Science, Department of Algorithmics and Software

email: [dariusz.myszor@polsl.pl](mailto:dariusz.myszor@polsl.pl)

<sup>b</sup> Silesian University of Technology's Academic High School in Gliwice

email: [michal.lasak@alogliwice.polsl.pl](mailto:michal.lasak@alogliwice.polsl.pl), [szymon.sadza@alogliwice.polsl.pl](mailto:szymon.sadza@alogliwice.polsl.pl)

**Abstract:** The article presents research on EEG-based screen numeric keyboard and performance measurement

**Key Words:** Brain-computer Interface, Neural, Brain activity detection

### 1. INTRODUCTION

The paper presents research focused on designing of an Brain-Computer-Interface-based (BCI) numeric keyboard interface for entering PIN numbers. Tests were performed to reveal the quality of the acquisition system. Additionally, subjective user feedback on system utilization was collected. UI of the application was created in Unity Engine. Data collecting device utilized in the work: NextMind allows for the acquisition of information about brain electrical activity and converts the data to easily interpretable control signals.

### 2. PROJECT ASSUMPTIONS

To perform tests on user-device interaction, certain assumptions were made: all tests were completed on the same hardware and software. In addition, all performed scenarios were identical between each subject.

### 3. DATA ACQUISITION

Electroencephalography (EEG) is typically a non-invasive method for detecting brain activity based on voltage fluctuations, primarily resulting from the orientation and distance to the source of the activity. The observable frequencies are in the range of 1 to 30 Hz [1].

A wide range of effects related to brain activity can be used to enable effective control of various processes, including [4] slow cortical potentials (SCP), stimulus-related synchronizations and desynchronizations, steady-state evoked potentials (SSEP), P300 wave.

From the point of view of Brain-Computer interfaces, steady-state evoked potentials (SSEP) are especially interesting. SSEPs are electrophysiological responses caused by exposure to stimuli of a specific frequency, resulting in the appearance of a component of a corresponding frequency in specific areas of the cerebral cortex. Depending on the nature of the interacting stimulus, the following steady-state evoked potentials are distinguished: auditory (steady-state auditory evoked potentials, SSAEP), visual (steady-state visual evoked potentials, SSVEP), and sensory (steady-state somatosensory evoked potentials, SSSEP). An important advantage of the SSEP effect is the short reaction time to the appearance of a stimulus, which ensures a high bandwidth of the brain-computer interface [5].

Such BCI interfaces are particularly interesting in supporting people with disabilities for rehabilitation and even communication purposes (e.g. BCI keyboards) [2] [3]

The Next Mind interface was chosen because of its ease of use, compact design, and available SDK, allowing seamless integration with the Unity Engine. The application of this device allowed to put the focus on the rapid prototyping of the UI of the on-screen keyboard application as well as simplified the process of data collection.

For the purpose of this research, the SSVEP effect was exploited [6]. An on-screen numeric keyboard was presented, and each button was assigned a different type of NextMind active asset (related to various texture patterns and texture blinking frequency). When the user gazes at a specific button in the occipital area of the brain, patterns in EEG signals emerge related to the specific active asset configuration. Thus, there is a way to determine the button on which the user is looking at so the selection of the proper button-related value.

#### 4. USER INTERFACE

A unified interface was created in the Unity Engine. The user was able to select numbers by looking at the buttons. The goal of the user was to enter a four-digit passcode (which was displayed in the top right corner of the screen). After the passcode was provided, the user had to accept the entered passcode by selecting the ENTER on-screen button. The time of entering a passcode was limited to 30 seconds. The information on what button the test subject was looking at was, as mentioned previously, obtained by an EEG sensor mounted to the back of the participant's scalp. The UI of the application is presented in Fig. 1 - 5.

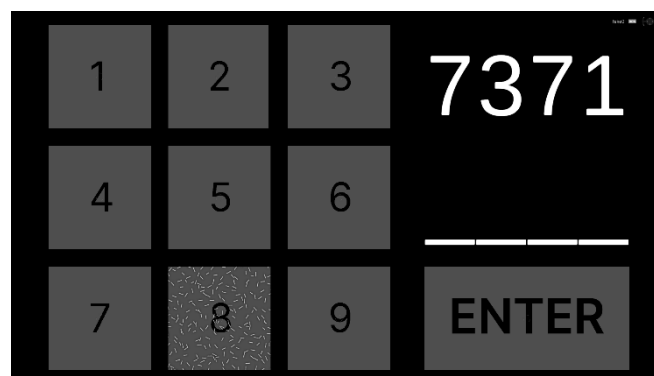


Figure 1: Before typing has started.

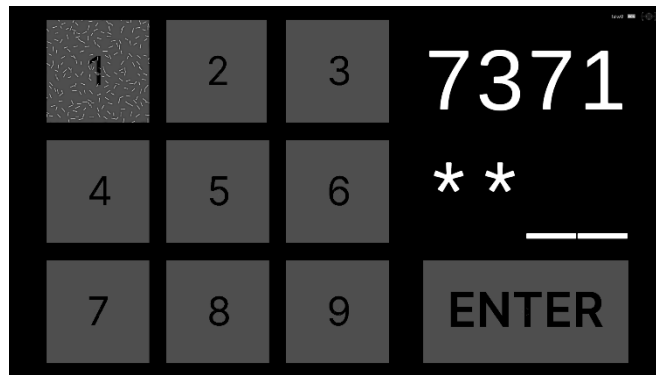


Figure 2: While typing.

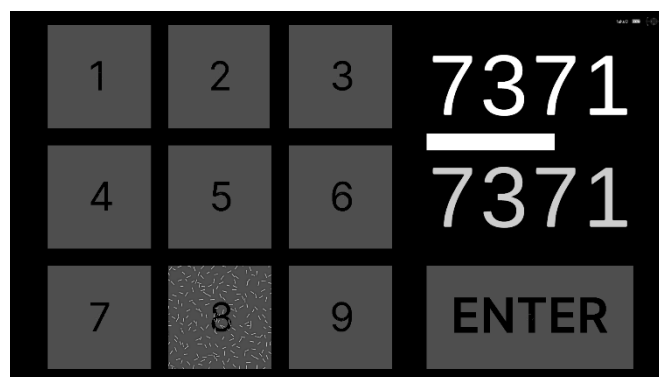


Figure 3: When written code matches the provided one.

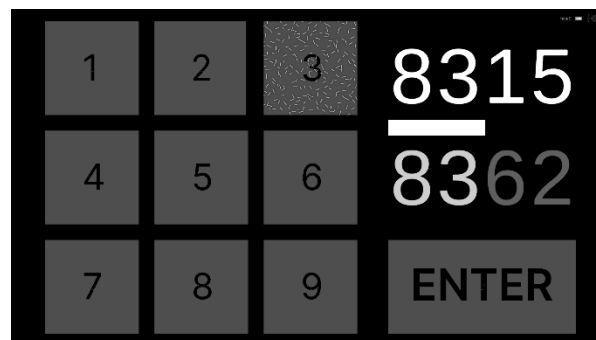


Figure 4: When written code does not match the provided one.

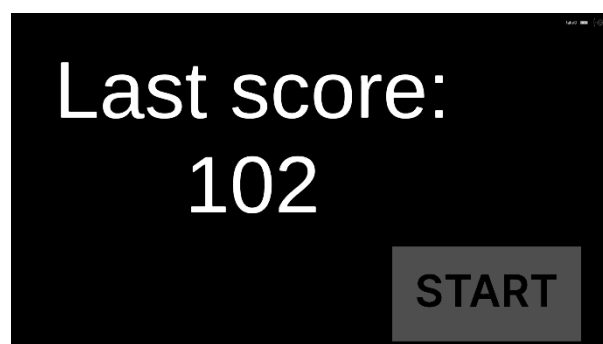


Figure 5: Display of total score after all tests has been completed.

The total score obtained by the user is calculated using the following formula:

$$Score = \frac{\sum_{i=1}^n (3 * 10^4 - t_i) * \frac{p_i}{c}}{100 * n}$$

where n is equal to the total number of tests, t is the time the test has taken, p is the amount of numbers being correct, and c is the total amount of numbers.

## 5. PERFORMANCE METRIC

To test whether a device/system, that the user is interacting with, is applicable in the real world or not, one cannot only judge based on the pure mathematical coefficients, but rather should observe the interaction of the device/system with the user, leading to a decent understanding of usefulness of such device. This is the reason why, while the tests were performed, two metrics were taken into account. The first one was the total score, which gives a good understanding of how well the test subject was able to cooperate with the test device. Second was the test subject itself and their own personal opinion after using the device.

## 6. TESTS

Tests were performed using NextMind's EEG and developed application. Before the test, volunteers went through the process of NextMind calibration. During test execution, the subjects were asked to enter the correct code ten times. When the test was over, the program calculated the Score using the provided formula, and participants were asked to rate their experience with the device. For every test to be replicable, they were performed in the same room, on the same hardware and software, with dim light, occluded windows, and complete silence.

## 7. RESULTS

Results seen in the experiment were not as prominent as expected (tab. 1), with an average total score of 69 points and an average personal opinion of 4/5. The biggest issue in the tests was the inconsistency of results, with a high of 165 and a low of -7 points that, despite the rather high score of 69 points on average, makes the conclusion of whether the technology is or is not suited for wider use, extremally hard to make. But, besides that, there was still a lot to conclude from. The most interesting measure turned out to be the paradoxically very high personal opinion mark that every test subject was to give after using the EEG sensor. The lowest observable score was 3/5, even though the total score of that test of -7 points was lacking significantly, and the highest personal score of 5/5, which was given twice, could be seen next to both 165 and 42 total score points. It is obvious that in order to draw any sensible conclusion, more tests need to be performed, the total score is too random for being a scientific data source, and the personal opinion score needs to be redesigned as it seems to have no linkage with the calculated scores.

Table 1. The performed tests on which results were formed.

Score, defined by the formula	User rating
165	4/5
42	5/5
76	4/5
-7	3/5

## BIBLIOGRAPHY

1. H.J. Craig, Electroencephalography: basic principles, clinical applications, and related fields. *Neurology* 67.11 (2006): 2092-2092.
2. D. Mattia, L. Astolfi, J. Toppi, M. Petti, F. Pichiorri i F. Cincotti, Interfacing brain and computer in neurorehabilitation, 4th International Winter Conference on Brain-Computer Interface (BCI), Yongpyong, 2016.
3. F. Pichiorri, G. Morone, M. Petti, J. Toppi, I. Pisotta, M. Molinari, S. Paolucci, M. Inghilleri, L. Astolfi, F. Cincotti i D. Mattia, „Brain–computer interface boosts motor imagery practice during stroke recovery,” *Annals of Neurology*, pp. 851-865, 2015.
4. C. S. Nam, A. Nijholt, F. Lotte, *Brain-Computer Interfaces Handbook: Technological and Theoretical Advances*, Boca Raton: CRC Press, 2018.
5. Ishizuka, Kazumi, Nobuaki Kobayashi, and Ken Saito. "High accuracy and short delay 1ch-ssvep quadcopter-BMI using deep learning." *Journal of Robotics and Mechatronics* 32.4 (2020): 738-744.
6. Nguyen, Trung-Hau, and Wan-Young Chung. "A single-channel SSVEP-based BCI speller using deep learning." *IEEE Access* 7 (2018): 1752-1763.



26th January 2024  
Gliwice, Poland

DEPARTMENT OF ENGINEERING MATERIALS AND BIOMATERIALS  
FACULTY OF MECHANICAL ENGINEERING  
SILESIA UNIVERSITY OF TECHNOLOGY

## INTERNATIONAL STUDENTS SCIENTIFIC CONFERENCE

### Efficient Data Loader for Training a Pyramid Stereo Matching Network on Synthetic CARLA-Generated Dataset

D. Myszor<sup>a</sup>, M. Paszkuta<sup>b</sup>, T. Kukuczka<sup>c</sup>, E. Szmyt<sup>d</sup>, D. Sobieraj P. Michalski<sup>f</sup>, K. Pawełczyk<sup>g</sup>, M. Polończyk<sup>g</sup>

<sup>a</sup> Silesian University of Technology, Faculty of Automatic Control, Electronics And Computer Science, Department of Algorithmics and Software

<sup>b</sup> Silesian University of Technology, Faculty of Automatic Control, Electronics And Computer Science, Department of Graphics, Computer Vision and Digital Systems

<sup>c</sup> Silesian University of Technology, Faculty of Automatic Control, Electronics And Computer Science, Department of Graphics, Department of Cybernetics, Nanotechnology and Data Processing

<sup>d</sup> Silesian University of Technology, Virtual Flying Student Research Club

<sup>f</sup> Opole University of Technology, Department of Informatics

<sup>g</sup> Autonomos Systems Sp. z o. o.  
email: [dariusz.myszor@polsl.pl](mailto:dariusz.myszor@polsl.pl)

**Abstract:** The article describes the implementation of a class intended to use data from the CARLA simulation environment to train the popular PSMNet neural network. Data processing from simulation stereoscopic cameras and a depth map sensor was also presented.

**Keywords:** neural network, PSMNet, CARLA, stereo vision

## 1. INTRODUCTION

Autonomous vehicles require spatial awareness to operate. The most valuable information is provided by lidars, a three-dimensional map of the vehicle's surroundings [3,4]. These devices provide precise information about the distance to points in 3D space[9,10]. However, obtained points are sparse, lidars have limited capabilities in the area of obtained data point resolution. Therefore, the lidar can omit smaller objects (especially ones further away from the sensor)[5,8] In addition, lidars are expensive devices that significantly influence the cost of the whole sensory system[6].

The solution to this issue can be utilising a set of global shutter cameras configured as stereoscopic pairs. Three-dimensional maps of the surroundings can be reconstructed based on the data from such a set. Cameras are significantly cheaper than lidars. At the same time, the resolution of acquired maps is significantly higher, and the distance to every point of the scene, registered by two cameras, can be obtained. Mathematical equations for depth reconstruction



from stereoscopic pairs are known [9]. However, a significant issue is the localisation of corresponding points in pictures taken from stereoscopic pairs[7].

Convolutional neural networks (CNNs) have found widespread applications in various domains, including image classification, image segmentation, object detection, and medical image analysis. Such networks can also be employed for the purpose of corresponding points recognition. They can provide information about the disparity, i.e. the distance in pixels between corresponding points on the left and right images (see fig. 1) [1]. Especially useful in this application are networks based on the Pyramid Stereo Matching concept, e.g., the PSMNet structure, which in 2018 year obtained first place in the KITTI ranking. The huge advantage of applying artificial neural networks is the method's robustness. Employed structures can cope well with a wide variety of conditions (such as operation environment, light and weather). However, it requires a significant amount of training data that might be tricky to obtain in real-life conditions. Therefore, simulators such as CARLA can be employed, allowing the creation of versatile training data sets[7].

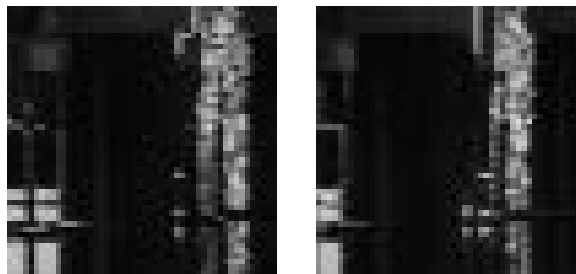


Figure 1. Red points show the actual location of the point in space after applying data from the disparity map, green point shows (in the image from the right camera) where the point would be if the same coordinates were used as in the image on the left (left camera).

## 2. PSMNET STRUCTURE

PSMNet is a deep neural network[1]. It utilises a pyramid structure to process multi-scale information. There are multiple stages, each of them processes input images at different scales. It allows the capture of local and global context. Images from the left and right cameras are processed separately. In the next step, the cost volume is constructed based on the concatenation of feature maps extracted from left and right images. Cost volume represents matching cost between patches in left and right images at various levels of disparity. Then, 3D convolutions process the cost volume. This approach allows to consider both spatial and disparity dimensions while discovering relations between pixels. At the network output, the disparity map is returned. One of the available cameras is selected before the training process (left or right). In relation to this selected camera, the disparity map is calculated. Importantly, disparity is provided for every pixel of the input image obtained from the selected camera. A disparity map represents the shift between pixels on the images obtained by the right and left cameras. The depth map represents the distance between the camera and the object (in meters). Disparity maps can be converted easily to distance maps if camera parameters and distance between cameras are known.

### 3. CARLA SIMULATOR

CARLA is an open-source simulator implemented to support autonomous driving systems' development, training, and validation[2]. CARLA provides a set of open digital assets (urban layouts, vehicles, buildings) that allow experiments to be conducted in realistic environments under various environmental conditions. The simulator introduces a high level of flexibility at the level of configuration. It also provides a set of sensors which can be employed for data gathering. In this research, we utilised two RGB cameras to construct a stereoscopic pair and depth detector, which was located in the same location as a left camera. The CARLA depth sensor, providing precise depth information for every pixel, was utilized to acquire a reference depth for the generated RGB images. All virtual sensors were synchronized using CARLA's synchronous mode. Images from the RGB cameras and reference depth were captured simultaneously and saved as PNG files with lossless compression. A 24-bit coding basis on RGB channels was used for depth coding.

The utilization of CARLA allowed for the creation of versatile datasets which were used for PSMNet training and evaluation.

### 4. DATASET LOADER

The PSMNet structure was implemented by the authors and published on the website <https://github.com/JiaRenChang/PSMNet>. Authors utilised Python language and PyTorch machine learning library for deep neural network development. The PSMNet repository comes with the default data loader for the KITTY[12] and Scene Flow[11] datasets, as utilized by the authors. To train and validate the PSMNet model using CARLA-generated data, a custom dataset loader class was developed. This class facilitates the reading of input PNG files containing RGB content, while also loading reference depth maps and dynamically converting them into disparity maps.



*Figure 2. The left image shows the output depth map from the CARLA simulator, while the right shows the normalised image.*

The depth map generated by the CARLA simulator is a 24-bit image mapped to 3 channels of the RGB colour space (see Fig. 2 top image). Such data can be decoded using the following formula:

$$depth_{norm} = \frac{R + G \cdot 256 + B \cdot 256^2}{256^3 - 1} \cdot 1000$$

In this equation, an order of bytes from less to more significant is visible (R->G->B). This equation converts CARLA format depth maps to maps for which individual pixels are distances expressed in meters (see Fig. 2 bottom image). The maximum distance that can be obtained is 1000 meters (this is the maximum value that can be obtained for the CARLA simulator).

The PSMNet network takes a pair of stereoscopic images as input, producing a disparity map. While this process necessitates the use of a reference disparity during the training phase, there is currently no sensor available that provides this type of data. Consequently, a corresponding code has been developed to convert the depth map into a disparity map, and the operation is described by the following formula:

$$disp = \frac{focal \cdot baseline}{Depth_{norm}},$$

baseline is the distance between the cameras in stereoscopic pair (expressed in meters). For simulation data, focal has the following equation:

$$focal = \frac{width}{2 \cdot \tan\left(\frac{FOV \cdot \pi}{360}\right)}$$

Where width is the number of horizontal image pixels, FOV is the horizontal camera field of view. Additional conditions were used to prevent undesirable errors occurring in the neural network:

$$disp = \begin{cases} 0, & disp < 0.5 \\ disp, & disp \geq 0.5 \end{cases}$$

This is necessary because such small shifts between corresponding points in the left and right images are misinterpreted by the artificial neural network and have a negative influence on the structure training process.

The implemented dataset loader class accepts the following arguments:

- list with absolute patches to left images,
- list with absolute patches to the right images,
- list with absolute patches to the depth map.

Corresponding left/right/depth data should have the same indexes in the respective lists. We used the PIL library to load images as well as depth maps. Images are loaded in RGB format. Depth maps are converted to disparity maps with the above-mentioned formulas. In the next step, camera images and disparity maps are cropped randomly with a target resolution of 256x512 pixels. In the further step, data are transferred to PyTorch tensor formats and sent to the PsmNet model. Our class inherits from the data.Dataset class, so it can be implemented when creating a DataLoader as a dataset, providing appropriate arguments. Dataset loader were made publicly available on GitHub (<https://github.com/TKukuczka/PSMNet-Carla-Loader>).

## 5. CONCLUSION

In this article, the motivation for the utilization of stereoscopic cameras for the purpose of depth, map generation as well as the application of simulation data for the purpose of depth estimation artificial neural network training were presented.

In addition, the internal functionality of the custom dataset loader class, which serves as a bridge between simulation-generated data and depth estimation artificial neural network (which was implemented by the authors and made publicly available on GitHub) was presented.

## 6. ACKNOWLEDGEMENTS

The publication/paper was based on the results of the project no. POIR.01.01.01-00-0123/20 co-financed by the European Union under the European Regional Development Fund - Smart Growth program 2014-2020.



Rzeczpospolita  
Polska



Unia Europejska  
Europejski Fundusz  
Rozwoju Regionalnego



## BIBLIOGRAPHY

1. CHANG, Jia-Ren; CHEN, Yong-Sheng. Pyramid stereo matching network. In: Proceedings of the IEEE conference on computer vision and pattern recognition. 2018. p. 5410-5418.
2. DOSOVITSKIY, Alexey, et al. CARLA: An open urban driving simulator. In: Conference on robot learning. PMLR, 2017. p. 1-16.
3. ROYO, Santiago; BALLESTA-GARCIA, Maria. An overview of lidar imaging systems for autonomous vehicles. Applied sciences, 2019, 9.19: 4093
4. LI, You; IBANEZ-GUZMAN, Javier. Lidar for autonomous driving: The principles, challenges, and trends for automotive lidar and perception systems. IEEE Signal Processing Magazine, 2020, 37.4: 50-61.
5. ZHANG, Yihuan, et al. An efficient LiDAR-based localization method for self-driving cars in dynamic environments. Robotica, 2022, 40.1: 38-55.
6. GÖHRING, Daniel, et al. Radar/lidar sensor fusion for car-following on highways. In: The 5th International Conference on Automation, Robotics and Applications. IEEE, 2011. p. 407-412
7. NIRANJAN, D. R., et al. Deep learning based object detection model for autonomous driving research using carla simulator. In: 2021 2nd international conference on smart electronics and communication (ICOSEC). IEEE, 2021. p. 1251-1258.
8. MOU, Shenyu, et al. An optimal lidar configuration approach for self-driving cars. arXiv preprint arXiv:1805.07843, 2018.
9. RASHED, Hazem, et al. Motion and depth augmented semantic segmentation for autonomous navigation. In: Proceedings of the IEEE/CVF Conference on Computer Vision and Pattern Recognition Workshops. 2019. p. 0-0.
10. IANCU, David-Traian, et al. Vehicle depth estimation for autonomous driving. UPB Scientific Bulletin, Series C: Electrical Engineering and Computer Science, 2021, 3-20

11. Mayer, Nikolaus et al. "A Large Dataset to Train Convolutional Networks for Disparity, Optical Flow, and Scene Flow Estimation." 2016 IEEE Conference on Computer Vision and Pattern Recognition (CVPR) (2015): 4040-4048.
12. M. Menze and A. Geiger, "Object scene flow for autonomous vehicles," 2015 IEEE Conference on Computer Vision and Pattern Recognition (CVPR), Boston, MA, USA, 2015, pp. 3061-3070, doi: 10.1109/CVPR.2015.7298925.



26th January 2024  
Gliwice, Poland

DEPARTMENT OF ENGINEERING MATERIALS AND BIOMATERIALS  
FACULTY OF MECHANICAL ENGINEERING  
SILESIA UNIVERSITY OF TECHNOLOGY

## INTERNATIONAL STUDENTS SCIENTIFIC CONFERENCE

### Designing and developing a station for testing the quality of EEG gels

D. Myszor<sup>a</sup>, J. Sarno<sup>b</sup>, P. Bartosz<sup>b</sup>, M. Wieczorek<sup>b</sup>, M. Wola<sup>b</sup>, K. Cichecka<sup>c</sup>, M. Łoś<sup>c</sup>,  
M. Polak<sup>c</sup>, N. Krzywda<sup>c</sup>

<sup>a</sup> Silesian University of Technology, Faculty of Automatic Control, Electronics and Computer Science, Department of Algorithmics and Software

<sup>b</sup> Silesian University of Technology, Faculty of Automatic Control, Electronics and Computer Science, Virtual Flying Student Research Group

<sup>c</sup> Silesian University of Technology, Faculty of Environmental and Energy Engineering, Virtual Flying Student Research Club  
email: [dariusz.myszor@polsl.pl](mailto:dariusz.myszor@polsl.pl)

**Abstract:** The article describes the design of a device for testing gels used in electroencephalogram (EEG) diagnosis. The device's purpose is to allow for test execution in consistent conditions with minimal time and effort required for the later processing of collected data.

**Keywords:** EEG, Gels, BCI, Electronics

## 1. INTRODUCTION

As part of the research project realized under the IDUB - "Inicjatywa Doskonałości - Uczelnia Badawcza", students designed and developed a device that would allow for simple and reliable testing of various EEG gels as well as various conditions that might or might not affect their effectiveness. Research on the quality of EEG devices and gels is often done only on human subjects, so creating a controlled environment that allows for reliable and repeatable tests can be vastly beneficial [1][2].

## 2. ELECTROENCEPHALOGRAPHIC GELS

Electroencephalogram (EEG) is an incredibly useful diagnosis tool for real-time monitoring of bio-electrical brain activity. However, the efficiency of collected data is often determined by the quality of used electrodes and conductive substances such as electroencephalography gels. Electrodes using gels have been proven to have the highest effectiveness [2]. In the past few years, new recipes and forms of said gels have been developed with the goal of improving their conductivity, stability, and patient comfort level. The goal of this research was to develop a device that would allow for reliable testing of the conductive

properties of EEG gels in consistent and controlled conditions, which, in turn, would allow a close study of the effects of external conditions on gels of various forms and compositions.

### **3. DEVICE STRUCTURE**

The device has been built in a modular way in order to make it open for upgrades in the future as well as modifications that would allow for tests focusing on other areas, for example, testing various EEG technologies or electrode types. Additionally, the device had to fulfill specific requirements in order to maintain the highest possible quality of collected data:

- the device should have the ability to control and maintain temperature,
- the device should additionally collect other environmental data,
- electromagnetic interferences produced by the device should be as little as possible,
- the device should allow for easy change of currently tested gel.

#### **3.1 Gel Testing Module**

The device's primary function is to test the efficiency of various forms of gels used for EEG devices. The sinusoidal function generator was attached to a copper plate to achieve this goal. The generator's configuration varied on a specific test at a given moment. An electrode with gel was attached to the plate via elastic fabric, and an actual EEG device (OpenBCI) was used to collect data generated this way. An EEG device was additionally connected directly to a sinusoidal function generator in order for both devices to use common electrical potential as a base level. The choice of copper for a plate resulted from two main concerns. The first one was to use a substance with high electrical conductivity, and the second concern was to use a substance that would be both chemically and biologically neutral, as the device was to be used for both organic and non-organic gels.

#### **3.2 Thermal Control Module**

The human body's natural temperature usually oscillates between 36.5 - 37.5 °C[3], but it can reach a broader range in certain situations. It's essential to test how gels will behave in thermal conditions close to those of human skin. Human skin temperature is noticeably higher than that of a typical room. That's why the heating system is sufficient to simulate human skin's temperature without a need for cooling. This was implemented via a high-resistance plate that functions as a heat generator and a set of high-precision digital thermal sensors. The concern about this system was due to potential electromagnetic interference caused by a heat generator switching on and off to maintain the temperature. A ceramic block was attached to the brass plate to mitigate this issue. The ceramic block was then isolated from the environment via a thick layer of styrofoam. The block is heated to the desired temperature before the main measurements and disabled as the data collection process starts. Data from thermal sensors is being collected the whole time during the gel testing so the effects of block cooling off could be recognised during data processing.

#### **3.3 Additional Sensors**

Temperature is not the only condition that might affect the gel and, consequently, collected data. Other conditions like air humidity or atmospheric pressure might affect the efficiency of gels. In order to avoid variations in those conditions that would distort collected data, additional sensors were put in place to be recorded alongside temperature during the measurements.

However, those data can only be passively evaluated to ensure there is no significant difference between various tests carried out on the electrodes and gels.

### 3.4 EMC Interference Mitigating

Signals registered via EEG devices usually have a voltage below  $100\mu\text{V}$ . In order to mimic real-life scenarios, the generated waves also have amplitudes within this range. However, the problem with measurements done on such a small voltage is its susceptibility to interference. Multiple measures were taken in order to minimise this issue, one of which is the usage of the ceramic block as a thermal battery instead of active heating, described in subsection 3.2. Additionally, the power supply and central controlling unit have been enclosed into a Faraday's cage and moved away from the EEG device and the plate to minimise their impact.

## 4. DATA PROCESSING

Collected data is being processed digitally using a dedicated app designed specifically for that purpose. In the first step, data from sensors is moved onto the same timeline as the main EEG measurements in order for a researcher to subjectively validate if the environmental changes, that naturally occurred during the data collection stage, are small enough to consider the collected data reliable. If the decision is positive, the Fourier transform is being conducted on an EEG dataset to isolate waves generated by a generator and discard any type of noise. Within the result, the peaks of sinusoidal waves are used as the final metric for the gel's quality.

## 5. APPLICATIONS

The created station can be used in many various applications. Reliably testing the influence of gels on signals received by EEG is one of them. Still, with accurate measurements of possible distortions in a signal, it is possible to create a correction mechanism that can significantly improve the quality of the data received from EEG. Such improvements can significantly boost the diagnostic capabilities of EEGs but also can help develop more reliable and complex brain-computer interfaces.

## 6. PLACE FOR FUTURE IMPROVEMENT

There are still certain improvements that could be introduced in the future. More noticeably, the brass plate can be replaced with a material that more faithfully emulates human skin in its thermal, bio-electrical and textural properties, allowing for even more precise data. Additionally, pairing the device with an environmental simulation chamber in order to control atmospheric pressure and air humidity would be useful for testing more closely the impact of those conditions on overall gels' effectiveness.

## BIBLIOGRAPHY

1. Radüntz, Thea. Signal quality evaluation of emerging EEG devices. *Frontiers in physiology*, 2018, 9: 98.



2. Mihajlović, Vojkan; Garcia-Molina, Gary; Peuscher, Jan. Dry and water-based EEG electrodes in SSVEP-based BCI applications. In: Biomedical Engineering Systems and Technologies: 5th International Joint Conference, BIOSTEC 2012, Vilamoura, Portugal, February 1-4, 2012, Revised Selected Papers 5. Springer Berlin Heidelberg, 2013. p. 23-40.
3. Hutchison, James S., et al. Hypothermia therapy after traumatic brain injury in children. *New England Journal of Medicine*, 2008, 358.23: 2447-2456.



26th January 2024  
Gliwice, Poland

DEPARTMENT OF ENGINEERING MATERIALS AND BIOMATERIALS  
FACULTY OF MECHANICAL ENGINEERING  
SILESIA UNIVERSITY OF TECHNOLOGY

## INTERNATIONAL STUDENTS SCIENTIFIC CONFERENCE

### **Numerical research of gear-lever of the planetary drive mechanisms of basic needles of warp knitting machines with the use of the software environment PRANS-PK**

V. Neimak<sup>a</sup>, O. Polishchuk<sup>a</sup>, T. Romanets<sup>a</sup>, S. Smutko<sup>a</sup>, M. Bonek<sup>b</sup>

<sup>a</sup> Khmelnytskyi National University, Faculty of Engineering, Transport and Architecture, Khmelnytskyi, Ukraine email: nejmakvit@gmail.com, opolishchuk71@gmail.com, tromanec@gmail.com, svsmutko@gmail.com.

<sup>b</sup> Silesian University of Technology, Faculty of Mechanical Engineering, Department of Engineering Materials and Biomaterials, Gliwice, Poland

**Abstract:** we proved the possibility of using gear-lever mechanisms as a drive of warp knitting machines based on satellite curves, which are able to reproduce these mechanisms. At the frequencies of rotation modern WKM presence of unbalanced masses leads to significant dynamic loads on the shafts and pillars mechanism. Unbalanced forces, variable in magnitude and direction, can cause vibration as individual units and the entire mechanism, with the most vibration caused by the inertia of the rotating masses and masses that move back and forth. This article presents the results of experimental studies of dynamic single-stage planetary gear-lever mechanism. The experimental stand and sensors for determination of reactions at pillars are worked out. Software LabVIEW is used for registration and data processing.

**Keywords:** gear-lever of the planetary mechanism, dynamic single-stage, balanced.

## 1. INTRODUCTION

In the laboratory of the Department of Machines and Apparatus of the Khmelnytskyi National University, one- and two-stage gear-lever planetary mechanisms for driving the working bodies of warp-knitting machines (WKM) were developed.

Works [1,2] proved the possibility of using gear-lever mechanisms as a drive for warp knitting machines based on satellite curves that are able to reproduce these mechanisms. However, the dynamics of these mechanisms at rotation frequencies at which modern warp knitting machines operate - more than 1500 rpm - have not been studied. At such rotation frequencies, the presence of unbalanced masses leads to significant dynamic loads on the shafts and supports of the mechanism. Unbalanced forces, variable in magnitude and direction, can cause vibration of both individual links and the entire mechanism as a whole, and the largest vibrations are caused by the inertial forces of rotating masses and reciprocating masses. In work [3], possible balancing options were analyzed and a number of measures were taken for this purpose. The next stage is the study of the dynamic loads of gear-lever planetary

mechanisms, in particular, the determination of the reactions in the supports that occur during movement. Determination and analysis of dynamic characteristics of gear-lever planetary mechanisms will make it possible to compare them with other mechanisms used as WKM drives, to develop and test methods for reducing dynamic loads.

## 2. OBJECTS AND METHODS OF RESEARCH

The next stage is the study of the dynamic loads of gear-lever planetary mechanisms, in particular, the determination of the reactions in the supports that occur during movement. Determination and analysis of dynamic characteristics of gear-lever planetary mechanisms will make it possible to compare them with other mechanisms used as WKM drives, to develop and test methods for reducing dynamic loads.

The kinematic diagram of the stand for experimental studies of dynamic loads of the gear-lever drive mechanism of the working bodies of warp knitting machines is presented in Figure 1. The worm gear 27 is driven from motor 1 through pulleys 2, 21 and belt 4, which in its turn with the help of pulleys 26 24 and belt 25 transmits revolutions to the shaft 5 of the installation.

A gear 8 is placed on the shaft 5, which is fastened with a screw 20. To synchronize the shafts 7 and 5, an intermediate wheel 9 is used, which is mounted on the intermediate shaft 6, and through the key, it transmits revolutions to the gear wheel 10. The eccentric gears 13 and 14 drive working bodies: connecting rod 15 and 16, needle guide 17, on which the needle 19 is fixed with the help of a screw 18. The counterweight 11 is attached to the shaft 7 with a key joint. The screw 12 fixes the finger, which is the axis of rotation of the central gear wheel 14. The counterweight 11 and the crank 22 serve to balance the mechanism. The geometric parameters of the counterweight 11 and the eccentric wheel 13 were obtained according to the method presented in [3].

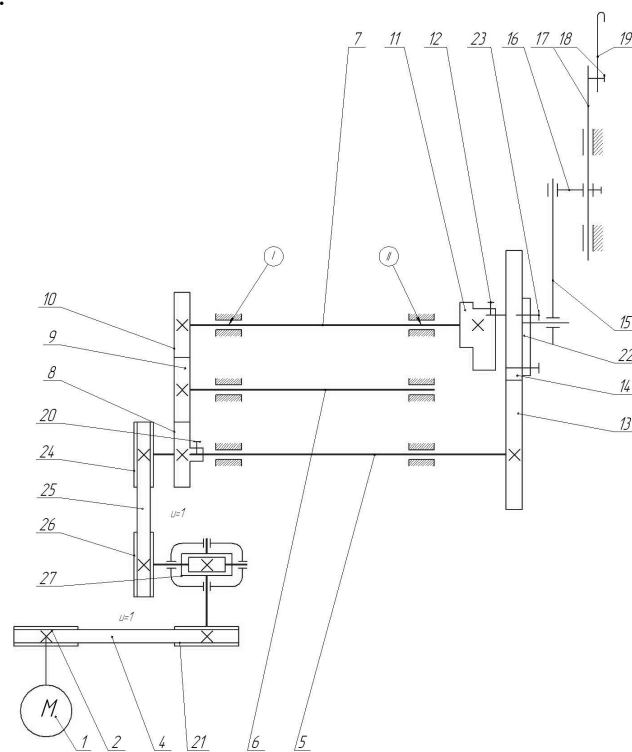


Figure 1. Kinematic scheme of the gear-lever drive mechanism of the working bodies of warp-knitting machines

Sensors for researching the reactions in the supports are placed in the places where the bearings of the shafts I, II are installed (Fig. 1). The experiment was carried out at a speed of rotation of the shaft of the central gear wheel (item 14) of 60 rpm.

To fix the reactions in the supports of the gear-lever planetary mechanism of the drive of the working bodies of the OVM, the sensor presented in Figure 2 has been developed. The elastic element is made of BROF10-1 bronze, the wall thickness is calculated in such a way that only elastic deformation occurs in it, for which it was carried out preliminary compression calculations. Tensor resistors KF 5P1-3-100-6-16 were used.

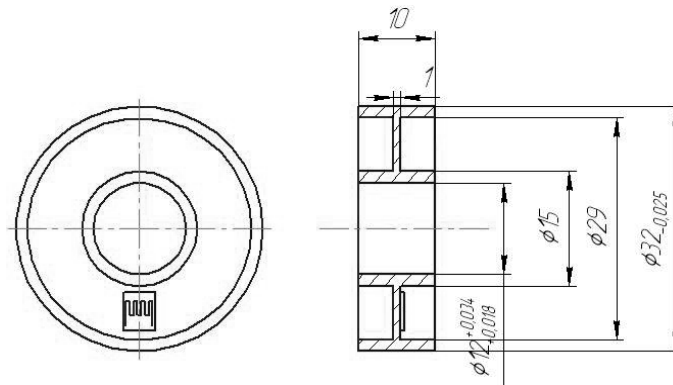


Figure 2. A sensor for determining reactions in resistances

The block diagram of the stand for registering force changes in the supports is presented in Figure 3. The ED electric motor drives the experimental setup. Reactions in the resistances are measured using tensor resistors of the KF 5P1-3-100-6-16 type, which are placed on the vertical plane of the sensor and connected to each other according to the bridge scheme.

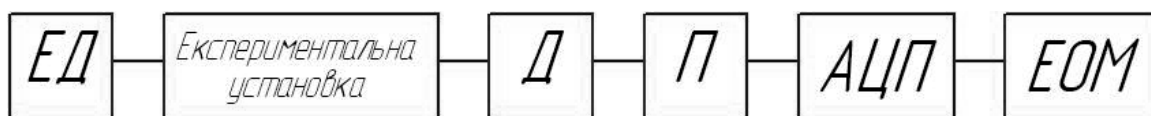


Figure 3. Block diagram of measurement of reactions in resistances

Signals from the D sensor through the LM358N amplifier and the USB-1009 analog-to-digital ADC converter are fed to the computer electronic computer, where they are processed using the LabVIEW software environment.

The graphical shell of the LabVIEW environment shows how the responses in resistances change over time.

When conducting a study of the dynamic characteristics of the gear-lever planetary drive mechanism of the working bodies of the OBM, the sensor was calibrated to determine the reactions in the supports, and the study was carried out using the LabVIEW software environment (Fig. 4).

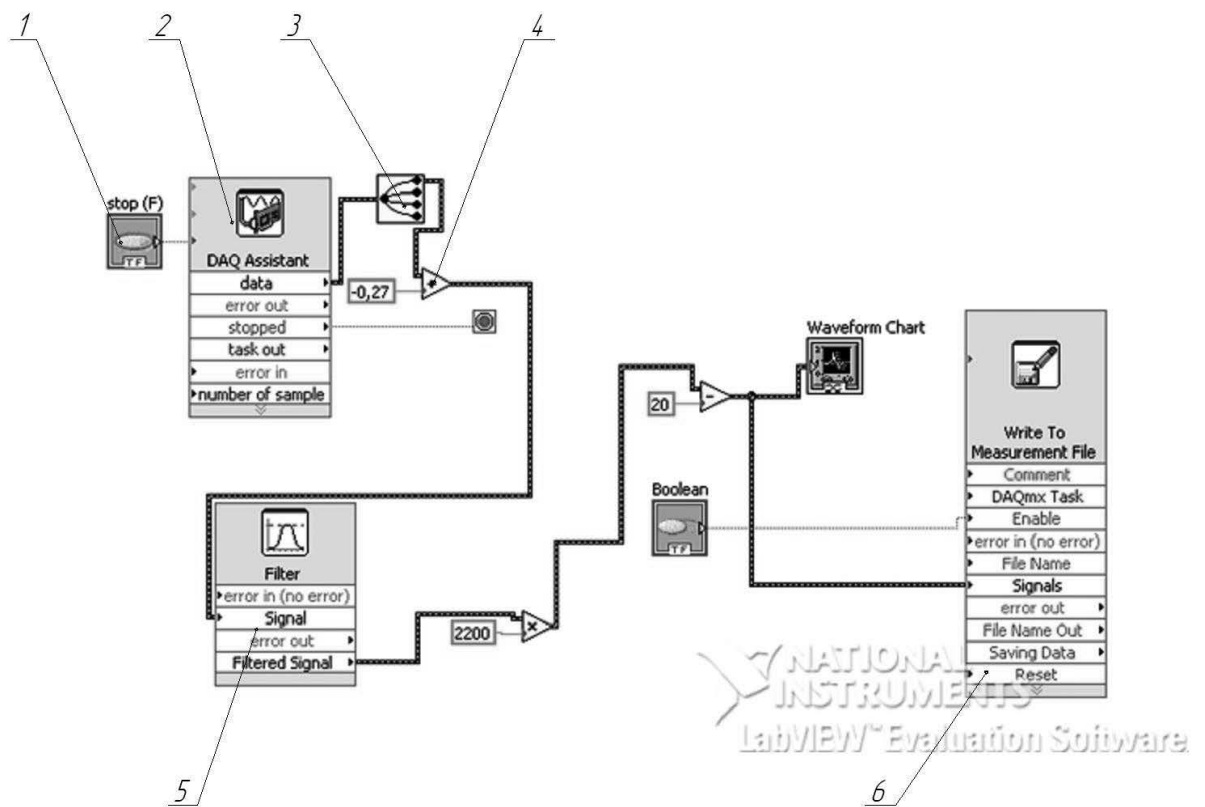
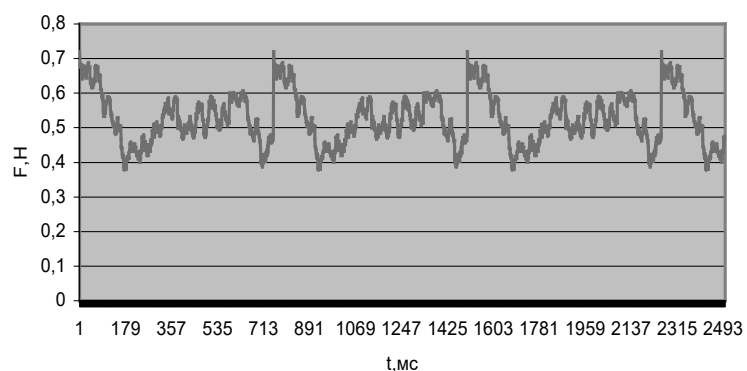


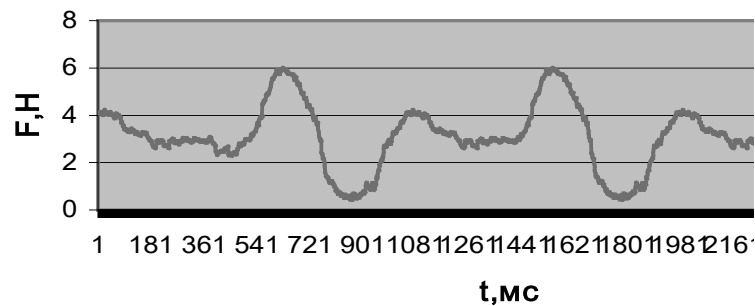
Figure 4. Scheme of the stand in the LabVIEW software environment, 1 – switch; 2 – analog-digital converter; 3- illuminator; 4- taring coefficients; 5 – filter; 6 – block of writing to files

### 3. RESULTS AND DISCUSSIONS

Figure 5 shows the results of experimental studies processed in the LabVIEW software environment.



a



b

Figure 5. Forces acting in the supports at a speed of 60 rpm: a- support I; b - support II

#### 4. CONCLUSIONS

The analysis of the results of the experimental data of the dynamic studies of the single-stage gear-lever planetary mechanism at 60 rpm, with the use of measures to balance the rotating masses proposed in [3] showed that the maximum reaction force in the supports is 5.9 N. In the future, it is necessary to conduct a cycle of experimental studies at working speeds and compare the results with the dynamic characteristics of the working bodies of modern WKM.

#### BIBLIOGRAPHY

1. Karelin V.S. Design of lever and gear-lever mechanisms / V.S. Karelin. – M.: Mechanical engineering, 1986. – 184 p.
2. Smutko S.V. Development of universal gear-important planetary mechanisms for the drive of hinged organs of the basic knitting machines: dissertation... candidate of technical sciences: 05.05.10 / Smutko Svitlana Valeriivna – Khmelnytsky, 2001. – 206 p.
3. Neimak V.S. Balancing of a single-stage gear-lever planetary mechanism / V.S. Neimak, G.B. Paraska. – Bulletin of the Khmelnytskyi National University. – 2004. – №5. – P.60-63.



26th January 2024  
Gliwice, Poland

DEPARTMENT OF ENGINEERING MATERIALS AND BIOMATERIALS  
FACULTY OF MECHANICAL ENGINEERING  
SILESIA UNIVERSITY OF TECHNOLOGY

## INTERNATIONAL STUDENTS SCIENTIFIC CONFERENCE

### Development of a material for 3D printing that ensures self-cooling

S. Nowak<sup>a</sup>, S. Bijański<sup>a</sup>, Ł. Hajduk<sup>b</sup>, P. Zawisza<sup>a</sup>, J. Wojnarowski<sup>a</sup>, M. Mikulski<sup>a</sup>,  
M.M. Szindler<sup>c</sup>, M. Szindler<sup>d</sup>, K. Wrześniowska<sup>e</sup>, J. Popis<sup>c</sup>

<sup>a</sup> Silesian University of Technology, Faculty of Mechanical Engineering

<sup>b</sup> Silesian University of Technology, Faculty of Transport and the Aviation Engineering

<sup>c</sup> Silesian University of Technology, Faculty of Mechanical Engineering, Department of Engineering Materials and Biomaterials

email: magdalena.szindler@polsl.pl

<sup>d</sup> Silesian University of Technology, Faculty of Mechanical Engineering, Scientific and Didactic Laboratory of Nanotechnology and Material Technologies

<sup>e</sup> Silesian University of Technology, Faculty of Mechanical Engineering, Department of Technological Process Automation and Integrated Manufacturing Systems

**Abstract:** The article presents the synthesis of material using sodium carbonate, calcium chloride, and citric acid, leading to controlled micro granule production through chemical reactions. The designed material has the physical properties of reflecting, retaining, or emitting infrared radiation, i.e., thermal radiation. Consequently, such a substance may have cooling properties, with the material coated with this substance may have a lower temperature compared to the surroundings. Microscopic analysis reveals a correlation between mixing time and particle size, where longer mixing periods result in smaller particles. This material can be used to create a suspension, from which elements will be 3D printed. The concept of a material cooling the environment combined with additive manufacturing through 3D printing may bring benefits in the form of rapid production of radiators with complex geometric shapes, whose production using other technologies is high-cost.

**Keywords:** 3D printing, self-cooling material, radiation cooling

## 1. INTRODUCTION

The first air conditioner was invented in 1902 in the workshop of inventor Willis Haviland Carrier. His invention was installed on a larger scale in 1925 in the Rivoli Theater building in Times Square and immediately became an image and commercial success [1]. According to the IEA report - "The Future of Cooling", a significant interest in this technology is expected by 2050, when it accounts for 10% of global electricity consumption, and in developing countries such as India the consumption is much higher [2]. One way to reduce the demand for electricity by lowering the temperature is radiative cooling. This phenomenon involves lowering the temperature of a given body below the temperature of the surrounding air due to intensive heat

radiation to the cooler atmosphere [3,4]. The problem is the energy supplied directly from the sun, which can provide nearly 1kW of energy per  $1\text{m}^2$ , so another aspect to focus on is the maximum level of solar reflection [5,6]. Another challenge is the cost and low efficiency of current methods of creating multilayer materials using the radiation-cooling effect [7]. This article presents the production of a material with specific physical properties, i.e. reflection, retention, or emission of infrared radiation, i.e. thermal radiation. Thanks to this, such a substance will have cooling properties in the environment, with non-toxic ingredients and at low costs [5]. This substance will be used as a suspension in 3D printing technology that reflects or stops emitting infrared light. 3D printing has been developing intensively in the industry in recent years because it enables quick, easy, and economical production of prototypes [8]. Due to low costs, it can also replace small-batch production with other methods, e.g. injection molding associated with high costs and technical difficulties related to making the matrix [9]. Due to the characteristics of the objects presented above, they require a special approach to their design, which prolongs and increases the costs of this process. The development of a material that will cool the surroundings and its use in additive technologies (3D printing) may bring benefits in the form of quick production of heat sinks with complex geometric shapes, the production of which using other technologies is high-cost [10,11]. In times of climate change, any opportunity to save energy and materials is a sought-after feature, and by producing this type of material, it will be possible to use less electricity for cooling [12].

## 2. MATERIALS AND METHODS

The mixture was prepared from 20g sodium carbonate ( $\text{Na}_2\text{CO}_3$ ) dissolved in 200 ml water, and 10g calcium chloride ( $\text{CaCl}_2$ ) dissolved in 100 ml water mixed with 3g citric acid ( $\text{HOC}(\text{CO}_2\text{H})(\text{CH}_2\text{CO}_2\text{H})_2$ ) dissolved in 30 ml water.  $\text{CaCl}_2$ , in contact with  $\text{CO}_2$  from the air, forms calcium carbonate in the form of irregular crystals, the addition of citric acid dissolves the formed crystals and allows calcium chloride to react with sodium carbonate and produce calcium carbonate micro granules in controlled and repeatable conditions. In this way, three mixtures were prepared with different mixing times. The mixtures were prepared using a magnetic stirrer. The first one was stirred for 1 minute, the second one for 5 minutes, and the third one was stirred for 10 minutes. After mixing, the solutions were placed in a laboratory dryer and dried for 2 h at  $100^\circ\text{C}$ . Additionally, after drying, the obtained powders were mixed in a weight ratio of 15/5/1, which means that 75% of the weight were particles obtained from the solution that was stirred for 1 min, 20% of the weight were particles obtained from the solution that was stirred for 5 min, and 5% of the weight were particles obtained from solution which was stirred for 10 min.

This proportion is advantageous due to the density of microspheres because spherical particles occupy most of the space in which they are located. The balls form in similar diameter have a dense configuration, taking up approximately 65-75%. The space between them, which takes in approximately 25-35%, can be filled by microspheres with smaller diameters [13].

All samples were observed with light ZEISS Axio Vert.A1 inverted metallurgical microscope. This microscope is capable of bright and darkfield illumination. Images registered at a magnification of 10, 20 and 50 times. The average particle diameter was determined.

The research was performed using a thermal imaging camera Flir T335. The thermal image resolution of this camera is  $320 \times 240$  pixels. The thermal sensitivity is  $<50$  mK. The range of measured temperature is  $(-20 \div +650)^\circ\text{C}$ . Images were analyzed using the Research IR software.



### 3. RESULTS

Figures 1, 2, and 3 show microscopic images of microspheres  $\text{CaCO}_3$  at 10, 20, and 50 times magnification, respectively. As the mixing time of the  $\text{CaCO}_3$  microspheres increases, nucleation increases, resulting in smaller diameters of the obtained particles. After 1 minute of stirring with a magnetic stirrer, the average particle size is  $8.1 \mu\text{m}$ , after 5 minutes  $6.8 \mu\text{m}$  and after 10 minutes they are the smallest and amount to  $4.3 \mu\text{m}$  (Table 1). Figures 1 (d), 2 (d), and 3 (d) show the mixture  $\text{CaCO}_3$ . The presence of particles of various sizes is visible.

Thermographic images were taken to record the ambient temperature and the temperature of the samples made. Images with a temperature scale were recorded in which cold colors mean a lower temperature and warm colors mean a higher temperature. Selected samples are shown in Figure 4. The point with the highest ambient temperature was  $22.2^\circ\text{C}$ . The average ambient temperature was  $20.7^\circ\text{C}$ . The substrate covered with a paste made of  $\text{CaCO}_3$  particles stirred for 1 minute was characterized by a temperature of  $18.6^\circ\text{C}$ . In turn, with the particles mixed for 10 minutes, it was characterized by a temperature of  $18.8^\circ\text{C}$ . The paste made from a mixture of these particles had the smallest effect and reduced the surface temperature to  $19.4^\circ\text{C}$ .

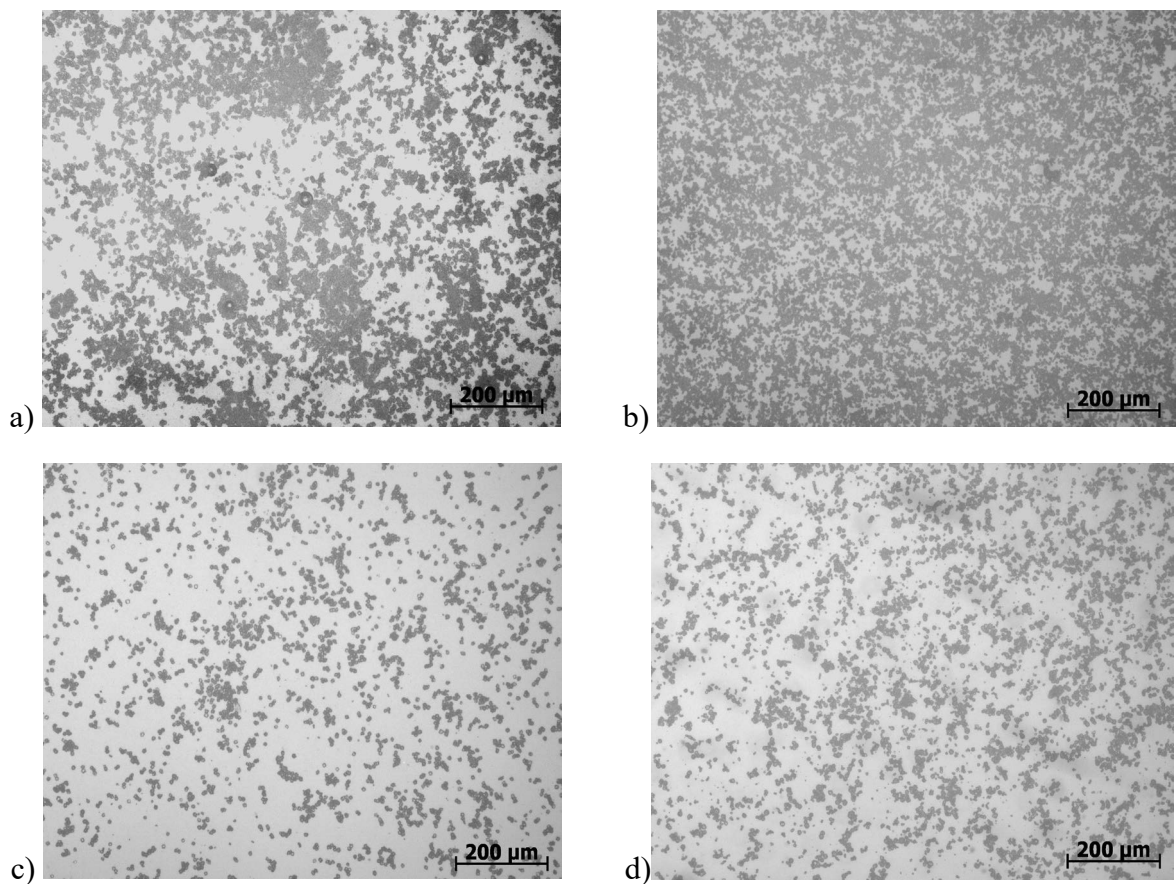


Figure 1. Images of particles formed by mixing for a) 1, b) 5, c) 10 minutes, and d) mixture; mag. 10x

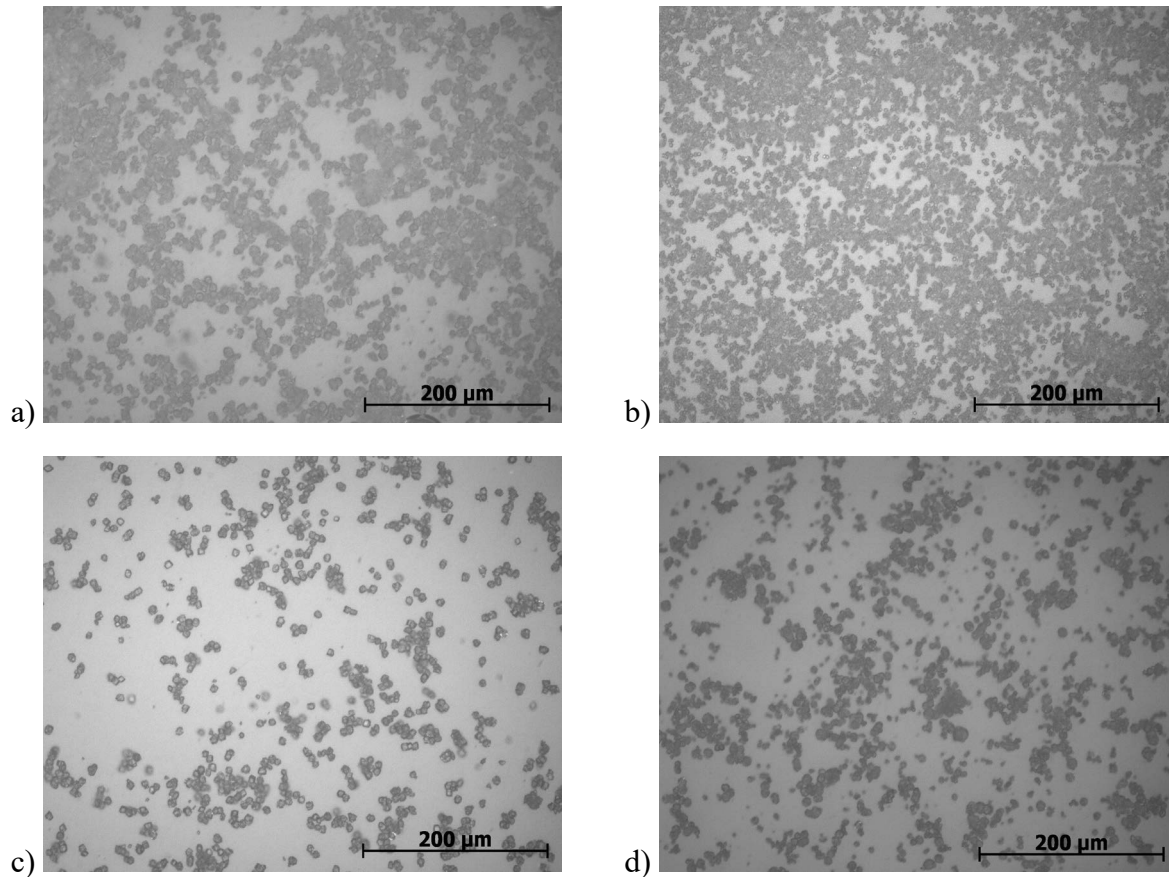


Figure 2. Images of particles formed by mixing for a) 1, b) 5, c) 10 minutes, and d) mixture mag. 20x

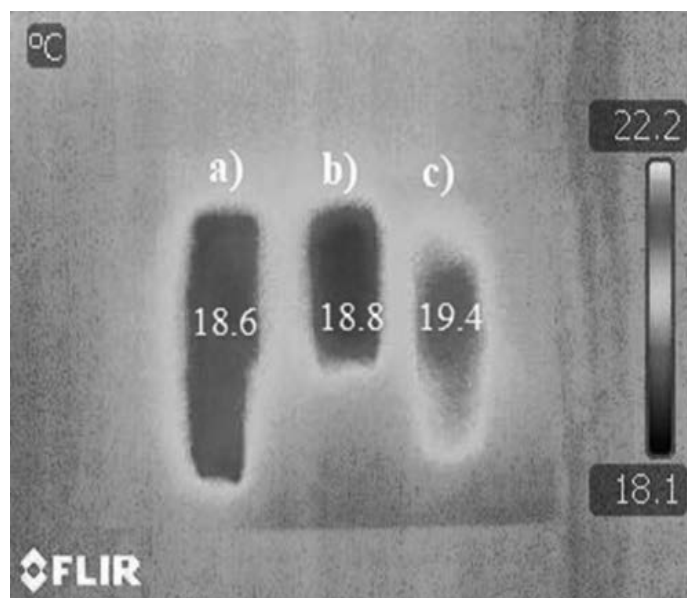


Figure 4. Thermographic image of samples prepared with a mixing time of: a) 1 min; b) 10 min; c) a mixture of a and b samples

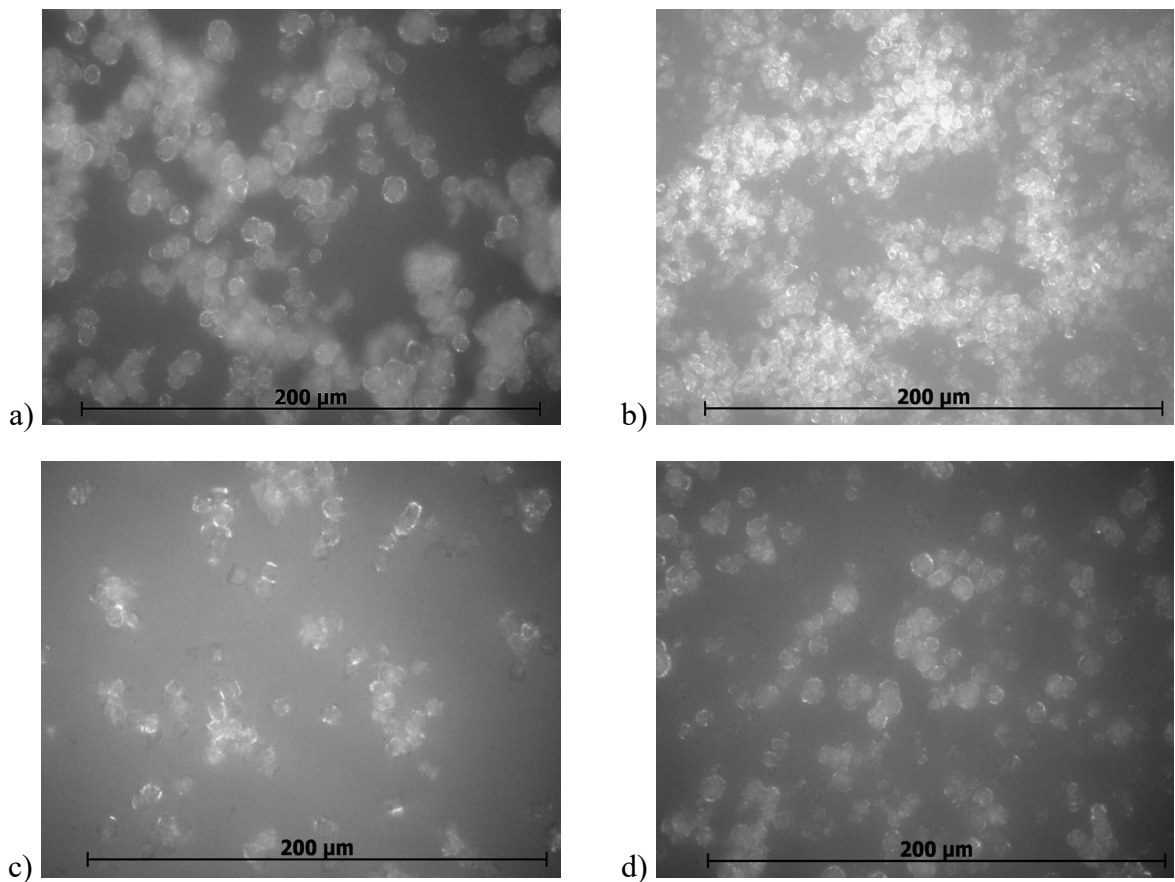


Figure 3. Images of particles formed by mixing for a) 1, b) 5, c) 10 minutes, and d) mixture mag. 50x

Table 1. The average particle sizes are mixed for different amounts of time

Mixing time [min]	Average particle
1	8.1
5	6.8
10	4.3

#### 4. CONCLUSIONS

Microspheres of smaller size can be obtained in a controlled manner by using a longer mixing time. After 1 minute of mixing, the average grain size is 8.1  $\mu\text{m}$ , after 5 minutes 6.8  $\mu\text{m}$ , after 10 minutes 4.3  $\mu\text{m}$ . The best results of thermographic tests were obtained for samples mixed for the shortest time (1 minute). Lowered surface temperature from an average ambient temperature of 22.7 to 18.6°C. This was certainly influenced by the size of the particles obtained, which increased with the shortening of the mixing time.

In a further stage of research, particle size optimization was planned. Then the suspension will be produced from the prepared material, which can be deposited on a surface or used to build three-dimensional elements using a 3D printer. The concept of a material that cools the surroundings combined with additive manufacturing using 3D printing may bring benefits in the form of rapid production of radiators with complex geometric shapes, the production of which using other technologies is high-cost.

## BIBLIOGRAPHY

1. How was air conditioning invented? The invention is over 100 years old (in Polish), online: <https://businessinsider.com.pl/technologie/nauka/historia-wynalazku-klimatyzacji-jak-powstala-kto-ja-wymyslil/8qzfcx4>, 2017.
2. The Future of Cooling, Opportunities for energy-efficient air conditioning, online: <https://www.iea.org/reports/the-future-of-cooling>
3. S. Fan, W. Li, Photonics and thermodynamics concepts in radiative cooling, *Nature Photonics* 16 (2022) 182–190.
4. B. Zhao, M. Hu, X. Ao, N. Chen, G. Pei, Radiative cooling: A review of fundamentals, materials, applications, and prospects, *Applied Energy* 236 (2019) 489-513.
5. X. Li, J. Peoples, Z. Huang, Z. Zhao, J. Qiu, X. Ruan, Full Daytime Sub-ambient Radiative Cooling in Commercial-like Paints with High Figure of Merit, *Cell Reports Physical Science* 1 (2020) <https://doi.org/10.1016/j.xcrp.2020.100221>.
6. D. Zhao, A. Aili, Y. Zhai, J. Lu, D. Kidd, G. Tan, X. Yin, R. Yang, Subambient Cooling of Water: Toward Real-World Applications of Daytime Radiative Cooling, *Joule* 3, 111–123 (2018), <https://doi.org/10.1016/j.joule.2018.10.006>.
7. Md. M. Hossain, M. Gu, Radiative Cooling: Principles, Progress, and Potentials, *Advanced Science* 3 (2016) <https://doi.org/10.1002/advs.201500360>.
8. V. Carlota, Soliquid is the startup doing large-scale 3D printing in suspension, <https://www.3dnatives.com/en/soliquid-3d-printing-suspension-090720194/>.
9. M. Zastrov, 3D printing gets bigger, faster and stronger, Research advances are changing the image of a once-niche technology. *nature* (2020) <https://www.nature.com/articles/d41586-020-00271-6>.
10. I. Karakurt, L. Lin, 3D printing technologies: techniques, materials, and post-processing, *Current Opinion in Chemical Engineering* 28 (2020) 134-143.
11. M. Korpela, N. Riikonen, H. Piili, A. Salminen, O. Nyrhilä, Additive Manufacturing—Past, Present, and the Future, *Technical, Economic and Societal Effects of Manufacturing 4.0* (2020) 17–41.
12. K. J. Miparanum, B. Albar, A. J. III Abando, Effects of functional fillers in the mechanical properties of 3D-printed polylactic acid using fused deposition modelling, *ScienceOpen Preprints*, DOI:10.14293/S2199-1006.1.SOR-.PPJZTVP.v1, 2022.
13. E. Skrzypczak, Z. Szepliński: Introduction to the physics of the atomic nucleus and elementary particles (in Polish), WN PWN, 2012.



26th January 2024  
Gliwice, Poland

DEPARTMENT OF ENGINEERING MATERIALS AND BIOMATERIALS  
FACULTY OF MECHANICAL ENGINEERING  
SILESIA UNIVERSITY OF TECHNOLOGY

## INTERNATIONAL STUDENTS SCIENTIFIC CONFERENCE

### **Computer programs supporting the design and modeling of injection molding technology**

J. Nowak<sup>a</sup>, A.J. Nowak<sup>b</sup>

<sup>a</sup>Graduate, Silesian University of Technology, Faculty of Mechanical Engineering Technology;  
<sup>b</sup> Silesian University of Technology, Faculty of Mechanical Engineering Technology, Scientific and Didactic Laboratory of Nanotechnology and Materials Technology, Faculty of Mechanical Engineering Technology, Silesian University of Technology, e-mail: [agnieszka.j.nowak@polsl.pl](mailto:agnieszka.j.nowak@polsl.pl)

**Abstract:** This work discusses selected simulation techniques for processing polymer materials and the possibilities of computer-aided design based on the most popular computer programs. The possibilities of computer programs dedicated to injection technology and those supporting design were discussed. Advantages and disadvantages were indicated.

**Keywords:** computer aided manufacturing, injection molding simulations, SolidWorks, Moldex3D

### **1. INTRODUCTION**

Nowadays, the world, thanks to the development of technology, is moving towards computerization and automation of almost every aspect of human life. It is closely related to the development of civilization. This is also the case in the process of satisfying consumer needs. The work of designers, constructors, technologists, and engineers is supported by specialized programs that allow for easier and faster design of a given detail and influence its efficient modification and optimization until a finished or semi-finished product is obtained. Plastics are widely used in almost every industry, e.g., medicine, electronics, electrical engineering, automotive, apparatus and machine parts, packaging, cosmetics, construction, etc. One of the most frequently used methods for serial and mass production of repeatable elements from polymer materials is injection molding. The most complicated aspect of this technology is injection molds. They are characterized by a complex shape, precision of workmanship, mechanical and physical properties, and must also meet the user's expectations related to reliability and functionality. Therefore, a detailed analysis of the plastics processing conditions related to the injection process is fundamental when designing them. With the development of injection molding technology and constantly growing customer expectations regarding the quality of manufactured elements, computer simulations in the initial stages of injection mold

design are now beneficial and popular. Through virtual simulations, it is possible to analyze the cavity filling, pressing, and cooling phases and observe the degree of mold deformation at individual stages. Injection molding is a popular method used in the multi-series production of details from thermoplastic polymer materials. That is why many companies commonly use software to simulate this process, such as Moldex3D. Moldex 3D is a CAE (Computer Aided Engineering) system created by the Taiwanese company CoreTech System. It is used for digital analysis of the injection process of thermoplastic and thermosetting plastics, which is very useful when designing both injection molds and molded parts. Thanks to it, you can determine the most critical parameters of the process, predict problems that may occur (making it easier to eliminate them already at the stage of designing the injection mold or detail), plan its correct course, and prevent defects in the finished product. It's related to a limit on the number of prototypes and samples produced by injection mold designers. They also allow for predicting the deformation of the molded part during cooling in the injection mold and after its removal. Moldex3D has modules where you can design additional cooling of the molding or pressure [1-8]

## **2. SIMULATION TECHNIQUES IN INJECTION MOLDING**

Plastic injection simulation programs are used nowadays in many companies. They support the work of mold designers, mold constructors, engineers, and technologists. Currently, some of the most popular programs in this field are Moldex3D, Cadmould, Ansys, and Moldflow Plastics Advisers. The advantages of these simulators are enormous. The programs are so refined that they allow you to predict problems that may occur during the injection process and facilitate their elimination already at the design stage of the injection mold or the detail itself. They help calculate important parameters needed when designing a mold, such as the cavity-filling and pressing and cooling phases. They allow you to reduce the number of physical prototypes produced and shorten the time of all stages of work from the beginning of design until obtaining the finished product. This is possible thanks to a large number of parameters that can be changed many times until satisfactory results are obtained. They prevent air traps from forming in the mold during injection molding. Thanks to extensive material databases with plastic injection simulation programs, as well as the ability to define and add your material to the database, it is possible to verify the material in simulation conditions - assessment of the finished molding with given injection parameters, as well as assessment of the cooling system or the location of injection channels. These simulators also help analyze the deformation of the molded part during its cooling in the injection mold and after its removal. All these advantages save material, time, and money [9-15].

There are already many plastic injection simulation programs on the market, and these are, for example, Moldex3D, Cadmould, Moldflow, ANSYS Polyflow, SIMPOE, TMConcept, PLANETS MoldStudio3D, REM3D. A brief description of several of them is presented below [11]. Moldex 3D is a CAE (Computer Aided Engineering) system created by the Taiwanese company CoreTech System. It is used for digital analysis of the injection process of thermoplastic and thermosetting plastics, which is very useful when designing both injection

molds and molded parts. Thanks to its functionality and innovation, it is used in many industrial sectors in which polymeric materials are used. Moldex3D is a paid program available in five different packages: eDesign Basic, Professional Basic, eDesign, Professional, Advanced, and IC Packaging, selected by customers depending on the advancement of their projects. Each module allows errors to be avoided when designing injection molds and moldings and optimizing the injection process. Moldex3D is highly intuitive and has a clear interface. The work begins by creating a new project and then importing its geometry previously created in CAD software e.g., SolidWorks, AutoCAD, CATIA, Fusion 360, etc. The program is based on STEP files, a universal, standard data exchange system between CAD, CAM, and CAE programs. This extension is not tied to any specific system. The program is characterized by a modular structure, where each module analyzes a different aspect of filling the mold cavity. Most modules can come in Shell or Solid (calculations of thin-walled or thick-walled elements). This program is systematically improved and expanded with new modules. Moldex3D allows you to create your mesh for the analyzed detail and also allows you to import a FEM mesh from other popular computing systems, e.g., Ansys, Femap, and Nastran. The order of performing the steps for different types of simulations and calculations is similar because the program does not allow you to proceed to the next stage of work if you have not completed all the previous necessary steps. Thanks to the cooperation of the creators of this software, from companies producing injection molding, granulates, a very well-developed material database distinguishes Moldex3D (Fig. 1).

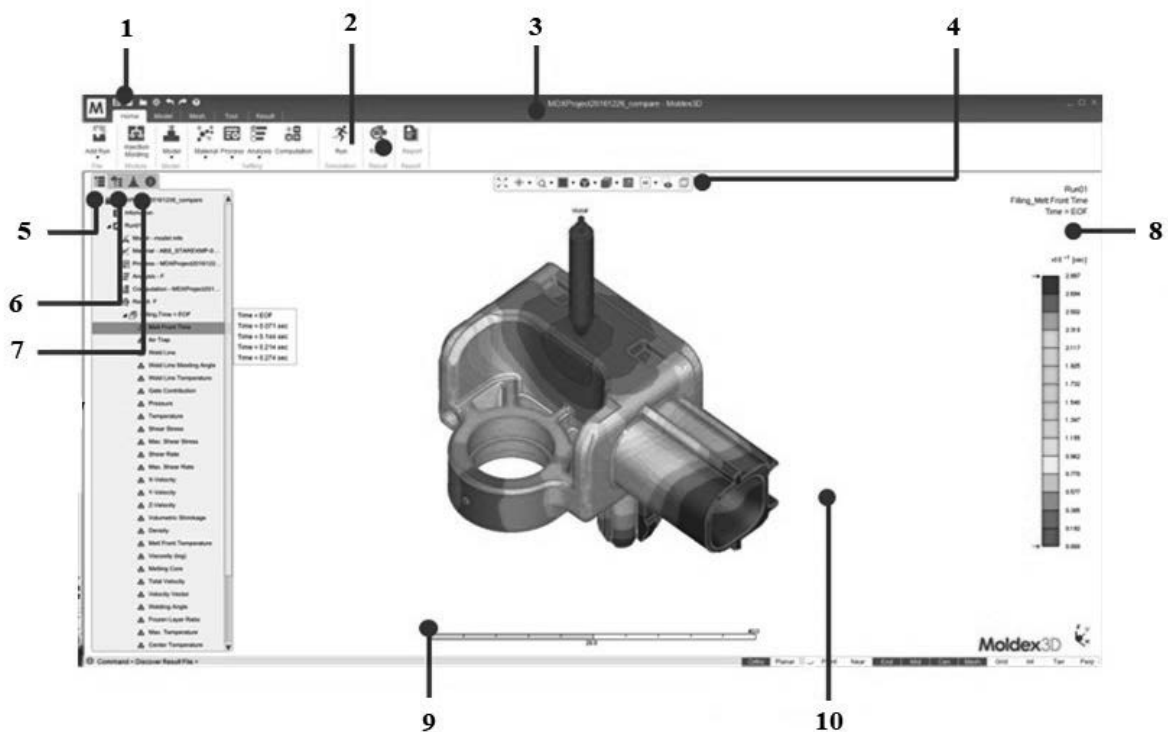


Figure 1. View of the Moldex3D program window with a description of some elements: 1-quick access bar; 2-menu ribbon; 3-project name; 4-view inspection tools;5-project tree; 6-tree models; 7-defect/error tree; 8-legend; 9-graphic scale; 10-graphic window [14]

Additionally, it is possible to individually define the properties of your material. The program has very high calculation accuracy and enables precise simulation of processes in

three dimensions, i.e., conditions close to reality, thanks to the Finite Volume Method (FVM). It also allows you to perform calculations and simulate all processes while filling the injection mold cavity. Moldex3D software supports a variety of molding and simulation techniques, such as Co-Injection Molding (CoIM), Bi-Injection Molding (BiIM), Gas/Water Assisted Injection Molding (GAIM/WAIM), Powder Injection Molding (PIM), Foam Injection Molding (FIM), chemical foam molding (CFM), compression molding (CM), and injection compression molding (ICM). It also allows you to adapt the process conditions to the conditions occurring when working on a real injection molding machine, and this is possible because the program database contains data from almost a thousand different devices of this type. In addition to parameters such as cycle time, temperature, and pressure, it is also possible to determine the deformation and shrinkage of the molded part and analyze the cooling process. The results of simulations and analyses are obtained in the form of animations, drawings, cross-sections, charts, or color scales on a 3D model [10-14].

### **3. COMPUTER-AIDED INJECTION MOLDING TECHNOLOGY**

The dynamic development of civilization contributed to the progress of computer technology. These devices have become everyday objects and are now used in almost every sphere of life. Modern computers can process a lot of information and perform many complex calculations in a short time. Thanks to this, many commercial and free programs have been created to facilitate the work of designers, constructors, engineers, and technologists. This led to the development of computer-aided manufacturing (CIM) (Computer Integrated Manufacturing), which is now an indispensable part of the industry. It includes computer technologies commonly known as CAx. These programs support all phases of the entire product lifecycle. They support meeting consumer needs, from design through analysis, optimization, and production planning to receiving the finished product. The advantage of using them is that they shorten the time from diagnosing the need to receiving the finished product and reduce design and manufacturing costs by reducing the number of prototypes and material losses. The family of CAx programs is constantly growing, but the most famous ones include [16-20]:

CAD (Computer Aided Design) it is one of the essential tools of every designer nowadays. This group includes all programs responsible for creating 2D drawings, 3D models and technical documentation, e.g., technical drawings based on designed three-dimensional models, also allow you to describe product parameters and perform various calculations. CAD systems are used for design e.g., parts of devices and machines, integrated circuits and electrical installations, and buildings. The most famous CAD programs are AutoCAD, SolidWorks, Autodesk Inventor, CATIA, and SolidEdge;

CAM (Computer Aided Manufacturing) - all systems designed to combine the design and manufacturing phases. They support the planning of production processes and the control of tool operation and material flow. CAM programs are also used to generate machine code for machining machines (e.g., lasers, milling machines, lathes, etc.) based on a model created in CAD programs in order to create a finished product from a semi-finished product. They also enable the creation of simulations of a given process, making it possible to check its correctness and select appropriate parameters. The family of CAM programs includes CAMWorks, AlphaCAM, SolidCAM;



CAE (Computer Aided Engineering) computer-aided engineering work - this group includes all programs supporting the engineer's work in design, construction, and engineering analyses, i.e., in the first phases of product development. They enable mechanical, thermal, and electromagnetic calculations to be performed. This means that thanks to CAE systems, it is possible to determine a product's technical and physical characteristics. They also enable computer simulation of fluid and gas flow, simulation of forming and casting processes, product and process optimization, and understanding the behavior of the finished product in real conditions. Examples of CAE programs include Creo (Pro/ENGINEER), KOMPAS 3D, DC-SOFTWARE, FEMAP;

CAQ (Computer Aided Quality Assurance) - as the name suggests, these are systems responsible for ensuring product quality throughout its life cycle. This group includes all programs supporting the planning of product quality standards, quality control, the completion of process data collection, and the implementation of measurement and quality control procedures. They also enable data analysis, supply control, supplier assessment, complaint management, documentation of inspection results, creation of reports on production processes, and process automation. The advantages of using CAQ systems are high quality of products, time savings, cost reduction, fast and efficient flow of information, reduction of the number of shortages and defects of finished products, collection of all data in one central database, real-time control over the process, significant improvement and continuous process improvement. Sample program: QDA;

CAP (Computer Aided Planning) - computer-aided planning - these are all programs and systems used in enterprise management. They support preparing work plans, assembly, inspection, and programming of measuring machines, machine tools, and robots. It contributes to better integration of people's activities and means of production. CAP systems provide data not only for production planning, but also for planning standard costs.

This is how all computer programs belonging to the group of supporting manufacturing (CIM) complement each other during the entire production process (Fig. 2).

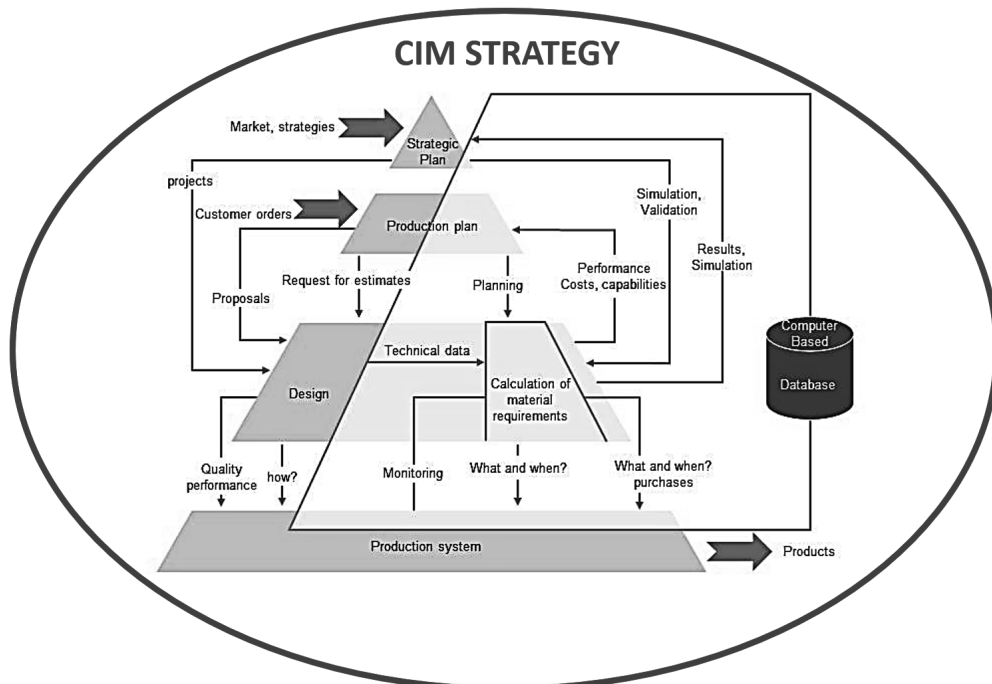


Figure 2. Model of the functioning structure of the CIM system [16]

This model allows for a thorough analysis of all functions of an industrial enterprise, taking into account both economic and technical tasks. This model takes into account two basic systems of an industrial enterprise [15]:

- logistics system - basic economic functions of production planning and control;
- technical system- basic technical functions focused on the product.

#### 4. EXAMPLES OF COMPUTER PROGRAMS SUPPORTING DESIGN

SolidWorks is a computer-aided design program developed by Jon Hirschtick and a group of engineers in 1993 the United States. The software's first version, SolidWorks 95, was released on November 11, 1995. The program gained many supporters among engineers in a very short time thanks to its ease of use. SolidWorks Corporation was bought out in 1997 for \$310 million by the giant French company Dassault Systèmes, which it still owns today. Since the development of SolidWorks 95,

The SOLIDWORKS program is available in commercial packages, i.e., SOLIDWORKS Standard, SOLIDWORKS Professional, SOLIDWORKS Premium, as well as in educational versions: SOLIDWORKS Education Edition, SOLIDWORKS Student Edition, SOLIDWORKS Student Access, SOLIDWORKS Student Trial, SOLIDWORKS for Startups, SOLIDWORKS Research. It runs on the Microsoft Windows operating system. SolidWorks is a program that allows for parametric modeling, meaning that the dimensions of a given detail can have mutual relationships and be changed at any time during design. The dimensions of the solid and the dimensions of all related documentation will change automatically. Based on the 3D model of solid parts, it is possible to create assemblies of up to several thousand elements, their technical drawings, motion and load simulations, and animations. And many analyses, e.g., static, thermal, nonlinear, fatigue, etc. The possibilities of the SolidWorks program depend on the purchased version. The software also allows for carrying out Finite Element Method FEM (FEM) analyses. It is an advanced method of solving complex systems of differential equations, which is based on the division of the domain, i.e., the object under study, into many simpler pieces (finite elements). It is also possible to perform CFD (Computational Fluid Dynamics) analysis. Computational fluid dynamics allows us to solve problems related to fluid flows. The SolidWorks program has rich material databases and libraries of ready-made elements. This software uses its special file formats for saving parts (.SLDPRT), assemblies (.SLDASM), and drawings (.SLDDRW). Additionally, it integrates very well with CAM programs. Its disadvantage is very high hardware requirements. On the market, it competes with programs such as Autodesk Inventor and Solid Edge [23, 24].

Nowadays, computer-aided design CAD systems are indispensable elements of the work of designers, constructors, technologists, and engineers. Their variety is huge. Initially, the abbreviation CAD came from the term Computer Aided Drafting. Initially, the effectiveness of these programs could have been higher. This was because computers did not offer the same possibilities as they do today, and CAD programs were still in use in the initial development phase. As computer hardware improved and offered more and more opportunities, CAD software was enhanced. Programs began to become more and more intuitive and had more functions. From the beginning, the precursor of CAD engineering software was the American company Autodesk, which created the AutoCAD software. Over the years, they have set higher and higher standards in this field, thanks to which they have won many prestigious awards and titles [8, 12].

Currently, the abbreviation CAD comes from the first letters of the English expression Computer-Aided Design. These programs allow you to create two-dimensional (2D) drawings or three-dimensional (3D) models of a given element. The designed three-dimensional models can be solid or surface. A solid model comprises solids to which we can provide physical parameters. The surface model consists of properly created surfaces that can be further shaped. CAD systems allow you to create complex assemblies by connecting simpler elements using bonds. Thanks to them, the elements are arranged and related to each other appropriately and specifically. Additionally, adding specific material from the program's material database to each designed element is possible. In addition to an extensive material library, they often also have extensive libraries of typical components. Thanks to special modules, CAD programs allow you to perform calculations and simulations. In addition, it is also possible to create technical documentation based on modeled two-dimensional or three-dimensional details that are created by projecting them on a plane model. Many programs are also equipped with visualization and animation tools to present the model to potential recipients. This makes it watchable from all sides and checks how it behaves in motion [16, 19].

## **5. SUMMARY**

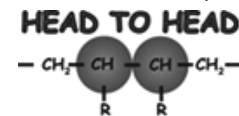
The advantages include a very intuitive interface already in almost every CAD program. This makes work easier and shortens the time needed to create a finished object. The main advantage of design-aided programs is the huge number of tools they offer, which makes it possible to create very complex ones and impressive projects. This software has several functions that enable the creation of complex details. An additional advantage is that they are expanded even more each year. Another advantage of these programs is the possibility of parametric design, which means that the parts of complex designs will adapt to each other after any changes, and the drawings will be updated. This increases the speed and efficiency of work. Most CAD programs have options that allow you to perform many different simulations and analyses of the finished details. The designed 3D model can be subjected to, for example, static analysis using the Finite Element Method, thermal analysis, non-linear analysis, fatigue analysis, etc. Thanks to them, we obtained a lot of helpful information, such as what stresses and deformations are caused by the load a given element will carry during operation. This analysis eliminates the risk of part damage in natural conditions. This allows you to eliminate defects in the final, finished product, predict how it will behave in natural conditions, shorten the design time, and reduce the number of prototypes produced. This minimizes the risk of mistakes or collisions and errors at the design stage. All these advantages also involve lower costs for the company, which is a huge additional advantage. CAD programs are also equipped with rich material databases available to all program users. Depending on the purchased software version, they often have extensive detailed databases and generators of typical parts. Thanks to this function, standard machine parts are placed in the project very quickly. Another advantage of programming aids is the ability to create complete technological documentation for each project. Production is based on it. Automatic insertion of views, dimensions, generation of sections, and details shortens the total project execution time. The essential thing is that the technical documentation is automatically updated when project changes occur. The advantages of design-aided programs undoubtedly include compatibility with other software, e.g., CAM [16-20].

The main disadvantage of design-aided programs is that purchasing their licenses is expensive. Buying it for a year is more advantageous than, for example, a month. The programs

also take up a lot of disk space and have high hardware requirements, so their efficient functioning requires a good and modern computer with high computing power [18-20].

*General thoughts:*

*This study was created thanks to the work carried out by members of the Student Scientific Club of Plastics and Composites Processing "HEAD TO HEAD" operating at the Scientific and Didactic Laboratory of Nanotechnology and Material Technologies at the Faculty of Mechanical Engineering.*



## BIBLIOGRAPHY

1. Blicharski M., Materials Engineering, ed. Scientific and Technical, Warsaw, 2012.
2. Broniewski T., Test methods and assessment of the properties of plastics, ed. Scientific and Technical, Warsaw, 2000.
3. Collective work edited by Wilczyński K., Plastics Processing, Publishing House of the Warsaw University of Technology, Warsaw, 2000.
4. Broniewski T., Kapko J., Płaczek W., Thomalla J., Methods and assessment of properties of plastics, ed. Scientific and Technical, Warsaw, 2000.
5. Guin I., Polymer Materials, ed. PWN, Warsaw, 2003.
6. <https://pubchem.ncbi.nlm.nih.gov/> [access 16.03.2023]
7. Collective work edited by Wilczyński K., Computer-aided design in plastics processing, Publishing House of the Warsaw University of Technology, Warsaw, 2014.
8. Maw-Ling W., Rong-Yeu Ch., Chia-Hsiang H., Molding simulation. Theory and Practice, Haser Publishers, Munich 2018.
9. [www.moldex3d.com.pl](http://www.moldex3d.com.pl) [access 10.01.2024]
10. <https://www.simcon.com/en/> [access 11.01.2024]
11. Bis J., Markiewicz R., Computer-aided CAD design. BASICS, ed. REA, Warsaw, 2009.
12. Werner Dankwort, C., Weidlich, Roland, Guenther, Birgit; Blaurock, Joerg E., Engineers' CAX education—it's not only CAD", Computer-Aided Design. 2004, 36 (14), : 1439–1450.
13. Nowakowski P., Selected computer techniques in design and manufacturing, Silesian University of Technology Publishers, Gliwice, 2006.
14. Sobańska, Cost accounting and management accounting, C.H. Publishing House Beck, Warsaw, 2003.
15. <https://eia.pg.edu.pl/documents/1189298/9869265/wyklad%201-2%20-%20Techniki%20CAx.pdf> [access 07.01.2024]
16. <https://www.slideteam.net/computer-integrated-manufacturing-cim-strategy-ppt-powerpoint-presentation-summary.html> [access 08.01.2024]
17. <https://www.solidworks.pl/> [dostęp 07.01.2024]
18. <https://www.autodesk.pl> [access 09.01.2024]
19. Jaskulski, AutoCAD 2018/LT2018/360+, Wydawnictwo Naukowe PWN, Warszawa, 2017.
20. <http://dsxcad.com/autodesk-autocad-zalety-i-wady-programu/> [access 09.01.2020]



26th January 2024  
Gliwice, Poland

DEPARTMENT OF ENGINEERING MATERIALS AND BIOMATERIALS  
FACULTY OF MECHANICAL ENGINEERING  
SILESIA UNIVERSITY OF TECHNOLOGY

## INTERNATIONAL STUDENTS SCIENTIFIC CONFERENCE

### Impact of laser surface modification in chosen fields

M. Paluch<sup>a</sup>, D. Gajczowska<sup>a</sup>, P. Cisowski<sup>a</sup>, M. Bonek<sup>b</sup>, E. Tillova<sup>c</sup>, U. Ozdemir<sup>d</sup>,  
O. Polishchuk<sup>e</sup>, B. Gitolendia<sup>f</sup>

<sup>a</sup> Student of Silesian University of Technology, Faculty of Mechanical Engineering, Department of Engineering Materials and Biomaterials, Gliwice, Poland

<sup>b</sup> Silesian University of Technology, Faculty of Mechanical Engineering, Department of Engineering Materials and Biomaterials, Gliwice, Poland

<sup>c</sup> University of Zilina, Faculty of Mechanical Engineering, Department of Materials Engineering, Slovak Republic

<sup>d</sup> Gazi University, Faculty of Technology, Metallurgical and Materials Engineering Department, Ankara, Turkey

<sup>f</sup> Georgian Technical University, Faculty of Transport Systems and Mechanical Engineering, Tbilisi, Georgia

**Abstract:** The article describes the various methods that laser surface modification has impacted or changed the chosen industry fields, focusing on additive manufacturing, polymers and computer-assisted manufacturing.

**Keywords:** metallurgy, laser surface treatment, polymers, biomaterials

### 1. LASER STEEL PROCESSING AND METALLURGICAL EXPERTISE

In today's dynamic industrial environment, research on the application of high-power lasers in steel processing constitutes an area of intense exploration that shapes the future of modern technologies. This field of investigation not only poses challenges for scientists in refining laser processes but also necessitates interdisciplinary collaboration, especially in the realm of metallurgical expertise. In the context of this dynamic research domain, the role of material structure analysis, mechanical properties, thermal effects, weld quality assessment, and connections, as well as laser surface processing and cutting of steel using high-power lasers, becomes pivotal.

Material Structure Analysis, a fundamental aspect of metallurgical expertise, is exceptionally crucial in the context of the structural evolution of metallic materials under the influence of intense heating and cooling generated by high-power lasers. Recent studies have observed that laser steel processing not only impacts microstructure but also macrostructure, emphasizing the need for a comprehensive understanding of these changes for effective design of industrial processes [1, 2].

### **1.1. Contemporary Challenges and Innovations in the Industrial of Lasers and Metallurgy**

The mechanical properties of materials in the context of high-power lasers become immensely significant, as the precise determination of the strength, hardness, and plasticity of steel directly influences the efficiency of machining processes. The application of metallography and mechanical properties testing allows for a more comprehensive understanding of the material's response to the laser beam, which is crucial for process optimization.

Thermal and Microstructural Effects generated during laser processes are an area where metallurgical expertise significantly impacts technological advancements. Localized microstructural changes, induced by intense thermal effects, require in-depth analysis to better comprehend the influence of laser processes on the durability and strength of steel under various thermal conditions.

Quality Assessment of Welds and Connections is another area where the synergy between metallurgical experts and researchers in high-power lasers brings substantial benefits. The development of modern welding techniques and the analysis of weld microstructure enable effective defect identification, thereby improving the quality of metallic connections.

Laser Surface Processing, encompassing techniques such as laser hardening or coating, is an area where metallurgical expertise plays a crucial role. Analyzing the microstructure post laser processing allows for the precise adjustment of processes, directly impacting the surface properties of steel, including hardness and wear resistance.

In the context of Laser Cutting of Steel, precision and cutting quality become even more complex challenges, where the analysis of the microstructure of cut edges is an integral part of metallurgical expertise. Optimizing the process to achieve desired effects requires profound knowledge in both laser technology and metallurgy. [3-6]

### **1.2. Sustainable Development in the Context of Laser Steel Processing: Ecological Perspective and the Role of Metallurgical Expertise**

The development of new steel processing technologies also necessitates a consideration of ecological aspects and sustainable development. Laser processes, while undeniably effective, must also be analyzed in terms of their impact on the natural environment. Here, once again, metallurgical expertise can play a crucial role in assessing the impact of processes on the longevity and resilience of steel over an extended time frame.

Collaboration between metallurgical experts and researchers in high-power lasers in the industry is a dynamic dialogue, where knowledge exchange is the key to revolutionary progress in the field of modern steel processing technologies. The integration of knowledge from both areas allows for a comprehensive understanding of the impact of lasers on the structure and properties of steel, simultaneously opening the doors to innovative solutions in the metallurgical industry, considering both process efficiency and their alignment with the principles of sustainable development [7].

## **2. SYNERGY BETWEEN ADDITIVE MANUFACTURING AND LASER STEEL PROCESSING**

In the face of contemporary challenges in materials engineering, the synergy between additive manufacturing and laser steel processing shapes the landscape of modern innovations.

This fusion of two research areas opens new possibilities for the industry, not only in terms of production efficiency but also concerning sustainable development and comprehensive improvement of engineering processes [8].

### **2.1. Analysis of Material Structure, Mechanical Properties and Thermal Effects in Additive Manufacturing and Laser Steel Processing Technologies**

Analysis of Material Structure and Mechanical Properties becomes a fundamental common point for both technologies. Understanding the microstructure of materials and their mechanical properties is a key element in effective materials engineering. In the case of additive manufacturing technologies, such as 3D metal printing, and laser steel processing, in-depth analysis of structure and mechanical properties forms the basis for precise process design.

Thermal and Microstructural Effects generated during processes in both technologies constitute a shared area of research. Thermal and microstructural changes resulting from both additive processes and laser steel processing require comprehensive analysis. Understanding microscopic transformations in the material structure during intense thermal processes is essential for achieving optimal results in the production of components and constructions [3-4, 9-10].

Quality Assessment of Prints and Connections, a common element in both fields, emphasizes the need for precise identification of defects and forecasting their impact on material strength. Whether in the case of layers applied in additive technologies or in the process of joining steel using lasers, the analysis of component quality becomes a key element in refining materials engineering processes.

Collaboration between Researchers in Additive Technologies and High-Power Laser Specialists is a modern exchange of knowledge leading to revolutionary advancements. The integration of knowledge from both areas enables a comprehensive understanding of the impact of lasers on the structure and properties of materials in the context of additive technologies and vice versa. This synergy allows for achieving the highest process efficiency while simultaneously considering the principles of sustainable development [8-10].

### **2.2. Synergy of Additive Manufacturing and Laser Steel Processing in Modern Materials Engineering**

As a result, the fusion of additive manufacturing and laser steel processing transcends the boundaries of traditional approaches, ushering in a new era of materials engineering. This collaborative approach not only brings innovative solutions but also shifts production paradigms, emphasizing precision, durability, and sustainable development. In this symbiosis, both fields mutually reinforce each other, paving the way for a prospective revolution in the realm of materials science.

An additional layer to this reflection is the advancement of new materials with exceptional properties applicable in both technologies. Innovative metallic alloys and composites, tailored to the specifics of additive processes and laser processing, introduce a new dimension to materials engineering. Their versatile application in the production of advanced aerospace, medical, or industrial components underscores the dynamic evolution of the field and its transformative potential.

Furthermore, the ecological aspect gains prominence in the context of both technologies. Implementing energy-efficient processes and materials in line with sustainable development principles becomes imperative for contemporary materials engineering. In this context,

the pursuit of waste minimization, efficient resource utilization, and emission reduction emerges as a crucial imperative [4, 10].

### **3. LASER INTERACTION WITH POLYMERS**

Understanding the dynamics between the interaction of lasers and polymers, as well as the physical and chemical changes taking place between the medium and the material lie at the heart of advanced manufacturing processes. Depending on various parameters, - the laser type, the parameters of the laser beam and the type of the polymer material chosen - the absorption of the thermal energy supplied by the laser can lead to melting, ablation and even decomposition of the surface. This comprehension serves as the foundation for precise adjustments, optimizing outcomes in various applications. The wavelength, power, and duration of the laser pulses are critical parameters that influence the interaction dynamics, making it imperative to tailor laser processing techniques to specific polymer materials [11-13].

#### **3.1. Laser Cutting and Engraving**

Laser cutting and engraving have revolutionized precision manufacturing across industries, especially in the fabrication of electronic components and complex packaging materials. CO2 lasers, due to their efficient energy absorption characteristics, are the most common choice

in these applications. In laser cutting, the focused beam cleanly slices through the polymer material, offering detailed and precise shapes with minimal thermal damage to the surface and the underlying layers of the polymer material. This non-contact method eliminates the need for physical tools, reducing wear and tear and enabling the creation of complex designs with higher precision than other methods.

In applications where high degree of precision is required, such as in the electronics industry, laser cutting has become indispensable, as the components are complex in both their shapes and sizes. Additionally, due to the minimal thermal impact, the quality of the finished product will be greater, with less imperfections and toolmarks. Laser engraving, as a related technique, provides a means to mark or decorate polymer surfaces with precision. It offers the same benefits as laser cutting – high degree of precision, low chance of surface degradation and the possibility to create complex designs without the need for dedicated tools [12-13].

#### **3.2. Laser Welding of Polymers**

Laser welding is a very advantageous technique in joining polymer components, particularly for thermoplastics. As a non-contact method, it allows for localized and controlled heating, minimizing the risk of thermal damage to the polymer. The optimization of laser welding parameters, including power, scanning speed, and beam focus, is paramount in achieving robust joints. Selecting the appropriate polymer material and ensuring its compatibility with the laser wavelength are additional considerations that influence the success of the welding process. Applications of laser welding abound in industries where precision and the preservation of material properties are crucial, especially in medical and biomedical manufacturing - the clean and controlled nature of laser welding ensures the integrity of the polymer components. Ongoing research aims to further refine and expand the capabilities of laser welding, addressing challenges and broadening its applicability across diverse polymer materials [13-14].



### **3.3. Surface Modification and Functionalization**

Laser processing extends beyond conventional cutting and welding to include precise surface modification of polymer materials. Laser ablation, a technique where material is selectively removed from the surface, allows for the creation of specific and designed microstructures, enhancing adhesion and wettability of the surface. Concurrently, laser-induced chemical reactions on the polymer surface enable targeted functionalization, introducing specific groups or patterns to enhance properties.

These surface modifications find many applications in medical and biomaterial fields, where tailored surface properties are critical. The controlled and localized nature of laser surface modification provides a level of precision unable to be met by more traditional methods. Research in this domain explores innovative applications, including the development of biomimetic surfaces and advanced coatings for medical devices [14-16].

### **3.4. Additive Manufacturing with Laser Processing**

The integration of laser processing with additive manufacturing has opened new frontiers in the production of polymer components such as Selective Laser Sintering (SLS) and Stereolithography (SLA). SLS and SLA methods are prominent examples of the development of additive manufacturing where lasers selectively fuse or polymerize layers of material to create three-dimensional structures. SLS utilizes powdered polymer material, sintered layer by layer with precision by the laser, while SLA cures liquid resin layer by layer to achieve the desired form. These technologies offer unprecedented design flexibility and precision in creating customized polymer structures tailored to the desired properties [17-18].

## **4. COMPUTER-AIDED MATERIAL PROCESSING IN LASER PROCESSES**

There are several uses for contemporary laser technology in a variety of industrial domains, including materials processing. High precision, speed, and versatility in material processing are the hallmarks of laser techniques. To guarantee the best outcomes, sophisticated laser processes call for sophisticated instruments and methods. Computer-Aided Material Processing (CAMP), which combines cutting-edge computer systems with laser technology, is being utilized more frequently for this reason [21,22].

### **4.1. Laser Process Simulation and Thermal Modelling**

Laser processes can be simulated before they are carried out with the use of computer-aided material processes. Through these simulations, the effects of different parameters on the process outcomes, such laser power, travel speed, exposure duration, and others, may be analysed.

This enables engineers to forecast outcomes and optimize process parameters before they start working physically. Additionally, by using these simulations, many situations may be virtually tested, which can drastically reduce costs, the likelihood of errors, and process times.

Heat generation is one of the essential components of laser operations, and it directly affects the outcome of the process. Thermal modelling, which enables the analysis of temperature distribution in the produced material, is made possible by computer-aided material processes. Because of this, the impact of heat on the microstructure and characteristics of the material may be anticipated and managed. In addition, thermal modelling makes it possible to identify

possible issues like deformations, cracks, and phase shifts that could arise from the laser process [21-23].

#### **4.2. Process Monitoring and Control**

Real-time laser process monitoring and control is another aspect of computer-aided material processing. Process variables like temperature, scanning speed, or laser beam quality can be tracked and changed instantly with the use of sensors and advanced vision systems. This reduces the possibility of mistakes and faulty goods while enabling a prompt response to altering processing circumstances. Data from multiple sensors positioned throughout the laser processing system are gathered and analysed in real-time. These sensors are capable of measuring temperature, power, location, and beam quality, among other factors. The computer system then processes and analyses the gathered data to offer feedback on the efficiency of the procedure. Modern vision systems are essential for keeping an eye on the precision and calibre of the laser process. Defect identification, process parameter verification, and material surface inspection are made possible by high-resolution cameras and imaging systems. Operators can identify irregularities and make the required modifications to guarantee ideal processing conditions thanks to this real-time visual feedback.

In computer-aided material processing, real-time monitoring and control together improve process efficiency, quality, and reliability overall. It lowers the possibility of errors, enhances the overall efficiency of the laser process, and enables quick reaction to changing circumstances [22,23].

### **5. NANOSTRUCTURED COATINGS PRODUCED BY LASER PROCESSES**

The use of laser technology in the creation and modification of nanostructured coatings has grown significantly in recent years. The special qualities of nanostructured coatings include high hardness, mechanical strength, wear resistance, and many more. Laser procedures allow for the exact generation and alteration of nanostructured coatings on a variety of materials. These processes include laser ablation, ultraviolet beam, laser deposition, and ion beam. We will go over a number of methods and uses for nanostructured coatings in laser processes in this chapter [24].

#### **5.1. Techniques for creating nanostructured coatings**

There are numerous methods for producing nanostructured coatings in laser operations, which allow for exact material surface manipulation and modification. Several of these methods that are common in the fields of materials science and nanotechnology will be covered in this chapter.

One of the most widely used methods for producing nanostructured coatings is laser ablation. It entails employing laser pulses to remove material from the target surface. The material evaporates or flakes off the surface due to the effect of laser radiation, leaving behind a nanostructured covering. Metals, ceramics, and polymer matrices are just a few of the substrates on which nanostructured layers can be produced using laser ablation. With this method, the form, depth, and chemical makeup of nanostructured coatings may all be precisely controlled.

Using a laser beam, the technique known as "laser deposition" enables the exact application of material layers to the substrate. This method involves feeding the starting material into the laser

action area in the form of a powder or gaseous stream. The substance melts or evaporates when exposed to laser radiation, depositing a nanostructured layer on the target surface. Nanostructured coatings can be precisely tailored in terms of thickness, chemical makeup, and structure using laser deposition. It is extensively employed in optical, electrical, and engineering thin-film coating techniques.

Additionally, surfaces can be altered and nanostructured coatings can be made using the ultraviolet (UV) beam. Concentrating the UV laser on the material's surface can change its structure and surface characteristics locally. UV lasers are used in ablative material removal, photolithography, photopolymerization, and microstructure formation, to name a few applications. High resolution and incredibly small size nanostructures can be produced with the use of a UV beam.

Another method for altering surfaces and producing nanostructured coatings is ion beam. Ion beams are made up of charged ions that are directed at a material's surface and accelerated by an electric field. Ions can alter the structure, chemical makeup, and surface characteristics after colliding with a surface. Ion implantation, material removal, nanostructure formation, and surface chemical alteration are all possible with ion beams. With this method, the distribution and depth of nanostructures on the surface may be precisely controlled.

There are numerous potentials in the fields of surface engineering, materials science, and nanotechnology for using the aforementioned methods to create nanostructured coatings in laser operations. They make it possible to precisely alter the composition, structure, and chemical characteristics of a material's nanoscale surface. By applying these methods, new materials with special qualities—like increased electrical conductivity, strength, and resistance to wear and tear—may be created [25-27].

## **ACKNOWLEDGEMENTS**

The work was created as a result of the project as part of project based learning - PBL, in the 10th competition under the Initiative of Excellence - Research University, Silesian University of Technology.

## **BIBLIOGRAPHY**

1. M. Płatek, A. Dudek, J. Ucieklak, Analiza materiałoznawcza deimplantowanego elementu endoprotezy stawu biodrowego, *Engineering of Biomaterials*, 2019.
2. J. Dobrzański, *Materiałoznawcza interpretacja trwałości stali dla energetyki*, Gliwice, 2016
3. Borek, A. Klimpel, R. Grzelka, S. Mucha, B. Ścibisz, *Technologie Laserowe Spawania, Wytwarzania i obróbki Ciepłej Warstw Wierzchnich. Weld. Tech. Rev.* 2013,
4. D. Panek, M. Bonek: *Obróbka laserowa warstwy wierzchniej stali austenitycznej*, *Prace Studenckich Kół Naukowych, Kongres Studenckich Kół Naukowych CO-KÓŁ*, Wydawnictwo Politechniki Śląskiej, Volume 13, 2007, 53-60.
5. J. Radziejewska, "Laserowa modyfikacja właściwości warstwy wierzchniej wspomagana nagniataniem", *Instytut Podstawowych Problemów Techniki Polskiej Akademii Nauk*, 2011.
6. D.A. Belforte - *Encyclopedia of Materials: Science and Technology*, 2001

7. Klimpel, D. Janicki, A. Lisiecki, Z. Wilk, Spawalnicze technologie laserowe. Przykłady zastosowania lasera diodowego dużej mocy, Biuletyn instytutu spawalnictwa w Gliwicach, 2008.
8. W. P. Napadłek, W. Chrzanowski, A. M. Woźniak, "Przyrostowe technologie 3D w odbudowie kształtu zużytych eksploatacyjnie łopat turbin parowych," Autobusy. Technika, Eksploatacja, Systemy Transportowe, vol. 18, 2017.
9. M. Karoluk, A. Pawlak, E. Chlebus. "Wykorzystanie technologii przyrostowej SLM w procesie przetwarzania stopu tytanu Ti-6Al-7Nb do zastosowań biomedycznych." Aktualne Problemy Biomechaniki, Volume 8, 2014, 81-86
10. J. Mikoś, "Przegląd technologii druku 3D jako produkcji dodatkowej (przyrostowa) do wykonywania prototypów małych maszyn elektrycznych." Maszyny Elektryczne: zeszyty problemowe, 2021.
11. S. C. Tjong, "Polymer Composites with Carbonaceous Nanofillers: Properties and Applications," Wiley, 2012.
12. J. Powell, "Introduction to Laser Technology," Institute of Physics Publishing, 2004.
13. C. Yu, Y. Huang, "Laser Welding of Plastics," John Wiley & Sons, 2018.
14. M. H. Lee, "Laser Processing of Engineering Materials: Principles, Procedure and Industrial Application," Elsevier, 2005.
15. P. Mathur, "Laser Surface Modification of Biomaterials: Techniques and Applications," Woodhead Publishing, 2016.
16. L. Gibson et al., "Additive Manufacturing Technologies: 3D Printing, Rapid Prototyping, and Direct Digital Manufacturing," Springer, 2015.
17. M. Brandt, "Introduction to Additive Manufacturing," CRC Press, 2019.
18. Gibson, D. W. Rosen, and B. Stucker, "Additive Manufacturing Technologies: Rapid Prototyping to Direct Digital Manufacturing," Springer, 2010.
19. S. Katayama, "Lasers in Materials Processing: A Bibliography of a Developing Technology," Elsevier, 1991.
20. P. Krawczyk, Wspomaganie komputerowe procesów technologicznych w mikroobróbce laserowej, Przegląd Mechaniczny, 2018.
21. M. Kowalski, Modelowanie numeryczne procesu cięcia laserowego dla blachy ze stopu aluminium, Czasopismo Techniczne, 2020.
22. X. Wang, Y. Liu, Computer-Aided Design and Simulation of Laser Processing, Springer, 2018.
23. B. Stępak, Wpływ parametrów procesu laserowego na właściwości powłok nanostrukturalnych, Materiały Inżynierskie, 2019.
24. J. Jasiński, Zastosowanie powłok nanostrukturalnych w medycynie, Technologia i Automatyzacja Procesów, 2021.
25. G. Thompson, Laser-Assisted Nanostructured Coatings: Processing, Characterization, and Properties, CRC Press.
26. Y. Zhang, Laser Surface Engineering: Processes and Applications, Woodhead Publishing.
27. X. Li, Laser Surface Modification of Biomaterials: Techniques and Applications, Elsevier.



26th January 2024  
Gliwice, Poland

DEPARTMENT OF ENGINEERING MATERIALS AND BIOMATERIALS  
FACULTY OF MECHANICAL ENGINEERING  
SILESIA UNIVERSITY OF TECHNOLOGY

## INTERNATIONAL STUDENTS SCIENTIFIC CONFERENCE

### **Point Cloud Acquisition Using Multiple Azure Kinect DK Sensors Based on ArUco Cube Spatial Calibration**

M. Paszkuta<sup>a</sup>, E. Szmyt<sup>b</sup>, T. Kukuczka<sup>c</sup>, D. Myszor<sup>d</sup>

<sup>a</sup> Silesian University of Technology, Faculty of Automatic Control, Electronics And Computer Science, Department of Graphics, Computer Vision and Digital Systems

<sup>b</sup> Silesian University of Technology, Virtual Flying Student Research Group

<sup>c</sup> Silesian University of Technology, Faculty of Automatic Control, Electronics And Computer Science, Department of Graphics, Department of Cybernetics, Nanotechnology and Data Processing

<sup>d</sup> Silesian University of Technology, Faculty of Automatic Control, Electronics And Computer Science, Department of Algorithmics and Software

email: [dariusz.myszor@polsl.pl](mailto:dariusz.myszor@polsl.pl)

**Abstract:** The article describes the synchronization of Azure Kinect DK sensors based on ArUco Cube, for the purpose of point of clouds acquired from many devices stitching.

**Keywords:** point cloud, calibration, Azure Kinect

## 1. INTRODUCTION

The Microsoft Azure Kinect DK is a device designed for spatial data acquisition, incorporating a range of sensors such as an RGB camera, IR camera, IMU sensors, ToF sensor, and a matrix of microphones. The Azure Kinect finds utility across a broad spectrum of applications, ranging from entertainment to medical usage. Its seamless compatibility with various Azure platform tools, libraries, and SDKs developed by Microsoft empowers users to harness motion tracking, skeleton extraction, voice recognition, and depth sensing capabilities across diverse domains. Notably, this sensor can be utilized for volumetric video acquisition in the form of point cloud sequences, achieving a frame rate of up to 30 Frames Per Second (FPS).

It is crucial to acknowledge that the depth and RGB sensors are positioned at a slight distance from each other, introducing a potential challenge of occlusions. Occlusions may occur when a foreground object obstructs the view of a portion of a background object for one of these sensors. To address this issue and enhance the generation of a dense point cloud representation while minimizing the risk of occlusions, the proposal of employing multiple sensor sets has been set forth [9, 10].

The configuration involving multiple synchronized devices could be employed to expand the acquisition area and reduce the likelihood of occlusion, thereby enhancing the comprehensive understanding of the scene. However, due to the necessity of precise extrinsic calibration involving six degrees of freedom for each sensor, data fusion is not a trivial task.

This article describes the approach to data fusion from multiple Azure Kinect DK devices, which was exploited in the vFly projects related to data acquisition stations, e.g., based on depth cameras applied to the problem of disparity map estimation.

## 2. HARDWARE CONFIGURATION

The Microsoft Azure Kinect DK represents a state-of-the-art spatial computing developer kit. It is equipped with a depth sensor that allows one to select between wide and narrow field-of-view (FOV)[1], a microphone array for speech and sound capture, an RGB video camera that provides a video stream aligned with the depth stream, an accelerometer and gyroscope, external synchronisation pins which allows to link multiple Kinect devices and synchronise data acquisition (fig. 1) [3]. In the area of software, the device provides models for vision and speech recognition and the ability to integrate with Azure AI Services [8].

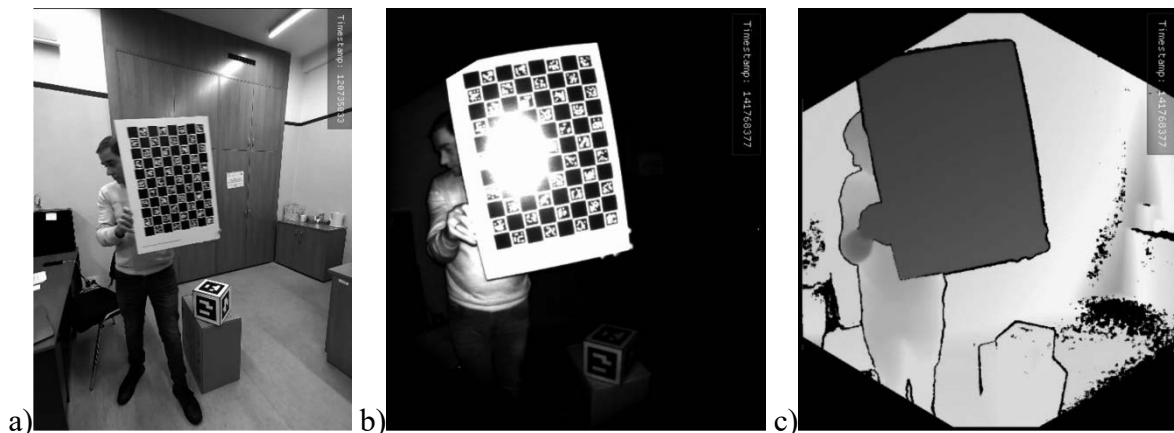


Figure 1. The example images obtained from Azure Kinect DK: a) RGB camera, b) IR camera, c) depth camera

An especially interesting functionality of the device is the depth sensor that provides information about the distance for every registered by the sensor point of the scene[1]. The resolution of the depth sensor is equal to 1MP; in combination with the price of the device, it is an interesting alternative to lidar devices, which can provide a similar resolution but for a higher price. In addition, Azure Kinect possess synchronisation pins that facilitate significantly synchronisation between devices and allow for simultaneous registration of data at the same time points. Popular solid-state devices rarely possess such a feature, which enforces the utilization of time-based approximate data synchronisation methods (based on RTC protocols).

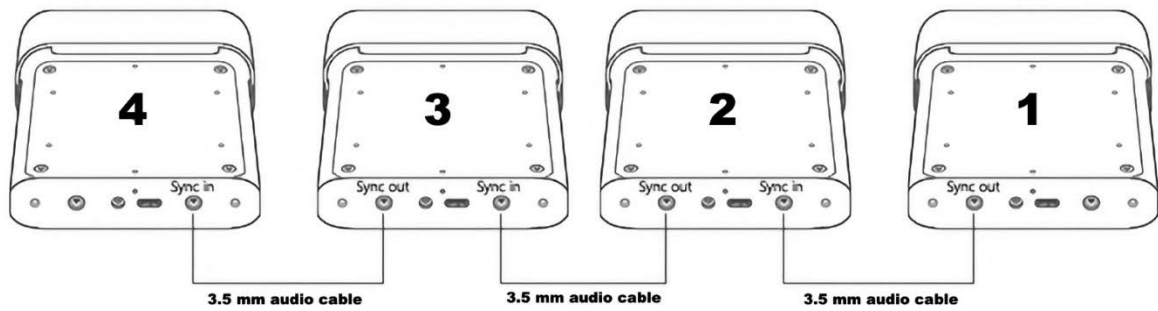


Figure 2. The Azure Kinect DK daisy-chain sync configuration schematic.

We used the daisy chain configuration to synchronize four devices (fig. 2 and fig.3). Azure Kinect DK offered hardware synchronization through the Sync In and Sync Out jacks. The first device provides the triggering signal for the subordinate devices, but the configuration with an external signal is also possible. We utilized a standard 3.5-mm jack audio cable that was 3 meters long. The Sync Out interface from the first device was connected to the Sync In of the second device, and so on. With this method, it is possible to connect up to eight subordinate devices. The Time-of-Flight (ToF) measurement is based on emitting laser light; therefore, devices with overlapping fields of view could interfere with one another.



Figure 3. Configuration of Azure Kinect DK sensors utilized for 360-degree 3D point cloud acquisition, featuring a visible ArUco cube used for spatial calibration.

### 3. SOFTWARE

To enable data fusion, the spatial relationship between Kinect devices must be determined. For this purpose, a cube with ArUco markers on its walls can be utilised [4, 6]. Each wall possesses a single ArUco marker. ArUco markers [11] are unique identification codes typically presented as black-and-white square patterns. This square alignment allows a computer vision system to identify and track the marker's position and orientation [7]. ArUco markers are almost always surrounded by white borders, which facilitate detection and recognition, even in challenging conditions. ArUco markers can be easily generated with the OpenCV - Open Computer Vision library (with generateMarkerImage static method from cv2.aruco class) [5].

The cube is utilized because sensors can be positioned at various locations in space. It is crucial to ensure that each RGB camera captures at least one cube wall with a visible ArUco marker. Each ArUco code corresponds to rotation and translation in relation to the center of the cube. These rotation and translation values are precalculated after assembling the ArUco cube and remain constant over time. As a result, these precalculated values can be embedded in the code or configuration file. The example RGB image, featuring the highlighted ArUco markers detected on the calibration cube, is depicted in fig. 4.



Figure 4. Example RGB image with the highlighted ArUco markers detected on the calibration cube

The first step is the designation of an intrinsic Kinect RGB camera matrix. It describes the relationship between points in three-dimensional space and their projections on a two-dimensional camera image plane (transforms 3D point's coordinates to 2D coordinates on camera image). The camera intrinsic matrix has the following form.

$$K = \begin{bmatrix} f_x & s & c_x \\ 0 & f_y & c_y \\ 0 & 0 & 1 \end{bmatrix}$$

where

- $f_x$  and  $f_y$  are focal lengths of the camera in x and y directions (expressed in pixels),
- $s$  is the skew coefficient,
- $c_x, c_y$  are the coordinates of the optical centre of the camera.

Lens distortion parameters are another important parameter of the acquisition system. They are presented as a vector

$$dist = (k_1, k_2, p_1, p_2, k_3)$$

where  $k_1, k_2, k_3$  are the radial distortion coefficients and  $p_1, p_2$  are the tangential distortion coefficients.



Parameters can be obtained with the camera calibration process during which a set of calibration images consisting of ArUco markers is registered, and features (corner coordinates, marker IDs) are extracted and passed to the OpenCV `calibrateCamera` method, which in turn returns (among other parameters) intrinsic camera matrix components as well as lens distortion parameters. It is done independently for every Kinect device utilised in the system because each individual RGB camera, even if built from the same components according to the same diagrams, is a subject of slight differences in component quality and their placement precision at the level of the assembly. On the other hand, a comparison of the coefficients embedded in the Kinect device by the manufacturer with these calculated based on the calibration process led us to the conclusion that the coefficients embedded in the device also present sufficient quality. Therefore, in the final solution, we applied coefficients embedded internally in the devices.

We predefine dictionaries that describe cube parameters such as cube wall rotation and offset of the cube centre.

```
self.DEFAULT_ROT = np.array([[0, 0, -1], [0, 1, 0], [1, 0, 0]])
# Dictionary used to map the ArUco ids to the corresponding specific rotations for each face of the cube
self.EUL_ROT_DICT = {
    94: np.matmul(np.array([[1, 0, 0], [0, 1, 0], [0, 0, 1]]), self.DEFAULT_ROT), # top
    95: np.matmul(np.array([[1, 0, 0], [0, 0, 1], [0, -1, 0]]), self.DEFAULT_ROT), # front
    99: np.matmul(np.array([[1, 0, 0], [0, 0, -1], [0, 1, 0]]), self.DEFAULT_ROT), # rear
    98: np.matmul(np.array([[0, 0, -1], [0, 1, 0], [1, 0, 0]]), self.DEFAULT_ROT), # right
    96: np.matmul(np.array([[0, 0, 1], [0, 1, 0], [-1, 0, 0]]), self.DEFAULT_ROT) # left
}
# Dictionary used to find the centroid of the cube given a face
self.CENTER_POINT_OFFSET_DICT = {
    94: np.float32([-self.cubeSize / 2., 0, 0]), # top
    95: np.float32([0, (self.cubeSize / 2.), 0]), # front
    99: np.float32([0, -(self.cubeSize / 2.), 0]), # rear
    98: np.float32([0, 0, (self.cubeSize / 2.)]), #right
    96: np.float32([0, 0, -(self.cubeSize / 2.)]) #left
}
```

Then, a set of Kinect devices is set up in the destination location, and a cube is registered with RGB cameras. Custom `Aruco_Detector` class is implemented, which initialises the object of the `ArucoDetector` class (from OpenCV library) based on default parameters (obtained with `cv2.aruco.DetectorParameters()`) and dictionary of ArUco codes utilised on the cube (obtained with `cv2.aruco.getPredefinedDictionary`). `ArucoDetector` class object is assigned to the variable `arucoDetector`. The `aruco_Detector` class also loads the camera intrinsic matrix and distortion matrix for each camera utilised in the system.

To obtain a final form of the optimal camera matrix for undistorting images, we execute `cv2.getOptimalNewCameraMatrix` method, with parameters: intrinsic matrix, distortion matrix, as well as the size of the input image.

Obtained calibration frames are converted to grayscale with `cv2.cvtColor` (`cv2.COLOR_BGR2GRAY` option) and delivered to the `arucoDetector.detectMarkers`. The method returns corners of the detected ArUco codes and respective identification values. Markers that do not have appropriate identification values are eliminated automatically by the code to rule out the ability to detect other markers that can be located on the scene but are not calibration markers.

If a single camera finds several markers, we select the best marker (i.e. the one with the greatest area). We refine the corner coordinates to sub-pixel accuracy with `cv2.cornerSubPix` method. Then, each camera's rotation and the translation vector are determined with `cv2.aruco.estimatePoseSingleMarkers` method (which takes an array of detected marker corners, intrinsic matrix and distortion vector as parameters). It allows us to estimate the pose of the marker in the camera coordinate system. The rotation vector is transformed into a rotation matrix with `cv2.Rodrigues` as rotation matrices are often more convenient to utilise. Then, we use `np.matmul` to multiply the rotation matrix with a predefined detected ArUco code rotation

(rotation in relation to the middle of the ArUco cube). That combines the rotation and translation information obtained from the ArUco marker with an additional translation offset (centroid\_offset). This transformation is necessary to convert the centroid from the local coordinate system of the ArUco marker to the camera coordinate system.

In the next step, we compose a homogenous transformation matrix consisting of a rotation matrix (that combines the rotation from the ArUco marker with a predefined rotation) as well as a translation vector obtained from `cv2.aruco.estimatePoseSingleMarkers`. An additional row  $[0, 0, 0, 1]$  is appended to the bottom of the matrix to make it a  $4 \times 4$  homogeneous transformation matrix. Then, we multiply the obtained homogeneous transformation matrix with the 3D centroid of the ArUco. As a result, we obtain the position of the centre of the cube in 3D space as well as a rotation matrix, which can be utilised later to modify the coordinates of points obtained by the depth camera and unify reference frames between the Kinect devices exploited in the system. Results of the system functionality for four Kinect sensors employed simultaneously were presented in fig. 5.

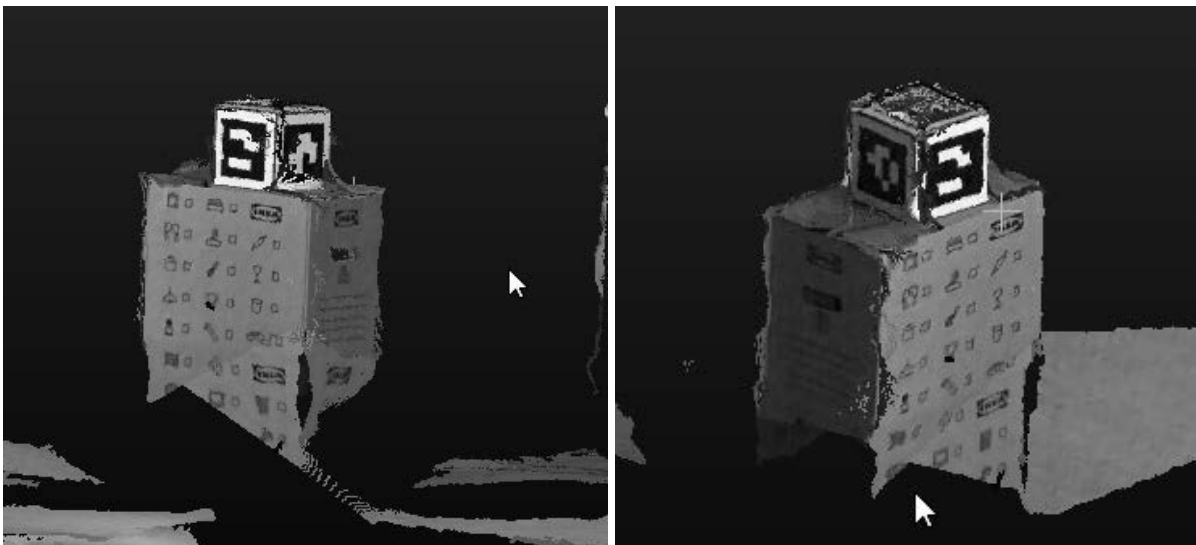


Figure 5. Example point cloud obtained using four synchronized and spatial calibrated Azure Kinect sensors

#### 4. SUMMARY

The pipeline that allows for data fusion obtained from multiple Azure Kinect is described in the article. Open source libraries, such as OpenCV, were applied, which facilitated the data processing process. Code was implemented in Python; therefore, it can be run on a wide variety of operating systems. The pipeline was utilised in the work of vFly Students Group during the realisation of a project related to a data acquisition station based on depth cameras.

#### BIBLIOGRAPHY

1. Andersen, Michael Riis, et al. "Kinect depth sensor evaluation for computer vision applications." *Aarhus University* (2012): 1-37.

2. Antico, Mauro, et al. "Postural control assessment via Microsoft Azure Kinect DK: An evaluation study." *Computer Methods and Programs in Biomedicine* 209 (2021): 106324.
3. Ayed, Ines, et al. "Vision-based serious games and virtual reality systems for motor rehabilitation: A review geared toward a research methodology." *International journal of medical informatics* 131 (2019): 103909.
4. Kalaitzakis, Michail, et al. "Fiducial markers for pose estimation: Overview, applications and experimental comparison of the artag, apriltag, aruco and stag markers." *Journal of Intelligent & Robotic Systems* 101 (2021): 1-26.
5. Haggui, Olfa, Matossouwé Agninoube Tchelim, and Baptiste Magnier. "A comparison of opencv algorithms for human tracking with a moving perspective camera." *2021 9th European Workshop on Visual Information Processing (EUVIP)*. IEEE, 2021.
6. S. Garrido-Jurado, R. Muñoz-Salinas, F. J. Madrid-Cuevas and M. J. Marín-Jiménez, "Automatic generation and detection of highly reliable fiducial markers under occlusion", *Pattern Recognit.*, vol. 47, no. 6, pp. 2280-2292, Jun. 2014.
7. Jun, Kooksung, et al. "Pathological gait classification using kinect v2 and gated recurrent neural networks." *IEEE Access* 8 (2020): 139881-139891.
8. Kurillo, Gregorij, et al. "Evaluating the accuracy of the azure kinect and kinect v2." *Sensors* 22.7 (2022): 2469.
9. Xing, Qing-Jun, et al. "Functional movement screen dataset collected with two azure kinect depth sensors." *Scientific Data* 9.1 (2022): 104.
10. Yuan, Zhilu, et al. "A survey on indoor 3D modeling and applications via RGB-D devices." *Frontiers of Information Technology & Electronic Engineering* 22.6 (2021): 815-826.
11. Garrido-Jurado, S., Muñoz-Salinas, R., Madrid-Cuevas, F. J., & Marín-Jiménez, M. J. (2014). Automatic generation and detection of highly reliable fiducial markers under occlusion. In *Pattern Recognition* (Vol. 47, Issue 6, pp. 2280–2292). Elsevier BV.



26th January 2024  
Gliwice, Poland

DEPARTMENT OF ENGINEERING MATERIALS AND BIOMATERIALS  
FACULTY OF MECHANICAL ENGINEERING  
SILESIA UNIVERSITY OF TECHNOLOGY

## INTERNATIONAL STUDENTS SCIENTIFIC CONFERENCE

### **Application of the NORAXON myoMotion system in the scope of 5S methodology applications**

W. Piętakiewicz<sup>a1</sup>, A. Sykała<sup>b1</sup>, P. Trybuszkiewicz<sup>b2</sup>, R. Trepia<sup>a2</sup>, K. Szczyrba<sup>a3</sup>, M. Roszak<sup>a</sup>, R. Michnik<sup>b3</sup>, M. Molenda<sup>c</sup>, A. Miller-Banas<sup>b4</sup>

<sup>a</sup> Silesian University of Technology, Faculty of Mechanical Engineering, Department of Engineering Materials and Biomaterials

email <sup>a1</sup>: wiktpie055@student.polsl.pl; email <sup>a2</sup>: rafatre774@student.polsl.pl; email

<sup>a3</sup>: kacpszc239@student.polsl.pl; email <sup>a4</sup>: marek.roszak@polsl.pl

<sup>b</sup> Silesian University of Technology, Faculty of Biomedical Engineering, Department of Biomechatronics

email <sup>b1</sup>: agnisyk881@student.polsl.pl; email <sup>b2</sup>: patrtry061@student.polsl.pl; email

<sup>b3</sup>: robert.michnik@polsl.pl; email <sup>b4</sup>: anna.miller-banas@polsl.pl

<sup>c</sup> Silesian University of Technology, Faculty of Organization and Management, Department of Economy and Informatics

email: michal.molenda@polsl.pl

**Abstract:** Effectiveness in the workplace determines an organization's ability to succeed. Workplace effectiveness concerns the quality of work performed, employee involvement, and achievement of goals. Clearly defining goals, providing appropriate tools, and providing job-specific training are particularly important. The 5S method allows you to effectively improve the efficiency of the workplace, especially when employees' suggestions are taken into account during its implementation. The myoMotion Noraxon system enables analysis of employee activities, which supports optimizing working conditions. The use of the Noraxon system - which was used for the first time for this type of analysis - supports the improvement of the workplace, allowing you to assess the effectiveness of the solutions used in the organization of the workplace.

**Keywords:** 5S, Kaizen, Continuous Improvement, System NORAXON, Assembly Station, Pen Assembly.

## 1. INTRODUCTION

Workplace efficiency is a crucial indicator for assessing the organization of the workplace. The workplace's effectiveness significantly impacts the entire organization's success, primarily by influencing the quality of work, employee involvement, and, consequently, achieving business goals. In this context, it is crucial to define the goals and requirements for individual workplaces, as well as to provide employees with appropriate tools and resources needed to perform tasks at

the workplace, including training, shaping the effectiveness of tasks at the workplace and employees' awareness of the importance of organizing the workplace, both in terms of performance, but also security aspects [1].

The efficiency of workplace organization can be significantly improved by using the 5S method. The implementation of the 5S method allows you to improve the efficiency of workplace organization effectively. However, to implement the necessary improvements by this method that contribute to increased efficiency, feedback from employees regarding the organization of the workplace should be taken into account. Employees are the best experts in their workplaces, so their opinions are extremely valuable, but it should be remembered that these opinions are subjective [2].

To assess the way of organizing work, the Noraxon myoMotion system was used, which allowed for the recording and analysis of activities performed by employees while performing a task at the workplace. The Noraxon MyoMotion system is a modern solution used for the first time in the study to assess workplace organizations' effectiveness in implementing the 5S method. The planned research allowed for the assessment of the impact of the organization of the workplace on the efficiency of the assembly process, as well as a detailed analysis of the employee's movements.

## **2. CHARACTERISTICS OF THE NORAXON SYSTEM**

Noraxon's myoMOTION system is a combination of hardware and software that enables recording human movement in a three-degree-of-freedom projection. A compact inertial measurement unit (IMU) placed on any human body segment precisely tracks its angular orientation in 3D. By placing individual IMU sensors on two adjacent body segments, an individual joint's range of motion (ROM) can be determined. The analysis can be extended from examining a single joint to simultaneously measuring the entire human body using 16 sensors placed for all major joints.

The myoMOTION sensors transmit a signal in the range of movement of the human body directly to the myoMOTION receiver to quantify angular changes in selected body segments.

The acquired data can then be analyzed using Noraxon MR3 software. The signal can be integrated with other biomechanical systems from Noraxon (EMG, video), Zebris (treadmills, platforms), and Medilogic (shoe insoles) [3,4].

Data that can be obtained using the MyoMotion system include:

1. Linear acceleration: The myoMotion system measures acceleration in three spatial axes (x, y, z). This allows the body's or limbs' acceleration to be tracked in different directions during movement.
2. Angular velocity: the system records angular velocity around three axes. This data helps analyze the rotation and rotational movement of individual body parts.
3. Orientation and tilt: Using data from the IMU sensors, the myoMotion system can determine the orientation of the body or limbs and their tilt in space.
4. Synchronization with other devices: The myoMotion system allows data to be synchronized with other measurement devices, such as motion analysis cameras, EMG (electromyography), or force platforms. This provides comprehensive data on body movement and function.

5. Biomechanical analysis: the data collected by the myoMotion system can be used to perform biomechanical analysis, including assessing movement patterns, postural analysis, and evaluating kinematic parameters during various activities or sports training.

Noraxon's myoMotion system is used in physiotherapy, sports, research, biomechanics, and many other areas where tracking body movement and analyzing kinematic parameters is essential. The data collected allows a detailed analysis of the movement, which is extremely helpful in diagnosis, therapy, sports training, or scientific research related to the movement performed by the subject.

IMU sensors can be used on specific body segments, such as the feet, lower legs, thighs, sacrum and torso, wrist, arm, and forearm. Future research may address the use of IMU sensors in these areas and their applications, including smartwatches. IMU sensors are widely used for movement analysis in sports and rehabilitation settings. They are providing valuable data on body movements and associated performance. They can also be used to accurately classify typical body positions such as standing, sitting, lying down, and sitting on the floor [5]. In addition, IMUs can measure spatio-temporal parameters such as step time, step length, and swing time, as well as spatio-temporal parameter variability and symmetry during walking [6]. IMUs can also track 3D spinal motion during spinal flexion extension and lateral flexion, providing low mean squared error and a strong correlation with motion capture hardware [7, 8].

The Noraxon myoMotion kit consists of:

- a number and type of sensors equal to the selected configuration;
- a signal receiver connected via USB;
- sensor charger;
- double-sided tape for mounting the sensors;
- accessory kit for attaching sensors (elastic straps);
- software for data recording and analysis.

The main advantages of the technology described above are that it is easy and quick to use, fully portable, and can be used with independent external cameras.

### 3. CHARACTERISTICS OF THE 5S METHOD

The 5S method is a systematic approach to workplace management originating from Japan, the use of which increases the level of productivity, quality and safety at the workplace. This is achieved by introducing principles and rules that ensure efficient functioning, segregation and discipline of employees [9].

The name of the method is an acronym derived from five Japanese words denoting the stages of implementing the 5S method [10-12]:

#### a) 1S – Sort - Seiri

It is the first step in the 5S methodology to organize the workplace. "Seiri" means selection, the process of sorting tools, materials, and other elements at the workplace, keeping only necessary items. This allows for increased transparency at the workplace, and the operator's attention is not distracted by unnecessary elements. At this stage, all items at the workstation are reviewed and grouped according to a specific system, eliminating those considered unnecessary.

Selection helps maintain cleanliness at the workplace, improves the efficiency of searching for and retrieving necessary parts or tools, and shortens operation time, increasing productivity at a given position. Unnecessary raw materials, broken tools, outdated data, and documents are eliminated, contributing to more effective resource management [10-12].

**b) 2S – Set in order - Seiton**

The second phase involves properly organizing items at the workplace. The main goal is to place items where they are most needed to increase work efficiency and safety. Employees should be encouraged to place items where they are used and improve visual management of the workplace.

An essential element of "Seiton" is to make everything needed for work visible. This makes it easier to identify and correct errors. Introducing visual controls is recommended at this stage, for example, by using tool boards, parts containers, or optimizing the design of the workplace. Implementation of the 2S principle includes segregating items and marking their storage locations. Tools used infrequently or occasionally should be placed outside the immediate use area. Storage places should be marked to enable quick identification, for example, with colored lines, signs, or tool boards.

Systematic and ergonomic arrangement of things increases work efficiency. Determining the best places and methods for storing and replenishing materials, tools, equipment, and information is essential. Visualization of the workplace, such as painting the floor or marking tools, helps maintain order and efficiency of work [10-12].

**c) 3S - Shine – Seiso**

This phase involves cyclical cleaning, which allows you to identify and eliminate sources of disorder and maintain cleanliness at the workplace. This stage begins with workplace reorganization, which requires carefully checking whether the previous 5S rules have been adequately applied. It is the employee's responsibility to keep the workstation clean every day. Inspection questions are used to assess the workplace for cleanliness, such as whether there are oil stains, dust, or metal filings around the workplace, whether the machine is clean, etc. Regular cleaning is a type of inspection that detects minor damage that may be a source of equipment failure and production losses.

Employee involvement in this process is crucial. Establishing a cleaning schedule and determining responsibility for cleaning specific areas is essential. It is emphasized that untidy and dirty work areas increase the risk of accidents, employee injuries, and potential customer complaints due to a product that does not meet the requirements. Therefore, it is recommended that this stage be implemented as a daily routine [10-12].

**d) 4S – Standardize – Seiketsu**

The fourth phase of 5S, "Seiketsu," or standardization, makes it easier to control the production process in the enterprise. Standardization involves creating consistent ways of carrying out tasks at a position by creating standardized procedures and rules.

The developed and implemented standard in the form of procedures and instructions helps maintain order at workstations. Standards developed by employees of a peculiar plant are internal documents and should be communicative, clear, and easy to understand.

Standards are a collection of the best experiences of employees in performing a specific operation. They specify the order in which activities should be performed to achieve the best results. Standardization sheets should be placed in permanent and visible places to ensure easy access. Actions consistent with the first three phases of 5S are essential to the method but cannot be used once or ad hoc. They should be characterized by continuity and systematicity, preventing employees from returning to old, unfavorable habits [10-12].

#### e) 5S - Sustain/self-discipline – Shitsuke

The fifth phase of the 5S methodology, self-discipline, is the key to maintaining the benefits of implementing this methodology. Self-discipline requires employees to change their habits and behavior to adhere to established standards. To achieve self-discipline, employees must be aware of the importance of safety, order, and cleanliness in the workplace, leading to fewer non-compliances, increased efficiency, and preventing accidents.

Introducing the 5S methodology requires self-discipline from employees with compliance with the principles of cyclic cleaning and segregation. This leads to an increase in workers' awareness, a reduction in the number of faulty products and processes and improved internal communication.

In the self-discipline process, it may be helpful to formally establish a system for presenting achievements, such as photos of the position before and after the introduction of the 5S methodology, or job evaluation sheets [10-12].

#### 4. ANALYSIS OF THE SCOPE FOR RESEARCH IN THE AREA OF WORKPLACE ORGANIZATION EFFICIENCY USING THE NORAXON MYOMOTION SYSTEM

Following an analysis of the research capabilities of the Noraxon myoMotion system, it was noted that it can also be used for research in the organization and quality management field. It can be used to assess the performance of employees during the implementation of the 5S methodology at a given workplace. For example, data from inertial sensors can be used to determine how much time employees spend looking for objects, what range of movements they perform, how far their reach is, and how often they make unnecessary movements.

The Noraxon system allows for the analysis of the acquired data in the following areas:

- **Time and distance of performed movements** - one of the critical factors affecting work efficiency is the duration of performed movements. This time depends on the organization of the workplace and the arrangement of individual elements of the workplace, where the critical role is played by the 2S (Seiton) phase. This has a direct impact on the time spent performing individual movements. Optimization of the workplace allows the efficiency of time use to be shaped, but it also involves energy expenditure associated with the implementation of the work, which concerns working comfort. The shorter the duration of the movement, the higher the work efficiency.
- **Frequency of movements** - another critical factor affecting work efficiency is the frequency of movements. If items in the workplace are regularly cleaned, which is the basis of the 3S phase - Seiso, and adequately organized, employees do not have to waste time looking for the necessary items, which reduces the frequency of inefficient movements. The rarer the movement, the less strain on the muscles and joints, which translates into the comfort of work and the employee's well-being.
- **Effective use of workspace** - Effective use of workspace can help increase the workstation's efficiency and impact the comfort of work. By implementing the 1S stage - Seiri, the available workspace at the workstation is increased, and the implementation of the 2S stage - Seiton allows for its optimization through the effective placement of tools and objects at the workstation.
- **Muscle loading** - Muscle loading can lead to pain and fatigue and, in the long term, to workers' occupational diseases. By applying the 4S stage, i.e., Seiketsu, unnecessary



movements are eliminated in each operation, but in many cases, defining an ergonomic assembly method is problematic because the development of the standard is based on the subjective feelings of the employee. In this place, the Noraxon myoMotion system can play a crucial role, which enables precise measurement of the muscle load of employees in actual working conditions. Thanks to this, objective analysis of anomalies occurring during the performance of activities, such as excessive muscle loading for a given movement in a given activity, is possible.

- **Level of ergonomics** - Ergonomics of the workplace have an impact on reducing muscle and joint load, preventing potential accidents, and shaping work efficiency. The operator works more efficiently by implementing the 2S Seiton stage because the machines, tools, and parts will be arranged appropriately and oriented. Thanks to standardization for individual workstations (4S Seiketsu), we maintain the repeatability of the actions performed by the operator at the workstation, and there is a possibility of continuous improvement of the workstation.
- **Evaluating the effectiveness of workstation organization in different business areas** - Noraxon myoMotion system can be used to evaluate the effectiveness of workstation organization and employees' adherence to the 5S (Shitsuke) method in different business areas, such as production or logistics.

Capturing the data mentioned above can be used to identify areas where implementing changes can improve workplace efficiency. For example, if workers spend a lot of time looking for items, a visual identification system can be introduced to make them easier to find during assembly operations. If workers move too far, the arrangement of items or workstation equipment can be changed. If workers make unnecessary movements, the process under analysis can be standardized. The effectiveness of the improvements can be verified by re-measuring using the Noraxon system sensors.

#### **Advantages of using Noraxon to analyse the implementation of the 5S method in the workplace:**

- **Accuracy:** the Noraxon myoMotion system is characterized by high accuracy. As a result, it provides reliable data that can be used to identify areas where performance can be improved.
- **Based on data:** Noraxon myoMotion system is characterized by high accuracy. It is possible to rely on accurate data, with a high resolution of the measurements taken, and not just on estimated values. This approach can avoid erroneous theses and the solutions built on them.
- **Efficient measurement time:** the Noraxon myoMotion system can record workers' movements over a more extended period without interfering with them. This provides reliable data that covers the entire work process without interfering.
- **A considerable amount of data for analysis:** the Noraxon system captures a vast amount of data that can be used for in-depth analysis of work organization performance and employee behaviour. This makes it possible to identify areas where productivity can be improved, considering criteria such as time, energy expenditure, ranges of movement, and repetition of movements.

#### **Disadvantages of using Noraxon when implementing 5S in the workplace:**

- **Cost:** The Noraxon MyoMotion system is relatively expensive. This may be a barrier to its widespread use.

- **Complicated:** the Noraxon myoMotion system is complicated to use. It is therefore necessary to train the employees who will use it.
- **Nuisance:** the Noraxon system requires 16 sensors to be worn on the worker, including three sensors taped directly to the body. This can be uncomfortable for some workers and infringe on their sphere of comfort. To guarantee the correct reading from the sensors of the NORAXON myoMotion system, it is necessary to place the sensor pullers in direct contact with the worker's body. Suppose a worker must wear a protective helmet or other personal protective equipment. In that case, it may not be possible to position the sensor to measure, for example, the position of the worker's head.
- **Interference:** the Noraxon system can be interfered with by metallic accessories such as jewelry, metal elements in the environment, or electronics. This can result in the need for frequent calibration of the system or even make testing impossible if too many factors in the environment lead to sensor interference.
- **Demanding data analysis:** the Noraxon system records large amounts of data that require analysis by specialists. This can be time-consuming and expensive.

### **Planning a study of the implementation of the 5S method in the workplace using the Noraxon system**

To plan the study, it is necessary to determine what data should be extracted from the Noraxon system and what process will be analyzed. Assuming that such a study is being carried out at an assembly station, for example, the Noraxon system for monitoring worker movements can be used to collect the following data:

- the duration of individual assembly operations,
- range of motion and ergonomics of the work, frequency of individual movements
- frequency of individual movements

Four trials were conducted to test the capabilities of the Noraxon myoMotion system, where improvements were implemented in each successive trial by the implementation phases of the 5S method.

The equipment of the research station included:

- table
- height-adjustable chair
- Two containers for NOK/OK products,
- assembly material – parts from disassembled automatic pens,
- bumpers for the edges of the assembly station,
- Assembly drawing,
- containers for pen elements,
- mounting mat,
- photos of NOK/OK products,
- work standardization sheet,
- laptop with appropriate software,
- Noraxon measurement system.

Assumptions for each trial:

1. **Incorrect Assembly:** If the operator notices that the assembly of the part is incorrect, he puts down the faulty pen and continues working. In this case, no correction is made, and the pen remains in the condition where the error was noticed.

2. Dropped Parts: In the case of dropped parts, the operator follows the dropped parts policy, i.e., classifies them as NOK.
3. Lack of Supervision: Direct supervision of the operator's actions during each test must be done.
4. Work Registration: Each trial is recorded using the Noraxon myoMotion system for later analysis.
5. Ergonomics of the workstation: Each operator adjusts the seat height to their needs before starting work.
6. Manual Preferences: Before starting the test, ask the operator whether he is right- or left-handed to adapt the workstation to his preferences.
7. Inspection of NOK parts: At each stage of the process, an inspection of pens marked as NOK is carried out.

The assembly station consisted of a table and a chair with a mechanism enabling seat height adjustment. The operator was able to adjust the height of the chair to his preferences. The table on which the pens were mounted in four attempts was in contact with a wall of uniform grey. The lighting at the workstation was evenly distributed.

The research tests carried out are characterized below:

#### **ATTEMPT I**

Before the test, an anthropometric analysis of the test subjects and their training in pen assembly was carried out. In the first attempt, the pen components were mixed and stacked in a single pile placed in the center of the assembly station. During the effort, the operator placed the assembled pens that the operator found to be compliant (OK) into a pile to their right, while the operator placed the pens found to be non-compliant (NOK) into a pile to the operator's left - the area for depositing OK and NOK products was not delimited.

#### **ATTEMPT II**

In the second attempt, the parts of the pens were sorted into separate piles for each part in a random sequence. In front of the operator at eye level, an overview photograph of the assembled pen was placed, showing each component in the correct orientation. As in the previous attempt, the operator placed the assembled pens that the operator found to be compliant (OK) into a pile to the operator's right, while the pens found to be non-compliant (NOK) were placed into a pile to the operator's left - the placement area for OK and NOK products was not delimited.

#### **ATTEMPT III**

In the third attempt, the parts of the pens were sorted and placed in containers in the same arrangement as in sample two. A transparent assembly mat was placed on the workstation to minimise the possibility of parts slipping, and a white sheet of paper was placed under the mat to unify the background. Bumpers were attached to the edges of the assembly workstation to prevent parts from sliding to the floor. Photographs of common mistakes during pen assembly were placed in front of the operator at eye level, along with comparisons of pens assembled correctly.

#### **ATTEMPT IV**

In the fourth attempt, the operator was trained in the pen assembly operation according to a developed work standard based on workers' observations and best practices from previous

attempts. The pen components were sorted and placed in containers within the operator's reach to pick up the components from left to right during pen assembly. The containers were inclined at a 30° angle to the desk surface. As in the previous attempt, photographs of common mistakes during pen assembly were placed in front of the operator at eye level, along with comparisons of pens assembled correctly.

The data collected in connection with the project according to the methodology outlined above produced data that will be analyzed in terms of the following parameters:

- changes during assembly operations,
- improving ergonomics and reducing muscle load,
- optimisation of movements and reduction of unnecessary activities,
- repetition of movements in individual attempts.

An experiment designed in this way will allow a reliable assessment of the impact of implementing the 5S methodology on workstation performance and the other criteria mentioned above.

## ACKNOWLEDGMENT

The study was developed as part of the Project Based Learning project entitled "Application of the NORAXON myoMotion system in the scope of 5S methodology applications." within the 10th edition of the Excellence Initiative Programme - Research University - Silesian University of Technology, in the academic year 2023-2024.

## BIBLIOGRAPHY

1. Karolina Kolińska, Adam Koliński. Zastosowanie standaryzacji pracy w celu poprawy efektywności produkcji, *Zeszyty Naukowe Politechniki Poznańskiej*, 2013, Nr 61
2. Manuela Ingaldi, Adam Pala. Improvement of the workplaces in chosen enterprise. *Archives of Engineering Knowledge Vol. 1, Issue 1, (2016) 45-49*
3. myoMOTION Hardware User Manual, [http://www.noraxon.com/wp-content/uploads/2015/05/P-6808-Rev-C-MyoMotion\\_Hardware\\_New-format.pdf](http://www.noraxon.com/wp-content/uploads/2015/05/P-6808-Rev-C-MyoMotion_Hardware_New-format.pdf)
4. Amadeusz Bartoszek, Artur Struzik, Sebastian Jaroszczyk, Marek Woźniewski, Bogdan Pietraszewski, Comparison of the optoelectronic BTS Smart system and IMU-based MyoMotion system for the assessment of gait variables, *Acta of Bioengineering and Biomechanics Vol. 24, No. 1, 2022*
5. Dylan Kobsar, Dylan Kobsar, Jesse M. Charlton, Calvin T.F. Tse, Jean-Francois Esculier, Angelo Graffos, Natasha M. Krowchuk, Daniel Thatcher, Michael A. Hunt, Validity and reliability of wearable inertial sensors in healthy adult walking: a systematic review and meta-analysis, *Journal of Neuroengineering and Rehabilitation (BioMed Central)*, 2020 – Vol. 17, Iss: 1, pp 1-21
6. Thurmon E. Lockhart, Rahul Soangra, Jian Zhang, Xuefang Wu, Wavelet based automated postural event detection and activity classification with single imu, *Biomedical sciences instrumentation*, 2013, Vol. 49, pp 224-233

7. K. H. E. Beange, Adrian D. C. Chan, R. B. Graham, Wearable sensor performance for clinical motion tracking of the lumbar spine, 2019, Vol. 42
8. Ryan B. Graham, Arnaud Dupeyron, Jaap H. van Dieën, Between-day reliability of IMU-derived spine control metrics in patients with low back pain, *Journal of Biomechanics*, 2020
9. CZAJKOWSKA, Klaudia. 5S jako metoda budowania przewagi konkurencyjnej. *Journal of Modern Management Process*, 2017, 2.2: 27-35.
10. MICHALSKA, Joanna; SZEWIECZEK, Danuta. The 5S methodology as a tool for improving the organization. *Journal of achievements in materials and manufacturing engineering*, 2007, 24.2: 211-214.
11. GALA, Beata; WOLNIAK, Radosław. Problemy wdrożenia praktyk 5s w przedsiębiorstwie przemysłowym problems of implementation 5s practices in an industrial company. *Management Systems in Production Engineering* No 4(12), 2013
12. AGRAHARI, R. S.; DANGLE, P. A.; CHANDRATRE, K. V. Implementation of 5S methodology in the small-scale industry: a case study. *International Journal of Scientific & Technology Research*, 2015, 4.4: 180-187.



26th January 2024  
Gliwice, Poland

DEPARTMENT OF ENGINEERING MATERIALS AND BIOMATERIALS  
FACULTY OF MECHANICAL ENGINEERING  
SILESIA UNIVERSITY OF TECHNOLOGY

## INTERNATIONAL STUDENTS SCIENTIFIC CONFERENCE

### **Personalized sensory accessories for children with disabilities manufactured with 3D printing technology**

A. Piątek<sup>a</sup>, W. Wyleżoła<sup>a</sup>, M. Słowiak<sup>b</sup>, Sz. Modliński<sup>b</sup>, A.J. Nowak<sup>c</sup>, W. Walke<sup>d</sup>, M. Król<sup>e</sup>

<sup>a</sup> Student, Silesian University of Technology, Faculty of Biomedical Engineering,

<sup>b</sup> Student, Silesian University of Technology, Faculty of Mechanical Engineering Technology,

<sup>c</sup> Silesian University of Technology, Faculty of Mechanical Engineering Technology, Scientific and Didactic Laboratory of Nanotechnology and Materials Technology, Faculty of Mechanical Engineering Technology, Silesian University of Technology,

<sup>e</sup> Silesian University of Technology, Department of Biomedical Engineering, Department of Biomaterials and Medical Device Engineering

<sup>f</sup> Silesian University of Technology, Department of Mechanical Engineering Technology, Department of Engineering and Biomedical Materials; e-mail: [agnieszka.j.nowak@polsl.pl](mailto:agnieszka.j.nowak@polsl.pl)

**Abstract:** The work presents the concept and process of manufacturing a sensory path dedicated to children with disabilities, using the 3D printing method. The purpose of the work is to present the essence of sensory accessories and the benefits of their use in the therapy of children with various disabilities. The work discusses the criteria for material selection, which should be safe for children, durable and at the same time adapted to sensory needs. In addition, the 3D printing process is described, focusing on emphasizing the precision of the manufacturing of individual components to ensure maximum therapeutic effect. The work includes two design concepts for the basic sensory elements, each of which has been described in detail and presented in the form of photos taken at the design stage in the relevant graphics programs.

**Keywords:** 3D printing, PLA, Sensory mat, Disability, Design, Inventor, SolidWorks

## **1. INTRODUCTION**

The production of sensory accessories for people with disabilities brings a number of benefits both to the people with disabilities themselves and to society as a whole. It improves the quality of life for people with disabilities by enabling stimulation of the senses through a variety of sensory stimuli, such as textures, sounds or colors. Sensory accessories are also an integral part of therapeutic programs, supporting the development of sensory skills, social competence and communication skills. With customization, through a variety of shapes, sizes and materials, as well as degrees of difficulty, these accessories contribute to the creation of products tailored to the needs of the specific requirements of people with disabilities [1,6].

In the context of manufacturing sensory accessories, it is worth noting that the practice focuses on diverse age groups, particularly children and adults. This division takes into account the specific needs and developmental stages of both groups. The manufacture of dedicated sensory accessories for children with disabilities brings unique benefits. Children during the developmental period particularly benefit from organoleptic or sensory stimulus senses, which affect their motor, emotional and social development. These accessories are designed for a variety of experiences, supporting children in developing cognitive skills and sensory integration. Adults with disabilities also benefit from sensory accessories that are tailored to their individual needs. Stimulation of the senses can help improve well-being or reduce stress. With a variety of shapes, materials and functions, sensory accessories for adults are becoming an integral part of strategies to support daily functioning. Common to both groups is that, sensory accessories not only serve practical therapeutic purposes, but also promote activity, social integration and better adaptation to the surrounding environment. In turn, this contributes to building a more integrated society.

Sensory accessories are a variety of objects and tools designed to stimulate the senses. Below are examples of such accessories [1,6,7]:

- sensory mats - mats of various textures, shapes and colors that provide a variety of sensory experiences,
- fidgets - small, portable gadgets that can be manipulated with the hands to help concentration and sensory regulation,
- sensory squeezers - soft toys that can be squeezed and then loosened back up,
- blankets with different textures - made of different materials, such as soft fleece fabric that mimics fur, or blankets with piping that provide a variety of tactile sensations,
- musical instruments with different sounds - instruments such as drums, xylophones or percussion instruments that allow exploration of sounds and rhythms.

These examples represent only a small fraction of the sensory accessories available. In practice, there are many other items that can be customized to meet individual user needs and preferences [7,8]. This article focuses on the design and manufacture of a sensory path, so it is this subject that will be described in detail. The manufacture of sensory paths is aimed at providing benefits to various groups of people, especially children and people with disabilities. The main task of sensory paths is to stimulate the senses, support motor development, sensory therapy by stimulating movement, motor coordination and muscle strength, thus also supporting overall physical development. In addition, the use of sensory accessories helps reduce stress, treat disorders and create pleasant experiences, lead out of traumas, fears, etc. [2]. In summary, sensory accessories are created to improve quality of life, promote development and provide therapeutic support.

## **2. ASSUMPTIONS AND STAGES OF ACTION**

Personalized sensory accessories, including therapeutic accessories, for children with motor and intellectual disabilities are primarily designed to be safe and tailored to the individual needs of a given child. The correct choice of material, color and geometry to support the development of a particular child, taking into account the child's age and the type and degree of disability, will bring tangible benefits to the achievements and development of individual children. Therapeutic toys and sensory accessories for children with intellectual disabilities were carefully designed to support motor skills, manual skills, visual memory and perceptiveness. In

addition, they were designed to best support the therapy and learning process of children with diverse limitations, such as cerebral palsy, Down syndrome and Asperger's syndrome. In this context, the process of designing and adapting the functional features of toys and therapeutic accessories to the specific individual needs of children with diagnosed conditions was crucial. Incremental technologies, especially 3D printing, were the answer to this individual approach and the search for optimal therapeutic solutions. This method, which is now a very important and rapidly growing branch of rapid design technology, made it possible to obtain accurate details from previously prepared 3D models. 3D printing, as one of the many methods of industrial and retail production, allowed for great dynamism in making changes and verifying design concepts. The combination of three-dimensional imaging and fabrication guaranteed a comprehensive approach to an individual child's needs. The project consisted of several stages (Fig.1), the first involving the preparation of design assumptions, including the selection and development of the geometry of therapeutic accessories in CAD software and the selection of safe thermoplastic and/or thermoplastic matrix composite materials. The next stage was technological testing, optimization of the geometry and function of the developed parts, and calibration of the manufacturing process. The next stage consisted of producing a package of standardized samples, including print, material and finishing parameters, consistent with the manufacturing assumptions of the finished parts. This stage also included full material characterization, conducting tests under laboratory conditions in accordance with applicable standards, and prototypes of the developed accessories were produced and subjected to performance testing.

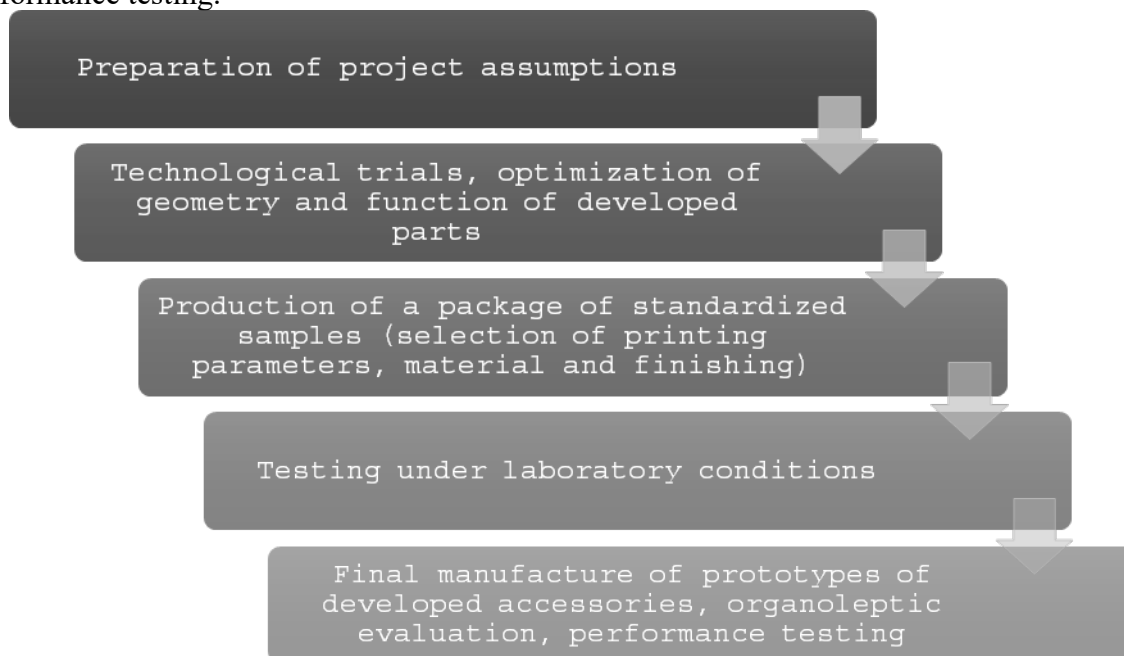
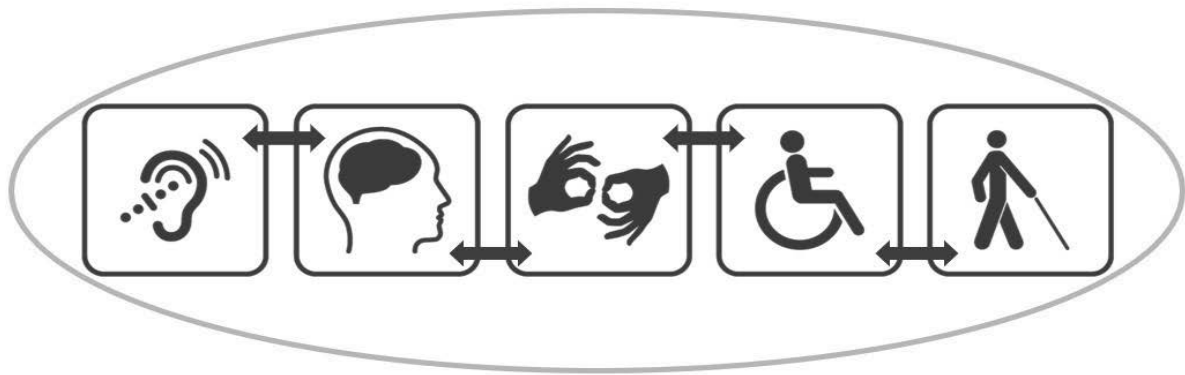


Figure 1. Stages of the project

In the process of designing the sensory elements, several key guidelines were emphasized to develop products that meet the highest quality standards and deliver therapeutic value to their users. In addition, safety of use was a priority from the design stage. Sensory elements are designed and manufactured to provide a safe space for users, eliminating potential risks associated with their use. Adaptation to the needs of individual children is a key element of the



designs developed. Each sensory element module is carefully tailored to meet the individual user's needs, both sensorially and functionally. The selection of materials, colors and geometry plays an important role in the manufacture of the sensory elements. Materials are selected that are safe for health and pleasant to the touch. Colors and shapes are carefully selected to stimulate the senses and generate therapeutic sensations. The age and type of disability of the child are taken into account to tailor accessories to specific age groups and specific developmental needs. Supporting appropriate motor skills is a key aspect of the designs. The mat modules are designed to activate movements and develop the users' motor skills. Developing manual skills and perceptiveness are other goals behind the design of the sensory elements. Through the variety of textures and shapes of the interactive elements, we support the development of these important skills. Through the use of appropriate stimuli and functions (Fig. 2), the accessories provide therapeutic support, helping in the rehabilitation process and the development of users' sensory abilities.



*Figure 2. Support on all levels of disability*

### **3. DESIGN**

As a result of a group discussion at the design stage, two concepts for sensory elements emerged. The decision was made to focus on both simultaneously in order to enrich the design with a variety of accessory applications. Despite the differences in concepts, the two share a common element, namely the method of attachment and the fact that each sensory mat consists of separate modules that are printed in their entirety using a 3D printer. Each of these modules is then combined with the others to create complex pathways, elements or sensory arrays. Two popular CAD (Computer-Aided Design) software environments were used in the design process, namely Inventor and SolidWorks. Inventor is a professional 3D design software developed by Autodesk. It is widely used in the engineering field, especially in the design of machinery, equipment and other mechanical components. Inventor offers a wide range of tools for 3D modeling, kit creation, technical drawings, stress analysis and motion simulation. It allows precise design of parts taking into account various materials and design parameters. Meanwhile, SolidWorks is another advanced CAD software, also popular in the engineering industry. SolidWorks offers comprehensive tools for 3D modeling, animation, stress analysis, technical drawing generation and simulation. It is used to design various types of structures, from simple components to complex assemblies. Both Inventor and SolidWorks use a parametric-type user interface, meaning users can define geometric and structural parameters, making it easy to adapt designs to changing requirements. Both environments offer extensive tools for creating models, assemblies and technical documentation. The posted Figure 3 shows

a common element of both sensory accessory concepts, namely an aluminum guide. Attaching the guide to the wall will allow the sensory element modules to be installed at a height that is accessible to people with disabilities, allowing them to use the modules at hand and eye level.



Figure 3. Aluminum guide a) V-SLOT 1120-SR-200; b) dimensions [5]

Two concepts of sensory elements were developed and described and illustrated in detail. Figures 4 and 5 show the first concept (sensory mat concept). Each module has a joint on the top edge, bottom edge and side edges.

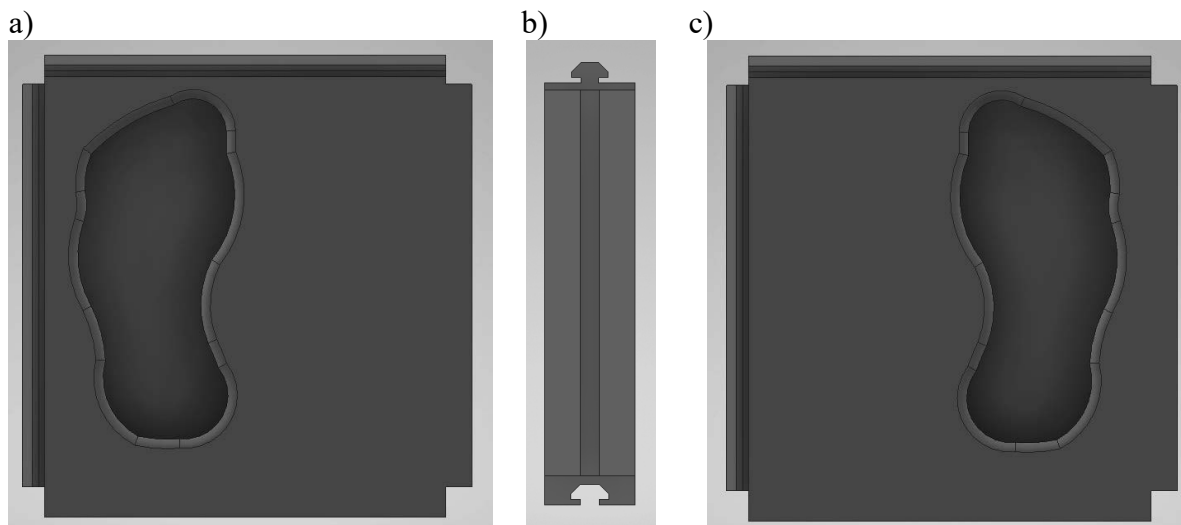
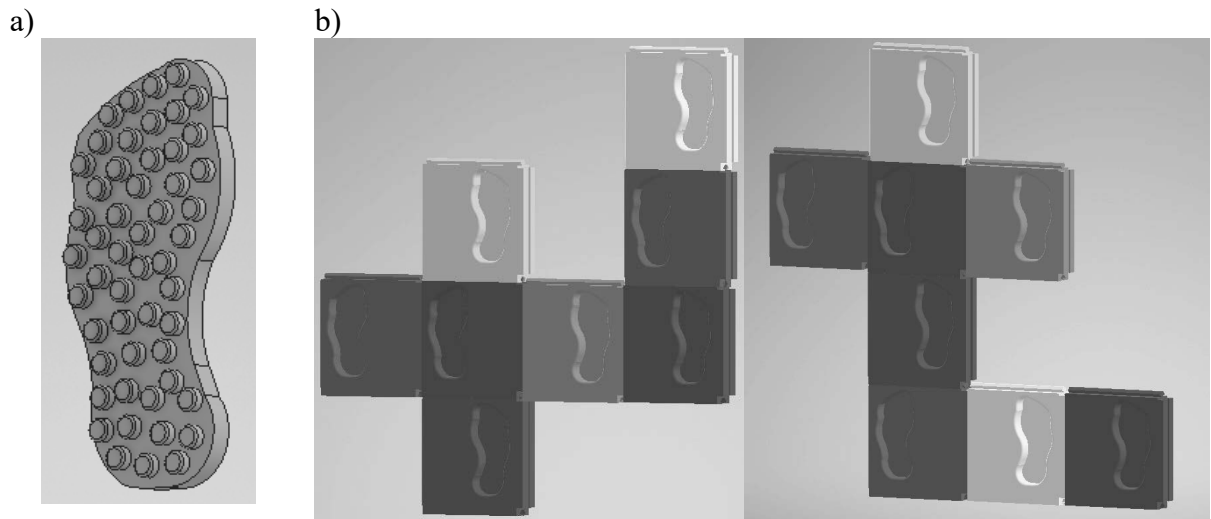


Figure 4. Example photos of sensory path component modules, views of: a) front, (b) side of left module and c) front of right module

The joints make it possible to create a path, that is, to add modules from every possible side (Figures 5). The main purpose of this concept is to create the aforementioned path on the ground. The tiles are designed so that their bottom surface is smooth, as it will be appropriately protected from slipping, so that the entire mat when placed on the ground is safe for the recipient. Figure No. 6 presents sample images of the second concept (sensory book). This concept differs significantly from the first, both in terms of the geometry of the modules and their purpose. In this case, the main goal was to create sensory elements that hang on the wall and are slid into a specially designed slide, as shown in Figure 3a. In addition, there is the

possibility of creating a "sensory book," seen in Figure 7. This interactive book would consist of modules that could be clipped sequentially one after the other into a suitably prepared rack, with the ability to slide out each module at any time. A major difference between the modules in the two concepts is the way they are connected to the slide. In the case of the first concept, the connection is located on the top surface of the module, while in the second concept it was placed on the rear surface. This is a consequence of the fact that the second concept does not involve setting the modules on the ground, which eliminates the need to equip them with anti-slip elements on the back surface of the tiles.



*Figure 5. (a) sample left-fill; (b) sample module assemblies*

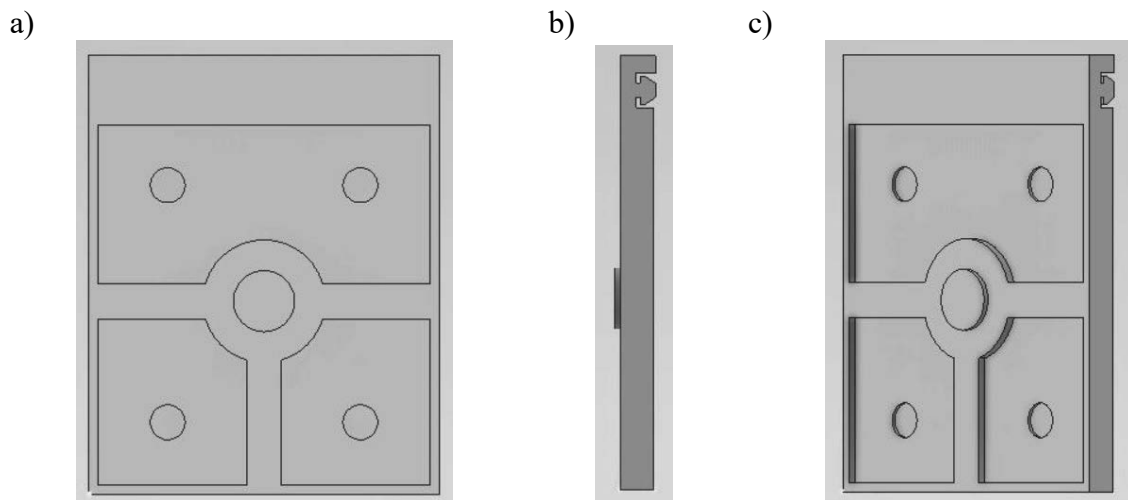


*Figure 6. Module of concept two: (a) front view, (b) side view, (c) front oblique view*

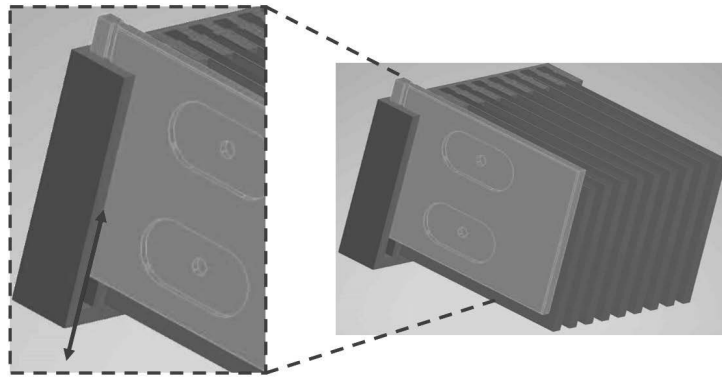


Figure. 7. Assembling the modules of concept two in the form of a sensory book

#### 4. MATERIALS AND PROTOTYPE MANUFACTURING

Sensory accessory modules in the first verification phase, will be manufactured from high-quality PLA. This material is durable and environmentally friendly, and will not only provide a solid structure for each module, but also an aesthetic appearance, adding a unique character to the whole. To enhance the sensory experience, the inserts will be made of flexible TPU or soft silicones. In addition, materials such as strings, yarns, unsharpened pebbles and cotton balls are planned to be attached to their surface. These materials will broaden the spectrum of receiving additional tactile sensations, which will directly translate into a wider impact on the senses of the receiving group. In addition, the modules, which are designed to be placed on the ground, will be equipped with a special anti-slip layer on the underside. This feature will protect the mat from accidental movement, ensuring stability and safety during use. This will allow users to freely explore different textures, confident that the mat will remain solidly in place. After the initial selection of a group of materials, it was decided to use incremental technologies in the manufacturing process. 3D printing in its broadest sense is an attractive manufacturing method because of the range of benefits and possibilities it offers. The ability to personalize and customize sensory components is one of the key aspects of this technology. 3D printing enables rapid prototyping and flexible manufacturing, which is important in the context of sensory accessories that require constant modification and improvement. The variety of materials available for 3D printing allows for the production of modules with varying textures and sensory properties, which is important when it comes to customizing them for specific therapies or user preferences [3].

Ultimately, the FFF method was chosen to produce the sensory accessories in the project due to several factors. One was that 3D printing using the FFF method allows the use of a variety of materials, including thermoplastics, elastomers, metallized filaments and many others. In addition, the FFF method typically has a relatively high printing speed, which allows for rapid production of prototypes and prints. Although other methods, such as SLA or SLS, offer higher resolution, 3D printing using the FFF method is sufficient for many applications, especially those that do not require very precise details [4]. The 3D printers on the equipment of the Nanotechnology and Materials Technology Science and Teaching Laboratory, mainly the Prusa i3 MK3 by Josef Prusa, were used to produce the prototypes. To prepare the g-code, software dedicated to this printer was used, viz: PrusaSlicer-2.6.1 (Fig. 8b).

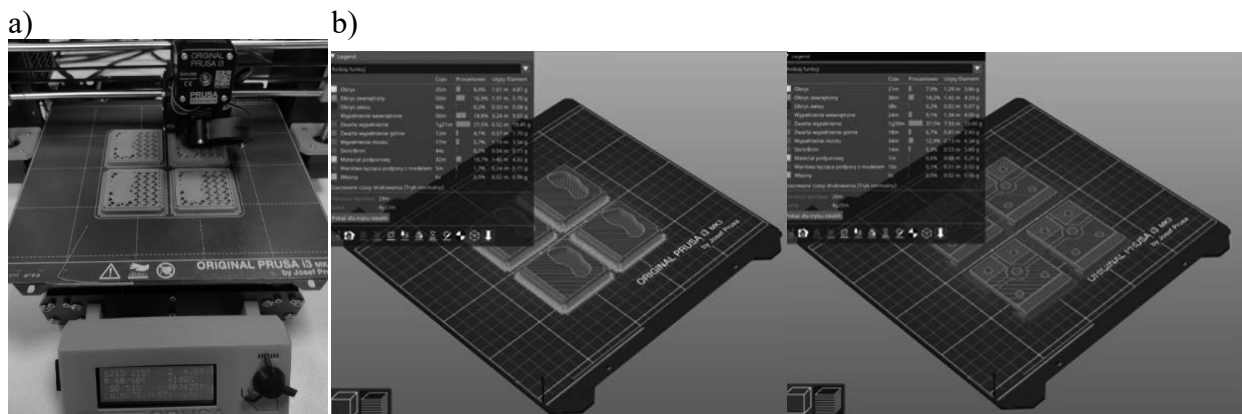


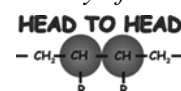
Figure. 9. The process of printing prototypes: a) prototypes in the printer workspace, b) the process of selecting print parameters

## 5. SUMMARY

The project is currently going through the prototype printing phase. After thorough verification of their correctness, it is planned to purchase an adequate amount of filament and the necessary additional materials for the production of full-size modules. At the same time, work is being carried out on filling the cavities in the modules, adjusting their surface in such a way as to ensure that the modules will become completely satisfactory sensory accessories. Due to the nature of the tasks carried out, the Scientific Circle of Plastics Processing and Composites "HEAD TO HEAD" has taken active cooperation with: The Association for the Disabled "Seven" in Katowice has existed continuously since 2011 and School and Kindergarten Complex No. 16 in Gliwice, which in 2020 included Primary School No. 23 and Municipal Kindergarten No. 23. These establishments are home to potential recipients and early testers of the developed as part of the project's variants. These places, full of the energy and joy of the younger generation, are the focus of efforts to create extraordinary spaces for the exploration and development of the senses. The designs of the sensory elements are particularly tailored to the age group up to 14 years, introducing children to the magical world of diverse sensory stimuli. Each module, each element of the mat is designed to create a safe and fascinating space that will stimulate the curiosity and development of the audience. In doing so, no age restrictions are placed. Although originally aimed at children, sensory accessories open the door to everyone, regardless of age. Therefore, with openness, sensory elements are also directed to adults, providing them with the opportunity to enjoy the benefits of the projects. Everyone, regardless of age or individual needs, deserves a unique sensory experience. Tailored to the specific requirements of schools and their students, Sensory Elements creates a unique space where joy, learning and exploration come together in harmony.

### General comments:

The present study was developed through the PBL project entitled. "Personalized sensory accessories for children with disabilities manufactured with 3D printing technology" implemented under the Excellence Initiative - Research University program. Order No. 55/2020 of the Rector of the Silesian University of Technology. The work was carried out by members of the "HEAD TO HEAD" Student Scientific Circle of Plastics and Composites Processing, operating at the Scientific and Teaching Laboratory of Nanotechnology and Materials Technology at the Faculty of Mechanical Engineering.



**BIBLIOGRAPHY**

1. Borkowska M.: Sensory integration in child development. Neurophysiological basics, Harmonia Publishing House, 2018
2. <https://www.medme.pl/artykuly/mata-sensoryczna-dla-dzieci-niemowlat,73660.html>, accessed: 28/12/2023
3. Budzik G., Woźniak J., Przeszłowski Ł.: 3D printing as an element of the future industry, G. Budzik, J. Woźniak, Ł. Przeszłowski, Rzeszow University of Technology, 2022
4. DOI: <https://doi.org/10.17814/mechanik.2017.3.46>
5. <https://allegro.pl/oferta/profil-aluminiowy-c-11x20-l-200cm-prowadnica-track-12939650334?fromVariant=12939632422>, accessed: 28.12.2023
6. Macg A.: The use of educational and therapeutic methods in working with children and adolescents with moderate, severe and profound intellectual disabilities, FOSZE Educational Publishing House, 2016
7. <https://nature-solution.com/zabawki-sensoryczne-dla-niemowlat-i-malych-dzieci-dlaczego-warto/>, accessed: 04.01.2024
8. <https://slimebox.pl/czym-jest-sensoryka>, accessed: 04.01.2024



26th January 2024  
Gliwice, Poland

DEPARTMENT OF ENGINEERING MATERIALS AND BIOMATERIALS  
FACULTY OF MECHANICAL ENGINEERING  
SILESIA UNIVERSITY OF TECHNOLOGY

## INTERNATIONAL STUDENTS SCIENTIFIC CONFERENCE

### Finite elements analysis of hip joint endoprosthesis

Jakub Polis<sup>a</sup>, Jakub Bicz<sup>a</sup>, Zuzanna Buchaj<sup>b</sup>, Rafał Szymik<sup>c</sup>, Zuzanna Zielińska<sup>c</sup>, Mateusz Szojda<sup>d</sup>, Agata Śliwa<sup>e</sup>, Marek Sroka<sup>e</sup>, Amadeusz Dziwis<sup>e</sup>, Wojciech Mikołajko<sup>e</sup>

<sup>a</sup> Student of Silesian University of Technology, Faculty of Mechanical Engineering  
email: jakupol064@student.polsl.pl; jakubic839@student.polsl.pl

<sup>b</sup> Student of Silesian University of Technology, Faculty of Biomedical Engineering  
email: zb301191@student.polsl.pl

<sup>c</sup> Student of Silesian University of Technology, Faculty of Materials Engineering  
e-mail: zz304779@student.polsl.pl; rs301942@student.polsl.pl

<sup>d</sup> Student of the Academic High School of the Silesian University of Technology in Gliwice  
email: matiszrojda@icloud.com

<sup>e</sup> Silesian University of Technology, Faculty of Mechanical Engineering, Department of Engineering Materials and Biomaterials

email: agata.sliwa@polsl.pl; marek.sroka@polsl.pl; amadeusz.dziwis@polsl.pl; wojciech.mikolajko@polsl.pl

**Abstract:** This paper presents an FEM analysis of the distribution of stresses, displacements and deformations resulting from the application of a specific force on a hip endoprosthesis, depending on the material used – which was Ti-6Al-4V alloy and steel 1.4541 (X6CrNiTi18-10). The analysis was carried out using SOLIDWORKS software. The points of highest stress and displacement were determined, as well as the value of the critical force at which deformation of the component occurs.

**Keywords:** hip endoprosthesis, FEM analysis, stresses, deformations.

### 1. INTRODUCTION

The development of modern materials used in medicine has naturally necessitated an increase in their quality, improvements to the biomaterials already in use and attempts to introduce them into medical practice [1].

When an implant is inserted into the human body, it is assumed that it will fulfil a specific function over the long term. By taking into account the stress distribution at the implant-bone interface, by ensuring a secure insertion into the bone, a good bonding and bone positioning with the correct implant configuration throughout the implant's lifespan, it is possible to create the conditions that accompany the normal healing process of a fractured bone [1].

Biomaterials are accepted by the human body and some of them (hydroxyapatite ceramics, bio-glass, modified carbon materials) permanently fuse with living tissues, participating in its

regeneration. According to the European Society for Biomaterials: "a biomaterial is any substance (other than a drug) or combination of substances of synthetic or natural origin, that can be used at any time, in whole or in part, to treat, augment or replace tissue of an organ, organ or body function" [1].

Implants are any medical devices made of one or more biomaterials, that can be placed inside the body, as well as partially or completely under the epithelial surface and can remain for a prolonged period of time in the body; they can be qualified based on the duration of their safe use for the patient's body [1].

In various types of medical literature, it is reported that at birth, the human body is made up of approximately 270 bones, and in adulthood this number will be reduced to 206, as some bones are fused together. The hip joint transfers the load from the upper body to the lower abdomen. The hip joint is a synovial joint that connects the lower limb to the trunk. It provides a wide range of movement and consists of an acetabulum and a synovial ball (femoral head). As the size of the femoral head increases, the range of movement increases with the joint. The hip joint can support the entire weight of the body while providing stability mainly during the movement of the trunk on the femur, which occurs during walking and running [2].

The head of the femur is articulated with the pelvis and provides the joint with varying degrees of freedom to aid joint movement. In cases of injury or trauma, and due to age, these joints have to be replaced with artificial implants. On the historical side, at the beginning of 1935, hip arthroplasty was an effective medical procedure, which was then used for all kinds of hip disorders. Currently, we can learn from many publications that total hip arthroplasty is widely known as one of the best advanced techniques in healthcare. In total hip endoprosthesis, the femoral head is separated from the acetabulum by inserting a bearing surface between the two parts. With this procedure, pain is drastically reduced and movement is restored. Stems are the main elements that provide stability after arthroplasty. The femoral head is fixed on the stem, followed by the acetabular cup and the posterior acetabulum. Currently, the success rate of hip arthroplasty is 10 years and 95% survival rate in patients over 70 years of age [2].

Since the beginning of hip replacement, various biomaterials have been used as bearing surfaces. The pair of bearings used by orthopaedic surgeons are 'metal on polyethylene' (MoP) and 'ceramic on polyethylene' (CoP), which are well known as hard-on-soft bearings; and 'metal on metal' (MoM), 'ceramic on ceramic' (CoC) and 'ceramic on metal' (CoM), which are well known as hard-on-hard bearings. Hard-on-soft bearings suffer long-term failures due to osteolysis caused by polyethylene wear [2].

The most commonly used endoprostheses in the treatment of degenerative diseases of the hip joint are total hip endoprostheses, classic cementless endoprostheses, usually made of molybdenum-chromium-cobalt alloys with a spatial titanium layer on the surface, imitating the structure of natural bone [3].

## 2. MATERIALS AND METHODOLOGY

The analysed component of a hip endoprosthesis is a head, neck assembly with an angle of  $135^\circ$  and a stem. Two models of the endoprosthesis are presented, made of Ti-6Al-4V alloy and 1.4541 steel, respectively. The main consideration is that the endoprosthesis should be able to carry a load of 2.300 N without losing its integrity. In addition, the material used should be biologically safe for the patient.



### 3. SELECTION OF MATERIALS

Ti-6Al-4V alloy is one of the most commonly used titanium alloys in biomedical applications. It exhibits a dual-phase structure, consisting of an  $\alpha$  phase, crystallizing in a hexagonal arrangement, and a  $\beta$  phase with a body-centered cubic structure. The  $\alpha+\beta$  alloys can be subjected to a precipitation hardening process – solution treatment, with subsequent aging – which allows to increase strength properties by 30-50%, while maintaining the Young's modulus value at a similar level [4,5].

Titanium alloys find a number of applications in prosthetics and medical technology - they are used, among other things, in the manufacture of dental implants, joint endoprotheses and screws and brackets used in orthopaedics. This is due to their favourable properties – such as high biocompatibility and corrosion resistance, and high specific strength. In addition, they exhibit Young's modulus values approximately 50% lower than those of stainless steel and cobalt alloys, while maintaining similar tensile strength values [5].

*Table 1. Chemical composition of Ti-6Al-4V alloy [8]*

Chemical element	Min [%]	Max [%]
V	3.5	4.5
Al	5.5	6.75
Fe	-	0.3
O	-	0.2
C	-	0.08
N	-	0.05
H	-	0.015
Y	-	0.005
Ti	Balance*	

\* The percentage of titanium is determined by difference and does not need to be determined or certified.

*Table 2. Selected mechanical and physical properties of Ti-6Al-4V alloy*

Elastic modulus [N/m <sup>2</sup> ]	1.0480031e+11
Poisson's ratio	0.31
Shear stress ratio [N/m <sup>2</sup> ]	4.1023807e+10
Specific mass [kg/m <sup>3</sup> ]	4428.784
Ultimate tensile strength [N/m <sup>2</sup> ]	1050000000
Yield strenght [N/m <sup>2</sup> ]	827370880
Thermal expansion coefficient [K]	9e-06
Thermal conductivity coefficient [W/(m*K)]	586.04
Specific heat [J/(kg*K)]	586.04

Titanium alloys have a higher corrosion resistance than stainless steels and cobalt alloys, which is one of the factors contributing to their high biocompatibility. The corrosion resistance of titanium is due to the formation, under the influence of the corrosive environment, of a passive

titanium oxide film on their surface, which protects against further oxidation. An important feature favouring the use of titanium for the manufacture of long-lasting implants is their ability, unique compared to other metallic biomaterials, to form a bond with bone [1,5,6].

The disadvantages of titanium alloys include their relatively low wear resistance. This is due to breakdown of oxide layer under loading conditions – leading to uneven wear of the material, resulting in increased surface roughness. Another problem is the risk of the release of vanadium and aluminium ions – with toxic and carcinogenic effects [7].

Second material used in simulation is a austenitic chromium-nickel stainless steel (X6CrNiTi18-10 steel). Stainless steels were, next to precious metals, the first materials used to manufacturing implants – they have been used since the 1930s. Nowadays, stainless steels are one of the most frequently used metal biomaterials – especially in the case of short-term implants. Their applications include wires used in dentistry, screws and plates used in orthopedics, but also – in the case of some types of steel, long-term implants such as joint endoprostheses and stents [1,5].

Their widespread use is determined by their relatively low cost, good availability and acceptable mechanical properties. However, a limiting factor for the use of stainless steel as a material for manufacturing of permanent implants is its relatively low corrosion resistance – compared to cobalt and titanium alloys. In the aggressive environment of body fluids, stainless steel implants may be subject to intergranular corrosion, as well as crevice corrosion. Furthermore, due to the simultaneous interaction of the corrosive environment and tensile stresses may occurs stress corrosion cracking – in case of which, stresses causing the cracks could be significantly lower than the yield and strength limits of the material. As a result, this contributes to a reduction in the fatigue strength of the implants. The steel used in the simulation is characterised by increased resistance to intergranular and crevice corrosion, thanks to the addition of titanium. Titanium, which has a higher affinity for carbon than chromium, binds the carbon in the steel, preventing the formation of chromium carbides at grain boundaries – and thus the depletion of chromium in the surrounding areas [1,4,5,10].

The factor, which is unfavourable to the use of steel as an endoprosthesis material, is also the high value of Young's modulus. Another particularly important problem is the risk of nickel and chromium being released into the body, which can occur through corrosion or abrasive wear. This can result in allergic reactions and, in extreme cases, metallosis, causing inflammation of the tissues surrounding the implant. In addition, both nickel and chromium exhibit toxic and carcinogenic properties [1,5,7].

Table 3. Chemical composition of steel 1.4541 (X6CrNiTi18-10) [10]

Chemical element	Min [%]	Max [%]
C	-	0.08
Si	-	1.0
Mn	-	2.0
P	-	0.045
S	-	0.03
Cr	17	19
Ni	9	12
Ti	-	0.7

Table 4. Selected mechanical and physical properties of steel 1.4541 (X6CrNiTi18-10)

Elastic modulus [N/m <sup>2</sup> ]	2e+11
Poisson's ratio	0,28
Shear stress ratio [N/m <sup>2</sup> ]	7.9e+10
Specific mass [kg/m <sup>3</sup> ]	7900
Ultimate tensile strength [N/m <sup>2</sup> ]	600000000
Yield strenght [N/m <sup>2</sup> ]	400000000
Thermal expansion coefficient [K]	1.1e-0,5
Thermal conductivity coefficient [W/(m*K)]	14
Specific heat [J/(kg*K)]	440

#### 4. CAD GEOMETRIC MODEL

A model of the hip endoprosthesis was made using SOLIDWORKS to carry out strength analysis by means of computer simulation. The designed hip endoprosthesis model is shown in Figure 1a.

#### 5. BOUNDARY CONDITIONS

The loading and boundary conditions used are in accordance with ASTM F2996-13 and ISO 7206 4:2010(E) [11]. The following boundary conditions were adopted in the computer simulation:

- A finite element mesh was superimposed on the hip endoprosthesis model (Figure 1b),
- A force of 2,300 N was applied, the value of which is derived from ASTM F2996-13 and ISO 7206-4:2010(E) (Figure 1c),
- The location of force application and immobilization geometry of the hip endoprosthesis model are shown in Figure 1c.

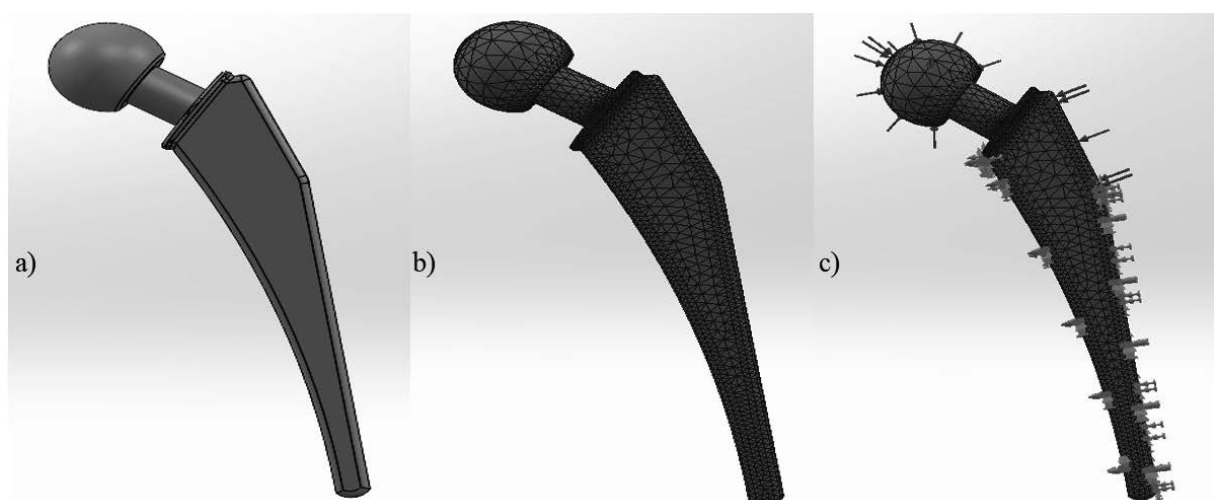


Figure 1. CAD model of hip endoprosthesis (a); with superimposed finite element mesh (b); with superimposed finite element mesh, visible direction of forces and immobilised endoprosthesis geometry (c)

## 6. ANALYSIS OF RESULTS

Numerical stress analysis was performed based on the Huber-Mises hypothesis. After loading the component, stress diagrams were obtained, the values of which are expressed in MPa. Figure 2 shows the distribution of stresses developed during the given loading.

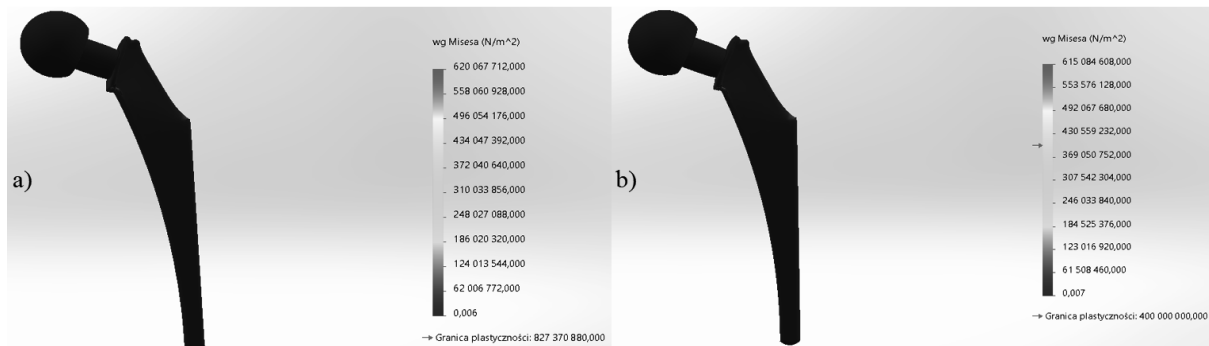


Figure 2. Huber-Mises stress reduction distribution for Ti-6Al-4V alloy (a) and steel 1.4541 (b)

The purpose of the subsequent computer simulation carried out was to determine the magnitude of the displacement under the application of a given force and to generate the displacement diagrams of the structure, which are shown in Figure 3. As a result of the load, the geometric dimensions of our model can change. The largest displacement in each material analysed occurred at the head surface of the endoprosthesis.

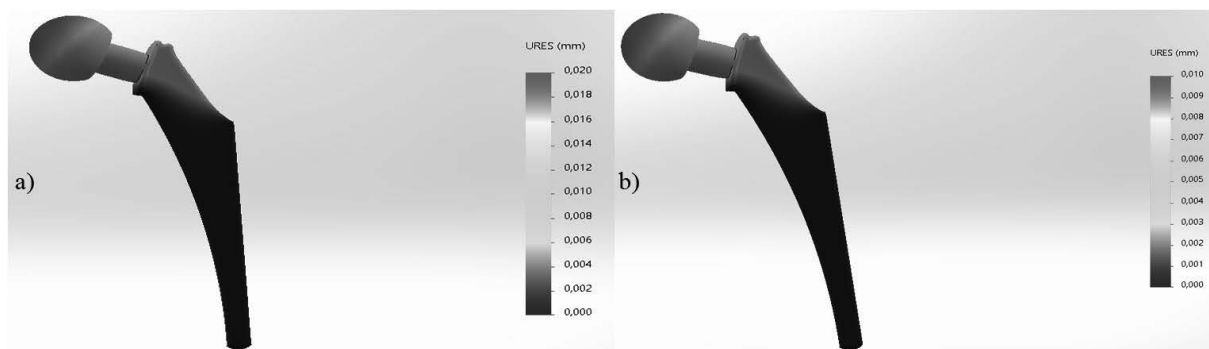


Figure 3. Displacement distribution for Ti-6Al-4V alloy (a) and steel 1.4541(b)

The last simulation carried out was to determine the critical force causing the deformation. Figure 4 shows the equivalent deformation represented by the largest force required to deform the axis.

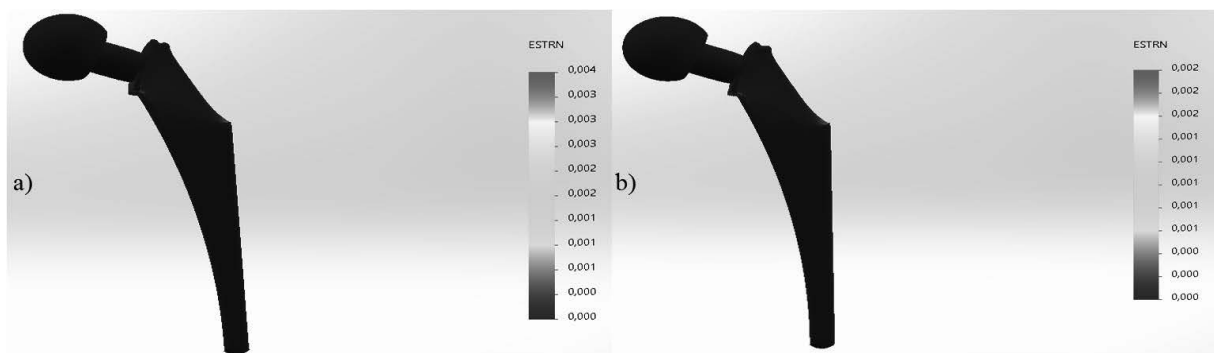


Figure 4. Equivalent deformation for Ti-6Al-4V alloy (a) and steel 1.4541 (b)

The overall results of the simulations performed are shown in Table 5.

Table 5. Summary of overall results from computer simulations carried out

Material used	Maximum stress value [MPa]	Maximum displacement [mm]	Maximum deformation value
Ti-6Al-4V alloy	620.067	0.020	0.004
Steel 1.4541 (X6CrNiTi18-10)	615.084	0.010	0.002

## 7. CONCLUSION

The results of the strength analysis indicate that both Ti-6Al-4V alloy and steel 1.4541 are suitable for use as hip joint endoprosthesis material – because, even under significant loading, exhibited negligible displacement and deformation values, with similar stresses values.

The highest stresses were obtained for the Ti-6Al-4V alloy. It is worth noting, however, that the difference between the materials analysed is negligible – it amount only 4.983 MPa.

A larger displacement was recorded for the model made of Ti-6Al-4V alloy. Its value is twice as high as when using 1.4541 steel.

The largest deformation was obtained for the model made of Ti-6Al-4V alloy – in the case of 1.4541 steel, it was twice as small.

Of the materials used in simulation, steel 1.4541 (X6CrNiTi18-10) can be considered as optimal material for hip endoprosthesis due to its satisfactory strength properties, resulting in the lowest values of displacement, deformation and stress for this material.

## ACKNOWLEDGEMENTS

The work was created as a result of the project as part of project based learning - PBL, in the X competition under the Initiative of Excellence - Research University, Silesian University of Technology.

**BIBLIOGRAPHY**

1. Świczko-Żurek B.: Biomateriały, Wydawnictwo Politechniki Gdańskiej, 2009.
2. Chethan K. N., Shyamasunder Bhat N., Zuber M., Satish Shenoy B.: Finite Element Analysis of Different Hip Implant Designs along with Femur under Static Loading Conditions. *Journal of Biomedical Physics & Engineering*, 2019.
3. <https://medicus-bonus.pl/staw-biodrowy-budowa-i-rodzaje-endoprotez/> - data dostępu 01.12.2023.
4. Dobrzański L.A., Podstawy nauki o materiałach i metaloznastwo, Wydawnictwo Naukowo-Techniczne, Warszawa, 2002.
5. Chen Q., Thouas G. A., Metallic implant biomaterials. *Materials Science and Engineering: R: Reports*, 87, 2015, p.1–57.
6. Manmeet Kaur, K. Singh, Review on titanium and titanium based alloys as biomaterials for orthopaedic applications, *Materials Science and Engineering: C*, volume 102, 2019, p.844-862.
7. Liyao Guo, Seyed Ataollah Naghavi, Ziqiang Wang, Swastina Nath Varma, Zhiwu Han, Zhongwen Yao, Ling Wang, Liqiang Wang, Chaozong Liu, On the design evolution of hip implants: A review, *Materials & Design* vol. 216, 2022, 110552.
8. <http://bqw.csstgc.com.cn/userfiles/04d50d7598c54325a4f12f868710a407/files/teckSolution/2019/11/Standard%20Specification%20for%20Wrought%20Titanium-6Aluminum-4Vanadium%20Alloy%20for%20Surgical%20Implant%20 Applications.pdf> - data dostępu 01.12.2023 r.
9. Gierzyńska-Dolna M., Wiśniewska-Weinert H., Adamus J., Tribologiczne i materiałowe uwarunkowania stosowania endoprotez stawowych, *Tribologia* 1, 2009, p.47-62.
10. <https://virgamet.pl/x6crniti1810-aisi-321-321h-x8crniti1810-z6cnt1810-1h18n9t-stal-nierdzewna> - data dostępu 01.12.2023 r.
11. Chethan K. N., Shyamasunder Bhat N., Zuber M., Satish Shenoy B., Finite element analysis of hip implant with varying in taper neck lengths under static loading conditions, *Computer Methods and Programs in Biomedicine*, 2021.



26th January 2024  
Gliwice, Poland

DEPARTMENT OF ENGINEERING MATERIALS AND BIOMATERIALS  
FACULTY OF MECHANICAL ENGINEERING  
SILESIA UNIVERSITY OF TECHNOLOGY

## INTERNATIONAL STUDENTS SCIENTIFIC CONFERENCE

### The influence of environmental conditions on the solar panel work

P. Radek<sup>a</sup>, M. Sładek<sup>a</sup>, P. Kołodziejczyk<sup>a</sup>, J. Tłołka<sup>a</sup>, S. Nowak<sup>b</sup>, G. Nowak<sup>cd</sup>, M.M. Szindler<sup>d</sup>, J. Popis<sup>c</sup>, M. Szindler

<sup>a</sup> Student of Silesian University of Technology, Faculty of Electrical Engineering, Akademicka 3, 44-100 Gliwice

<sup>b</sup> Student of Silesian University of Technology Faculty of Mechanical Engineering, Konarskiego 18a, 44-100 Gliwice

<sup>c</sup> Łukasiewicz Research Network – Krakow Institute of Technology, Centre of Biomedical Engineering, Zabrze, Poland

<sup>d</sup> Silesian University of Technology, Faculty of Biomedical Engineering, Department of Biomaterials and Medical Devices Engineering, Zabrze, Poland

<sup>e</sup> Silesian University of Technology, Faculty of Mechanical Engineering, Department of Engineering Materials and Biomaterials, Gliwice, Poland

<sup>f</sup> Silesian University of Technology, Faculty of Mechanical Engineering, Didactic Laboratory of Nanotechnology and Material Technologies, Gliwice, Poland

E-mail (corresponding author): [magdalena.szindler@polsl.pl](mailto:magdalena.szindler@polsl.pl)

**Abstract:** The article presents the influence of weather conditions and surroundings on the operation of a solar panel located in Gliwice. As part of the research, a system was constructed in which a 100 W solar panel was connected to a portable power generator, with a current-voltage meter connected between them. The work of the panel was observed and analyzed in the following months of 2023. The best months turned out to be June and July, when 15.3 kW and 14.9 kW were produced, respectively. In total, in 2023 it was possible to produce over 93kW from a 100W solar panel. As the number of sunny hours per month increased, the amount of energy produced increased, while the average monthly cloud cover had a negative impact on its work.

**Keywords:** photovoltaics, solar panels, environmental conditions

## 1. INTRODUCTION

The solar panels work depending on where they are installed in different environmental conditions. For example, the number of sunny hours in Poland is 1600, of which only 15% are fully sunny hours. Annual resources of solar energy on horizontal surfaces in Poland are estimated at approximately 1100 kWh/m<sup>2</sup> to 1,250 kWh/m<sup>2</sup> per year, of which 780 kWh/m<sup>2</sup> falls in the months from April to September [1-7]. The amount of solar energy that reaches the panels and can be processed depends on many factors (e.g. installation location, average daily

temperature, cloud cover, pollution, etc.). To make it possible to compare different PV modules, their ratings are provided for standard atmospheric conditions, i.e. STC (Standard Test Conditions) [5-9]. However, the actual working conditions differ from the standard ones, which determine, among others: nominal power or efficiency. Therefore, most reputable manufacturers increasingly provide normal conditions, i.e. NOCT (Normal Operating Cell Temperature), next to STC conditions. The data for NOCT conditions are much closer to those achieved by an operating photovoltaic installation. Therefore, in an extremely rapidly changing climate, it is extremely important to create up-to-date databases of atmospheric conditions affecting the operation of solar panels not only globally but also locally [4-12].

Many people who are considering installing a photovoltaic installation are afraid that the impact of weather on photovoltaic panels may limit their effectiveness and efficiency. Does the variability of seasons affect photovoltaics, especially when the number of sunny days in Poland is not as impressive as in other latitudes. Therefore, the scientific goal of the article was to examine the impact of the location and environmental conditions in Gliwice and the surrounding area on the operation of the solar panel.

## 2. MATERIALS AND METHODS

The 100W monocrystalline silicon photovoltaic panel from Jackery company was used for the research. The ethylene tetrafluoroethylene (ETFE) laminated case extends the lifespan of the solar panel, and weighs in total just 4 kilograms. It's lightweight, foldable, IP65 waterproof-rated, and easy to carry around for taking on outdoor applications. The technical parameters of the photovoltaic panel used in the tests are presented in Table 1.

The panel was connected to the Jackery Explorer 500 Portable Power Station. This station is equipped with a 518 Wh (24 Ah, 21.6 V) lithium-ion battery. A current-voltage meter is connected between the photovoltaic panel and the station (Figure 1). The system was set to the south and measurements were taken at two times: morning and afternoon. This enabled readings in 2023 and its assessment in terms of obtaining energy from the sun in Gliwice, Poland.

*Table 1. Technical parameters of the photovoltaic panel used in the tests*

<b>Model</b>	SolarSaga 100
<b>Peak Power</b>	100 W
<b>Cell Efficiency</b>	23%
<b>Power Voltage</b>	18V
<b>Power Current</b>	5.55A
<b>Open Circuit Voltage</b>	21.6V
<b>Short Circuit Current</b>	6.1A
<b>Operating Temperature Range</b>	-10÷65°C
<b>Dimensions (unfolded)</b>	1220x535x5mm
<b>Dimensions (folded)</b>	610x535x35mm



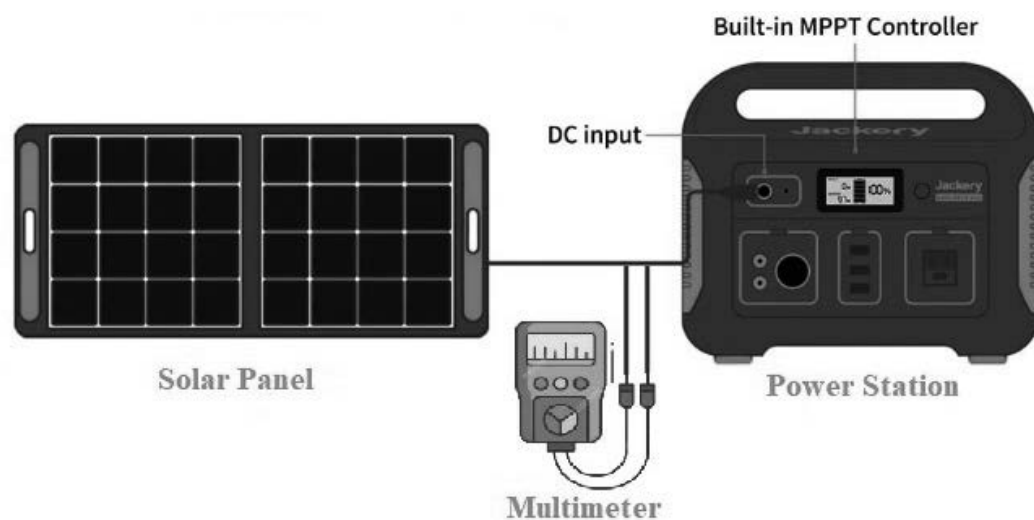


Figure 1. Scheme of the system for obtaining and recording energy from a solar panel.

### 3. RESULTS

Figure 2 shows the amount of power obtained from a 100W Jackery solar panel in 2023 divided into months. In 6 months, we managed to produce power of over 10kW. The best months turned out to be June and July, when 15.3 kW and 14.9 kW were produced, respectively. In total, in 2023 it was possible to produce over 93kW from a 100W solar panel.

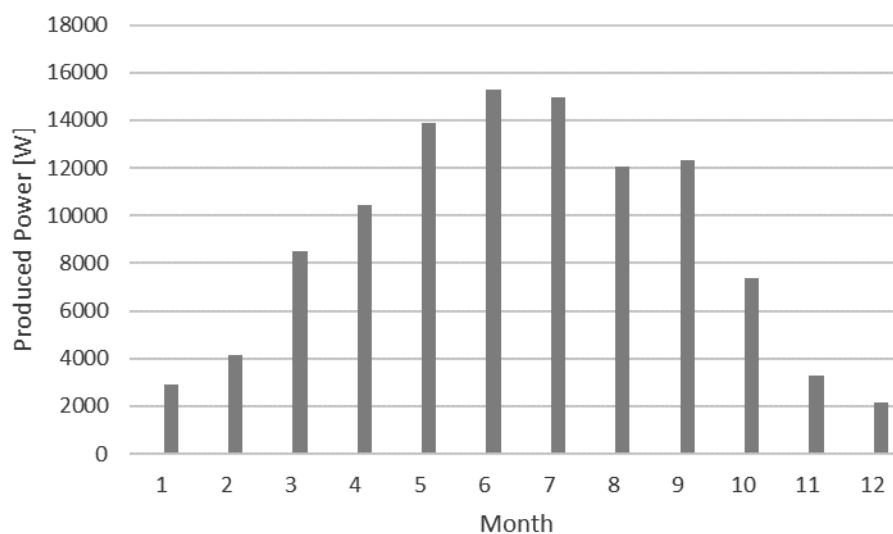


Figure 2. Energy produced by a 100W solar panel in 2023 divided by month

Figure 3 shows the impact of the number of sunny hours on the power produced. Despite the tendency that the amount of power produced increases with the increase in the number of sunny hours, it is not a linear trend. It is also influenced by other factors, such as the number of days in a month, ambient temperature, etc. The number of sunny days exceeding 120 in month enabled

the production of power exceeding 10kW. In turn, Figure 4 shows the impact of average monthly cloud cover on the power produced by the solar panel. Although there is a downward trend with increasing cloud cover, it is also not a linear trend. As in the previous case, other conditions also influence this. Cloud cover of up to 50% enabled effective energy harvesting.

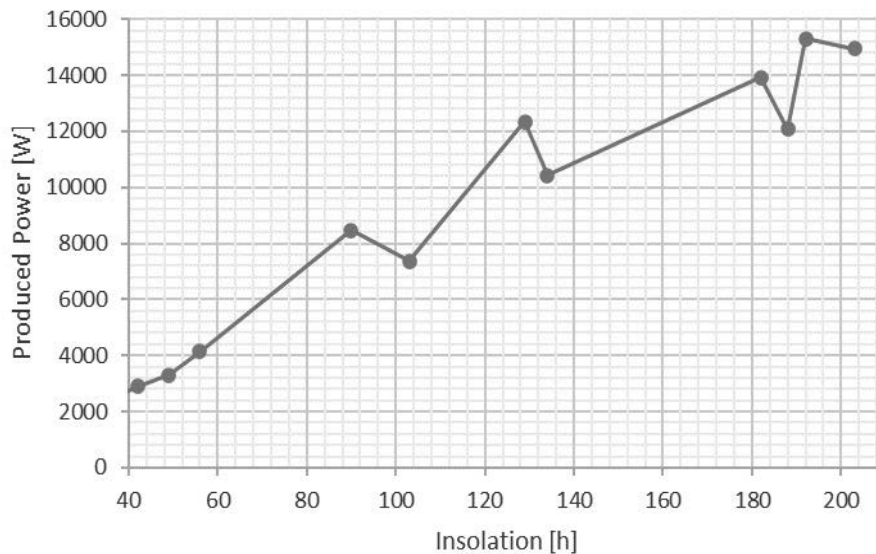


Figure 3. The influence of the number of sunny days in a month on the power produced by a solar panel

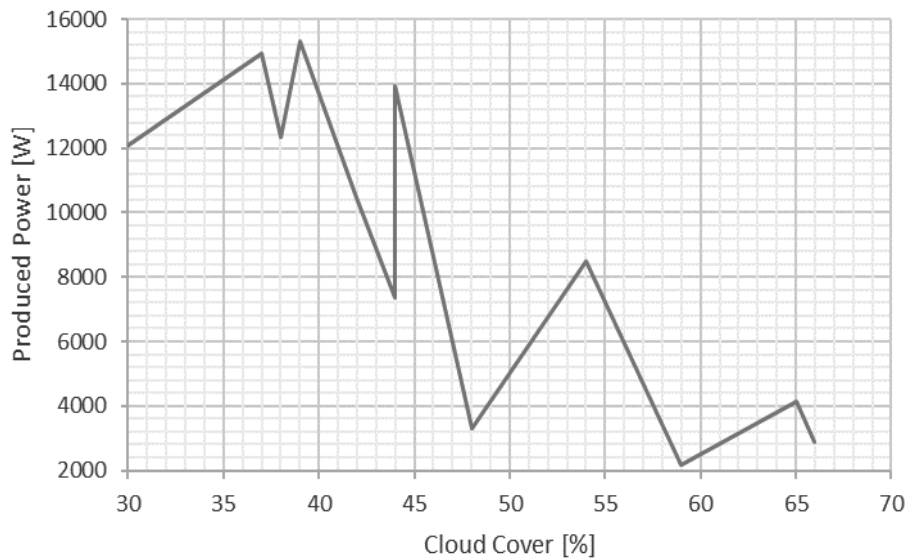


Figure 4. The influence of the average degree of cloudiness in a month on the power produced by the solar panel

#### 4. CONCLUSIONS

As part of the article, a portable station for obtaining and recording electricity using solar panels was developed. The influence of weather conditions in Gliwice on the operation of the solar panel was observed. For 6 months in 2023, it was possible to obtain over 10kW of electricity per month from a 100W solar panel. In total, in 2023 it was possible to produce over 93kW from a 100W solar panel. As the number of sunny hours per month increased, the amount of energy produced increased, while the average monthly cloud cover had a negative impact on its work.

#### BIBLIOGRAPHY

1. A. Gholami, M. Ameri, et. al. Impact of harsh weather conditions on solar photovoltaic cell temperature: Experimental analysis and thermal-optical modeling, *Solar Energy* 252 (2023) 176-194.
2. A.Y. Al-Hasan, A new correlation for direct beam solar radiation received by photovoltaic panel with sand dust accumulated on its surface, *Solar Energy* 63/5 (1998) 323-333.
3. N.S. Beattie, Understanding the effects of sand and dust accumulation on photovoltaic modules, *Renewable Energy* 48 (2012) 448-452.
4. E.D. Clarke, *Solar energy and weather*, John Wiley & Sons Ltd on behalf of Royal Meteorological Society (2022) 73-92.
5. S. Ghazi, The effect of weather conditions on the efficiency of PV panels in southeast of UK, *Renewable Energy* 69 (2014) 50-59.
6. B. Igliński, G. Piechota, et al., The assessment of solar photovoltaic in Poland: the photovoltaics potential, perspectives and development, *Clean Technologies and Environmental* 25 (2023) 281–298.
7. M. Dzikuć, A. Piwowski, et. al. The importance and potential of photovoltaics in the context of low-carbon development in Poland, *Energy Storage and Saving* 1/3 (2022) 162-165.
8. J. Rudniak, Comparison of local solar radiation parameters with data from a typical meteorological year, *Thermal Science and Engineering Progress* 16 (2022) 2-8.
9. C. Coskun, Z. Oktay, Estimation of monthly solar radiation distribution for solar energy system analysis, *Energy* 36/2 1319-1323.
10. R. Gnatowska, E. Moryń-Kucharczyk, The place of photovoltaics in Poland's energy mix, *Energies*, 14 (2021) 1471- 1477.
11. B. Igliński, U. Kielkowska, G. Piechota, et al., Can energy self-sufficiency be achieved? Case study of Warmińsko-Mazurskie Voivodeship (Poland), *Clean Technologies and Environmental Policy* 23 (2021) 2061-2081.
12. J. Duda, R. Kusa, Development of Roadmap for Photovoltaic Solar Technologies and Market in Poland, *Energies* 15/1 (2022), 174-178.



26th June 2023  
Gliwice, Poland

DEPARTMENT OF ENGINEERING MATERIALS AND BIOMATERIALS  
FACULTY OF MECHANICAL ENGINEERING  
SILESIA UNIVERSITY OF TECHNOLOGY

## INTERNATIONAL STUDENTS SCIENTIFIC CONFERENCE

### Recycled filament- a review

M. Rejek<sup>a</sup>, S. Jędrzejewski<sup>b</sup>, Ł. Kołodziej<sup>c</sup>, D. Markusik<sup>d</sup>, D. Tatar<sup>e</sup>,  
A. Woszczak<sup>f</sup>, B. Chadzima<sup>g</sup>, M. Król<sup>h</sup>, A. J. Nowak<sup>i</sup>

<sup>a</sup> Studentka kierunku Mechanika i Budowa Maszyn: Technologie Spawalnicze,  
e-mail: monirej772@student.polsl.pl,

<sup>b</sup> Student kierunku Inżynieria Materiałowa, e-mail: szymjed659@student.polsl.pl

<sup>c</sup> Student kierunku Technologia Chemiczna: Technologia Polimerów i Tworzyw Sztucznych,  
e-mail: lukakol625@student.polsl.pl,

<sup>d</sup> Student kierunku Automatyka i Robotyka Przemysłowa: Zintegrowane systemy wytwarzania,  
e-mail: dorimar256@student.polsl.pl,

<sup>e</sup> Student kierunku Inżynieria Materiałowa, e-mail: danitat271@student.polsl.pl,

<sup>f</sup> Student kierunku Inżynieria Materiałowa, e-mail: adamwos244@student.polsl.pl

<sup>g</sup> Research Centre UNIZA, University of Zilina, Univerzitna 8215/1, 010 26 Zilina, Slovakia

<sup>h</sup> Politechnika Śląska, Wydział Mechaniczny Technologiczny, Katedra Materiałów  
Inżynierskich i Biomedycznych, e-mail: mariusz.krol@polsl.pl,

<sup>i</sup> Politechnika Śląska Wydział Mechaniczny Technologiczny, Laboratorium Naukowo  
Dydaktyczne Nanotechnologii i Technologii Materiałowych, ul. Towarowa 7a, 44-100 Gliwice;  
e-mail: agnieszka.j.nowak@polsl.pl

**Abstract:** The progress in recycling materials for 3D printing has been ongoing, with researchers and industry professionals exploring various approaches to enhance sustainability in additive manufacturing. Companies and individuals have been experimenting with tools and machines that can grind down plastic prints into pellets, which can then be extruded to create new filament. Some companies are working on closed-loop systems where plastic waste generated during 3D printing processes is collected, processed, and reused within the same manufacturing environment. This approach aims to reduce overall material waste. The work presented here provides an overview of the materials used in recycling to produce a new filament for 3d printing using the FFF technique. Presented the achievements to date in the field of plastic recycling. It's important to note that the progress in recycling materials for 3D printing is a dynamic field, and new developments may have occurred.

**Keywords:** recycled filament, fused filament fabrication, waste material,

### 1. INTRODUCTION

To begin with, it is important to clarify the concept of what is recycled filament? Filament recycling is the process of converting used plastic printing threads into new materials for

production. By recovering and recycling filaments, it is possible to reduce the environmental impact. Plastic extrusion is a vital element in 3D printing and filament manufacturing. Understanding the process of creating custom filaments involves working with plastic pellets, incorporating pigments, and carefully controlling the melting and feeding through a nozzle. Making filament for 3D printing involves a straightforward yet precise process. It starts with selecting the appropriate plastic pellets and mixing them with pigments to achieve the desired color. After this, the mixture is melted and fed through a nozzle, ensuring consistent diameter and quality. Finally, the filament is spooled up and ready for use in 3D printing.

- Selecting Plastic Pellets - choosing the right type of plastic pellets is crucial for achieving the desired filament properties.
- Mixing and Melting - incorporating pigments and precisely melting the plastic mixture is essential for color and quality control.
- Nozzle Feeding and Spooling - the melted material is carefully fed through a nozzle to ensure consistent diameter and then spooled up for use in 3D printing.

The raw material for most 3D printing filament comes in the form of plastic pellets. These pellets are available in different grades, each with unique properties tailored for specific applications. Choosing the right grade of plastic pellets is essential for ensuring the filament's performance and characteristics meet the intended purpose.

Depending on the specific application, it's crucial to select from various grades of plastic pellets that differ in properties. Factors such as strength, flexibility, and temperature resistance play a significant role in choosing the appropriate plastic grade:

- strength - some plastic grades offer exceptional strength, suitable for structural components and load-bearing parts.
- flexibility - flexibility is important for creating parts that require bending and deformation without breaking.
- temperature resistance - certain grades exhibit high-temperature resistance, ideal for applications subjected to heat stress.

To achieve specific characteristics in 3D printed parts, it's essential to tailor the filament properties. This includes considerations such as color, transparency, tensile strength, and heat resistance:

- color - customizing filament colors to match design specifications.
- transparency - creating transparent filaments for see-through applications.
- tensile Strength - modifying filament properties to withstand varying forces and loads.
- heat resistance - developing filaments capable of withstanding high-temperature environments.

Plastic extrusion is a key element in 3D printing and filament production. Making filament for 3D printing is fundamentally not too hard. It is necessary to have plastic pellets, mix them with some pigments, melt and feed through a nozzle, and spool everything up. The raw material for most 3D printing filament comes in the form of plastic pellets. Depending on application, material can be selected between a various grades of differing in properties.

Before diving into custom filament creation, it's crucial to identify which types of plastics can be recycled and repurposed for filament production (Figure 1 and 2).

Polymer Name	POLYETHYLENE TEREPHTHALATE	HIGH-DENSITY POLYETHYLENE	POLYVINYL CHLORIDE	LOW-DENSITY POLYETHYLENE	POLYPROPYLENE	POLYSTYRENE	All other plastics, including acrylic, fiberglass, nylon, polycarbonate, and polylactic acid (a bioplastic)
Resin Identification Code							
Abbreviation	PET or PETE	HDPE	PVC	LDPE	PP	PS	OTHER
Recyclable?	Commonly Recycled	Commonly Recycled	Sometimes Recycled	Sometimes Recycled	Occasionally Recycled	Commonly Recycled (but difficult to do)	Difficult to Recycle
Percentage Recycled Annually			<1%"/>				
How Long to Decompose Under Perfect Conditions							Majority of these plastics: <b>never</b> Polylactic acid: <b>6 months</b>
Maximum Temperature	70°C (158°F)	120°C (248°F)	70°C (158°F)	80°C (176°F)	135°C (275°F)	90°C (194°F)	Polycarbonate: 135°C (275°F) Polylactic acid: 150°C (302°F)
Brittleness Temperature	-40°C (-40°F)	-100°C (-148°F)	-30°C (-22°F)	-100°C (-148°F)	0°C (32°F)	-20°C (-4°F)	Polycarbonate: -135°C (-211°F) Polylactic acid: 60°C (140°F)
Toxicity Level							
Most Commonly Leached Toxin(s)	Antimony Oxide, Bromine, Diazomethane, Lead Oxide, Nickel Ethylene Oxide, and Benzene	Chromium Oxide, Benzoyl Peroxide, Hexane, and Cyclohexane	Benzene, Carbon Tetrachloride, 1,2-Dichloroethane, Phthalates, Ethylene Oxide, Lead Chromate, Methyl Acrylate, Methanol, Phthalic Anhydride, Tetrahydrofuran, and Tribasic Lead Sulfate, Mercury, Cadmium, Bisphenol A (BPA)	Benzene, Chromium Oxide, Cumene Hydroperoxide, And Tert-butyl Hydroperoxide	Methanol, 2,6-di-tert-Butyl-4-Methyl Phenol, and Nickel Dibutyl Dithiocarbamate	Styrene, Ethylbenzene, Benzene, Ethylene, Carbon Tetrachloride, Polyvinyl Alcohol, Antimony Oxide, and Tert-butyl Hydroperoxide, Benzoquinone	BPA, BPS, as well as all other toxins mentioned

Figure 2. Types of recyclable plastic materials

**PLA (Polylactic Acid)** filament is a recyclable, natural thermoplastic polyester that is derived from renewable resources such as corn starch or sugar cane. The filament is biodegradable under certain conditions with high heat capacity and high mechanical strength. It can be melted without significant damage and does not emit toxins or fumes. PLA is an easy-to-use 3D printing material for many who are just starting their journey. It can be printed at low temperatures, does not require heated beds or environmentally controlled build chambers, and can be purchased in filament form at a low cost. PLA does, however, exhibit low heat resistance relative to other 3D printing materials, and may not meet the mechanical requirements of your application due to its mediocre strength properties. PLA parts may perform adequately for less-demanding applications, but should carefully be considered when higher functionality is required.

**ABS (Acrylonitrile Butadiene Styrene)** is one of the most commonly used 3D printing thermoplastic alongside PLA. Generally, ABS, is easy to process and ideal for rapid prototyping. Because of its superior ductility, strength, and thermal stability, it can be machined more easily and used mechanically in certain applications. Its heat resistance property amongst other great properties often make it the go-to material candidate for a broad range of applications.

**TPU (Thermoplastic Polyurethane)** is an elastic and rubbery 3D printer filament. It is used in many different industries for its excellent features. TPU has excellent layer adhesion, and the

shape maintains stability during the cooling process. So it is easier to print than other flexible materials like TPE. The main features of TPU are: 1. Abrasion resistance 2. High flexibility 3. Durability 4. Chemical resistance 5. High strength 6. Medium heat resistance

**HDPE (High-Density Polyethylene)** is a type of polyethylene known for its resistance to chemicals, rigidity, and good wear resistance. It is often used to create containers, pipes, and durable mechanical parts. HDPE extrusion requires higher temperatures and specific settings to achieve good layer adhesion. HDPE is a thermoplastic polymer made from petroleum. It has high intermolecular forces and greater stiffness than low-density polyethylene, with the result that the tensile strength is greater; compared to the latter, moreover, it is also harder and more opaque and can withstand higher temperatures. It is one of the most common materials in everyday life: in fact, HDPE accounts for 40% of the total volume of world production of plastic materials and is easily available in many commonly used articles such as detergent drums, bottle caps, containers of various types and folding chairs, as well as being also present in water pipes and telecommunications cables.

**PETG (Polyethylene Terephthalate modified with Glycol)** is a commonly used technical material, popular among 3D printer users for its low price and good printability. It's tenacious, with good temperature resistance; PETG is most commonly used for printing various mechanical parts, holders, clamps, and waterproof parts (thanks to great layer adhesion). PETG has a glossy surface, adheres greatly to a print sheet, and does not shrink or warp (it has very little thermal expansion), therefore it's suitable for printing large models. Plus, its high tenacity and flexibility often prevent it from breaking. Due to good temperature resistance, PETG parts are suitable both for interior and most exterior use (with temperatures below 80 °C).

The letter G in PETG means that it's modified with glycol during the manufacturing process. Glycol makes PET less brittle, easier to print, and more transparent for translucent prints. Of course, you can print also with PET filaments without glycol. However, printing with only PET is challenging and does not offer any advantage whatsoever.

One of the important indexes of materials is Melt Flow Index (MFI) (Figure 3). The Melt Flow Index is a measure of the ease with which a thermoplastic polymer can be melted and extruded under specific conditions. It is a crucial parameter in assessing the processability and flow properties of plastic materials. MFI is particularly important in industries where polymers are used for various applications, such as injection molding and extrusion. A low melt flow index means high viscosity and is what you want for extrusion because the filament needs to keep its shape.

A high melt flow index means a low viscosity and is, for example, used in injection molding, where the material needs to flow into every last bit of the mold easily. In summary, the Melt Flow Index provides a quantitative measure of a polymer's flow characteristics during the molten state, offering valuable information for manufacturers to optimize processing conditions and ensure the quality of the end product.

a)



b)



c)



d)



e)

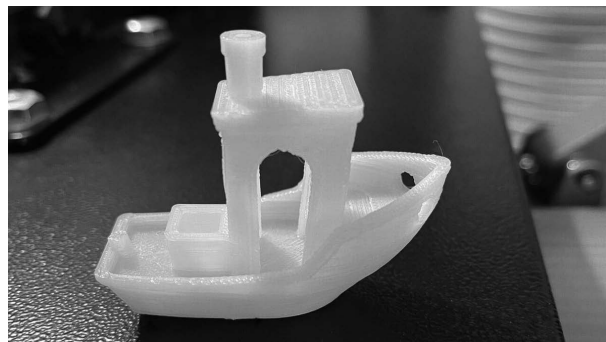


Figure 2. Examples of materials application in FDM printing: a) PLA, b) PETG, c) ABS, d) TPU, e) HDPE



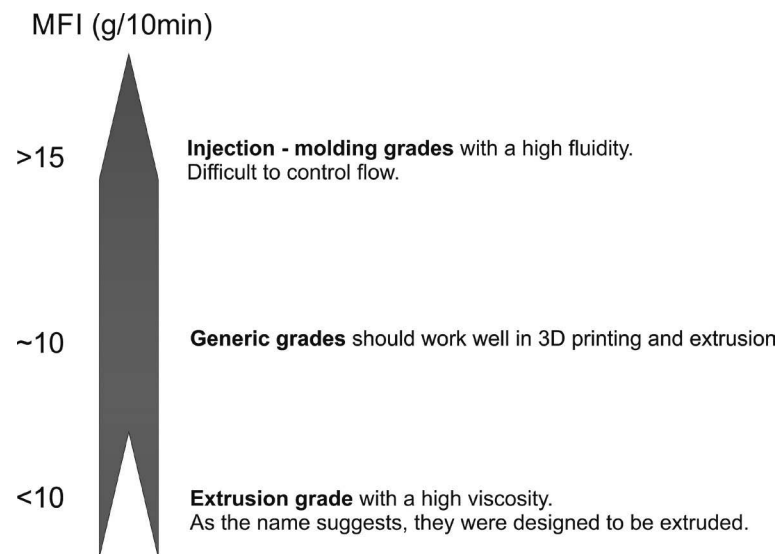


Figure 3. The Melt Flow Index rate [4]

Progress is currently underway to recycle a wide range of materials. To date, a number of studies have been performed to determine the effect of the amount of recyclate on the properties of the newly obtained filament. Thus, in the work Falkowska P., Jędrzejewski S., Tatar D. et al. [6] successfully processing for the production of new filament, recyclate from old failed prints was obtained, processed into pellets and mixed with new PLA pellets to produce new PLA filament doped with 30%, 50% and 70% recyclate. The new filament produced in this way was used to make static tensile test specimens. Based on the study, it was found that as the percentage of recyclate increases, the strength of the parts made from the new recyclate doped filament decreases by about 13% (Figure 4).

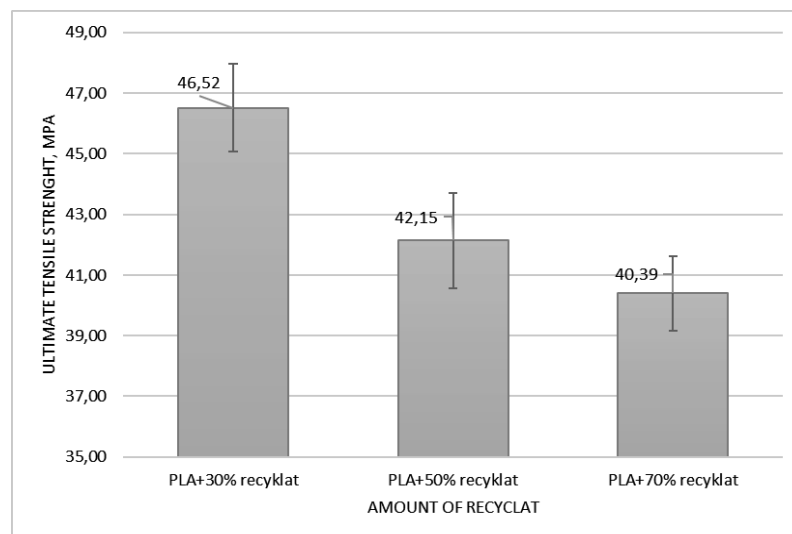


Figure 4. Effect of recyclate proportion on mechanical properties of components [5]

In work Falkowska P., Olszowska M., Krawczyk A. et al. [6] took a closer look at 3D printing. Recyclate was obtained from old failed prints and a new type of biodegradable PLA filament doped with 10% recyclate was produced. Tensile strength tests were then carried out to compare the properties between the regular filament and the doped recyclate. It was stated

that the application of recycled PLA as a raw material could be a viable means of re-manufacturing. Such PLA regranulate would work well for the production of products that do not have strict mechanical property requirements. It is safe to say that by using a relatively low percentage of recycled PLA (<10%) mixed with original PLA, one can produce a material almost identical to that of 100% virgin PLA, may represent a future strategy for sustainable PLA management (Figure 5).

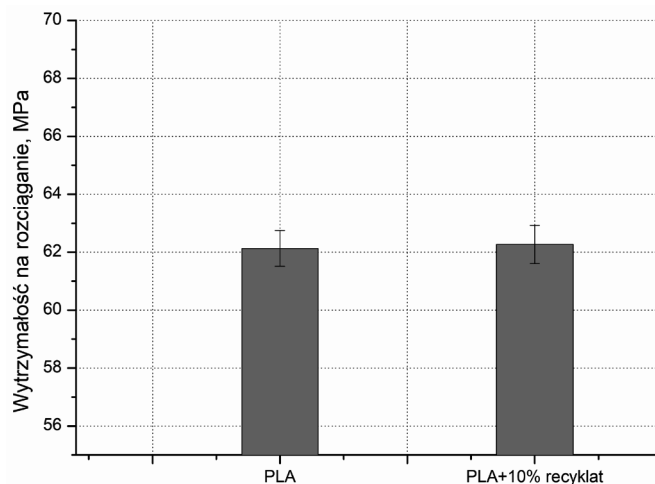


Figure 5. Comparison of print properties from PLA and PLA doped with recycilate [6]

From other hand C.G. Schirmeister, T. Hees et. al. [7] improved Young's modulus, tensile strength and surface quality of 3D printed HDPE by varying 3D printing parameters like temperature and diameter of the nozzle, extrusion rate, build plate temperature, and build plate material. For the first time additive manufactured HDPE and injection-molded HDPE exhibit similar mechanical properties with exception of elongation at break. Excellent fusion of the extruded polymer strands and the absence of anisotropy are achieved, as verified by microscopic imaging and measuring the tensile strength parallel and perpendicular to the 3D printing direction. The well-known shrinkage and adhesion problems typical for FFF of HDPE are overcome by selecting the appropriate build plate material and by adjusting the FFF process parameters. Among a great variety of materials, SEBS as build plate material affords excellent adhesion to HDPE during the entire manufacturing process and enables facile detachment of the printed object by peeling and bending without damaging the print object. HDPE filaments suitable for FFF are readily available by HDPE extrusion. In conventional FFF processes, printing causes voids that indicate poor adhesion between the strands. This drastically impairs both mechanical and optical properties and accounts for massive anisotropy of the mechanical properties which are highly dependent on the printing direction and pathways. To prevent void formation and to compensate shrinkage due to HDPE crystallization during solidification the extrusion rate is gradually increased during printing from a filling grade of 100 to 107 %. Moreover, in an optimized FFF process, significantly improved mechanical properties, lack of anisotropy and improved surface are achieved at an extrusion temperature of 220 °C for a nozzle with 0.8mm diameter and 240 °C for a nozzle with a diameter of 0.4 mm. Both nozzle diameter and printing speed impact surface quality but do not impair mechanical properties. According to tensile testing parallel (0°) and perpendicular (90°) to the printing direction no massive influence of the printing direction is detected, whereas most state-of-the-art printed HDPE samples lose their strength at an angle of 90°. Nevertheless, this progress made in FFF

printing of HDPE represents an important step to expand the range of materials in extrusion-based additive manufacturing and include semi-crystalline hydrocarbon materials which hold great promise for the development of sustainable additive manufacturing (Figure 6).

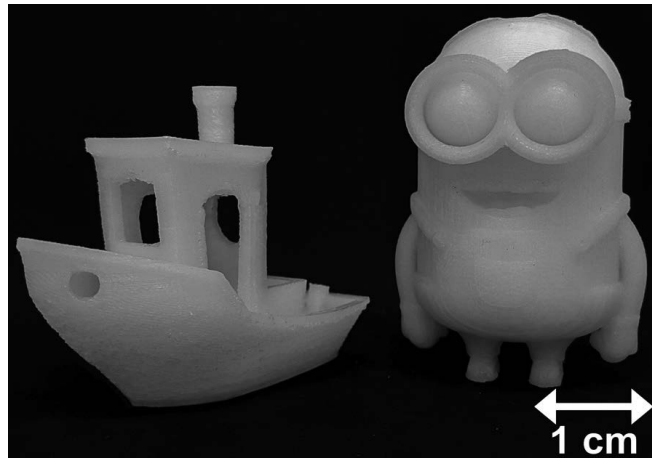


Figure 6. More complex print objects demonstrating dimensional accuracy by FFF printing of HDPE with optimized conditions on a SEBS plate and adjusted amount of extruded polymer melt.

One of the interested research done in last few months was done by engineers from Felfil company where used mussels shells to create new compounds is a very good way to reuse waste from the food chain (Figure 7). In fact, extruding "clam filament" was successful and good for a regular 3D printer. They used about 20% ground shells; the remaining 80% was PLA. Increasing the percentage of clam shells still allowed extrusion, but then the printer jammed. Moreover, the resulting filament had a pleasant sheen due to the microscopic parts of the shells and a gray color. Even though the percentage of shells used in the filament may seem small, the numbers are impressive on a large scale: the major shellfish producers in Europe range from 65,000 tons per year (Italy) to 200,000 (Spain), while per capita consumption ranges from 200 grams to 4 kg. What's more, the seafood industry discards more than 7 million tons of shellfish each year, and most of it ends up in the sea or in landfills. Therefore, being able to reuse some of the waste to create new filament could be a great solution [2].



Figure 7. Partially organic filament [8]

## 2. SUMMARY

Filament recycling is a key step towards a more sustainable and greener future. Thanks to advances in technology and innovation, more and more people have the opportunity to participate in this process, creating new and valuable products.

The world of 3D printing continues to evolve with the introduction of innovative filament materials. Cutting-edge options, ranging from composite filaments to flexible and dissolvable filaments, open new avenues for creativity and practical applications.

Recycling of filaments give possibilities to exploring new filament materials. Integrating different materials to enhance properties and create new possibilities, like:

- composite filaments - integrating different materials to enhance properties and create new possibilities.
- flexible filaments - developing filaments that offer flexibility and resilience for specialized applications.
- dissolvable filaments - creating support structures that can be dissolved, allowing for complex and intricate designs.

It's essential to note that the future of recycling in 3D printing will depend on ongoing research, technological advancements, market demand, and environmental considerations. As sustainability becomes a more significant focus across industries, the 3D printing community is likely to see continuous improvements in recycling practices and materials.

## ACKNOWLEDGEMENT

The present study was produced as part of the activities of the Student Research Group "GYROID" operating at the Department of Engineering and Biomedical Materials at the Faculty of Mechanical Engineering, Silesian University of Technology in Gliwice.

The thesis was developed as a result of a project within project-oriented education-PBL, in competition X within the Excellence Initiative - Research University programme, Silesian University of Technology.

The publication is result of cooperation within the Visegrad Scholarship Program 2023/2024.



## LITERATURE

1. [www.3devo.com](http://www.3devo.com)
2. [www.felfil.com](http://www.felfil.com)
3. <https://help.prusa3d.com/>,
4. <https://support.3devo.com/>
5. Falkowska P., Jędrzejewski S., Tatar D. [i in.], Badania własności wytrzymałościowych filamentów domieszkowanych recyklatem, TalentDetector2023\_Summer : International Students Scientific Conference, Brenna, Poland, 26th June 2023 / Bonek Mirosław (red.), Prace Katedry Materiałów Inżynierskich i Biomedycznych, 2023, Gliwice, Politechnika Śląska, s.209-215, ISBN 978-83-65138-38-5

6. Falkowska P., Olszowska M., Krawczyk A. [i in.], Własności wytrzymałościowe filamentu domieszkowanego recyklatem, TalentDetector2023\_Winter : International Students Scientific Conference, 27th January 2023 / Bonek Mirosław (red.), Prace Katedry Materiałów Inżynierskich i Biomedycznych, 2023, Gliwice, Politechnika Śląska, s.158-166, ISBN 978-83-65138-34-7
7. C.G. Schirmeister, T. Hees, E. H. Licht, R. Mülhaupt, 3D printing of high density polyethylene by fused filament fabrication, Additive Manufacturing 28 (2019) 152–159
8. <https://felfil.com/a-dinner-with-felfil-filament-with-mussels-shells>



26th January 2024  
Gliwice, Poland

DEPARTMENT OF ENGINEERING MATERIALS AND BIOMATERIALS  
FACULTY OF MECHANICAL ENGINEERING  
SILESIA UNIVERSITY OF TECHNOLOGY

## INTERNATIONAL STUDENTS SCIENTIFIC CONFERENCE

### Investigation of the mechanical properties of components manufactured from recycled high-density polyethylene

M. Rejek<sup>a</sup>, S. Jędrzejewski<sup>b</sup>, Ł. Kołodziej<sup>c</sup>, D. Markusik<sup>d</sup>, D. Tatar<sup>e</sup>,  
A. Woszczak<sup>f</sup>, B. Chadzima<sup>g</sup>, M. Król<sup>h</sup>, A.J. Nowak<sup>i</sup>

<sup>a</sup> Studentka kierunku Mechanika i Budowa Maszyn: Technologie Spawalnicze, e-mail: monirej772@student.polsl.pl,

<sup>b</sup> Student kierunku Inżynieria Materiałowa, e-mail: szymjed659@student.polsl.pl

<sup>c</sup> Student kierunku Technologia Chemiczna: Technologia Polimerów i Tworzyw Sztucznych, e-mail: lukakol625@student.polsl.pl,

<sup>d</sup> Student kierunku Automatyka i Robotyka Przemysłowa: Zintegrowane systemy wytwarzania, e-mail: dorimar256@student.polsl.pl,

<sup>e</sup> Student kierunku Inżynieria Materiałowa, e-mail: danitat271@student.polsl.pl,

<sup>f</sup> Student kierunku Inżynieria Materiałowa, e-mail: adamwos244@student.polsl.pl

<sup>g</sup> Research Centre UNIZA, University of Zilina, Univerzitna 8215/1, 010 26 Zilina, Slovakia

<sup>h</sup> Politechnika Śląska, Wydział Mechaniczny Technologiczny, Katedra Materiałów Inżynierskich i Biomedycznych, e-mail: mariusz.krol@polsl.pl,

<sup>i</sup> Politechnika Śląska Wydział Mechaniczny Technologiczny, Laboratorium Naukowo Dydaktyczne Nanotechnologii i Technologii Materiałowych, ul. Towarowa 7a, 44-100 Gliwice; e-mail: agnieszka.j.nowak@polsl.pl

**Abstract:** This paper presents the results of tests on a high-density polyethylene filament and a recycled high-density polyethylene filament obtained by shredding water bottle caps. The comparison of the produced materials was based on the results of tensile strength tests carried out in the materials testing laboratory. The aim of the study was to provide an overview of recycled FFF printing filaments produced using HDPE.

**Keywords:** HDPE, 3D printing, Fused Filament Fabrication, recycled materials, recycled filament

## 1. INTRODUCTION

Additive manufacturing technologies introduce a novel aspect to polymer processing, offering significant potential for sustainable, lightweight construction and the creation of intricate, multifunctional material systems in a single processing step [1-5]. *High-density polyethylene* (HDPE), a type of polymer, is commonly used in the production of fibers for devices utilized in additive methods. HDPE is a soft, flexible thermoplastic material derived from petroleum and is part of the polyolefins group, which is solely composed of carbon and hydrogen molecules. The fundamental building blocks of the polymer chains are long -C-C-C

chains [6]. The production of 1 kg of HDPE requires 1.75 kg of petroleum, which is converted into energy and raw materials [7]. HDPE is known for its high durability, making it a popular choice in the food and cosmetic industries for items such as milk bottles, bottle caps, and certain cosmetic packaging. The density of HDPE typically falls between 0.942 to 0.965 g/cm<sup>3</sup>, and the material can shrink anywhere from 1.5% to 3%.

The majority of plastic recycling involves homogeneous recycling, which pertains to the recycling of homogeneous polymers. This type of recycling is applicable to items gathered through differentiated collection or separated post-collection from similar items made of different polymers [8].

## 2. AIM OF THE RESEARCH

This work aimed to create a filament composed of HDPE, incorporating 30% HDPE recyclate, and to assess the mechanical characteristics of parts fabricated from this newly formulated filament. The recyclate was made up of pulverized caps. The evaluation of mechanical attributes was conducted through tensile strength examinations.

## 3. MATERIALS AND METHODS

The research material was a filament made from commercially pure high-density polyethylene (HDPE) granulate, granulate, and 30% pulverized caps sourced from drinking water bottles. Before grinding, the caps were meticulously cleaned and subsequently dried. The Felfil Shredder, a polymer material shredder, was employed for the grinding process, which was performed thrice to yield granulate with a smaller fraction. The prepared granulate, now containing fragments of crushed caps, was mixed with HDPE granulate. Using the Felfil Evo Extruder, a new filament was extruded with a controlled diameter in the 1.68-1.78 mm range. This, in conjunction with the Felfil Spooler device, facilitated the creation of a filament from the recyclate (Fig. 1).

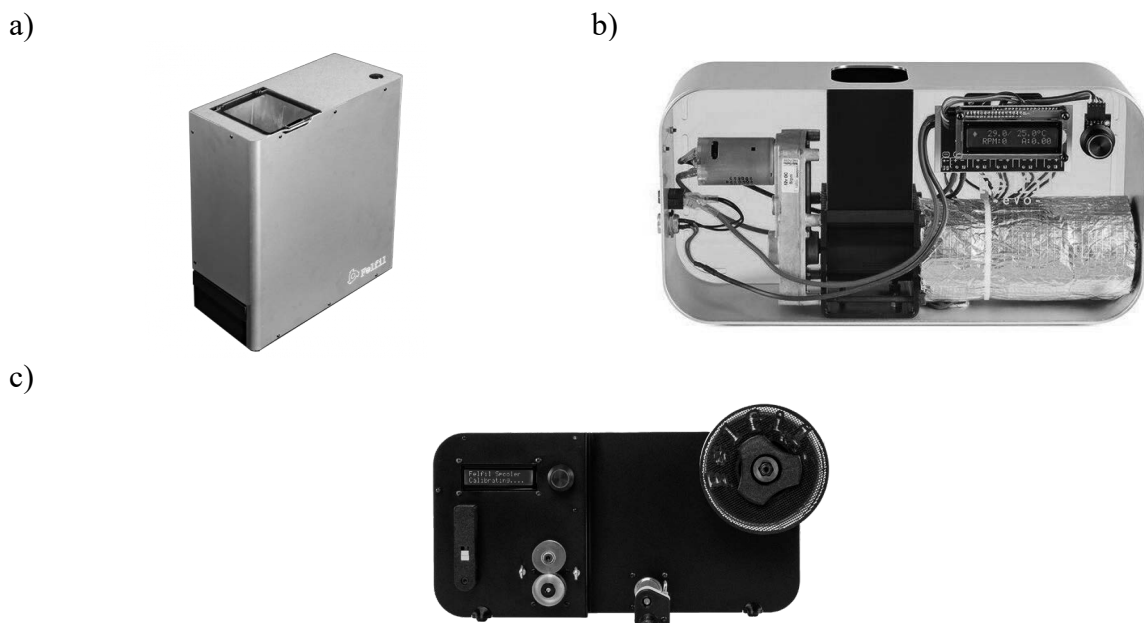


*Figure 1. Felfil Evo devices for filament production: a) shredder, b) filament extrusion system, c) spooler [9]*

The 3D Evo Composer 350 system was used to extrude a filament with 30% recycle (Fig. 2). The extrusion process took place at a temperature range of 170 to 180 °C with the screw speed of the extruder (RPM) being 6.1 r/min. The exact manufacturing parameters are presented in Table 1.

*Table 1. Processing parameters of 3D Evo Composer 350 extruder heating zones; RPM - revolutions of the extruder screw per minute*

	Value	Unit
H4	180	°C
H3	180	°C
H2	175	°C
H1	170	°C
RPM	6.1	r/min
Cooling Fan power	100	%

Before spooling, the HDPE filament thread undergoes cooling. This operation aims to prevent thread deformation onto the spool during the material spooling process. For this purpose, a cooling model of the 3D EVO brand was used. Using fans set at the outlet of the nozzle results in more significant deformation of the thread cross-section when using high blowing velocity. The operations and devices used allowed the diameter of the HDPE filament to be stabilized in the range of approx. 1.75 mm.

a)



b)



*Figure 2. a) 3D Evo Composer 350 device [10], b) processed granules from bottle caps*

From the obtained material, specimens for tensile strength tests were made using the FlashForge Creator 2 printer (Fig. 3). Several samples were produced for each type of material for tensile strength testing. For pure HDPE (marked as HDPE 100), 5 samples were prepared, and for HDPE with 30% recycled material (marked as HDPE 70/30), 7 samples were prepared. The printer used to develop the normalized tensile test specimens had an enclosed chamber, allowing the printing process to be carried out under stable conditions. A PS sheet working platform was used to increase the adhesion of the printed specimens to the substrate. Temperature of nozzle was set at 220 °C.



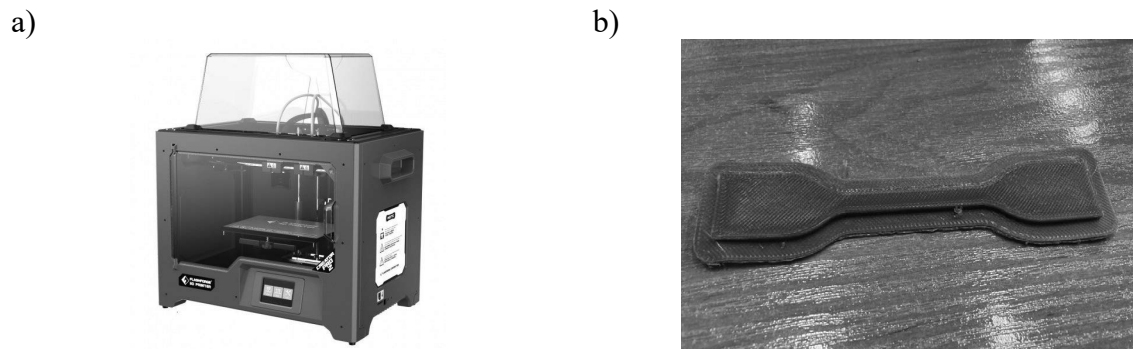


*Figure. 3. a) FlashForge Creator 2 3D printer [11] b) A specimen for strength testing printed on the 3D FlashForge Creator 2 with HDPE containing 30% recycled HDPE.*

Tensile strength tests were conducted on a Zwick/Roell Z020 device in accordance with the PN-EN ISO 527 standard. Special fixtures were mounted to conduct a static tensile test.



*Figure 4. Holders for conducting a static tensile test mounted on the Zwick/Roell Z020 device.*

#### **4. RESULTS AND DISCUSSION**

As a result of extruding the filament thread on the 3D Evo Composer device, a chart (Fig. 5) of the material diameter variation over time was obtained. At the beginning of the process, the variation in the diameter of the thread was significant, but after a period of approximately 1800 seconds, the diameter of cross-sectional size was normalized. Deviations from the specified size in the further time range were small and did not result in deformation of the produced material.

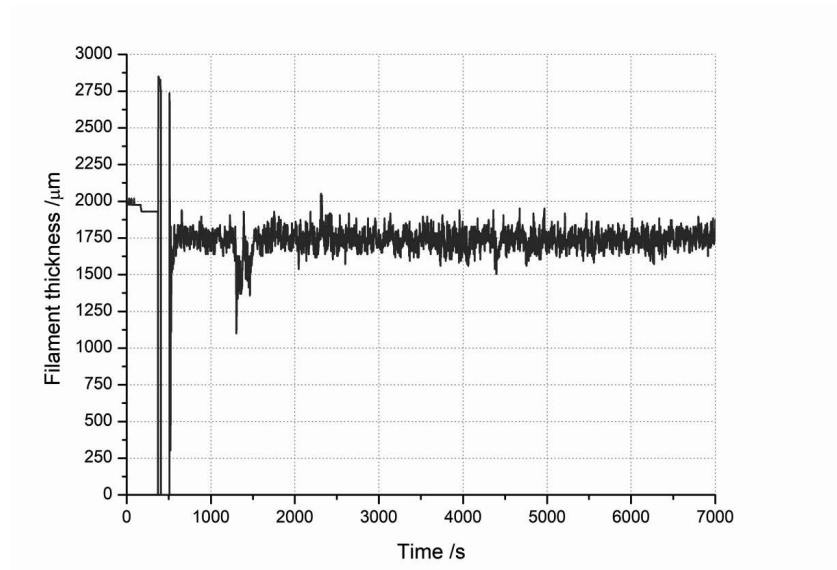


Figure 5. Chart from the 3D Evo Composer 350 program depicting the variability of the extruded material diameter over time.

As a result of performing a static tensile test on the Zwick/Roell Z020 strength testing machine, the following results were obtained and are presented in Table 2. The highest tensile strength value (21.46 MPa) is exhibited by the sample labelled HDPE 70/30 5. Meanwhile, the highest elongation value (11.04%) was achieved by the sample labelled HDPE 100 1.

Table 2. Strength test results for HDPE 100 and HDPE 70/30 samples.

Sample	$\sigma$ [MPa]	$\epsilon$ [%]
HDPE 70/30 1	17.26	8.01
HDPE 70/30 2	19.01	8.27
HDPE 70/30 3	17.31	11.03
HDPE 70/30 4	18.84	8.90
HDPE 70/30 5	21.46	8.26
HDPE 70/30 6	18.38	8.59
HDPE 70/30 7	18.47	8.91
HDPE 100 1	16.40	11.04
HDPE 100 2	17.97	8.90
HDPE 100 3	19.40	9.53
HDPE 100 4	17.50	9.03
HDPE 100 5	15.69	10.70

The averaged results of the tensile strength test are presented numerically in Table 3. Samples labelled as HDPE 70/30 show a 6.86% higher tensile strength; however, in terms of elongation, they achieve results 10.06% worse than samples labelled as HDPE 100.

Table 3. Averaged strength test results for HDPE 100 and HDPE 70/30 samples.

Sample	avg $\sigma$ [MPa]	avg $\epsilon$ [%]
HDPE 70/30	18.67	8.85
HDPE 100	17.39	9.84

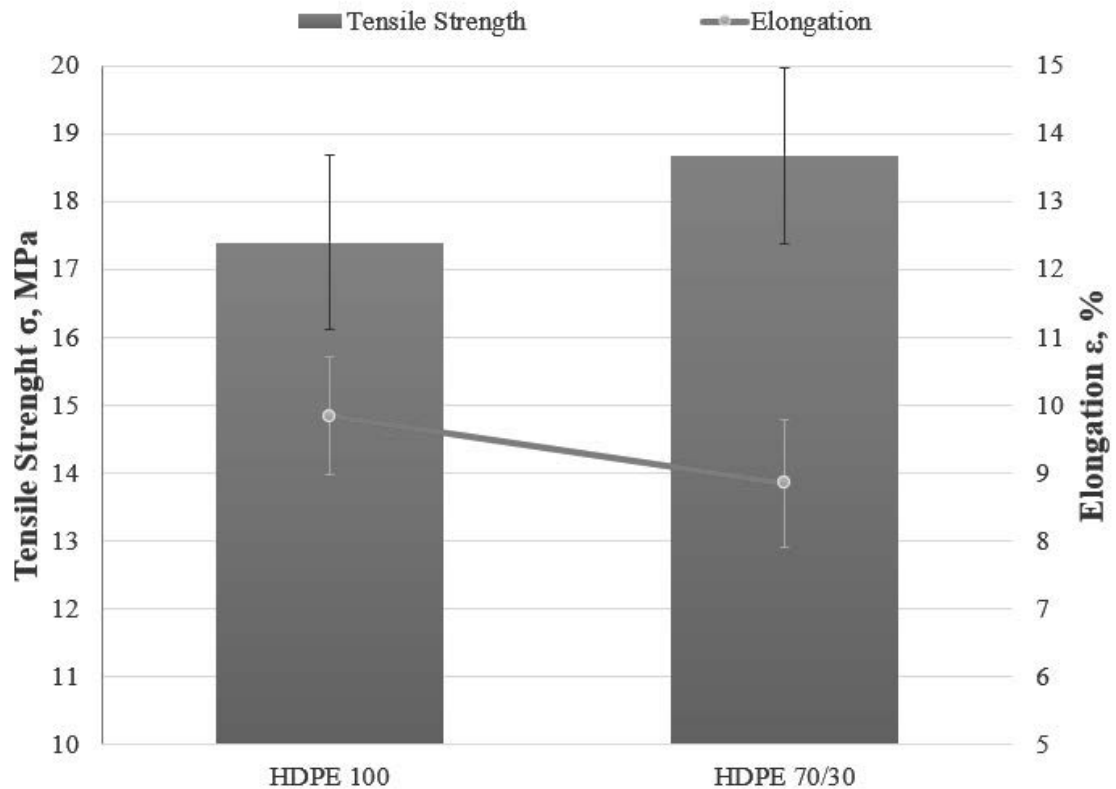


Figure 6. Average results of tensile strength test for HDPE 70/30 and HDPE.

## 5. CONCLUSIONS

The research aimed to develop a filament from HDPE, in which 30% consisted of recycled HDPE derived from shredded caps of water bottles. The production process involved cleaning, drying, and grinding the caps, then extruding the granulate into filament using the Felfil Evo extruder and Composer 350.

Analysis of filament diameter variability showed stabilization after approximately 1800 seconds, confirming the effectiveness of the process. Tensile strength tests compared two samples: HDPE 70/30 (with 30% recycled HDPE) and pure HDPE 100. The results indicated that HDPE 70/30 achieved a higher average tensile strength but had lower elongation at break than HDPE 100.

The mechanical properties of HDPE 70/30 showed similar values, suggesting good reproducibility of the recycled filament. A comparison with pure HDPE 100 showed that the recycled filament could have comparable or even better mechanical properties. The slight

increase in mechanical properties may be due to using additives or stabilizers in the cap manufacturing process.

The stability of the filament's diameter was achieved by using appropriate operations and equipment, such as the Felfil Evo and Composer extruder systems. Mechanical tests confirmed that the manufacturing process and equipment contributed to successfully producing a stable HDPE filament with the desired mechanical properties.

The study's conclusions suggest that a filament with 30% recycled HDPE can be successfully extruded and used in a new printing process, opening up the potential of using recycled materials to produce 3D printing filaments without compromising mechanical properties.

## ACKNOWLEDGEMENT

The present study was produced as part of the activities of the Student Research Group "GYROID" operating at the Department of Engineering and Biomedical Materials at the Faculty of Mechanical Engineering, Silesian University of Technology in Gliwice.

The thesis was developed as a result of a project within project-oriented education-PBL, in competition X within the Excellence Initiative - Research University programme, Silesian University of Technology.

The publication is result of cooperation within the Visegrad Scholarship Program 2023/2024.



## LITERATURE

1. T.D. Ngo, A. Kashani, G. Imbalzano, K.T.Q. Nguyen, D. Hui, Additive manufacturing (3D printing): a review of materials, methods, applications and challenges, *Composites Part B Eng.*, 143 (2018), Pages 172-196.
2. S. Singh, S. Ramakrishna, R. Singh, Material issues in additive manufacturing: a review, *Journal of Manufacturing Processes*, 25 (2017), Pages 185-200.
3. J.W. Stansbury, M.J. Idacavage, 3D printing with polymers: challenges among expanding options and opportunities, *Dental Materials*, 2 (1) (2016), Pages 54-64.
4. S.A.M. Tofail, E.P. Koumoulos, A. Bandyopadhyay, S. Bose, L. O'Donoghue, C. Charitidis, Additive manufacturing: scientific and technological challenges, market uptake and opportunities, *Materials Today*, Volume 21 (1) (2018), Pages 22-37.
5. C. G. Schirmeister, T. Hees, E. H. Licht, R. Mülhaupt, 3D printing of high density polyethylene by fused filament fabrication, *Additive Manufacturing*, Volume 28 (2019), Pages 152-159.
6. Novigo Films, Co to są poliolefiny i jakie mają zastosowanie? (Online) <https://novigofilms.com/co-to-sa-poliolefiny-i-jakie-maja-zastosowanie/>, data dostępu: 6.12.2023
7. S. Kumar, A. K. Panda, R.K. Singh, A review on tertiary recycling of high-density polyethylene to fuel, *Resources, Conservation and Recycling*, Volume 55, Issue 11 (2011), Pages 893-910.

8. M. Kostadinova Loutcheva, M. Proietto, N. Jilov, F.P. La Mantia, Recycling of high density polyethylene containers, *Polymer Degradation and Stability*, Volume 57, Issue 1 (1997), Pages 77-81.
9. Felfil Evo - wyłaczarka włókien (Online) <https://www.na3d.pl/p/3208/felfil-evo-wytlaczarka-wlokien>, data dostępu: 5.12.2023
10. <https://www.3devo.com/>, data dostępu: 5.12.2023
11. Drukarka 3D - Flashforge Creator Pro 2 - IDEX dual-extruder (Online) <https://botland.com.pl/produkty-wycofane/16740-drukarka-3d-flashforge-creator-pro-2-idex-dual-extruder-6971940403616.html>, data dostępu: 5.12.2023



26th January 2024  
Gliwice, Poland

DEPARTMENT OF ENGINEERING MATERIALS AND BIOMATERIALS  
FACULTY OF MECHANICAL ENGINEERING  
SILESIA UNIVERSITY OF TECHNOLOGY

## INTERNATIONAL STUDENTS SCIENTIFIC CONFERENCE

### Wpływ teksturowania laserowego na własności tribologiczne Poli-eter-eter ketonu

K. Roskosz<sup>a</sup>, O. Bialas<sup>b\*</sup>

<sup>a</sup> TPNL Kamil Roskosz, ul. Krawiecka 18, 47-480 Pietrowice Wielkie

<sup>b</sup> Politechnika Śląska, Laboratorium Naukowo-Dydaktyczne Nanotechnologii i Technologii Materiałowych, ul. Towarowa 7a, 44-100 Gliwice

\*email: [oktawian.bialas@polsl.pl](mailto:oktawian.bialas@polsl.pl)

**Streszczenie:** Celem niniejszej pracy badawczej było ocenienie wpływu modyfikacji powierzchniowej polimeru medycznego typu PEEK na wartość współczynnika tarcia, mającego krytyczny wpływ na trwałość produktu w narażeniu na siły ścierające występujące w kontakcie materiał implantowany – kość. Przeprowadzono obróbkę powierzchniową materiału w stanie wyjściowym za pomocą mikroteksturowania laserowego w szeregu parametrów procesowych. Otrzymane materiały scharakteryzowano pod kątem topografii powierzchni przed oraz po obróbce, a następnie oznaczono współczynnik tarcia wykorzystując badania tribologiczne w odmianie metody pin-on-disc. W szereg technik miroskopowych włączono mikroskopię świetlną oraz stereoskopową wraz z rekonstrukcją obrazu w przestrzeni trójwymiarowej. Otrzymane wyniki badań pozwoliły na pozytywną ocenę materiałów modyfikowanych laserowo w zakresie obniżenia współczynnika tarcia po obróbce w stosunku do materiału rodzimego. Analiza śladów wytarcia pozwoliła na ocenę stopnia zużycia mikrotekstury w warunkach zużycia ściernego. Mikrostopowanie laserowe pozwala na obniżenie współczynnika tarcia.

**Abstract:** The aim of this research was to assess the impact of surface modification of a medical polymer of the PEEK type on the friction coefficient, which has a critical influence on the durability of the product exposed to abrasive forces occurring in contact with the implanted material – bone. Surface treatment of the material in its initial state was performed using laser microtexturing with a series of process parameters. The obtained materials were characterized for surface topography before and after processing, and then the friction coefficient was determined using tribological tests in the pin-on-disc method variant. Various microscopic techniques, including light microscopy and stereoscopy with image reconstruction in three-dimensional space, were employed. The research results allowed for a positive assessment of laser-modified materials in terms of reducing the friction coefficient after processing compared to the native material. Wear track analysis enabled the evaluation of the degree of microtexture wear under abrasive wear conditions. Laser microstructuring allows for a reduction in the friction coefficient.

**Słowa kluczowe:** mikroobróbka laserowa, PEEK, własności tribologiczne

## 1. WSTĘP

Polieteroeteroketon (PEEK) to polimer termoplastyczny o strukturze częściowo krystalicznej, który ma pochodzenie organiczne [1–4]. Pierwsze prace nad tym materiałem rozpoczęły się w 1978 roku, ale jego wprowadzenie na rynek miało miejsce na początku lat 80. ubiegłego wieku. Dzięki swoim doskonałym właściwościom termicznym i mechanicznym, a także wyjątkowej trwałości i odporności chemicznej, PEEK jest używany do produkcji części maszyn i różnych urządzeń, ze względu na swoje dobre właściwości ślizgowe. Mimo że PEEK jest uważany za polimer o właściwościach termicznych, maksymalna temperatura eksploatacji wynosi 260°C, a temperatura przetwarzania osiąga do 400°C. Biokompatybilność wyrobów wykonanych z PEEK była znana od lat 80 [5,6]. XX wieku, jednak pierwszy raz znalazły one zastosowanie w implantologii jako dyski lędźwiowe kręgosłupa i wszczepiono je pacjentom w latach 90. Ze względu na swoją lekkość, niski koszt produkcji i zdolność do tworzenia precyzyjnych implantów, coraz częściej zastępują one tytan i jego stopy. Wytwarzanie implantów z PEEK coraz częściej wykorzystuje technologię druku 3D, co znacząco przyspiesza proces produkcji odpowiednich komponentów. Inną zaletą materiałów PEEK w porównaniu z tytanem jest ich elastyczność, która wynosi 120 GPa w przypadku tytanu, co może prowadzić do kumulacji naprężeń i powodować dyskomfort u pacjenta. Implanty z PEEK charakteryzują się niskim modułem sprężystości, który wynosi od 3 do 4 GPa, w przeciwieństwie do ludzkiej kości korowej, na przykład kości udowej, która ma średnio 18 GPa. Modyfikacja PEEK wprowadza szeroki zakres różnorodnych właściwości chemicznych, odporność chemiczną i biokompatybilność, sprawia to, że ten materiał staje się niezawodny, ekonomiczny i powszechnie dostępny, co zwiększa jego atrakcyjność [7–9]. Z uwagi na swoje własności ślizgowe w niniejszej pracy podjęto próbę jeszcze większego obniżenia współczynnika tarcia występującego w konwencjonalnie ciętym przy pomocy tokarki materiale typu PEEK. Niniejsze badania obejmują wykorzystanie technologii mikroobróbki laserowej oraz wytworzenia mikrotekstury wiązką lasera, która może zapewnić odkładanie się w rowkach utworzonych przez wiązkę laserową produktów tarcia, co nie pozwoli na niestabilne zachowanie się materiału w warunkach tarcia suchego a także wydłuży cykl życia produktu wykonanego z materiału PEEK [7,10]. W szereg badań włączono analizę morfologii powierzchni przy użyciu mikroskopu stereoskopowego oraz przeprowadzono badania tribologiczne mające na celu oznaczenie własności współczynnika tarcia w funkcji dystansu przebytego przez przeciwpróbkę.

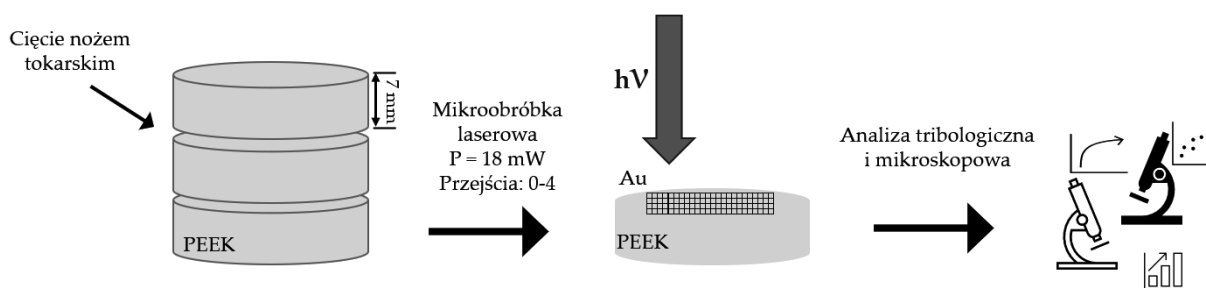
## 2. METODYKA

Pręty wykonane z Poli-eter-eter-ketonu (PEEK) (Mitsubishi Chemical Advanced Materials, Lenzburg, Switzerland) o średnicy 32 mm [5]. Pocięto na plastry o grubości 7 mm a następnie oczyszczono i odłuszczone. Jednorodne wyrównanie i przygotowanie powierzchni jest niezbędne do przeprowadzenia analizy porównawczej [6].

Tabela 1 parametry mikroobróbki laserowej

Wariant	Częstotliwość [Hz]	Prędkość ruchu wiązki [mm/s]	Liczba przejść	Średnica wiązki [ $\mu\text{m}$ ]
P2	400	1	2	~30
P4	400		4	

Następnie próbki zostały poddane obróbce laserowej w mikroteksturze kratownicy o boku 250  $\mu\text{m}$ . Wiązka lasera oddziaływała na materiał z mocą 18 mW oraz przy prędkości posuwu równej 1 mm/s w ilości przejść lasera 2x oraz 4x. Eksperyment został przeprowadzony przy użyciu lasera pikosekundowego A-355 Laser Micromachining system (Oxford Lasers, Didcot, UK), o długości fali 355 nm i maksymalnej mocy 48 mW. Metodę badań zobrazowano na niniejszym schemacie (Rys 1). Parametry obróbki laserowej zaprezentowano w tabeli 1



Rysunek 1 Schemat metodyki wytworzenia materiału do badań

Ocenę mikrostruktury przeprowadzono z użyciem mikroskopu stereoskopowego Leica DVM6 (Leica, Wetzlar, Germany) z wykorzystaniem obserwacji w polu jasnym techniką światła odbitego. Dodatkowo, w celu zobrazowania mikrotekstury pod kątem geometrii użyto funkcji rekonstrukcji obrazu w przestrzeni 3D. Próbkę w stanie wyjściowym oraz po mikrostrukturyzacji w ustalonych warunkach procesowych zostały poddane badaniu trybologicznemu w odmianie metody pin-on-disc wykorzystując urządzenie CSM tribometer (CSM Instruments, Needham, MA, USA) z penetratorem w formie kulki o średnicy 5 mm wykonanej z  $\text{Al}_2\text{O}_3$ . Do badania założono następujące parametry (Tab 2):

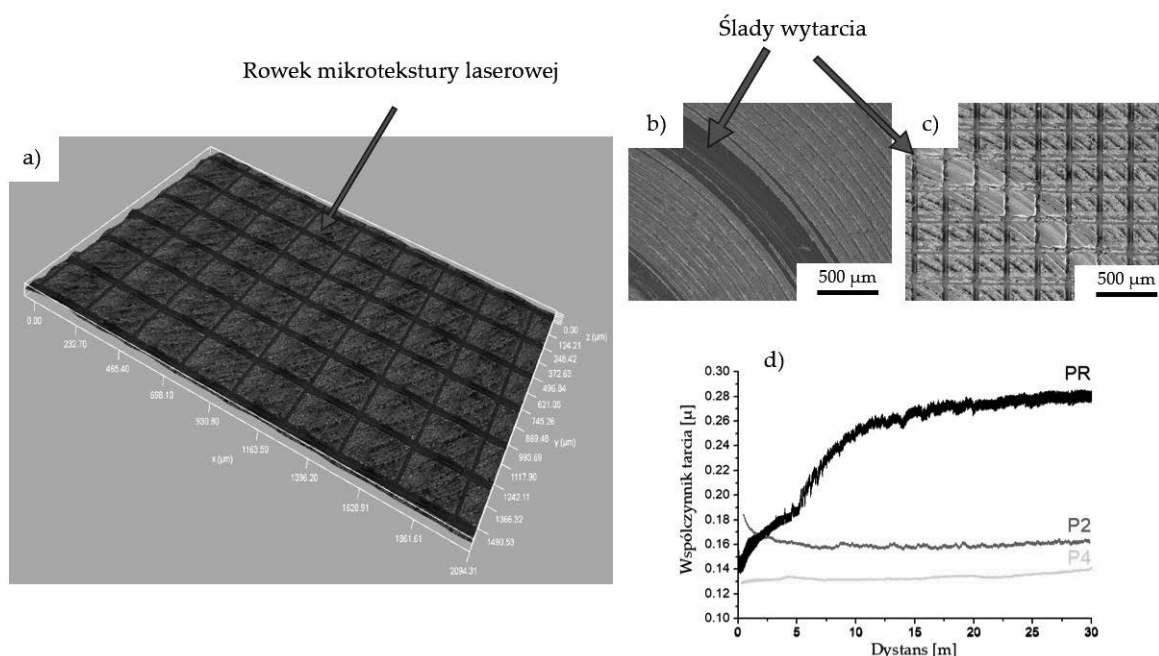
Tabela 2 parametry badania trybologicznego

Częstotliwość próbkowania [Hz]	Czas trwania testu [min]	Temperatura [ $^{\circ}\text{C}$ ]	Wilgotność [%]	Obciążenie [N]	Promień [mm]	Dystans [m]	Prędkość liniowa [cm/s]
3	40	25	60	15	3	30	2.5



### 3. WYNIKI

W toku badań materiał poddano analizie za pomocą mikroskopii świetlnej stereoskopowej w próbkach rodzimych zaobserwowano topografię powierzchni o kształcie okręgów odpowiadającą cięciu przy użyciu noża tokarskiego. W przypadku próbek po obróbce laserowej zaobserwowano powtarzalną, jednorodną strukturę geometryczną w postaci kratownicy powstałej poprzez mikroteksturowanie laserowe. Rowki żłobione przy użyciu wiązki lasera posiadają zagłębienia mogące być rezerwuarem produktów tarcia. Po przeprowadzeniu badań tribologicznych ujawniono różne przebiegi krzywych na wykresach zależności współczynnika tarcia od przebytego dystansu. Najwyższy współczynnik tarcia, wrastający w wraz z przebytem dystansem rejestruje się dla próbki PR (Próbka rodzima). Współczynnik tarcia stabilizuje się na wartości  $0.28 \mu$ . Próbki po mikroteksturyzacji laserowej wykazują znacznie obniżony współczynnik tarcia stabilizujący się na poziomie odpowiednio  $0.16$  oraz  $0.14$  dla próbki P2 oraz P4. Istotnie, materiał posiadający geometryczną mikroteksturę poprzez możliwość utrzymania w zagłębieniach produktów tarcia charakteryzuje się obniżonym współczynnikiem tarcia. Spadek współczynnika tarcia jest zależny od głębokości rowków mikrotekstury, sterowanej w niniejszym eksperymencie poprzez ilość przejść wiązki laserowej. Analiza mikrostrukturalna próbek po badaniach tribologicznych nie ujawniła degradacji mikrotekstury laserowej, co pozwala stwierdzić, że mikrotekstura utrzymuje swoje cechy użytkowe w parametrach badania, w przyszłości należy poprowadzić badania aż do uzyskania całkowitej degradacji tekstury celem określenia możliwej długości czasu pracy potencjalnego urządzenia wykonanego z tak obrobionego materiału. Wyniki przedstawiono na rys 2.



Rys 2 Rekonstrukcja 3D powierzchni próbki mikroteksturowanej laserowo (a), powierzchnia próbki rodzimej po badaniu tribologicznym (b), reprezentatywna powierzchnia próbki po mikroobróbce laserowej oraz po badaniu tribologicznym (c), wykres zależności współczynnika tarcia od przebytego dystansu przeciwpróbki (d)

#### 4. WNIOSKI

Po przeprowadzeniu badań nad powierzchniową modyfikacją powierzchni próbek PEEK wykorzystując obróbkę laserową można wystrósować następujące wnioski:

- Mikroobróbka laserowa z użyciem urządzenia emitującego źródło monochromatycznej wiązki fotonów o pikosekundowym czasie emisji pozwala na wykonanie mikrotekstury na materiale PEEK o dużej powtarzalności wraz z precyzyjnym określeniem parametrów procesowych obróbki
- Wytworzony materiał charakteryzuje się obniżonym współczynnikiem tarcia co potencjalnie wydłuża cykl życia produktu poddanego takiej obróbce powierzchniowej
- Założone parametry badania nie doprowadziły do całkowitej degradacji mikrotekstury, charakteryzuje się ona dużą trwałością i w przyszłych badaniach powinno się zmienić parametry badań tribologicznych celem doprowadzenia do degradacji tekstury a następnie oszacowania potencjalnego czasu zużycia materiału.

#### BIBLIOGRAFIA

- [1] Bialas, O., Lis, M., Woźniak, A., and Adamiak, M., 2021, "Laser Superficial Fusion of Gold Nanoparticles with PEEK Polymer for Cardiovascular Application," *Materials*, 14(4), p. 971.
- [2] Liber-Kneć, A., and Łagan, S. D., 2011, *Ćwiczenia laboratoryjne z biomateriałów: pomoc dydaktyczna*, Politechnika Krakowska, Kraków.
- [3] Marciniak, J. and Politechnika Śląska (Gliwice), 1996, *Biomateriały*, Wydawnictwo Politechniki Śląskiej, Gliwice.
- [4] Ozwoniarek, J., Wiśniewska-Weinert, H., Lisowski, J., and Kędzia, Ł., 2007, "Nowe Rozwiązania w Zakresie Biotribologii i Biomateriałów. Cz. 2 Stanowisko Do Badań Zużyciowych Elementów Endoprotez Stawu Biodrowego," *Obróbka Plastyczna Metali*, T. 18, nr 1, pp. 35–40.
- [5] "https://www.ensingerplastics.com/en/shapes/high-performance-plastics/peek (03.01.2021)."
- [6] Voyiadjis, G. Z., Samadi-Dooki, A., and Malekmoitei, L., 2017, "Nanoindentation of High Performance Semicrystalline Polymers: A Case Study on PEEK," *Polymer Testing*, 61, pp. 57–64.
- [7] Kurtz, S. M., and Devine, J. N., 2007, "PEEK Biomaterials in Trauma, Orthopedic, and Spinal Implants," *Biomaterials*, 28(32), pp. 4845–4869.
- [8] Panayotov, I. V., Orti, V., Cuisinier, F., and Yachouh, J., 2016, "Polyetheretherketone (PEEK) for Medical Applications," *J Mater Sci: Mater Med*, 27(7), p. 118.
- [9] Ma, R., and Tang, T., 2014, "Current Strategies to Improve the Bioactivity of PEEK," *IJMS*, 15(4), pp. 5426–5445.
- [10] Riveiro, A., Soto, R., Comesaña, R., Boutinguiza, M., del Val, J., Quintero, F., Lusquiños, F., and Pou, J., 2012, "Laser Surface Modification of PEEK," *Applied Surface Science*, 258(23), pp. 9437–9442.



26th January 2024  
Gliwice, Poland

DEPARTMENT OF ENGINEERING MATERIALS AND BIOMATERIALS  
FACULTY OF MECHANICAL ENGINEERING  
SILESIA UNIVERSITY OF TECHNOLOGY

## INTERNATIONAL STUDENTS SCIENTIFIC CONFERENCE

### **Laser jako innowacyjne narzędzie do cięcia stali w wielkogabarytowych konstrukcjach**

T. Setnik <sup>a</sup>, J. Płocica <sup>a</sup>, M. Bonek <sup>b</sup>

<sup>a</sup> Uczeń V Liceum Ogólnokształcące z Oddziałami Dwujęzycznymi im. Andrzeja Struga w Gliwicach, email: rozer0902@gmail.com

<sup>b</sup> Politechnika Śląska, Wydział Mechaniczny Technologiczny, Katedra Materiałów Inżynierskich i Biomedycznych  
email: mirosław.bonek@polsl.pl

**Streszczenie:** Artykuł omawia użycie technologii laserowej jako metody cięcia stali w wielkogabarytowych konstrukcjach. Technologia cięcia laserowego pozwala na duże udogodnienia w pracy, między innymi krótszy czas wykonywania operacji z porównywalną jakością krawędzi cięcia, większą możliwością manipulowania kształtem wycinanego elementu, precyzyjniejszym cięciem czy też mniejszym użyciem energii i zasobów materialnych.

#### **WPROWADZENIE**

Przy wielkogabarytowych konstrukcjach w wielu przypadkach potrzebna jest niezrównana precyzja. Często, niedokładność rzędu, nawet 1mm może spowodować brak oczekiwanego efektu co w rezultacie zwiększy koszty produkcji, materiałów itp. Tutaj z pomocą przychodzi technologia laserowa która w ostatnim czasie bardzo się rozwinęła przez co możemy ją stosować w prozaicznych czynnościach, ale także znajdujemy dlań zastosowanie w ważnych dziedzinach. Bez tej technologii nie byłoby np. Platform morskich, zaawansowanych statków kosmicznych lub współczesnych samochodów i to właśnie przez cięcie laserowe niedokładności przy cięciu stają się tak nieznaczące, że straty stały się bardzo niewielkie. Przy wielkogabarytowych konstrukcjach dzięki technologii laserowej możemy bardzo dokładnie wycinać elementy konstrukcji więc gdy już wycięte elementy będziemy składać w całość będą one pasowały bardzo dobrze, a szczeliny na poszczególnych łączeniach będzie niewidoczna, dlatego w tym artykule spróbujemy przedstawić państwu, dlaczego cięcie laserowe jest tak innowacyjne przy budowie wielkogabarytowych konstrukcji.

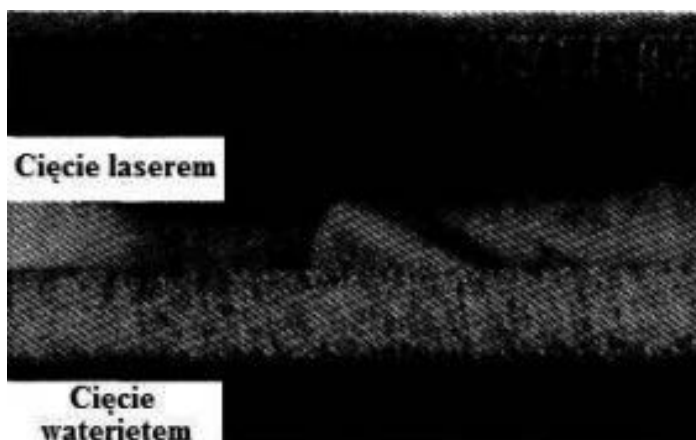
#### **ZASADA DZIAŁANIA LASERÓW W CIĘCIU STALI**

Do cięcia stali wykorzystuje się dwa typy cięcia laserowego, pierwszym jest cięcie przez topienie i wydmuchiwanie. Polega ono na topieniu stali i natychmiastowym wydmuchiwaniu

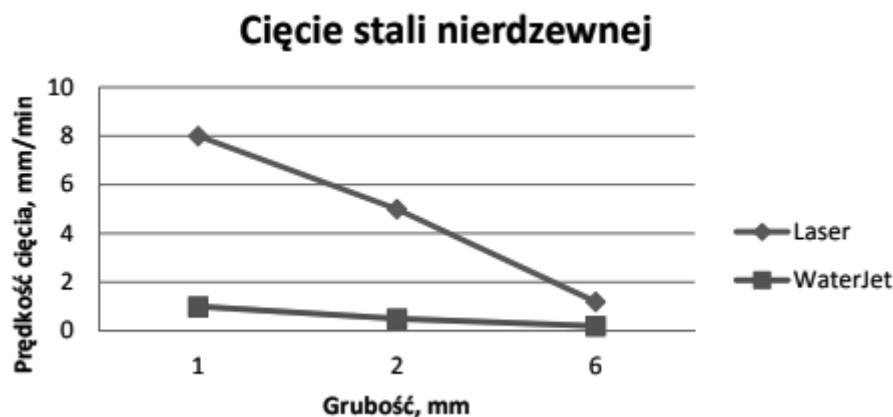
jej przez gaz ochronny. Wykorzystanie gazu ochronnego w dużym stopniu obniża zapotrzebowanie energii. Ten typ cięcia wykorzystuje się głównie do cięcia stali nierdzewnych. Drugim rodzajem cięcia laserowego wykorzystywanych przy cięciu stali jest cięcie przez wypalanie. Metoda ta jest podobna do topienia i wydmuchiwania, materiał poddawany jest działaniu skupionej wiązce, która topi materiał, jednocześnie przez powstałą szczelinę przepuszcza się gaz reaktywny, najczęściej tlen lub jego mieszanki, gaz reaguje z wydmuchiwanym materiałem spalając się. Metodę tą wykorzystuje się do stali węglowej [1].

## PRECYZJA, DOKŁADNOŚĆ I PRĘDKOŚĆ

Precyzja i dokładność cięcia laserowego są nieporównywalnie lepsza do między innymi cięcia wodą lub plazmą, jest też niezwykle szybki pomimo wysokiej precyzji, pozwala to na znaczne zmniejszenie kosztów, które zmniejszane są jeszcze bardziej przez brak potrzeby stosowania wody oraz ścierniwa. W porównaniu do cięcia wodą, dzięki cięciu laserowemu można uzyskać porównywalną jakość krawędzi cięcia w znacząco krótszym czasie (rys. 1 i 2) [1].



Rys. 1. Tekstura powierzchni cięcia stali nierdzewnej o grubości 2 mm [1]



Rys. 2. Porównanie prędkości cięcia stali nierdzewnej [1]

## **ZASTOSOWANIE W RÓŻNYCH BRANŻACH**

Wielkogabarytowe konstrukcje mogą nam się jawić w różnych branżach np.

### *-Przemysł budowlany*

W budownictwie laserowe cięcie stali wykorzystuje się do produkcji elementów konstrukcyjnych, takich jak belki, słupy, kształtki czy platformy. Duże i precyzyjne cięcia pozwalają na skonstruowanie solidnych i trwałych struktur co za tym idzie konstrukcja mostów i hal przemysłowych i innych dużych obiektów infrastrukturalnych.

### *-Przemysł energetyczny*

W sektorze energetycznym laserowe cięcie stali jest stosowane podczas konstrukcji dla elektrowni, zarówno konwencjonalnych, jak i odnawialnych. Stalowe ramy, podpory, które są wycinane z dużą precyzją przez co znacznie zwiększa się wydajność i trwałość infrastruktury energetycznej.

### *-przemysł lotniczy i kosmiczny*

Przy produkcji statków kosmicznych kontrola nad kształtami jest kluczowa, bo nawet najmniejszy błąd może doprowadzić do rozszczelnienia kadłuba w przestrzeni kosmicznej, ale przy budowie zwykłych samolotów pasażerskich można zwiększyć aerodynamiczność kadłuba co zmniejszy koszty użytkowania.

### *-przemysł morski*

Bez cięcia laserowego statki i platformy morskie byłyby bardziej podatne na korozję a cięcie laserowe skutecznie temu zapobiega przez dokładniejsze wycięcie i lepsze dopasowanie kształtu do wymaganego projektu.

### *-przemysł motoryzacyjny*

W produkcji pojazdów laserowe cięcie sprawdza się bardzo dobrze podczas wycinania elementów ramy i karoserii oraz bardziej skomplikowanych elementów oraz cięcie laserowe umożliwia na uzyskanie lekkich a jednocześnie wytrzymałych konstrukcji.

### *-przemysł petrochemiczny*

W sektorze petrochemicznym, gdzie konieczne są trwałe konstrukcje odporniejsze na ekstremalne warunki, laserowe cięcie stali jest używane do produkcji rurociągów, zbiorników i innych instalacji.

To są tylko nieliczne z wielu działów przemysłu w jakich cięcie laserowe ma zastosowanie dla wielkogabarytowych konstrukcji.

## **OPTIMALIZACJA KOSZTÓW I SUROWCÓW**

### *Kompresowanie wzorów i minimalizacja odpadów:*

Cięcie laserowe pozwala na efektywne ułożenie wzorów na arkuszu materiału, minimalizując przerwy między nimi. Zaawansowane oprogramowanie Computer Aided Design/ Computer Aided Manufacturing analizuje dostępny materiał i automatycznie zoptymalizuje

rozmieszczenie wzorów w taki sposób, aby zminimalizować straty materiałowe. Dzięki temu możliwe jest efektywne wykorzystanie każdej powierzchni arkusza, co przekłada się na redukcję zużywanych surowców.

#### *Automatyczne układanie wzorów:*

Nowoczesne systemy laserowe są często wyposażone w zaawansowane funkcje automatycznego układania wzorów. Komputer analizuje kształty i wielkości poszczególnych elementów do wycięcia oraz dostępny materiał, a następnie samodzielnie ustala optymalne rozmieszczenie wzorów na arkuszu. Ten proces automatyczny eliminuje konieczność ręcznego planowania układu, co znacznie przyspiesza proces produkcji.

#### *Redukcja odpadów i oszczędności surowców:*

Dzięki precyzyjnemu cięciu laserowemu, minimalizacji odstępów między wzorami oraz optymalnemu wykorzystaniu materiału, ilość odpadów generowanych podczas procesu produkcji jest znacznie mniejsza. Redukcja strat materiałowych przekłada się bezpośrednio na oszczędności surowców, co ma istotne znaczenie zarówno dla aspektów ekologicznych, jak i ekonomicznych przedsiębiorstwa.

#### *Optymalizacja czasu produkcji:*

Korzystając z zaawansowanego oprogramowania, można zoptymalizować czas cięcia poprzez inteligentne rozmieszczenie wzorów w taki sposób, aby minimalizować przejścia lasera między poszczególnymi elementami. Redukcja czasu pustego oraz optymalne ułożenie wzorów skutkują skróceniem całkowitego czasu produkcji, co ma bezpośredni wpływ na koszty operacyjne przedsiębiorstwa.

#### *Elastyczność i dostosowywanie do zmian:*

Automatyzacja procesów w cięciu laserowym pozwala na elastyczne dostosowywanie się do zmian w zamówieniach czy projektach. W razie potrzeby można łatwo modyfikować programy cięcia, a system automatycznie przystosuje się do nowych parametrów produkcji, co umożliwia skuteczne reagowanie na zmieniające się warunki rynkowe.

## **AUTOMATYZACJA I PROGRAMOWALNOŚĆ**

Automatyzacja i programowalność w procesie cięcia laserowego przynoszą dodatkowe korzyści, które dalej wpływają na efektywność produkcji w różnych branżach:

#### *Wszechstronność produkcji:*

Dzięki automatyzacji i programowalności, procesy cięcia laserowego można łatwo dostosować do różnych projektów i wymagań. Maszyny laserowe mogą obsługiwać różnorodne materiały i grubości, umożliwiając produkcję różnorodnych komponentów.

#### *Szybkie dostosowanie do zmiany projektu:*

W przypadku zmiany projektu lub potrzeby wprowadzenia nowych elementów, automatyzacja umożliwia szybkie dostosowanie programów bez konieczności długotrwałej zmiany ustawień maszyny. To znacznie przyspiesza proces przygotowania do produkcji.

#### *Eliminacja błędów ludzkich:*

Automatyzacja redukuje ryzyko błędów ludzkich, co jest szczególnie ważne przy produkcji masowej. Maszyny laserowe działają zgodnie z dokładnie zaprogramowanymi parametrami, co minimalizuje ryzyko pomyłek.

*Zwiększenie wydajności:*

Automatyczne systemy mogą pracować niemal bez przerwy, co znacznie zwiększa wydajność produkcji w porównaniu do manualnych metod. Długotrwała praca maszyn poza godzinami roboczymi przekłada się na skrócenie czasu produkcji.

*Optymalizacja ułożenia wzorów na materiale:*

Programowalność pozwala na optymalne ułożenie wzorów na arkuszu materiału. Systemy: Computer Aided Design/ Computer Aided Manufacturing mogą zoptymalizować rozmieszczenie elementów, minimalizując odpady i poprawiając efektywność wykorzystania surowców.

*Skalowalność produkcji:*

Dzięki programowalności i automatyzacji, produkcję można łatwo skalować w zależności od zapotrzebowania. Systemy te pozwalają na elastyczne dostosowanie produkcji do zmieniających się warunków rynkowych.

*Łatwość monitorowania i kontroli:*

Automatyczne systemy są łatwiejsze do monitorowania w czasie rzeczywistym. Operatorzy mogą śledzić postęp produkcji, monitorować jakość cięcia i szybko reagować na ewentualne problemy.

## **PODSUMOWANIE**

Przedstawione argumenty zarysowują szerokie zastosowanie technologii cięcia laserowego podczas produkcji wielkogabarytowych konstrukcji. Widać dobitnie, że technologia cięcia laserowego jest stosowana przy cięciu bardzo dużych elementów oraz tych niewielkich przez co sprawdza się ona na wielu etapach produkcji. Produkcja tak wielkich konstrukcji jak np. Platforma morską stałaby się bardzo ciężka bez użycia technologii cięcia laserowego i już w tym momencie ta technologia jest bardzo rozwinięta oraz stale znajdujemy dla niej nowe zastosowania. Warto dodać, że technologia cięcia laserowego cały czas się rozwija więc w niedalekiej przyszłości inne wielkogabarytowe konstrukcje znajdą dla niej zastosowanie.

## **PODZIĘKOWANIE**

Praca powstała w wyniku realizacji projektu realizowanego z uczniami szkoły ponadpodstawowej w ramach kształcenia zorientowanego projektowo - PBL, w ramach programu Inicjatywa Doskonałości – Uczelnia Badawcza, Politechnika Śląska.

**BIBLIOGRAFIA**

1. K. Musiła, K. Studnik, M. Bonek, Cięcie laserowe, Gliwice, 2014.
2. Wikipedia, Cięcia laserowe, strona internetowa:  
[https://pl.wikipedia.org/wiki/Cięcie\\_laserowe](https://pl.wikipedia.org/wiki/Cięcie_laserowe)
3. J. LeGrand, 5 ways to improve your flow of laser-cut parts, 2019, strona internetowa:  
<https://www.thefabricator.com/thefabricator/article/lasercutting/5-ways-to-improve-your-flow-of-laser-cut-parts>
4. <https://www.newtechsolutions.pl/systemy-cad-i-cam-roznice-i-zastosowanie>
5. <https://dps-software.pl/wytwarzanie/alphacam/>





26th January 2024  
Gliwice, Poland

DEPARTMENT OF ENGINEERING MATERIALS AND BIOMATERIALS  
FACULTY OF MECHANICAL ENGINEERING  
SILESIA UNIVERSITY OF TECHNOLOGY

## INTERNATIONAL STUDENTS SCIENTIFIC CONFERENCE

### The use of smart coatings as corrosion protection in the automotive industry

G. Sikorski <sup>a</sup>, R. Łosoń <sup>a</sup>, J. Zawadzki <sup>a</sup>, M. Bonek <sup>b</sup>

<sup>a</sup> Student of Silesian University of Technology, Faculty of Mechanical Engineering

<sup>b</sup> Silesian University of Technology, Faculty of Mechanical Engineering, Department of Engineering Materials and Biomaterials  
email: mirosław.bonek@polsl.pl

**Abstract:** The article discusses the development of smart coatings, including shape memory polymers and nano-scale coatings, in the context of addressing challenges related to corrosion and improving durability. It presents solutions based on research collaboration and hybrid coatings to enhance effectiveness.

**Keywords:** automotive, smart coatings, corrosion

### 1. INTRODUCTION TO THE PROBLEMS OF CORROSION IN THE AUTOMOTIVE INDUSTRY AND THE IMPORTANCE OF THE USE OF ANTI-CORROSION COATINGS

Corrosion is the process of material degradation through chemical reaction with its surroundings. In the automotive industry, corrosion is one of the main problems associated with vehicle use. The causes of corrosion are diverse and can result from moisture, salts, acids, bases, gases, or mechanical factors. In the case of vehicles, corrosion often results from the use of road salt, which is used to remove snow and ice during winter. Mechanical damage to protective coatings, such as paint or anti-corrosion coatings can also accelerate corrosion.

The consequences of corrosion in the automotive industry are very serious. Corrosion can weaken the vehicle's structure and affect its safety. Corrosion can also lead to mechanical failures, such as brake failure, which can be very dangerous on the road.

The impact of corrosion on the automotive industry is significant. Car manufacturers aim to minimize the risk of corrosion in their vehicles, as it can lead to failure and, ultimately, claims from customers. Therefore, car manufacturers use various methods to protect against corrosion, such as anti-corrosion coatings, galvanization, or the use of materials with high corrosion resistance. Meanwhile, in automotive service centers, particular attention is paid to detecting and repairing corrosion spots, which can prolong the life of the vehicle and ensure the safety of the driver and passengers.

### 1.1. The importance of using anti-corrosion coatings

The use of anti-corrosion coatings in the automotive industry has many benefits for both vehicle manufacturers and users. Below are the most important ones:

- Increased vehicle durability - anti-corrosion coatings protect the car body from external factors such as moisture, road salt, acid rain, or other chemical substances. By limiting corrosion, the car body is less susceptible to damage and can last longer.
- Ensuring driver and passenger safety - corrosion can weaken the vehicle's structure and ultimately lead to breakdowns, which pose a safety risk to the driver and passengers. The use of anti-corrosion coatings can help prevent such situations.
- Reducing repair and maintenance costs - if the car body is protected by an anti-corrosion coating, it requires less frequent maintenance and repairs than vehicles that are not protected. Reducing repair and maintenance costs translates into lower vehicle maintenance costs.
- Improving the manufacturer's image - car manufacturers who use effective corrosion protection methods have a better reputation among customers. Customers expect their car to be durable and reliable, and the use of anti-corrosion coatings helps meet those expectations.

### 1.2. The history of using anti-corrosion coatings in the automotive industry

The first car models had metal bodies that were prone to corrosion. To prevent corrosion, various methods were used, such as:

- Painting - car bodies were covered with paint that was supposed to protect metal from corrosion. However, the paint was prone to chipping and damage, which led to unprotected areas.
- Galvanizing - used in the 1930s, involved covering the car body with a layer of zinc, which was supposed to protect the metal from corrosion. However, this process was expensive and time-consuming, which limited its popularity.
- Oxidizing - this method involved covering metal with a layer of oxides, which protected the metal from corrosion. However, this process was not effective enough and did not provide long-lasting protection against corrosion.

### 1.3 Challenges related to preventing corrosion in the automotive industry

One of the challenges for manufacturers of anti-corrosion coatings is to provide products that will be effective for a long time and at the same time will be safe for the environment. Many countries are introducing increasingly restrictive regulations regarding the use of chemical substances, which forces manufacturers to change the formulas of their coatings and search for more environmentally friendly solutions.

Another challenge is to provide effective anti-corrosion protection for increasingly complex car designs. Electric, hybrid, and automated cars have many additional components that are susceptible to corrosion, such as batteries, electric motors, and other electronic elements. Therefore, manufacturers must develop special anti-corrosion coatings that are able to protect these components from corrosion.

## **2. THE USE OF SMART COATINGS AS CORROSION PROTECTION IN THE AUTOMOTIVE INDUSTRY**

Researchers are working on creating new coatings because the car industry needs coatings that are super good at protecting and fixing themselves, and are also eco-friendly. They want these coatings to be smart, so they can actively protect against damage from things like scratches or rust, making them last longer. There are different ways they're trying to make these smart and self-healing coatings. They're adding tiny capsules that have healing stuff inside, using special polymers that remember their shape or have blood vessel-like properties, and using certain materials that can heal themselves. Using both organic and inorganic materials for these coatings is attractive because it's cost-effective and simple, making it a good choice for cars [1].

Nowadays, protective coatings for things like cars need to be smart and react to any damage caused by the environment. They should be able to fix themselves, sticking back together and going back to how they were before. This is really important to make sure things like metal parts in cars last a long time, especially in places with tough chemicals. These coatings are made to actively protect metals from rust and fix themselves. Right now, the focus is on making coatings that can do a lot of things and react to different signals – they call them "smart" coatings. When something happens, like exposure to water, salty stuff, changes in acidity, scratches, or changes in temperature, these coatings can automatically control rust and keep the metal safe. It's like the coating knows what to do when something goes wrong, making it work better [2].

### **2.1. Definition of smart shape memory polymers coating**

Protective coatings for metal are like special layers that are a mix of different materials. These materials have different parts that determine how they work, like their chemical makeup, structure at different scales (big and small), and how they act on surfaces. The main part of this coating is called the binder, and it's like the glue that sticks everything together. This binder is crucial because it makes a strong barrier to stop water and other stuff from getting in, and it also sticks well to the metal. How well it works depends on its special properties, like the kind of material it's made of and how it's connected.

There's also something called pigments in these coatings. They're like tiny particles that can be really small or even microscopic. They're not just there for looks – they can protect, serve a purpose, or make things look good. The way they're made, their size, shape, amount, and where they are in the coating all affect how well they do their job and how they mix with the binder.

These protective coatings usually have multiple layers, like a primer, topcoat, and sometimes something in the middle. Each layer has a specific job (see Figure 1). To make sure these coatings stick well and protect the metal, you have to get the metal ready first. This can be done by rubbing it or treating it with special chemicals, like coatings that convert chromate/phosphate, anodization, sol-gel coatings, or using a mix of these methods. This is especially important when dealing with coatings on aluminum alloys [4].

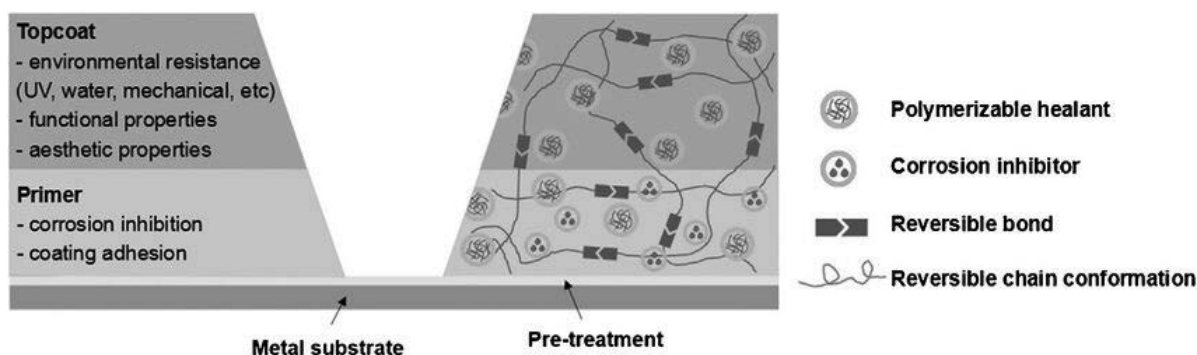


Figure 1. Basic structure and functions of a coating system and major self-healing mechanisms [4].

## 2.2. Smart nano-scale container anticorrosive coating for car bodies

To make metal surfaces more resistant to corrosion, a new type of self-repairing coatings has been developed. Traditional coatings primarily rely on creating a barrier to shield metal from corrosion. However, this protective mechanism can be compromised when the coating gets damaged and is exposed to corrosive electrolytes. One way to create effective coatings in the presence of corrosive electrolytes is by using corrosion inhibitors. These inhibitors can be classified into three types based on the mechanism they use to control the corrosion process: anodic, cathodic, and mixed inhibitors. The effectiveness of an inhibitor depends on its solubility, where very low solubility can result in poor passivating behavior on the metal substrate.

High solubility of inhibitors can have two drawbacks. Firstly, the inhibitor may be quickly washed out from the coating. Secondly, osmotic pressure can lead to blistering and delamination of the active surface, ultimately causing destruction of the passive layer. Consequently, adding active inhibitors at high concentrations in conventional processes is not practical. However, modern coatings have addressed this challenge by utilizing nanoscale containers to transport active agents like inhibitors. In this method, the active inhibitor is loaded into a nanocontainer with a permeable shell, enabling controlled release of the active agents into the coating matrix. Alternatively, the passive layer can be infused with active agents, but this may lead to instability and reduced self-repairing activity due to interaction between the active materials and the coating matrix. However, these issues can be avoided in systems loaded with nanocontainers as the coating matrix doesn't directly contact the active agents. This system is illustrated schematically in Figure 2 [5].

To keep active materials in a confined state, nanocontainers are evenly spread throughout a coating matrix. These nanocontainers are designed to release their contents in response to specific signals or environmental changes. The effectiveness of the anticorrosion performance of nanocontainers largely relies on their permeability and compatibility with the coating matrix. It is recommended to use nanocontainers within the size range of 300-400 nm, as larger sizes may lead to the formation of large hollow cavities in the coating matrix, significantly reducing the protective properties of the coating. The mechanism by which nanocontainers release active agents and protect attacked areas of the metal surface from corrosive electrolytes, forming a passive layer, is schematically depicted in Figure 3 (Shchukin et al., 2007) [5].

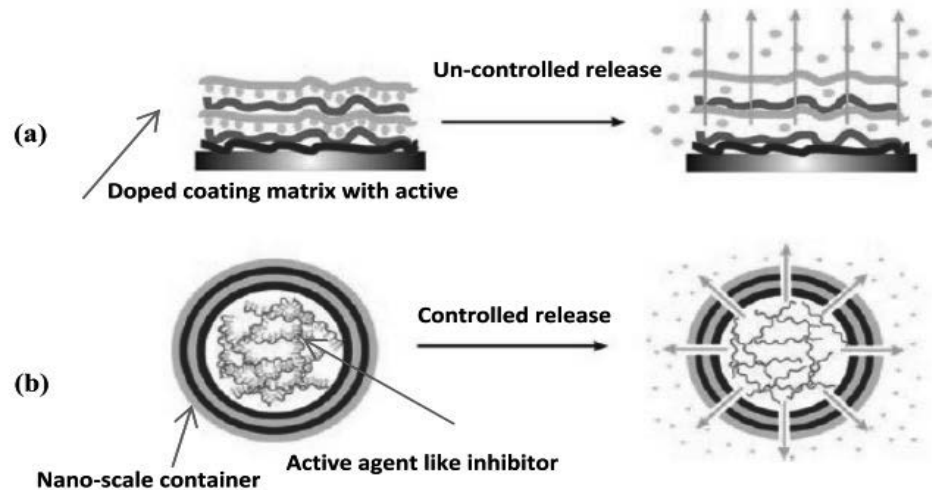


Figure 2. Active material is embedded in the “passive” matrix of the coating (a) and active material is encapsulated into nanocontainers (b). [5]

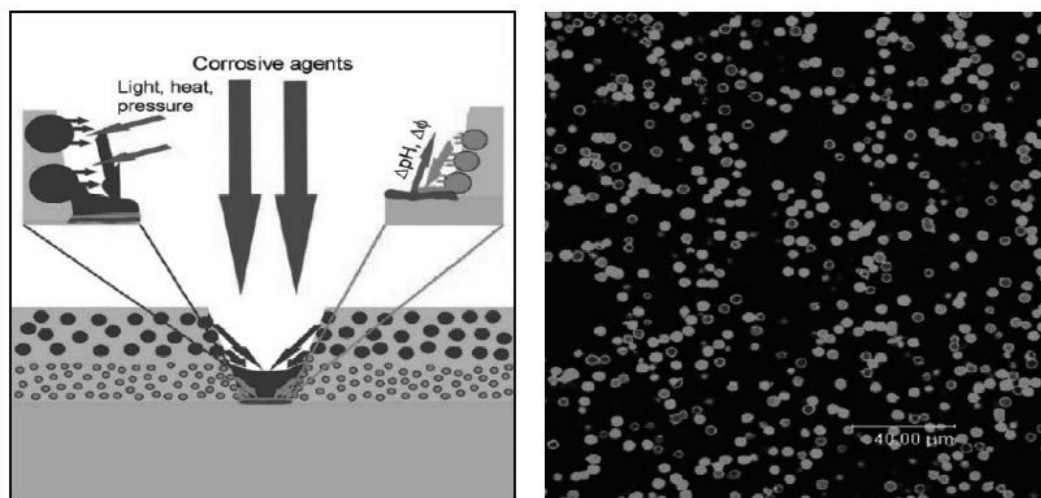


Figure 3. Schematic illustration of self-repairing mechanism of nanocontainers when metal is exposed to corrosive electrolyte. [5]

### 2.3. Comparison of smart shape memory polymers and Smart nano-scale container anticorrosive coating

Shape memory polymers and smart nano-scale container anticorrosive coatings are two innovative materials that have the potential to revolutionize the automotive industry. Both materials have unique properties that make them valuable in different applications.

Both materials have advantages in the automotive industry. SMPs can change their shape and return to their original shape, making them ideal for use in self-healing materials. This means that if a part made from SMP is damaged, it can repair itself, reducing the need for costly repairs or replacements. Additionally, SMPs can be used in sensors and actuators, which can improve the performance of a vehicle.

Smart nano-scale container anticorrosive coatings provide protection against corrosion for car bodies, which is a significant issue in the automotive industry. Corrosion can cause damage to the body of a car, reducing its lifespan and affecting its performance. The use of smart nano-scale container anticorrosive coatings can prevent this damage and extend the life of a vehicle.

However, both materials have limitations as well. SMPs are currently expensive to produce, which makes them less accessible for widespread use. Additionally, their performance can be affected by environmental factors, such as temperature and humidity. Smart nano-scale container anticorrosive coatings, on the other hand, may not be as effective in preventing corrosion in areas with high exposure to salt, such as coastal regions.

#### **2.4. The problems and possible solutions of using smart coatings as corrosion protection in the automotive industry.**

The automotive industry has been facing severe challenges related to corrosion, and smart coatings have been seen as a promising solution. However, the use of smart coatings as corrosion protection in the automotive industry is not without challenges.

##### **2.4.1. Compatibility issues**

Smart coatings face compatibility challenges when used in the automotive industry since they must be able to adhere to different materials, including metals, plastics, and composites. This obstacle has limited the widespread use of smart coatings in industry.

One solution to this challenge is to invest in research and development to improve the compatibility of these coatings with different materials used in vehicle manufacturing. Collaborating with material suppliers to develop smart coatings that are specifically designed to adhere to various materials can also be effective.

##### **2.4.2. Durability issues**

Smart coatings provide advanced features like self-healing and self-cleaning abilities, but they are frequently less durable than traditional coatings due to these features. This could be an issue in the automotive industry, where cars are subjected to harsh conditions, including corrosive agents such as salt, moisture, and chemicals, and smart coatings may not be able to withstand them.

Developing hybrid coatings that combine the self-healing and self-cleaning abilities of smart coatings with the durability of traditional coatings is a promising approach.

##### **2.4.3. High cost**

Another significant challenge associated with the use of smart coatings is the high cost. Smart coatings require advanced materials and technologies, which make them more expensive than traditional coatings. This cost factor has been a significant barrier to the widespread adoption of smart coatings in the automotive industry, where cost is a crucial consideration.

One solution to this challenge is to invest in research and development to reduce the cost of producing smart coatings by exploring more cost-effective materials and manufacturing techniques. Collaborating with suppliers to negotiate lower prices for raw materials and equipment can also help reduce the cost of these coatings.

#### **2.4.4. Application issues**

The application of smart coatings is more complex than traditional coatings. Smart coatings often require specialized equipment and techniques, and the application process is more time-consuming. In the fast-paced automotive industry, where time is of the essence, this can be a significant issue. Additionally, the application of smart coatings requires skilled personnel, and the training of personnel can be costly.

One possible solution is to develop simplified application techniques that require less specialized equipment and personnel training. Investing in automation technology to improve the efficiency of the application process can also help reduce the time and labor required to apply smart coatings.

### **3. CONCLUSION**

Corrosion is a significant issue in the automotive industry, with various types of corrosion affecting different components of a vehicle. The prevention and control of corrosion in automobiles are critical for maintaining vehicle safety and prolonging the life of the car. Car manufacturers and automotive service centers need to take corrosion seriously and implement appropriate prevention and control measures to ensure the safety and satisfaction of their customers. By using effective protection methods and repairing corrosion spots, the negative impact of corrosion on the automotive industry can be reduced, ultimately leading to a safer and more durable vehicle for drivers and passengers.

The use of smart anti-corrosion coatings in the automotive industry is a promising approach to improving vehicle lifespan and reducing maintenance costs. However, addressing the challenges associated with these coatings is essential to ensure their effective use. Investing in research and development, collaborating with suppliers and material manufacturers, and exploring new technologies and techniques are some possible solutions to these challenges. By implementing these solutions, the automotive industry can fully realize the potential benefits of using smart anti-corrosion coatings.

While shape memory polymers and smart nano-scale container anticorrosive coatings are two innovative materials with unique properties and applications, they serve different purposes in the automotive industry. SMPs have the potential to improve the performance of vehicles through their use of sensors and actuators, as well as their self-healing properties. Smart nano-scale container anticorrosive coatings, on the other hand, can protect car bodies from corrosion and extend the lifespan of vehicles. Both materials have limitations, but their advantages make them valuable for use in the automotive industry.

### **ACKNOWLEDGEMENT**

The work was created as a result of the project of the Student Scientific Circle “Laser Surface Treatment” operating at the Department of Engineering Materials and Biomaterials at the Faculty of Mechanical Engineering, Silesian University of Technology.

**BIBLIOGRAPHY**

1. Zhang, F., Ju, P., Pan, M., Zhang, D., Huang, Y., Li, G., & Li, X. (2018). Self-healing mechanisms in smart protective coatings: a review. *Corrosion Science*. doi: 10.1016/j.corsci.2018.08.005
2. Stankiewicz, A., Szczygieł, I. & Szczygieł, B. Self-healing coatings in anti-corrosion applications. *JMater Sci* 48, 8041–8051 (2013)
3. Fan Zhang, Pengfei Ju, Mengqiu Pan, Dawei Zhang, Yao Huang, Guoliang Li, Xiaogang Li, Self-healing mechanisms in smart protective coatings: A review,
4. *The Role of Nanotechnology in Automotive Industries*. Mohsen Mohseni, Bahram Ramezanzadeh, Hossein Yari and Mohsen Moazzami Gudarzi
5. Shchukin, D. and Möhwald, H. (2007), Self-Repairing Coatings Containing Active Nanoreservoirs. *Small*, 3: 926-943.





26th January 2024  
Gliwice, Poland

DEPARTMENT OF ENGINEERING MATERIALS AND BIOMATERIALS  
FACULTY OF MECHANICAL ENGINEERING  
SILESIA UNIVERSITY OF TECHNOLOGY

## INTERNATIONAL STUDENTS SCIENTIFIC CONFERENCE

### Comparison of surface topography and electrical properties of crystalline silicon solar cells (part I)

B. Śmieszek<sup>a</sup>, W. Pelka<sup>a</sup>, O. Płaczek<sup>a</sup>, M. Musztyfaga-Staszuk<sup>b</sup>, A. Drygała<sup>c</sup>, J. Popis<sup>c</sup>, M. Staszuk<sup>c</sup>

<sup>a</sup> Pupil, Complex of Communication Schools, Warszawska 35, 44-100 Gliwice, Poland

<sup>b</sup> Silesian University of Technology, Faculty of Mechanical Engineering, Welding Department, Konarskiego 18a, 44-100 Gliwice, Poland

<sup>c</sup> Silesian University of Technology, Department of Engineering Materials and Biomaterials, Konarskiego 18a, 44-100 Gliwice, Poland

email: malgorzata.musztyfaga@polsl.pl

**Abstract:** The study aims to compare the obtained results of the electrical (contact resistance and resistivity between the emitter and the front metallization grid) and microstructural properties of two types of crystalline silicon solar cells.

**Keywords:** crystalline silicon solar cells, front electrode, electrical parameters

## 1. INTRODUCTION

### 1.1. Renewable energy sources (RES)

Renewable energy sources (RES) are resources where energy has been created and using them does not cause long-lasting deficiency [1]:

- *Solar energy* – the energy of the sun's radiation that is converted into electricity thanks to solar cells or into heat by using solar collectors.
- *Wind energy* – kinetic energy of the moving air masses. Wind power converts this energy into electricity by turbines.
- *Water energy* - which uses the mechanical energy of flowing water. An example is a hydroelectric power plant located on a river that converts this energy into electricity by hydrogenators.
- *Geothermal energy* - which uses heat energy from the inside of the Earth. It is used to heat water at homes by using heat pumps or to produce electricity.
- *Biomass energy* - which uses different organic plant materials like straw, municipal wastes, and biofuels.

The Sun is a star of middle magnitude. In astronomic terminology is called a “*yellow dwarf*”. In a shorter time than one hour, the sun emits such an amount of energy as mankind

uses in the term of one year [2,3]. Within all sources of energy mentioned earlier, we connect the biggest hope with solar power engineering [4,5].

One of the technologies enabling the harnessing of solar energy is photovoltaic technology, which allows for the direct conversion of solar radiation into electricity. No other method of energy acquisition is as clean, environmentally friendly, and universally applicable. Nevertheless, it is necessary to install special photovoltaic devices, thanks to which it is possible to convert solar energy into electricity. However, this involves costs. Photovoltaic systems can deliver electricity through devices and/or power grids. Big reliability, the silence of work, and minimal impact on the environment are characteristic advantages of that process. Therefore, it is important to take up issues related to improving the performance of materials for photovoltaic applications in research [4-8].

## 1.2. Classification of photovoltaic cells

Photovoltaic cells can be classified according to:

### ▪ First generation

The I-generation solar cells are mainly based on crystalline silicon. They are divided into monocrystalline and multicrystalline silicon solar cells. At present, silicon is the basis for about 90% of global solar cell production. This is due to the widespread occurrence of silicon and its semiconductor properties. The scheme of an I-generation solar cell is shown in Figure 1. Monocrystalline silicon solar cells (mono-Si) have the highest efficiency of converting solar energy into electricity, which can range from about 15% to over 24%. Multicrystalline silicon solar cells (multi-Si) have a slightly low efficiency, which can range from about 13% to 18% [9,10,13].

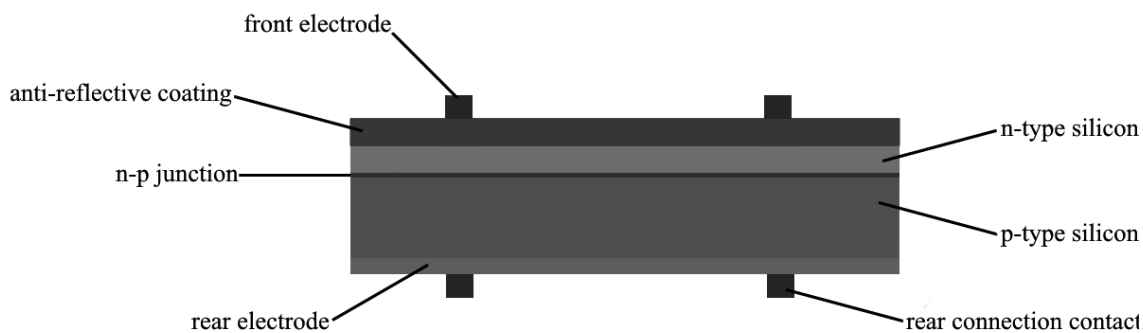


Figure 1. The scheme of a first-generation solar cell (example) [9].

### ▪ Second generation

The II-generation solar cells are based on thin-film production technology. These include thin-film cells made of cadmium telluride (CdTe), semiconductors composed of copper, selenium, indium, gallium (CIGS), amorphous silicon. Thin-film solar cells are characterized by a very thin (1-3  $\mu\text{m}$ ) layer of semiconductor. The II-generation solar cells are characterized by high efficiency, some reach up to 23%, which is worse efficiency than in the case of monocrystalline silicon solar cells, but they are cheaper to produce [9,10,13].

### ▪ Third generation

The III-generation solar cells are based on the production of devices composed of several materials. Third-generation solar cells are designed to achieve high power-conversion

efficiency while being low-cost to produce. These are dye-sensitized solar cells, perovskite-based cells, organic photovoltaics, quantum dot solar cells, and tandem solar cells, a stacked form of different materials utilizing a maximum solar spectrum to achieve high power conversion efficiency [9,10,13].

### 1.3. Technology of producing silicon cells

Currently, the most popular base material for the production of solar cells is crystalline silicon. The most important reason for the use of silicon is that the cells based on them achieve high efficiency at constantly decreasing costs. Silicon is common in nature, which means that there is no fear of its deficiency with the growing scale of production. The technologies used to make crystalline silicon-based cells have been widely known for many years [11, 14,15]. The scheme of the individual technological steps is shown in Figure 2.

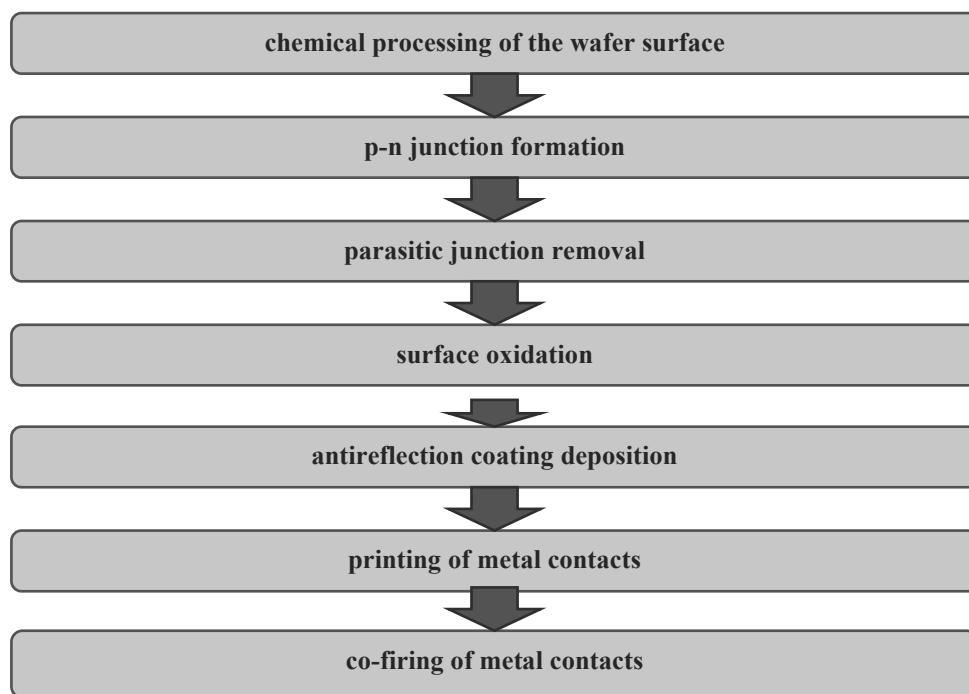


Figure 2. The scheme of individual technological steps in the solar cell production (example) [11,12].

The paper presents a series of mono- and multicrystalline silicon solar cells with front metallization produced by a conventional method (through co-firing it in a belt furnace), and next to compare their structure, and electrical properties.

## 2. MATERIAL

The material parameters of silicon used to produce the solar cells examined in this work are summarized in Table 1. These were mono- and multicrystalline silicon wafers from Deutsche

Solar AG. Solar cells were made with the same technology. The front electrode was deposited from commercial paste PV19B using screen-printing method and co-fired at 920°C in a belt furnace.

Table 1. Parameter of crystalline silicon

Conductivity	type p
Dopant	bor
The thickness of the wafer	200 ± 30 μm
Surface area	5 cm x 5 cm
Resistivity	1 ÷ 3 Ω·cm

### 3. METHODOLOGY

Measurements of selected parts of solar cells were made using a measuring station equipped with a Corescan device, which was designed by SunLab. As a part of the research, two operating modes of the device were used: Core scan (Contact Resistance Scan) and LBIC (Light Beam Induced Current). The Core scan mode using the PD (Potential Differences) method allows for mapping the contact resistance  $R_c$  and resistivity  $\rho_c$  between the emitter and the front metallization grid of solar cell. The measurement was performed at current density 30 mA/cm<sup>2</sup>. However, this is a destructive method. By the LBIC method, the distribution of the short-circuit current is obtained, without damage to the tested cell. Both methods allow the presentation of the obtained result in the form of 2D and 3D graphic figures.

The surface topography of the front contacts was performed using the ZEISS SUPRA 35 scanning electron microscope (SEM). The analysis of the chemical composition of the front electrode and the surface of solar cells was performed using the method of energy dispersive X-ray spectroscopy (EDS).

### 4. RESULTS

#### 4.1. Electrical properties

The results of the electrical properties measurements of the investigated samples obtained applying a Corescan device using the PD method are summarized in Table 2.

Table 2. Parameters of contact resistance and resistivity between the emitter and the front metallization grid of solar cell, where  $T_M$  – temperature of co-firing metalization,  $V$  - voltage

Solar cell number	Silicon type	$T_M$ [°C]	$V$ [mV]	$R_c$ [Ωcm]	$\rho_c$ [mΩcm <sup>2</sup> ]
1	Monocrystalline	920	8.3	2.5	30
2	Multicrystalline			5	60

Based on the obtained results, it was found that solar cells were characterized by a low value of contact resistance on the connection metal-semiconductor. For a monocrystalline silicon solar cell, were obtained twice the low value of contact resistance and resistivity, using the

same voltage value. Figure 3 shows the results of the measurement of the short-circuit current distribution in silicon solar cells using a Corescan device by the LBIC method. The differences in the distribution of the short-circuit current can be attributed to areas with a reduced lifetime of carriers. In the case of short-circuit current distribution on the surface of a monocrystalline solar cell, it was found that it is more uniform and ranges from 25 to 30 mA/cm<sup>2</sup>. However, in the case of the distribution of the short-circuit current on the surface of a multicrystalline silicon solar cell, it was found that it is less uniform and is in the range between 25 and 45 mA/cm<sup>2</sup>.

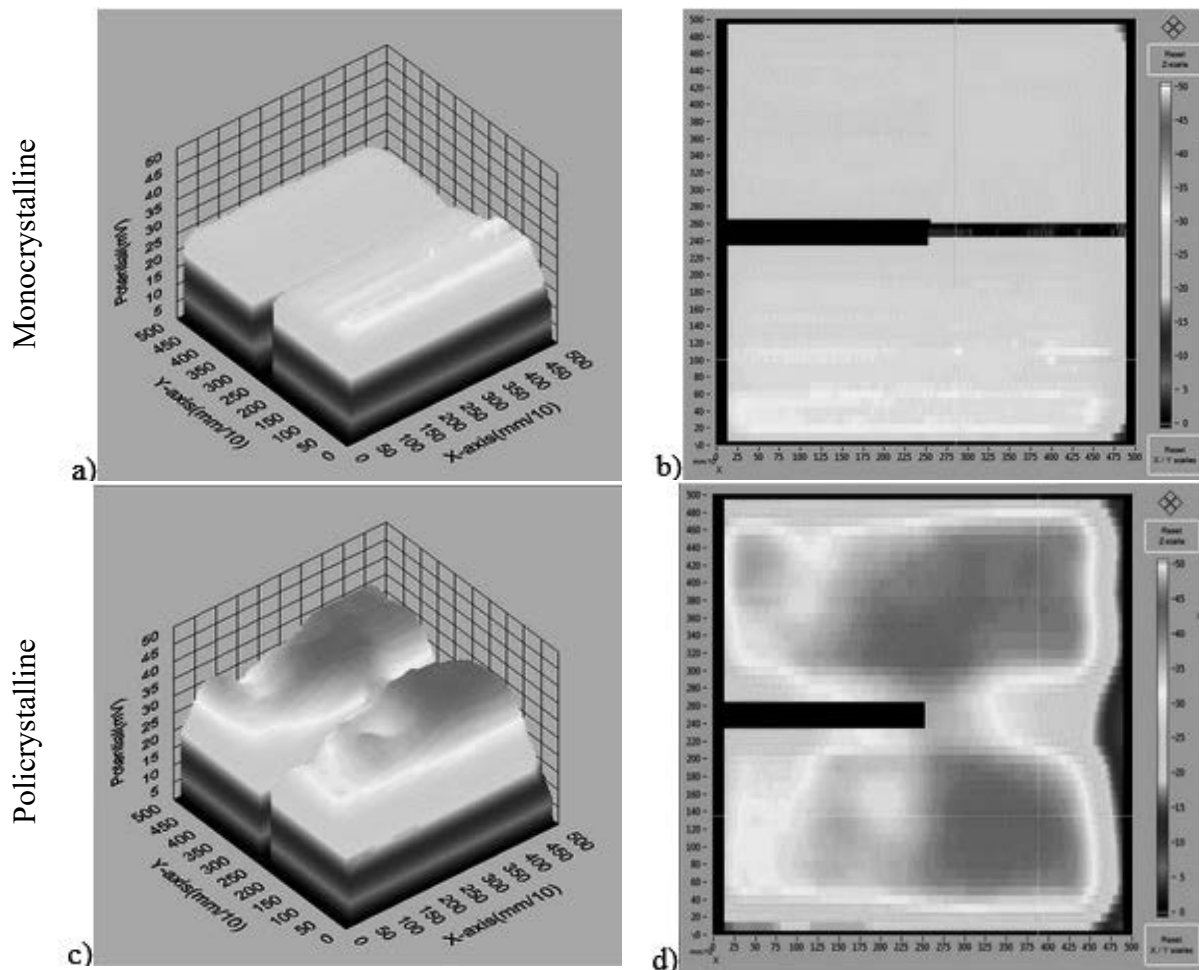


Figure 3. The short-circuit current distribution on the surface of a solar cell: 3D (a, c) and (b, d) 2D image.

#### 4.2. Microstructural properties

Surface observations in a scanning electron microscope at magnifications of the 10 000x the front electrode applied from a commercial paste and co-fired in a belt furnace on the surface of mono- and multicrystalline silicon solar cells are shown in Figure 4. Microscopic observations show that the morphology of the front electrodes shows a porous structure containing a dense grid of connections between the agglomerates of grains (Figure 4.)

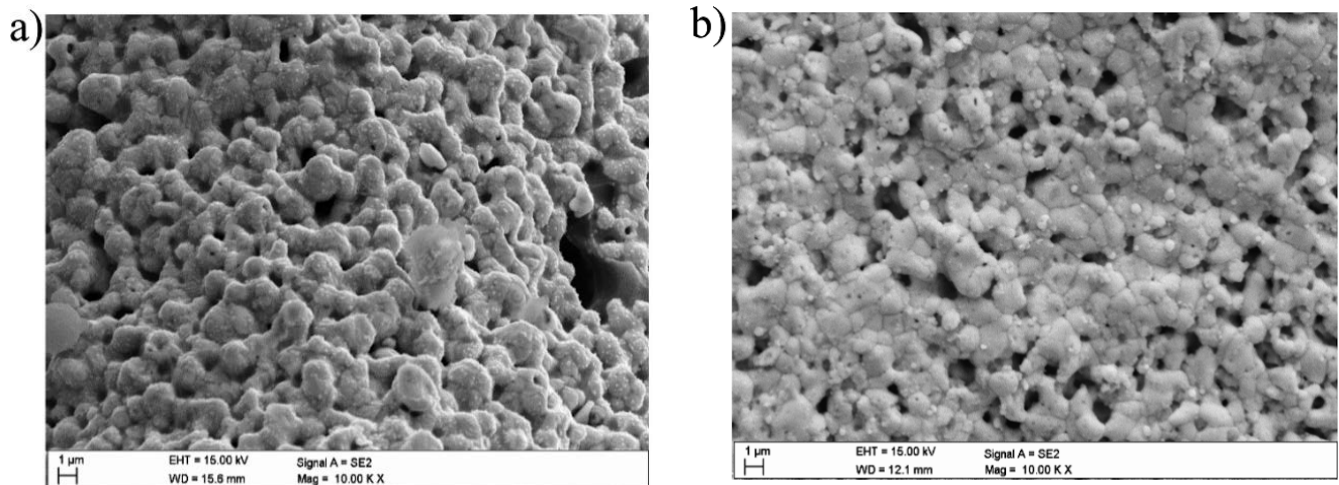


Figure 4. Topography of the front electrode surface made of PV 19B paste manufactured on the a) monocrystalline and b) multicrystalline silicon (SEM)

Microscopic observations with chemical composition analysis confirm the presence of elements suitable for the substrate (element Si) with deposited layers and the front electrode (mainly the element Ag) of solar cells (Figures 5 and 6).

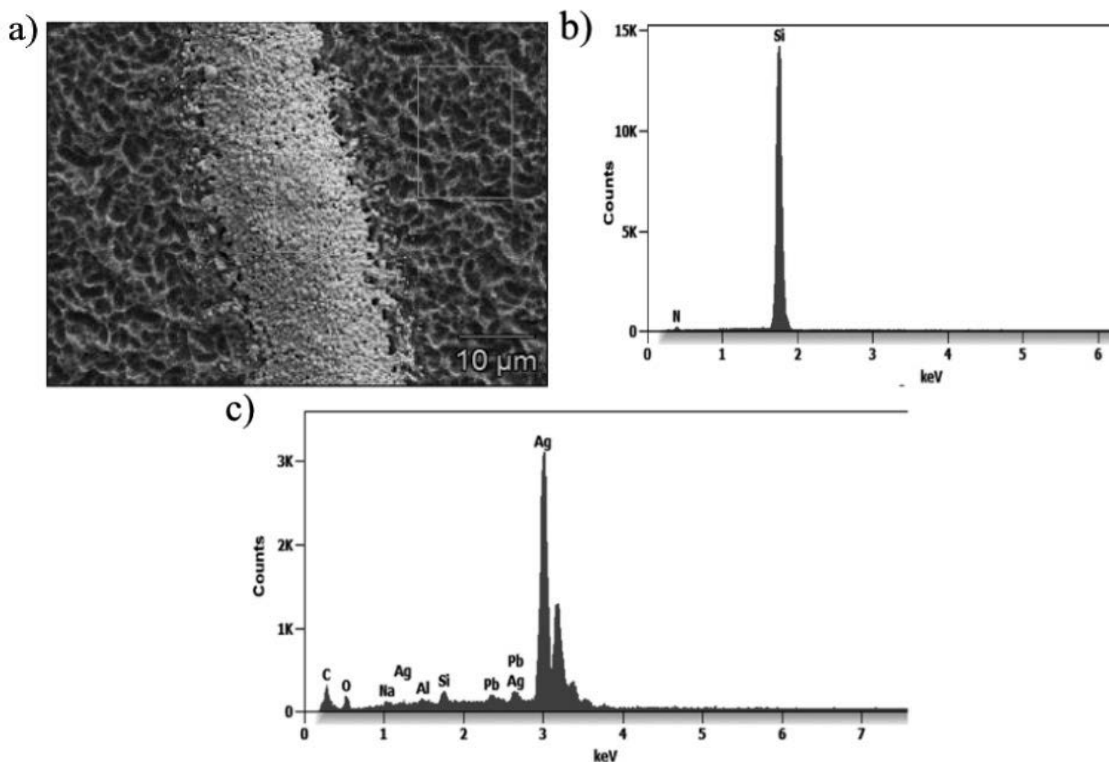


Figure 5. a) Topography of a monocrystalline silicon solar cell and EDS microanalysis from the area: b) 1 (silicon with deposited layers) c) 2 (front electrode)

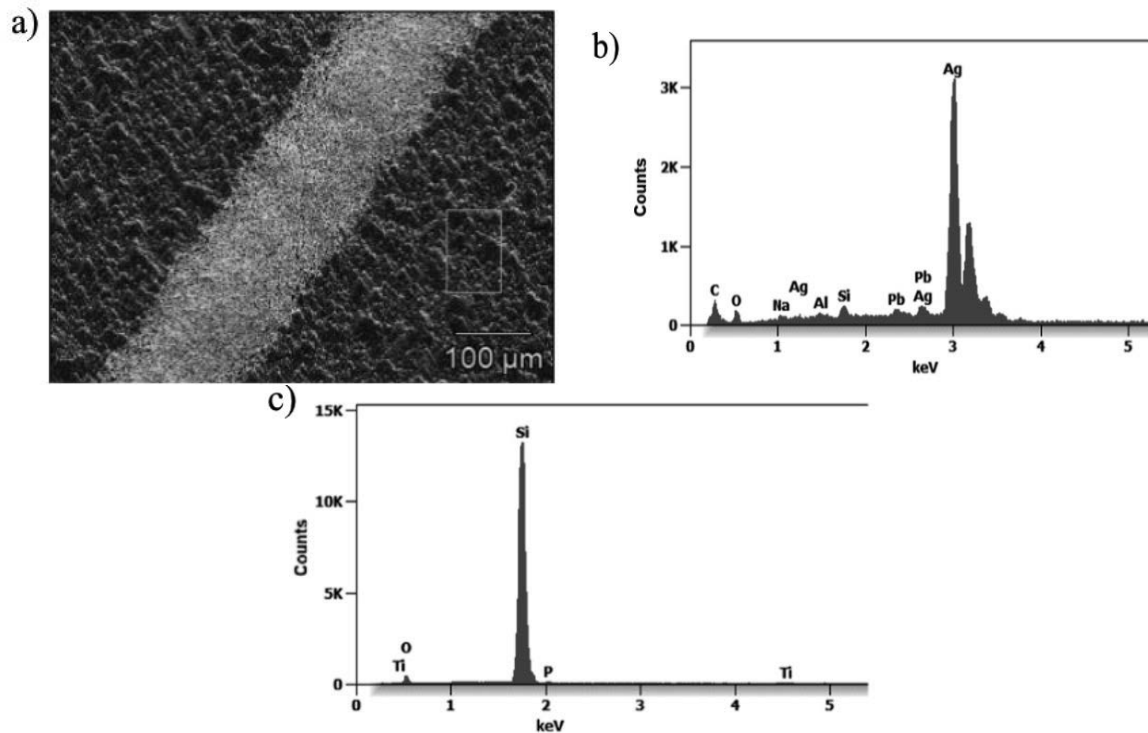


Figure 6. a) Topography of a multicrystalline silicon solar cell and EDS microanalysis from the area: b) 1 (silicon with deposited layers) c) 2 (front electrode)

## 5. SUMMARY

Based on the results of the study, it was found, that the solar cells produced with a front electrode manufactured from commercial paste PV19B co-fired at 920°C in a belt furnace in one mono- and multicrystalline silicon-based process showed some differences in the results measurements of electrical properties. The lowest value of contact resistance ( $R_c=2.5 \Omega\text{cm}$ ) and resistivity ( $\rho_c=30 \text{ m}\Omega\text{cm}^2$ ) were obtained for a monocrystalline silicon solar cell. Additionally, a more uniform distribution of short-circuit current on the surface (range from 25 to 30  $\text{mA}/\text{cm}^2$ ) was obtained for this type of solar cell. However, in the case of structural studies, it was found that the morphology of the front electrodes shows a porous structure containing a dense network of connections between agglomerates of grains. The analysis of the chemical composition also confirmed the presence of elements suitable for the deposited layers and the front electrode.

The subject matter is part of the priority research area of the Silesian University of Technology „Climate and environmental protection, modern energy” which includes a direct reference to research related to photovoltaics, and, special attention was paid to improvement of solar cells efficiency.

## ACKNOWLEDGMENTS

The work was created as a result of a project carried out with secondary school pupils as a part of the Excellence Initiative - Research University program, Silesian University of Technology.

## BIBLIOGRAPHY

1. P. Tyrpa, K. Frączek, P. Pilarski, *Odnawialne źródła energii*, 2017.
2. [www.sharp.eu/cps/rde/xchg/pl/hs.xsl/-/html/photovoltaic.html](http://www.sharp.eu/cps/rde/xchg/pl/hs.xsl/-/html/photovoltaic.html)
3. R. Loska, A. Drygała, *Zastosowanie krzemowych ogniw słonecznych w systemach fotowoltaicznych*, PSKN, Nr 21, Gliwice, 2009.
4. M.T. Sarniak, *Podstawy fotowoltaiki*, OWPW, Warszawa, 2008.
5. Drygała A., *Wpływ teksturowania laserowego na własności fotowoltaiczne krzemu polikrystalicznego*, Praca doktorska, Biblioteka Główna Politechniki Śląskiej, Gliwice, 2007.
6. J. A. Januszka, A. Drygała, L.A. Dobrzański, *Moduły fotowoltaiczne – sposób na tanią energię elektryczną*. Materiały Konferencyjne XXXVI Szkoły Inżynierii Materiałowej, Kraków-Krynica, 2008, 287-291.
7. L.A. Dobrzański, *Niemetalowe materiały inżynierskie*, Wydawnictwo Politechniki Śląskiej, Gliwice, 2008.
8. L.A. Dobrzański, *Materiały inżynierskie i projektowanie materiałowe: podstawy nauki o materiałach i metaloznawstwo*”, Wyd. 2, zm. i uzupeł., WNT, Warszawa, 2006.
9. B. Szymański, *Instalacje fotowoltaiczne*, Wydanie VII, Kraków 2018.
10. [https://zielonestrefy.pl/materiały-stosowane-w-fotowoltaiceIwAR35oenMCR2VlvV8Wa/?fbclid=i0bL\\_PfPSpIGFIkayHnhVqgDJyrBhVS7yEiZ38-](https://zielonestrefy.pl/materiały-stosowane-w-fotowoltaiceIwAR35oenMCR2VlvV8Wa/?fbclid=i0bL_PfPSpIGFIkayHnhVqgDJyrBhVS7yEiZ38-)
11. K. Drabczyk, P. Panek, M. Lipiński, P. Zięba, *Ogniwa fotowoltaiczne na bazie krzemu krystalicznego w aspekcie technologii przemysłowych*, I Krajowa Konferencja Fotowoltaiki, 2009, Krynica-Zdrój.
12. P. Panek, M. Lipiński, E. Bełtowska-Lehman, K. Drabczyk, R. Ciach, *Industrial technology of multicrystalline silicon solar cells*, *Opto-Electronic Review* 17 (2), 2009.
13. A. Mroziński, J. B. Flizikowski, *Inżynieria instalacji fotowoltaicznych*, Wydawnictwo Grafpol Agnieszka Blicharz-Krupińska, 2016.
14. J. Paska, R. Bielas, M. Bartecka, *Odnawialne źródła energii w Polsce-rozwoj i perspektywy*, Politechnika Lubelska, 2017.
15. M. Muszyfaga-Staszuk, *Nowe kompozyty na bazie miedzi w zastosowaniu do wytwarzania krzemowych ogniw fotowoltaicznych*, Monografia, Wydawnictwo Politechniki Śląskiej, vol. 778, 2019.





26th January 2024  
Gliwice, Poland

DEPARTMENT OF ENGINEERING MATERIALS AND BIOMATERIALS  
FACULTY OF MECHANICAL ENGINEERING  
SILESIA UNIVERSITY OF TECHNOLOGY

## INTERNATIONAL STUDENTS SCIENTIFIC CONFERENCE

### Quality management of the laser cutting process in the manufacture of stainless steel parts

Iu. Sokolan <sup>a</sup>, K. Sokolan <sup>b</sup>, P. Maidan <sup>c</sup>, O. Polishchuk <sup>d</sup>, M. Bonek <sup>e</sup>

<sup>a</sup> Khmelnytskyi National University, Faculty of Engineering Mechanics, Khmelnytskyi, Ukraine  
email: sokolan.julia@gmail.com.

<sup>b</sup> Khmelnytskyi National University, Faculty of Engineering Mechanics, Khmelnytskyi, Ukraine  
email: sokolan.kateryna@gmail.com .

<sup>c</sup> Khmelnytskyi National University, Faculty of Engineering Mechanics, Khmelnytskyi, Ukraine  
email: maidanp@khnmu.edu.ua.

<sup>d</sup> Khmelnytskyi National University, Faculty of Engineering Mechanics, Khmelnytskyi, Ukraine  
email: opolishchuk71@gmail.com.

<sup>e</sup> Silesian University of Technology, Faculty of Mechanical Engineering, Department of Engineering Materials and Biomaterials, Gliwice, Poland

**Abstract:** Increasing the efficiency of the laser cutting process, as well as its flexibility and quality, can reduce production costs. Machining stainless steel is associated with a number of difficulties, which, in turn, are caused by the material's properties. That is why laser cutting is one of the most effective methods of processing stainless steel. The quality of manufactured parts is inextricably linked to cutting modes. The paper envisages the optimisation of stainless steel laser cutting modes using the Taguchi method. Such parameters of the cut as roughness, heat affected zone, and geometric shape deviation were studied. The studies were carried out on a Smart 3015 laser cutting machine. The control variables of laser cutting according to the Taguchi method and their influence on the response variables were determined. According to the results of the studies, it was found that the smallest deviations in geometric shape, thermal impact zone, and surface roughness are achieved at a laser speed of 40 cm/min, laser power of 1000 W, frequency of 50 Hz, and gas pressure of 0.5 MPa. In addition, the percentage effect of each cutting parameter on the response variables was determined. A study using the Taguchi method showed that 80-90% of the influence is exerted by the laser power.

**Keywords:** laser cutting, laser cutting modes, orthogonal array, Taguchi method, stainless steel, roughness, geometric shape deviation, heat affected zone.

## 1. INTRODUCTION

The use of laser technology is a progressive trend in mechanical engineering that has developed significantly in recent years. The use of laser radiation is effective in the aviation and

automotive industries, as well as in specialized industries involving the use of hard-to-process materials. The capabilities of a focused laser beam as a universal tool are unique [1].

Stainless steel is widely used in construction, industry and engineering systems. For parts such as fittings, flanges, stainless pipes, etc., it is the main raw material for manufacturing.

The machining of stainless steel is associated with a number of difficulties, which, in turn, are caused by the material's properties. These challenges include:

- rapid wear of the cutting tool;
- the need for constant chip removal;
- increase in material density during deformation [2].

## 2. FORMULATION OF THE PROBLEM

To maintain the established level of quality of manufacturing parts and high productivity of the laser cutting process itself, it is important to select the optimal cutting parameters. These parameters affect the characteristics of the finished parts, which is reflected in the roughness of the surface, the width of the slot, and the size of the heat affected zone.

The aim of the study is to optimize such laser cutting parameters as laser frequency and power, cutting speed and gas pressure using the Taguchi method.

## 3. PRESENTING MAIN MATERIAL

Taguchi methods are statistical methods aimed at improving the quality of manufactured parts. These methods are widely used to improve the quality of manufactured parts in engineering and biotechnology [3]. The Taguchi method offers a systematic and fairly simple approach to optimizing productivity in manufacturing. The main purpose of this method is to improve the quality of products, regardless of their application, or to minimize productivity variations and processes to achieve target performance indicators.

The Taguchi method uses a number of variables, namely:

- control variables (denoted by  $X$ ) are variables that can be controlled during the manufacturing of a part;
- noise variables (denoted by  $Z$ ) are variables that are impossible or too difficult to control in the production of a part. Such noise variables can cause changes in the  $Y$  response variables and lead to a loss of quality in the manufactured product;
- response variables (denoted by  $Y$ ) - represent performance characteristics and control functions.

The procedure for applying the Taguchi method is summarized in Fig. 1. The Taguchi method estimates the average performance by intersecting two arrays: an outer array created for noise variables and an inner array created on the basis of control variables. The loss function is mainly used to measure the loss of quality that can be associated with a deviation from the target performance value and has the form:

$$L(y) = k \cdot (y - T)^2, \quad (1)$$

where  $L(y)$  is the value of the loss function;  $y$  is the quality indicator to be measured;  $k$  is the scale factor;  $T$  is the nominal value of the quality indicator.

According to the Taguchi method, the value of the averaged indicators is calculated using Formula 2, the standard deviation is calculated using Formula 3, and the response is calculated using Formula 4.

$$L(y) = \log\left(\frac{\sum y^2}{n}\right), \tag{2}$$

$$L(y) = \log\left(\frac{\sum \frac{1}{y^2}}{n}\right), \tag{3}$$

$$L(y) = \log\left(\frac{y^2}{s^2 y}\right), \tag{4}$$

where  $n$  is the number of studies conducted;  $y$  is the results of the respective response variables;  $s^2 y$  is the variance of  $y$ .

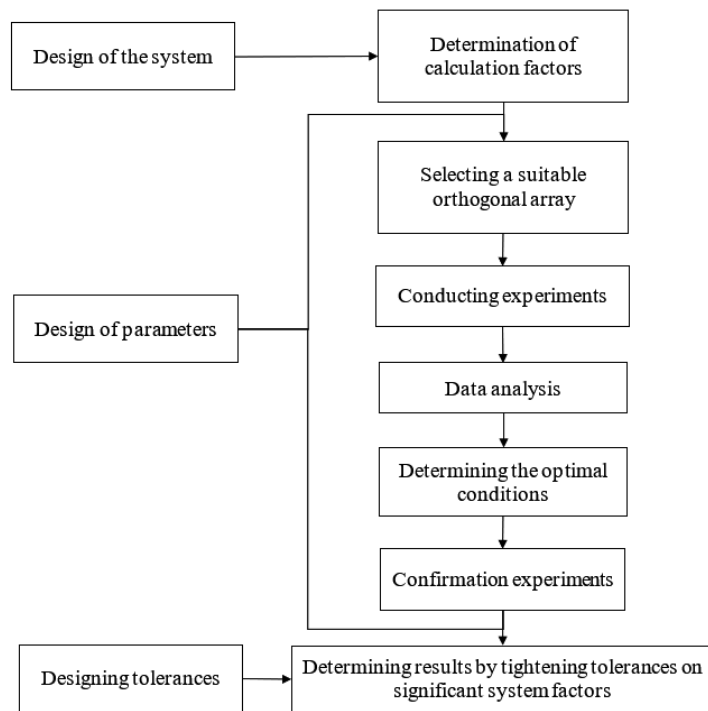


Figure 1 – Stages of research by the method of orthogonal arrays

The Smart 3015 machine was used to obtain the experimental results. The research was carried out for the process of laser cutting of thick sheet metal parts.

The parameters of the Taguchi method studies were the heat affected zone (HAZ), average surface roughness ( $R_a$ ), and depth of cut ( $t_a$ ). The cutting speed (cm/min), laser power (W), gas pressure (MPa), and laser frequency (Hz) were selected as control variables according to the Taguchi method. The above factors according to the Taguchi method will be used at three levels, which are shown in Table 1. An array of the L27 type was chosen as an orthogonal array. This array is characterized by the presence of 27 rows, which correspond to the number of experiments (27 times).

Experimental studies were carried out on plates made of 08X16H11M3 material, the width and length of which were 50 mm and the thickness was 3 mm (Fig. 2, a). A laser cut was made in the plates, in which, after the cut, the width of the cut, the roughness on the surface of the cut, and the TEM were measured (Fig. 2, b). The results of the experimental studies are given in Table 2.

When a part is cut, a geometric shape deviation can form on the edges, in this case a taper, which was calculated using the formula:

$$K = \frac{(a_{top} - a_{bottom}) \cdot 180}{t_{sheet} \cdot 2\pi}, \quad (5)$$

where  $t_{sheet}$  is the thickness of the sheet, mm;  $a_{top}$  is the width of the upper part of the opening, mm;  $a_{bottom}$  is the width of the lower part of the opening, mm; K is the taper, deg.

Table 1 - Assigning levels to control variables using the Taguchi method

Variables	Levels		
	1	2	3
Cutting speed, cm/min	40	20	10
Frequency, Hz	125	75	25
Pressure, MPa	1,5	1	0,5
Laser power, W	2000	1500	1000

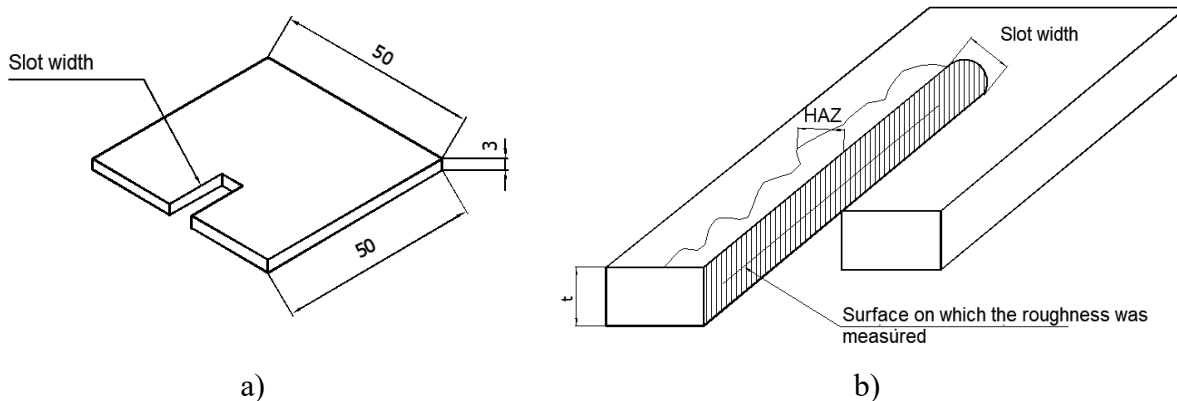


Figure 2 - Sample for the study:

a - dimensions of the sample; b - measurements of the slot elements

Based on the experimental data obtained, the corresponding orthogonal arrays were constructed using the Taguchi method, an example of which is shown in Table 3. The variables are cutting speed (X1), frequency (X2), gas pressure (X3), and laser power (X4). Three interactions are also investigated - X1 and X4, X3 and X1, and X1 and X2. After that, the obtained experimental values were subjected to analysis of variance, which is a mandatory step in using the Taguchi method [3, 4].

At the first stage of the dispersion analysis, the variation ratio (S/N) of the quality characteristics of the laser cutting process is calculated. Next, the degree of freedom (denoted by DOF) is calculated. The total sum of squares (SS) is calculated using the formula [3]:

$$SS = (\sum y_n) - \frac{T^2}{n}, \tag{6}$$

where  $n$  is the number of trials;  $T$  is the total value of the variation ratio;  $y_n$  is the value of the response variable in experiment  $n$ .

The influence of various factors is taken into account when calculating the sum of squares using the formula:

$$SS(X1) = \frac{X13^2}{9} + \frac{X12^2}{9} + \frac{X11^2}{9} - \frac{T^2}{n}. \tag{7}$$

Table 2 - Results of experimental studies to determine the deviation of the geometric shape of the opening

Run	Average taper, K deg.	1 level	Bottom	Top	2 level	Bottom	Top	3 level	Bottom	Top
1	2	3	4	5	6	7	8	9	10	11
1	1,46	1,33	0,35	0,49	1,45	0,33	0,48	1,6	0,32	0,49
2	1,35	1,2	0,33	0,45	1,55	0,26	0,43	1,3	0,32	0,46
3	1,49	1,23	0,26	0,39	1,75	0,21	0,4	1,5	0,31	0,47
4	0,8	0,74	0,41	0,49	0,68	0,42	0,49	0,98	0,38	0,49
5	0,84	0,89	0,3	0,39	0,87	0,3	0,39	0,77	0,28	0,36
6	0,9	0,95	0,31	0,41	0,89	0,31	0,41	0,88	0,38	0,47
7	0,74	0,87	0,36	0,45	0,71	0,21	0,45	0,66	0,39	0,46
8	0,74	0,73	0,3	0,37	0,88	0,37	0,3	0,62	0,3	0,36
9	0,7	0,65	0,37	0,43	0,59	0,23	0,43	0,87	0,32	0,41
10	0,77	0,88	0,3	0,39	0,78	0,33	0,32	0,67	0,18	0,25
11	0,76	0,86	0,33	0,42	0,66	0,28	0,4	0,77	0,3	0,38
12	0,85	0,94	0,31	0,41	0,75	0,33	0,36	0,88	0,16	0,25
13	0,54	0,66	0,29	0,36	0,57	0,19	0,25	0,41	0,18	0,23
14	0,55	0,54	0,39	0,45	0,65	0,28	0,35	0,46	0,32	0,37
15	0,55	0,67	0,27	0,34	0,45	0,31	0,36	0,55	0,26	0,32
16	0,48	0,45	0,28	0,33	0,41	0,17	0,21	0,59	0,21	0,28
17	0,4	0,39	0,39	0,43	0,45	0,24	0,29	0,38	0,24	0,28
18	0,45	0,98	0,33	0,37	0,42	0,18	0,23	0,57	0,28	0,34
19	0,32	0,36	0,33	0,36	0,31	0,16	0,2	0,29	0,18	0,22
20	0,41	0,51	0,33	0,38	0,32	0,33	0,37	0,41	0,33	0,37
21	0,21	0,22	0,18	0,21	0,19	0,34	0,36	0,23	0,18	0,21
22	0,3	0,32	0,19	0,23	0,31	0,2	0,23	0,27	0,2	0,23
23	0,34	0,41	0,21	0,25	0,34	0,28	0,32	0,27	0,33	0,36
24	0,22	0,27	0,22	0,25	0,22	0,25	0,27	0,18	0,18	0,2
25	0,26	0,33	0,14	0,18	0,22	0,21	0,24	0,25	0,21	0,24
26	0,23	0,19	0,15	0,17	0,3	0,18	0,21	0,22	0,23	0,25
27	0,32	0,35	0,14	0,18	0,33	0,18	0,21	0,28	0,27	0,3

The error in the calculation of the sum of squares is calculated using the formula:

$$SS(\varepsilon) = SS - SS(X1). \quad (8)$$

The calculation of the mean square, denoted by  $VV$ , is performed using the formula:

$$VV = SS(X1) - DOF(X1). \quad (8)$$

The  $F$  value is calculated using the formula [3]:

$$F = \frac{L_s}{SS(\varepsilon)}. \quad (9)$$

where  $L_s$  is the root mean square value calculated according to formula 3.

Table 3 - Dispersion analysis of taper

Cutting parameter	Variable ratio			P	SS	VV	F	DOF
	1	2	3					
X1 Cutting speed	55,5	46,2	39,1					2
X2 Frequency	53,8	43,7	43,4					2
X3 Gas pressure	26,9	51,9	62,1	11,61	72,7	36,39	10,88	2
X4 Laser power	2,45	41,5	96,9	79,86	500,9	250,4	74,88	2
X1X2	46,0	45,6	49,3				0,89	4
X1X3	47,0	43,0	50,9				4,1	4
X1X4	45,9	42,7	52,3				5,2	4
Error				8,53		3,34	53,5	16
Total				100			627,2	26

The percentage of contribution of a particular level parameter to its impact on the response variables is calculated as follows:

$$P(X1) = \frac{SS(X1)}{SS} \cdot 100\%. \quad (10)$$

#### 4. THE RESULT OF WORK

The results of the dispersion analysis of the roughness, heat affected zone, and deviation of the geometric shape of the slot are shown in Tables 3-5. As can be seen from Table 3-5, in the process of laser cutting, the parameter X4, which corresponds to the laser power, has the greatest influence on the characteristics of roughness, taper of the slot and the HAZ. Parameter X4 has 80-90% of the influence. Parameter X3, which corresponds to the gas pressure when performing laser cutting of stainless steel, has about 10% of the influence.

To simplify the perception of the digital values obtained as a result of assessing the impact of laser cutting modes on the characteristics of the slot, three-dimensional graphs were constructed, which are shown in Figs. 3-5.

After analyzing the results of reducing the response variables (slot surface roughness, geometric shape deviation, and thermal impact zone) using the Taguchi method, the optimal cutting conditions for stainless steel 08X16H11M3 were determined, which are shown in Table 6.

Table 4 - Dispersion analysis of the slot surface roughness

Cutting parameter	Variable ratio			P	SS	VV	F	DOF
	1	2	3					
X1 Cutting speed	57,5	53,3	56,2		1,02			2
X2 Frequency	53,9	57,9	55,2		0,92			2
X3 Gas pressure	62,3	55,3	49,3	10,39	9,3	4,67	14,23	2
X4 Laser power	74,5	54,8	37,7	83,76	75,3	37,65	114,7	2
X1X2	57,9	56,5	52,6		1,6			4
X1X3	55,1	55,5	56,5		0,1			4
X1X4	55,3	55,2	56,4		0,09			4
Error				5,85	5,25	0,32		16
Total				100	89,9			26

Table 5 - Dispersion analysis of the heat affected zone

Cutting parameter	Variable ratio			P	SS	VV	F	DOF
	1	2	3					
X1 Cutting speed	2,3	2,3	2,7		0,015			2
X2 Frequency	2,3	2,5	2,5		0,004			2

X3 Gas pressure	2,9	2,5	1,9	9,64	0,059	0,03		2
X4 Laser power	4,2	2,0	1,2	85,59	0,53	0,26		2
X1X2	2,5	2,4	2,4		0,0018			4
X1X3	2,4	2,5	2,4		0,0003			4
X1X4	2,4	2,4	2,5		0,00026			4
Error				4,77	0,0296	0,0019		16
Total				100	0,6196			26

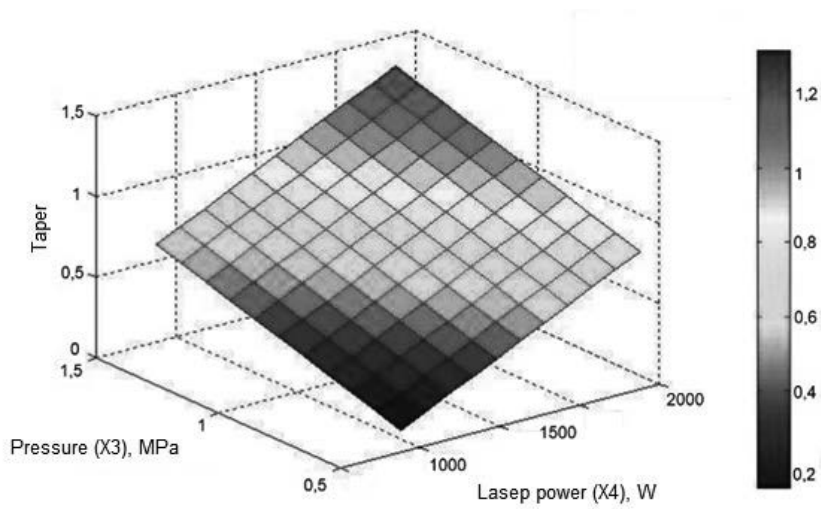


Figure 3 - Taper of the slot with varying laser power and gas pressure

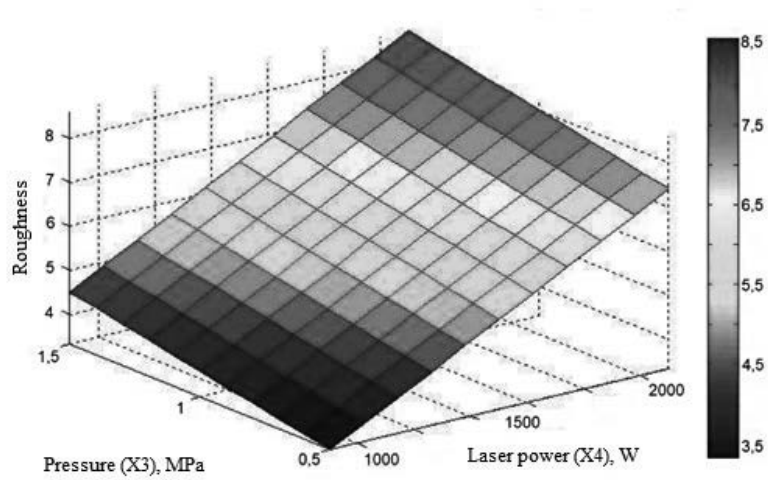


Figure 4 - Average roughness of the slot surface with varying laser power and pressure



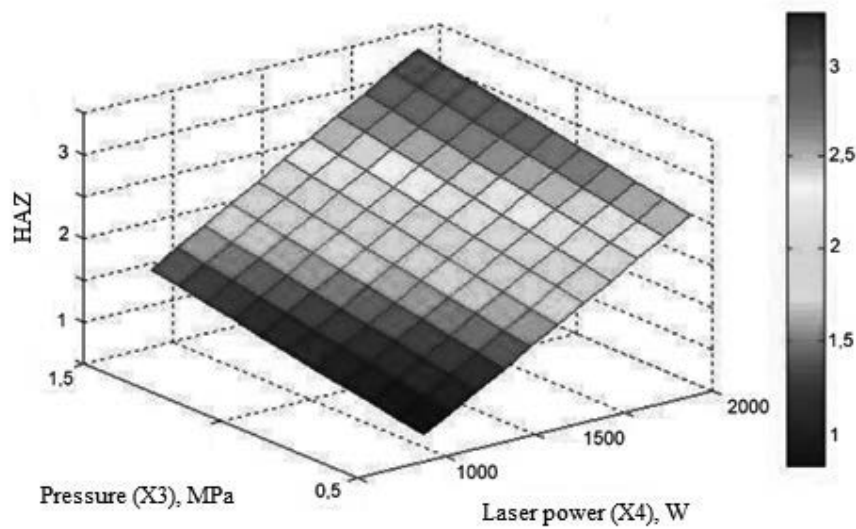


Figure 5 - Heat affected zone when changing laser pressure and power

Table 6 - Optimal cutting conditions for stainless steel 08X16H11M3 determined by the Taguchi method

Control variables (X)	Response variables (Y)			The optimum cutting parameter
	Taper	Roughness	HAZ	
Cutting speed X1, cm/min	40	-	-	40
Frequency X2, Hz	75	25	-	50
Gas pressure X3, MPa	0,5	0,5	0,5	0,5
Laser power X4, W	1000	1000	1000	1000

As can be seen from Table 6, for all response variables, the most optimal control variable X4, which corresponds to the laser power, is 1000 W. Similarly, for all response variables, the most optimal value of the control variable X3, which corresponds to the gas pressure, is 0.5 MPa.

In the case of the cutting speed, it has a negligible effect on the mean surface roughness and the RTV, so it can be neglected for these response variables. Therefore, the optimal value is the value at which the best slot taper, i.e. the control variable X1, which corresponds to the cutting speed, is 40 cm/min.

### 5. CONCLUSIONS

In this work, the possibility of using the orthogonal array method as a tool for optimizing the parameters of laser cutting of stainless steel 08X16H11M3 was investigated. According to the results of the study, the optimal laser cutting modes were established, namely: cutting speed 40 cm/min, laser power 1000 W, frequency 50 Hz, gas pressure 0.5 MPa.

**BIBLIOGRAPHY**

1. Pupan L.I. Laser technologies in mechanical engineering: a textbook for students of the speciality "Applied Mechanics" of full-time, part-time and distance learning / L.I. Pupan. - Kharkiv: NTU "KhPI", 2020. 109 p.
2. Types of stainless steel processing. Access mode: <https://westa.kiev.ua/ua/vidy-obrabotki-nerzhaveushej-stali>
3. Bendell A. Taguchi Methods / A. Bendell - Springer Dordrecht. - 2009. - 212 p.
4. Roy K.R. Design of Experiments Using the Taguchi Approach: 16 Steps to Product and Process Improvement / K.R. Roy. - Wiley-Interscience. - 2001. - 560 p.
5. HGstar Smart3015 machine. Access mode: <https://www.hg-star.com/ru/budget-laser-cutting-machine/>



26th January 2024  
Gliwice, Poland

DEPARTMENT OF ENGINEERING MATERIALS AND BIOMATERIALS  
FACULTY OF MECHANICAL ENGINEERING  
SILESIA UNIVERSITY OF TECHNOLOGY

## INTERNATIONAL STUDENTS SCIENTIFIC CONFERENCE

### Ewolucja mikrostruktury złącza spawanego ze stali X10CrWMoVNb9-2 po wyżarzaniu przez 10000h

K. Sówka<sup>1,2</sup>, M. Sroka<sup>1</sup>

<sup>1</sup> Silesian University of Technology, Department of Engineering Materials and Biomaterials, S. Konarskiego 18A, 44-100 Gliwice, Poland.

<sup>2</sup> ZRE Katowice, Gen. Jankego 13, 40-615 Katowice, Poland  
e-mail: marek.sroka@polsl.pl, karol.sowka@polsl.pl

**Streszczenie:** W artykule opisano wpływ wyżarzania w temperaturze 600 i 650°C przez 10.000 h na jednoimienne złącze spawane ze stali X10CrWMoVNb9-2. Wyżarzanie próbek prowadzono w piecu wielopróbkowym, bez przyłożonego obciążenia do badanych próbek. Przeprowadzono obserwacje mikrostruktury strefy wpływu ciepła złącza w stanie wyjściowym i po wyżarzaniu wykorzystując metodę mikroskopii skaningowej.

**Abstract:** The paper presents the effect of annealing at 600 and 650°C for 10.000 h on a similar welded pipe joint made of X10CrWMoVNb9-2 steel. Annealing of the samples was carried out in multi-sample furnace, with no load applied to the tested samples. Observations of the microstructure in the initial state and after annealing were made using the scanning microscopy method.

**Słowa kluczowe:** X10CrWMoVNb9-2, P92, złącze spawane jednoimienne, spoina, mikrostruktura, wyżarzanie

#### 1. WSTĘP

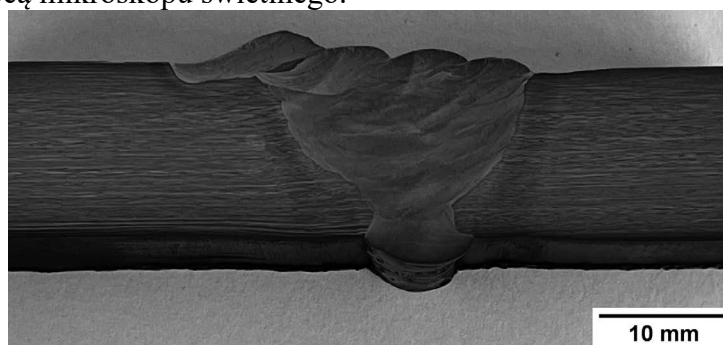
W kontekście zapewnienia niezawodności nowoczesnych jednostek energetycznych o parametrach nadkrytycznych konieczne jest ciągle poszerzanie wiedzy na temat stanu materiału złącza spawanego. Konstrukcja takich kotłów wymaga przeprowadzania szczegółowych okresowych badań w celu dokładnego określenia wytrzymałości poszczególnych komponentów ciśnieniowych. Szczególnie istotne jest to w przypadku elementów o najwyższych parametrach eksploatacyjnych, głównie są to rurociągi i kolektory pary, czyli elementy pracujące powyżej temperatury granicznej. W przypadku elementów, które nie są ogrzewane od zewnątrz spalinami, to właśnie proces pełzania okazuje się być dominującym czynnikiem wpływającym na degradację tychże komponentów [1-4].

Wnioski z przeprowadzonych badań mogą posłużyć do doskonalenia procesów produkcyjnych, wybierania optymalnych materiałów oraz opracowania skutecznych strategii eksploatacyjnych, co w rezultacie przyczyni się do wydłużenia żywotności i efektywności kotłów pracujących w warunkach nadkrytycznych i ultranadkrytycznych.

Badana stal, czyli X10CrWMoVNb9-2 to stal o strukturze martenzytycznej, należąca do grupy stali charakteryzującej się 9% zawartością chromu. Stosowana jest na urządzenia ciśnieniowe pracujące w wysokich parametrach roboczych pary. Powstała na drodze modyfikacji stali T9, czyli X10CrMo91 (poprzez dodatek stopowy wanadu i niobu) a następnie ewolucji stali T/P91, czyli X10CrMoVNb9-1 (poprzez dodatek wolframu, obniżenie zawartości molibdenu oraz inne mikrodotądki stopowe) [5-11].

## 2. MATERIAŁ DO BADAŃ

Materiał do badań stanowiły rurowe złącza spawane, na bazie rur do zastosowań ciśnieniowych wg EN 10216-2. Badano rury w typoszeregu 76,1x20,0 mm i gatunku stali X10CrWMoVNb9-2 (nazwa skrócona wg ASTM to T/P92). W tabeli 1 zestawiono składy chemiczne: rur oraz materiałów dodatkowych do spawania zgodnie z normą PN-EN 10216-2, PN-EN ISO 3580, PN-EN ISO 21952. Rysunek 1 przedstawia zdjęcie makro złącza spawanego wykonana za pomocą mikroskopu świetlnego.



Rysunek 1. Badane złącze spawane, LM

Figure 1. Tested welded joint, LM

Tabela 1. Skład chemiczny materiałów użytych do wykonania złącza

Table 1. Chemical composition of materials used to make the joint

Skład chemiczny składowych badanego złącza spawanego (wt-%)										
Norma materiałowa	Gatunek	C	Si	Mn	P max	S max	Nb	Ti	V	Zr
PN-EN 10216-2: Rury stalowe bez szwu do zastosowań ciśnieniowych	X10CrWMoVNb9-2 1.4901	0,07 to 0,13	≤ 0,50	0,30 to 0,60	0,02	0,01	0,04 to 0,09	0,01 max	0,15 to 0,25	0,01 max
		Cr	Mo	Ni	N	B	Al tot	Cu	W	
		8,5 to 9,5	0,30 to 0,60	≤ 0,40	0,030 to 0,070	0,001 to 0,006	≤ 0,02	-	1,50 to 2,00	
Norma materiałowa	Gatunek	C	Si	Mn	Cr	Ni	Mo	V	Nb	W
PN-EN ISO 3580: Materiały dodatkowe do spawania - elektrody otulone dla stali odpornych na pełzanie	X10CrWMoVNb9-2 1.4901	0,10	0,30	0,50	8,60	0,50	0,40	0,20	0,05	1,50
Material norm	Gatunek	C	Si	Mn	Cr	Mo	Ni	W	V	Nb
PN-EN ISO 21952: Materiały dodatkowe do spawania - druty, pręty i stopiwa dla stali odpornych na pełzanie	X10CrWMoVNb9-2 1.4901	0,10	0,30	0,70	8,60	0,55	0,70	1,60	0,20	0,04

Przetop złącza, czyli warstwę graniową złącza wykonano za pomocą metody 141 – GTAW (z ang.: Gas Tungsten Arc Welding) czyli spawanie nietopliwą elektrodą wolframową z materiałem dodatkowym w postaci litego drutu oraz w gazowej osłonie grani w postaci 100% argonu. Kolejne warstwy, czyli warstwy wypełniające oraz lico zostały wykonane metodą 111 – SMAW (z ang.: Shielded Metal Arc Welding) czyli spawanie elektrodą otuloną. Takie połączenie metod spawania zapewnia wysoką jakość złącza spawanego, jest to typowe

rozwiązanie stosowane dla odpowiedzialnych komponentów energetyki, jakimi niewątpliwie są rurociągi wysokoprężne [12].

Spawanie złącza wykonano zachowując parametry takie jak: temperatura międzyścięgowa między 200 a 250°C, prędkość podgrzewania do wyżarzania, czas wyżarzania wynoszący 180 minut w temperaturze między 750 a 770°C oraz na koniec odpowiednia prędkość chłodzenia po wyżarzaniu wynosząca od 100 do 300°C/h. Takie parametry zapewniają możliwie najlepsze właściwości technologiczne złącza w stanie wyjściowym.

### 3. METODY BADAWCZE

Celem badań było porównanie próbek pod kątem mikrostruktury strefy wpływu ciepła złącza spawanego w stanie wyjściowym oraz po symulacji w warunkach odpowiadającym rzeczywistym parametrom pracy rurociągu. Wykonane złącza spawane zostały pocięte wzdłużnie, przygotowano z nich próbki do badań mikrostrukturalnych w stanie dostawy, próbki do wyżarzania przez 10.000h w temperaturze 600°C oraz próbki do wyżarzania przez 10.000h w temperaturze 650°C. Wyżarzanie próbek odbywało się w piecach produkcji własnej Sieci Badawczej Łukasiewicz – Górnośląski Instytut Technologiczny w Gliwicach.

Obserwacje mikrostruktury materiału złącza wykonanego ze stali P92 przeprowadzono na zglądach metalograficznych z ujawnieniem stref złącza. Zgłady wykonano na przekroju poprzecznym wycinków złącza poprzez szlifowanie i polerowanie mechaniczne oraz trawienie.

Badania mikrostruktury materiału w stanie dostawy oraz po wyżarzaniu przez 10.000h w temperaturze 600 i 650°C przeprowadzono za pomocą wysokorozdzielczego elektronowego mikroskopu skaningowego (SEM) JSM-7200F firmy JEOL, który jest wyposażony w detektory EDS (Octane Elite Super) i EBSD (Hikari Plus) firmy EDAX.



Rysunek 2. Mikroskopu skaningowy JSM-7200F firmy JEOL  
*Figure 2. Scanning microscope JSM-7200F firmy JEOL*

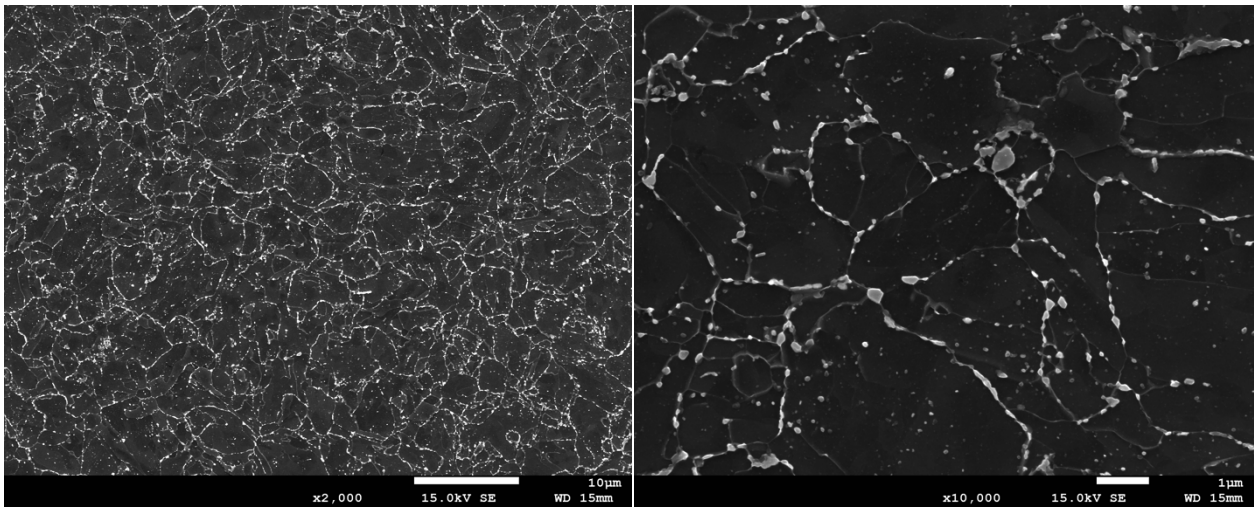
### 4. WYNIKI BADAŃ

Obserwacje materiału rodzimego w stanie dostawy dla obu stron złącza wykazały strukturę odpuszczonego martenzytu listwowego z bardzo drobnymi wydzieleniami typu  $M_{23}C_6$  po granicach ziaren byłego austenitu i listwach martenzytu, co jest prawidłowe dla stanu wyjściowego badanej stali [2,3,10,11]. W niniejszym opracowaniu zestawiono zmiany mikrostrukturalne dla strefy wpływu ciepła badanego złącza.

Badania mikrostruktury złącza spawanego po wyżarzaniu w temperaturze 600°C przez 10.000h wykazały niezwykle zbliżoną strukturę do stanu wyjściowego tzn. strukturę odpuszczonego martenzytu listwowego z zauważalnym, jednakże bardzo nieznacznym wzrostem wielkości wydzieliń, głównie po granicach ziaren byłego austenitu.

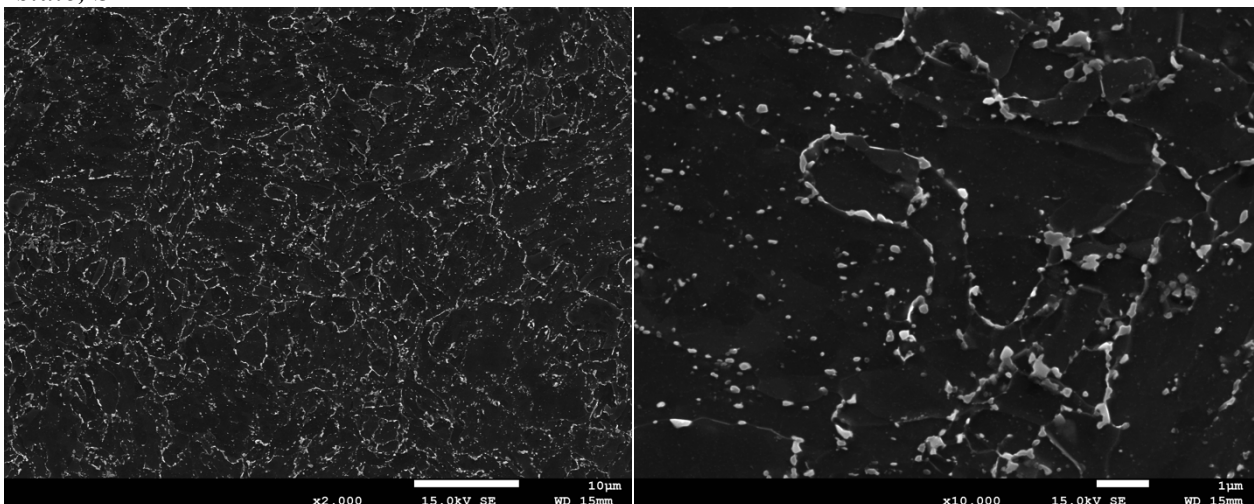
Badania mikrostruktury złącza spawanego po wyżarzaniu w temperaturze 650°C przez 10.000h wykazały, iż obrazy mikrostruktury różnią się od próbek wyżarzanych w 600°C. Zauważono wzrost wielkości pojedynczych wydzieliń oraz lokalną ich koagulację.

Wyniki badań mikrostrukturalnych zaprezentowano na rysunkach: stan wyjściowy (rysunek 3), stan po wyżarzaniu przez 10000h w 600°C (rysunek 4) oraz stan po wyżarzaniu przez 10000h w 650°C (rysunek 5).



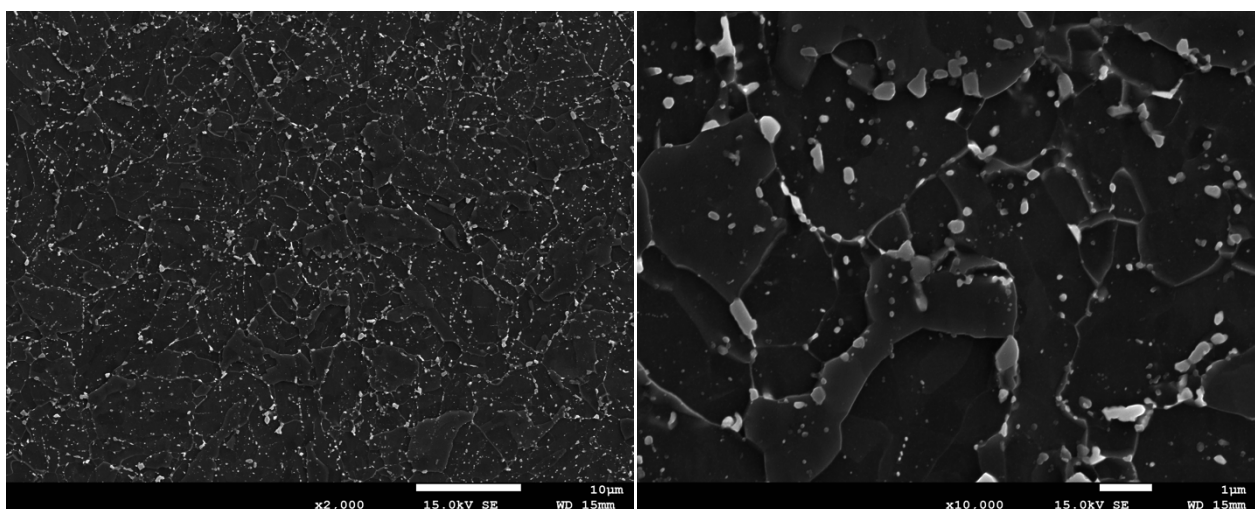
Rysunek 3. Mikrostruktura strefy wpływu ciepła złącza X10CrWMoVNb9-2 w stanie wyjściowym, SEM

*Figure 3. Microstructure of the heat affected zone of the X10CrWMoVNb9-2 joint in the initial state, SEM*



Rysunek 4. Mikrostruktura strefy wpływu ciepła złącza X10CrWMoVNb9-2 po wyżarzaniu w 600°C przez 10.000h, SEM

*Figure 4. Microstructure of the heat affected zone of the X10CrWMoVNb9-2 joint after annealing at 600°C for 10,000 h, SEM*



Rysunek 5. Mikrostruktura strefy wpływu ciepła złącza X10CrWMoVNb9-2 po wyżarzaniu w 650°C przez 10.000h, SEM

*Figure 5. Microstructure of the heat affected zone of the X10CrWMoVNb9-2 joint after annealing at 650°C for 10,000 h, SEM*

## 5. WNIOSKI

Badania mikrostrukturalne nie ujawniły obecności pustek, mikropęknięć oraz nieciągłości strefy wpływu ciepła badanego złącza.

Wyżarzanie rurowego złącza spawanego ze stali X10CrWMoVNb9-2 przez 10.000 godzin w temperaturze 600°C wykazało, że w mikrostrukturze zaobserwowano jedynie nieznaczne zmiany w postaci procesów wydzieleniowych, głównie wzdłuż granic ziaren dawnego austenitu i listew martenzytycznych.

Wyżarzanie przez 10.000 godzin w temperaturze 650°C złącza spawanego wykonanego ze stali X10CrWMoVNb9-2 potwierdziło dane literaturowe, że dynamika degradacji materiału w mikrostrukturze była większa niż w temperaturze 600°C. Zaobserwowano szybszy wzrost wielkości wydzieleń i ich koagulację wzdłuż granic ziaren byłego austenitu oraz po granicach listew martenzytu.

## 6. BIBLIOGRAFIA

1. A. Zieliński, G. Golański, M. Sroka, Evolution of the microstructure and mechanical properties of HR3C austenitic stainless steel after ageing for up to 30,000 h at 650–750 °C, *Materials Science and Engineering: A* 796 (2020) 139944.
2. A. Hernas, J. Dobrzański, J. Pasternak, S. Fudali, Characteristics of the new generation of materials for the energy sector. Publishing house of the Silesian University of Technology (2015).
3. A. Zieliński, Trwałość eksploatacyjna żarowytrzymałych stali o osnowie ferrytycznej w warunkach długotrwałego oddziaływania temperatury, 2016, ISBN: 978-83-938130-4-9.
4. A. Zieliński, J. Dobrzański, H. Paszkowska, Zmiany struktury i własności mechanicznych w wyniku równoczesnego oddziaływania temperatury, naprężenia i czasu

- stali 9–12% Cr na elementy krytyczne kotłów o parametrach nadkrytycznych pracujących w warunkach pełzania, *Prace Instytutu Metalurgii Żelaza*, 2011, 63, 60-62.
5. Guo X., Gong J., Jiang Y., Wang X., Zhao Y.: Microstructures and high-temperature mechanical properties in 9Cr-0.5 Mo-1.8 W-VNb steel after aging at 650° C, *Materials at High Temperatures*, 2015, 32, (6), 566-574.
  6. Dobrzański J., Hernas A., Pasternak J., Zieliński A.: Microstructure and mechanical properties characteristics of welded joints made of creep-resistant steel with 12%Cr, V, W and Co additions. Fifth International Conference on Advances in Material Technology for Fossil Power Plants. Marco Island, Florida USA. EPRI, 3-5 October 2007.
  7. J. Zhang, D. B.SH., L. X.M., Q. G.L. and Z. Y., Microstructure evolution of P92 steel weld metal after service for 8000h, 2017.
  8. K. Bumjoon, J. Chanseo, L. Byeongsoo, Creep behavior and microstructural damage of martensitic P92 steel weldment, *Materials Science and Engineering: A* 483–484, 2008, 544-546.
  9. A. Zieliński, M. Sroka, M. Miczka, A. Śliwa, Forecasting the Particle Diameter Size Distribution in P92 (X10CrWMoVNb9-2) Steel After Long-Term Ageing at 600 and 650°C, *Archives of Metallurgy and Materials*. 2016, 61, (2A), s. 753–760.
  10. N. Saini, R.S. Mulik, M. Mohan Mahapatra, Study on the effect of ageing on laves phase evolution and their effect on mechanical properties of P92 steel, *Materials Science and Engineering: A* 716, 2018, 179-188.
  11. F Abe, T Horiuchi, M Taneike, K Sawada, Stabilization of martensitic microstructure in advanced 9Cr steel during creep at high temperature, *Materials Science and Engineering: A*, Volume 378, Issues 1–2, 2004, Pages 299-303.
  12. K. Ferenc, Spawalnictwo, WNT, 2015, ISBN 978-83-7926-064-5, 29-37.





26th January 2024  
Gliwice, Poland

DEPARTMENT OF ENGINEERING MATERIALS AND BIOMATERIALS  
FACULTY OF MECHANICAL ENGINEERING  
SILESIA UNIVERSITY OF TECHNOLOGY

## INTERNATIONAL STUDENTS SCIENTIFIC CONFERENCE

### Wpływ obróbki cieplno-plastycznej na konduktywność miedzi chromowej

M. Szafran<sup>a</sup>, M.M. Krupiński<sup>b</sup>, W. Borek<sup>c</sup>, M. Krupiński<sup>c,\*</sup>

<sup>a</sup> Politechnika Śląska, Wydział Elektryczny, Inżynieria Ogólna

<sup>b</sup> Wieloprofilowy Zespół Szkół, 42-600 Tarnowskie Góry, ul. Sienkiewicza 6

<sup>c</sup> Politechnika Śląska, Wydział Mechaniczny Technologiczny, Katedra Materiałów Inżynierskich i Biomedycznych, 44-100 Gliwice, ul. Konarskiego 18a

\*e-mail: mariusz.krupinski@polsl.pl

**Streszczenie:** Celem pracy było określenie wpływu odkształcenia plastycznego na mikrostrukturę i własności stopu CuCr1. W pracy wykonano analizę termiczno-derywacyjną z zastosowaniem urządzenia UMSA MT-5 (Universal Metallurgical Simulator and Analyzer). Wykonano również badania mikrostruktury z zastosowaniem mikroskopii świetlnej oraz badania twardości i konduktywności.

**Abstract:** The aim of the work was study the influence of plastic deformation on microstructure and properties of the CuCr1 alloy. In the work, thermal-derivative analysis was performed using the UMSA MT-5 (Universal Metallurgical Simulator and Analyzer) device. Microstructure tests were performed using light microscopy, electrical conductivity, as well as hardness tests.

**Słowo kluczowe:** Cu-Cr, analiza termiczno-derywacyjna, odkształcenie plastyczne, mikrostruktura, konduktywność.

#### 1. WSTĘP

Stopy miedzi są jednym z najważniejszych materiałów stosowanych w przemyśle elektrycznym i elektronicznym ze względu na swoją wysoką konduktywność. Konduktywność jest miarą zdolności materiału do przewodzenia prądu elektrycznego. Zdecydowany wpływ na jej wartość w przypadku stopów miedzi ma mikrostruktura stopu, która zależy od kinetyki krystalizacji oraz zastosowanych procesów obróbki [1].

Dodatki stopowe mają wpływ na mikrostrukturę, rozmiar ziaren oraz ilość wystąpień faz międzymetalicznych. Jednym z efektów stosowania dodatków stopowych może być przyspieszenie procesu krystalizacji, co prowadzi do powstania drobniejszych ziaren i bardziej równoosiowej mikrostruktury. Inne dodatki, takie jak chrom, mogą spowolnić ten proces, co pozwala na bardziej kontrolowane formowanie struktury krystalicznej. Dodatki te wpływają również na temperaturę topnienia oraz zakres temperatur, w których zachodzi proces krystalizacji. Skład chemiczny stopu może mieć znaczący wpływ na przewodność. Regularna struktura krystaliczna stopów miedzi ułatwia swobodny ruch elektronów, dzięki czemu materiał ten wykazuje się wysoką konduktywnością elektryczną [2,3].

Czysta miedź jest metalem o wysokiej przewodności elektrycznej, jednak dodatek chromu powoduje rozdrobnienie mikrostruktury, co wpływa na zmniejszenie przewodności elektrycznej stopu [4]. Dyspersyjne fazy chromu w osnowie fazy  $\alpha$ , powodują utrudnienie ruchu dyslokacji, dzięki czemu wzrasta twardość oraz wytrzymałość mechaniczna stopu. Podczas procesu odkształcenia plastycznego, struktura stopu ulega zmianom, co również wpływa na jej właściwości fizyczne. Powstanie defektów strukturalnych, takich jak dyslokacje utrudniają swobodny przepływ elektronów przez materiał, co prowadzi do wzrostu oporu elektrycznego. Zmniejszenie wielkości ziarna prowadzi do zwiększenia liczby granic ziaren, które stanowią dodatkową przeszkodę dla przepływu prądu elektrycznego [5].

## 2. MATERIAŁY I METODYKA BADAŃ

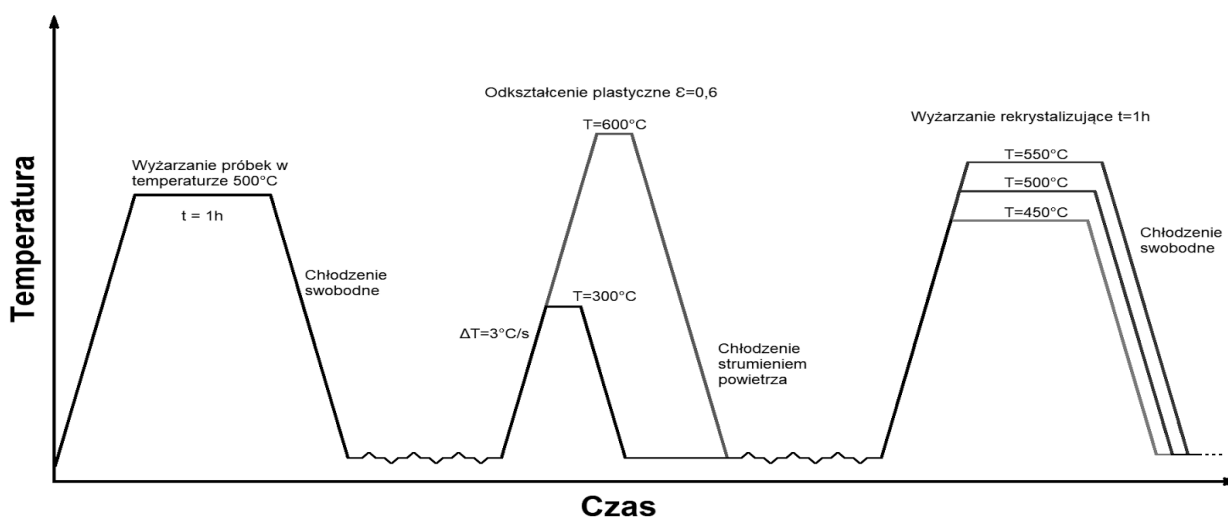
Wpływ obróbki cieplno-plastycznej na mikrostrukturę i własności wykonano dla stopu CuCr1. W celu określenia zależności między składem chemicznym, przebiegiem krystalizacji, punktami charakterystycznymi krzepnącego stopu, wykonano analizę termiczno-derywacyjną zrealizowaną z zastosowaniem stanowiska UMSA MT5 przy parametrach topienia zamieszczonych w tabeli 1. Do pomiaru temperatury zastosowano termopary typu K, które umieszczono w węźle cieplnym. Stop topiono w tyglach grafitowych i stosowano atmosferę ochronną w postaci Ar, na powierzchnię wewnętrzną tygla naniesiono zawiesinę BN.

Tabela 1. Parametry topienia.

Table 1. Melting parameters.

Moc generatora [W]	Zastosowana moc grzania do mocy maksymalnej [%]	Temperatura wygrzewania [°C]	Czas wygrzewania [s]
2200	75	1185	900

Do badań zależności pomiędzy zastosowanym odkształceniem plastycznym i obróbką cieplną, a twardością i konduktywnością stopu użyto próbek walcowych o wymiarach  $\Phi=12$  mm oraz  $h=12$  mm. Stop miedzi poddany został wstępnemu wyżarzaniu w temperaturze 500°C przez godzinę, z zastosowaniem atmosfery ochronnej argonu. Odkształcenie plastyczne na zimno oraz na gorąco, zrealizowane zostało przy pomocy symulatora obróbki cieplno-plastycznej Gleeble 3800. Do pomiaru temperatury w trakcie odkształcenia plastycznego zastosowano termopary typu K, które zostały zakute w uprzednio nawierconych otworach. Między kowadełka z węgla wolframu, a badaną próbkę zastosowano podkładki z folii tantalowej oraz smar wysokotemperaturowy na bazie niklu. Miało to na celu zmniejszenie tarcia jak również polepszenie kontaktu między kowadełkami, a próbką. Odkształcenie plastyczne wykonano w próżni, w celu ochrony stopu przed utlenieniem. Stop odkształcony został z gniosem 60%. Parametry obróbki cieplno-plastycznej przedstawiono na rysunku 1.



Rysunek 1. Schemat obróbki cieplnej i cieplno-plastycznej.

Figure 1. Diagram of heat and thermo-plastic treatment.

Wprowadzone oznaczenia przy zastosowaniu odpowiednich procesów obróbki cieplno-plastycznej zamieszczono w tabeli 2.

Tabela 2. Oznaczenia w zależności od zastosowanej obróbki cieplno-plastycznej.

Table 2. Markings depending on used type of thermoplastic treatment.

Oznaczenie stopu	Temperatura odształcenia plastycznego, °C	Temperatura wyżarzania rekrytalizującego, °C
CuCr1/300(OP)	300	-
CuCr1/600(OP)	600	-
CuCr1/300(OP)/450(W)	300	450
CuCr1/300(OP)/500(W)	300	500
CuCr1/300(OP)/550(W)	300	550

OP – obróbka plastyczna; W - wyżarzanie

W celu zbadania wpływu parametrów procesu obróbki cieplno-plastycznej na własności, wykonano:

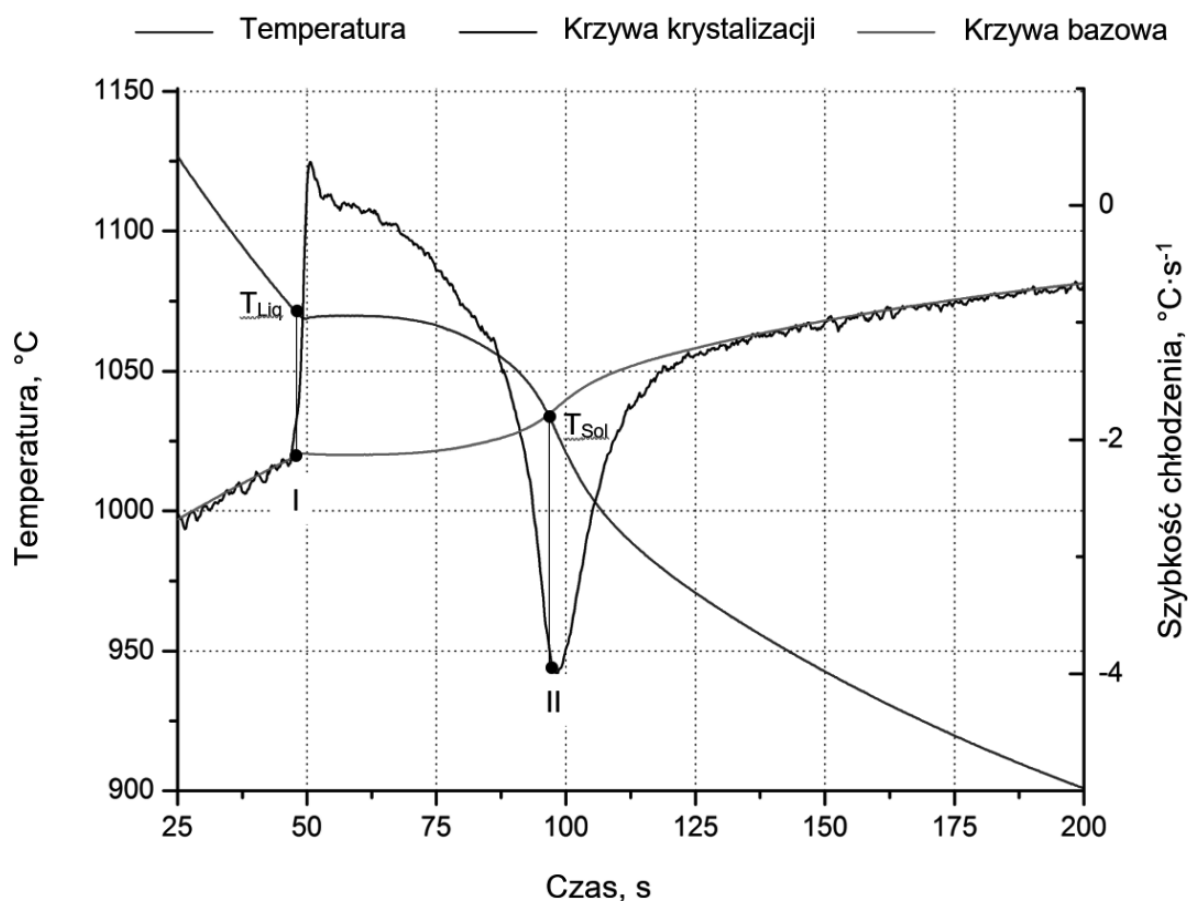
- analizę mikrostruktury, która została wykonana z zastosowaniem mikroskopu optycznego Axio Observer firmy ZEISS. Zgłady polerowano sukniem MD-Nap oraz zawiesiną diamentową 1  $\mu\text{m}$  firmy Struers. Trawienie wykonano z zastosowaniem odczynnika: 2g  $\text{K}_2\text{Cr}_2\text{O}_7$  na 100 $\text{cm}^3$   $\text{H}_2\text{O}$  i 4 $\text{cm}^3$   $\text{NaCl}$  oraz 8 $\text{cm}^3$   $\text{H}_2\text{SO}_4$  w czasie 10s.
- badanie konduktywności stopu wykonano za pomocą Sigmascope SMP350 z sondą FS40.
- statyczne badanie twardości metodą Vickersa (HV5), wykonano przy zastosowaniu urządzenia Future Tech FM-ARS 900 (czas 10 s).

### 3. WYNIKI

#### 3.1. Analiza termiczno-derywacyjna

Zastosowanie analizy termiczno-derywacyjnej umożliwiło wyznaczenie temperatury początku ( $T_{Liq}$ ) oraz końca ( $T_{Sol}$ ) krzepnięcia stopu. Na rysunku 2 przedstawiono krzywą chłodzenia, krzywą derywacyjną oraz krzywą bazową dla stopu CuCr1. Na krzywej derywacyjnej widoczne są punkty charakterystyczne (I) początek krzepnięcia, punkt (II) koniec krzepnięcia (rys. 2). Na podstawie przebiegu krzywej chłodzenia, krzywej derywacyjnej wyznaczono temperaturę początku ( $T_{Liq} = 1071^{\circ}\text{C}$ ) oraz końca krzepnięcia ( $T_{Sol} = 1033^{\circ}\text{C}$ ) dla badanego stopu. Szybkość chłodzenia (CR - Cooling Rate) obliczono z zależności:

$$CR = \frac{T_{Liq} - T_{Sol}}{t_{Sol} - t_{Liq}} \text{ [}^{\circ}\text{C} \cdot \text{s}^{-1}\text{]} \quad (1)$$



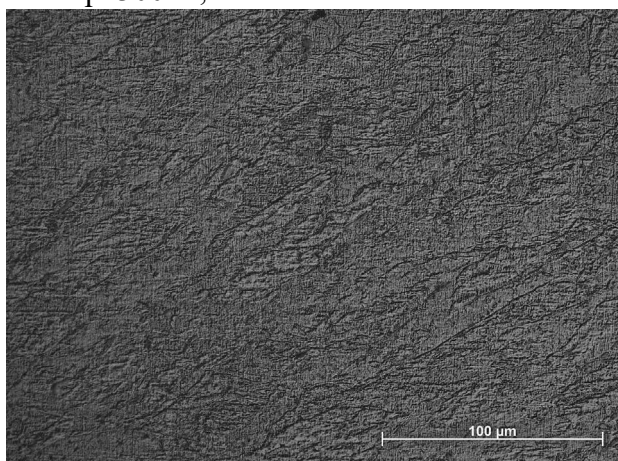
Rysunek 2. Krzywa chłodzenia, krzywa derywacyjna oraz krzywa bazowa dla stopu CuCr1,  $CR = 0.7^{\circ}\text{C} \cdot \text{s}^{-1}$

Figure 2. Cooling curve, derivation curve and base curve for CuCr1 alloy,  $CR = 0.7^{\circ}\text{C} \cdot \text{s}^{-1}$

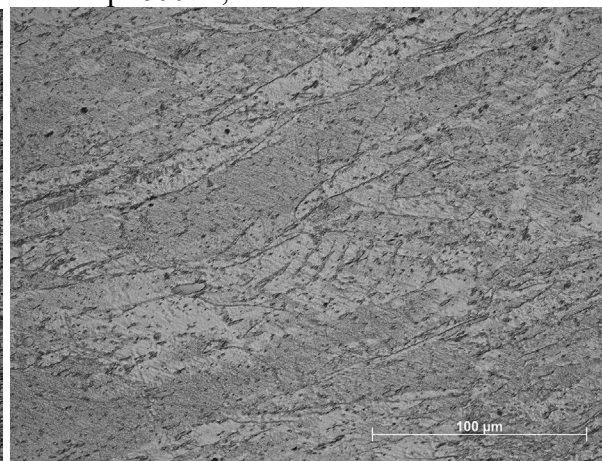
### 3.2. Analiza mikrostruktury

Mikrostruktura po analizie termiczno-derywacyjnej zamieszczona została na rys. 3d, widoczne są dendryty oraz drobne fazy chromu na granicy fazy  $\alpha$ . Mikrostrukturę stopu w różnym stanie obróbki cieplno-plastycznej przedstawiono na rysunku 3 a-c. Na rys. 3a widoczna jest typowa mikrostruktura powstająca w wyniku odkształcenia plastycznego na zimno z licznymi pasmami poślizgu i bliźniakami. Mikrostruktura stopu odkształconego w temperaturze 600°C cechuje się wydłużonym kształtem ziaren (rys. 3b). W strukturze stopu odkształconego plastycznie w temperaturze 300°C i wyżarzonego w temperaturze 550°C (rys. 3c), zaobserwować można ziarna fazy  $\alpha$  wraz z fazą chromu (#1) na granicy ziaren.

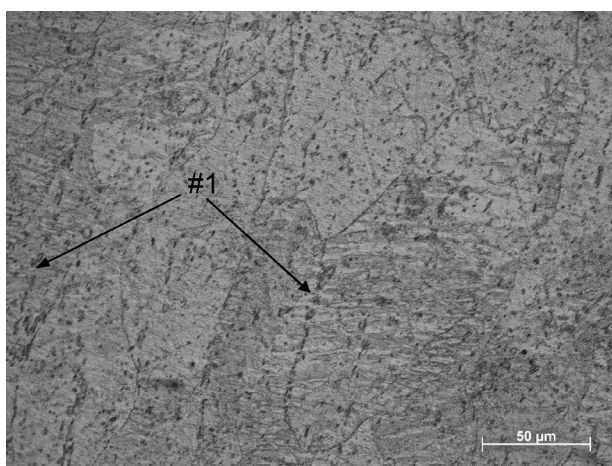
a) CuCr1 odkształcona plastycznie w temp. 300°C,



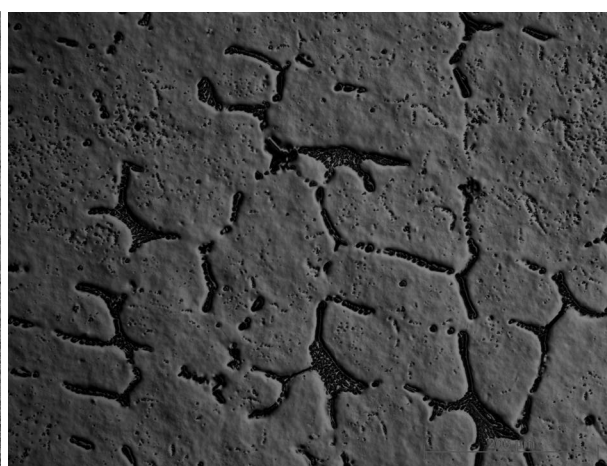
b) CuCr1 odkształcona plastycznie w temp. 600°C,



c) CuCr1 odkształcona plastycznie w temp. 300°C, wyżarzone w temp.



d) CuCr1 po ADT



Rysunek 3. Mikrostruktura stopu CuCr1  
Figure 3. Microstructure of CuCr1 alloy

### 3.3. Twardość i konduktywność

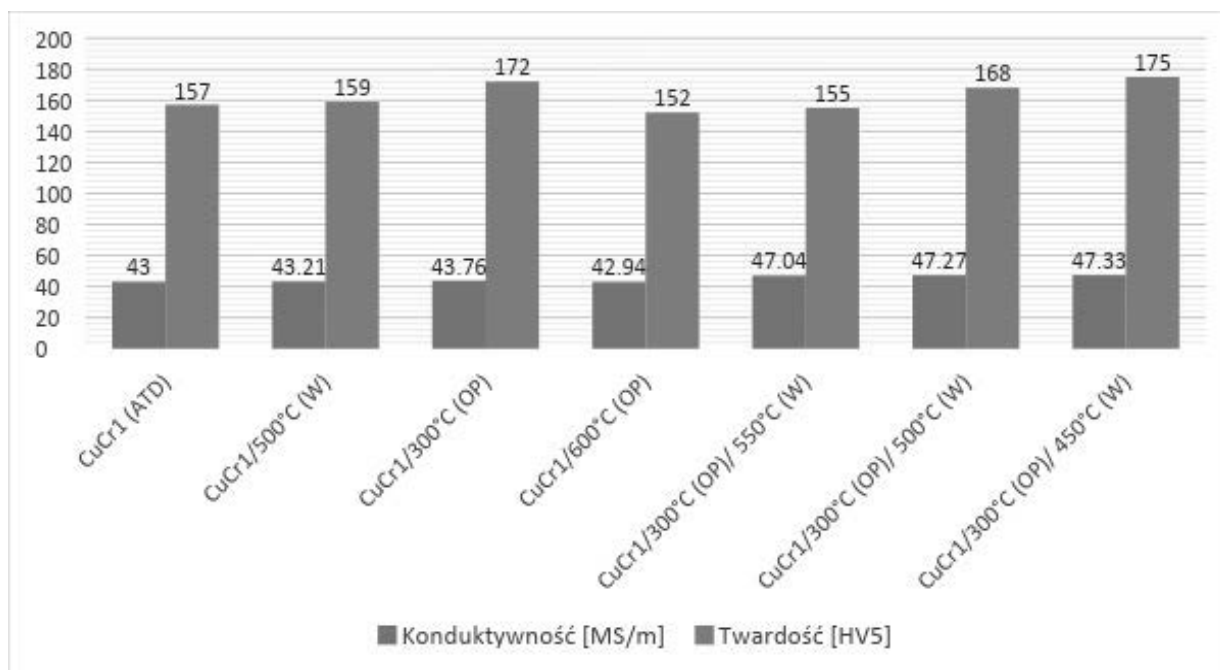
Wyniki badań twardości oraz konduktywności wraz z odchyleniem standardowym zamieszczono w tabeli 3 oraz przedstawiono graficznie na rys. 4. Odształcenie plastycznie stopu na zimno powoduje umocnienie, zaobserwować można wzrost twardości o ok. 8%, natomiast konduktywność pozostaje na niezmiennym poziomie w porównaniu do stopu po analizie termiczno-derywacyjnej. Wyżarzanie rekrytalizujące stopu powoduje wzrost konduktywności o ok. 9%, natomiast spadek twardości ok. 10% następuje dla temperatury 550°C w porównaniu do twardości w stanie odształconym na zimno.

Tabela 3. Średnie wartości konduktywności i twardości stopu.

Table 3. Average values of conductivity and hardness of the alloy.

Stan stopu	Średnia konduktywność, MS/m	Odchylenie standardowe	Średnia twardość, HV <sub>5</sub>	Odchylenie standardowe
CuCr1/500(W)	43.21	0.29	159	1.15
CuCr1/300(OP)	43.76	5.49	172	4.84
CuCr1/600(OP)	42.94	3.37	152	5.75
CuCr1/300(OP)/450(W)	47.33	0.22	175	6.45
CuCr1/300(OP)/500(W)	47.27	0.09	168	2.93
CuCr1/300(OP)/550(W)	47.04	0.05	155	2.14

OP – obróbka plastyczna; W - wyżarzanie



Rysunek 4. Graficzne przedstawienie średnich wartości konduktywności i twardości stopu.

Figure 4. Graphical representation of the average conductivity and hardness values of the alloy.

### 3. WYNIKI

Obecność chromu w stopie miedzi chromowej CuCr1 ma znaczący wpływ na jej mikrostrukturę. Krzepnący na granicy osnowy fazy  $\alpha$  chrom, powoduje wzrost twardości oraz zmniejszenie konduktywności stopu w porównaniu do czystej miedzi (58.58 MS/m [6]).

Obróbka plastyczna na zimno w temperaturze 300°C z 60% stopniem gniotu, powoduje zwiększenie twardości stopu o około 8% w porównaniu z twardością stopu po analizie termiczno-derywacyjnej. Wynika to z umocnienia powstałego przez zmiany morfologii mikrostruktury oraz powstanie defektów w mikrostrukturze stopu. Proces wyżarzania stopu CuCr1 uprzednio odkształconego plastycznie na zimno powoduje wzrost konduktywności o ok. 4 MS/m. Podczas wyżarzania w temperaturze 550°C następuje spadek twardości, ale nie ma to znaczącego wpływu na konduktywność. Obróbka plastyczna na gorąco powoduje nieznaczny spadek konduktywności oraz spadek twardości o ok 4% w porównaniu z stopem nie poddanym obróbce plastycznej.

## **PODZIĘKOWANIE**

Praca powstała w wyniku realizacji projektu w ramach kształcenia zorientowanego projektowo - PBL, w konkursie X w ramach programu Inicjatywa Doskonałości – Uczelnia Badawcza, Wydział Mechaniczny Technologiczny, Politechnika Śląska.

## **LITERATURA**

1. Z. Rdzawski monografia “Miedź stopowa” Wydawnictwo Politechniki Śląskiej Gliwice 2009.
2. B. Krupińska, W. Borek, M. Krupiński, T. Karkoszka, The Influence of Ag on the Microstructure and Properties of Cu-Ni-Si, *Materials* 13 (2020) 3416.
3. Deutsches Kupferinstitut Berufsverband “Low-Alloyed Copper Alloys“.
4. M. Krancy, Rozprawa doktorska “Uszlachetnianie miedzi oraz stopów Cu-Cr preparatami utleniająco - modyfikującymi w aspekcie poprawy przewodności elektrycznej” AGH 2019.
5. H. Jiang, L. Peng, X. Mi, H. Guo, H. Xie, D. Liu, F. Liu, Z. Yang “Simultaneously enhancing the strength and electrical conductivity of Cu-Ni-Sn alloy through plastic deformation of an intermetallic compound” *Materials & Design* Volume 235 (2023) 112445.
6. S. Fassbinder, Miedź w elektrotechnice - Praktyczne zastosowania materiałów przewodzących, Niemiecki Instytut Miedzi (2010).



26th January 2024  
Gliwice, Poland

DEPARTMENT OF ENGINEERING MATERIALS AND BIOMATERIALS  
FACULTY OF MECHANICAL ENGINEERING  
SILESIA UNIVERSITY OF TECHNOLOGY

## INTERNATIONAL STUDENTS SCIENTIFIC CONFERENCE

### Technologie laserowe w przemyśle

S. Szeja <sup>a</sup>, A. Zyzik <sup>a</sup>, M. Volkmer <sup>a</sup>, M. Bonek <sup>b</sup>

<sup>a</sup> Student Politechniki Śląskiej, Wydział Elektryczny  
email: szymsze085@student.polsl.pl

<sup>b</sup> Politechnika Śląska, Wydział Mechaniczny Technologiczny, Katedra Materiałów Inżynierskich i Biomedycznych  
email: mirosław.bonek@polsl.pl

**Streszczenie:** W artykule opisano technologie laserów przemysłowych, ich rodzaje, sposób komunikacji z maszynami laserowymi oraz budowę układów optycznych laserów spawalniczych związane z laserami, ich rodzaje, sposoby obróbki materiału oraz budowie i układów optycznych laserów spawalniczych.

**Abstract:** The article describes the technologies of industrial lasers, their types, the method of communication with laser machines and the construction of optical systems of welding lasers. related to lasers, their types, methods of material processing and the construction and optical systems of welding lasers.

**Słowa kluczowe:** laser, obróbka materiału, promieniowanie, budowa lasera

### 1. WSTĘP

W ostatnich latach tego wieku technologia laserowa mocno się rozwija i postęp w odkrywaniu nowych oraz optymalizacji używanych do dziś technologii będzie trwał jeszcze przez wiele kolejnych lat. Technologia laserowa pozwala na obróbkę materiałów metalowych w postaci cięcia, spawania, przetapiania czy obróbki cieplnej. Znacznym problemem przy wykorzystywaniu laserów do obróbek materiałowych były koszty związane z ich obsługą i utrzymaniem w porównaniu do znanych już klasycznych sposobów spawania lub cięcia metali. Najnowsze rozwiązania technologiczne laserów włóknowych i tarczowych umożliwiają realistyczne wykorzystanie laserów w przemyśle. Ze względu na proste oraz lekkie konstrukcje głowic laserowych pozwalają na optymalizację automatyzacji i robotyzacji prac na materiałach metalowych przy produkcji masowej i seryjnej. W wielu gałęziach takiego przemysłu lasery ugruntowały swoje miejsce jako niezastąpione narzędzia jako wysokojakościowe oraz ekonomiczne metody obróbki materiałowej.

### 2. PROMIENIOWANIE LASEROWE

Promieniowanie laserowe reprezentuje specyficzny rodzaj promieniowania elektromagnetycznego, znany również jako światło laserowe. W dziedzinie nauk ścisłych



termin "światło" odnosi się do zakresu fal elektromagnetycznych (kwantów) o długości fali mieszczącej się w przedziale od 10,0 [nm] do 1,0 [mm], obejmującego podczerwień, światło widzialne i ultrafiolet. Generacja światła laserowego zachodzi w specjalnych urządzeniach zwanych generatorami laserowymi, gdzie dochodzi do przejść energetycznych atomów między stanami o wyższej i niższej energii w ośrodku czynnym lasera. W przypadku laserów o dużej mocy, substancje gazowe lub stałe stanowią główny medium aktywne.[5]

Promieniowanie laserowe jest rezultatem emisji wymuszonej i charakteryzuje się wysoką spójnością czasową i przestrzenną (koherencją), a także wąskim zakresem długości fali (monochromatycznością). Kluczowymi cechami promieniowania laserowego są:

- Minimalna rozbieżność wiązki, spowodowana spójnością, koherencją, uporządkowaniem przestrzennym i czasowym, równością fazową oraz jednorodnością amplitudową powierzchni falowych drgań elektromagnetycznych,
- Monochromatyczność; na przykład, w laserze rubinowym szerokość linii widmowej zazwyczaj nie przekracza 0,01 [nm]. Z kolei lasery gazowe CO<sub>2</sub> wyróżniają się bardzo wąską linią widmową, a teoretyczna szerokość prążka jest rzędu setnych części [nm],
- Równoległość; w laserach stałych rozbieżność wiązki nie przekracza zwykle 10 miliradianów, podczas gdy w laserach CO<sub>2</sub> utrzymuje się poniżej 2-5 miliradianów,
- Duża energia promieniowania; laserów emitujących impulsowe i udarowe (PM - Pulse Mode, GP - Giant Pulse Mode) charakteryzuje się gęstością energii impulsów rzędu  $10^4 - 10^7$  [J/mm<sup>2</sup>], przy czasach impulsów rzędu milisekund, a gęstość mocy osiąga  $10^9 + 10^{11}$  [W/mm<sup>2</sup>], gdy czasy impulsów są rzędu pikosekund. W przypadku laserów emitujących promieniowanie ciągłe (CW - Continuous Wave Mode), gęstości mocy sytuują się w zakresie od  $10^3$  do  $10^7$  [W/mm<sup>2</sup>].

### 3. RODZAJE LASERÓW PRZEMYSŁOWYCH

Do obróbki laserowej wykorzystuje się wiele rodzajów laserów przemysłowych, z których każdy jest dopasowany do konkretnych zastosowań ze względu na właściwości oraz charakterystyki promieniowania laserowego. Poniżej przedstawiono zestawienie najczęściej wykorzystywanych odmian wraz z ich zastosowaniem.

**Laser Kryształiczny** – Obecnie najbardziej wykorzystywany laser w przemyśle, w którym jako medium aktywne do wytworzenia wiązki używa się ciała stałego najczęściej kryształu stworzonego z granatu itrowo-glinowego, który domieszkowany jest neodymem. Medium pobudzone jest za pomocą energii zewnętrznej, powodując przejście atomów do wyższych stanów energetycznych. Przy powrocie do niższych emitują fotony. Proces zachodzi wewnątrz rezonatora posiadającego zwierciadło na każdym z dwóch końców, powodując wzmocnienie i utrzymanie fali świetlnej poprzez wielokrotne odbicia. Proces ten prowadzi do emisji spójnej wiązki laserowej. Ta odmiana lasera znajduje zastosowanie w cięciu, spawaniu oraz znakowaniu metali.[4]

**Laser gazowy CO<sub>2</sub>** – Inaczej nazywany też molekularnym, jest to laser bazujący na mieszance gazowej dwutlenku węgla, która aktywowana jest elektrycznie w wyniku wyładowań. Pobudzając w ten sposób fotony doprowadza się do powstania światła wewnątrz rezonatora, które odbijane wielokrotnie od zwierciadeł prowadzi w końcu do emisji spójnej, ukierunkowanej wiązki laserowej. Biorąc pod uwagę długość fali, lasery te doskonale nadają się do obróbki materiałów niemetalicznych takich jak, drewno, akryl, szkło, guma. Ze względu

na wysoką wydajność oraz bardzo dobrą jakość promieniowania najczęściej wykorzystywany jest do grawerowania. [3]

**Laser diodowy** - laser, którego obszarem czynnym jest półprzewodnik, najczęściej w postaci złącza P-N, w którym obszar czynny pompowany jest przez przepływający prąd elektryczny. Wprowadzając nośniki ładunku, czyli elektrony i dziury, doprowadzamy do rekombinacji ładunku w wyniku czego powstają fotony. Fotony mają określoną energię co odpowiada określonej długości fali. Analogicznie od innych laserów fotony wielokrotnie odbijają się od zwierciadeł krańcowych tak długo aż wystąpią odpowiednie warunki do emisji spójnej wiązki laserowej poprzez jedno z częściowo przezroczystych zwierciadeł. Najbardziej perspektywiczny z punktu widzenia zastosowania ze względu na dużą moc, małe wymiary. Wykorzystywany najczęściej w łączności światłowodowej, urządzenia pomiarowe takie jak dalmierz czy napędy CD. [3]

**Laser rubinowy** – kolejny laser wykorzystujący ciało stałe jako ośrodek czynny, tym ciałem jest rubin, który w odpowiednim połączeniu zapewnia występowanie trójpoziomowego układu stanów energetycznych. Laser ten skonstruowano jako pierwszy, bo już w 1960 roku. Fotony emitowane w wyniku emisji spontanicznej, które poruszają się wzdłuż osi wywołują emisję wymuszoną, poprzez wielokrotne odbijanie się od krańcowych zwierciadeł. W ten sposób liczba fotonów gwałtownie rośnie i uciekając przez częściowo odbijającą powierzchnię zwierciadeł tworzą wiązkę laserową. Stosuje się go w naukach ścisłych, laboratoriach oraz eksperymentach. [3]

Ponad to w laserach przemysłowych kluczową rolę pełni elektronika, która odpowiada za sterowanie, modulacje i monitorowanie procesów związanych z generacją wiązki laserowej. Jak i zasilaniem czy też sterowanie robotami, które w obecnym czasie są szeroko wykorzystywane w procesie obróbki. Oto kilka kluczowych elementów, w których jest wykorzystywana: [1,2]

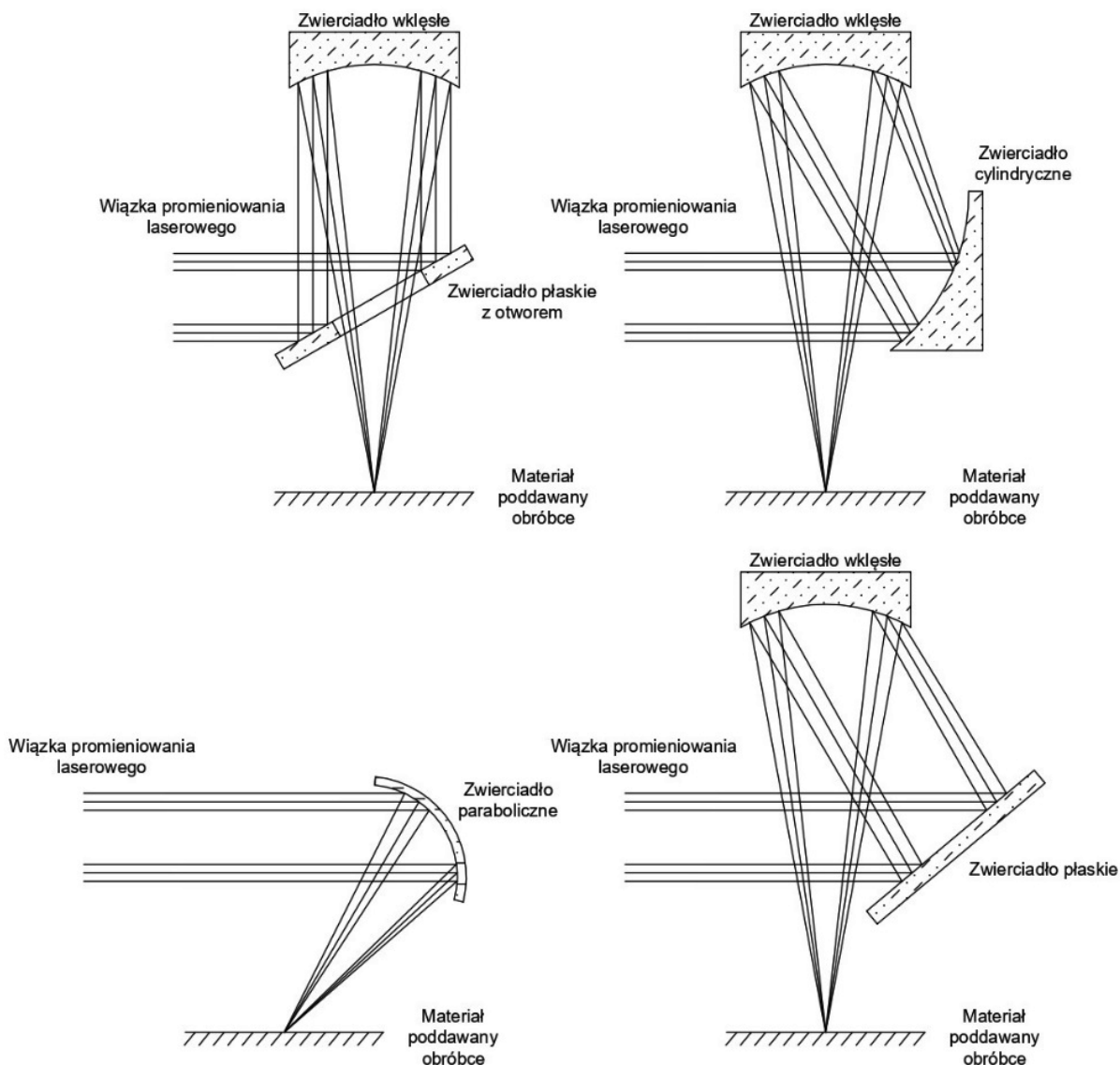
**Zasilanie i układy sterowania** – odpowiada za dostarczanie odpowiednich napięć i prądów do komponentów lasera, takich jak diody, elementy aktywne, czujniki, układy optyczne czy też roboty, które zajmują się umiejscowieniem próbki, oraz późniejszą manipulacją w trakcie procesu obrabiania. Układy sterowania natomiast odpowiadają za regulację parametrów pracy np. moc, częstotliwość. [1,2]

**Układy chłodzenia** – lasery generują ciepło, które negatywnie może wpłynąć na wydajność procesu oraz na trwałość. Elektronika steruje układami chłodzenia takimi jak wentylatory, odsysacze czy też układy chłodzenia cieczą. [1,2]

**Komunikacja i zdalne sterowanie** – w obecnie używanych laserach do obsługi stosowane są interfejsy komunikacyjne, takie jak Ethernet, Rs-232, które umożliwiają zdalne sterowanie procesami oraz ich kontrole. Dodatkowo umożliwiają one ciągłą komunikację oraz diagnostykę z urządzeniem.

#### 4. UKŁADY OPTYCZNE W LASERACH

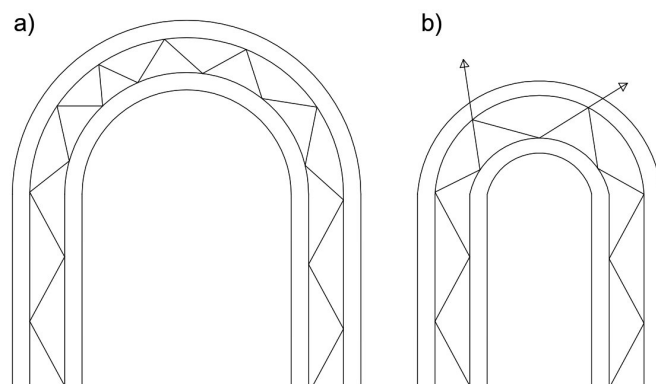
Nie we wszystkich przypadkach maszyn laserowych wiązka promieniowania laserowego jest doprowadzana za pomocą światłowodów. Wiązka laserów CO<sub>2</sub> wymaga wykorzystania odpowiednich układów optycznych, które również zależą od mocy lasera, gdyż dla mocy wiązki lasera większej od 5,0 kW wiązka ma przekrój pierścieniowy, który wymaga wykorzystania specjalnych głowic optycznych ogniskujących wiązkę pierścieniową lasera CO<sub>2</sub> o dużej mocy.



Rysunek 1. Uprozczone schematy głowic optycznych laserów  $CO_2$  o dużej mocy działających na wiązkę laserową pierścieniową.

Pozostałe lasery zazwyczaj korzystają z technologii światłowody w celu doprowadzenia wiązki lasera z generatora promieniowania lasera do miejsca obróbki. Znormalizowana konstrukcja światłowodu składa się z cienkiej rurki stalowej pokrytej osłoną z tworzywa sztucznego, dodatkowo wzmocnionego siatką stalową. Głównym zadaniem takiej konstrukcji jest ochrona przewodu światłowodu od zmęczenia mechanicznego. Dokończeniem konstrukcji światłowodu jest włókno optyczne umiejscowione wewnątrz cienkościennej rurki osłonowej z sztucznego tworzywa. Jako dodatkową ochronę w przypadku przerwania lub rozcięcia światłowodu stosuje się ochronny przewód elektryczny, który ma na celu natychmiastowe przerwanie pracy generatora promieniowania laserowego.

Mimo zastosowania odpowiednich powłok objających wiązkę promieniowania laserowego, nadmierne zgięcie przewodu może skutkować tym, że część energii lasera przebiję powłokę i zacznie prowadzić do uszkodzenia przewodu światłowodu (zjawisko częściowego odbicia).



Rysunek 2. Kąt zgięcia przewodu światłowodowego; a) poprawne przewodzenie wiązki laserowej, b) przegięcie przewodu światłowodowego, skutkujące przebiciem osłony światłowodowego przez część energii lasera (zmęczenie mechaniczne).

## 1. PODSUMOWANIE

Lasery są obecnie jedynym dostępnym źródłem energii o gęstości mocy nawet ponad  $10^9$ - $10^{11}$  [W/cm<sup>2</sup>] w normalnych warunkach atmosferycznych. Tak duże gęstości mocy oraz możliwość dokładnego sterowania wiązką promieniowania laserowego umożliwiają bardzo dokładne nagrzewanie z szybkościami dochodzącymi do  $10^6$  [°C/s] a następnie topienie, a nawet odparowanie wszystkich znanych materiałów inżynierskich. Stąd też lasery już od kilkudziesięciu lat są stosowane w wielu gałęziach przemysłu do automatycznego lub zrobotyzowanego spawania, napawania, stopowania, przetapiania, powierzchniowej obróbki cieplnej, lutowania twardego i lutowania miękkiego, cięcia, przebijania, żłobienia, ablacji, a szczególnie w przemyśle: samochodowym, lotniczym, energetycznym, okrętowym czy zbrojeniowym, ale również w medycynie, geodezji i elektronice.

## PODZIĘKOWANIE

Praca powstała w wyniku realizacji projektu w ramach kształcenia zorientowanego projektowo - PBL, w konkursie X w ramach programu Inicjatywa Doskonałości – Uczelnia Badawcza, Politechnika Śląska.

## LITERATURA

- [1] Barczyk J, Kłosowiak M.: Robotyzacja cięcia laserowego, *Pomiary Automatyka Robotyka*, 6/2005
- [2] Ciecierska B, Kluz R.: *Obróbka laserowa powierzchni z wykorzystaniem robota przemysłowego*, Warszawa, 2014
- [3] Bryl R.: *Podstawy działania laserów oraz ich zastosowania*, Uniwersytet Wrocławski
- [4] Wójciuk K.: *Klasyfikacja laserów pod względem ośrodka czynnego i ich praktyczne zastosowanie*, <http://laboratoria.net>
- [5] Klimpel A.: *Technologie laserowe: spawanie, napawanie, stopowanie, obróbka cieplna i cięcie*, Wydawnictwo Politechniki Śląskiej, Gliwice 2012



26th January 2024  
Gliwice, Poland

DEPARTMENT OF ENGINEERING MATERIALS AND BIOMATERIALS  
FACULTY OF MECHANICAL ENGINEERING  
SILESIA UNIVERSITY OF TECHNOLOGY

## INTERNATIONAL STUDENTS SCIENTIFIC CONFERENCE

### Morphology of Polymer Clay Nanocomposite Fibres

Y.M. Tsekpo <sup>1</sup>, W. Smok <sup>1</sup>, P. Jarka <sup>1</sup> and T. Tanski <sup>1</sup>

<sup>a</sup> Silesian University of Technology, Faculty of Mechanical Engineering, Department of Engineering Materials and Biomaterials  
email: yao.tsekpo@polsl.pl

**Abstract:** This paper aims to prepare PMMA clay nanocomposite fibers using electrospinning technology from a solution containing poly(methyl methacrylate) (PMMA), N, N-Dimethylformamide (DMF), nano-bentonite and magnetite (Fe<sub>3</sub>O<sub>4</sub>) nanoparticles. Four types of nanofibers were produced; pristine PMMA and three composite mats with a 10% concentration of nanoparticles in a 5wt.% solution of PMMA in DMF. The morphology of the resultant nanofibers was analyzed using a scanning electron microscope (SEM). The results obtained revealed that the average fiber diameters obtained were between 203.06 nm – 309.66 nm. The results imply that the material is suitable for application as a membrane or filter.

**Keywords:** morphology, polymer, nanofibers, magnetite, bentonite

### 1. INTRODUCTION

Nanocomposites are new materials that contain nanoscale fillers, such as silica and carbon black, which are frequently used as reinforcement in rubber or polymer technologies. These materials offer good qualities and properties at a low level of filler reinforcement because of their unique physical characteristics, which include enlarged surface area, architecture, functions, surface energy, and a high strength-to-weight ratio[1]. Minerals known as nanoclays, which have unique morphologies, structures, and chemical compositions, are used as nanofillers. Interlayers between the layered aluminosilicates known as nanoclays are merely a few nanometers thick. In nanotechnology, nanoclays are known as 2D nanomaterials[2].

The use of clays in a variety of polymeric matrix materials can be traced back to Prof. A. Blumstein's studies in the 1960s on polymer chains based on methyl methacrylate on montmorillonite (MMT) clay[3]. Advanced polymeric/nanoclay composites for aeronautical and biomedical applications were inspired by the nylon-6/silicate clay nanocomposites developed by the Toyota research team. Bentonite clay, clay nanocomposites, and copolymers based on polyurethane provide enhanced characteristics such as biodegradability and antibacterial activity in addition to mechanical strength[4].

One method for producing materials for a variety of uses, such as environmental cleanup and protection, is electrospinning. It is utilized in several industries, including sensors, composite reinforcement, biomedical devices, and universal membranes[5]. Because of their small diameter, electrospun nanofibers are porous and have enormous surface areas. Polymer characteristics, tip-to-collector distance, voltage intensity, flow rate, collecting roller speed, temperature, and humidity are some of the variables influencing fiber production. The electric field produced by the electrospinning process causes the diameter of the fluid jets to decrease.

This work reports the electrospinning method in the preparation of PMMA/Bentonite/Magnetite composite nanofibers. The work highlights the effects of nano-bentonite and magnetite nanoparticles on morphology and optical properties, and it illustrates the creative application of nano-reinforcement in electrospun mats.

## 2. MATERIALS AND METHOD

Bentonite clay powder (<50 nm, Sigma-Aldrich) was utilized straight out of the package without any additional purification. Iron oxide ( $\text{Fe}_3\text{O}_4$ ) nanoparticles were also made using green synthesized, following the instructions provided by Tsekpo et al. [6]. Poly (methyl methacrylate) (PMMA, 99%,  $M_w=9600000$ ) and N, N-Dimethylformamide (DMF, 99.8% purity) were purchased from Sigma Aldrich.

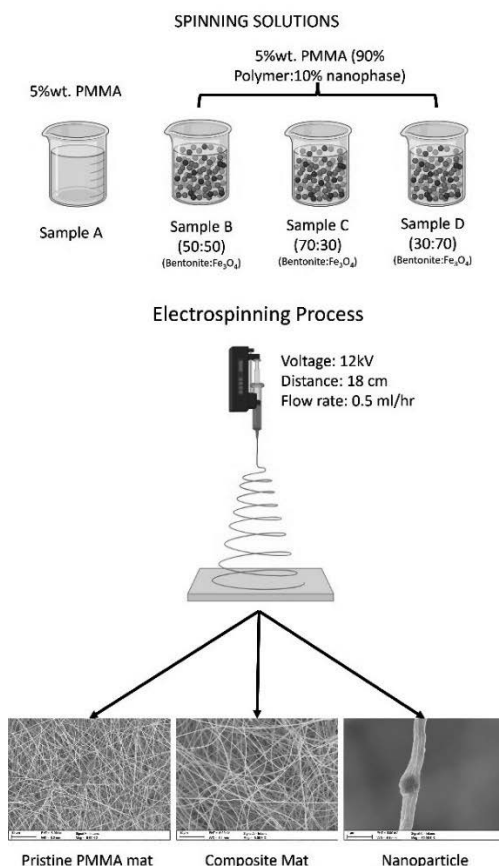


Figure 1. Schematic of Methodology

The final products were PMMA/DMF/Bentonite/Fe<sub>3</sub>O<sub>4</sub> solutions with a 5% concentration of PMMA and a 10% concentration of nanoparticles mixed in different bentonite ratios. To break nanoparticle agglomerates, reinforcing phase was added to DMF, and the solution was sonified for 15 minutes. The polymer was added and mixed for 24 hours at room temperature. The solution was placed in a sterile syringe, and the polymer and composite nanofibers were obtained using the electrospinning method using the FLOW—Nanotechnology Solutions Electrospinner 2.2.0-500 device.

A scanning electron microscope (SEM, SUPRA 35 by ZEISS, Germany) with the EDAX Trident XM4 series X-ray spectrometer (EDX) was used to observe the morphology of the prepared fibrous mat. EDX on the SEM was only used in the examination of the prepared fibrous mats.

### 3. RESULTS AND DISCUSSION

SEM images of PMMA fibers, composite fibers formed from solutions with varying nanophase ratios, and their elemental makeup are presented in the study.

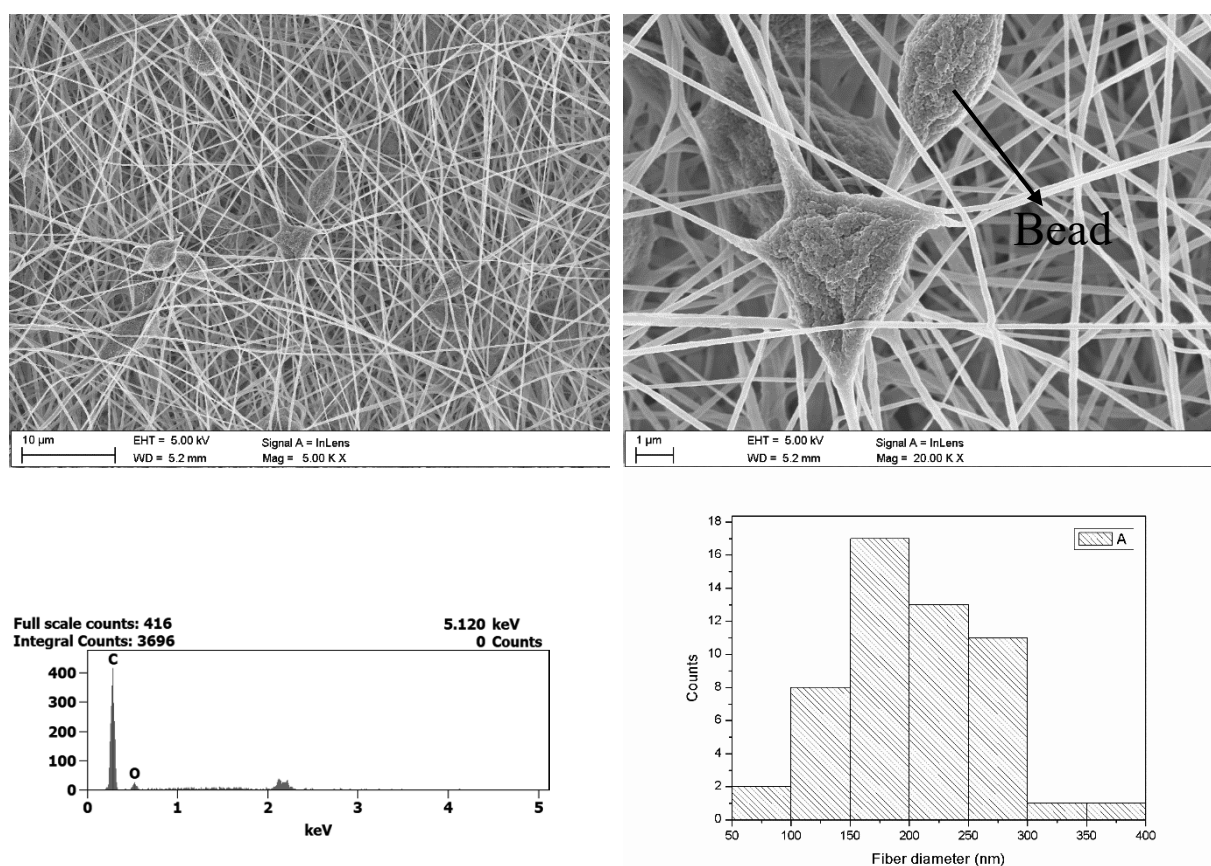


Figure 2. Image, Fibre distribution and EDX spectra of Sample A

ImageJ was used to estimate the nanofibers' average diameters. Smooth fibers were evident, and the fibers made from immaculate PMMA were attained in the nano regime. Because of the low concentration of PMMA utilized in the electrospinning process, which lowers the spinning solution's viscosity and results in less polymer chain entanglement, beads were seen. As a result of electrostatic scattering and the electrospaying action, beads are formed. The elements carbon and oxygen were detected by the EDX analysis.

Table 1. Average fibre diameter for samples produced.

Sample	Average Fibre Diameter (nm)	Standard Deviation
A	203.06	52.28
B	277.38	79.27
C	328.10	99.97
D	309.66	63.26

When compared to pristine fibers, the diameter of composite PMMA fibers increases upon the introduction of nanophase. There are fewer beads and an agglomerated nanophase, and the fibers are clean and homogeneous in shape. However, because of the variation in the nanophase's particle shape, the composite fibers are rougher. The higher viscosity of the doped solution is responsible for the diameter increase. This phenomenon causes the concentration of the spinnable polymer in the spinning solution to decrease while the concentration of solids in the solution increases, giving rise to viscoelastic characteristics.

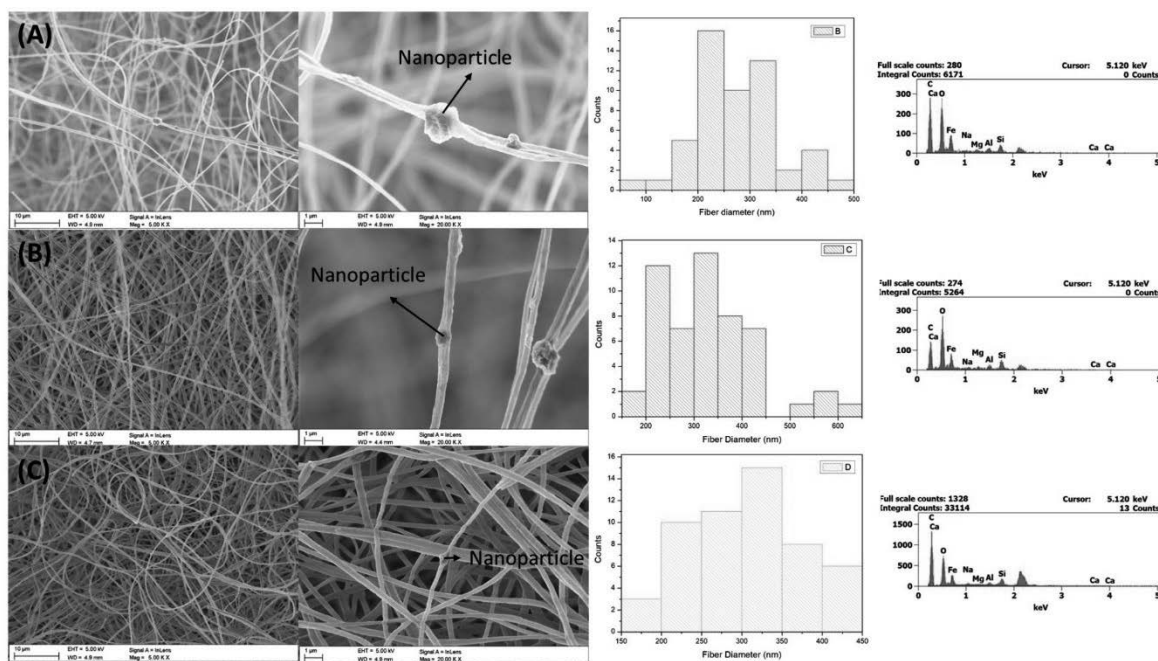


Figure 3. Image, Fibre distribution and EDX spectra of (a) Sample B (b)Sample C and (C) Sample D



#### 4. CONCLUSION

In summary, creating nanofibrous mats by electrospinning from solution is explained in this study. The process used enables the production of PMMA polymer fibers and PMMA/Bentonite/Fe<sub>3</sub>O<sub>4</sub> composite fibers with the concentrations depicted in Figure 1. The fibers obtained were in the nano regime, as shown by the analysis of the micrograph of the fibrous PMMA and composite mat. The addition of the nanophase resulted in the production of fibers with larger diameters. This happened because the spinning solution's viscosity was increased by the presence of nanoparticles, which increased the amount of solids in the solution and improved its conductivity. The results obtained imply that the material is suitable for a membrane or filter.

#### BIBLIOGRAPHY

1. S. Murugesan, T. Scheibel, Copolymer/Clay Nanocomposites for Biomedical Applications, *Adv Funct Mater* 30 (2020) 1908101. <https://doi.org/10.1002/adfm.201908101>.
2. R. Iravani, C. An, Y. Adamian, M. Mohammadi, A review on the use of nanoclay adsorbents in environmental pollution control, *Water Air Soil Pollut* 233 (2022) 109.
3. A. Blumstein, Polymerization of adsorbed monolayers. I. Preparation of the clay-polymer complex, *J Polym Sci A* 3 (1965) 2653–2664.
4. Y. Lvov, B. Guo, R.F. Fakhrullin, Functional polymer composites with nanoclays, Royal Society of Chemistry, 2016.
5. A. Yang, R. Gao, H. Yang, Application of layered nanoclay in electrochemical energy: Current status and future, *EnergyChem* 3 (2021) 100062.
6. Y.M. Tsekpo, A.N.S. Appiah, L.N.W. Damoah, D. Amusah, E. Annan, Fabrication, Properties, and Performance of Polymer-Clay Nanocomposites for Organic Dye Removal from Aqueous Media, *Adsorption Science and Technology* 2023 (2023). <https://doi.org/10.1155/2023/5683415>.



26th January 2024  
Gliwice, Poland

DEPARTMENT OF ENGINEERING MATERIALS AND BIOMATERIALS  
FACULTY OF MECHANICAL ENGINEERING  
SILESIA UNIVERSITY OF TECHNOLOGY

## INTERNATIONAL STUDENTS SCIENTIFIC CONFERENCE

### The system for collecting data on failures in the maintenance department

D. Wala<sup>a</sup>, M. Spilka<sup>b</sup>

<sup>a</sup> Student, Silesian University of Technology, Faculty of Mechanical Engineering, Department of Engineering Materials and Biomaterials, Management and Production Engineering  
email: dariwal151@student.polsl.pl

<sup>b</sup> Silesian University of Technology, Faculty of Mechanical Engineering, Department of Engineering Materials and Biomaterials  
email: monika.spilka@polsl.pl

**Abstract:** The article presents the application that enables employees to report information about failures to the existing database. The collected data can serve as information for the analytical team, which can easily draw conclusions and then use them as input for quality diagnostic tools or as ready information to support decision-making within the company.

**Keywords:** total productive maintenance, manufacturing company, database, failure, data collection system, application

### 1. INTRODUCTION

Lean management is now the foundation of modern manufacturing plants. The existence of tools such as Total Productive Maintenance (TPM) creates a new culture in the workplace, based on empowering and mobilizing employees to perform additional tasks in areas where they are competent. According to TPM principles, individuals spending the most time with machines should have a greater role in the decision-making process within the company. Decision-making should always be preceded by a proper analysis of collected data, which is often inadequately standardized due to the complexity of the problem. Inaccuracies in data sets lead to drawing incorrect conclusions, which in turn result in flawed decisions. Therefore, companies should have a flexible approach to the initial stages of the decision-making process. Flexibility in this regard should involve collecting a large number of parameters, allowing greater freedom in choosing their combinations to deduce the source of occurring failures.

Various types of IT tools play a crucial role in supporting production management and data collection processes. In the market, many companies offer software licenses to support production systems. Some companies also choose to develop their own software. Both of these solutions incur significant costs and are associated with many drawbacks, as those responsible for licensing or software development are often not directly involved in the specifics of a given process, which may lead to overlooking critical details. A solution to the above problem is to enhance the flexibility of creating applications that support the production system by using

low-code platforms. These platforms enable the creation of necessary tools even by individuals with limited programming knowledge. An ideal environment for such tasks is Microsoft SharePoint, which allows easy integration of spreadsheets across various platforms. The package includes tools such as Power Apps, which serve as creators for the mentioned applications. Practically every large manufacturing company uses Microsoft tools, making such solutions cost-effective. This approach also eliminates personnel issues, as the Office suite is widely used, and a significant portion of employees, after training, will be able to use it efficiently.

## **2. COLLECTING DATA ON THE CAUSES OF ACCIDENTS**

Accurate recognition of the workplace, job specifics, and the origins of failures should form the basis for activities undertaken by the analytical-decision-making team. However, in practice, this is often limited, leading to decisions that may not be accurate and fail to eliminate the true cause of failures. The "Gemba walk," suggested in literature and rooted in Lean Manufacturing methodology, aims to physically and personally familiarize individuals with the issues at workstations. However, in a global context, it may not fulfill its task because the number of failures and areas where they occur usually exceeds the decision-makers' capabilities. An alternative to the "Gemba walk" is an approach based solely on reports, limited statistics, or measurement data collected in specific segments of production lines. In such cases, significant entities that are the actual cause of failures may go unnoticed, increasing the analysis time and the risk of errors [1,2].

The Total Productive Maintenance tool and its effective implementation on the production floor provide a solid foundation for introducing a new data collection system. The implementation of each pillar of this methodology not only changes the work culture but also helps in implementing new tools, primarily supporting the maintenance department. Employees focused on continuous improvement in quality, increased efficiency, and waste reduction will be more willing to adapt to new responsibilities imposed on them. While TPM is often associated with transferring machine responsibilities from the maintenance department to production operators, it is justified to shift the duty of acquiring data about failures from the analytical-decision-making team to the repairing employees. The essence of this action is to empower mechanics to determine the cause of the failure after the repair has been made [3].

In addition to identifying the cause of the failure, employees would be obligated to fill out a short form containing basic information about the failure and the actions taken. Enabling the submission of such a report should be flexible and mobile, with a mobile application being the most convenient and efficient option. Designing such an application and integrating it with the database would pose a challenge for the implementation team and would require support from the IT department. However, creating an application in a low-code creator that allows easy integration with the database could save a lot of financial resources and time. The Microsoft SharePoint platform allows creators to build functional tools, so it can be used to create an application with a built-in form, from which data will be exported to the database. The basic database can be the Lists platform, which can be integrated with Power Apps in real-time. Since both tools complement each other well, it is worthwhile to use them when creating the system presented in Figure 1.

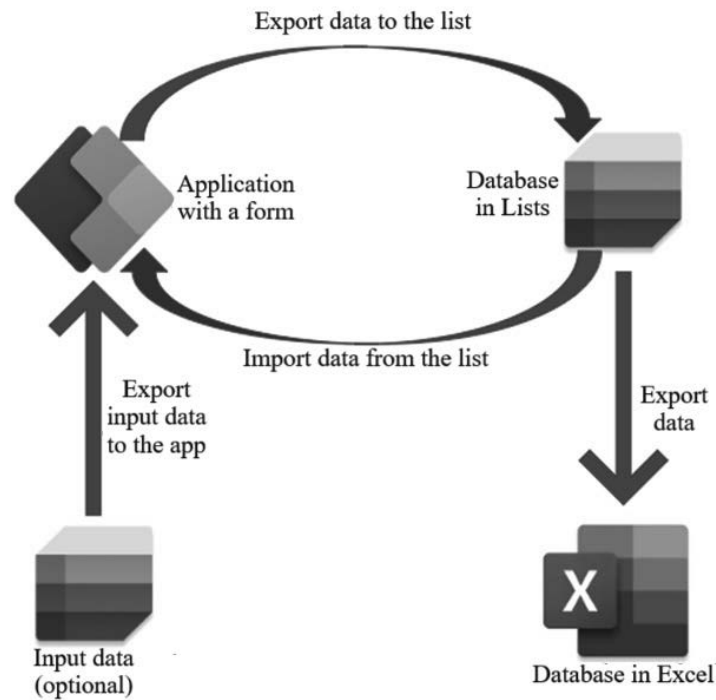


Figure 1. Relationships between SharePoint sheets

### 2.1. Designing a mobile application

The mentioned Power Apps creator enables the creation of a form (depicted in Figure 2) containing various user input data entry forms. The selection of a specific data input window is closely dependent on the tasks that the given information is intended to fulfill. In the application example, the following input data forms were applied:

**Text input** – an option used in places where entering template content would be ineffective. An example is the "Fault Description" field, the completion of which requires the employee's own ingenuity, making it impossible to establish a drop-down list due to the infinite possibilities. Another problematic field is "Listed Items" because, thanks to the application's integration capabilities with databases, it is possible to create a drop-down list containing all components of the production station. However, this solution is not optimal as, due to the large number of items entered into the system, the employee would spend much more time selecting the appropriate items. Text input is also used in windows requiring entry of time expressed in minutes.

**Dropdown list** – a solution allowing the user to choose from available options. Replacing the manual text entry function with a dropdown list benefits both the data enterer and the analytical team. The entering employee saves time by choosing one of the available options. This field, however, holds particular value for the analytical team because the lack of differences in entered data eliminates the need to correct discrepancies between specific entries and prevents the possibility of omitting any data in further analysis.

Conditional dropdown list – technically does not differ from a regular dropdown list, but the introduction of a logical condition significantly streamlines the work of the data enterer and eliminates the risk of them making certain mistakes. An ideal example of using a conditional dropdown list is the dependency of the "workplace" dropdown list on the "Line." After choosing the appropriate line, only those positions corresponding to that line will appear in the dropdown list for selecting the position.

Figure 2. View of the application's main page

Each window that appears in the form carries specific information that can be utilized during analysis. However, the most crucial item is the dropdown list "Fault Cause," which includes seven predefined causes of failure. This is an adopted classifying value to categorize potential causes in a general sense. The aim is to limit the time spent by the form filler contemplating the perfect option, guiding analysts towards the suggested range of causes. A more detailed description should be provided in the "Fault Description" text field. The decision was made to highlight the following seven causes of failure and add an "other" option. The scope of classified causes is as follows:

- Operator mistake – behavior that led to a failure due to non-compliance with workstation instructions or provided recommendations;
- Component wear – premature wear of a machine's mechanism part before the scheduled maintenance or service period;
- Improper maintenance – failure of maintenance personnel to adhere to the maintenance schedule or the quality of actions taken;
- Production defects of the element – defects not resulting from assembly, use, or maintenance of the machine. This also applies to machine software if it is still in its proprietary version;

- Faulty assembly – failure resulting from the incorrect installation of an element whose quality is correct;
- Design error – concerns situations arising from a wrongly designed process;
- Contamination – the presence of unauthorized elements in the employee's or machine's workspace that directly affected the failure;
- Other – difficult to determine or unspecified causes.

The editing form window also includes two buttons, with the "Submit Report" button being particularly significant. This button is associated with a code containing the function of exporting the data entered by the employee to the linked Microsoft Lists sheet as a single row. In addition to visible data, the button also exports information about the filler, the date of the report (a numerical Unix value formatted to a value understood by Microsoft Excel as a date), and the generated report ID code. After performing these functions, the button clears the form and displays a message that the report has been submitted.

The second button is "Edit," which takes the user to another window of the application (Figure 3), containing an archive of reports with the ability to edit them in case of errors. The window contains a list of previous reports and a panel allowing their editing. The "Overwrite" button corrects the selected row in the Lists database sheet and sends the user a message about the successful operation of overwriting the content. The arrow visible in the editing window is a button that causes a return to the form window.

The screenshot displays a mobile application interface. On the left, there is a vertical list of report entries, each containing a date, a line number, and a name (Dariusz Wala). The selected entry is 202310040815, LP, Dariusz Wala. To the right of this list is a form for editing the selected report. The form fields are: LP (202310040815), Line (L5), Workplace (L5S1), Failure cause (Production defects of the), Failure description (Faulty tolerance of the gear), Has the ticket been rep... (No), and Was the production line... (No). At the bottom of the form, there is a dark button labeled "Overwrite" and a curved arrow icon pointing back to the list.

Figure 3. View of the application's second page

### **3. SUMMARY**

The data collection process should be appropriately organized and flexible to minimize the possibility of making incorrect decisions. Considering the involvement of maintenance personnel in filling out failure forms, which would be automatically formatted into a tabular database, can be a valuable step. This database would serve as essential information for the analytical team. The tools provided by Microsoft SharePoint offer a cost-effective, flexible, and efficient way to achieve this goal.

### **BIBLIOGRAPHY**

1. M. Pradziadowicz, A. Zaremba, Lean Management – współczesna metoda systemu produkcji, *Studia Zarządzania i Finansów Wyższej Szkoły Bankowej w Poznaniu*, 13 (2017) 51-60.
2. R. Wolniak, Gemba–japońska technika zarządzania, *Przegląd organizacji* 7-8 (2003) 22-25.
3. D.R. Kiran, *Total quality management: Key concepts and case studies*, Butterworth-Heinemann, 2016.



26th January 2024  
Gliwice, Poland

DEPARTMENT OF ENGINEERING MATERIALS AND BIOMATERIALS  
FACULTY OF MECHANICAL ENGINEERING  
SILESIAAN UNIVERSITY OF TECHNOLOGY

## INTERNATIONAL STUDENTS SCIENTIFIC CONFERENCE

### Development of a hand prosthesis model using Reverse Engineering

Ł. Wantuch<sup>a</sup>, M. M. Szindler<sup>b</sup>

<sup>a</sup> Member of the LabTech Scientific Club, Silesian University of Technology, Faculty of Mechanical Engineering and Technology

<sup>b</sup> Silesian University of Technology, Faculty of Mechanical Engineering and Technology, Department of Engineering Materials and Biomedical Engineering  
email: magdalena.szindler@polsl.pl

**Abstract:** This article presents the development of a model for a prosthetic hand using reverse engineering. Reverse engineering tools were employed to create a model of a hand prosthesis, followed by the development of moving parts and the printing of a finger model using a 3D printer. The hand was scanned using 3D scanners. The model was created in SolidWorks, and moving parts were designed in SolidWorks too, and printed on SLA 3D printer, Form 3+.

**Keywords:** reverse engineering, scanning methodology, prostheses, CAD/CAM

#### 1. INTRODUCTION

Each year in Poland, over 15,000 people lose an upper or lower limb through amputation. This result is eight times higher than, for example, in Spain, and the number of amputations increases every year. In the European Union, Poland ranks among the leaders in terms of amputations performed. The causes of amputation include: transport and agricultural accidents, explosions, frostbite, burns, electric shocks, and due to cancer or vascular diseases. It should be emphasized that amputation is a radical treatment method that deprives the patient of the ability to fully perceive stimuli from the environment and the prehensile factor. This makes it difficult to carry out simple everyday activities and often leads to mental health problems [1-4].

As a result of the development of the field of prosthetics, many attempts have been made to create upper and lower limb prostheses that are most convenient for patients and make every day functioning easier. As a consequence of the combination of reverse engineering and medicine, it is possible to create prostheses quickly [1-7].

Reverse engineering is a technology that introduces significant changes in the field of medicine. With this technology, it is possible to understand how a specific object was created, what materials were used, and how it functions. Real shapes of the object can be obtained and utilized for 3D modelling, followed by processes such as 3D printing. This technique allows the creation of a prosthetic hand, replacing a part of the musculoskeletal system, or producing implants tailored to the patient's anatomical dimensions [3-10].

In reverse engineering, several aspects should be taken into account that influence the selection of the method of collecting data about the processed object and influence the course of the reverse engineering stages. These factors are: the number of parts to be scanned - single or



many, the size of the element to be scanned - small or large, the complexity of the part whether the element has a simple or more complex structure, the material of the physical model - hard or soft, the texture of the part - matte or glossy, the required accuracy and part geometry – the outer, inner part of the element [4-13].

Dimensioning involves measuring an object using traditional measuring tools and recording the measurements in a technical drawing, and then developing a 3D model based on the previously taken dimensions. This method provides information about the object, precisely determines the features of the object, the form and dimensions of the element. This technique is used when the shape of the object is simple and measurement is easy [8-15].

Scanning technologies record information about an object without physical contact with the item. Scanners use lasers, optics, cameras and point sensors to record object data. These devices currently enable full analysis of the measurement by recording up to 2 million points, and the measurement duration is about a second [8-17].

Medicine is a field in which continuous development is needed to improve the lives of people suffering from diseases, illnesses and various disabilities. Modern technologies and techniques stand against the development of medicine, which enable the improvement of the functioning of patients with various ailments. These technologies include reverse engineering. The main applications of reverse engineering in medicine are the creation of implants and prostheses with more or less complex shapes, reconstruction of body parts, changes in prostheses, analysing products, replacing hard-to-reach parts for medical equipment and creating models of organs for simulating surgery. Using spatial scanners used in reverse engineering, it is possible to produce, for example, implants and prostheses. Thanks to precise measurements of scanners and sending the point cloud to CAD systems, it is possible to produce elements that are individually prepared to meet the patient's requirements [11-21].

Reverse engineering tools were employed to create a model of a hand prosthesis, followed by the development of moving parts and the printing of a finger model using a 3D printer. As part of the research, a finger prosthesis with movable elements was scanned, modelled and manufactured.

## **2. METHODOLOGY AND SOFTWARE USED FOR RESEARCH**

The first stage in the manufacture of the prosthesis was to scan the hand on the Creality CR Scan 01 laser scanner. This scanner features two scanning methods: with a rotary table and hand scanning. No markers are required to read out the geometry of the component. The recommended scanning distance is between 400 and 900 mm. The resolution of the scanner is 500 microns and the accuracy of 10 frames per second is 100 microns. When scanning the hand, the correct distance should be maintained and the correct light level selected. The hand should be kept still during the scan and the person performing the scan should not make any sudden movements and should hold the scanner in the right in the correct position to view the scan and the camera image on the monitor [5-7]. During the scanning process, the scanner can lost its way, at which point the scanner had to be returned to the point where it read the image. Several attempts were made to scan. The scan covers a large area, shown on figure 1. In the next step, redundant areas of the scan were truncated and the hand itself was extracted. The trimming of the scan was done in CR Studio. In figure 2 the extracted hand can be seen, with few imperfections. A second scan of the hand was performed. The 3D scanner used was the Shining Einscan Pro HD characterised by higher scanning accuracy, scanning speed and high

resolution. The scan was performed in manual mode. Unlike the first scan, it is not in colour. ExScan Pro software was used to record the point cloud. The result of the scan is shown in figure 3.

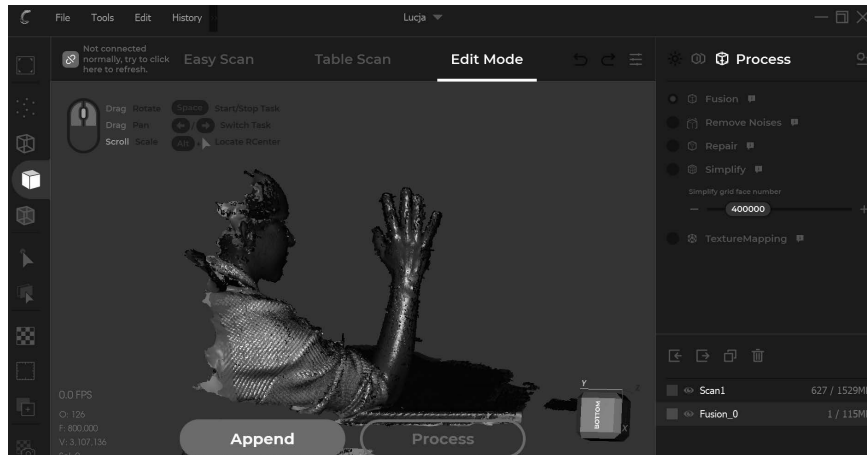


Figure 1. Scanning result prepared on Creality CR Scan 01 laser scanner.

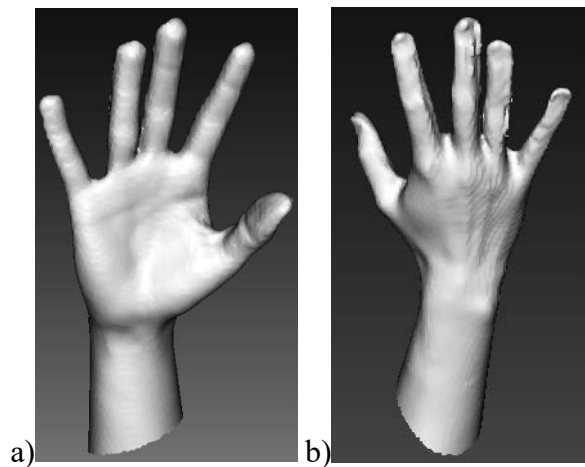


Figure 2. The scan image obtained using by Creality CR Scan 01: a) inner; b) outer hand part.

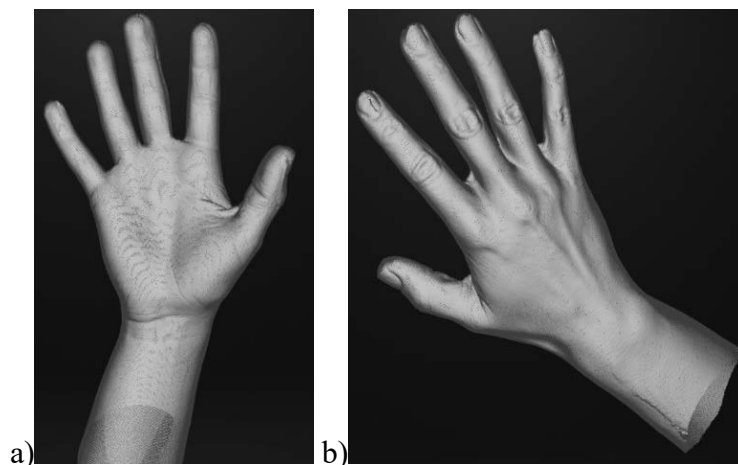


Figure 3. The scan image obtained using by Einscan Pro HD: a) inner; b) outer hand part.

After scanning, the differences in scans were noted. The Einscan scanner scanned faster and more accurately compared to CR Scan. The quality of the scan from the Einscan scanner is much better, even fingerprints are visible, the scan from the CR Scan is of good quality but not as accurate. It was decided to further process the scan, which was taken on an EinScan Pro HD scanner. Thanks to the EXscan Pro software the point cloud was generated. The CAD programme for further processing was SolidWorks. SolidWorks was opened and the ScanTo3D add-in was run, so the point cloud file was read out. A mesh was created from the point cloud. In the next step, a surface model of the hand was created. The surface creator function was used for this. The initial surface model was inaccurate and contained unfilled areas (Figure 4). The surface model was once again created from the mesh, the areas that were not filled were made smaller, with the help of the "surface fill" tool, the cavities in the model were filled, shown in figure 5. Figure 6 show the surface model, after changes have been made and filling in of unfilled surfaces.



Figure 4. Preliminary surface model

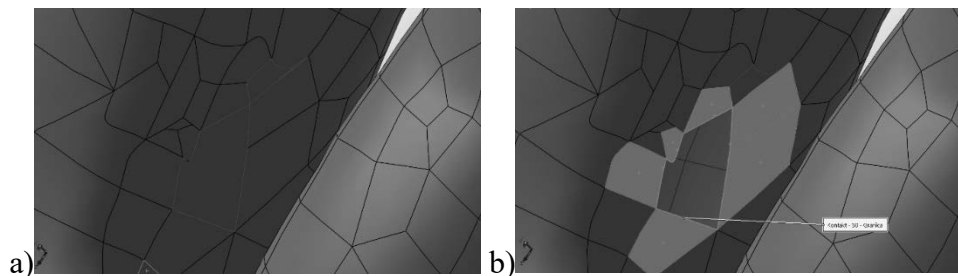


Figure 5. Surface filling a) unfilled surface, b) surface after using the "surface filling" function.

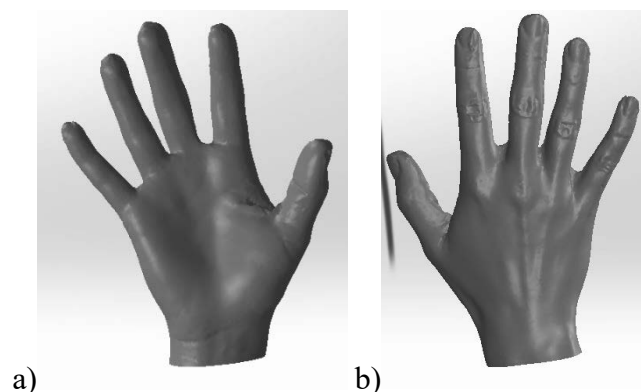


Figure 6. Surface model image: a) inner; b) outer hand part.

### 3. PREPARATION OF MOVING PARTS AND PRINTING OF FINGER ELEMENTS

Thanks to a number of features in SolidWorks including: add plane, sketchpad, cutout, extract base addition, the moving parts were created. The moving parts were then refined so as not to cause the moving part to bend in every direction. In the human hand, the joint has an adequate range of movement. In the design of the hand model, the moving parts were altered so that they were not hypermobile. The refined moving parts were developed on the index finger, shown on Figure 7.

The next step was to print the moving parts on a 3D printer. It was decided to use a printer using photopolymer resins. SLA technology is based on photopolymerisation. The component is created by selectively curing the resin with laser light. Before printing, PreForm software was used to prepare the model for printing; thanks to this software, it is possible to determine the printing parameters, the position of the support structures, which are responsible for keeping the component on the working platform and for maintaining the correct shape of the printed component. There is also a preview of how the component will be printed layer by layer and the printing time for the component is indicated. The model was printed in transparent resin and the print time for the component was approximately 6h. The model was printed on a FormLabs Form 3+ printer (Figure 8a), which is characterised by fast printing and high accuracy of printed parts. The printed part was then transferred to a device that cleans the part after printing (Figure 8b).

The model was then transferred to the Formlabs Cure unit (Figure 9), which is a UV exposure and print curing station. The unit controls the given temperature and exposure time. The FormLabs Cure is designed for post-processing and processing of models printed using SLA technology.

After several of the above-mentioned steps, a finished finger model was created. An important part in 3D printing is post-processing. Once the finished model was removed from the FormLabs Cure, the removal of the support structures proceeded. Once these were removed, the printed tubes were fitted to the holes and inserted into their intended location. By applying post-processing and fitting the tubes, the correct functioning of the moving parts was checked. All stages of post-processing were illustrated in figure 10 and figure 11.

After checking the accuracy of the moving parts, it was found that they do not bend towards the dorsal side of the hand i.e. an improvement has been made to the moving part but the direction in which the finger should bend could have a greater range of movement. In order to improve this, the moving parts should be set deeper and the excess material cut out to increase the range of movement. After printing, it was noted that the moving parts could be embedded deeper and thicker to be more robust.

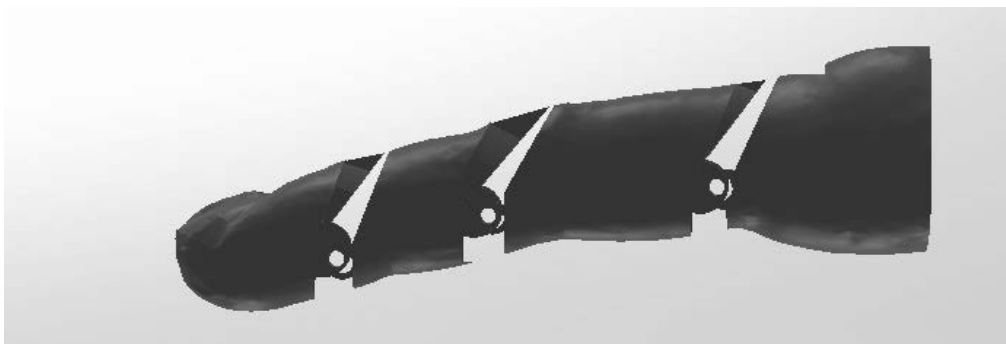


Figure 7. Mobile parts in the index finger.

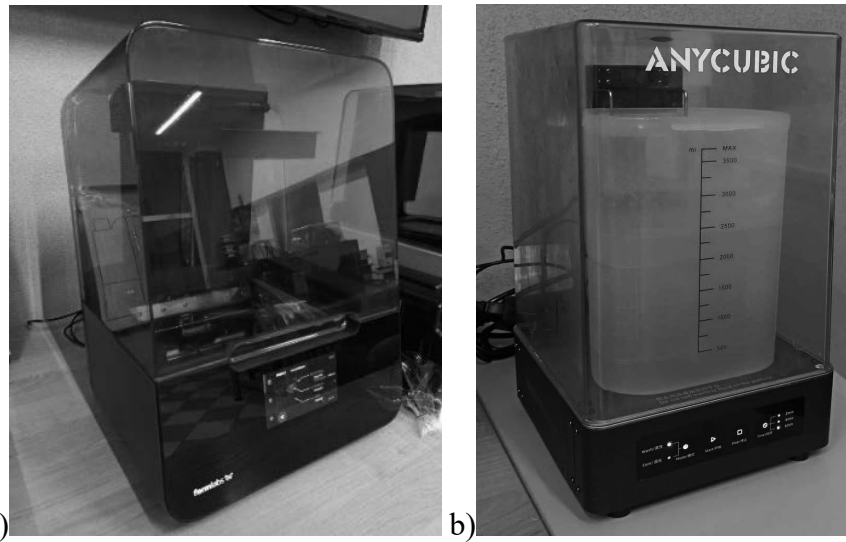


Figure 8. Devices used to print finger elements: a) FormLabs printer; b) print cleaning unit.

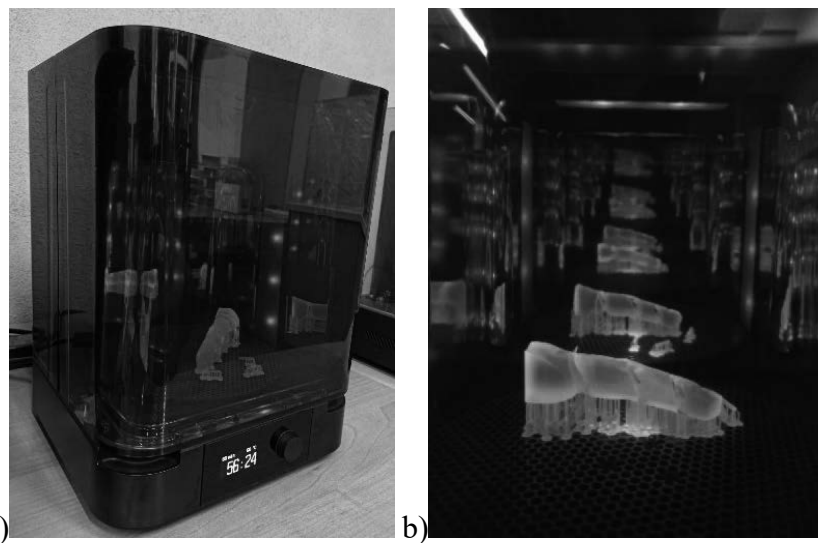


Figure 9. FormLabs Cure device: a) external view of the device; b) internal view of the device.

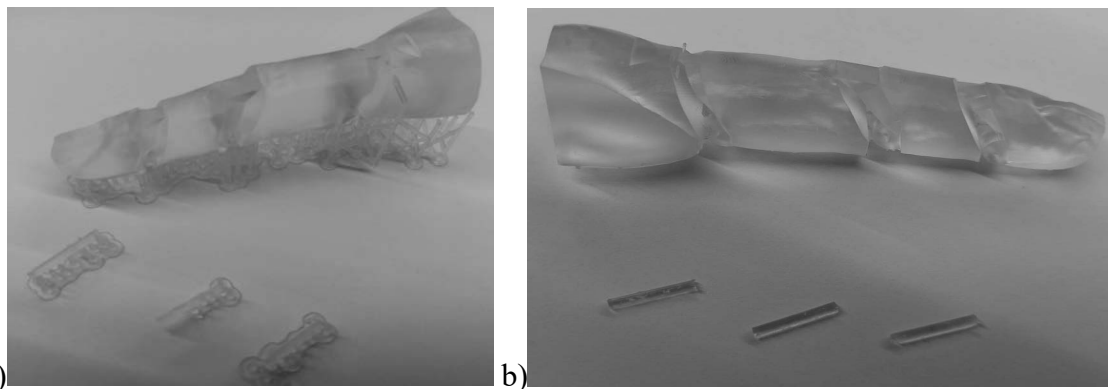


Figure 10. Printed finger elements: a) with support; b) after removal of supporting structures.

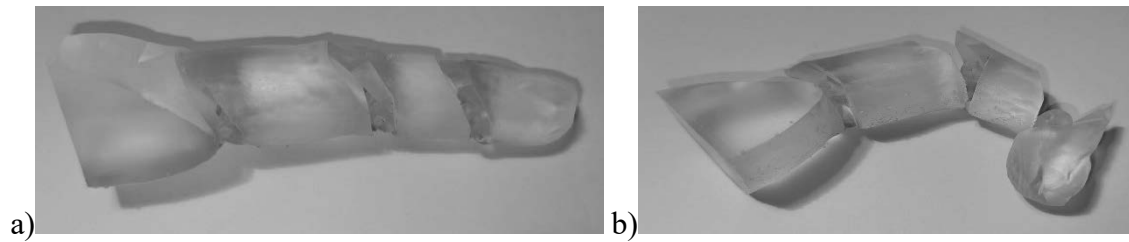


Figure 11. Assembled finger elements: a) with moving parts; b) with bent moving parts.

## CONCLUSIONS

Reverse engineering facilitates information gathering about a specific element through dimensioning and scanning, enabling the replication and improvement of the element. The use of reverse engineering tools made it possible to create a model of a hand prosthesis. The integration of spatial scanners, CAD/CAM systems, and medical tools allows for innovative solutions that enhance the lives of disabled or differently-abled individuals, impacting their daily functioning.

After scanning, the differences in scans were noted. The Einscan scanner scanned faster and more accurately compared to CR Scan. The quality of the scan from the Einscan scanner is much better, even fingerprints are visible, the scan from the CR Scan is of good quality but not as accurate. After several steps, a finished finger model was created. An important part in 3D printing is post-processing. By applying post-processing and fitting the tubes, the correct functioning of the moving parts was checked.

In conclusion, this article demonstrates that reverse engineering enables the development of a hand prosthesis model, emphasizing the importance of combining various technologies to achieve modern solutions in different scientific fields. The study highlights the usefulness of reverse engineering tools, particularly spatial scanners, in obtaining anatomical dimensions for creating individualized prosthetics. Reverse engineering finds application in prosthetics, dentistry, surgery, and orthopaedics. Reverse engineering synergizes well with CAD/CAM programs, allowing model improvements, and 3D printing technology facilitates the creation of physically accurate models, enabling the assessment of quality and functionality.

## BIBLIOGRAPHY

1. S. Grycuk, Designing and strength tests of upper limb prosthesis, *Acta Bio-Optica et Informatica Medica Inżynieria Biomedyczna*: nr. 24/2, s. 74-78, 2018.
2. P. Z. Filipek, A. Kociubiński, P. A. Mazurek, T. N. Kołtunowicz, J. Majcher, S. Styła: *Problemy Współczesnej Inżynierii. Wybrane zagadnienia elektrotechniki i informatyki w przemyśle i medycynie*. Politechnika Lubelska, Lublin, 2020.
3. M. Skowrońska, J. Sadowska, M. Kromka-Szydek: Model dłoni w programie CATIA V5 z uwzględnieniem parametrów ruchliwości ręki. *Aktualne Problemy Biomechaniki*: nr. 5, s. 133-136, 2011.
4. J. S. Tutak, B. Klatka: Bioniczna proteza dłoni. *Acta Bio-Optica Art Informatica Medica Inżynieria Biomedyczna*: vol. 22, nr. 1, s. 24-30, 2016.
5. P. Siemiński, G. Budzik, *Techniki przyrostowe. Druk 3D. Drukarki 3D*, Wydawnictwo Politechniki Warszawskiej, 2015

6. P. J. Dytrych, P. Borkowski, G.E. Dytrych Projekt: Protezy kciuka dla dziecka z zespołem Nagera wykonane metodą druku 3D. *Neurol Dziec*; nr. 26, 52: s. 45-54, 2017.
7. V. Raja, K.J. Fernandes: *Reverse Engineering. An Industrial Perspective*. Wydawnictwo Springer – Verlag London Limited, 2008
8. J. Bochnia: Zastosowanie skanowania 3D w inżynierii odwrotnej. *Mechanik*: nr. 3, s. 194-196, 2019.
9. V. G. Macefield, T. P. Knellwolf, Functional properties of human muscle spindles. *Journal of Neurophysiology*. 2018;120(2):452–467. doi: 10.1152/jn.00071.2018.
10. K. Gładysz, J. Szydłowska, O. Żuchnik, O. Król, P. Kwiatkowski, B. Kuczyńska, M. Czelej, A. Kłos, K. Gieroba, M. Szydłowski. Biodruk 3D jako przyszłość medycyny regeneracyjnej i nadzieja dla transplantologii. *Health and Sport*: nr. 13(1), s.38-44, 2023.
11. F. Zajac, Muscle and tendon: properties, models, scaling, and application to biomechanics and motor control. *Critical Reviews in Biomedical Engineering*. 1989;17(4):359–411.
12. A. Dawood, B. Marti Marti, V. Sauret-Jackson, A. Darwood: 3D printing in dentistry. *British dental journal*: 219/11, s. 521-529, 2015.
13. M. Žujović , R. Obradović , I. Rakonjac, J. Milošević: 3D Printing Technologies in Architectural Design and Construction: A Systematic Literature Review. *Buildings*: nr. 12/1319, s. 1-24, 2022.
14. M. Ziółkowska, P. Radek, et.al., Electrically conductive light-curing resins used in 3D printing, *TalentDetector2023 Winter: International Students Scientific Conference, Prace Katedry Materiałów Inżynierskich i Biomedycznych, 2023, Gliwice, Politechnika Śląska, s. 582-587.*
15. R. S. Johansson, J. R. Flanagan Coding and use of tactile signals from the fingertips in object manipulation tasks. *Nature Reviews. Neuroscience*. 2009;10(5):345–359. doi: 10.1038/nrn2621.
16. M. Ziółkowska, P. Kołodziejczyk, M. Sładek, et.al., Analiza skanowanego trójwymiarowego obrazu elementu przestrzennego i możliwości jego powielania w technologii addytywno-subtraktywnej, *TalentDetector2023 Winter: International Students Scientific Conference, Prace Katedry Materiałów Inżynierskich i Biomedycznych, 2023, Gliwice, Politechnika Śląska, s.572-581,*
17. N. Shahrudin , P. Koshy , J. Alipal , M.H.A. Kadir , T.C. Lee: Challenges of 3D printing technology for manufacturing biomedical products: A case study of Malaysian manufacturing firms. *Heliyon*: nr. 6, s. 2-14, 2020.
18. S. H. Sun, H. W. Chiang, M.L. Lee: Adaptive direct slicing of a commercial CAD model for use in rapid prototyping. *Int J Adv Manuf Technol*: nr. 34 s. 689-701, 2007.
19. M. Wolny, P. Ziobro, D. Więcek: Praktyczne zastosowania inżynierii odwrotnej. s.237-246
20. S. Sikorski, P. Duda, K. Dulęba, Z. Wróbel: Zastosowanie inżynierii odwrotnej w modelowaniu protez stawów. *Mechanik*: nr. 12, s. 1912-1913, 2016.
21. <https://www.3dnatives.com/en/laser-3d-scanner-vs-structured-light-3d-scanner-080820194/> (dostęp 03.11.2023r.)



26th January 2024  
Gliwice, Poland

DEPARTMENT OF ENGINEERING MATERIALS AND BIOMATERIALS  
FACULTY OF MECHANICAL ENGINEERING  
SILESIA UNIVERSITY OF TECHNOLOGY

## INTERNATIONAL STUDENTS SCIENTIFIC CONFERENCE

### The corrosion resistance of electro-deposited zinc coatings applied to the structural steel

J. Wiczorek<sup>a</sup>, J. Nosiadek<sup>b</sup>, M. Milewski<sup>b</sup>, K. Pepel<sup>b</sup>, T. Markefka<sup>b</sup>, J. Krawczyk<sup>b</sup>, M. Bodio<sup>b</sup>, W. Pakieła<sup>c</sup>, A. Zarychta<sup>c</sup>, A. Drygala<sup>c</sup>, B. Grzegorzczak<sup>c</sup>, J. Kubisztal<sup>d</sup>, K. Gołombek<sup>e</sup>, S. Lesz<sup>c</sup>

<sup>a</sup>Student, Silesian University of Technology, Faculty of Automatic Control, Electronics and Computer Science, Akademicka 16, 44-100 Gliwice, Poland,  
email: jw306100@student.polsl.pl

<sup>b</sup>Student, Silesian University of Technology, Faculty of Mechanical Engineering, 18a Konarskiego Street, 44-100 Gliwice, Poland,  
email: jn307433@student.polsl.pl, mm308741@student.polsl.pl, kp308739@student.polsl.pl, tm307426@student.polsl.pl, jk308486@student.polsl.pl

<sup>c</sup>Silesian University of Technology, Faculty of Mechanical Engineering, Department of Engineering Materials and Biomaterials, 18a Konarskiego Street, 44-100 Gliwice, Poland,  
email: sabina.lesz@polsl.pl, adam.zarychta@polsl.pl, aleksandra.drygala@polsl.pl

<sup>d</sup>University of Silesia, Institute of Materials Engineering, 1A, 75 Pułku Piechoty Street, Chorzów 41-500, Poland,  
email: julian.kubisztal@us.edu.pl

<sup>e</sup>Silesian University of Technology, Materials Research Laboratory, Silesian University of Technology, 18a Konarskiego St, 44-100 Gliwice, Poland,  
e-mail: klaudiusz.golombek@polsl.pl

**Abstract:** The paper presents the corrosion resistance of zinc coating on DC01 steel, studied by open circuit potential, potentiodynamic polarization measurements, and scanning electron microscope, for different electro-deposition conditions.

**Keywords:** electrogalvanizing, zinc coating, corrosion resistance, SEM method

## 1. INTRODUCTION

The European standard EN 10139 DC01, refers to a low-carbon, cold-rolled steel, with specific mechanical and chemical properties [1]. It is characterized by a low carbon content, making it soft and easy to bend and shape. This type of steel is popular in the metallurgical production, of sheet metal products.

DC01 steel finds application in various fields, including the production of: casings, automotive sheets, metal components, and metal constructions, and across different branches of industry, where high-quality surface sheets and good formability are required. DC01 steel,



being one of the popular types of steel, like many other metal materials alloys, faces challenges related to susceptibility to corrosion [2].

Corrosion is defined as the damage of metals and alloys through chemical or electrochemical interaction with their surrounding environment. It may lead to a loss of strength and durability [3-14].

In the case of DC01 steel, its susceptibility to corrosion primarily arises from the carbon content and other chemical components (Table 1), which can react with moisture and chemicals present in the environment. To minimize the risk of corrosion, it is crucial to provide adequate protection to the surface of DC01 steel. Regular maintenance and conservation play a key role in preserving the mechanical and aesthetic properties of DC01 steel, especially in conditions where corrosive factors such as moisture, salt, or acids are present. In industrial practice, awareness of susceptibility to corrosion is a significant element in material management, and appropriate protective measures can significantly extend the durability and functionality of structures made from this steel. To protect against corrosion, we can use various methods, such as coating protection (non-metallic and metallic coatings) or electrochemical protection (cathode, anodic). From a practical point of view, the most important application of anodic metallic coatings is galvanizing, i.e. covering steel with a zinc coating. The vast majority of metal coatings are applied by immersion in molten metal, called flame coating, or electrolytically from an aqueous electrolyte solution by electrolysis [15].

Coatings are widely used to protect metal alloys from corrosion. Still, their performance depends, on how much they physically restrict the approach of water and oxygen, to the coating/substrate interface. Zinc-based galvanic coatings can prevent corrosion by providing good sacrificial protection, in the initial stage of service life. However, under an acidic and saline environment, these coatings may deteriorate rapidly, limiting their protection capability.

In this study we examine the impact of zinc coating applied, using the electrogalvanizing process on the corrosion resistance of DC01 steel.

## 2. MATERIALS AND METHODS

### 2.1 Sample specification

Test samples were cut out from a DC01 steel sheet (Table 1) and subjected to the zinc electrogalvanizing process.

*Table 1. Chemical composition of DC01 steel*

Symbol classification	Numeric classification	European norm	C %	Si %	Mn %	P %	S %	Ti %	Al %	Nb %
DC01	1.0330	EN10139	≤0.12	-	≤0.60	≤0.045	≤0.045	-	-	-

The electroplating was carried out in an alkaline bath. The bath consists of sodium hydroxide at a concentration of 120 to 160 g/dm<sup>3</sup>, with zinc content ranging from 9 to 13 g/dm<sup>3</sup>. Additionally, a carrier, brightener, and softener supplied by an external company were used in the bath. All zinc coatings were obtained at a temperature of 24 °C. For deposition, current densities of 1.7 A/dm<sup>2</sup>, 2.1 A/dm<sup>2</sup>, and 2.5 A/dm<sup>2</sup> were used. The electroplating time, for all samples was 80 minutes [4]. The base sample was not subjected to

the zinc plating process. In the designation of test samples, T - means the deposition time expressed in minutes, while D - means the deposition current density, expressed in A/dm<sup>2</sup>.

The galvanizing process was conducted on a suspended, automated line utilizing an alkaline bath. The hanging line is in the shape of the letter "U" and is divided into a surface preparation station on one side, a transfer station in the middle, and a zinc coating zone on the other side. Loading and unloading are done manually, after which the entire cycle is automated and computer-controlled. Initially, surface cleaning and pickling took place in HCl and H<sub>3</sub>PO<sub>4</sub>, with hydrochloric acid content ranging from 100 to 180 g/dm<sup>3</sup> and phosphoric acid content from 50 to 80 g/dm<sup>3</sup>. Subsequently, rinsing with demineralized water occurs, followed by electrochemical degreasing in NaOH, where the sodium hydroxide concentration is 220 to 260 g/dm<sup>3</sup>. Cleaning and pickling are carried out at temperatures ranging from 30 to 40 °C, while degreasing occurs in the temperature range of 40 to 50 °C. After surface degreasing, the material is rinsed again, and in the next stage, pickling is performed, involving the removal of oxide layers from the surface. This process is carried out in a hydrochloric acid solution with a concentration of 120 to 160 g/dm<sup>3</sup>. Additional assisting agents were used for each of these processes [4].

## 2.2 Experimental

The microstructural analysis was performed, for the DC01 steel samples using the Zeiss Axio Observer Z1m optical microscope Carl Zeiss.

The thickness of the zinc coatings was determined using the ultrasonic gauge KARL DEUTSCH EWP 2026. The gauge allows for measuring the thickness of non-magnetic coatings on magnetic substrates. Additionally, random samples were subjected to measurements using the DELTASCOPE FMP30 thickness gauge, from Fischer (magnetic induction method according to DIN EN ISO 2178), with an accuracy of ±0.5 μm.

Electrochemical measurements of the zinc coatings and DC01 steel were carried out using a PARSTAT 2273 electrochemical workstation. All experiments were performed after 90 minutes of immersion of samples in a 5 wt.% NaCl solution, at a temperature of 25 °C. For corrosion tests, a conventional 3-electrode cell configuration was used in which zinc coating or DC01 steel was used as the working electrode, a saturated calomel electrode (SCE) as a reference, and platinum mesh as a counter electrode. Polarization curves were recorded at a scan rate of 10 mV/min in a potential range of ± 150 mV, vs open circuit potential (OCP). Potentiodynamic polarization curves were recorded at a 60 mV/min scan rate, with a potential range from -150 mV vs. OCP to +100 mV.

The surface samples, after electrochemical tests and cleaning in distilled water, were revealed with a scanning electron microscope Zeiss SUPRA 25, Carl Zeiss, operating at 20 kV, working in SE mode. Specimens, for microstructural observations, were prepared using standard metallographic procedures. They were mechanically ground with SiC paper, up to 2000 grids, then polished with a diamond paste, and finally etched in 5% Nital.

## 3. RESULTS AND DISCUSSION

The structure of the DC01 steel has been presented in Fig. 1. Because of the random orientation of Zn coating grains, the etching speed is selective.

The results of the coating's thickness measurement, determined either by gauge KARL DEUTSCH EWP 2026 or the DELTASCOPE FMP30 are summarized in Table 2.

Table 2. Measurement data determined the thicknesses of zinc coatings

Process parameters		Measured thicknesses of zinc coatings, $\mu\text{m}$
Galvanizing time $T$ , min	Current density $D$ , $\text{A}/\text{dm}^2$	
80	1.7	17.1
80	2.1	19.2
80	2.5	36.6

Open circuit potential, versus time, registered for zinc coatings and DC01 steel in 5 wt.% NaCl solution was presented in Fig. 2.

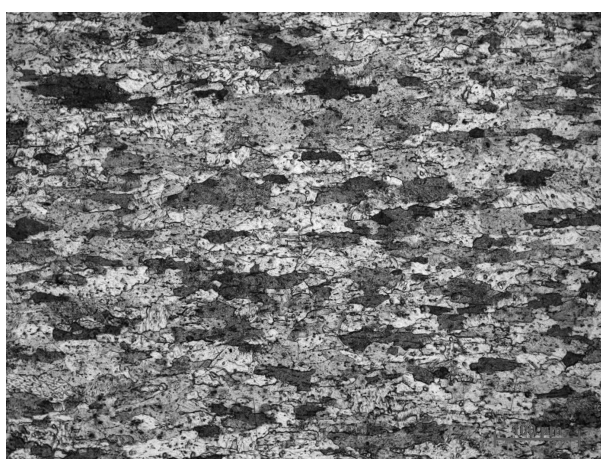


Figure 1. The structure of the DC01 steel

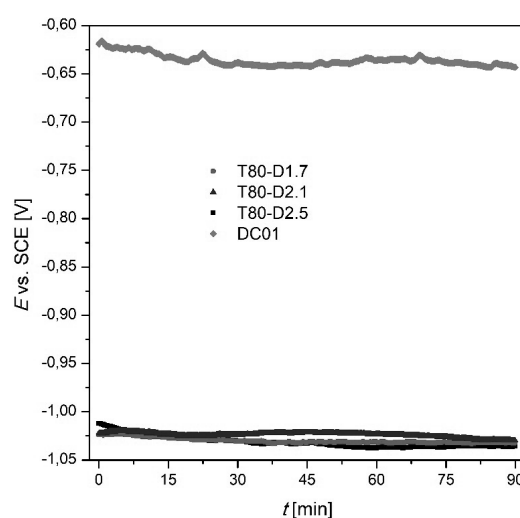


Figure 2. Open circuit potential versus time registered for zinc coatings and DC01 steel in 5 wt.% NaCl solution

Without forced current, zinc coating acts as the anode, and the steel substrate serves as the cathode. The dissolution process occurs on the coating, while the reduction process takes place on the substrate because DC01 as the mild low-carbon steel is more noble (less active) than zinc (it has a higher potential in the galvanic series).

Polarization curves, registered for zinc coatings and DC01 steel in 5 wt.% NaCl solution was presented in Fig. 3. Electrochemical parameters obtained for the zinc coatings and DC01 steel were matched in Table 2. The lack of passive range, in the Tafel curves (Fig. 3), was observed, only the dissolution of the Zn coating - was visible. Zn coatings are characterized by comparable corrosion resistance, which is confirmed, by the quantitative data in Table 3. The corrosion potential  $E_{\text{corr}}$  correlates, with the thickness of applied zinc coatings. The curve obtained for DC01 steel (base sample) indicates a higher  $E_{\text{corr}}$  in comparison with zinc coatings. DC01 steel exhibits a lower tendency to corrosion in a 5 wt.% NaCl solution, compared to zinc, which stems from its position in the galvanic series, where iron ( $E^\circ = -0.44\text{V}$ ) is less active than zinc ( $E^\circ = -0.76$ ). As can be seen in the drawing and the data in Table 3, the corrosion potential determined for the T80-D2.5 sample is the lowest. However, the corrosion current is the largest, which indicates that the sample is characterized by the lowest corrosion resistance of all samples. Metals with lower potentials, are more electrochemically active, making them more

prone to oxidation, and less conducive to reduction. Conversely, metals with higher potentials, exhibit the opposite phenomenon, being less prone to oxidation, and more easily reduced. As long as zinc remains undissolved, it protects DC01 steel, from corrosion processes.

Potentiodynamic polarization curves registered for zinc coatings and DC01 steel in 5 wt.% NaCl solution was presented in Fig. 4.

Table 3. Electrochemical parameters obtained for the zinc coatings and DC01 steel. Uncertainties of the determined parameters are shown in round brackets.

Sample	$E_{\text{corr}}$ [mV vs SCE]	$j_{\text{corr}}$ [ $\mu\text{A cm}^{-2}$ ]	$b_a$ [mV dec $^{-1}$ ]	$b_c$ [mV dec $^{-1}$ ]	$v_{\text{corr}}$ [ $\mu\text{m year}^{-1}$ ]
DC01	-605.9(2)	6.28(5)	89.2(4)	1549(112)	72.9(5)
T80-D1.7	-1029.1(1)	0.80(1)	21.4(1)	730(34)	12.0(2)
T80-D2.1	-1052.7(2)	0.57(1)	28.9(1)	365(10)	8.5(1)
T80-D2.5	-1073.2(3)	0.82(2)	30.8(1)	646(49)	12.3(2)

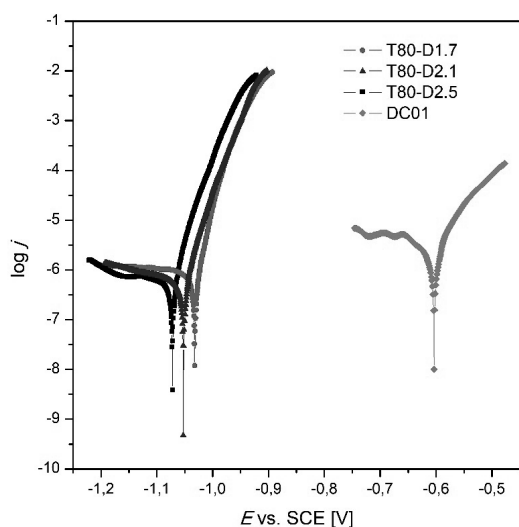


Figure 3. Polarization curves registered for zinc coatings and DC01 steel in 5 wt.% NaCl solution

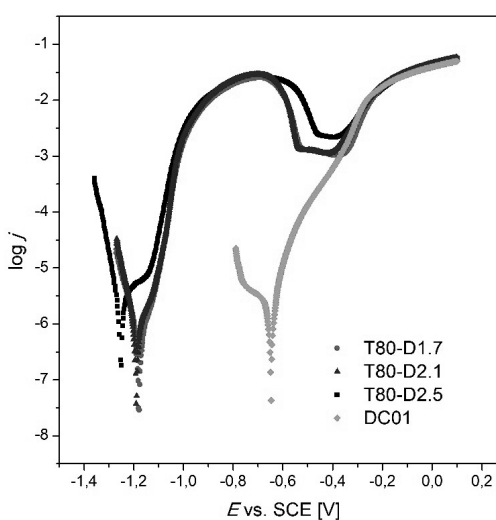


Figure 4. Potentiodynamic polarization curves registered for zinc coatings and DC01 steel in 5 wt.% NaCl solution

The curves shown in Fig. 4 were measured in a wide range of potentials in the anode direction. The dissolving of the tested coatings is visible up to the complete vanishing of the coatings then unprotected the DC01 steel substrate starts to dissolve. A thicker coating layer (black line) means a longer time for its dissolving (longer time of substrate corrosion protection). As long as zinc coating exists steel substrate is protected from corrosion processes. Fe is a more noble metal material than Zn in the electrochemical series. Random crystallographic orientations of zinc grains are responsible for the uneven dissolution rate of the DC01 surface (compare Fig. 1, Fig. 5, and Fig. 6). Figures 6 and 7 clearly show the corrosion products of the zinc coating, which is related to the thickness of the coating.

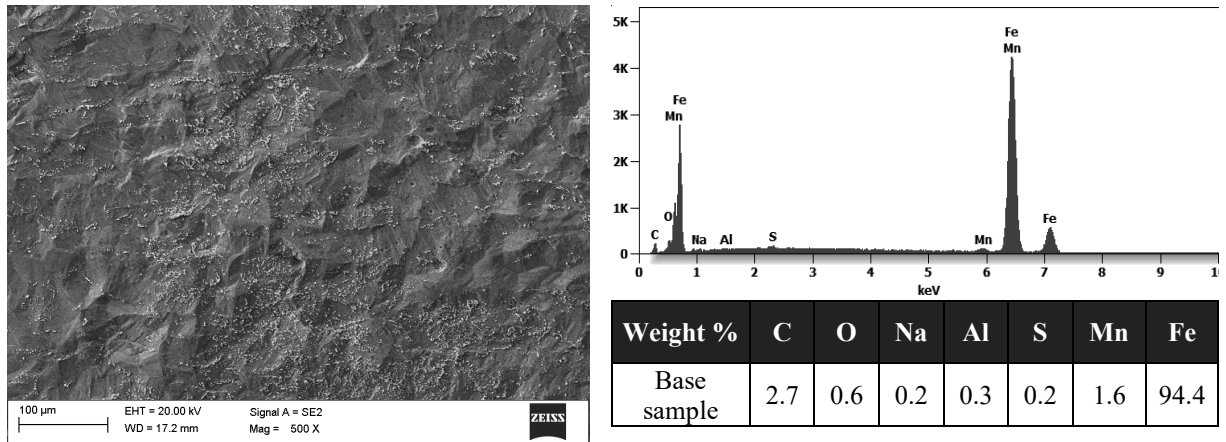


Figure 5. SEM scan of corroded DC01 base sample with EDS analysis

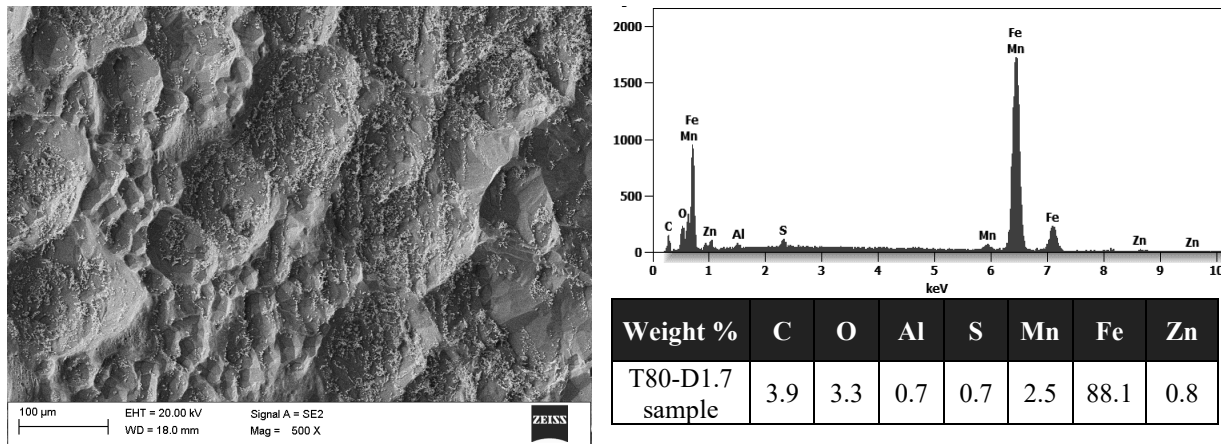


Figure 6. SEM scan of corroded T80-D1.7 sample with EDS analysis

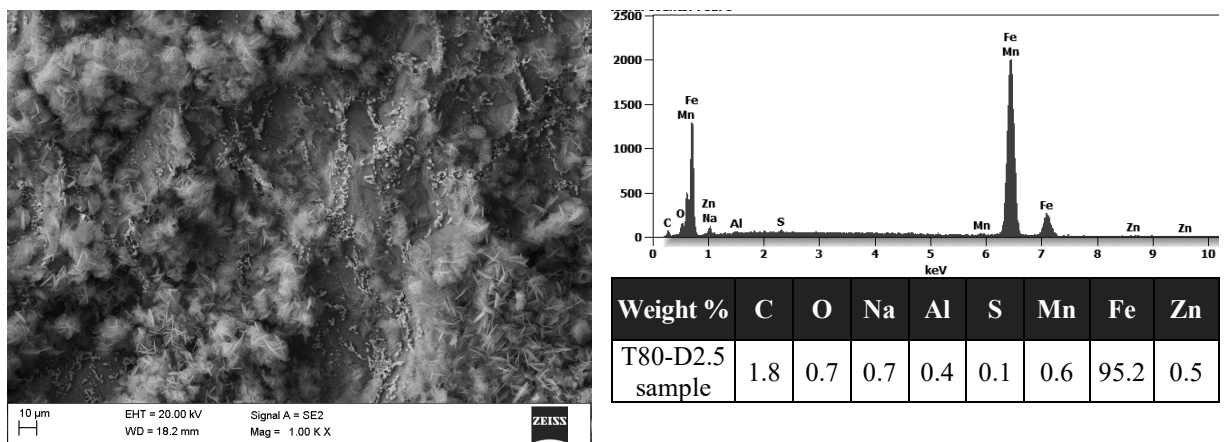


Figure 7. SEM scan of corroded T80-D2.5 sample with EDS analysis

#### 4. CONCLUSIONS

The following conclusions can be drawn from the present study:

- The sample labelled "T80-D2.1" exhibited the highest corrosion resistance. This suggests, that the thickness of the zinc coating, influences the effectiveness of corrosion protection.
- The differences between the zinc-coated samples were minimal, indicating that there might be certain optimal galvanizing conditions, that provide sufficient protection.
- The DC01 samples, i.e., without an additional zinc coating, showed slight corrosion resistance in 5 wt.% NaCl. This confirms, that corrosion protection derived solely from the DC01 material is limited.
- All samples experienced complete corrosion, after the total erosion of the zinc layer. After that corrosion resistance aligned with the baseline sample, suggesting that despite zinc layer corrosion, the metal's properties were not lost.

#### ACKNOWLEDGMENTS

The work was carried out as part of project-oriented education – PBL (Project-Based Learning) - 10th edition – of the Excellence Initiative - Research University program in the scope of the project entitled: "Corrosion resistance of zinc coatings produced by electrolytic method on structural steel".

#### BIBLIOGRAPHY

1. European norm EN 10130/10139.
2. R. Trojnar, D. Solipiwo, M. Bodio, A. Widak, M. Łągiewka, J. Popis, W. Pakieła, B. Grzegorzczak, J. Wyrwał, A. Zarychta, S. Lesz, Wpływ gęstości prądu i czasu nakładania na grubość antykorozyjnych powłok cynkowych, TalentDetector2023\_Summer: International Students Scientific Conference, Brenna, Poland, 26th June 2023, Bonek Mirosław (Red.), Prace Katedry Materiałów Inżynierskich i Biomedycznych, 2023, Gliwice, Politechnika Śląska, (2023) 687-698.
3. M. Pochrzast, J. Marciniak, W. Walke, M. Kaczmarek, J. Szewczenko, S. Loska, Zastosowanie Elektrochemicznej Spektroskopii Impedancyjnej do oceny stopu Ti-6Al-4V stosowanego w Ortopedii, Inżynieria Biomateriałów, 106-108 (2011) 149-153.
4. A. Jażdżewska, Impedancyjne monitorowanie szybkości korozji w układach wodnych z zastosowaniem inhibitorów korozji. Rozprawa doktorska. Politechnika Gdańska. Wydział Chemiczny. Gdańsk 2017.
5. A. Kadhim, A.A. Al-Amiery, R. Alazawi, M.K.S. Al-Ghezi and R.H. Abass, Corrosion inhibitors. Int. J. Corros. Scale Inhib., 10 (1) (2021) 54–67.
6. A. Meroufel, S. Touzain, EIS characterization of new zinc-rich powder coatings. Progress in Organic Coatings 59 (2007) 197–205.
7. L. A. Hernandez-Alvarado, L. S. Hernandez, S. L. Rodriguez-Reyna, Evaluation of Corrosion Behavior of Galvanized Steel Treated with Conventional Conversion Coatings

- and a Chromate-Free Organic Inhibitor. *International Journal of Corrosion* Volume 2012, Article ID 368130.
8. J. A. Cabral-Miramontes, D. M. Bastidas, M. A. Baltazar, P. Zambrano-Robledo, J. M. Bastidas, F. M. Almeraya-Calderón, C. Gaona-Tiburcio, Corrosion behavior of Zn-TiO<sub>2</sub> and Zn-ZnO Electrodeposited Coatings in 3.5% NaCl solution. *Int. J. Electrochem. Sci.*, 14 (2019) 4226 – 4239.
  9. J. Y. Chen, Z. Y. Hu, Z. X. Li, X. L. Wang, C. D. Gu, J. P. Tu, Non- chromate conversion process for zinc coating with durable hydrophobicity and enhanced corrosion resistance. *Biosurf. Biotribol.* 8 (3) (2022) 266–277.
  10. R. A. Dharanendra, M. Shet Prakash, S. Sreenivasa, S. Shivakumara Electrochemical corrosion behaviour of zinc and zinc-reduced graphene oxide coatings on mild steel in 3.5% NaCl solution. *Bull. Mater. Sci.* 45 (2022) 149.
  11. M. Cheng Li, L. L. Jiang, W. Q. Zhang, Y. H. Qian, S. Z. Luo, J. N. Shen, Electrochemical corrosion behavior of nanocrystalline zinc coatings in 3.5% NaCl solutions. *J. Solid State Electrochem.* 11 (2007) 1319–1325.
  12. H. I. Ünala, S. Zorb, H. M. Gökerçila, Corrosion Behavior of Zn and Ni Coated Carbon Steels in 3% NaCl. ISSN 20702051, *Protection of Metals and Physical Chemistry of Surfaces* 49 (5) (2013) 591–596.
  13. K. Akhtar, S.A. Khan, S.B. Khan, A.M. Asiri, Scanning Electron Microscopy: Principle and Applications in Nanomaterials Characterization. In: Sharma, S. (eds) *Handbook of Materials Characterization*. Springer, Cham (2018).
  14. A. Bai, K-L. Yang, H-L. Chen, Y. Hong, and S-B. Chang, High current density on electroplating smooth alkaline zinc, Coating, MATEC Web of Conferences 123, ICPMMT, 00024 (2017 ) DOI: 10.1051/mateconf/201712300024.
  15. S. Zehra, M. Mobin, R. Aslam, CHAPTER 2 - Corrosion prevention and protection methods, Editor(s): L. Guo, C. Verma, D. Zhang, *Eco-Friendly Corrosion Inhibitors*, Elsevier (2022) 13-26.



26th June 2023  
Gliwice, Poland

DEPARTMENT OF ENGINEERING MATERIALS AND BIOMATERIALS  
FACULTY OF MECHANICAL ENGINEERING  
SILESIA UNIVERSITY OF TECHNOLOGY

## INTERNATIONAL STUDENTS SCIENTIFIC CONFERENCE

### Optimization of the CuTi4 alloy melting and casting process

K. Wiśniewski<sup>a</sup>, Z. Rdzawski<sup>a</sup>, W. Głuchowski<sup>a</sup>, M. Łagoda<sup>a</sup>, M. Musztyfaga-Staszuk<sup>b</sup>

<sup>a</sup> Łukasiewicz Research Network – Institute of Non Ferrous Metals, Centre of Advanced Material Technologies

email: krzysztof.wisniewski@imn.lukasiewicz.gov.pl

<sup>b</sup> Silesian University of Technology, Faculty of Mechanical Engineering, Department of Welding Engineering

email: malgorzata.musztyfaga-staszuk@polsl.pl

**Abstract:** The article presents the technological assumptions for melting and casting a copper alloy with the addition of Ti 4% mass, guaranteeing to obtain ingots with the desired macro and microstructure, as well as properties conducive to further plastic working.

**Keywords:** copper, titanium, CuTi alloys, welding, casting.

### 1. INTRODUCTION

The development of IT has had a strong impact on the pace of keeping up with the growing demand for reliable electrical, macro, and microelectronics products, not only in quantitative but also qualitative terms. This trend necessitates the use of improved material solutions. In the material sphere, a significant share is made up of copper alloys characterized by favorable sets of mechanical, physicochemical properties and their stability under variable conditions of mechanical, thermal, force, current loads, etc. Hence, many scientific and research institutes as well as enterprises, both large and small, with a sophisticated profile production, working on achieving the most favorable sets of functional properties for selected copper alloys.

Among these alloys, copper-titanium alloys, both two-component and multi-component, cover a special place. By reviewing the previous [1-3] and the latest literature [4-8], it can be concluded that interest in copper alloys, including CuTi alloys, is constantly increasing. The search for new, more favorable properties of these alloys does not stop and is constantly growing. These requirements are related not only to ensuring appropriate shapes and dimensions, but above all to achieving the appropriate microstructure of the alloy, guaranteeing compliance with these requirements for larger quantities of semi-finished products made of this alloy, not only in terms of test samples, but above all on a "quarter industrial" scale. An important role in this process is played by the optimal melting and casting of the material, which guarantees obtaining a good-quality casting with the intended chemical composition, macro and microstructure.



## 2. METHODOLOGY

Melting and casting of the CuTi4 alloy were performed in a VIM-LAB 50-60 induction vacuum furnace in an argon atmosphere.

The observation of macro and microstructure was carried out using a Keyence VHX-7000 light microscope and a Zeiss Gemini 1525 scanning microscope, equipped with a Quantax XFlash®6 Bruker Nano X-ray spectrometer (EDS SD). To reveal the structure, the samples were etched with the reagent  $H_2SO_4 + NaCl + K_2Cr_2O_2 + water$ .

The Vickers hardness of the cast material was tested using a Future-Tech FM-700 hardness tester. Conductivity was measured based on the complex impedance of the measurement probe using the Foerster SIGMATEST device.

## 3. THE PROCESS OF MELTING AND CASTING THE CuTi4 ALLOY

To obtain a casting with the lowest possible share of impurities, the input material consisted of pure ingredients, consisting of oxygen-free copper in the form of flat bars and pure titanium in the form of a strip - Figure 1.



Figure 1. Input material for the CuTi4 alloy melting and casting process

The mass of the melting charge was set at 8 kg, ensuring a concentration of 4% by mass of titanium in the copper matrix. Titanium tape was wrapped around copper cathodes. The purpose of creating this type of package was to minimize the risk of titanium floating on the surface of the molten copper.

The charge was melted in an induction vacuum furnace, in a ceramic crucible. The method of placing the charge in the crucible is shown in Figure 2.

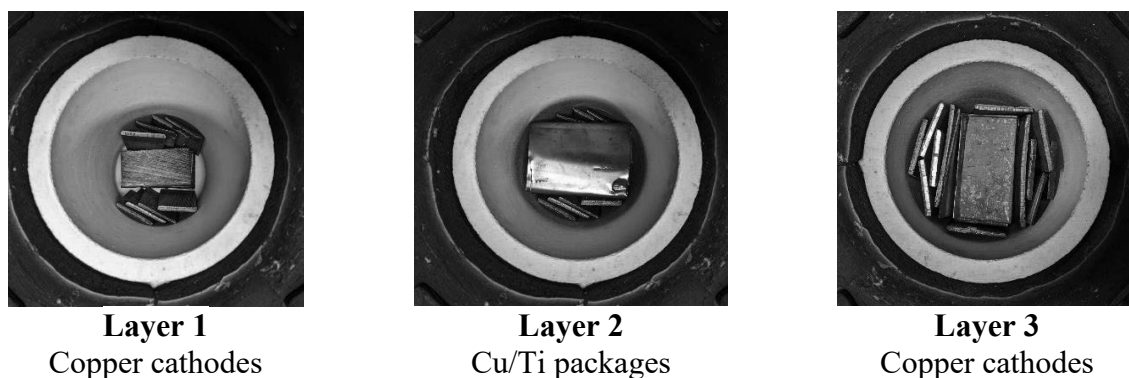


Figure 2. The method of placing the melting charge in the crucible

After placing the charge in the crucible and closing the furnace chamber, the vacuum pump was turned on and the heating process at the set temperature has started. The vacuum pump was turned on until the pyrometer directed at the surface of the charge indicated a temperature of approximately 1000°C. The charge was then observed to slide, which suggested its melting in the lower layers, and occurred approximately 30 minutes after the start of heating. During this time, the vacuum pump was able to continuously remove oxygen as well as possible gases and other impurities from the furnace chamber. Then the vacuum pump was turned off and argon was introduced into the furnace chamber. After this treatment, the heating process was continued until the pyrometer directed at the surface of the charge indicated the target temperature. From that moment, the material was heated for the appropriate time, after which the casting process began.

The material was cast into two graphite crucibles through a specially constructed extension (funnel), the appearance of which is shown in Figure 3.

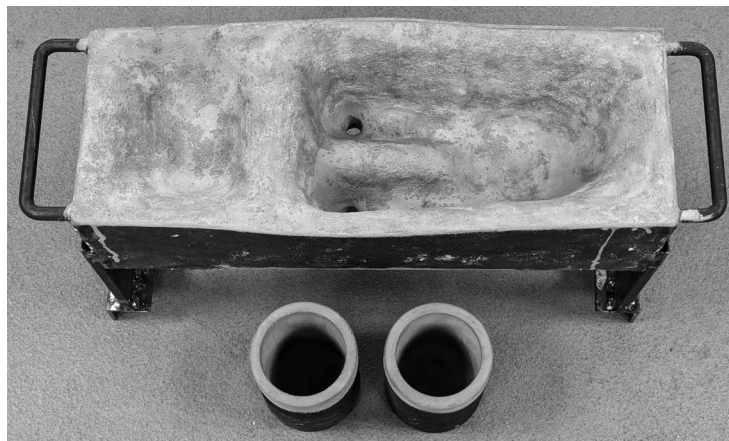


Figure 3. The appearance of a two-hole extension (funnel), and graphite crucibles

Casting the material through an extension constructed in this way, facilitated the uniform supply of liquid metal to the crucibles, and created more favorable conditions for the crystallization of the cast alloy. Figure 4 shows a view of cast CuTi4 ingots.



Figure 4. Casted CuTi4 ingots, diameter  $\varnothing$ 68 mm

Then, the chemical composition of the obtained ingots was tested. Samples were taken from two areas of the ingot: from the bottom (the foot of the ingot) and the top (the head of the ingot), to better assess the uniformity of the chemical composition throughout the entire volume of the material. The average results of the analysis are presented in Table 1.

Table 1. CuTi4 ingots - the average results of the chemical composition analysis

Sample	Element, content [%]				
	Cu	Ti	Si	P	Fe
<b>Bottom (foot of the ingot)</b>	95.7	4.29	-	-	0.02
<b>Top (head of the ingot)</b>	95.3	4.45	0.15	0.05	0.02

The obtained chemical composition was close to the intended, and was homogeneous, based on measurements made in the two extreme areas of the ingot (bottom and top). It is estimated that the slightly higher-than-expected titanium content resulted from the heterogeneity of the material immediately after melting and was treated as an acceptable measurement tolerance.

#### 4. MACRO AND MICROSTRUCTURE ANALYSIS AFTER CASTING

From a cast CuTi4 ingot with a diameter of 68 mm, a 10 mm thick sample was cut from a suitable place and used for metallographic tests. These tests were carried out on the sample surface perpendicular to the casting direction. An example image of the macrostructure is shown in Figure 5. Figures 6-8 show images of the microstructure from the edge, intermediate and central zones of the ingot.

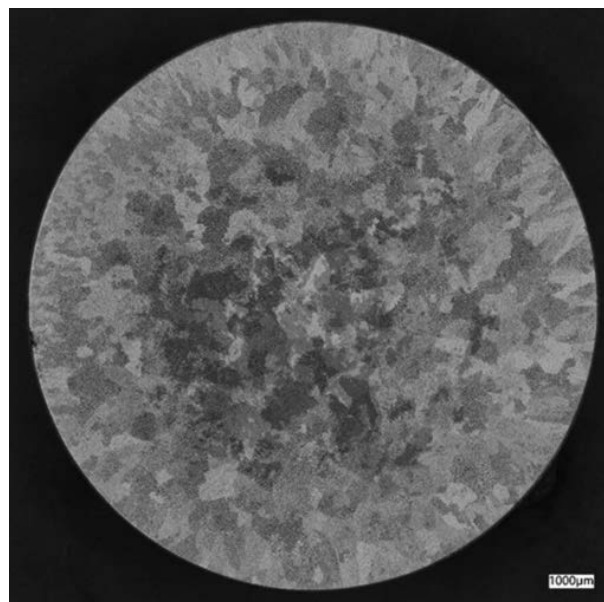


Figure 5. Macrostructure of CuTi4 ingot. Light microscopy, etched specimen

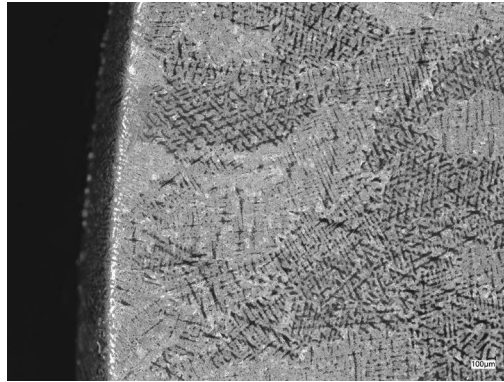


Figure 6. Microstructure of the CuTi4 ingot from the edge area. Light microscopy, etched sample

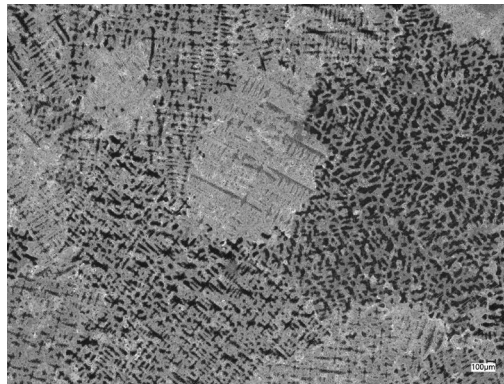


Figure 7. Microstructure of the CuTi4 ingot from the intermediate area. Light microscopy, etched sample



Figure 8. Microstructure of the CuTi4 ingot from the central area. Light microscopy, etched sample

The presented images show the typical appearance of the macrostructure after casting, for many copper alloy samples with a circular cross-section. The outer zone is characterized by the formation of a layer of dendritic crystals directed towards the center of the ingot. In the central zone, significant differences in the structure of the resulting crystallites are observed, which form differently oriented, very fine groups of dendrites, which may indicate the heterogeneous and varied solubility of titanium in the copper matrix.

Figures 9-10 show example microstructure images obtained using scanning microscopy.

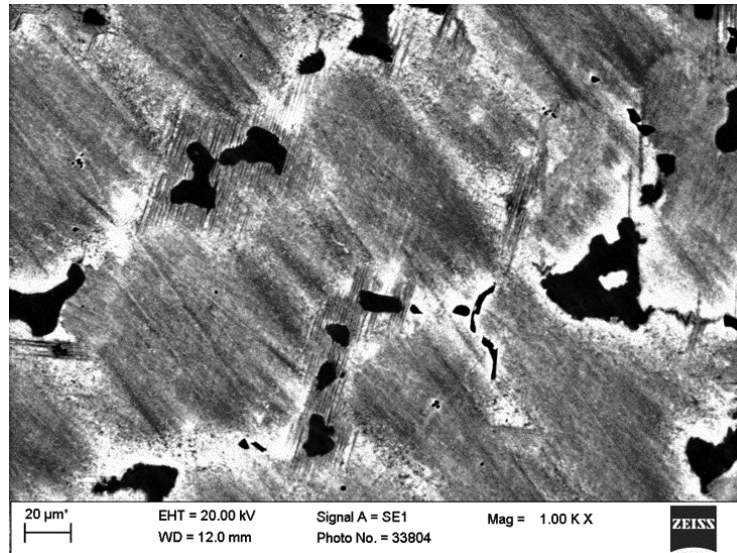
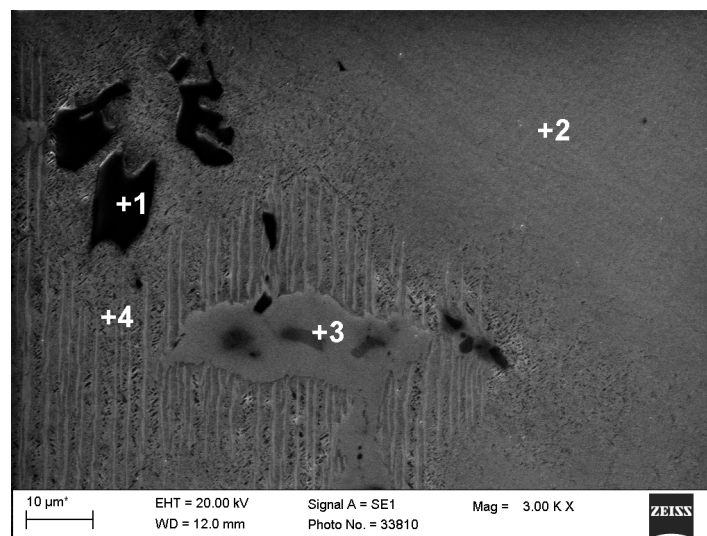


Figure 9. Microstructure of the CuTi4 ingot, edge area (SEM, polished specimen), 1000x



Rys. 10. Microstructure of the CuTi4 ingot, central area (SEM, polished sample), microanalysis (% mass), 2000x

**P1:** Cu=5.21; Ti=71.86; Si=18.32 ; **P2:** Cu=98.36; Ti=1.64  
**P3:** Cu=82.30; Ti=17.70 ; **P4:** Cu=95.53; Ti=4.47

At 1000x magnification (Fig. 9), the effects of the dissolution of Ti in the copper matrix can be seen in the area of some titanium particles, in the form of parallel plates. This is probably the result of heterogeneous nucleation of the equilibrium phase  $\beta'$ -Cu<sub>4</sub>Ti, which could be caused by the process of free solidification of the alloy in the crucibles. Fig. 10 shows an example image of the microstructure from the central area, at 3000x magnification, along with a point analysis of the chemical composition. These studies confirm the heterogeneity of titanium dissolution in the copper matrix and the possibility of nucleation, modulation formation (spinodal decomposition) and phase separation during the crystallization of the ingot.

## 5. HARDNESS AND ELECTRICAL CONDUCTIVITY TESTING

Hardness and conductivity measurements were made on the cross-section of a 10 mm thick sample. Measurements were made in several areas, as shown in Figure 11. Hardness measurements were carried out using the Vickers method, while conductivity measurements were made based on the complex impedance of the measurement probe, using the Foerster SIGMATEST device. The obtained results of hardness and conductivity measurement are presented in Table 2.

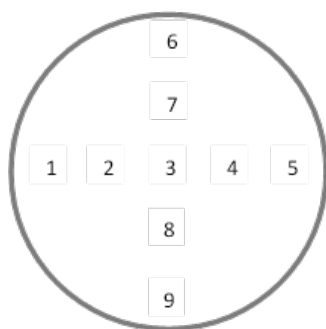


Figure 11. Illustration of a cross-section of a CuTi<sub>4</sub> ingot, indicating the hardness and electrical conductivity measurement areas

Table 2. Results of measurements of hardness and electrical conductivity of CuTi<sub>4</sub> ingot

	Measurement area								
	1	2	3	4	5	6	7	8	9
Electrical conductivity [Ms/m]	7.963	7.527	7.966	8.052	7.892	7.815	7.975	7.939	7.846
Hardness [HV]	189	144	169	156	197	187	152	169	193

The average measured conductivity of the CuTi<sub>4</sub> ingot in the as-cast condition was 7.9 MS/m. Hardness measured by the Vickers method showed a higher value in the edge area of the ingot, where it was approximately 190 HV (measurement location 1, 5, 6, 9). The intermediate and central zones of the ingot were characterized by lower hardness, on average approximately 160 HV.

## 6. CONCLUSION

Melting and casting the CuTi4 alloy using an induction vacuum furnace, high-purity input materials, and a specially constructed extension (funnel), allowed for obtaining high-quality ingots with the desired chemical composition. Analysis of the macro and microstructure of the cast material, performed using light and electron microscopy, showed a dendritic casting structure, that is typical for cylindrical copper alloy ingots.

To improve the casting structure and, as a result, increase the material's susceptibility to plastic working, the next necessary step is to perform homogenizing annealing at an appropriately selected temperature and time. This issue will be the subject of further research in this area.

## ACKNOWLEDGMENTS

The presented research results were obtained as a result of research work carried out in Łukasiewicz – IMN, Gliwice.

## BIBLIOGRAPHY

1. Z. Rdzawski, Miedź stopowa, Monografia, Wydawnictwo Politechniki Śląskiej, 2009.
2. J. Konieczny, Z. Rdzawski, Influence of cold working on microstructure and properties of annealing CuTi4 alloy, *Journal of Achievements in Materials and Manufacturing Engineering*, Volume 55, 2012.
3. R. Markandeya, S. Nagarjuna, D.S. Sarma, Precipitation hardening of Cu–Ti–Cr alloys, *Materials Science and Engineering*, Volume 371, 2004.
4. W. Głuchowski, Opracowanie założeń procesowych wytwarzania stopów miedzi z dodatkiem tytanu, Badania subwencyjne nr 0404135003, nr sprawozdania 8426/G/2023, Łukasiewicz-IMN, 2023. Niepublikowane.
5. B. Rouxel, C. Cayron, J. Bernard, P. Sanders, R. E. Logé, Micro-addition of Fe in highly alloyed Cu-Ti alloys to improve both formability and strength, *Materials & Design* 213, 2022.
6. W. Liu, X. Chen, T. Ahmad, C. Zhou, X. Xiao, H. Wang, B. Yang, Microstructure and mechanical properties of Cu-Ti alloys with ultrahigh strength and high ductility by thermo-mechanical treatment, *Material Science and Engineering*, Volume 835, 2022.
7. L. Huang, Z. Cui, X. Meng, X. Zhang, X. Zhang, X. Song, N. Tang, Z. Xiao, Q. Lei, Z. Li, Effect of microelements on the microstructure evolution and properties of ultrahigh strength Cu-Ti alloys, *Material Science and Engineering*, Volume 823, 2021.
8. Y. Liao, C. Guo, C. Zhou, W. Xie, B. Yang, H. Wang, Stability of the metastable B'-Cu<sub>4</sub>Ti phase in Cu-Ti alloys: Role of the Ti content, *Materials Characterization*, Volume 203, 2023.



26th January 2024  
Gliwice, Poland

DEPARTMENT OF ENGINEERING MATERIALS AND BIOMATERIALS  
FACULTY OF MECHANICAL ENGINEERING  
SILESIA UNIVERSITY OF TECHNOLOGY

## INTERNATIONAL STUDENTS SCIENTIFIC CONFERENCE

### **Biomaterials, Bioceramic Materials, and Metals for Bone Scaffold Formation and Scaffold Fabrication Methodologies**

Sichale Worku <sup>a</sup>, Mirosław Bonek <sup>b</sup>

<sup>a</sup> Silesian University of Technology, Faculty of Mechanical Engineering, Department of Engineering Materials and Biomaterials

email: Sichale.Fita@polsl.pl

<sup>b</sup> Silesian University of Technology, Faculty of Mechanical Engineering, Department of Engineering Materials and Biomaterials

email: miroslaw.bonek@polsl.pl

**Abstract:** Bio-ceramic materials have surfaced as a highly promising pathway for the manufacturing of bone scaffolds, owing to their biocompatibility and structural similarity to actual bone. This review article discusses the application of these materials and the methodology used in the production process. Again, we emphasize the importance of metals and bio-ceramic materials in the advancement of bone scaffold fabrication. It showcases their potential to enhance tissue regeneration and facilitate the healing process in orthopaedic and reconstructive procedures.

**Keyword:** Bioceramic material, scaffold, orthopaedic.

## 1. INTRODUCTION

The total number of bone-related diseases and disorders has increased significantly in recent years at the global level [1]. According to 2018 data, more than two million bone transplants are performed every year across the world to correct bone defects, making it one of the most common regenerative activities [2]. Expected soon, this trend is projected to increase twice, particularly posing a higher risk to the elderly and overweight people [1]. Bones have healing and regenerative potential; however, the process of bone healing alone is insufficient to address extensive bone deficiencies resulting from variables such as advanced age, traffic accidents, nonunion fractures, bone tumour removal, and other causes. These issues pose significant challenges in the field of orthopaedics and can have detrimental effects on both health and quality of life [3]. On the other hand, minor bone injuries in humans are known to heal themselves. However, large-scale bone defects may be extremely harmful to one's health.

Bone healing is now possible due to medical advancements in technology as shown in Figure 1.1 below. Since biodegradable scaffolds can break down naturally, there is less need for extra surgical procedures to remove them, which makes them a popular choice in the domains of bone regeneration and clinical therapies [4]. The most widely used biodegradable



scaffold materials currently are bio-ceramics, polymers, and metals [5]. Metallic cellular solids made of biocompatible metals such as titanium, stainless steel, or cobalt-chromium have attracted attention because they are strong, reliable, and safe for living things. Their three-dimensional structures help tissue grow back in orthopaedic implants, heart stents, and other tissue-engineering cellular materials by supporting it and making it stronger [6].

Metals such as magnesium and zinc, along with their respective alloys, increase the mechanical characteristics of materials. However, the degradation process of those materials is naturally unstable and poses difficulties in terms of control [7]. Polymeric materials, like polylactic acid (PLA), polycaprolactone (PCL), various hydrogels, and collagen, demonstrate excellent biocompatibility. However, their mechanical strength is quite weak, and it is difficult to regulate their rate of degradation. On the other hand, bioceramic materials, like bioactive glass and hydroxyapatite, have remarkable biocompatibility. Furthermore, the  $\text{Ca}^{2+}$ ,  $\text{Zn}^{2+}$ ,  $\text{Mg}^{2+}$ ,  $(\text{PO}_4)^{3-}$ , and  $(\text{SiO}_3)^{2-}$  ions generated during breakdown might stimulate the growth and specialization of bone cells [8], [9]. Many of them have a modulus of strength comparable to that of human bones. However, the materials' poor mechanical qualities limit their potential applications [10].

Bone is a multiphasic structure that contains collagen, blood vessels, and bone marrow to be the soft material. The main inorganic phase of tissue is hydroxyapatite (HAp) ( $\text{Ca}_5(\text{PO}_4)_3(\text{OH})$ ) [11]. Bone healing is complex and influenced by numerous factors, including mechanical, chemical, and electrical stimuli [12]. Filling a bone scaffold is one of the most efficient approaches to treating bone defects [13]. Bone regeneration is complex, as it requires the consideration of molecular, biochemical, mechanical, and cellular factors [14]. An effective bone scaffold should possess suitable mechanical qualities, biological activity, degradability, angiogenesis, and the ability to kill or prevent tumour cell growth of tumour cells [15]. Additionally, it should exhibit porosity that helps with nutrient absorption. The application of additive manufacturing technology allows the production of bone-filled scaffolds that possess complex shapes, internal pores, and controlled porosity [16]. Interlinked macropores are important to provide enough space for cellular functions, nutrition transportation, and cell-to-cell communication [17].

The primary objective of this review is to examine various materials used for the manufacture of scaffolds as shown on figure 1.2 and to suggest suitable materials for the manufacturing of bone scaffolds. Additionally, the review aims to propose the approaches employed in this field. Considering the importance of correcting bone defects, it is essential to develop a scaffold that is very precise and exhibits exceptional cell behaviours.

### **1.1 Materials and methodologies have been used for scaffold generation**

Traditional manufacturing methods, like as die casting and gas foaming, are frequently employed in the construction of scaffolds. However, these traditional methods are not sufficiently efficient for producing micro complex structures [18]. The application of different smart materials in 3D printing has been utilized in the fields of soft robotics, electrochemical energy storage, food science, biomedicine, and biomanufacturing [19]. The AM (Additive Manufacturing) field covers numerous approaches, including Binder Jetting, Directed Energy Deposition, Material Extrusion, Material Jetting, Powder Bed Fusion, Sheet Lamination, and Vat Photopolymerization.

Material extrusion (ME) is the most common additive manufacturing (AM) process, having minimal costs for equipment and feedstock costs, and can work with a wide variety of materials. ME has been widely used in various applications and works with a wide range of materials such as polymers, metals, bio and food items, ceramics, and composite materials. Nevertheless, components produced by ME may have unfavourable internal voids caused by insufficient material filling within the layers of the part [20]. Laser-powered bed fusion used for WE43( $\alpha$ -Mg, Y<sub>2</sub>O<sub>3</sub>, and MgRE precipitate) with energy input and scanning strategy and results in good properties and in vitro and in vivo investigations [21].

Porous Ti6Al4V scaffolds with different pore sizes were manufactured by selective laser melting technology [22]. The physiological characteristics and osseointegration capacities of the scaffolds were evaluated using a series of in vitro and in vivo tests. Bionic manufacturing techniques are used to create porous polymer PEEK scaffolds, which are covered with a stable layer of hydroxyapatite (HA). These extremely porous PEEK@HA scaffolds promoted the integration of bone tissue in living organisms, rats [23]. A titanium alloy scaffold with structural specifications for rabbits that are comparable to those of human bones was designed and prepared. It enhances its osseointegration-promoting effects by bio modifying [24].

A biomimetic-graded TPMS scaffold from Ti6Al4V was created by having a changeable pore size [25]. This scaffold possesses mechanical properties, specifically an elastic modulus and yield strength, that are within the required range for bone tissue. An aerogel scaffold [26] from a combination of poly (ethylene glycol) diacrylate (PEGDA), Pluronic F127, and Lithium phenyl-2,4,6 trimethylbenzoylphosphinate (LAP). This mixture showed good mechanical and biological qualities. Finally, to produce bone-like porous scaffolds, two different types of ceramic scaffolds with different levels of porosity, specifically octagon and rhombus scaffolds, were created using Digital Lighting Process technology [27] which resulted in good porosity, mechanical properties, and good fluid flow inside. Scientific research on biodegradable scaffolds has seen a substantial surge in recent years. However, there have been not much of studies investigating the degradation of composite bio-ceramic scaffolds [28].

## 2. BIOCERAMIC MATERIALS FOR SCAFFOLD MANUFACTURING

### 2.1 Calcium Phosphate and Hydroxyapatite-based bioceramic

The primary component of bone is calcium phosphate. Despite extensive studies exploring the search for the ideal synthetic bone, no suitable scaffold material has yet been found [29]. To improve the mechanical qualities of calcium phosphate, iron doping has been discovered to enhance osteogenic potential. Fe<sup>2+</sup>,<sup>3+</sup>-doped  $\beta$ -tricalcium phosphate scaffold in vivo found that after implantation, osteoblasts and osteocytes proliferated and formed new bone with a network of capillaries [30]. Similar outcomes have also been reported by [31] by synthesising superparamagnetic nanoparticles by introducing Fe<sup>2+</sup> and Fe<sup>3+</sup> ions into the hydroxyapatite structure.

Porous hydroxyapatite (HA) bone repair scaffolds with controlled architecture and porosity are challenging to manufacture and lack sufficient osteoinductive activity, limiting their wider clinical application. The clinical applicability of porous hydroxyapatite (HA) bone repair scaffolds is limited due to their difficult manufacturing process and insufficient osteoinductive activity [32]. However, by combining 3D printing and aerogel technologies, alginate-HA aerogel scaffolds were effectively created with a precise and unique nanostructure.

Using the DLP 3D printing technique, a porous graphene oxide / hydroxyapatite, GO / HA composite scaffold combined with different ratios of GO nanosheet is produced to promote cell adhesion, proliferation, pore structure, and osteogenic differentiation of Rat bone marrow mesenchymal stem cells (rBMSCs) [32]. Porous hydroxyapatite (HA) scaffolds manufactured by a contemporary 3D printing technique called VAT photopolymerization and the structure inspired by trabecular bone, namely the Gyroid-Triply periodic minimal surface pattern (TPMS), and finally implanted in a clinically relevant large animal model (sheep femur) [33].

## 2.2 Calcium-based bioceramic

Calcium silicate (CaSi) is a suitable substrate for bone tissue engineering due to its ability to release bioactive ions such as  $\text{Si}^{4+}$  and  $\text{Ca}^{2+}$ , which facilitate the process of bone regeneration [34]. However, CS porous scaffolds were manufactured using 3DIP technology, which offers a promising alternative to existing bone scaffolds with notable advantages [34]. The binder jetting is utilized to create scaffolds composed of barium titanate and bioactive glass 45S5 bioactive glass. Piezoelectric ( $\text{BaTiO}_3$ ) and bioactive (45S5® Bioglass) biomaterials possess mechanical properties like those of spongy bone seen in the human body [35]. The mechanical properties of the 3D-jetted  $\text{BaTiO}_3$  scaffolds were improved better than those of a  $\text{BaTiO}_3$ -hydroxyapatite ( $\text{BaTiO}_3/\text{HA}$ ) composite that had been discovered [36]. The bioactive scaffold of a combination of interconnected porous scaffolds made of magnesium-doped wollastonite (CSi-Mg) with a surface layer of nanohydroxyapatite (n-HA) [37].

Biodegradable composite ceramic scaffolds containing  $\text{MgO}$  and  $\text{Ca}_3(\text{PO}_4)_2$  were manufactured by a vat photopolymerization process, and the results showed that the strength of the 80 MPa sample was similar to that of cortical bones. Tetra calcium phosphate (TTCP) and Whitlockite (WH) with poly (methyl methacrylate) (PMMA) cement were incorporated to create a new bone cement called TTCP/WH. Its characteristics were evaluated and analyzed in vitro, as well as in the rabbit ilium. The results showed that the TTCP/WH cement exhibited a higher osteoconductive compared to the bioinert PMMA bone cement [38]. Borate bioactive glass/polycaprolactone (BBG/PCL) composite scaffolds with different BBG contents were fabricated using selective laser sintering for critical-sized bone defects (CSBD), customized porous scaffold rabbit radius size. Results with sufficient mechanical strength to maintain the integrity of the scaffold structure during a relatively long repair of CSBD repair [39].

## 3. CONCLUSION

The application of bioceramic materials in bone scaffold fabrication advances regenerative medicine and orthopaedic therapy. Their precise manufacture assures biocompatibility and structural integrity, which are important for human integration. Natural bio-ceramics promote tissue regeneration and offer mechanical support as bone. These scaffolds can solve bone tissue engineering problems with appropriate material selection and manufacturing. Although long-term efficacy and safety in vivo studies are needed, bio ceramics and innovative manufacturing methods show a transformative approach to bone healing, reconstructive surgeries, and patient quality of life.

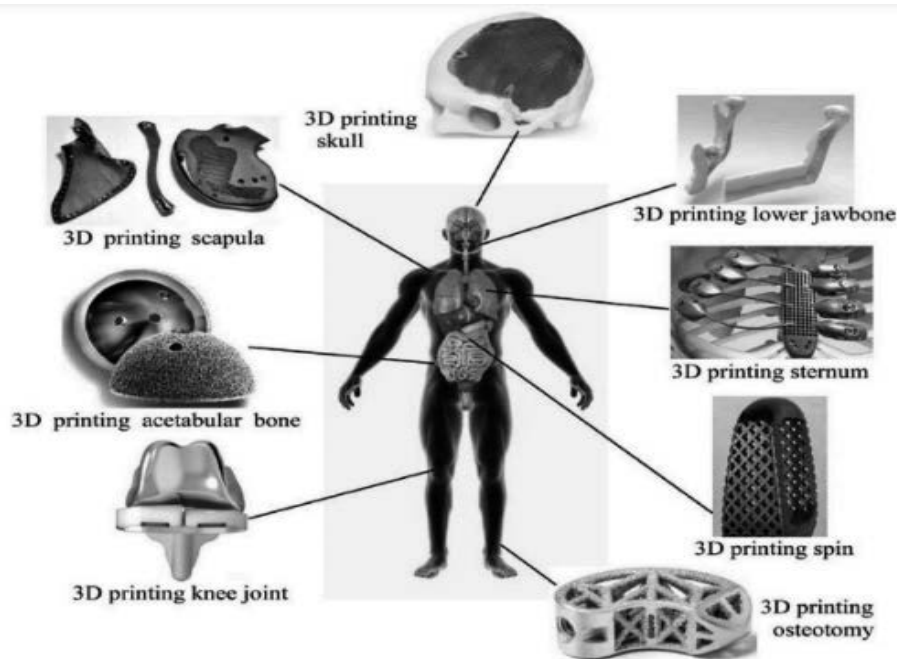


Figure 1. Picture demonstrating various kinds of body implants

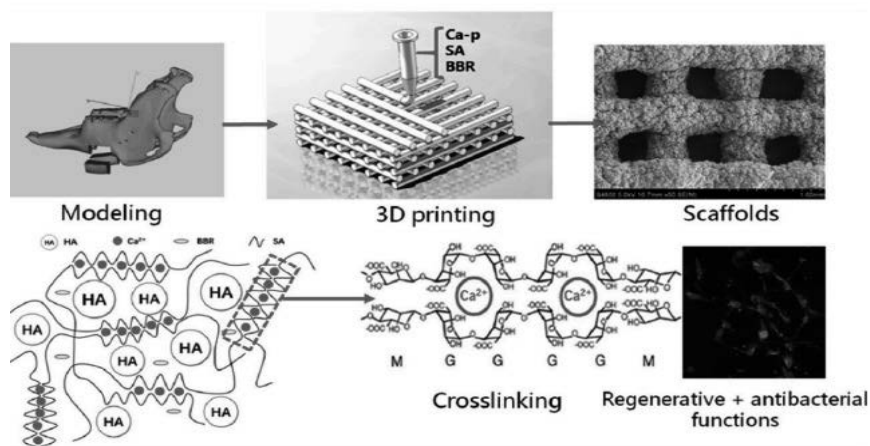


Figure 2. Schematic diagram of the scaffold fabrication process

## BIBLIOGRAPY

- [1] S. Kargozar, P. B. Milan, F. Baino, and M. Mozafari, "Nanoengineered biomaterials for bone/dental regeneration," in *Nanoengineered Biomaterials for Regenerative Medicine*, Elsevier, 2018, pp. 13–38. doi: 10.1016/B978-0-12-813355-2.00002-8.
- [2] C. K. E. F. Caoimhe Kiernan, "Chapter 6 Endochondral Ossification Recapitulating Bone Development for Bone Defect Repair," 2018.
- [3] M. Qasim, D. S. Chae, and N. Lee, "Advancements and frontiers in nano-based 3d and 4d scaffolds for bone and cartilage tissue engineering," *Int J Nanomedicine*, vol. 14, pp. 4333–4351, 2019, doi: 10.2147/IJN.S209431.

- [4] M. Ge *et al.*, “Additive manufacturing a novel bioceramic bone scaffold with MgO/Ca<sub>3</sub>(PO<sub>4</sub>)<sub>2</sub>: Microstructure, mechanical property and controllable degradation behavior,” *Journal of Materials Research and Technology*, vol. 27, pp. 2249–2263, Nov. 2023, doi: 10.1016/j.jmrt.2023.10.083.
- [5] M. P. Nikolova and M. S. Chavali, “Recent advances in biomaterials for 3D scaffolds: A review,” *Bioact Mater*, vol. 4, pp. 271–292, Dec. 2019, doi: 10.1016/j.bioactmat.2019.10.005.
- [6] E. Marin, “Forged to heal: The role of metallic cellular solids in bone tissue engineering,” *Mater Today Bio*, vol. 23, Dec. 2023, doi: 10.1016/j.mtbio.2023.100777.
- [7] C. Pan *et al.*, “Corrosion resistance and biocompatibility of magnesium alloy modified by alkali heating treatment followed by the immobilization of poly (ethylene glycol), fibronectin and heparin,” *Materials Science and Engineering C*, vol. 70, pp. 438–449, Jan. 2017, doi: 10.1016/j.msec.2016.09.028.
- [8] N. H. Radwan, M. Nasr, R. A. H. Ishak, N. F. Abdeltawab, and G. A. S. Awad, “Chitosan-calcium phosphate composite scaffolds for control of post-operative osteomyelitis: Fabrication, characterization, and in vitro–in vivo evaluation,” *Carbohydr Polym*, vol. 244, Sep. 2020, doi: 10.1016/j.carbpol.2020.116482.
- [9] A. Kumar *et al.*, “Load-bearing biodegradable PCL-PGA-beta TCP scaffolds for bone tissue regeneration,” *J Biomed Mater Res B Appl Biomater*, vol. 109, no. 2, pp. 193–200, Feb. 2021, doi: 10.1002/jbm.b.34691.
- [10] S. C. Wu, H. C. Hsu, S. K. Hsu, W. H. Wang, and W. F. Ho, “Preparation and characterization of four different compositions of calcium phosphate scaffolds for bone tissue engineering,” *Mater Charact*, vol. 62, no. 5, pp. 526–534, May 2011, doi: 10.1016/j.matchar.2011.03.014.
- [11] R. Z. Legeros, “Properties of Osteoconductive Biomaterials: Calcium Phosphates List of Abbreviations Used BMP bone morphogenetic protein ECM extracellular matrix MSC mesenchymal stem cell,” 2002.
- [12] C. Polley *et al.*, “3D printing of piezoelectric and bioactive barium titanate-bioactive glass scaffolds for bone tissue engineering,” *Mater Today Bio*, vol. 21, Aug. 2023, doi: 10.1016/j.mtbio.2023.100719.
- [13] H. Belaid *et al.*, “Development of new biocompatible 3D printed graphene oxide-based scaffolds,” *Materials Science and Engineering C*, vol. 110, May 2020, doi: 10.1016/j.msec.2019.110595.
- [14] A. Suleman, P. P. D. Kondiah, M. Mabrouk, and Y. E. Choonara, “The Application of 3D-Printing and Nanotechnology for the Targeted Treatment of Osteosarcoma,” *Frontiers in Materials*, vol. 8, Frontiers Media S.A., Jul. 01, 2021. doi: 10.3389/fmats.2021.668834.
- [15] H. Shao *et al.*, “3D-printed magnesium-doped wollastonite/nano-hydroxyapatite bioceramic scaffolds with high strength and anti-tumor property,” *Mater Des*, vol. 225, Jan. 2023, doi: 10.1016/j.matdes.2022.111464.
- [16] Y. Yang *et al.*, “3D-printed polycaprolactone-chitosan based drug delivery implants for personalized administration,” *Mater Des*, vol. 214, Feb. 2022, doi: 10.1016/j.matdes.2022.110394.
- [17] H. Ma *et al.*, “3D printing of biomaterials with mussel-inspired nanostructures for tumor therapy and tissue regeneration,” *Biomaterials*, vol. 111, pp. 138–148, Dec. 2016, doi: 10.1016/j.biomaterials.2016.10.005.

- [18] V. P. Meshalkin and A. V. Belyakov, "Methods used for the compaction and molding of ceramic matrix composites reinforced with carbon nanotubes," *Processes*, vol. 8, no. 8. MDPI AG, Aug. 01, 2020. doi: 10.3390/PR8081004.
- [19] M. Shahbazi, H. Jäger, R. Ettelaie, A. Mohammadi, and P. Asghartabar Kashi, "Multimaterial 3D printing of self-assembling smart thermo-responsive polymers into 4D printed objects: A review," *Additive Manufacturing*, vol. 71. Elsevier B.V., Jun. 05, 2023. doi: 10.1016/j.addma.2023.103598.
- [20] X. Sun, M. Mazur, and C. T. Cheng, "A review of void reduction strategies in material extrusion-based additive manufacturing," *Additive Manufacturing*, vol. 67. Elsevier B.V., Apr. 05, 2023. doi: 10.1016/j.addma.2023.103463.
- [21] J. Liu *et al.*, "Biodegradable magnesium alloy WE43 porous scaffolds fabricated by laser powder bed fusion for orthopedic applications: Process optimization, in vitro and in vivo investigation," *Bioact Mater*, vol. 16, pp. 301–319, Oct. 2022, doi: 10.1016/j.bioactmat.2022.02.020.
- [22] Z. Wang *et al.*, "Biomimetic design strategy of complex porous structure based on 3D printing Ti-6Al-4V scaffolds for enhanced osseointegration," *Mater Des*, vol. 218, Jun. 2022, doi: 10.1016/j.matdes.2022.110721.
- [23] M. Yakufu, Z. Wang, J. Liu, and P. Zhang, "Bionic manufacturing strategy of hydroxyapatite-coated polyether ether ketone scaffolds for promoting mineralization and osseointegration," *Mater Des*, vol. 223, Nov. 2022, doi: 10.1016/j.matdes.2022.111193.
- [24] Z. Che *et al.*, "Bifunctionalized hydrogels promote angiogenesis and osseointegration at the interface of three-dimensionally printed porous titanium scaffolds," *Mater Des*, vol. 223, Nov. 2022, doi: 10.1016/j.matdes.2022.111118.
- [25] J. Zhang *et al.*, "Design of a biomimetic graded TPMS scaffold with quantitatively adjustable pore size," *Mater Des*, vol. 218, Jun. 2022, doi: 10.1016/j.matdes.2022.110665.
- [26] Z. Wang *et al.*, "Fabrication of aerogel scaffolds with adjustable macro/micro-pore structure through 3D printing and sacrificial template method for tissue engineering," *Mater Des*, vol. 217, May 2022, doi: 10.1016/j.matdes.2022.110662.
- [27] H. Lei *et al.*, "Rational design and additive manufacturing of alumina-based lattice structures for bone implant," *Mater Des*, vol. 221, Sep. 2022, doi: 10.1016/j.matdes.2022.111003.
- [28] W. Liu, Z. Huan, C. Wu, Z. Zhou, and J. Chang, "High-strength calcium silicate-incorporated magnesium phosphate bone cement with osteogenic potential for orthopedic application," *Compos B Eng*, vol. 247, Dec. 2022, doi: 10.1016/j.compositesb.2022.110324.
- [29] A. D. Anastasiou *et al.*, "Exogenous mineralization of hard tissues using photo-absorptive minerals and femto-second lasers; the case of dental enamel," *Acta Biomater*, vol. 71, pp. 86–95, Apr. 2018, doi: 10.1016/j.actbio.2018.02.012.
- [30] A. Manchón *et al.*, "A new iron calcium phosphate material to improve the osteoconductive properties of a biodegradable ceramic: A study in rabbit calvaria," *Biomedical Materials (Bristol)*, vol. 10, no. 5, Oct. 2015, doi: 10.1088/1748-6041/10/5/055012.
- [31] S. Panseri *et al.*, "Intrinsically superparamagnetic Fe-hydroxyapatite nanoparticles positively influence osteoblast-like cell behaviour," *J Nanobiotechnology*, vol. 10, Jul. 2012, doi: 10.1186/1477-3155-10-32.

- [32] H. Zhao, H. Xing, Q. Lai, Y. Zhao, Q. Chen, and B. Zou, "Additive manufacturing of graphene oxide/hydroxyapatite bioceramic scaffolds with reinforced osteoinductivity based on digital light processing technology," *Mater Des*, vol. 223, Nov. 2022, doi: 10.1016/j.matdes.2022.111231.
- [33] I. Bouakaz, C. Drouet, D. Grossin, E. Cobraiville, and G. Nolens, "Hydroxyapatite 3D-printed scaffolds with Gyroid-Triply periodic minimal surface porous structure: Fabrication and an in vivo pilot study in sheep," *Acta Biomater*, vol. 170, pp. 580–595, Oct. 2023, doi: 10.1016/j.actbio.2023.08.041.
- [34] K. Liu *et al.*, "Effect of polycaprolactone impregnation on the properties of calcium silicate scaffolds fabricated by 3D printing," *Mater Des*, vol. 220, Aug. 2022, doi: 10.1016/j.matdes.2022.110856.
- [35] T. Distler *et al.*, "Polymer-Bioactive Glass Composite Filaments for 3D Scaffold Manufacturing by Fused Deposition Modeling: Fabrication and Characterization," *Front Bioeng Biotechnol*, vol. 8, Jun. 2020, doi: 10.3389/fbioe.2020.00552.
- [36] C. Polley *et al.*, "3D printing of piezoelectric barium titanate-hydroxyapatite scaffolds with interconnected porosity for bone tissue engineering," *Materials*, vol. 13, no. 7, Apr. 2020, doi: 10.3390/MA13071773.
- [37] H. Shao *et al.*, "3D-printed magnesium-doped wollastonite/nano-hydroxyapatite bioceramic scaffolds with high strength and anti-tumor property," *Mater Des*, vol. 225, Jan. 2023, doi: 10.1016/j.matdes.2022.111464.
- [38] Q. Z. Liu *et al.*, "Bioactive magnesium-based whitlockite ceramic as bone cement additives for enhancing osseointegration and bone regeneration," *Mater Des*, vol. 229, May 2023, doi: 10.1016/j.matdes.2023.111914.
- [39] J. Han *et al.*, "Biodegradable BBG/PCL composite scaffolds fabricated by selective laser sintering for directed regeneration of critical-sized bone defects," *Mater Des*, vol. 225, Jan. 2023, doi: 10.1016/j.matdes.2022.111543.



26th January 2024  
Gliwice, Poland

DEPARTMENT OF ENGINEERING MATERIALS AND BIOMATERIALS  
FACULTY OF MECHANICAL ENGINEERING  
SILESIA UNIVERSITY OF TECHNOLOGY

## INTERNATIONAL STUDENTS SCIENTIFIC CONFERENCE

### Torch Holder Design and Thermal Analysis of Hybrid Welding Machine

C. Yıldız<sup>a</sup>, S. Korucu<sup>b</sup>

<sup>a</sup>Gazi University , Faculty of Technology , Department of Manufacturing Engineering, Ankara, Turkey

<sup>b</sup>Gazi University , Faculty of Technology , Department of Manufacturing Engineering, Ankara, Turkey, email: skorucu@gazi.edu.tr

**Abstract:** TIG-MIG hybrid welding equipment is becoming more and more suitable for serial production. In this study, a torch holder, which allows the TIG and MIG torches to be held stationary, has been designed to be more advanced and suitable for angled welding processes. The temperature of the weld pool was simulated through the design ANSYS program and thermal analysis was carried out by finite element method. In further studies, designs and analyzes for mechanization in TIG-MIG hybrid welding equipment will be carried out.

**Keywords:** TIG, MIG, hybrid, welding, manufacturing, finite, element

#### 1. WHAT IS TIG-MIG HYBRID WELDING?

TIG-MIG Hybrid welding consists of TIG and MIG welds applied simultaneously and in the same direction in the same weld zone and a double welding arc formed in the specified zone. This results in a more stable arc and faster weldability. It has lower heat input and higher metal deposition rate compared to conventional welding methods. [1-3]

In recent years, hybridization of conventional TIG and MIG welding process has been tried to achieve better welding speed. The TIG-MIG Hybrid arc welding process is reported to have a 17 to 44% higher weld metal deposition rate compared to the conventional TIG welding process [4].

In conventional TIG-MIG welding processes, a higher speed of defect-free weld metal deposition is expected to achieve high productivity. However, an increase in the weld metal deposition rate will lead to an increase in heat input, which will result in undesirable metallurgical transformations in the heat affected zone (HAZ) of the base metal. Therefore, the amount of weld metal deposition can be increased as much as HAZ transformations allow [5].

#### 2. TIG-MIG WELDING MECHANISM

The TIG-MIG Hybrid welding mechanism keeps the welding torches stationary and prevents torch movement and torch axis slippage during the welding process. These prepared mechanisms have a skeleton for the holding of the torches and the passage of the torch hoses.



The mechanisms can move in 3 axes (x, y, z) with the help of motors and thus make additive manufacturing possible.

### 2.1 Torch Holder in Mechanism

The torch holder, one of the most important parts of the hybrid welding mechanism, ensures that the welding torches perform the welding process on the same axis and at a constant angle. By adjusting the distance between the torches, the distance between the welding arcs can be changed.

The torch holder is also used to adjust the distance of the torches from the base material. In this way, the distance of the torches to the base material can be adjusted independently of each other and the change in the properties of the weld metal can be analyzed. As a result, in the TIG-MIG hybrid welding mechanism, the filler material, Ampere, Voltage values are important, as well as the distance between the torches, the angle between the torches and the distance to the base material are also effective on the metallurgical and mechanical properties of the weld metal.

The torch holder plays an important role in the hybrid welding mechanism, so a new design was made and analyzed.

### 3. DESIGN OF TORCH HOLDER

The role and importance of the torch holder in the hybrid welding mechanism has been mentioned in the previous sections. In the literature researches, it has been seen that the torch holder part of the torch holder cannot be angled or fixed angle holders are used as the deficiency of the experimental setups. For this reason, the design phase was realized with a torch holder approach that can move in more than one axis.

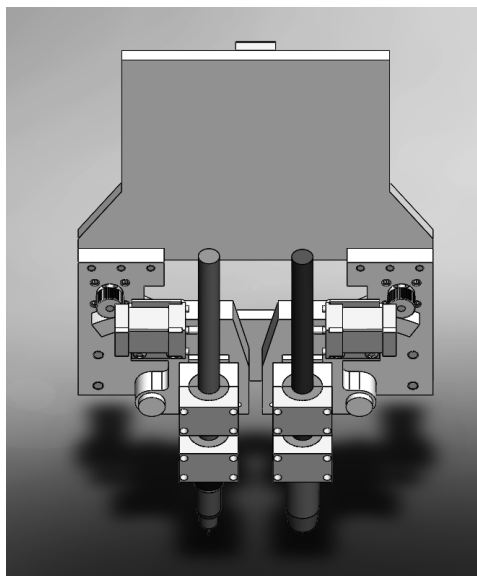


Figure 1. Torch holder design

This mechanism, which can move in more than one axis, allows the TIG torch, which acts as a pre-annealer, to perform a single-sided annealing task. The ability of the torches to move in more than one axis will increase the angular movements of the torches relative to each other, enabling experiments to be diversified.

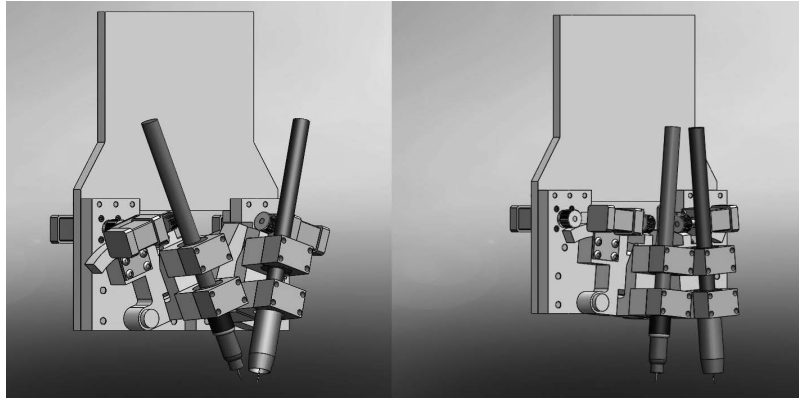


Figure 2. Torch holder mechanism x axis move

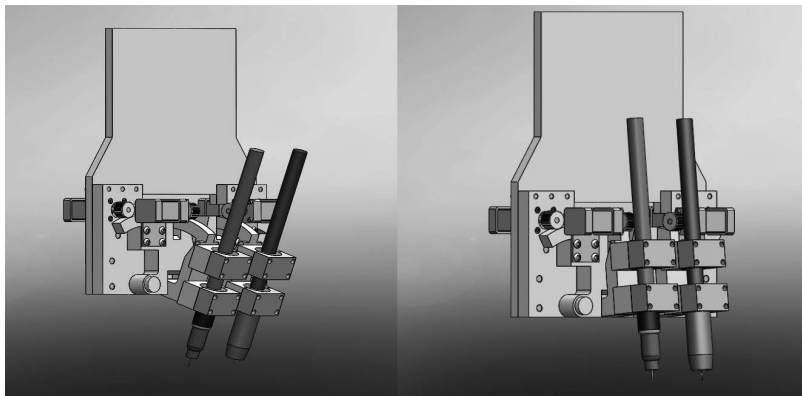


Figure 3. Torch holder mechanism y axis move

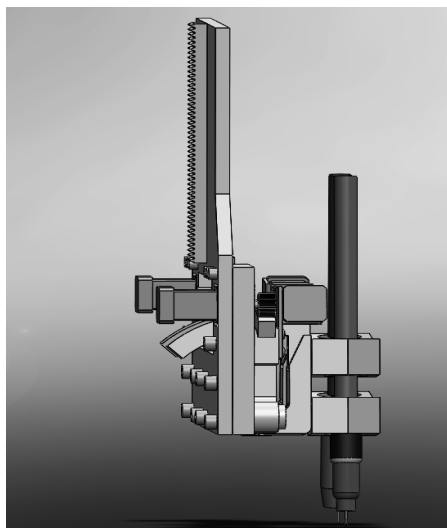


Figure 4. Torch holder mechanism z axis move

The movements of the torches on the torch carrier in the x, y, z axes are carried out precisely by means of servo motors and gears. In this way, the desired dimensions are determined more easily and parameter diversity is provided.

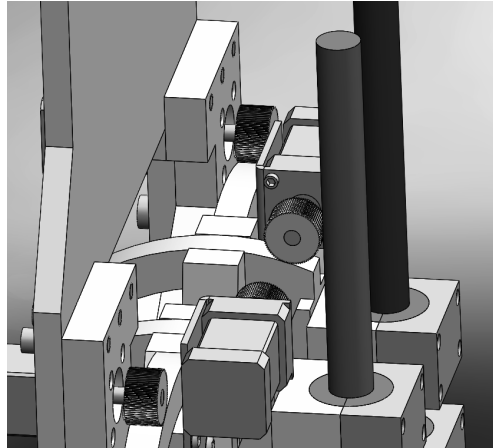


Figure 5. Adjustment of x,y axis movement with servo motors

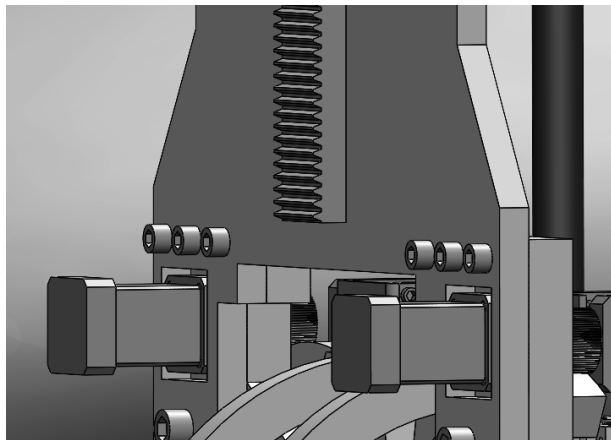


Figure 6. Adjustment of z axis movement with servo motors

#### 4. THERMAL ANALYSIS

The hybrid welding zone has a welding pool that has more force compared to conventional welding methods. The most important feature of this pool is that it can contain both MIG and TIG welding arc in the pool at the same time.

In hybrid welding, the joining process with the additional metal is carried out by MIG welding. The separation of the liquid metal falling into the weld pool from the welding wire occurs at a temperature of approximately 1800 °K. The liquid metal drop reaches a maximum temperature of 3500 °K and an average temperature of 2800 °K. [6]

The designed torch holder was transferred to the test environment by simulating the maximum temperature of the welding pool. The welded plate dimensions are 300\*150\*10 mm and the welded plates are 316 stainless steel. The welding process was carried out up to half of the

plate length. In the simulation process, the weld pool was considered moving and the mechanism was moved in the welding direction throughout the welding process.

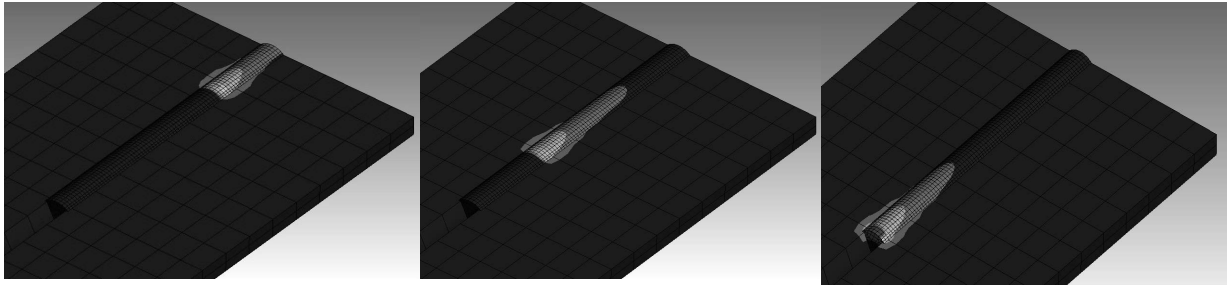


Figure 7. Welding line progression.

Afterwards, the analysis modeling of the mechanism moving in the welding direction and the material to be welded were prepared by SOLIDWORKS and ANSYS Workbench programs.

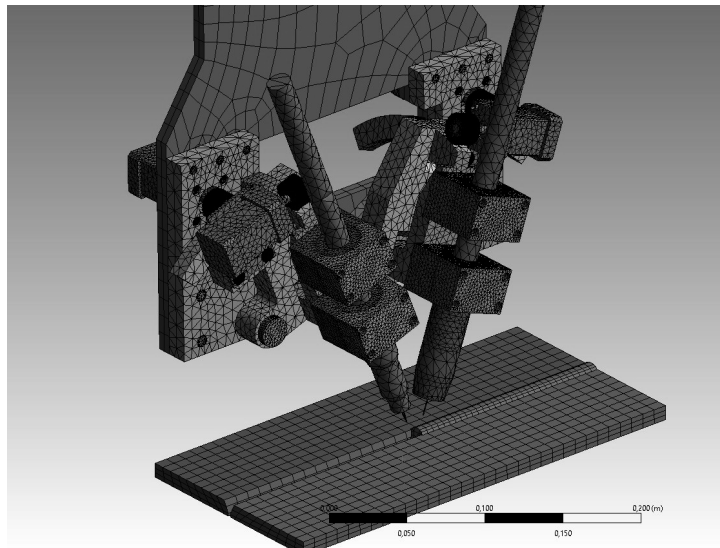


Figure 8. Experimental setup

In the experimental design, the distance between the TIG and MIG torches was 40 degrees, the distance between the torches was 14 mm and the distance of the torches to the welding plate was 10 mm.

## 5. RESULT AND DISCUSSIONS

The results obtained according to the prepared experimental environment are as follows;

In the experiment where TIG and MIG welding arcs worked in the same welding pool, the welding pool temperature was simulated as 3326 °C (3600 °K). At the end of the welding process, the minimum temperature of the welded plates was 376.3 °C in the welding direction.

In the HAZ (Heat Affected Zone) region, the temperature was measured instantaneously between 1014°C and 661°C. The temperature in the test environment was set at 22°C. The change in the temperature of the experimental environment affects the cooling rate of the weld and therefore the temperature gradient.

The maximum temperature measured on the torch holder mechanism is 314 °C. This temperature was measured on the first clamps holding the torches and on the bottom surface of the plate carrying the torch holder apparatus.

The reason why the torch holder is underheated is that the heat transmitted during the welding process encounters more than one surface.

No geometrical distortion of the torch holder was observed in the experiment.

## 6. CONCLUSION

This designed experimental setup partially reflects realistic welding conditions. The simulation is considered as a fully functioning system and welding machines are included in this idea.

Welding spatter is ignored and could not be simulated in the program. For this reason, the design will be corrected in future studies in order not to prevent the system from working by taking into account the jumps.

In this first design, a torch holder that can work on more axes was considered and the design was realized. In future studies, more independent designs such as a welding robot arm will be considered.

The torch holder, which is designed entirely from structural steel, can be improved by using different material types in areas where heat transfer is high in future studies.

Conventional designs of welding torches currently perform many welding operations. However, torch designs should be changed in hybrid welding mechanisms.

## BIBLIOGRAPHY

1. X. Meng, G. Qin, Y. Zhang, B. Fu, and Z. Zou, "High speed TIG–MAG hybrid arc welding of mild steel plate," *J. Mater. Process. Technol.*, vol. 214 (11), 2417–2424 (2014).
2. C. Schneider, C. Lisboa, R. Silva, R. Lermen, "Optimizing the Parameters of TIGMIG/MAG Hybrid Welding on the Geometry of Bead welding using the Taguchi Method", *J. Manuf. Mater. Process.*, vol. 1 (2), 14, (2017).
3. Ö. Güçlü., T. Fındık, U. Özdemir, C. Yıldız, "TIG-MIG hibrit ark kaynak yönetimi ile birleştirilen AISI304 malzemelerin mekanik ve metalurjik özelliklerinin incelenmesi," 6 th International Conference on Welding Technologies and Exhibition (ICWET'21) , Hatay, Turkey, 325-333 (2021)
4. S. Lu, Yi, Chen, X. Shi, Yu, Li, and Y. M. Chen, Jinsong, Kvidahl, Lee, Zhang, "Double-electrode arc welding process: Principle, variants, control and developments," *J. Manuf. Process.*, vol. 16, no. 1, 93–108 (2014).
5. Han, Yu, et al. "Numerical simulation of arc and droplet behaviors in TIG-MIG hybrid welding." *Materials* 13.20 (2020): 4520.
6. J. Chen, C. S. Wu, and M. A. Chen, "Improvement of welding heat source models for TIG-MIG hybrid welding process," *J. Manuf. Process.*, vol. 16, no. 4, 485–493 (2014).



26th January 2024  
Gliwice, Poland

DEPARTMENT OF ENGINEERING MATERIALS AND BIOMATERIALS  
FACULTY OF MECHANICAL ENGINEERING  
SILESIA UNIVERSITY OF TECHNOLOGY

## INTERNATIONAL STUDENTS SCIENTIFIC CONFERENCE

### **Structural and mechanical properties of an innovative composite coating for intense abrasive wear**

J. Żuławska<sup>a</sup>, M. Wnętrzak<sup>a</sup>, M. Dziergas<sup>a</sup>, B. Siedlaczek<sup>a</sup>, A. Czupryński<sup>a,\*</sup>, W. Kwaśny<sup>a</sup>

<sup>a</sup> Silesian University of Technology, Faculty of Mechanical Engineering, Department of Welding Engineering

\*email: artur.czuprynski@polsl.pl

**Abstract:** This article presents research on the structural and mechanical properties of an innovative metal matrix composite (MMC) coating designed for use in conditions of intense metal-mineral abrasive wear. The layer, which is intended to protect the working surface of drilling tools used in the oil and natural gas extraction sector, was padded using the multi-run technique on a sheet made of AISI 4715 low-alloy structural steel by Laser Direct Metal Deposition (LDMD) using a high-power fiber laser (FL). An innovative cobalt alloy matrix powder with a ceramic reinforcement of crushed titanium carbide (TiC) and tungsten-coated synthetic polycrystalline diamond (PCD) was used as the surfacing material. The influence of the preheating temperature of the base material on the susceptibility to cracking and abrasive wear of the composite coating was assessed. The structural properties of the coating were characterized by using methods such as optical microscopy and scanning electron microscopy (SEM). The mechanical properties of the hardfaced coating were assessed on the basis of the results of a metal-mineral abrasive wear resistance test, hardness measurement, and the observation of the abrasion area. The results of laboratory tests showed a slight dissolution of the tungsten coating protecting the synthetic PCD particles and the transfer of its components into the metallic matrix of the composite. Moreover, it was proved that an increase in the preheating temperature of the base material prior to welding has a positive effect on reducing the susceptibility of the coating to cracking, and increasing the resistance to abrasive wear.

**Keywords:** LDMD, cladding, deposition, titanium carbide, synthetic polycrystalline diamond

## 1. INTRODUCTION

Laser Direct Metal Deposition (LDMD) hardfacing—with direct feeding of metallic powder to the weld pool—is a very modern and advanced welding technology. The idea behind the process is to slightly melt the surface of the material with a heat source, a laser beam generated by a high-power laser, and simultaneously deliver a stream of metal powder to the weld pool through a nozzle. The additional material supplied from outside then becomes the main component of the produced coating, and as a result of the high temperature of the process, it melts with the substrate. The coatings produced using this method exhibit excellent

metallurgical bonding to the substrate, low dilution (i.e., low mixing between the clad material and the substrate material, high density, little or no cracking and good mechanical properties. The LDMD technique and other types of laser surfacing can produce coatings from almost any metal material, both on new and regenerated elements, which are used in the following industries: aerospace, energy, petrochemical, automotive, and medical [1,2].

Recently, there has been a great deal of interest in the use of the laser cladding method to produce composite surface layers on the surface of components made of ferrous and nonferrous alloys [3,4]. Metal matrix composites (MMCs), due to their properties such as high hardness, excellent wear and corrosion resistance, are currently the most interesting—in terms of research and being the most desirable materials in industrial applications—group of additional materials for laser surfacing [5,6]. The combinations of metal matrix and reinforcing particles are very diverse, and the most popular are composites based on iron, nickel, cobalt, magnesium and aluminum alloys in combination with reinforcing particles such as tungsten carbide (WC) [7,8], silicon carbide (SiC) [9], boron carbide (B<sub>4</sub>C) [10] and titanium carbide (TiC) [11], the latter being used in this study.

The aim of the study was to determine the effect of the preheating temperature of the base material on the structure, susceptibility to cracking, and abrasion resistance of a laser welded coating consisting of composite powder in a cobalt alloy matrix. A novelty in the presented results is the development of an innovative composition of the matrix reinforcement consisting of a composite containing super-hard phases in the form of ceramic particles from finely crushed TiC and spherical particles made of synthetic PCD, the latter being protected against thermal decomposition with a tungsten coating. Our results showed that there is a possibility of producing a composite laser welded coating using the ceramic reinforcement—the cobalt matrix phase system, the microstructure and abrasive properties of which are appropriate to protect the working surface three-cone toothed bits [12]. Currently, laser surfacing of the working surface of drilling cutter teeth is not used under production conditions. Typically, these elements are protected against wear by hardfacing using the oxyacetylene welding (OAW) method with a composite stick (tubular electrode) with a powder core. The implementation of the LMD surfacing technology in place of the gas surfacing technique used up to now for this industrial application may contribute to an improvement in the quality of surface layers by minimizing noncompliance, stresses, and welding deformations, as well as the share of base metal dilution in the weld, even to levels below 3%. In addition, it will allow for obtaining the required chemical composition of the padding weld to be already obtained in the first layer, contributing to greater production efficiency resulting from the automation and robotization of the padding process, and allowing for the finishing time of the padded surface to be shortened.

## **2. MATERIALS AND METHODS**

### **2.1. Materials**

The material used for surfacing was an innovative metallic powder of the Co<sub>3</sub> alloy group (Höganäs AB, Höganäs, Sweden) according to EN 147000 [13], characterized by an increased weight fraction of carbon (up to 3%) and tungsten (up to 14%). The metal powder that constituted the composite matrix material was mechanically mixed in a Turbula T2F laboratory turbulent mixer (Glen Mills Inc., Clifton, NJ, USA). The powder consisted of a hard reinforcing phase composed of crushed sharp-edged titanium carbide TiC and spherical

synthetic polycrystalline diamond PCD (Harmony Industry Diamond, Zhengzhou, China) with a tungsten coating. The proportion of the reinforcing phase components to the metal matrix components was 60% to 40% by weight with the hard phase content composed of 90% TiC with a particle size ranging from 140 to 250  $\mu\text{m}$  and 10% PCD with a particle size of 180  $\mu\text{m}$ . The chemical composition of the composite powder, claimed by patent P.435997 [14], is presented in Table 1. The base material was a low alloy structural steel of AISI 4715 (Table 2).

Table 1. Chemical composition of AISI 4715 low-alloy structural steel according to manufacturer data (TimkenSteel Ltd., Canton, OH, USA)

Element, wt.(%)									
Fe	C	Mn	Cr	Mo	Ni	Si	P	S	CEV <sup>1</sup>
Bal.	0.12–0.18	0.65–0.95	0.40–0.70	0.45–0.60	0.65–1.00	0.15–0.35	$\leq 0.015$	$\leq 0.015$	0.66

<sup>1</sup> CEV—Carbon Equivalent Value.

Table 2. Chemical composition of powder

Chemical Composition of the Matrix, wt. (%)									Ceramic Reinforcement of the Matrix, wt.(%)	
Co	Cr	W	Ni	Fe	Mn	Mo	C	Si	TiC	PCD-W
Bal.	24–28	12–14	$\leq 3$	$< 5$	$\leq 2$	$\leq 1$	2.5–3	$\leq 1$	90	10

Notes: Carbide to matrix ratio: 60/40 wt. (%).

## 2.2. Laser Processing

The laser powder surfacing process was carried out using the LDMD technique—with direct feeding of the composite powder to the weld pool—on a robotic stand equipped with a modern surfacing system using a YLS-4000 ytterbium fiber laser system (IPG Photonics Corporation, Oxford, MA, USA) with a wavelength of  $\lambda=1070$  nm and a maximum laser beam power of 4000 W mounted on a REIS RV30-26 six-axis robot (Reis Robotics, Obernburg am Main, Germany), Figure 1. The diameter of the laser spot at the focal plane, 20 mm from the nozzle tip, measured with a UFF100 Laserscope (Prometec GmbH, Aachen, Germany), was 5 mm, with energy distribution in the TEM01\* beam. The powder cladding set-up consisted of a computer-controlled powder feeding system and a coaxial cladding nozzle integrated with a Computerized Numerical Control (CNC) five-axis gantry. Coaxial powder injection was realized by using nozzle gas, carrier gas and shielding gas—Argon 5.0 (99.999%). Cladding was performed at the following gas flow rates: nozzle gas (Ar) = 15 L/min, carrier gas (Ar) = 2.8 L/min and shielding gas (Ar) = 12 L/min. In order to determine the range of optimum surfacing parameters, a series of single-run padding welds was carried out with laser power values of 1400, 1600, 1800, 2000 and 2200 W with a surface speed from 4 to 12 mm/s and a powder feed rate from 15 to 30 g/min. The optimum parameters for the surfacing of the composite coating (Table 3) were defined as the parameters that ensured a uniform distribution of the powder across the entire surface of the liquid metal in the weld pool, the correct depth of fusion  $g < 2$  mm, a layer height  $h < 5$  mm and a percentage of dilution of the base metal in the surface layer  $D < 5\%$  (Figure 2).



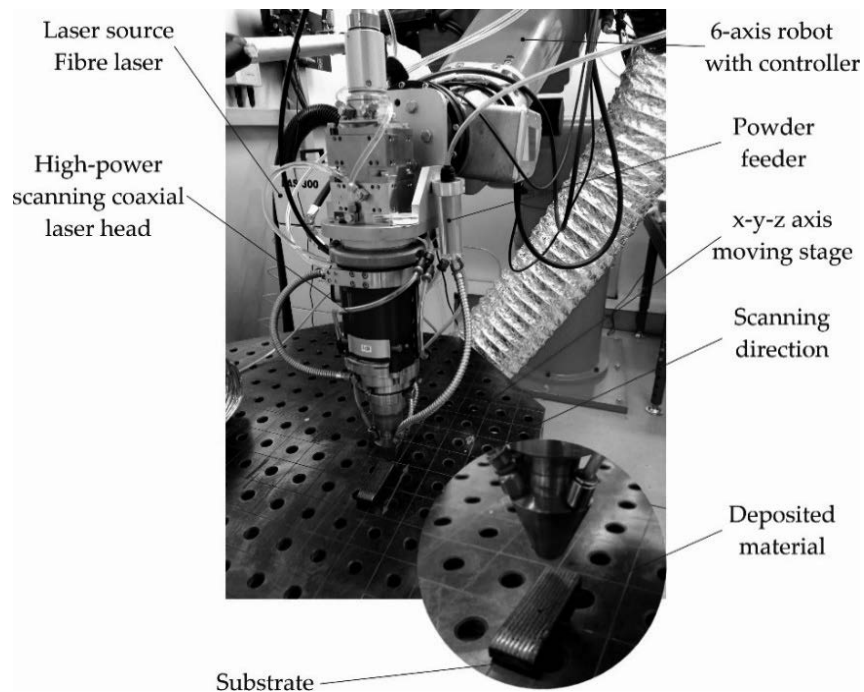


Figure 1. View of the test stand used for robotic surfacing with the LDMD

Table 3. Parameters for laser surfacing with Co3+TiC+PCD powder on AISI 4715 steel

Process Parameters	Value of the Parameter
Laser Power (W)	1800
Scanning Speed (mm/s)	8
Laser Spot Size, (mm)	5
Powder Feed Rate (g/min)	24
Overlap Ratio (%)	33
Heat Input <sup>1</sup> (J/mm)	225

<sup>1</sup> defined as the laser power divided by the scanning speed.

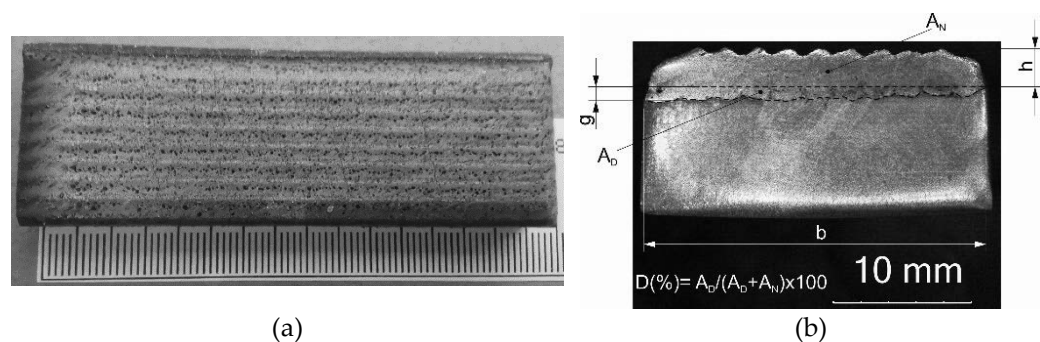


Figure 2. LDMD coating with composite powder: (a) a view from the face of the padding welds, (b) a cross section of the coating

Test samples were produced with dimensions of  $75 \times 25 \times 10$  mm—in a series of three, welded either without or with preheating of the substrate using an oxyacetylene torch to temperatures of 100, 200 or 300 °C, and the samples were marked with the symbols T0 (no heating), T100, T200 or T300, respectively.

### 2.3. Methodology of Research

In order to assess the quality of the surfacing welds and to determine the number of cracks in the surfacing layers at different preheating temperatures of the substrate, non-destructive testing i.e., visual tests (VT) and penetration tests (PT) were carried out. The structural and mechanical properties were determined on the basis of the analysis of the results of macro- and microscopic metallographic tests, and hardness measurements as well as metal-mineral abrasive wear resistance tests.

## 3. RESULTS AND DISCUSSION

### 3.1. Non-Destructive Testing Results

Non-destructive testing of laser-welded composite layers of cobalt Co3 powder containing of TiC and PCD ceramic particles on the substrate of low-alloy AISI 4715 structural steel allowed the type, location and size of surface imperfections to be determined. The results of penetration tests of surface coatings without heating or with preheating of the base material to temperatures of 100, 200 or 300 °C are shown in Figure 3.

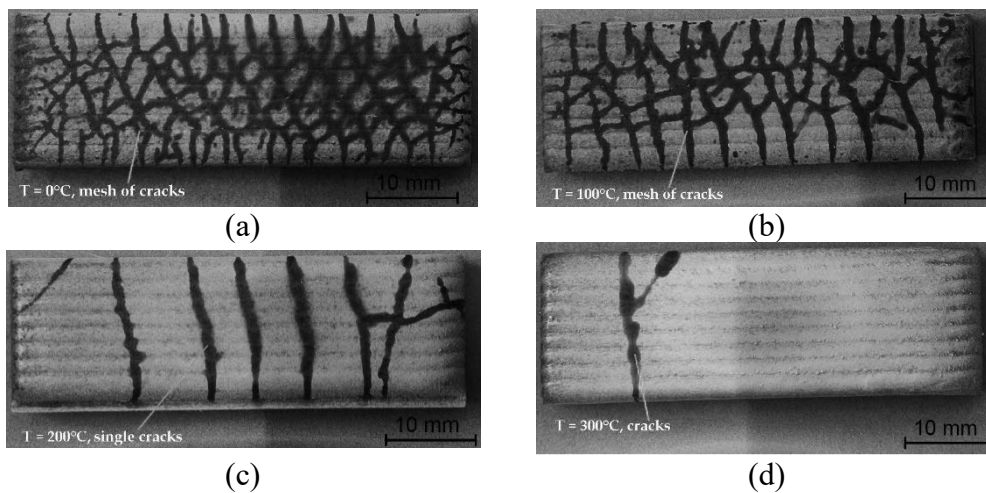


Figure 3. View of the coating laser-welded with composite powder after penetration tests (PT): (a) surfacing without heating, surfacing with preheating of the base material to temperatures of (b) 100 °C, (c) 200 °C, (d) 300 °C

In terms of the quality of workmanship, the coatings were characterized by a high regularity of the outer plane and the symmetry of the successive overlapping, weld beads. VT and PT of the surface of the layers showed only the presence of radial cracks (1051) and transverse cracks (1021). The lack of preheating of the substrate before surfacing resulted in the appearance of a dense network of cracks, Figure 3a. Increasing the preheating temperature to 100 °C caused the crack mesh density to decrease, and in the temperature range from 200 to 300 °C, a significant reduction was observed in the number of cracks in the layer. Only single cracks were detected spreading throughout the coating width in a line perpendicular to the welding direction, Figure 3c–d. A higher content of matrix alloying additives and a higher proportion of hard phase ceramic particles reinforcing the composite contributed to an increase in abrasion resistance, but at the same time increased the tendency for surface cracks to form in the padding weld.

Cracks appeared during cooling due to the difference in the thermal expansion coefficients of the base material and the padding weld material [15]. The cracks most often penetrated deep into the base material and in no way weakened the adhesion of the surface coating. The effect of the preheating temperature of the base material before surfacing on the number of cracks in the composite layer is shown in Figure 4.

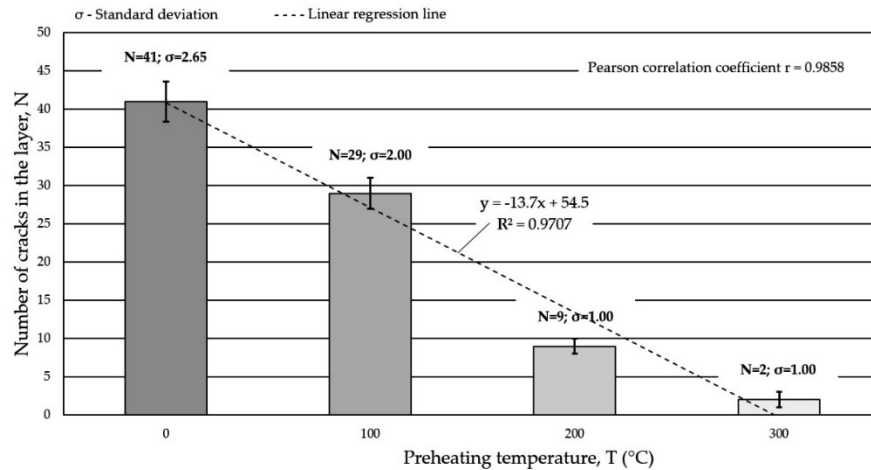


Figure 4. Influence of the preheating temperature of the base material before surfacing on the number of cracks in the composite layer

### 3.2. Metallographic Test Results

The results of microscopic metallographic observations of the composite coating allowed the matrix structure as well as the type, distribution and dimensions of the ceramic reinforcement to be determined. SEM observations were carried out at 80, 500 and 1500 times magnification. Secondary Electron (SE) as well as Back Scattered Electron (BSE) detectors were used for image acquisition, the latter to more clearly show the chemical contrast, ensuring the highest image quality. For detailed structural analysis of the areas containing carbide reinforcement particles, a transmission electron microscope (TEM) was used to determine the grain size, structural defects and cracks in the TiC and PCD particles. The examples results of the microscopic observations are shown in Figure 5.

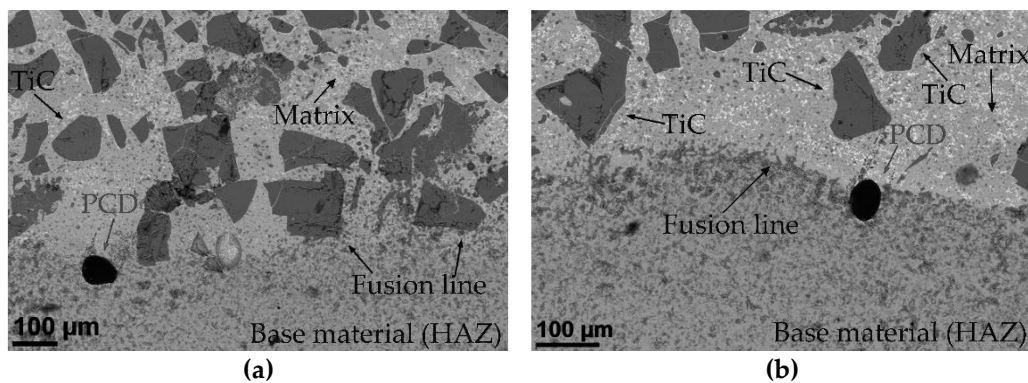


Figure 5. Area of the composite shell fusion line. SEM images (BSE detector): (a) left side of the coating section and (b) right side of the coating section

### 3.3. Hardness Measurements' Test Results

Measurements of the hardness of the outer surface and the cross-section of the coating are presented in Table 4 and Figure 6.

Table 4. Results of Rockwell C hardness measurement on the outer surface of the coating laser welded with Co<sub>3</sub>+TiC+PCD composite powder on AISI 4715 low-alloy structural steel

Specimen number	Hardnesses, (HRC)					Average hardness of the tested samples	Standard deviation	Dilution ratio, (%)
	Measurement point number 1	2	3	4	5			
T 0	59.8	61.8	60.9	61.7	60.3	60.9	0.9	2.6
T 100	60.4	59.5	61.2	59.2	60.0	60.1	0.8	3.3
T 200	60.2	57.9	59.4	58.7	59.9	59.2	0.9	6.5
T 300	57.4	58.5	59.7	59.0	58.8	58.7	0.8	8.2

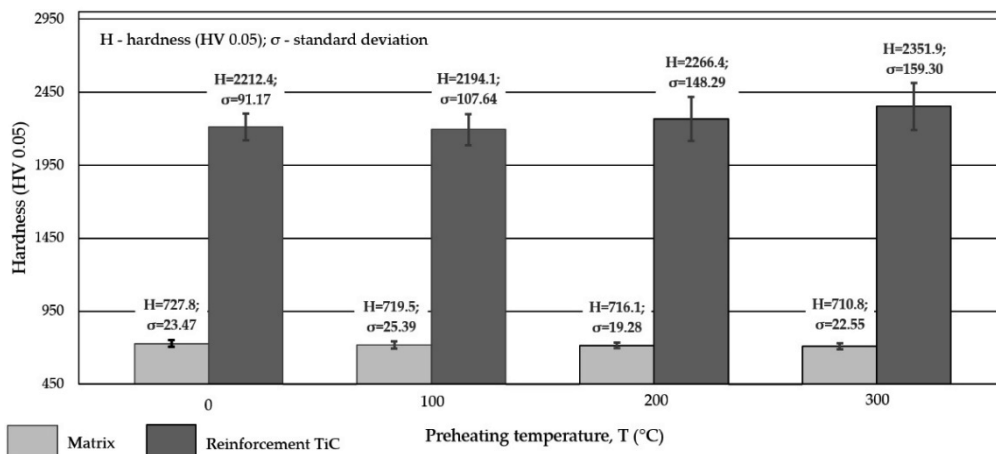


Figure 6. HV hardness measurement results on the cross-section of the coating laser-padded with Co<sub>3</sub>+TiC+PCD-W composite powder on AISI 4715 low-alloy structural steel

The results of the tests presented in Table 4 show that, even in the case of a large share of the base material in the padding weld, the hardness measurements on the surface of the layer show only a slight downward trend. The share of base material did not affect the final microhardness of the alloy matrix (Figure 6), and thus did not affect the overall hardness of the coating.

### 3.4. Abrasive Wear Test Results

The metal-mineral abrasion resistance of the composite coating was determined by calculating its average volume loss after the ASTM G65 test, Table 5. The results obtained were related to the average share of the base metal dilution in the surface layer, Table 4. The character of the abrasive wear of the top coat was assessed on the basis of visual tests (Figure 7), determining the average height of the abrasion area profile depending on the preheating temperature of the base material, Figure 8.

Table 5. The results of the metal-mineral abrasive wear resistance test of the composite coating welded with the LDMD method according to ASTM G65

Specimen Designation	Mass before Test, (g)	Mass after Test, (g)	Mass Loss, (g)	Average Mass Loss, (g)	Clad Layer Density, (g/cm <sup>3</sup> )	Average Volume Loss, (mm <sup>3</sup> )
No preheating						
T 0_1	149.8935	149.8203	0.0732	0.0806	5.7785	13.9482
T 0_2	149.8704	149.7824	0.0880			
Preheating temperature, T = 100 °C						
T 100_1	149.4675	149.3991	0.0684	0.0613	6.0176	10.1867
T 100_2	150.2985	150.2443	0.0542			
Preheating temperature, T = 200 °C						
T 200_1	150.8568	150.8377	0.0191	0.0184	6.3805	2.8837
T 200_2	149.7372	149.7195	0.0177			
Preheating temperature, T = 300 °C						
T 300_1	149.9748	149.9639	0.0109	0.0101	6.6169	1.5263
T 300_2	149.8394	149.8301	0.0093			

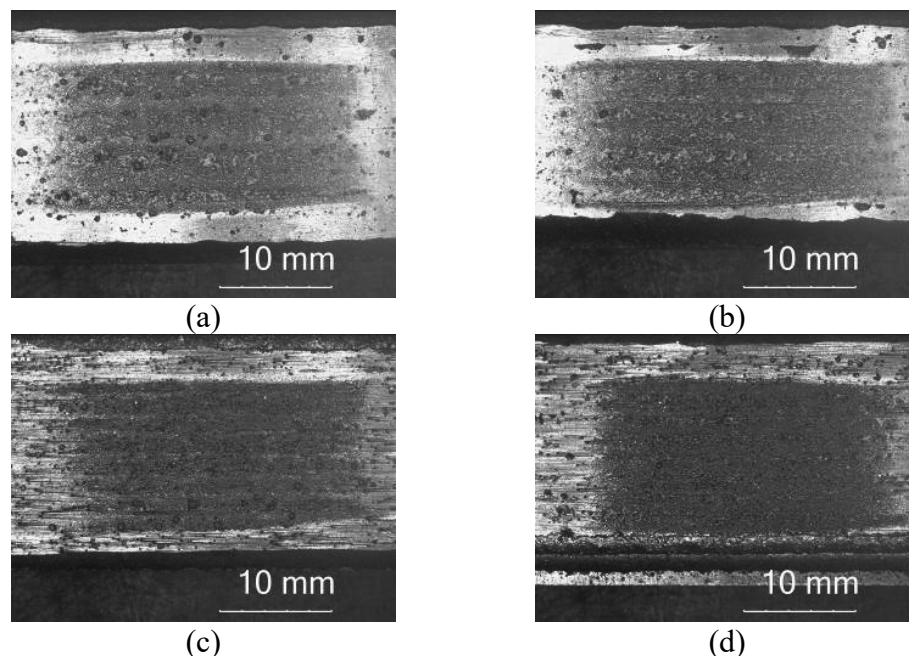


Figure 7. View of the surface of the abrasion area after the metal-mineral abrasion test of a composite coating welded by LDMD: (a) without heating the substrate and with heating to a temperature of: (b) T = 100 °C, (c) T = 200 °C, (d) T = 300 °C

The metal-mineral abrasion test according to ASTM G65, Procedure A, was carried out under medium stress because the sand grains after their interaction with the surface of the test sample were only partially crushed. The mass loss of the composite coating after the abrasive test decreased with increasing preheating temperature of the base material and density of the padding weld. The maximum mass loss of the composite coating, which exceeded 0.08 g, was recorded for the sample made without preheating the base material before padding, and the smallest for the padded coating with preheating the base material to 300 °C.

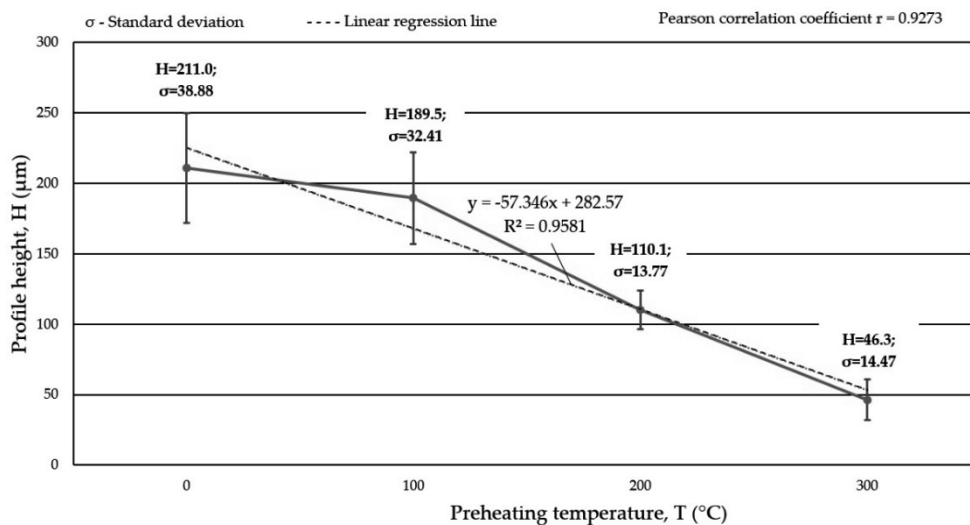


Figure 8. Dependence of the height of the profile of the abrasion area of the composite coating surface on the preheating temperature of the substrate material

#### 4. CONCLUSIONS

The purpose of this research was to assess the effect of the preheating temperature of the base material—low-alloy structural steel of grade AISI 4715—on the susceptibility to cracking, resistance to metal-mineral abrasive wear and metallographic structure LDMD coating, which was innovative in terms of its chemical composition and the type of hard matrix reinforcement phase. In the case analyzed, the substrate material was a low-alloy structural steel AISI 4715 for which the chemical equivalent of carbon  $CEV = 0.65\%$ . It is assumed that, with  $CEV$  values higher than  $0.60\%$ , steel is considered difficult to weld, and therefore requires the use of additional treatments regardless of the size and weight of the element being welded. Then, precautions such as preheating the material and maintaining this temperature throughout the surfacing process should be applied. After surfacing, it is also recommended to cool the element very slowly using heating mats, as well as often additional heat treatment. Preheating and meeting the temperature regime during surfacing, especially large components such as a drill bit with milled teeth, are critical factors in terms of surfacing efficiency and weld quality. This treatment allows for an increase in the speed of surfacing, a better melting and flow of the alloy, and a reduction in the likelihood of thermal decomposition of the carbide phase. The results allow us to conclude that the selected chemical composition of the metallic phases as well as the type, amount and size of the hard phase particles of the developed composite powder allow for high accuracy, repeatability of dosing and near perfect melting with the use of laser powder deposition systems. Preheating the base material above  $300\text{ }^{\circ}\text{C}$  significantly reduces the susceptibility to cracking and porosity of the metal deposit, reduces internal stresses in the TiC (preventing particle brittleness) and significantly increases resistance to metal-mineral abrasive wear. The process of LDMD with direct feeding of the powder to the weld pool helps to maintain the structural and thermal stability of the synthetic PCD particles. The tungsten from the protective coating of the PCD particles slightly enriches the matrix of the composite and does not significantly increase the hardness measured on the outer surface and the cross section of the surface coating.

**FUNDING:** The research was carried out thanks to the co-financing of project-oriented education – PBL edition. X, as part of the Excellence Initiative – Research University programme

## **BIBLIOGRAPHY**

1. S. Bhattacharya, G.P. Dinda, A.K. Dasgupta, J. Mazumder, Microstructural evolution of AISI 4340 steel during Direct Metal Deposition process. *Mater. Sci. Eng. A* 2011, 528, 2309–2318.
2. A. Lisiecki, Study of Optical Properties of Surface Layers Produced by Laser Surface Melting and Laser Surface Nitriding of Titanium Alloy. *Materials* 2019, 12, 3112.
3. S. Yang, W. Liu, M. Zhong, Z. Wang, TiC reinforced composite coating produced by powder feeding laser cladding, *Mater. Lett.* 2004, 58, 24, 2958–2962.
4. Zhang, P.; Pang, Y.; Yu, M. Effects of WC Particle Types on the Microstructures and Properties of WC-Reinforced Ni60 Composite Coatings Produced by Laser Cladding. *Metals* 2019, 9, 583.
5. V.V. Popov, A. Pismenny, N. Larianovsky, A. Lapteva, D. Safranchik, Corrosion Resistance of Al–CNT Metal Matrix Composites. *Materials* 2021, 14, 3530.
6. K. Senthil Kumar, S. Karthikeyan, R. Gokul Rahesh, Experimental investigation of wear characteristics of aluminium metal matrix composites, *Mater. Today Proc.* 2020, 33, 139–3142.
7. A. Czupryński, Comparison of Properties of Hardfaced Layers Made by a Metal-Core-Covered Tubular Electrode with a Special Chemical Composition. *Materials* 2020, 13, 5445.
8. J. Yang, F. Liu, X. Miao, F. Yang, Influence of laser cladding process on the magnetic properties of WC–FeNiCr metal–matrix composite coatings. *J. Mater. Process. Technol.* 2012, 212, 1862–1868.
9. Q. Li, G.M. Song, Y.Z. Zhang, T.C. Lei, W.Z. Chen, Microstructure and dry sliding wear behavior of laser clad Ni-based alloy coating with the addition of SiC. *Wear* 2003, 254, 222–229.
10. X. Niu, M.J. Chao, X.W. Zhou, D.S. Wang, B. Yuan, Research on in-situ synthesis of B<sub>4</sub>C particulate reinforced Ni-based composite coatings by laser cladding. *Chin. J. Lasers* 2005, 32, 1583–1588.
11. J. Nurminen, J. Näkki, P. Vuoristo, Microstructure and properties of hard and wear resistant MMC coatings deposited by laser cladding. *Int. J. Refract. Hard Mater.* 2009, 27, 472–478.
12. A. Czupryński, Microstructure and Abrasive Wear Resistance of Metal Matrix Composite Coatings Deposited on Steel Grade AISI 4715 by Powder Plasma Transferred Arc Welding Part 1. Mechanical and Structural Properties of a Cobalt-Based Alloy Surface Layer Reinforced with Particles of Titanium Carbide and Synthetic Metal–Diamond Composite. *Materials* 2021, 14, 2382.
13. EN 14700. Welding Consumables. In *Welding Consumables for Hardfacing*; CEN: Brussels, Belgium, 2014.
14. A. Czupryński Artur, M. Stawarz, PL Patent P.435997, 2020.
15. A. Czupryński, M. Żuk, Matrix Composite Coatings Deposited on AISI 4715 Steel by Powder Plasma-Transferred Arc Welding. Part 3. Comparison of the Brittle Fracture Resistance of Wear-Resistant Composite Layers Surfaced Using the PPTAW Method. *Materials* 2021, 14, 6066.



26th January 2024  
Gliwice, Poland

DEPARTMENT OF ENGINEERING MATERIALS AND BIOMATERIALS  
FACULTY OF MECHANICAL ENGINEERING  
SILESIA UNIVERSITY OF TECHNOLOGY

## INTERNATIONAL STUDENTS SCIENTIFIC CONFERENCE

### **Biopolymers as coating materials for zinc alloys and their biological evaluation**

M. Żydowicz<sup>a,c</sup>, L. Ochocka<sup>a,c</sup>, S. Bober<sup>a,c</sup>, M. Gawlas<sup>b</sup>, M. Rzepiela<sup>b</sup>, K. Cesarz-Andraczke<sup>b</sup>, M. Nitszke<sup>a</sup>, M. Adamiec-Organiściok<sup>a</sup>, M. Skonieczna<sup>a</sup>

<sup>a</sup> Silesian University of Technology, Faculty of Automation, Electronics and Computer Science, Department of Engineering and Systems Biology

email: mz300749@student.polsl.pl

<sup>b</sup> Silesian University of Technology, Faculty of Mechanical Engineering, Department of Engineering Materials and Biomaterials

email: katarzyna.cesarz-andraczke@polsl.pl

<sup>c</sup> Student Science Club of Engineering and Systems Biology at the Center of Biotechnology, Silesian University of Technology, Krzywoustego 8, 44-100 Gliwice, Poland

**Abstract:** The article presents the methodology for producing biopolymers, examining their structure and cytotoxicity to human cells in in vitro tests. The produced biopolymers may have potential application as a coating material on zinc alloys for the purposes of regenerative medicine and implantology.

**Keywords:** biopolymers, biomaterials, cytotoxicity, biological assessment, in vitro tests

### **1. INTRODUCTION**

Many different macromolecules are used in medicine. One of them are polymers - natural or synthetic. Polymers in medicine are widespread in many fields, e.g. dentistry, surgery, implantology. The most commonly used polymer is polyvinyl chloride (PVC), which is used in blood collection and transfusion kits, for transfusing fluids during peritoneal dialysis, and for the production of catheters, probes, tubing, drains, urine and secretion reservoirs. However, polystyrene (PS) is used to produce artificial teeth and jaw prostheses. In addition, polymers are used to produce devices, instruments and apparatus used externally, e.g. laparoscopes, electrodes, drains. It is also worth mentioning prosthetic limbs and facial parts. Polymers are divided into natural and artificial (man-made). In medicine, the former are used, for example, for the reconstruction of joint surfaces - collagen, for fibrinogen implants in urology and vascular surgery - fibrinogen, for tissue fusion - silk, and for sealing synthetic blood vessels - chitin. Synthetic polymers are also used in medicine. Vascular prostheses are made of polyesters, e.g. PET - polyethylene terephthalate. Silicone rubber is used to produce artificial heart valve components, and silicone resins are used to cover blood vessel prostheses and brain dural prostheses. Biodegradable polymers are also an important group and are decomposed by



microorganisms into carbon monoxide (IV) and water. They demonstrate the ability to degrade in the body at a set rate, depending on many factors. The most well-known are aliphatic polyesters - polylactide and poly(butylene succinate). Their main applications include endoprosthetics, wound dressing and the production of matrices for tissue regeneration [1]. Caseins are a group of proteins found mainly in cow's milk. Casein currently has a small and very specific application in medicine, such as alginate-casein-WS2 microspheres replacing bone graft with a synthetic one [2] or in the production of polycaprolactone fibers as a wound healing material [3]. They are glycoproteins with two cysteines that form intermolecular disulfide bonds. Unlike other proteins, casein has a random three-dimensional structure and does not form crystals, which is evidence of the lack of a homogeneous tertiary structure and an unstable secondary structure[4]. There are four subtypes of casein:  $\alpha$ S1,  $\alpha$ S2,  $\beta$  and  $\kappa$ , with the  $\alpha$ S1 and  $\alpha$ S2 types making up the largest portion in milk[3]. All these subtypes differ in their properties[4]. Polylactide (PLA) is an aliphatic polyester obtained from natural raw materials - lactic acid or lactide. Materials made from it have a variety of properties, from soft and flexible to hard and durable. The mechanism of polylactide degradation in the human body is very similar to the degradation in the natural environment. This polymer is converted into CO<sub>2</sub> and water, which is why it is considered biodegradable and non-toxic. PLA is used to make dressing materials, surgical threads, bone implants, connectors and screws for connecting bones. An important possibility of PLA is its use as a drug carrier during the so-called "targeted therapy"[5]. In the case of zinc alloys, as potentially resorbable materials, there is a challenge in controlling its degradation rate, because they are characterized by an irregular degradation process. This process starts at the alloy surface, so it is necessary to use a protective coating, such as a self-healing casein coating. Zinc alloys, being studied in the context of their potential use as resorbable implant materials, require the development of effective strategies to control the degradation process and the introduction of innovative solutions, such as self-healing coatings, to improve their suitability in the field of implantology [6].

## **2. MATERIALS AND METHODOLOGY**

The biopolymers were produced in laboratory conditions using casein and polylactide. Polylactide was dissolved in dichloromethane at room temperature to obtain solutions with the following concentrations: 0.5, 1 and 2%. The casein solution was heated until it became a homogeneous mixture. Control samples were prepared without the use of casein, which contained polylactide only. In the next step, 2 ml of casein solution was added to 10 ml of dissolved polylactide, stirred with a magnetic stirrer for about 2 minutes at room temperature, and then poured to the bottom of 3 cm diameter dishes and left to set spontaneously. Before biological research began, the obtained biopolymers were observed under a stereoscopic microscope to examine their structure. Magnifications of 25x and 50x were used. The final stage of the research was the biological evaluation of the obtained biopolymers. Each biopolymer was divided into 4 equal parts and then sterilized by surface brightening using a UVC lamp, dose 100 j/m. Osteosarcoma cells, U2OS (ATTC), were seeded at  $10 \times 10^4$  in 2 ml of DMEM-F12 medium (supplemented with 10% bovine serum, FBS and antibiotics) on the prepared fragments of materials. The cultures were incubated for another 72 hours in a 12-well plate (seeding area 3.8 cm<sup>2</sup>). After incubation, the cells were fixed with 70% ethanol, then rinsed with water, dried, and kept in a refrigerator until microscopic analysis. The fixed cells on the materials were labeled with Dapi stain (SlowFade™ Gold Antifade Mountant with DAPI, Thermo Fisher), and then the signal was captured using an Olympus FluoView FV1000™

confocal microscope (Olympus LS, Tokyo, Japan), in the Blue channel 365/430 nm. A magnification of 10x was used.

### 3. RESEARCH RESULTS

The results of structural observations of biopolymers performed using a stereoscopic microscope are shown in Figures 1 and 2.

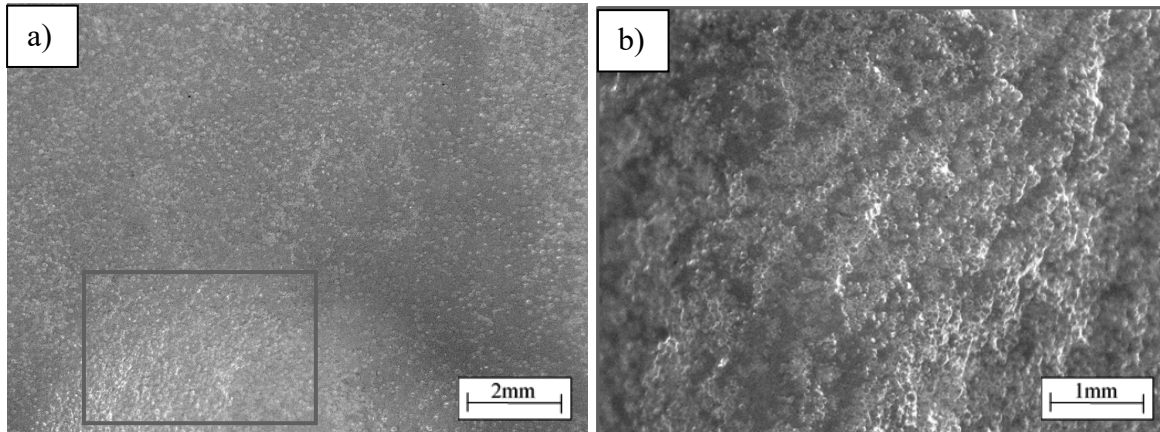


*Figure 1. Image for 0.5% PLA with the addition of 2% casein at 25x (a) and 50x (b) magnification.*

Structural observations of biopolymers performed using a stereoscopic microscope showed that a rough, bubble-like structure was obtained only for samples with a lower PLA content - 0.5%. For the remaining samples, no such structures were observed - they remained completely uniform.

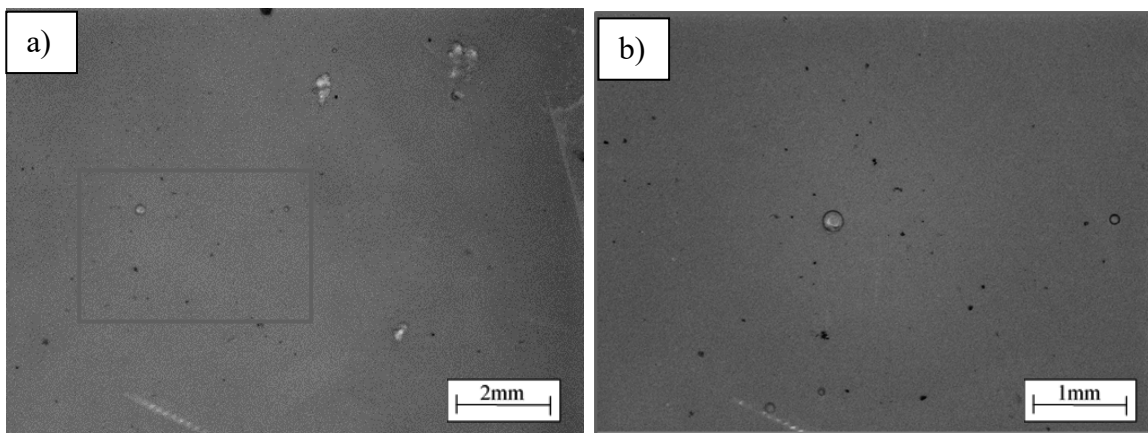


*Figure 2. Image for 0.5% PLA at 25x (a) and 50x (b) magnification.*

The results of biological evaluation tests performed using a confocal microscope at 10x magnification are shown in Figure 3.

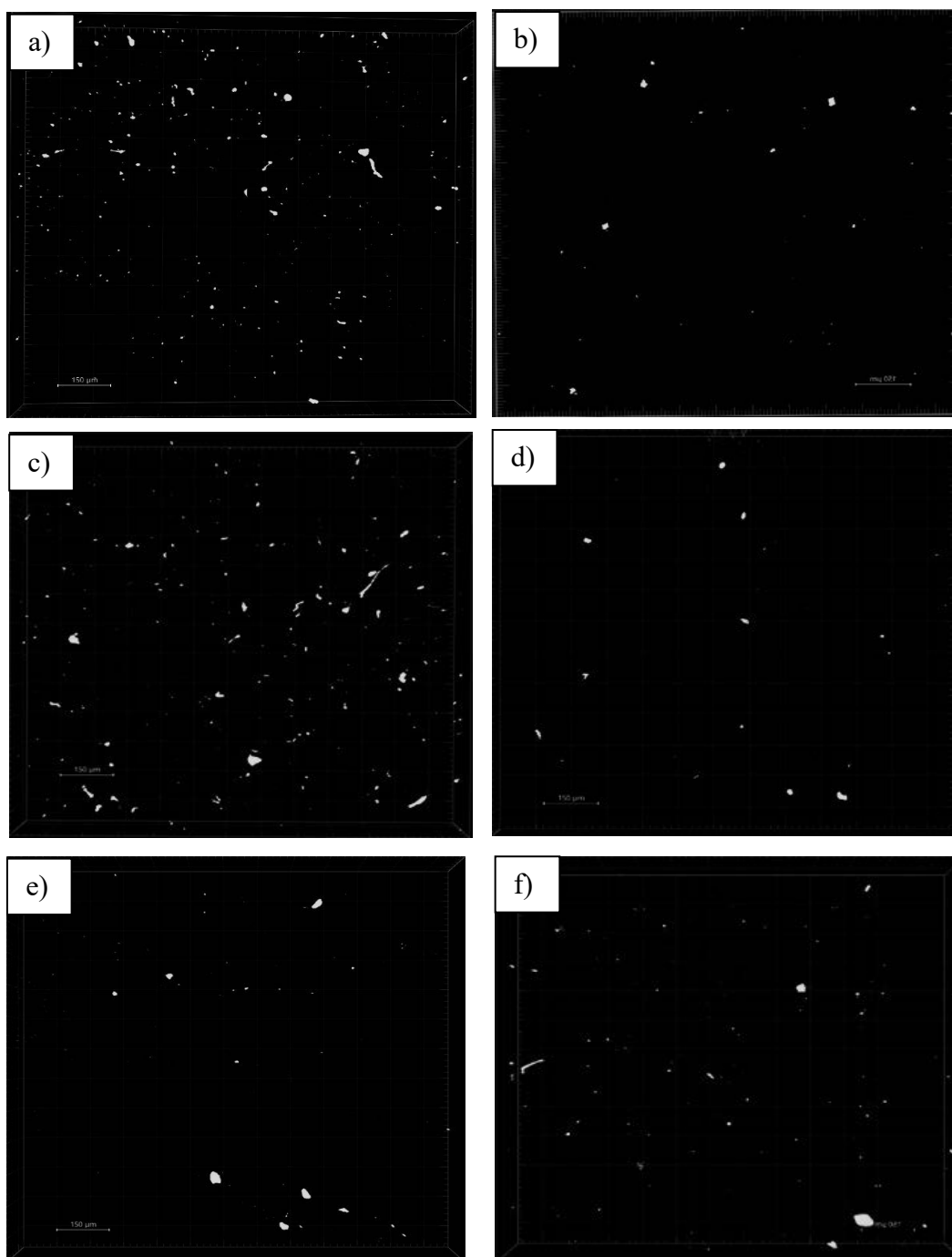


Figure 3. Biological test results for: a) 0.5% PLA, b) 0.5% PLA + 2 ml casein glue, c) 1% PLA, d) 1% PLA + 2% casein, e) 2% PLA, f) 2% PLA + 2% casein

The results of studies using a confocal microscope show a greater number of labeled cell nuclei of the U2OS line in the case of biopolymers containing only 0.5 or 1% of PLA. After adding casein glue or casein, the number of cells growing on the materials and dye-marked nuclei was lower. Opposite conclusions can be obtained in the case of 2% PLA samples - more nuclei were observed in the case of the sample containing additional casein.

#### 4. SUMMARY

Cells were seeded on each of the samples produced and kept alive for 72 hours. However, the sample of 0.5% PLA + 2% casein had too brittle and delicate structure and was damaged; such a low concentration of PLA with the addition of casein can be excluded from further research. The most promising results using casein were obtained with the 2% PLA sample. In conclusion, the PLA surface may be an optimal environment for the growth of osteosarcoma, U2OS, cells. When using casein, the most optimal concentration of PLA for the modification of the tested surfaces is 2%. Wyniki dostarczyły cennych wniosków i pozwoliły ukierunkować dalsze badania z wykorzystaniem PLA i kazeiny, jako biopolimerów do potencjalnego wykorzystania w modyfikacji implantów biomateriałami

#### BIBLIOGRAPHY

1. E. Olędzka, M. Sobczak, W. L. Kołodziejski, Polimery w medycynie — przegląd dotychczasowych osiągnięć, Polimery 11—12 (2007) 793—916.
2. P. A. Dalavi, A. Prabhu, M. Sajida, S. Murugan, V. Jayachandran, Casein-assisted exfoliation of tungsten disulfide nanosheets for biomedical applications, Colloids and Surfaces B: Biointerfaces, 232 (2023) 113595.
3. J. Ahmed, E. Guler, G. Sinemcan Ozcan, M. Emin Cam, S. Homer-Vanniasinkam, M. Edirisinghe Casein fibres for wound healing. Journal of The Royal Society Interface 20(2023) 0166.
4. P. Siročić, A., Kratošil L. Krehula, Z. Katančić, Z. Hrnjak-Murčić Characterization of Casein Fractions – Comparison of Commercial Casein and Casein Extracted from Cow's Milk. Chem. Biochem. Eng. Q., 30 (4) (2016) 501–509.
5. P. Ruśkowski, A. Gadomska-Gajadhur, Polilaktyd w zastosowaniach medycznych. Tworzywa Sztuczne w Przemysle, 2 (2017) 32-35.
6. K. Cesarz-Andraczke, B. Tuncay, W. Pakieła, Z. Brytan, M. Skonieczna, J. Bidulská, R. Bidulsky, The Biocompatibility and Self-Healing Effect of a Biopolymer's Coating on Zn Alloy for Biomedical Applications, Materials 16 (2023), 7486.

*The work was created as a result of the Project Based Learning (PBL) project titled: Production of biopolymers and their biological assessment.*